Faculty of Aerospace Engineering

Adaptive Incremental Backstepping Flight Control

Applied to an F-16 aircraft model

P. van Gils

May 7, 2015

Delft University of Technology

Challenge the future

Adaptive Incremental Backstepping Flight Control

Applied to an F-16 aircraft model

Master of Science Thesis

For obtaining the degree of Master of Science in Aerospace Engineering
at Delft University of Technology

P. van Gils

May 7, 2015

Faculty of Aerospace Engineering · Delft University of Technology

TU Delft

Delft University of Technology

Delft University Of Technology
Department Of
Control and Simulation

The undersigned hereby certify that they have read and recommend to the Faculty of Aerospace Engineering for acceptance a thesis entitled **"Adaptive Incremental Backstepping Flight Control"** by **P. van Gils** in partial fulfillment of the requirements for the degree of **Master of Science**.

Dated: May 7, 2015

Readers:

Prof. dr. ir. J. A. Mulder

Dr. ir. Q. P. Chu

Dr. ir. E. van Kampen

Dr. ir. C. C. de Visser

Ir. J. H. Breeman

Acknowledgments

This master thesis presents the conclusion of a period of self-fulfilling and mind-opening studies at the Delft University of Technology. An achievement that would not have been possible without the assistance and guidance of several individuals to whom I owe genuine gratitude and respect. Although it is impossible to list everyone here, I would like to mention some in particular.

First of all, I would like to express my sincere gratitude to my supervisor Dr. ir. Ping Chu for guiding me towards the topic of this thesis and for providing me insight and expertise that greatly assisted this research. Ping always had time for discussions on a wide variety of subjects.

Besides my supervisor, I would like to thank Prof. dr. ir. Bob Mulder, Dr. ir. Erik-Jan van Kampen, Dr. ir. Coen de Visser and Ir. Jan Breeman for taking place in my thesis committee.

I would like to emphasize my deep gratitude for the help obtained from Prof. dr. ir. Max Mulder during my studies at the Delft University of Technology. He opened the door to the Control & Simulation Division and assisted me in obtaining a very interesting internship position at Boeing Research & Technology in Madrid.

Many thanks go to my fellow students for the great time during graduation. Discussions helped to gain insights into a variety of other topics explored in the Control & Simulation Division. In particular I would like to thank Victor Ho, Sander van Lochem and Rick de Vries for all the interesting discussions and fun we have had in our office.

Last, but most definitely not least, I would like to thank my family and friends for their unconditional support and encouragement during my studies.

Delft University of Technology,
May 7, 2015

Pieter van Gils

Contents

List of Figures

List of Tables

Acronyms

ABS	Adaptive Backstepping
ADI	Approximate Dynamic Inversion
AF	Auxiliary Filter
AFTFC	Active Fault Tolerant Flight Control
AMI	Aerodynamic Model Identification
ANDI	Adaptive Nonlinear Dynamic Inversion
ASE	Aircraft State Estimator
BS	Backstepping
CA	Control Allocation
CF	Command Filter
CFD	Computational Fluid Dynamics
CLF	Control Lyapunov Function
DUT	Delft University of Technology
EASA	European Aviation Safety Agency
EKF	Extended Kalman Filter
FA	Function Approximator
FDI	Fault Detection and Isolation
FEP	Flight Envelope Protection
FTC	Fault Tolerant Control
FTFC	Fault Tolerant Flight Control
GPS	Global Positioning System
I&I	Immersion and Invariance
IBS	Incremental Backstepping
IEKF	Iterated Extended Kalman Filter
IIABS	Immersion and Invariance Adaptive Backstepping
IIAIBS	Immersion and Invariance Adaptive Incremental Backstepping
INDI	Incremental Nonlinear Dynamic Inversion

IPE	Incremental Parameter Estimator
IPEBS	Incremental Parameter Estimation Backstepping
IPEIBS	Incremental Parameter Estimation Incremental Backstepping
IUKF	Iterated Unscented Kalman Filter
KF	Kalman Filter
LCF	Lyapunov Candidate Function
LOC-I	Loss Of Control In-flight
LS	Least-Squares
LSABS	Least-Squares Adaptive Backstepping
LSAIBS	Least-Squares Adaptive Incremental Backstepping
MIMO	Multiple-Input and Multiple-Output
NDI	Nonlinear Dynamic Inversion
NN	Neural Network
OLS	Ordinary Least-Squares
OPBB	Ordinary Polynomial Basis Based
PE	Persistent Excitation
PFTFC	Passive Fault Tolerant Flight Control
PID	Proportional-Integral-Derivative
RLS	Recursive Least-Squares
RMSD	Root-Mean-Square Deviation
SBB	Sensor-Based Backstepping
SVD	Singular Value Decomposition
TF	Tuning Function
TFABS	Tuning Functions Adaptive Backstepping
TFAIBS	Tuning Functions Adaptive Incremental Backstepping
TLS	Total Least-Squares
TSM	Two-Step Method
TSS	Time-Scale Separation
UAV	Unmanned Aerial Vehicle
UKF	Unscented Kalman Filter
VTOL	Vertical Take-Off and Landing
WLS	Weighted Least-Squares

List of Symbols

Greek Symbols

α	Aerodynamic angle of attack
$\alpha_\star$	Stabilizing control law
β	Sideslip angle
$\beta_\star$	Continuous function
$\gamma_\star$	Adaptation gain
Γ	Inertia term
$\Gamma_\star$	Adaptation gain matrix
Δx	Incremental variable, that is, $\Delta x = x - x_0$
$\delta_\star$	Control surface deflection
ϵ	Positive constant
ζ	Damping ratio
θ	Pitch angle
$\theta_\star$	(Unknown) parameter
$\hat{\theta}_\star$	Estimated parameter
$\tilde{\theta}_\star$	Parameter estimation error
λ	Forgetting factor
$\xi_\star$	Estimator state
ξ	Dummy variable for integration
ρ	Stabilizing function
ρ	Air density

$\sigma_\star$	Parameter estimation error
ϕ	Roll angle
$\varphi_\star$	Regressor function
τ	Time constant
$\chi_\star$	State of the stable linear filter
χ	Dummy variable for integration
$\omega_{n,\star}$	Command filter natural frequency

Roman Symbols

A_x	Specific force along X-body axis
A_y	Specific force along Y-body axis
A_z	Specific force along Z-body axis
a	Speed of sound
b	Wing span
$C_\star$	Control or stability derivative
$C_\star$	Control gain matrix
C^k	The space of functions with k continuous derivatives
$c_\star$	Control gain
$c_\star$	Inertia term
$\bar{c}$	Wing mean aerodynamic chord
F_T	Engine thrust force
F_{mag}	Magnitude scaling
F_{var}	Variable scaling
$f_\star$	Frequency
g	Acceleration due to gravity
$g_\star$	Component of the acceleration due to gravity
h	Altitude
$I_\star$	Moment of inertia
I_N	N $\times$ N identity matrix
J	Cost function
$K_\star$	Kalman gain
k	Coefficient of friction
L	Positive constant
$\bar{L}$	Total aerodynamic moment about X-body axis

$\mathcal{M}$	Manifold
M	Mach number
$\bar{M}$	Total aerodynamic moment about Y-body axis
m	Mass
$\bar{N}$	Total aerodynamic moment about Z-body axis
$P_\star$	Covariance matrix
p	Airplane roll rate about X-body axis
p_s	Airplane roll rate about X-stability axis
q	Airplane roll rate about Y-body axis
q_s	Airplane roll rate about Y-stability axis
$\bar{q}$	Free-stream dynamic pressure
$\mathbb{R}$	Set of real numbers
r	Airplane roll rate about Z-body axis
r_s	Airplane roll rate about Z-stability axis
S	Wing area
s	Laplace operator
$\mathbb{T}_{sb}$	Transformation matrix from body-fixed reference frame to stability reference frame
T	Temperature
u	Component of airplane velocity along X-body axis
$u_\star$	Control input
$\mathcal{V}_\star$	(Control) Lyapunov Function
V_T	Total velocity
v	Virtual control law
v	Component of airplane velocity along Y-body axis
W	Continuous function
w	Component of airplane velocity along Z-body axis
$w_\star$	Update law
$X_\star$	Laplace transform of system state variable $x_\star$
$\bar{X}$	Total aerodynamic force along X-body axis
$x_\star$	System state variable
x_{cg}	Center-of-gravity location
$\bar{Y}$	Total aerodynamic force along Y-body axis
$y_\star$	Output state variable

$\bar{Z}$	Total aerodynamic force along Z-body axis
$z_\star$	Tracking error
$\bar{z}_\star$	Compensated tracking error

Subscripts

0	Part of the aerodynamic force or moment that is independent of the control surface
0	Sea level
b	Body-fixed reference frame
e	Equilibrium
k	Time step
M	Magnitude
n	Natural frequency
pf	Prefilter
R	Rate
r, ref	Reference
s	Sampling
s	Stability-axes reference frame

Superscripts

$\dagger$	Conjugate transpose
0	Raw signal
T	Transpose

Chapter 1

Introduction

According to the European Aviation Safety Agency (EASA), the highest number of fatal accidents involving airplanes operated by EASA Member States in the last 10 years are due to Loss Of Control In-flight (LOC-I) (European Aviation Safety Agency, 2013). This can be attributed to pilot error, technical malfunctioning, or a combination thereof. The accident rate of Unmanned Aerial Vehicles (UAVs) lies much higher compared to that of manned aircraft (Williams, 2004). About 80 percent of the flight incidents concerning UAVs are due to faults affecting propulsion, flight control surfaces, or sensors (Schaefer, 2003).

These findings underline the research relevance of Fault Tolerant Flight Control (FTFC), which has become feasible since the eighties due to the increase in available computational power. Previous research on flight accidents and their corresponding FTFC strategies suggests that an aircraft, under many post-failure circumstances, can still achieve a certain level of flight performance with the remaining valid control effectors (Smaili, Breeman, Lombaerts, & Joosten, 2006; Lombaerts, Smaili, et al., 2009; Lombaerts, Huisman, Chu, Mulder, & Joosten, 2009). Therefore, aviation safety can be improved by increasing the survivability of damaged (unmanned) aircraft by implementing FTFC systems.

Traditionally, and even today, gain-scheduling of linear feedback controllers is applied to achieve stabilization and satisfactory tracking performance of aircraft over a wide range of flight conditions. Because the dynamic behavior of an aircraft changes throughout the flight envelope, many different linear flight control laws must be designed for each region. In flight envelope regions with significant nonlinearities, or in case of failures (e.g. structural damage), gain-scheduling is not able to provide accurate tracking performance because this control strategy is based on linearized and nominal aircraft models (Sonneveldt, 2010; Falkena, 2012). Next, it is difficult to guarantee satisfactory stability and tracking performance over the complete flight envelope (Sonneveldt, 2010). At last, gain-scheduling of linear controllers is an extensive task. The main reason why this control strategy is still applied nowadays is because it is based on well-developed classical linear control theory. Furthermore, certification authorities are used to dealing with them.

Nonlinear and model-based control methods such as Nonlinear Dynamic Inversion (NDI) and Backstepping (BS) do not suffer from the drawbacks of gain-scheduled linear controllers. The idea behind these techniques is to cancel (part of) the nonlinear aircraft dynamics and to derive a control law for the resulting system. These methods have been successfully applied in off-line and on-line applications to control aircraft (Sonneveldt, 2010; Lombaerts, 2010; van Oort, 2011; Falkena, 2012). Backstepping is a design method that is, in contrary to NDI, based on Lyapunov stability theory. This can be a major benefit for certification of BS control laws, because the goals of global asymptotic stabilization and tracking can be guaranteed. Furthermore, BS is flexible in the choice of control law and can avoid wasteful cancellations as opposed to NDI (Sonneveldt, 2010). Because the flexible and Lyapunov-based BS control method offers many benefits compared to NDI and gain-scheduled linear control, this thesis focuses on reconfigurable *Backstepping* control laws.

However, because BS is a *model-based* control strategy, it is sensitive to model uncertainties. To make the BS control approach fault tolerant, which is of paramount importance for safety-critical systems such as aircraft, several approaches have been taken. In the literature survey (see Appendix A) the following promising fault tolerant approaches based on BS have been encountered:

1. Incremental Backstepping (Acquatella, 2011; Koschorke, 2012);
2. Sensor-Based Backstepping (Falkena, van Oort, & Chu, 2011; Falkena, Borst, van Oort, & Chu, 2013; Galrinho, de Visser, Chu, van Kampen, & Walpot, 2013);
3. Tuning Functions Adaptive Backstepping (Sonneveldt, Chu, & Mulder, 2007; Choi & Bang, 2011; Farrell, Polycarpou, Djapic, & Sharma, 2012);
4. Immersion and Invariance Adaptive Backstepping (Astolfi & Ortega, 2003; Hu & Zhang, 2013; Ali, Chu, van Kampen, & de Visser, 2014);
5. Least-Squares Adaptive Backstepping (van Oort, Sonneveldt, Chu, & Mulder, 2007).

The literature survey of the preliminary thesis report has shown some blind spots in the Adaptive Backstepping (ABS) theory. First of all, a comprehensive comparison study of the closed-loop performance and sensitivity to parametric uncertainties of these adaptive controllers does currently not exist. It is impossible to compare the performance of these control laws on basis of the existing literature, because different models and reference signals have been used. Next, most literature does not address the sensitivity of the developed controllers to sensor dynamics and noise. Because the ultimate goal is to use FTFC systems to increase the aviation safety, it is of paramount importance to evaluate the performance of these Adaptive Control laws in a practical context. At last, in some of the literature only the closed-loop performance of the adaptive controller is addressed, and not the performance of the parameter estimator itself. Although it is not necessary that the parameters converge to their true values for satisfactory closed-loop performance, Control Allocation (CA) modules require accurate estimates of the control effectiveness parameters.

From the motivation put above, the research question of this master thesis is formulated as follows:

> ***How do the different Adaptive Backstepping Flight Control approaches perform in practical applications under parametric uncertainties of the aircraft model?***

The results of this thesis research will contribute towards the further development of FTFC systems. The originality of this thesis shows in three ways. First, a comprehensive comparison study of the closed-loop performance and sensitivity to parametric uncertainties of these adaptive controllers is provided. Second, to the best knowledge of the author, Incremental Backstepping (IBS) control has not earlier been combined with Least-Squares (LS) and Tuning Function (TF) parameter estimators. At last, the sensitivity of the developed controllers to sensor dynamics and noise is addressed.

The Appendices of this report, starting from page 47, contain the literature study on FTFC and the preliminary thesis report. In this preliminary analysis use have been made of a simple nonlinear pendulum model to allow for an initial evaluation of the different BS control laws. This model has been selected because it is simple and therefore the complexity of the derivations is minimized. Furthermore, the pendulum model consists of two states such that the recursive approach of the BS method can be illustrated. The model, as well as the derived control laws, have been implemented in the `Matlab/Simulink` environment to generate simulation results.

Based on the conclusions of the preliminary analysis, the paper of this thesis uses an accurate high-fidelity aerodynamic Lockheed Martin F-16 `Matlab/Simulink` software package for further analysis of the ABS control laws, see Chapter 2. According to (Sonneveldt, 2010), this highly nonlinear model is currently the most accurate dynamic aircraft model available. The model is augmented with sensor dynamics and noise in order to make the simulations more realistic. Next, the nonlinear ABS control laws are derived and implemented in the software. The control laws as well as the tracking performance, parameter estimation errors and stability properties are compared and conclusions are drawn. The recommendations for future research, based on the findings of the current work, finally complete the research.

Chapter 2

Scientific Paper

Adaptive Incremental Backstepping Flight Control for a High-Performance Aircraft with Uncertainties

P. van Gils* and Q. P. Chu†

Delft University of Technology, P.O. Box 5058, 2600 GB Delft, The Netherlands

This paper deals with the development of Adaptive Incremental Backstepping control laws for a high-performance aircraft model (F-16), in order to make the airplane robustly seek references in roll rate and angle of attack at a constant airspeed while minimizing sideslip. An Incremental Backstepping scheme that relies on estimates of the angular accelerations and measurements of the current control deflections is used to reduce the dependency on the on-board aircraft model. The contribution of this paper is the design and evaluation of three parameter estimators to handle the remaining uncertainties. The estimators that are evaluated in this research are based on Tuning Functions, Least-Squares and Immersion & Invariance. It is shown that the Incremental Backstepping controller is not only more robust to uncertainties in the system dynamics compared to Backstepping, but is also more robust to uncertainties in the control effectiveness matrix. Furthermore, by augmenting the Incremental control law with on-line parameter update laws, the tracking performance of the uncertain F-16 model is significantly increased. The results of this study show the great potential of Adaptive Incremental Backstepping control in increasing the survivability of damaged aircraft.

Nomenclature

A_x, A_y, A_z	Specific forces along X_b, Y_b and Z_b-axis, m/s^2
b	Wing span, m
$C_\star$	Control or stability derivative
$c_\star$	Inertia term
$\bar{c}$	Wing mean aerodynamic chord, m
F_T	Engine thrust force, N
g	Acceleration due to gravity, m/s^2
$I_\star$	Moment of inertia, kgm^2
$\bar{L}, \bar{M}, \bar{N}$	Aerodynamic moments about X_b, Y_b, Z_b-axis, Nm
M	Mach number
m	Mass, kg
p, q, r	Roll rate about X_b, Y_b and Z_b-axis, rad/s
p_s, q_s, r_s	Roll rate about X_s, Y_s and Z_s-axis, rad/s
$\bar{q}$	Free-stream dynamic pressure, Pa
S	Wing area, m^2
s	Laplace operator
u, v, w	Velocities along X_b, Y_b and Z_b-axis, m/s
V_T	Total velocity, m/s
$\bar{X}, \bar{Y}, \bar{Z}$	Aerodynamic forces along X_b, Y_b and Z_b-axis, N
$x_\star$	System state variable
x_{cg}	Center-of-gravity location
$z_\star$	Tracking error
$\bar{z}_\star$	Compensated tracking error
α	Aerodynamic angle of attack, rad
β	Sideslip angle, rad
Δx	Incremental variable, that is, $\Delta x = x - x_0$
$\delta_e, \delta_a, \delta_r$	Elevator, aileron and rudder deflection, rad
$\theta_\star$	(Unknown) parameter
ρ	Air density, kg/m^3
ϕ, θ, ψ	Roll, pitch and heading angle, rad
$\varphi_\star$	Regressor function

Subscripts

b	Body-fixed reference frame
pf	Prefilter
ref	Reference
s	Stability-axes reference frame

Superscripts

0	Raw signal
T	Transpose

*M.Sc. Student, Faculty of Aerospace Engineering, Control and Simulation Division, 2626 HS Delft, The Netherlands.
†Associate Professor, Faculty of Aerospace Engineering, Control and Simulation Division, 2626 HS Delft, The Netherlands.

I. Introduction

According to the European Aviation Safety Agency (EASA), the highest number of fatal accidents involving airplanes operated by EASA Member States in the last 10 years are due to Loss Of Control In-flight (LOCI).[1] This can be attributed to pilot error, technical malfunctioning, or a combination thereof. The accident rate of Unmanned Aerial Vehicles (UAVs) lies much higher compared to that of manned aircraft.[2] About 80 percent of the flight incidents concerning UAVs are due to faults affecting propulsion, flight control surfaces, or sensors.[3]

These findings underline the research relevance of Fault Tolerant Flight Control (FTFC), which has become feasible since the eighties due to the increase in available computational power. Previous research on flight accidents and their corresponding FTFC strategies suggests that an aircraft, under many post-failure circumstances, can still achieve a certain level of flight performance with the remaining valid control effectors.[4–6] Therefore, aviation safety can be improved by increasing the survivability of damaged (unmanned) aircraft by implementing FTFC systems.

Traditionally, and even today, gain-scheduling of linear feedback controllers is applied to achieve stabilization and satisfactory tracking performance of aircraft over a wide range of flight conditions. Because the dynamic behavior of an aircraft changes throughout the flight envelope, many different linear flight control laws must be designed for each region. In flight envelope regions with significant nonlinearities, or in case of failures (e.g. structural damage), gain-scheduling is not able to provide accurate tracking performance because this control strategy is based on linearized and nominal aircraft models.[7,8] Next, it is difficult to guarantee satisfactory stability and tracking performance over the complete flight envelope.[7] At last, gain-scheduling of linear controllers is an extensive task. The main reason why this control strategy is still applied nowadays is because it is based on well-developed classical linear control theory. Furthermore, certification authorities are used to dealing with them.

Nonlinear and model-based control methods such as Nonlinear Dynamic Inversion (NDI) and Backstepping (BS) do not suffer from the drawbacks of gain-scheduled linear controllers. The idea behind these techniques is to cancel (part of) the nonlinear aircraft dynamics and to derive a control law for the resulting system. These methods have been successfully applied in off-line and on-line applications to control aircraft.[7–10] Backstepping is a design method that is, in contrary to NDI, based on Lyapunov stability theory. This can be a major benefit for certification of BS control laws, because the goals of global asymptotic stabilization and tracking can be guaranteed. Furthermore, BS is flexible in the choice of control law and can avoid wasteful cancellations as opposed to NDI.[7] Because the flexible and Lyapunov-based BS control method offers many benefits compared to NDI and gain-scheduled linear control, this paper focuses on reconfigurable *Backstepping* control laws.

The BS control approach has been augmented with command filters in the literature[11–14] to obviate the need for analytic computation of virtual control derivatives, which becomes very tedious when working with high-order systems. Furthermore, these filters eliminate the Backstepping's restriction to nonlinear systems of a lower triangular form. Finally, they improve the performance of Lyapunov-based parameter update laws by implementing magnitude, rate and bandwidth constraints on the (virtual) controls.

However, because Command-Filtered BS is a *model-based* control strategy, it is sensitive to model uncertainties. To make the BS control approach fault tolerant, which is of paramount importance for safety-critical systems such as aircraft, these control methods have been applied in an incremental[8,15,16] and in a sensor-based form.[17–19] The advantage of these approaches is that the dependency on the on-board aircraft model is reduced by using measurements or estimates of the state derivatives and current actuator states. Another approach is that of Adaptive Backstepping (ABS), which uses parameter update laws to guarantee closed-loop stability of uncertain systems. Earlier research has combined BS control with update laws based on Least-Squares (LS),[6,20] Lyapunov functions[11,21,22] and Immersion and Invariance (I&I).[23–26]

The approach of Incremental Backstepping (IBS) has been augmented with command filters and I&I update laws in Ali, Chu, Van Kampen and De Visser.[26] By using an incremental control law, the estimator now only has to estimate the aircraft control derivatives. The advantage of this approach is that the computational complexity is significantly reduced with respect to ABS. In this reference only a small uncertainty has been introduced in the pitching moment control derivative to evaluate the I&I identifier. Furthermore, the improvements in robustness thanks to the I&I estimator appear to be marginal; according to the authors this is likely due to the lack of a detailed regressor model in the identifier.

A comparison study of the closed-loop performance and sensitivity to parametric uncertainties of these ABS controllers does currently not exist. Moreover, most literature does not address the sensitivity of the developed controllers to sensor noise and dynamics. Because the ultimate goal is to use FTFC systems to increase the aviation safety, it is of paramount importance to evaluate the performance of these Adaptive Control laws in a practical context.

This paper deals with the development of three Command-Filtered Adaptive IBS control laws for a high-performance aircraft model (F-16) with a large flight envelope. The control objective is to make the airplane robustly seek references in roll rate and angle of attack at a constant airspeed while minimizing sideslip. However, first a *non-adaptive* Command-Filtered BS controller is derived that forms the baseline control system of this research. Next, in order to cope with the uncertainties introduced by the aerodynamic forces and moments, IBS is applied. The contribution of this paper is the design and evaluation of three distinct estimators to handle the remaining unknown parameters. First of all, the integrated Lyapunov-based Tuning Functions (TFs) approach is evaluated. Second, the Recursive Least-Squares (RLS) algorithm is implemented to obtain estimates of the unknown parameters. This results in a modular approach that is based on the certainty equivalence principle.[10,27] Finally, an I&I identifier is evaluated that includes more detailed regressor models compared to Ali *et al.*[26] To the best knowledge of the authors of this paper, IBS control has not earlier been combined with LS and TF parameter estimators. Because the designed controllers and estimators heavily rely on sensor measurements; sensor dynamics and noise are simulated to evaluate the control approaches on an uncertain F-16 aircraft model.

The paper outline is as follows: Section II discusses the nonlinear F-16 aircraft model that is used in this paper. Next, the design of the flight controllers and parameter estimators is described in Section III. The performance of these controllers is verified through `Matlab/Simulink` simulations in Section IV and the paper is concluded in Section V. Finally, the Appendices contain more information on the F-16 model and additional simulation results.

II. Nonlinear F-16 Aircraft Model

In this study the nonlinear F-16 low-fidelity aircraft model of Russell[28] is used to evaluate five BS control laws. This highly nonlinear model is currently the most accurate dynamic aircraft model available.[7] Assumptions and limitations for this model are:[29]

1. The aircraft is a rigid body;
2. The earth is flat and non-rotating and regarded as an inertial reference;
3. The mass is constant during the time interval over which the motion is considered;
4. The mass distribution of the aircraft is symmetric relative to the X_bOZ_b-plane, this implies that $I_{yz} = I_{xy} = 0$;
5. The thrust produced by the engine, F_T, acts through the center of gravity and along the X_b-axis;
6. The engine angular momentum has been neglected;
7. The leading edge flap is not implemented;
8. The horizontal tail has only symmetric deflection;
9. Speed brakes are not used;
10. There is a complete decoupling between the longitudinal and the lateral-directional equations.

The low-fidelity F-16 model is valid for the following flight envelope: $-10 \leq \alpha \leq 45$ degrees, $-30 \leq \beta \leq 30$ degrees and $0.1 \leq M \leq 0.6$.

II.A. Equations of Motion

With the given assumptions, the force equations of motion referenced to a body-fixed reference frame are given by[30]

$$\dot{u} = rv - qw - g\sin\theta + \frac{\bar{X}}{m} + \frac{F_T}{m} \tag{1a}$$
$$\dot{v} = pw - ru + g\cos\theta\sin\phi + \frac{\bar{Y}}{m} \tag{1b}$$
$$\dot{w} = qu - pv + g\cos\theta\cos\phi + \frac{\bar{Z}}{m}\,, \tag{1c}$$

where the aerodynamic forces are defined as

$$\bar{X} \equiv \bar{q}SC_{X,T} \tag{2a}$$
$$\bar{Y} \equiv \bar{q}SC_{Y,T} \tag{2b}$$
$$\bar{Z} \equiv \bar{q}SC_{Z,T}\,. \tag{2c}$$

where $\bar{q} = \rho V_T^2/2$ is the free-stream dynamic pressure. The moment equations of motion referenced to a body-fixed reference frame are given by[31]

$$\dot{p} = (c_1 r + c_2 p)q + c_3\bar{L} + c_4\bar{N} \tag{3a}$$
$$\dot{q} = c_5 pr - c_6\left(p^2 - r^2\right) + c_7\bar{M} \tag{3b}$$
$$\dot{r} = (c_8 p - c_2 r)q + c_4\bar{L} + c_9\bar{N}\,, \tag{3c}$$

where the moments of inertia are defined as

$$\Gamma c_1 = (I_y - I_z)I_z - I_{xz}^2 \qquad \Gamma c_4 = I_{xz} \qquad c_7 = \frac{1}{I_y} \tag{4a}$$
$$\Gamma c_2 = (I_x - I_y + I_z)I_{xz} \qquad c_5 = \frac{I_z - I_x}{I_y} \qquad \Gamma c_8 = I_x(I_x - I_y) + I_{xz}^2 \tag{4b}$$
$$\Gamma c_3 = I_z \qquad c_6 = \frac{I_{xz}}{I_y} \qquad \Gamma c_9 = I_x\,, \tag{4c}$$

with $\Gamma = I_x I_z - I_{xz}^2$. The aerodynamic moments are defined as

$$\bar{L} \equiv \bar{q}SbC_{L,T} \tag{5a}$$
$$\bar{M} \equiv \bar{q}SbC_{M,T} \tag{5b}$$
$$\bar{N} \equiv \bar{q}SbC_{N,T}\,. \tag{5c}$$

In Appendix A the total coefficient equations are listed that are used to sum the various aerodynamic contributions to a given force or moment coefficient of the F-16 model.

II.B. Atmospheric Model

An approximation of the International Standard Atmosphere is used for the atmospheric data:[32]

$$T = T_0 - 0.0065h\,, \qquad \text{for } 0 \leq h \leq 11,000 \tag{6a}$$
$$T = 216.65\,, \qquad \text{for } h > 11,000 \tag{6b}$$
$$\rho = \rho_0 e^{-\frac{g}{287.05T}h} \tag{6c}$$
$$a = \sqrt{1.4 \times 287.05T}\,, \tag{6d}$$

where $T_0 = 288.15\,\mathrm{K}$ and $\rho_0 = 1.225\,\mathrm{kg/m^3}$ are respectively the temperature and air density at sea level. The aircraft's altitude h is given in meters, the current temperature T in Kelvin, the speed of sound a in m/s and $g = 9.81\,\mathrm{m/s^2}$ is the acceleration due to gravity. Wind and atmospheric turbulence have not been modeled.

II.C. Control Variables

The control variables used in this study are the engine thrust force F_T, elevator δ_e, aileron δ_a and rudder δ_r. The control inputs are magnitude and rate limited and are implemented as first-order, low-pass filters with unity low-frequency (DC) gain and time constants τ, see Table 1.

Table 1. Actuator dynamics of the control inputs.[28]

Control	Units	Min.	Max.	Rate limit	τ [s]
Elevator	deg	-25	25	± 60 deg/s	0.0495
Ailerons	deg	-21.5	21.5	± 80 deg/s	0.0495
Rudder	deg	-30	30	± 120 deg/s	0.0495
Thrust	lbs	1 000	19 000	± 10 000 lbs/s	1.0

II.D. Aerodynamic Model

An overview of the total aerodynamic force and moment coefficients is given in Table 2. These coefficients are used to sum the various aerodynamic contributions to the given force or moment. In Appendix A a complete overview of the total coefficient equations can be found. As can be seen, coefficients $C_{X,T}$ and $C_{M,T}$ are not affine with respect to the elevator deflection; this has consequences for the BS control approach as we will see later on. The aerodynamic data of the F-16 model consists of a set of multi-dimensional data tables based on wind-tunnel measurements.[30,31] Linear interpolation is performed in between the data points.

Table 2. Force and moment coefficients for the F-16 model.[31] The aerodynamic coefficients in bold font are not affine in the control input.

Force coefficients		
X-axis force coefficient	$\boldsymbol{C_{X,T}}$	$= f(\alpha, \delta_e)$
Y-axis force coefficient	$C_{Y,T}$	$= f(\alpha, \beta) + g\delta_a + h\delta_r$
Z-axis force coefficient	$C_{Z,T}$	$= f(\alpha) + g(\alpha, \beta)\delta_e$
Moment coefficients		
Rolling-moment coefficient	$C_{L,T}$	$= f(\alpha, \beta) + g(\alpha, \beta)\delta_a + h(\alpha, \beta)\delta_r$
Pitching-moment coefficient	$\boldsymbol{C_{M,T}}$	$= f(\alpha, \beta, \delta_e)$
Yawing-moment coefficient	$C_{N,T}$	$= f(\alpha, \beta) + g(\alpha, \beta)\delta_a + h(\alpha, \beta)\delta_r$

II.E. Sensors

The F-16 model has been augmented with air data, inertial and attitude sensors to allow for more realistic simulations:[33]

- Air data sensors (V_T, $\bar{q}$, α, β)

$$H(s) = \frac{1}{0.02s + 1}\,. \tag{7}$$

- Inertial sensors (p, q, r, A_x, A_y, A_z)

$$H(s) = \frac{0.0001903s^2 + 0.005346s + 1}{0.0004942s^2 + 0.03082s + 1}\,. \tag{8}$$

- Attitude sensors (ϕ, θ)

$$H(s) = \frac{1}{0.00104s^2 + 0.0323s + 1}\,. \tag{9}$$

In addition to the sensor dynamics, independent zero-mean Gaussian noise has been added to the measurements. The selected noise standard deviations are given in Table 3. It has been assumed that the actuator dynamics are known, or equivalently, that the actuator positions are perfectly measured.

Table 3. Standard deviations of the measurement noise.

V_T	$\bar{q}$	α, β	p, q, r	A_x, A_y, A_z	ϕ, θ
1 m/s	50 Pa	0.1 deg	0.01 deg/s	0.01 m/s^2	0.1 deg

II.F. Aircraft Dynamics used for Control

In this paper control laws for an F-16 model are designed, in order to make the airplane robustly seek references in roll rate p_s and angle of attack α at a constant airspeed V_T while minimizing sideslip β. The angle of attack α is a typical control variable for high-performance aircraft because it is closely coupled to the normal acceleration.[34] The advantage of rolling around the stability X_s-axis instead of the body X_b-axis is that it reduces the amount of sideslip during a roll, especially at high angles of attack.[13] Summarizing, the task of the control system is to make sure that

$$V_T = V_{T,ref} \tag{10a}$$
$$\alpha = \alpha_{ref} \tag{10b}$$
$$\beta = 0 \tag{10c}$$
$$p_s = p_{s,ref}\ , \tag{10d}$$

is an asymptotic equilibrium. To avoid unachievable commands due to the actuator constraints, first-order lag prefilters are used to obtain the reference signals, e.g.

$$H_{pf,\alpha}(s) = \frac{\alpha_{ref}(s)}{\alpha_{(auto)pilot}(s)} = \frac{1}{\sigma_\alpha s + 1}\ . \tag{11}$$

The prefilter time constants $\sigma_\star$ are chosen to allow for fast tracking while avoiding command saturation as much as possible. The prefilters are also used to obtain the time derivatives of the reference signals, which are required by the BS control law as we will see later see on.

With the control objective set as Eq. (10), it is more convenient to express the force equations (see Eq. (1)) in the wind-axes reference frame. This implies the following transformations:[29]

$$V_T = \sqrt{u^2+v^2+w^2} \qquad\qquad u = V_T \cos\alpha\cos\beta \tag{12a}$$
$$\alpha = \arctan\frac{w}{u} \qquad \Leftrightarrow \qquad v = V_T \sin\beta \tag{12b}$$
$$\beta = \arcsin\frac{v}{V_T} \qquad\qquad w = V_T \sin\alpha\cos\beta\,. \tag{12c}$$

Taking the time derivative of V_T, α and β results in

$$\dot{V}_T = \frac{u\dot{u}+v\dot{v}+w\dot{w}}{V_T} \tag{13a}$$
$$\dot{\alpha} = \frac{u\dot{w}-w\dot{u}}{u^2+w^2} \tag{13b}$$
$$\dot{\beta} = \frac{\dot{v}V_T - v\dot{V}_T}{V_T^2\cos\beta}\,. \tag{13c}$$

Substituting Eqs. (1) and (12) into Eq. (13) gives the force equations in the wind-axes reference frame:

$$\dot{V}_T = \frac{1}{m}\big[\bar{X}\cos\alpha\cos\beta + \bar{Y}\sin\beta + \bar{Z}\sin\alpha\cos\beta + F_T\cos\alpha\cos\beta + mg_1\big] \tag{14a}$$
$$\dot{\alpha} = q - p\cos\alpha\tan\beta - r\sin\alpha\tan\beta + \frac{1}{mV_T\cos\beta}\big[-\bar{X}\sin\alpha + \bar{Z}\cos\alpha - F_T\sin\alpha + mg_3\big] \tag{14b}$$
$$\dot{\beta} = p\sin\alpha - r\cos\alpha + \frac{1}{mV_t}\big[-\bar{X}\cos\alpha\sin\beta + \bar{Y}\cos\beta - \bar{Z}\sin\alpha\sin\beta - F_T\cos\alpha\sin\beta + mg_2\big]\,, \tag{14c}$$

where the gravity components g_1, g_2 and g_3 are defined by

$$g_1 = g\big[-\cos\alpha\cos\beta\sin\theta + \sin\beta\sin\phi\cos\theta + \sin\alpha\cos\beta\cos\phi\cos\theta\big] \tag{15a}$$
$$g_2 = g\big[\cos\alpha\sin\beta\sin\theta + \cos\beta\sin\phi\cos\theta - \sin\alpha\sin\beta\cos\phi\cos\theta\big] \tag{15b}$$
$$g_3 = g\big[\sin\alpha\sin\theta + \cos\alpha\cos\phi\cos\theta\big]\,. \tag{15c}$$

By using the transformation matrix $\mathbb{T}_{sb}$ from the body rotation rates to the stability-axes rotation rates:[29]

$$\begin{bmatrix} p_s \\ q_s \\ r_s \end{bmatrix} = \underbrace{\begin{bmatrix} \cos\alpha & 0 & \sin\alpha \\ 0 & 1 & 0 \\ -\sin\alpha & 0 & \cos\alpha \end{bmatrix}}_{\mathbb{T}_{sb}} \begin{bmatrix} p \\ q \\ r \end{bmatrix}, \tag{16}$$

we can write Eq. (14) as

$$\dot{V}_T = \frac{1}{m}\big[\bar{X}\cos\alpha\cos\beta + \bar{Y}\sin\beta + \bar{Z}\sin\alpha\cos\beta + F_T\cos\alpha\cos\beta + mg_1\big] \tag{17a}$$
$$\dot{\alpha} = q_s - p_s\tan\beta + \frac{1}{mV_T\cos\beta}\big[-\bar{X}\sin\alpha + \bar{Z}\cos\alpha - F_T\sin\alpha + mg_3\big] \tag{17b}$$
$$\dot{\beta} = -r_s + \frac{1}{mV_t}\big[-\bar{X}\cos\alpha\sin\beta + \bar{Y}\cos\beta - \bar{Z}\sin\alpha\sin\beta - F_T\cos\alpha\sin\beta + mg_2\big]. \tag{17c}$$

Taking the time derivative of Eq. (16) and substituting Eq. (3) results in

$$\begin{bmatrix} \dot{p}_s \\ \dot{q}_s \\ \dot{r}_s \end{bmatrix} = \mathbb{T}_{sb} \begin{bmatrix} (c_1 r + c_2 p)q + c_3\bar{L} + c_4\bar{N} \\ c_5 pr - c_6\big(p^2 - r^2\big) + c_7\bar{M} \\ (c_8 p - c_2 r)q + c_4\bar{L} + c_9\bar{N} \end{bmatrix} + \begin{bmatrix} r_s \\ 0 \\ -p_s \end{bmatrix}\dot{\alpha}\,. \tag{18}$$

By selecting the states as

$$\boldsymbol{x}_1 = \begin{bmatrix} V_T \\ \alpha \\ \beta \end{bmatrix}, \qquad \boldsymbol{x}_2 = \begin{bmatrix} p_s \\ q_s \\ r_s \end{bmatrix}, \tag{19}$$

we can write Eqs. (17) and (18) as respectively

$$\dot{\boldsymbol{x}}_1 = \boldsymbol{f}_1 + G_1 \begin{bmatrix} F_T \\ q_s \\ r_s \end{bmatrix} \tag{20a}$$
$$\dot{\boldsymbol{x}}_2 = \boldsymbol{f}_2 + \big(H_2 + D_2 G_2\big) \begin{bmatrix} \delta_e \\ \delta_a \\ \delta_r \end{bmatrix}, \tag{20b}$$

where

$$
\boldsymbol{f}_1 = \begin{bmatrix} \frac{1}{m}\Big[\bar{X}\cos\alpha\cos\beta + \bar{Y}\sin\beta + \bar{Z}\sin\alpha\cos\beta + mg_1\Big] \\ -p_s\tan\beta + \frac{1}{mV_T\cos\beta}\Big[\bar{Z}\cos\alpha - \big(\bar{X}+F_T\big)\sin\alpha + mg_3\Big] \\ \frac{1}{mV_T}\Big[-\big(\bar{X}+F_T\big)\cos\alpha\sin\beta + \bar{Y}\cos\beta - \bar{Z}\sin\alpha\sin\beta + mg_2\Big] \end{bmatrix} \tag{21a}
$$

$$
G_1 = \begin{bmatrix} \frac{\cos\alpha\cos\beta}{m} & 0 & 0 \\ 0 & 1 & 0 \\ 0 & 0 & -1 \end{bmatrix} \tag{21b}
$$

$$
\begin{aligned}
\boldsymbol{f}_2 = &\begin{bmatrix} r_s\Big[q_s - p_s\tan\beta + \frac{1}{mV_T\cos\beta}\big(-\bar{X}_0\sin\alpha + \bar{Z}_0\cos\alpha - F_T\sin\alpha + mg_3\big)\Big] \\ 0 \\ -p_s\Big[q_s - p_s\tan\beta + \frac{1}{mV_T\cos\beta}\big(-\bar{X}_0\sin\alpha + \bar{Z}_0\cos\alpha - F_T\sin\alpha + mg_3\big)\Big] \end{bmatrix} \\
&+ \mathbb{T}_{sb}\begin{bmatrix} (c_1 r + c_2 p)q \\ c_5 pr - c_6\big(p^2 - r^2\big) \\ (c_8 p - c_2 r)q \end{bmatrix} + D_2\begin{bmatrix} \bar{L}_0 \\ \bar{M}_0 \\ \bar{N}_0 \end{bmatrix}
\end{aligned} \tag{21c}
$$

$$
H_2 = \begin{bmatrix} \frac{r_s}{mV_T\cos\beta}\big[\bar{Z}_{\delta_e}\cos\alpha - \bar{X}_{\delta_e}\sin\alpha\big] & 0 & 0 \\ 0 & 0 & 0 \\ \frac{-p_s}{mV_T\cos\beta}\big[\bar{Z}_{\delta_e}\cos\alpha - \bar{X}_{\delta_e}\sin\alpha\big] & 0 & 0 \end{bmatrix} \tag{21d}
$$

$$
D_2 = \mathbb{T}_{sb}\begin{bmatrix} c_3 & 0 & c_4 \\ 0 & c_7 & 0 \\ c_4 & 0 & c_9 \end{bmatrix}, \quad G_2 = \begin{bmatrix} 0 & \bar{L}_{\delta_a} & \bar{L}_{\delta_r} \\ \bar{M}_{\delta_e} & 0 & 0 \\ 0 & \bar{N}_{\delta_a} & \bar{N}_{\delta_r} \end{bmatrix}. \tag{21e}
$$

Note that the aerodynamic forces and moments have been split in a part that is independent of the control variables and a part that is linearly dependent on the control variables:

$$
\bar{X} = \bar{X}_0 + \bar{X}_{\delta_e}\delta_e \tag{22a}
$$
$$
\bar{Y} = \bar{Y}_0 + \bar{Y}_{\delta_a}\delta_a + \bar{Y}_{\delta_r}\delta_r \tag{22b}
$$
$$
\bar{Z} = \bar{Z}_0 + \bar{Z}_{\delta_e}\delta_e \tag{22c}
$$

$$
\bar{L} = \bar{L}_0 + \bar{L}_{\delta_a}\delta_a + \bar{L}_{\delta_r}\delta_r \tag{22d}
$$
$$
\bar{M} = \bar{M}_0 + \bar{M}_{\delta_e}\delta_e \tag{22e}
$$
$$
\bar{N} = \bar{N}_0 + \bar{N}_{\delta_a}\delta_a + \bar{N}_{\delta_r}\delta_r\,. \tag{22f}
$$

III. Flight Control Design

III.A. Backstepping

In the BS control approach,[7,27,34] the tracking error states are defined as

$$\boldsymbol{z}_1 = \begin{bmatrix} z_{11} \\ z_{12} \\ z_{13} \end{bmatrix} = \begin{bmatrix} V_T \\ \alpha \\ \beta \end{bmatrix} - \begin{bmatrix} V_T \\ \alpha \\ \beta \end{bmatrix}_{ref} = \boldsymbol{x}_1 - \boldsymbol{x}_{1,ref} \tag{23a}$$

$$\boldsymbol{z}_2 = \begin{bmatrix} z_{21} \\ z_{22} \\ z_{23} \end{bmatrix} = \begin{bmatrix} p_s \\ q_s \\ r_s \end{bmatrix} - \begin{bmatrix} p_s \\ q_s \\ r_s \end{bmatrix}_{ref} = \boldsymbol{x}_2 - \boldsymbol{x}_{2,ref}\,, \tag{23b}$$

where $q_{s,ref}$ and $r_{s,ref}$ are the intermediate control laws that will be defined by the BS controller. The remaining reference variables are obtained from the prefilters (see Eq. (11)). For the BS control approach including command filters,[11–14] the *modified* tracking errors are now defined as

$$\bar{\boldsymbol{z}}_i = \begin{bmatrix} \bar{z}_{i,1} \\ \bar{z}_{i,2} \\ \bar{z}_{i,3} \end{bmatrix} = \begin{bmatrix} z_{i,1} \\ z_{i,2} \\ z_{i,3} \end{bmatrix} - \begin{bmatrix} \chi_{i,1} \\ \chi_{i,2} \\ \chi_{i,3} \end{bmatrix} = \boldsymbol{z}_i - \boldsymbol{\chi}_i\,, \quad i = 1, 2\,, \tag{24}$$

where $\boldsymbol{\chi}_i$ will be defined later on. Backstepping is a *recursive* design approach; therefore we start by considering the $\boldsymbol{x}_1$-subsystem in Section III.A.1 and then move on to subsystem $\boldsymbol{x}_2$ in Section III.A.2. Finally, Section III.A.3 contains the proof that shows that the developed control law accomplishes control objective Eq. (10).

III.A.1. Outer loop control design

The dynamics of modified tracking error $\bar{\boldsymbol{z}}_1$ are given by

$$\dot{\bar{\boldsymbol{z}}}_1 = \boldsymbol{f}_1 + G_1 \begin{bmatrix} F_T \\ q_s \\ r_s \end{bmatrix} - \dot{\boldsymbol{x}}_{1,ref} - \dot{\boldsymbol{\chi}}_1\,. \tag{25}$$

By using measurements of the specific forces:

$$A_x = \frac{\bar{X} + F_T}{m}\,, \quad A_y = \frac{\bar{Y}}{m}\,, \quad A_z = \frac{\bar{Z}}{m}\,, \tag{26}$$

the number of required on-board model parameters can be reduced.[6] Ideally, this would mean that the vector $\boldsymbol{f}_1$ is no longer dependent on the aerodynamic forces $\left(\bar{X}, \bar{Y}, \bar{Z}\right)$. However, it is not allowed to rewrite $\dot{V}_T$ in terms of the specific force A_x, otherwise the control input F_T does not appear explicitly in the dynamics. Therefore vector $\boldsymbol{f}_1$ changes to:

$$\boldsymbol{f}_{1,m} = \begin{bmatrix} \frac{\bar{X}}{m}\cos\alpha\cos\beta + A_y \sin\beta + A_z \sin\alpha\cos\beta + g_1 \\ -p_s \tan\beta + \frac{1}{V_T\cos\beta}\left(A_z\cos\alpha - A_x\sin\alpha + g_3\right) \\ \frac{1}{V_T}\left(-A_x\cos\alpha\sin\beta + A_y\cos\beta - A_z\sin\alpha\sin\beta + g_2\right) \end{bmatrix}. \tag{27}$$

The raw *real* control F_T^0 and the raw *virtual* controls $q_{s,ref}^0$ and $r_{s,ref}^0$ are defined as

$$\begin{bmatrix} F_T \\ q_{s,ref} \\ r_{s,ref} \end{bmatrix}^0 = G_1^{-1}\left(-C_1\boldsymbol{z}_1 - \hat{\boldsymbol{f}}_{1,m} + \begin{bmatrix} \dot{V}_T \\ \dot{\alpha} \\ \dot{\beta} \end{bmatrix}_{ref}\right) - \begin{bmatrix} 0 \\ \chi_{22} \\ \chi_{23} \end{bmatrix}, \tag{28}$$

where C_1 is a positive diagonal matrix and where $\hat{\boldsymbol{f}}_{1,m}$ denotes the estimate of $\boldsymbol{f}_{1,m}$. Note from Eq. (21b) that matrix G_1 becomes singular when $\alpha = k\pi/2$ or $\beta = k\pi/2$ with k a non-zero integer. Fortunately, these values for α and β are not located in the flight envelope for which the F-16 model is valid (see Section II).

The raw (virtual) control vector $\begin{bmatrix} F_T^0 & q_{s,ref}^0 & r_{s,ref}^0 \end{bmatrix}^T$ is led through command filters[13,14,35] to obtain the vector $\begin{bmatrix} F_T & q_{s,ref} & r_{s,ref} \end{bmatrix}^T$ and its time derivative. The effect that the use of these command filters have on the tracking error $\boldsymbol{z}_1$ is estimated by the stable linear filter:

$$\begin{bmatrix} \dot{\chi}_{11} \\ \dot{\chi}_{12} \\ \dot{\chi}_{13} \end{bmatrix} = -C_1 \begin{bmatrix} \chi_{11} \\ \chi_{12} \\ \chi_{13} \end{bmatrix} + G_1 \left(\begin{bmatrix} F_T \\ q_{s_{ref}} \\ r_{s_{ref}} \end{bmatrix} - \begin{bmatrix} F_T \\ q_{s_{ref}} \\ r_{s_{ref}} \end{bmatrix}^0 \right), \tag{29}$$

with zero initial conditions, that is, $\boldsymbol{\chi}_1(0) = \mathbf{0}$.

III.A.2. Inner loop control design

The dynamics of modified tracking error $\bar{\boldsymbol{z}}_2$ are given by

$$\dot{\bar{\boldsymbol{z}}}_2 = \boldsymbol{f}_2 + \big(H_2 + D_2 G_2\big)\boldsymbol{u} - \dot{\boldsymbol{x}}_{2,ref} - \dot{\boldsymbol{\chi}}_2\,, \tag{30}$$

where we have assumed that control signal $\boldsymbol{u}$ equals the primary control deflections $[\delta_e, \delta_a, \delta_r]^T$, that is, actuator dynamics have been neglected. This is a valid assumption because the primary control actuator dynamics on the F-16 model are much faster than the plant dynamics. The use of these primary control deflections to control p_s and q_s through $\dot{\alpha}$ will now be neglected, because these surfaces are primarily *moment* generators instead of *force* generators.[34,36] Consequently, matrix H_2 is completely removed, which results in the following expression:

$$\dot{\bar{\boldsymbol{z}}}_2 = \boldsymbol{f}_2 + D_2 G_2 \boldsymbol{u} - \dot{\boldsymbol{x}}_{2,ref} - \dot{\boldsymbol{\chi}}_2\,. \tag{31}$$

Applying the Command-Filtered BS procedure[11–14] to this simplified vector equation yields the following raw BS control law:

$$D_2 \hat{G}_2 \boldsymbol{u}^0 = D_2 \hat{G}_2 \begin{bmatrix} \delta_e \\ \delta_a \\ \delta_r \end{bmatrix}^0 = -C_2 \boldsymbol{z}_2 - \hat{\boldsymbol{f}}_2 + \begin{bmatrix} \dot{p}_s \\ \dot{q}_s \\ \dot{r}_s \end{bmatrix}_{ref} - G_1 \begin{bmatrix} 0 \\ \bar{z}_{12} \\ \bar{z}_{13} \end{bmatrix}, \tag{32}$$

where C_2 is a positive diagonal matrix and where $\hat{\boldsymbol{f}}_2$ and $\hat{G}_2$ denote the estimates of respectively vector $\boldsymbol{f}_2$ and matrix G_2. The time derivative $\dot{p}_{s,ref}$ is obtained from the prefilter, while $\dot{q}_{s,ref}$ and $\dot{r}_{s,ref}$ are obtained from the command filters. Because the F-16 model that is used in this research is not over-actuated, $D_2 G_2$ is a square matrix. If this would not be the case, some form of control allocation would be required.[9,37] Note from Eq. (21e) that matrix G_2 is always of full rank as long as the primary control surfaces remain operable.

The raw control vector $\begin{bmatrix} \delta_e^0 & \delta_a^0 & \delta_r^0 \end{bmatrix}^T$ is led through command filters to obtain the vector $\begin{bmatrix} \delta_e & \delta_a & \delta_r \end{bmatrix}^T$. The effect that the use of these command filters have on the tracking error $\boldsymbol{z}_2$ is estimated by the stable linear filter:

$$\begin{bmatrix} \dot{\chi}_{21} \\ \dot{\chi}_{22} \\ \dot{\chi}_{23} \end{bmatrix} = -C_2 \begin{bmatrix} \chi_{21} \\ \chi_{22} \\ \chi_{23} \end{bmatrix} + D_2 \hat{G}_2 \left(\begin{bmatrix} \delta_e \\ \delta_a \\ \delta_r \end{bmatrix} - \begin{bmatrix} \delta_e \\ \delta_a \\ \delta_r \end{bmatrix}^0 \right), \tag{33}$$

with zero initial conditions, that is, $\boldsymbol{\chi}_2(0) = \mathbf{0}$. The command filters that transform the raw signals $(F_T, q_{s,ref}, r_{s,ref}, \delta_e, \delta_a, \delta_r)^0$ to produce magnitude, rate and bandwidth-limited signals and their derivatives are selected to be second-order, low-pass filters with unity low-frequency (DC) gain and bandwidth ω_n:[13,14,35]

$$\begin{bmatrix} \dot{q}_1 \\ \dot{q}_2 \end{bmatrix} = \begin{bmatrix} q_2 \\ 2\zeta\omega_n \left(S_R \left\{ \frac{\omega_n^2}{2\zeta\omega_n} \left[S_M \left(x_{i,ref}^0 \right) - q_1 \right] \right\} - q_2 \right) \end{bmatrix} \tag{34a}$$

$$\begin{bmatrix} x_{i,ref} \\ \dot{x}_{i,ref} \end{bmatrix} = \begin{bmatrix} q_1 \\ q_2 \end{bmatrix}, \tag{34b}$$

with initial conditions:

$$q_1(0) = \alpha_1\left(z_{i-1}(0), x_{i-1,ref}(0)\right) \tag{35a}$$
$$q_2(0) = 0\,. \tag{35b}$$

The saturation functions S_M and S_R are defined similarly as

$$S_M(x) = \begin{cases} M & \text{if} \quad x \;\ge M \\ x & \text{if} \quad |x| < M \\ -M & \text{if} \quad x \;\le M\,. \end{cases} \tag{36}$$

The reason for using low-pass *second-order* filters is to suppress noise of the output signal and its time derivative, while minimizing the time delay between the input and output.

The controller structure developed in this section can be seen in Figure 1. In this diagram CF 1 and CF 2 represent the Command Filters Eq. (34). The BS outer and inner loop blocks correspond to respectively Eqs. (28) and (32). The estimator update laws will be designed in Sections III.C to III.E.

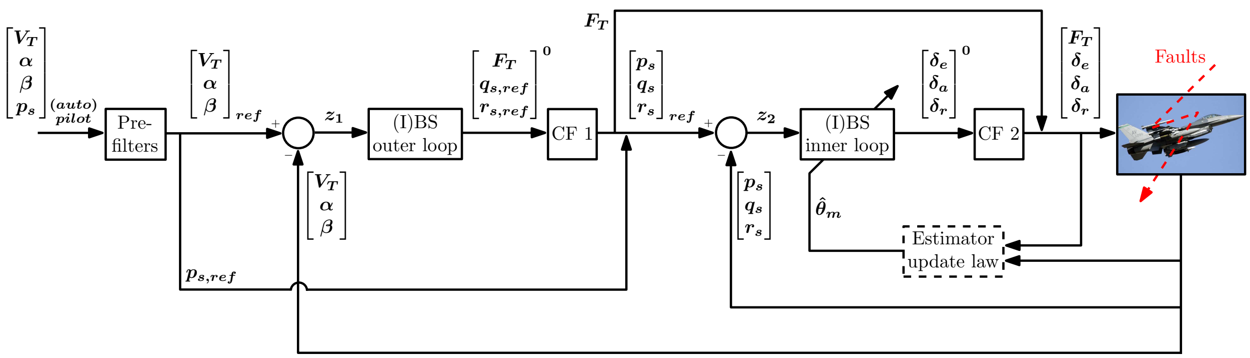

Figure 1. Command-Filtered (Adaptive Incremental) Backstepping controller structure.

III.A.3. Proof of stability

If we assume that $\hat{\boldsymbol{f}}_{1,m} = \boldsymbol{f}_{1,m}$, $\hat{\boldsymbol{f}}_2 = \boldsymbol{f}_2$ and $\hat{G}_2 = G_2$, then stability can be proved on basis of the following control Lyapunov function:

$$\mathcal{V}(\bar{\boldsymbol{z}}) = \frac{1}{2}\bar{\boldsymbol{z}}_1^T\bar{\boldsymbol{z}}_1 + \frac{1}{2}\bar{\boldsymbol{z}}_2^T\bar{\boldsymbol{z}}_2\,. \tag{37}$$

Taking the time derivative of $\mathcal{V}$ along Eqs. (25) and (31) results in

$$\begin{aligned}
\dot{\mathcal{V}} &= \bar{\boldsymbol{z}}_1^T\Big\{\boldsymbol{f}_1 + G_1\begin{bmatrix}F_T & q_s & r_s\end{bmatrix}^T - \dot{\boldsymbol{x}}_{1,ref} - \dot{\boldsymbol{\chi}}_1\Big\} + \bar{\boldsymbol{z}}_2^T\Big\{\boldsymbol{f}_2 + D_2G_2\boldsymbol{u} - \dot{\boldsymbol{x}}_{2,ref} - \dot{\boldsymbol{\chi}}_2\Big\} \\
&= \bar{\boldsymbol{z}}_1^T\Big\{\boldsymbol{f}_1 + G_1\begin{bmatrix}F_T & q_{s_{ref}} & r_{s_{ref}}\end{bmatrix}^T + G_1\begin{bmatrix}0 & z_{22} & z_{23}\end{bmatrix}^T - \dot{\boldsymbol{x}}_{1,ref} - \dot{\boldsymbol{\chi}}_1\Big\} \\
&+ \bar{\boldsymbol{z}}_2^T\Big\{\boldsymbol{f}_2 + D_2G_2\boldsymbol{u} - \dot{\boldsymbol{x}}_{2,ref} - \dot{\boldsymbol{\chi}}_2\Big\} \\
&= \bar{\boldsymbol{z}}_1^T\Big\{\boldsymbol{f}_1 + G_1\begin{bmatrix}F_T^0 & q_{s,ref}^0 & r_{s,ref}^0\end{bmatrix}^T + G_1\begin{bmatrix}0 & z_{22} & z_{23}\end{bmatrix}^T - \dot{\boldsymbol{x}}_{1,ref} + C_1\boldsymbol{\chi}_1\Big\} \\
&+ \bar{\boldsymbol{z}}_2^T\Big\{\boldsymbol{f}_2 + D_2G_2\boldsymbol{u}^0 - \dot{\boldsymbol{x}}_{2,ref} + C_2\boldsymbol{\chi}_2\Big\} \\
&= \bar{\boldsymbol{z}}_1^T\Big\{-C_1\boldsymbol{z}_1 + C_1\boldsymbol{\chi}_1 + G_1\begin{bmatrix}0 & \bar{z}_{22} & \bar{z}_{23}\end{bmatrix}^T\Big\} + \bar{\boldsymbol{z}}_2^T\Big\{-C_2\boldsymbol{z}_2 + C_2\boldsymbol{\chi}_2 - G_1\begin{bmatrix}0 & \bar{z}_{12} & \bar{z}_{13}\end{bmatrix}^T\Big\} \\
&= \bar{\boldsymbol{z}}_1^T\Big\{-C_1\bar{\boldsymbol{z}}_1 + G_1\begin{bmatrix}0 & \bar{z}_{22} & \bar{z}_{23}\end{bmatrix}^T\Big\} + \bar{\boldsymbol{z}}_2^T\Big\{-C_2\bar{\boldsymbol{z}}_2 - G_1\begin{bmatrix}0 & \bar{z}_{12} & \bar{z}_{13}\end{bmatrix}^T\Big\} \\
&= -\bar{\boldsymbol{z}}_1^T C_1\bar{\boldsymbol{z}}_1 - \bar{\boldsymbol{z}}_2^T C_2\bar{\boldsymbol{z}}_2\,.
\end{aligned} \tag{38}$$

By the theorem of *LaSalle-Yoshizawa* (see e.g. Theorem B.9 in Sonneveldt[7]) it now follows that the equilibrium $\bar{\boldsymbol{z}} = \mathbf{0}$ is globally uniformly asymptotically stable. Note that this derivation only guarantees desirable properties for the *modified* tracking error $\bar{\boldsymbol{z}}$ and not the *actual* tracking error $\boldsymbol{z}$. According to Farrell, Sharma and Polycarpou,[38] in the absence of physical limitations (i.e. magnitude, rate, and bandwidth constraints on the commanded states $\boldsymbol{x}_{i,ref}$ for $i = 1, 2$ and control $\boldsymbol{u}$), convergence of the tracking error $\boldsymbol{z}$ is still guaranteed. When the inputs are too aggressive, the implemented limits can come into effect. During such a period $\boldsymbol{z}$ and $\boldsymbol{\chi}$ become nonzero because the desired control signals are not able to be implemented. However, the $\boldsymbol{\chi}$-signals and therefore also the tracking error $\boldsymbol{z}$ will remain bounded, because $\boldsymbol{\chi}$ is the output of a stable linear system with a bounded input. When the limits are no longer in effect, the tracking error $\boldsymbol{z}$ will converge to $\mathbf{0}$.

III.A.4. Approximations of non-affine force and moment coefficients

In the derivations of the aircraft dynamics used for control, the aerodynamic forces and moments have been split in a part that is independent of the control variables and a part that is linearly dependent on the control variables (see Eq. (22)). However, the aerodynamic data tables for aerodynamic coefficients $C_{X,T}$ and $C_{M,T}$ are not affine in the input vector $\boldsymbol{u}$:

$$C_{X,T} = C_X(\alpha, \delta_e) + \frac{q\bar{c}}{2V_T} C_{X_q}(\alpha) \tag{39a}$$

$$C_{M,T} = C_{Z,T}[x_{cg_r} - x_{cg}] + \frac{q\bar{c}}{2V_T} C_{M_q}(\alpha) + C_M(\alpha, \delta_e)\,, \tag{39b}$$

where

$$C_{Z,T} = \delta C_{Z_{\delta_e}}(\alpha, \beta) \left(\frac{\delta_e}{25}\right) + \frac{q\bar{c}}{2V_T} C_{Z_q}(\alpha)\,, \tag{40}$$

and where the coefficients C_X, C_{X_q}, C_{M_q}, C_M, $\delta C_{Z_{\delta_e}}$ and C_{Z_q} are given in tabular form for $-10 \leq \alpha \leq 45$, $-30 \leq \beta \leq 30$ and $-24 \leq \delta_e \leq 24$ degrees. Therefore aerodynamic coefficients C_X and C_M have been approximated by polynomials with degree r in α and degree s in δ_e. The total degree of the polynomial is the maximum of r and s. For aerodynamic coefficient C_M we have:

$$C_M(\alpha, \delta_e) \cong \hat{C}_M(\alpha, \delta_e) = \sum_{i=0}^{r} \sum_{j=0}^{s} p_{ij} \alpha^i \delta_e^j\,, \quad i + j \leq max(r, s)\,, \tag{41}$$

where $\hat{C}_M$ is the approximation of C_M and p_{ij} are constant coefficients. By following the definitions of Eq. (22), this approximation is written in a part that is independent of the control variable δ_e and a part that is linearly dependent on δ_e:

$$\hat{C}_M(\alpha, \delta_e) = \hat{C}_{M_0}(\alpha) + \hat{C}_{M_{\alpha,\delta_e}}(\alpha, \delta_e)\delta_e\,, \tag{42}$$

where

$$\hat{C}_{M_0}(\alpha) = \sum_{i=0}^{r} p_{i0} \alpha^i \tag{43a}$$

$$\hat{C}_{M_{\alpha,\delta_e}}(\alpha, \delta_e) = \sum_{i=0}^{r-1} \sum_{j=1}^{s} p_{ij} \alpha^i \delta_e^{j-1}\,, \quad i + j \leq max(r, s)\,. \tag{43b}$$

Note that $\hat{C}_{M_{\alpha,\delta_e}}(\alpha, \delta_e)$ is a function of δ_e, which is possible because the current δ_e is already available from the corresponding command filter. The coefficients p_{ij} have been determined by obtaining a linear least-squares fit of the polynomial to the aerodynamic data table of the F-16 model. The order of the $\hat{C}_M$ and $\hat{C}_X$ polynomials have been selected to ensure a good fit and to prevent instability of the models. This has resulted in polynomial orders of $(r, s) = (5, 3)$ and $(r, s) = (4, 2)$ for respectively coefficient $\hat{C}_M$ and $\hat{C}_X$. Plots of the polynomial approximations can be seen in Appendix B.

III.B. Incremental Backstepping

Incremental Backstepping[8,15,16] is applied to reduce the dependency on the on-board aircraft model compared to conventional BS control. The derivations for subsystem $\boldsymbol{x}_1$ remain exactly the same as in Section III.A.1, because this subsystem is assumed to be fully known. Therefore we directly move on to the inner loop dynamics:

$$\dot{\boldsymbol{x}}_2 = \boldsymbol{f}_2(\boldsymbol{x}) + D_2(\boldsymbol{x})G_2(\boldsymbol{x},\boldsymbol{u})\boldsymbol{u}\,, \tag{44}$$

where $\boldsymbol{f}_2$, D_2 and G_2 are given by Eqs. (21c) to (21e). Taking the first-order Taylor series expansion around the current solution $[\boldsymbol{x}_0, \boldsymbol{u}_0]$ results in

$$\begin{aligned}\dot{\boldsymbol{x}}_2 \cong\ & \boldsymbol{f}_2(\boldsymbol{x}_0) + D_2(\boldsymbol{x}_0)G_2(\boldsymbol{x}_0,\boldsymbol{u}_0)\boldsymbol{u}_0 + \frac{\partial}{\partial \boldsymbol{x}}\left[\boldsymbol{f}_2(\boldsymbol{x}) + D_2(\boldsymbol{x})G_2(\boldsymbol{x},\boldsymbol{u})\boldsymbol{u}\right]\Big|_{\substack{\boldsymbol{x}=\boldsymbol{x}_0\\ \boldsymbol{u}=\boldsymbol{u}_0}}(\boldsymbol{x}-\boldsymbol{x}_0) \\ &+ \frac{\partial}{\partial \boldsymbol{u}}\left[D_2(\boldsymbol{x})G_2(\boldsymbol{x},\boldsymbol{u})\boldsymbol{u}\right]\Big|_{\substack{\boldsymbol{x}=\boldsymbol{x}_0\\ \boldsymbol{u}=\boldsymbol{u}_0}}(\boldsymbol{u}-\boldsymbol{u}_0)\,,\end{aligned} \tag{45}$$

where $\boldsymbol{x} = \begin{bmatrix}\boldsymbol{x}_1^T & \boldsymbol{x}_2^T\end{bmatrix}^T$. The linearization error is small when the sampling rate is sufficiently high. Equation (45) can be written as

$$\dot{\boldsymbol{x}}_2 \cong \dot{\boldsymbol{x}}_{2,0} + A_{2,0}\Delta\boldsymbol{x} + B_{2,0}\Delta\boldsymbol{u}\,, \tag{46}$$

where

$$\Delta\boldsymbol{x} = \boldsymbol{x} - \boldsymbol{x}_0\,, \quad \Delta\boldsymbol{u} = \boldsymbol{u} - \boldsymbol{u}_0 \tag{47a}$$

$$A_{2,0} = \frac{\partial}{\partial \boldsymbol{x}}\left[\boldsymbol{f}_2(\boldsymbol{x}) + D_2(\boldsymbol{x})G_2(\boldsymbol{x},\boldsymbol{u})\boldsymbol{u}\right]\Big|_{\substack{\boldsymbol{x}=\boldsymbol{x}_0\\ \boldsymbol{u}=\boldsymbol{u}_0}} \tag{47b}$$

$$B_{2,0} = \frac{\partial}{\partial \boldsymbol{u}}\left[D_2(\boldsymbol{x})G_2(\boldsymbol{x},\boldsymbol{u})\boldsymbol{u}\right]\Big|_{\substack{\boldsymbol{x}=\boldsymbol{x}_0\\ \boldsymbol{u}=\boldsymbol{u}_0}} = D_2(\boldsymbol{x}_0)\left[G_2(\boldsymbol{x}_0,\boldsymbol{u}_0) + \frac{\partial G_2(\boldsymbol{x},\boldsymbol{u})}{\partial \boldsymbol{u}}\Big|_{\substack{\boldsymbol{x}=\boldsymbol{x}_0\\ \boldsymbol{u}=\boldsymbol{u}_0}}\boldsymbol{u}_0\right]. \tag{47c}$$

The vectors $\Delta\boldsymbol{x}$ and $\Delta\boldsymbol{u}$ are known as respectively the *incremental state vector* and the *incremental control input*. Note from Eqs. (21e) and (42) that we obtain the following approximation:

$$\hat{G}_2 + \frac{\partial \hat{G}_2}{\partial \boldsymbol{u}} = \bar{q}Sb\begin{bmatrix} 0 & \hat{C}_{L_{\delta_a}} & \hat{C}_{L_{\delta_r}} \\ \hat{C}_{M_{\alpha,\delta_e}} + \frac{\partial \hat{C}_{M_{\alpha,\delta_e}}}{\partial \delta_e}\delta_e & 0 & 0 \\ 0 & \hat{C}_{N_{\delta_a}} & \hat{C}_{N_{\delta_r}}\end{bmatrix}, \tag{48}$$

where we now introduce the following parameter estimate for notational convenience:

$$\hat{C}_{M_{\delta_e}} \equiv \frac{\partial \hat{C}_M}{\partial \delta_e} = \hat{C}_{M_{\alpha,\delta_e}} + \frac{\partial \hat{C}_{M_{\alpha,\delta_e}}}{\partial \delta_e}\delta_e\,. \tag{49}$$

If we assume a sufficiently time-scale separated system, that is the increment in state $\Delta\boldsymbol{x}$ is much smaller than the increment in both state derivative $\Delta\dot{\boldsymbol{x}}_2$ and input $\Delta\boldsymbol{u}$, we can neglect the former.[8,39–41] This is allowed because the deflections of the control surfaces directly effect the angular accelerations, while the angular rates only change by integrating these angular accelerations. Hence Eq. (46) can be further simplified as follows:

$$\dot{\boldsymbol{x}}_2 \cong \dot{\boldsymbol{x}}_{2,0} + B_{2,0}(\boldsymbol{x}_0,\boldsymbol{u}_0)\Delta\boldsymbol{u}\,. \tag{50}$$

Applying the Command-Filtered BS procedure[11–14] to this simplified vector equation yields the following incremental BS control law:

$$\hat{B}_{2,0}(\boldsymbol{x}_0,\boldsymbol{u}_0)\Delta\boldsymbol{u}^0 = -C_2\boldsymbol{z}_2 + \begin{bmatrix}\dot{p}_s\\ \dot{q}_s\\ \dot{r}_s\end{bmatrix}_{ref} - \begin{bmatrix}\dot{p}_{s_0}\\ \dot{q}_{s_0}\\ \dot{r}_{s_0}\end{bmatrix} - G_1\begin{bmatrix}0\\ \bar{z}_{12}\\ \bar{z}_{13}\end{bmatrix}, \tag{51}$$

where C_2 is a positive diagonal matrix and where $\hat{B}_{2,0}$ denotes the estimate of $B_{2,0}$. The time derivative $\dot{p}_{s,ref}$ is obtained from the prefilter, while $\dot{q}_{s,ref}$ and $\dot{r}_{s,ref}$ are obtained from the command filters. Because the F-16 model is not over-actuated, $B_{2,0}$ is a square matrix. If this would not be the case, some form of control allocation would be required.[9,37] Note from Eqs. (21e) and (47c) that matrix $B_{2,0}$ is always of full rank as long as the primary control surfaces remain operable.

The current control deflections $\boldsymbol{u}_0$ have to be added to the incremental raw control signal $\Delta \boldsymbol{u}^0$ to get the total raw input vector $\boldsymbol{u}^0$. The final commanded deflections $\boldsymbol{u}$ for the F-16 aircraft are subsequently obtained using command filters. The effect that the use of these command filters have on the tracking error $\boldsymbol{z}_2$ is estimated by the stable linear filter

$$\begin{bmatrix} \dot{\chi}_{21} \\ \dot{\chi}_{22} \\ \dot{\chi}_{23} \end{bmatrix} = -C_2 \begin{bmatrix} \chi_{21} \\ \chi_{22} \\ \chi_{23} \end{bmatrix} + \hat{B}_{2,0} \left(\begin{bmatrix} \delta_e \\ \delta_a \\ \delta_r \end{bmatrix} - \begin{bmatrix} \delta_e \\ \delta_a \\ \delta_r \end{bmatrix}^0 \right), \tag{52}$$

with zero initial conditions, that is, $\boldsymbol{\chi}_2(0) = \mathbf{0}$. If the sampling rate is sufficiently high, and we assume that $\hat{\boldsymbol{f}}_{1,m} = \boldsymbol{f}_{1,m}$ and $\hat{B}_{2,0} = B_{2,0}$, i.e. we only deal with uncertainties in the system dynamics $\boldsymbol{f}_2$, then stability can be proved similar as in Section III.A.3.

If we compare IBS control law Eq. (51) with conventional BS controller Eq. (32), we can see that the incremental controller uses sensor measurements or estimates of the angular acceleration and the current control deflections to reduce the sensitivity to uncertainties and possibly model mismatch of the system dynamics $\boldsymbol{f}_2$. This is a huge improvement, because now we no longer need knowledge of the largest part of the aerodynamic model, the location of the center of gravity and the moments of inertia in order to control the F-16 aircraft.

Note that Ali[42] and Simplício, Pavel, Van Kampen and Chu[41] state that for sufficiently high update rate, closed-loop stability of incremental control law Eq. (51) is still guaranteed even when uncertainties are introduced in the control effectiveness matrix $B_{2,0}$. However, this conclusion was obtained by neglecting the difference between two consecutive measurements of the state vector derivative, which is *not* allowed because this would also imply that $\Delta \boldsymbol{u} = \mathbf{0}$. Therefore, without the availability of simulation results or further theoretical analysis, nothing can be said about the robustness properties of the IBS controller with respect to uncertainties in the control effectiveness matrix $B_{2,0}$.

III.C. Tuning Functions Adaptive Incremental Backstepping

As seen in the previous section, IBS control law Eq. (51) improves the robustness of the closed-loop system with respect to conventional BS by reducing its dependency on the exact knowledge of the plant dynamics $\boldsymbol{f}_2$. However, the IBS controller still requires accurate knowledge of the control effectiveness matrix $B_{2,0}$. In this section the incremental control law is augmented with Lyapunov-based update laws[11,21,22] to guarantee closed-loop stability even when uncertainties are introduced in the control effectiveness matrix $B_{2,0}$. By using an incremental control law, the estimator now only has to estimate the aircraft control derivatives.

The derivations for subsystem $\boldsymbol{x}_1$ remain exactly the same as in Section III.A.1, because this subsystem is assumed to be fully known. Therefore we directly move on to the outer loop control design in Section III.C.1. The proof that shows that the Tuning Functions Adaptive Incremental Backstepping (TFAIBS) controller guarantees closed-loop stability in case of inner loop uncertainties can be found in Section III.C.2. Finally in Section III.C.3, function approximators are defined to estimate an unknown parameter.

III.C.1. Outer loop control design

In the previous section we have seen that if the sampling rate is sufficiently high, the $\boldsymbol{x}_2$-subsystem can be written as

$$\dot{\boldsymbol{x}}_2 \cong \dot{\boldsymbol{x}}_{2,0} + B_{2,0}(\boldsymbol{x}_0, \boldsymbol{u}_0)\Delta \boldsymbol{u}\,, \tag{50 revisited}$$

where $B_{2,0}$ is defined by Eq. (47c) and contains uncertainties. The dynamics of modified tracking error $\bar{\boldsymbol{z}}_2$ are now given by

$$\dot{\bar{\boldsymbol{z}}}_2 \cong \dot{\boldsymbol{x}}_{2,0} + B_{2,0}(\boldsymbol{x}_0, \boldsymbol{u}_0)\Delta \boldsymbol{u} - \dot{\boldsymbol{x}}_{2,ref} - \dot{\boldsymbol{\chi}}_2\,. \tag{53}$$

Similar as in the previous section, the desired incremental control law and the stable linear filter are defined by respectively Eqs. (51) and (52). The estimation error is now introduced:

$$\tilde{B}_{2,0} = B_{2,0} - \hat{B}_{2,0}\,, \tag{54}$$

where the estimate $\hat{B}_{2,0}$ is defined as

$$\hat{\boldsymbol{b}}_{2j} = \Phi^T_{b_{2j}}(\boldsymbol{x})\hat{\boldsymbol{\theta}}_{b_{2j}}\,, \quad \text{for } j = 1, 2, 3\,, \tag{55}$$

where $\hat{\boldsymbol{b}}_{2j}$ represents the jth column of $\hat{B}_{2,0}$, $\Phi^T_{b_{2j}}$ are the known regressor functions and $\hat{\boldsymbol{\theta}}_{b_{2j}}$ are vectors with time-varying adaptive estimates. It is assumed that there exists a *constant* vector $\boldsymbol{\theta}_{b_{2j}}$ such that

$$\boldsymbol{b}_{2j} = \Phi^T_{b_{2j}}(\boldsymbol{x})\boldsymbol{\theta}_{b_{2j}}\,. \tag{56}$$

Now the parameter estimation errors can be defined as

$$\tilde{\boldsymbol{\theta}}_{b_{2j}} = \boldsymbol{\theta}_{b_{2j}} - \hat{\boldsymbol{\theta}}_{b_{2j}} \quad \rightarrow \quad \dot{\tilde{\boldsymbol{\theta}}}_{b_{2j}} = -\dot{\hat{\boldsymbol{\theta}}}_{b_{2j}}\,. \tag{57}$$

The following Lyapunov-based TFs[11,21,22] are selected to obtain the time-varying adaptive estimates $\hat{\boldsymbol{\theta}}_{b_{2j}}$:

$$\dot{\hat{\boldsymbol{\theta}}}_{b_{2j}} = \mathcal{P}_{b_{2j}}\Big[\Gamma_{b_{2j}}\Phi_{b_{2j}}(\boldsymbol{x}_0)\bar{\boldsymbol{z}}_2\Delta u_j\Big]\,, \tag{58}$$

where $\mathcal{P}_{b_{2j}}$ is a projection operator[7,27] to ensure that full rank of $\hat{B}_{2,0}$ is always maintained, $\Gamma_{b_{2j}}$ are positive diagonal matrices containing the adaptation gains and Δu_j is the jth element of $\Delta\boldsymbol{u}$. Note that the vectors $\hat{\boldsymbol{\theta}}_{b_{2j}}$ for $j = 1, 2, 3$ contain respectively the time-varying adaptive estimates of the control derivatives with respect to the elevator, aileron and rudder. Also note that the Lyapunov-based update law Eq. (58) is a function of the *modified* tracking error $\bar{\boldsymbol{z}}_2$ instead of the *actual* tracking error $\boldsymbol{z}_2$, this prevents the estimator to "unlearn" as soon as the input is saturated.

III.C.2. Proof of stability

If the sampling rate is sufficiently high, and we assume that $\hat{\boldsymbol{f}}_{1,m} = \boldsymbol{f}_{1,m}$, i.e. we only deal with uncertainties in the inner loop (vector equation $\boldsymbol{f}_2$ and matrix $B_{2,0}$), then stability can be proved on basis of the following control Lyapunov function:

$$\mathcal{V}(\bar{\boldsymbol{z}}) = \frac{1}{2}\bar{\boldsymbol{z}}_1^T\bar{\boldsymbol{z}}_1 + \frac{1}{2}\bar{\boldsymbol{z}}_2^T\bar{\boldsymbol{z}}_2 + \frac{1}{2}\sum_{j=1}^{3}\tilde{\boldsymbol{\theta}}^T_{b_{2j}}\Gamma^{-1}_{b_{2j}}\tilde{\boldsymbol{\theta}}_{b_{2j}}\,. \tag{59}$$

Taking the time derivative of $\mathcal{V}$ along the trajectories of Eqs. (25), (53) and (57) yields

$$\begin{aligned}
\dot{\mathcal{V}} = {} & \bar{\boldsymbol{z}}_1^T\Big\{\boldsymbol{f}_1 + G_1\begin{bmatrix}F_T & q_s & r_s\end{bmatrix}^T - \dot{\boldsymbol{x}}_{1,ref} - \dot{\boldsymbol{\chi}}_1\Big\} + \bar{\boldsymbol{z}}_2^T\Big\{\dot{\boldsymbol{x}}_{2,0} + \big(\tilde{B}_{2,0} + \hat{B}_{2,0}\big)\Delta\boldsymbol{u} - \dot{\boldsymbol{x}}_{2,ref} - \dot{\boldsymbol{\chi}}_2\Big\} \\
& -\sum_{j=1}^{3}\tilde{\boldsymbol{\theta}}^T_{b_{2j}}\Gamma^{-1}_{b_{2j}}\dot{\hat{\boldsymbol{\theta}}}_{b_{2j}} \qquad\qquad (60) \\
= {} & \bar{\boldsymbol{z}}_1^T\Big\{\boldsymbol{f}_1 + G_1\begin{bmatrix}F_T & q_{s_{ref}} & r_{s_{ref}}\end{bmatrix}^T + G_1\begin{bmatrix}0 & z_{22} & z_{23}\end{bmatrix}^T - \dot{\boldsymbol{x}}_{1,ref} - \dot{\boldsymbol{\chi}}_1\Big\} \\
& + \bar{\boldsymbol{z}}_2^T\Big\{\dot{\boldsymbol{x}}_{2,0} + \tilde{B}_{2,0}\Delta\boldsymbol{u} + \hat{B}_{2,0}\big(u^0 - u_0\big) - \dot{\boldsymbol{x}}_{2,ref} + C_2\boldsymbol{\chi}_2\Big\} - \sum_{j=1}^{3}\tilde{\boldsymbol{\theta}}^T_{b_{2j}}\Gamma^{-1}_{b_{2j}}\dot{\hat{\boldsymbol{\theta}}}_{b_{2j}} \\
= {} & \bar{\boldsymbol{z}}_1^T\Big\{\boldsymbol{f}_1 + G_1\begin{bmatrix}F_T & q_{s_{ref}} & r_{s_{ref}}\end{bmatrix}^T + G_1\begin{bmatrix}0 & z_{22} & z_{23}\end{bmatrix}^T - \dot{\boldsymbol{x}}_{1,ref} - \dot{\boldsymbol{\chi}}_1\Big\} \\
& + \bar{\boldsymbol{z}}_2^T\Big\{ - C_2\boldsymbol{z}_2 + \tilde{B}_{2,0}\Delta\boldsymbol{u} - G_1\begin{bmatrix}0 & \bar{z}_{12} & \bar{z}_{13}\end{bmatrix}^T + C_2\boldsymbol{\chi}_2\Big\} - \sum_{j=1}^{3}\tilde{\boldsymbol{\theta}}^T_{b_{2j}}\Gamma^{-1}_{b_{2j}}\dot{\hat{\boldsymbol{\theta}}}_{b_{2j}} \\
= {} & \bar{\boldsymbol{z}}_1^T\Big\{\boldsymbol{f}_1 + G_1\begin{bmatrix}F^0_T & q^0_{s_{ref}} & r^0_{s_{ref}}\end{bmatrix}^T + G_1\begin{bmatrix}0 & z_{22} & z_{23}\end{bmatrix}^T - \dot{\boldsymbol{x}}_{1,ref} + C_1\boldsymbol{\chi}_1\Big\} \\
& + \bar{\boldsymbol{z}}_2^T\Big\{ - C_2\bar{\boldsymbol{z}}_2 - G_1\begin{bmatrix}0 & \bar{z}_{12} & \bar{z}_{13}\end{bmatrix}^T\Big\} - \sum_{j=1}^{3}\tilde{\boldsymbol{\theta}}^T_{b_{2j}}\Gamma^{-1}_{b_{2j}}\Big\{\dot{\hat{\boldsymbol{\theta}}}_{b_{2j}} - \Gamma_{b_{2j}}\Phi_{b_{2j}}\bar{\boldsymbol{z}}_2\Delta u_j\Big\} \\
= {} & \bar{\boldsymbol{z}}_1^T\Big\{ - C_1\boldsymbol{z}_1 + G_1\begin{bmatrix}0 & \bar{z}_{22} & \bar{z}_{23}\end{bmatrix}\Big\} + \bar{\boldsymbol{z}}_2^T\Big\{ - C_2\bar{\boldsymbol{z}}_2 - G_1\begin{bmatrix}0 & \bar{z}_{12} & \bar{z}_{13}\end{bmatrix}^T\Big\} \\
= {} & -\bar{\boldsymbol{z}}_1^T C_1\bar{\boldsymbol{z}}_1 - \bar{\boldsymbol{z}}_2^T C_2\bar{\boldsymbol{z}}_2\,.
\end{aligned}$$

The exact same result was obtained in Eq. (38), thus we can draw the same conclusions on the stability properties of the tracking errors as in Section III.A.3. Note that the parameter estimation error is completely canceled in Eq. (60) by selecting the parameter update law as Eq. (58), therefore we cannot guarantee that the parameter estimate $\hat{\boldsymbol{\theta}}_{b_{2j}}$ actually converges to the real parameter $\boldsymbol{\theta}_{b_{2j}}$. All we can conclude from Eqs. (59) and (60) with respect to the parameter estimation error $\tilde{\boldsymbol{\theta}}_{b_{2j}}$ is that it is bounded. In Krstić[43] it is proven that convergence of the parameter estimate to a constant value is always achieved. In case of Persistent Excitation (PE), the parameter estimate converges to the actual parameter. The requirement of PE basically means that the reference signal must be "rich enough", i.e. "contain enough frequencies" for the parameter estimation error to converge to zero.[44]

III.C.3. *Estimating unknown control derivative* $C_{M_{\delta_e}}$

The regressor functions Φ and parameter vectors $\hat{\boldsymbol{\theta}}$ in update law Eq. (58) have not yet been specified. The non-dimensional aerodynamic coefficients of the F-16 model are available as aerodynamic data tables that are functions of flight parameters such as the angle of attack α and the sideslip angle β. In order to apply the TFs approach, these lookup tables have to be approximated in a parametric form.

In this paper a time-varying uncertainty in the pitching moment coefficient $C_M(\alpha, \delta_e)$ will be introduced in order to evaluate the (adaptive, incremental) BS control laws. Note from Eqs. (22e) and (48) that an uncertainty in coefficient $C_M(\alpha, \delta_e)$ results in an uncertain C_{M_0} and $C_{M_{\delta_e}}$ coefficient. Because incremental control law Eq. (51) is robust to uncertainties in C_{M_0}, we only need to estimate control derivative $C_{M_{\delta_e}}$ (see Eq. (49) for the definition of this coefficient). The following three function approximators that are linear-in-the-parameters will be used for estimation of the uncertain control derivative $C_{M_{\delta_e}}$:

$$\hat{C}_{M_{\delta_e,1}} = a_0 \tag{61a}$$

$$\hat{C}_{M_{\delta_e,2}} = b_0 + b_1\alpha + b_2\delta_e \tag{61b}$$

$$\hat{C}_{M_{\delta_e,3}} = c_0 + c_1\alpha + c_2\delta_e + c_3\alpha^2 + c_4\alpha\delta_e + c_5\delta_e^2\,, \tag{61c}$$

where the coefficients $(a_0, b_\star, c_\star)$ are estimated using TFs Eq. (58). The corresponding regressor functions Φ and parameter vectors $\hat{\boldsymbol{\theta}}$ are given by

$$\Phi^T_{b_{21,1}} = \bar{q}SbD_2 \begin{bmatrix} 0 \\ 1 \\ 0 \end{bmatrix}, \quad \Phi^T_{b_{21,2}} = \bar{q}SbD_2 \begin{bmatrix} 0 & 0 & 0 \\ 1 & \alpha & \delta_e \\ 0 & 0 & 0 \end{bmatrix}, \quad \Phi^T_{b_{21,3}} = \bar{q}SbD_2 \begin{bmatrix} 0 & 0 & 0 & 0 & 0 & 0 \\ 1 & \alpha & \delta_e & \alpha^2 & \alpha\delta_e & \delta_e^2 \\ 0 & 0 & 0 & 0 & 0 & 0 \end{bmatrix} \tag{62a}$$

$$\hat{\theta}_{b_{21,1}} = a_0, \qquad \hat{\boldsymbol{\theta}}_{b_{21,2}} = \begin{bmatrix} b_0 & b_1 & b_2 \end{bmatrix}, \qquad \hat{\boldsymbol{\theta}}_{b_{21,3}} = \begin{bmatrix} c_0 & c_1 & c_2 & c_3 & c_4 & c_5 \end{bmatrix}. \tag{62b}$$

For example, the TF update law corresponding to the first function approximator now follows from Eqs. (58) and (62):

$$\dot{\hat{C}}_{M_{\delta_e,1}} = \dot{\hat{\theta}}_{b_{21,1}} = \mathcal{P}_{b_{21}}\left[\Gamma_{b_{21,1}}\bar{q}Sbc_7\bar{z}_{22}\Delta\delta_e\right], \tag{63}$$

where $\Gamma_{b_{21,1}}$ is in this case a *scalar* adaptation gain.

III.D. Least-Squares Adaptive Incremental Backstepping

As seen in Section III.B, the IBS control law Eq. (51) improves the robustness of the closed-loop system with respect to conventional BS by reducing its dependency on the exact knowledge of the plant dynamics $\boldsymbol{f}_2$. However, the IBS controller still requires accurate knowledge of the control effectiveness matrix $B_{2,0}$. In this section the incremental control law is augmented with update laws based on Least-Squares[6,20] to estimate matrix $B_{2,0}$. By using an incremental control law, the estimator now only has to estimate the aircraft control derivatives.

The derivations for subsystem $\boldsymbol{x}_1$ remain exactly the same as in Section III.A.1, because this subsystem is assumed to be fully known. Therefore we directly move on to the outer loop control design:

$$\dot{\boldsymbol{x}}_2 \cong \dot{\boldsymbol{x}}_{2,0} + B_{2,0}(\boldsymbol{x}_0, \boldsymbol{u}_0)\Delta\boldsymbol{u}\,, \tag{50 revisited}$$

where $B_{2,0}$ is defined by Eq. (47c) and contains uncertainties. Similar as in the previous section, the desired incremental control law and the stable linear filter are defined by respectively Eqs. (51) and (52). Again, it is assumed that there exists a vector $\boldsymbol{\theta}_{b_{2j}}$ such that

$$\boldsymbol{b}_{2j} = \Phi^T_{b_{2j}}(\boldsymbol{x})\boldsymbol{\theta}_{b_{2j}}\,, \quad \text{for } j = 1, 2, 3\,, \tag{64}$$

where $\boldsymbol{b}_{2j}$ represents the jth column of $B_{2,0}$, $\Phi^T_{b_{2j}}$ are the known regressor functions and $\boldsymbol{\theta}_{b_{2j}}$ is an unknown constant vector. Now Eq. (50) can be written as

$$\Delta\dot{\boldsymbol{x}}_2 \cong \begin{bmatrix}\Phi^T_{b_{21}}(\boldsymbol{x}_0)\Delta\delta_e & \Phi^T_{b_{22}}(\boldsymbol{x}_0)\Delta\delta_a & \Phi^T_{b_{23}}(\boldsymbol{x}_0)\Delta\delta_r\end{bmatrix}\begin{bmatrix}\boldsymbol{\theta}_{b_{21}}\\ \boldsymbol{\theta}_{b_{22}}\\ \boldsymbol{\theta}_{b_{23}}\end{bmatrix}, \tag{65}$$

where $\Delta\dot{\boldsymbol{x}}_2 = \dot{\boldsymbol{x}}_2 - \dot{\boldsymbol{x}}_{2,0}$. At time k the following vector equation can be constructed by using the past N measurements:

$$\boldsymbol{y} \cong A\boldsymbol{\theta}\,, \tag{66}$$

where

$$\boldsymbol{y} = \begin{bmatrix}\Delta\dot{x}_{2,k-N} & \cdots & \Delta\dot{x}_{2,k-1} & \Delta\dot{x}_{2,k}\end{bmatrix}^T, \qquad \boldsymbol{\theta} = \begin{bmatrix}\boldsymbol{\theta}^T_{b_{21}} & \boldsymbol{\theta}^T_{b_{22}} & \boldsymbol{\theta}^T_{b_{23}}\end{bmatrix}^T, \tag{67a}$$

$$A = \begin{bmatrix}\Phi^T_{b_{21}}(\boldsymbol{x}_{k-N-1})\Delta\delta_{e,k-N} & \Phi^T_{b_{22}}(\boldsymbol{x}_{k-N-1})\Delta\delta_{a,k-N} & \Phi^T_{b_{23}}(\boldsymbol{x}_{k-N-1})\Delta\delta_{r,k-N}\\ \vdots & \vdots & \vdots\\ \Phi^T_{b_{21}}(\boldsymbol{x}_{k-2})\Delta\delta_{e,k-1} & \Phi^T_{b_{22}}(\boldsymbol{x}_{k-2})\Delta\delta_{a,k-1} & \Phi^T_{b_{23}}(\boldsymbol{x}_{k-2})\Delta\delta_{r,k-1}\\ \Phi^T_{b_{21}}(\boldsymbol{x}_{k-1})\Delta\delta_{e,k} & \Phi^T_{b_{22}}(\boldsymbol{x}_{k-1})\Delta\delta_{a,k} & \Phi^T_{b_{23}}(\boldsymbol{x}_{k-1})\Delta\delta_{r,k}\end{bmatrix}. \tag{67b}$$

If we assume measurements or estimates of $\dot{\boldsymbol{x}}_2$, $\boldsymbol{x}$ and $\boldsymbol{u}$ are available, then the unknown parameters can be estimated on-line by the efficient RLS algorithm with *exponential* forgetting:[45]

$$\hat{\boldsymbol{\theta}}_{k+1} = \mathcal{P}\Big[\hat{\boldsymbol{\theta}}_k + K_{k+1}\big(y_{k+1} - \boldsymbol{a}_{k+1}\hat{\boldsymbol{\theta}}_k\big)\Big] \tag{68a}$$

$$K_{k+1} = P_k\boldsymbol{a}^T_{k+1}\left(\boldsymbol{a}_{k+1}P_k\boldsymbol{a}^T_{k+1} + \lambda\right)^{-1} \tag{68b}$$

$$P_{k+1} = \frac{1}{\lambda}\left(I_N - K_{k+1}\boldsymbol{a}_{k+1}\right)P_k\,, \tag{68c}$$

where

$$A_{k+1} = \begin{bmatrix}A_k & \boldsymbol{a}_{k+1}\end{bmatrix}^T \tag{69a}$$

$$\boldsymbol{y}_k = \begin{bmatrix}y_1 & y_2 & \ldots & y_k\end{bmatrix}^T \tag{69b}$$

$$\boldsymbol{y}_{k+1} = \begin{bmatrix}\boldsymbol{y}^T_k & y_{k+1}\end{bmatrix}^T, \tag{69c}$$

and where $\mathcal{P}$ represents the parameter projection operator to prevent singularity problems, $\boldsymbol{a}$ the regression vector, K the Kalman gain, P the covariance matrix and λ the forgetting factor for which we have $0 < \lambda \leq 1$. Setting $\lambda = 1$ corresponds to "no forgetting" and estimating constant coefficients. Setting $\lambda < 1$ implies that past measurements are less significant for parameter estimation and can be "forgotten". $\lambda < 1$ should be set to estimate time-varying coefficients. Note that for this estimation procedure an initial parameter estimate and covariance matrix need to be provided.

A well-known problem of the RLS estimator utilizing forgetting is that the covariance matrix grows without bounds when the reference signal is non-persistently exciting. This causes unbounded noise sensitivity and leads to numerical difficulties.[46–48] One approach to avoid covariance windup is to use a *variable* forgetting factor, which changes the forgetting factor from a value slightly less than one to the value of one when the system is working in the steady state for a longer time. Another problem of the RLS estimator is that of saturation, in which the covariance matrix, which can be seen as an adaptation gain of the algorithm, tends to approach a *small* positive constant when the parameter estimates converge. This reduces the ability of the identifier to adjust to abrupt changes in the system parameters. This problem can be overcome by decreasing the forgetting factor, however, this increases the sensitivity of the estimator to noise and modeling error. Furthermore, a smaller forgetting factor increases the covariance windup problem. A better approach to prevent estimator saturation is that of covariance resetting[6,7,49] or by introducing a variable forgetting factor.[47,50]

Note that no formal proof is included for the Least-Squares Adaptive Incremental Backstepping (LSAIBS) controller that guarantees closed-loop stability in case of inner loop uncertainties. If the real-time identification routine is not able to provide accurate estimates of the control derivatives, then the possibility exists that this control approach leads to an unsatisfactory result. Therefore, robust BS could be considered for application in this context.[51–53] Another option is to include nonlinear damping terms in the control law to robustify the design against parameter estimation errors.[49] In this research it has been assumed that sufficiently accurate estimates are supplied by the estimator, such that the natural dynamics of the system are successfully canceled by selection of incremental control law Eq. (51). Generally, the more accurate the parameter estimates, the better the cancellation of the dynamics, and with that, the higher the performance of the controller.[54]

In this paper a time-varying uncertainty in the pitching moment coefficient $C_M(\alpha, \delta_e)$ will be introduced in order to evaluate the (adaptive, incremental) BS control laws. Note from Eqs. (22e) and (48) that an uncertainty in coefficient $C_M(\alpha, \delta_e)$ results in an uncertain C_{M_0} and $C_{M_{\delta_e}}$ coefficient. Because incremental control law Eq. (51) is robust to uncertainties in C_{M_0}, we only need to estimate control derivative $C_{M_{\delta_e}}$ (see Eq. (49) for the definition of this coefficient). The three function approximators that will be used for estimation of this uncertain control derivative $C_{M_{\delta_e}}$ are given in Eq. (61). Note that every row of Eq. (66) is a vector equation. In order to estimate the control efficiency $C_{M_{\delta_e}}$, we only need to consider the second vector equation:

$$\underbrace{\begin{bmatrix} \Delta\dot{x}_{2,2,k-N} \\ \vdots \\ \Delta\dot{x}_{2,2,k-1} \\ \Delta\dot{x}_{2,2,k} \end{bmatrix}}_{\boldsymbol{y}} \cong \underbrace{\begin{bmatrix} \Phi^T_{b_{21}}(\boldsymbol{x}_{k-N-1})\Delta\delta_{e,k-N} \\ \vdots \\ \Phi^T_{b_{21}}(\boldsymbol{x}_{k-2})\Delta\delta_{e,k-1} \\ \Phi^T_{b_{21}}(\boldsymbol{x}_{k-1})\Delta\delta_{e,k} \end{bmatrix}}_{A} \boldsymbol{\theta}_{b_{21}} \,. \tag{70}$$

Now the unknown parameter vector $\boldsymbol{\theta}_{b_{21}}$ can be estimated on-line by the RLS algorithm Eq. (68). Note that the regressor functions $\Phi_{b_{21}}$ and parameter vectors $\hat{\boldsymbol{\theta}}_{b_{21}}$ that correspond to function approximations Eq. (61) are given by Eq. (62).

III.E. Immersion & Invariance Adaptive Incremental Backstepping

As seen in Section III.B, the IBS control law Eq. (51) improves the robustness of the closed-loop system with respect to conventional BS by reducing its dependency on the exact knowledge of the plant dynamics $\boldsymbol{f}_2$. However, the IBS controller still requires accurate knowledge of the control effectiveness matrix $B_{2,0}$. In this section the incremental control law is augmented with update laws based on I&I[23–26] to guarantee closed-loop stability even when uncertainties are introduced in the control effectiveness matrix $B_{2,0}$. By using an incremental control law, the estimator now only has to estimate the aircraft control derivatives.

The derivations for subsystem $\boldsymbol{x}_1$ remain exactly the same as in Section III.A.1, because this subsystem is assumed to be fully known. Therefore we directly move on to the outer loop control design in Section III.E.1. The proof that shows that the I&I estimator obtains asymptotically converging estimates of each unknown term can be found in Section III.E.2. Finally in Section III.E.3, update laws are defined to estimate an unknown parameter.

III.E.1. Outer loop control design

In the previous section we have seen that when we assume a sufficiently high sampling rate, the $\boldsymbol{x}_2$-subsystem can be written as

$$\dot{\boldsymbol{x}}_2 \cong \dot{\boldsymbol{x}}_{2,0} + B_{2,0}(\boldsymbol{x}_0, \boldsymbol{u}_0)\Delta\boldsymbol{u}\,, \tag{50 revisited}$$

where $B_{2,0}$ is defined by Eq. (47c) and contains uncertainties. Similar as in the previous two sections, the desired incremental control law and the stable linear filter are defined by respectively Eqs. (51) and (52). It is assumed that Eq. (50) can be written as follows to facilitate the design procedure of the I&I estimator:

$$\dot{x}_{2,i} = f_i + \boldsymbol{\varphi}_i(\boldsymbol{x}_1, x_{2,1}, \ldots, x_{2,i}, \Delta\boldsymbol{u})^T\boldsymbol{\theta}\,, \qquad \text{for } i = 1,2,3 \tag{71a}$$

$$\dot{\boldsymbol{\xi}}_i = \boldsymbol{w}_i\,, \tag{71b}$$

where $\dot{\boldsymbol{x}}_{2,0} = [f_1 \;\; f_2 \;\; f_3]^T$, $\boldsymbol{\varphi}_i \in \mathbb{R}^r$ are the smooth and known regressor functions, $\boldsymbol{\theta} \in \mathbb{R}^r$ is a vector with unknown *constant* parameters, $\boldsymbol{\xi}_i \in \mathbb{R}^r$ is the estimator state and $\boldsymbol{w}_i \in \mathbb{R}^r$ is the update law to be determined. The design of the *overparameterized* I&I estimator of order $3r$ starts by defining the estimation errors as

$$\boldsymbol{\sigma}_i = \boldsymbol{\xi}_i + \boldsymbol{\beta}_i\left(\boldsymbol{x}_1, x_{2,1}, \ldots, x_{2,i}, \Delta\boldsymbol{u}\right) - \boldsymbol{\theta}\,, \qquad \text{for } i = 1,2,3\,, \tag{72}$$

where $\boldsymbol{\beta}_i(\cdot)$ are continuous functions yet to be specified. The dynamics of the estimation error are given by

$$\begin{aligned}
\dot{\boldsymbol{\sigma}}_i &= \dot{\boldsymbol{\xi}}_i + \dot{\boldsymbol{\beta}}_i\left(\boldsymbol{x}_1, x_{2,1}, \ldots, x_{2,i}, \Delta\boldsymbol{u}\right) \\
&= \boldsymbol{w}_i + \frac{\partial \boldsymbol{\beta}_i}{\partial \boldsymbol{x}_1}\dot{\boldsymbol{x}}_1 + \sum_{j=1}^{i}\frac{\partial \boldsymbol{\beta}_i}{\partial x_{2,j}}\dot{x}_{2,j} + \sum_{k=1}^{3}\frac{\partial \boldsymbol{\beta}_i}{\partial \Delta u_k}\Delta\dot{u}_k \\
&= \boldsymbol{w}_i + \frac{\partial \boldsymbol{\beta}_i}{\partial \boldsymbol{x}_1}\dot{\boldsymbol{x}}_1 + \sum_{j=1}^{i}\frac{\partial \boldsymbol{\beta}_i}{\partial x_{2,j}}\left[f_j + \boldsymbol{\varphi}_j^T\left(\boldsymbol{\xi}_i + \boldsymbol{\beta}_i - \boldsymbol{\sigma}_i\right)\right] + \sum_{k=1}^{3}\frac{\partial \boldsymbol{\beta}_i}{\partial \Delta u_k}\Delta\dot{u}_k\,.
\end{aligned} \tag{73}$$

The update law $\boldsymbol{w}_i$ is selected as

$$\boldsymbol{w}_i = -\frac{\partial \boldsymbol{\beta}_i}{\partial \boldsymbol{x}_1}\dot{\boldsymbol{x}}_1 - \sum_{j=1}^{i}\frac{\partial \boldsymbol{\beta}_i}{\partial x_{2,j}}\left[f_j + \boldsymbol{\varphi}_j^T\left(\boldsymbol{\xi}_i + \boldsymbol{\beta}_i\right)\right] - \sum_{k=1}^{3}\frac{\partial \boldsymbol{\beta}_i}{\partial \Delta u_k}\Delta\dot{u}_k\,, \tag{74}$$

which yields the following estimation error dynamics

$$\dot{\boldsymbol{\sigma}}_i = -\sum_{j=1}^{i}\frac{\partial \boldsymbol{\beta}_i}{\partial x_{2,j}}\boldsymbol{\varphi}_j^T\boldsymbol{\sigma}_i\,. \tag{75}$$

Note that the update law $\boldsymbol{w}_i$ is selected such that the estimation error dynamics Eq. (75) have an equilibrium at zero. In order to obtain an asymptotically converging estimate of each unknown term $\boldsymbol{\varphi}_i^T\boldsymbol{\theta}$, we can select the $\boldsymbol{\beta}_i$-functions as:[7,55]

$$\boldsymbol{\beta}_i(\boldsymbol{x}_1, x_{2,1}, \ldots, x_{2,i}, \Delta\boldsymbol{u}) = \Gamma_i\int_0^{x_{2,i}}\boldsymbol{\varphi}_i(\boldsymbol{x}_1, x_{2,1}, \ldots, x_{2,i-1}, \chi, \Delta\boldsymbol{u})\,d\chi + \boldsymbol{\epsilon}_i(x_{2,i})\,, \tag{76}$$

where Γ_i is a *positive* diagonal matrix containing the update gain parameters and where $\boldsymbol{\epsilon}_i$ are continuously differentiable functions that satisfy the partial differential matrix inequality:

$$F_i(\boldsymbol{x}_1, x_{2,1}, \ldots, x_{2,i}, \Delta\boldsymbol{u})^T + F_i(\boldsymbol{x}_1, x_{2,1}, \ldots, x_{2,i}, \Delta\boldsymbol{u}) \geq 0\,, \qquad \text{for } i = 2,3\,, \tag{77}$$

where

$$\begin{aligned}
F_i(\boldsymbol{x}_1, x_{2,1}, \ldots, x_{2,i}, \Delta\boldsymbol{u}) = \Gamma_i\sum_{j=1}^{i-1}\frac{\partial}{\partial x_{2,j}}&\left[\int_0^{x_{2,i}}\boldsymbol{\varphi}_i(\boldsymbol{x}_1, x_{2,1}, \ldots, x_{2,i-1}, \chi, \Delta\boldsymbol{u})\,d\chi\right]\boldsymbol{\varphi}_j(\boldsymbol{x}_1, x_{2,1}, \ldots, x_{2,j}, \Delta\boldsymbol{u})^T \\
&+ \frac{\partial \boldsymbol{\epsilon}_i}{\partial x_{2,i}}\boldsymbol{\varphi}_i(\boldsymbol{x}_1, x_{2,1}, \ldots, x_{2,i}, \Delta\boldsymbol{u})^T\,.
\end{aligned} \tag{78}$$

In the special case in which $\boldsymbol{\varphi}_i(\cdot)$ is *not* a function of $x_{2,l}$ for $i \neq l$ and $l = 1,2,3$, the trivial solution $\boldsymbol{\epsilon}_i(x_{2,i}) = \boldsymbol{0}$ satisfies inequality (77). The same simplification occurs when only one of the functions $\boldsymbol{\varphi}_i(\cdot)$ is non-zero. In general, it is not easy to find functions $\boldsymbol{\epsilon}_i$ that satisfy Eq. (78). The problem of finding the $\boldsymbol{\epsilon}_i$-functions can be prevented by using dynamic scaling and output filters.[7,56]

III.E.2. Proof of stability

In order to prove that the I&I estimator consisting of Eqs. (74) and (76) yields an asymptotically converging estimate of each unknown term $\boldsymbol{\varphi}_i^T\boldsymbol{\theta}$, we consider the following Lyapunov function:

$$\mathcal{V}(\boldsymbol{\sigma}) = \sum_{i=1}^{3} \boldsymbol{\sigma}_i^T \boldsymbol{\sigma}_i \,. \tag{79}$$

Taking the time derivative of $\mathcal{V}$ along the trajectories of Eq. (75) yields

$$\dot{\mathcal{V}} = -2\sum_{i=1}^{3} \boldsymbol{\sigma}_i^T \left[\sum_{j=1}^{i} \frac{\partial \boldsymbol{\beta}_i}{\partial x_{2,j}} \boldsymbol{\varphi}_j^T\right] \boldsymbol{\sigma}_i \,. \tag{80}$$

Note that the term between the square brackets can be written as

$$\begin{aligned}
\sum_{j=1}^{i} \frac{\partial \boldsymbol{\beta}_i}{\partial x_{2,j}} \boldsymbol{\varphi}_j^T &= \sum_{j=1}^{i-1} \frac{\partial}{\partial x_{2,j}} \left[\Gamma_i \int_0^{x_{2,i}} \boldsymbol{\varphi}_i(\boldsymbol{x}_1, x_{2,1}, \ldots, x_{2,i-1}, \chi, \Delta\boldsymbol{u}) d\chi\right] \boldsymbol{\varphi}_j(\boldsymbol{x}_1, x_{2,1}, \ldots, x_{2,j}, \Delta\boldsymbol{u})^T \\
&+ \frac{\partial}{\partial x_{2,i}} \left[\Gamma_i \int_0^{x_{2,i}} \boldsymbol{\varphi}_i(\boldsymbol{x}_1, x_{2,1}, \ldots, x_{2,i-1}, \chi, \Delta\boldsymbol{u}) d\chi + \boldsymbol{\epsilon}_i(x_{2,i})\right] \boldsymbol{\varphi}_i(\boldsymbol{x}_1, x_{2,1}, \ldots, x_{2,i}, \Delta\boldsymbol{u})^T \\
&= \sum_{j=1}^{i-1} \frac{\partial}{\partial x_{2,j}} \left[\Gamma_i \int_0^{x_{2,i}} \boldsymbol{\varphi}_i(\boldsymbol{x}_1, x_{2,1}, \ldots, x_{2,i-1}, \chi, \Delta\boldsymbol{u}) d\chi\right] \boldsymbol{\varphi}_j(\boldsymbol{x}_1, x_{2,1}, \ldots, x_{2,j}, \Delta\boldsymbol{u})^T \\
&+ \Gamma_i \boldsymbol{\varphi}_i(\boldsymbol{x}_1, x_{2,1}, \ldots, x_{2,i}, \Delta\boldsymbol{u}) \boldsymbol{\varphi}_i(\boldsymbol{x}_1, x_{2,1}, \ldots, x_{2,i}, \Delta\boldsymbol{u})^T + \frac{\partial \boldsymbol{\epsilon}_i(x_{2,i})}{\partial x_{2,i}} \boldsymbol{\varphi}_i(\boldsymbol{x}_1, x_{2,1}, \ldots, x_{2,i}, \Delta\boldsymbol{u})^T \\
&= \Gamma_i \boldsymbol{\varphi}_i(\boldsymbol{x}_1, x_{2,1}, \ldots, x_{2,i}, \Delta\boldsymbol{u}) \boldsymbol{\varphi}_i(\boldsymbol{x}_1, x_{2,1}, \ldots, x_{2,i}, \Delta\boldsymbol{u})^T + F_i \,.
\end{aligned} \tag{81}$$

Therefore the time derivative of $\mathcal{V}$ along the trajectories of Eq. (75) becomes

$$\begin{aligned}
\dot{\mathcal{V}} &= -2\sum_{i=1}^{3} \boldsymbol{\sigma}_i^T \Big[\Gamma_i \boldsymbol{\varphi}_i(\boldsymbol{x}_1, x_{2,1}, \ldots, x_{2,i}, \Delta\boldsymbol{u}) \boldsymbol{\varphi}_i(\boldsymbol{x}_1, x_{2,1}, \ldots, x_{2,i}, \Delta\boldsymbol{u})^T + F_i\Big] \boldsymbol{\sigma}_i \\
&= -2\sum_{i=1}^{3} \boldsymbol{\sigma}_i^T \Big[\Gamma_i \boldsymbol{\varphi}_i(\boldsymbol{x}_1, x_{2,1}, \ldots, x_{2,i}, \Delta\boldsymbol{u}) \boldsymbol{\varphi}_i(\boldsymbol{x}_1, x_{2,1}, \ldots, x_{2,i}, \Delta\boldsymbol{u})^T + 0.5F_i^T + 0.5F_i\Big] \boldsymbol{\sigma}_i \\
&\leq -2\sum_{i=1}^{3} \boldsymbol{\varphi}_i(\boldsymbol{x}_1, x_{2,1}, \ldots, x_{2,i}, \Delta\boldsymbol{u})^T \Gamma_i \boldsymbol{\sigma}_i \boldsymbol{\varphi}_i(\boldsymbol{x}_1, x_{2,1}, \ldots, x_{2,i}, \Delta\boldsymbol{u})^T \boldsymbol{\sigma}_i \,,
\end{aligned} \tag{82}$$

where $\boldsymbol{\sigma}_i^T F_i \boldsymbol{\sigma}_i = \boldsymbol{\sigma}_i^T \left[0.5F_i^T + 0.5F_i\right] \boldsymbol{\sigma}_i$ and Eq. (77) were used. By the theorem of *LaSalle-Yoshizawa* it now follows that an asymptotically converging estimate of the unknown term $\boldsymbol{\varphi}_i^T\boldsymbol{\theta}$ is obtained. Stability of the closed-loop system with IBS control law Eq. (51) and the I&I based estimator introduced in this section can be proved by using the following Lyapunov function $\mathcal{V}(\bar{\boldsymbol{z}}, \boldsymbol{\sigma}) = \sum_{j=1}^{2} \bar{\boldsymbol{z}}_j^T \bar{\boldsymbol{z}}_j + \sum_{i=1}^{3} \boldsymbol{\sigma}_i^T \boldsymbol{\sigma}_i$, see e.g. Sonneveldt.[7]

III.E.3. Estimating unknown control derivative $C_{M_{\delta_e}}$

In this paper a time-varying uncertainty in the pitching moment coefficient $C_M(\alpha, \delta_e)$ will be introduced in order to evaluate the (adaptive, incremental) BS control laws. Note from Eqs. (22e) and (48) that an uncertainty in coefficient $C_M(\alpha, \delta_e)$ results in an uncertain C_{M_0} and $C_{M_{\delta_e}}$ coefficient. Because incremental control law Eq. (51) is robust to uncertainties in C_{M_0}, we only need to estimate control derivative $C_{M_{\delta_e}}$ (see Eq. (49) for the definition of this coefficient). The three function approximators that will be used for estimation of this uncertain control derivative $C_{M_{\delta_e}}$ are given in Eq. (61). For constant function approximator (1) we have the following regressor function:

$$\varphi_{2,1} = c_7 \bar{q} S b \Delta\delta_e \,. \tag{83}$$

We are dealing with only one uncertain equation, therefore the trivial solution $\epsilon_2(x_{2,2}) = 0$ satisfies inequality (77). Substituting regressor $\varphi_{2,1}$ into Eq. (76) yields

$$\begin{aligned}\beta_{2,1}(\boldsymbol{x}_1, x_{2,1}, x_{2,2}, \Delta\boldsymbol{u}) &= \Gamma_{2,1}\int_0^{x_{2,2}} \varphi_{2,1}\left(\boldsymbol{x}_1, x_{2,1}, \chi, \Delta\boldsymbol{u}\right) d\chi \\ &= \Gamma_{2,1}\varphi_{2,1}x_{2,2}\,,\end{aligned} \tag{84}$$

where $\Gamma_{2,1}$ is now a *scalar* adaptation gain. Following from Eq. (74), the update law becomes

$$\begin{aligned}\dot{\xi}_{2,1} &= -\sum_{j=1}^{2}\frac{\partial\beta_{2,1}}{\partial x_{2,j}}\dot{x}_{2,j} - \sum_{k=1}^{3}\frac{\partial\beta_{2,1}}{\partial\Delta u_k}\Delta\dot{u}_k - \frac{\partial\beta_{2,1}}{\partial\bar{q}}\dot{\bar{q}} \\ &= -\Gamma_{2,1}\varphi_{2,1}\left[f_2 + \varphi_{2,1}(\xi_{2,1} + \beta_{2,1})\right] - \Gamma_{2,1}c_7 Sbx_{2,2}\left(\bar{q}\Delta\dot{\delta}_e + \dot{\bar{q}}\Delta\delta_e\right).\end{aligned} \tag{85}$$

Note that one additional term involving $\dot{\bar{q}}$ arises because the dynamic pressure $\bar{q}(t)$, which is an auxiliary state of the F-16 aircraft model, appears in regressor Eq. (83). In the I&I approach the estimation error is defined as

$$\sigma_{2,1} = \hat{C}_{M_{\delta_e}} - C_{M_{\delta_e}} = \xi_{2,1} + \beta_{2,1} - C_{M_{\delta_e}}\,. \tag{86}$$

Therefore the estimate of the control efficiency $C_{M_{\delta_e}}$ is now given by

$$\hat{C}_{M_{\delta_e}} = \mathcal{P}\left[\xi_{2,1} + \Gamma_{2,1}\varphi_{2,1}x_{2,2}\right], \tag{87}$$

where $\mathcal{P}$ represents the parameter projection operator to prevent singularities of IBS control law Eq. (51). The dynamics of the estimation error $\sigma_{2,1}$ can now be derived:

$$\begin{aligned}\dot{\sigma}_{2,1} &= \dot{\xi}_{2,1} + \frac{\partial\beta_{2,1}}{\partial x_{2,2}}\dot{x}_{2,2} + \frac{\partial\beta_{2,1}}{\partial\Delta\delta_e}\Delta\dot{\delta}_e + \frac{\partial\beta_{2,1}}{\partial\bar{q}}\dot{\bar{q}} \\ &= \dot{\xi}_{2,1} + \Gamma_{2,1}\varphi_{2,1}\left[f_2 + \varphi_{2,1}(\xi_{2,1} + \beta_{2,1} - \sigma_{2,1})\right] + \Gamma_{2,1}c_7\bar{q}Sbx_{2,2}\Delta\dot{\delta}_e + \Gamma_{2,1}c_7 Sb\Delta\delta_e x_{2,2}\dot{\bar{q}} \\ &= -\Gamma_{2,1}\varphi_{2,1}^2\sigma_{2,1}\,.\end{aligned} \tag{88}$$

Note that the same result for the estimation error dynamics can be obtained by using Eq. (75). As can be seen from Eq. (88), the dynamics of the parameter estimation error $\sigma_{2,1}$ are described by a first-order linear ordinary, homogeneous differential equation with a time-varying coefficient. The well-known solution to this differential equation is

$$\sigma_{2,1}(t) = \sigma_{2,1}(0)e^{-\Gamma_{2,1}\int_0^t \varphi_{2,1}(\xi)^2\, d\xi}\,, \tag{89}$$

which indicates that the parameter estimation error is a monotonically non-increasing function. In the same way the update laws for the second and third function approximator of Eq. (61) have been derived, see Appendix D. Overparameterization for all derived I&I estimators is eliminated since we are dealing with only one uncertain equation. Note that the parameter estimation errors that correspond to the non-constant function approximators are no longer monotonically non-increasing functions. Also note that the derived I&I update laws in this paper are significantly different from those in Ali *et al.*[26] and Sun,[57] where the update laws $\dot{\xi}_\star$ (in the referred literature denoted as $\dot{\hat{C}}_{\star_{\delta_\star}}$) are *incorrectly* obtained by setting them equal to the time derivative of $\beta_{\star_{\delta_\star}}$.

IV. Simulation Results

All simulations have been run with a fixed sampling frequency of 100 Hz and the `ode5 (Dormand-Prince)` solver of `Matlab/Simulink`. The F-16 model has been trimmed in a steady level flight at an altitude of 5000 m and a total velocity of 170 m/s. The resulting trim values can be found in Table 4. The parameters of the command filters are obtained from Sonneveldt, Chu and Mulder,[11] see Table 5. The time constants for the first-order lag prefilters (see Eq. (11)) have been set as $\sigma_\alpha = \sigma_{p_s} = 0.3$ s.

In none of the simulations the sign of the parameter estimate $\hat{C}_{M_{\delta_e}}$ changes, therefore there was no need to implement parameter projection operators $\mathcal{P}$ to prevent singularities of incremental control law Eq. (51) in the domain of operation.

In Section IV.A simulation results of the conventional BS controller are analyzed. Subsequently in Section IV.B, the robustness properties of the IBS controller are compared with those of the BS controller. Finally in Section IV.C, the *adaptive* control laws are simulated to see whether they are able to increase the closed-loop performance of the *uncertain* F-16 model compared to the (incremental) BS control laws.

Table 4. Trim values (steady level flight)

F_T	δ_e	δ_a	δ_r	α	V_T	h
1903 lbs	−0.7 deg	0 deg	0 deg	3.3 deg	170 m/s	5000 m

Table 5. Command filter parameters

Command variable	ω_n (rad/s)	ζ	Mag. limit	Rate limit
F_T	2	1	[1000, 19 000] lbs	± 10 000 lbs/s
q_s	10	1	± 20 deg/s	–
r_s	10	1	± 25 deg/s	–
δ_e	40.4	1	± 25 deg	± 60 deg/s
δ_a	40.4	1	± 21.5 deg	± 80 deg/s
δ_r	40.4	1	± 30 deg	± 120 deg/s

IV.A. Backstepping

For the BS control approach we need to select three control gains for the inner loop and three gains for the outer loop. As we have seen in Section III.A, the Lyapunov stability theory only requires the control gains to be larger than zero. One option to find these gains is to make use of reference and linearized models for which the characteristics of the roll mode, the short period mode and the Dutch roll mode are specified.[34] However, because the goal of this paper is to evaluate three approaches to adaptive incremental BS control, handling characteristics of the closed-loop system are of less importance. Therefore the gains of the BS have been found through experimental tuning, see Table 6.

Table 6. Backstepping control gains

c_{11}	c_{12}	c_{13}	c_{21}	c_{22}	c_{23}
0.5	3	4	1.5	12	8

From the simulations of the BS controller (see Figures 2 to 5) can be concluded that the polynomial approximations of aerodynamic coefficients C_M and C_X result in accurate tracking performance for the angle of attack α and roll rate p_s when no additional uncertainties are introduced. Furthermore, the sideslip angle β is successfully minimized. As can be seen, the total velocity V_T does not accurately follow the reference value. This is because the orientation of the aircraft is not controlled during the maneuver, and therefore it becomes physically impossible to keep V_T constant, see also Figures 3 and 4. Nevertheless, the thrust control loop is able to keep the F-16 model within the flight envelope for which the aerodynamic data is valid.

To evaluate the robustness of this controller, uncertainties in all the aerodynamic damping coefficients are introduced. In reality such uncertainties might be caused due to structural damage. Two types of uncertainties are considered:[58]

- Magnitude scaling. In this case the actual coefficients are obtained by scaling the *magnitude* of the nominal coefficient from the look-up table:

$$C_{\star_{act}}(\boldsymbol{x}) = [1 + F_{mag}]C_{\star_{nom}}(\boldsymbol{x})\,. \tag{90}$$

- Variable scaling. In this case the actual coefficients are obtained by scaling the *independent variable* of the nominal coefficient from the look-up table:

$$C_{\star_{act}}(\boldsymbol{x}) = C_{\star_{nom}}\left([1 + F_{var}]\boldsymbol{x}\right), \tag{91}$$

where F is the uncertainty factor and $\boldsymbol{x}$ denotes the state variables such as α and β.

From Figure 2 can be seen that the controller is not able to track the reference signals accurately when the damping coefficients used by the controller deviate from the actual damping coefficients. This is as expected because BS controller Eq. (32) highly relies on correct on-board parameters.

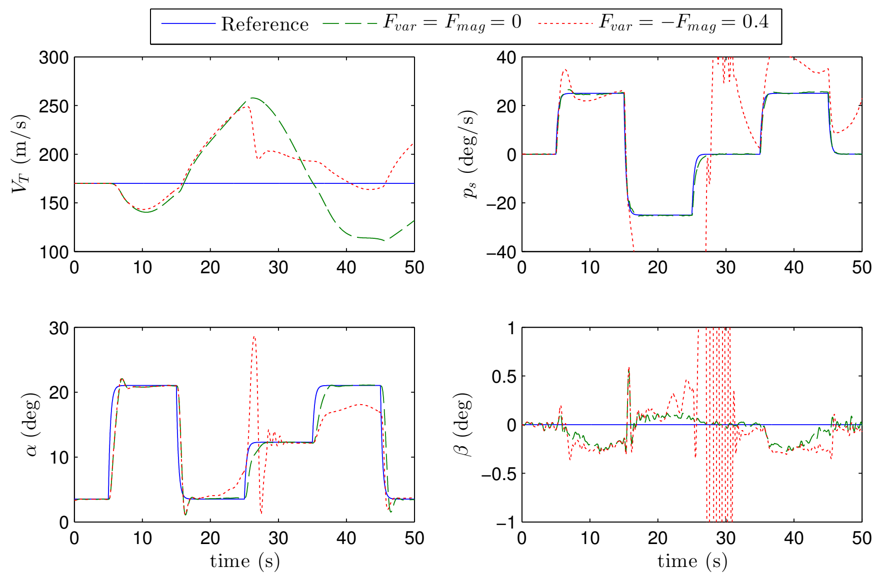

Figure 2. Tracking performance of the Backstepping controller with and without uncertainties in the aerodynamic damping coefficients.

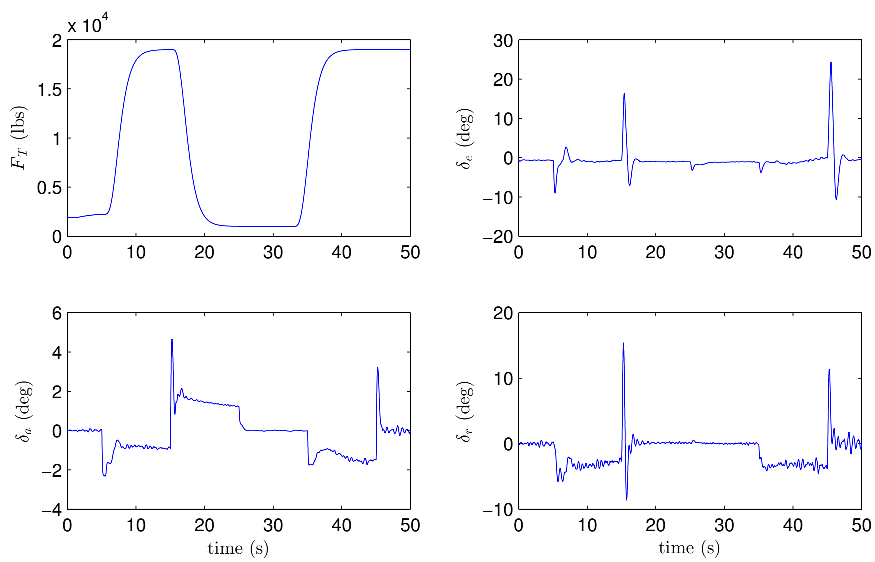

Figure 3. Control variables of the F-16 model for the simulation with $F_{var} = F_{mag} = 0$.

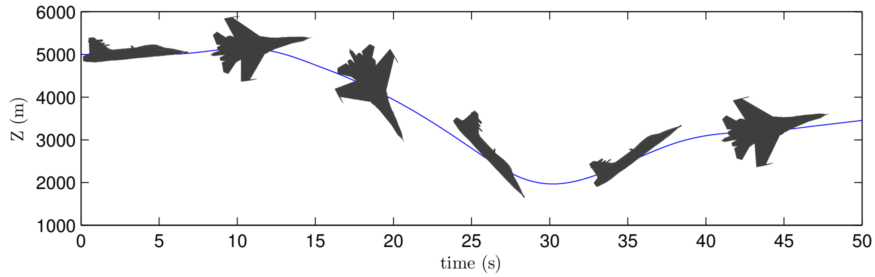

Figure 4. Altitude and orientation of the F-16 model for the simulation with $F_{var} = F_{mag} = 0$.

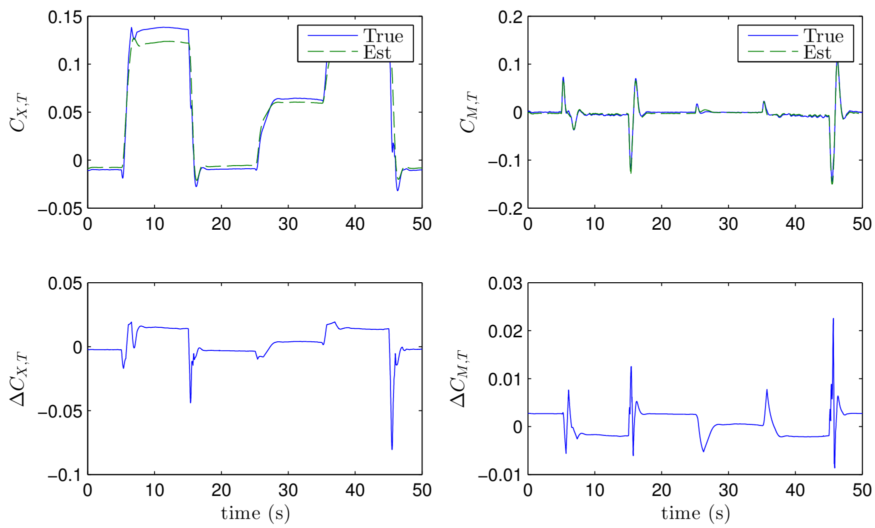

Figure 5. True and estimated values of aerodynamic coefficients $C_{X,T}$ and $C_{M,T}$ for the simulation with $F_{var} = F_{mag} = 0$.

IV.B. Incremental Backstepping

Similar as for the conventional BS controller, the IBS control gains have been found through experimental tuning, see Table 7. The angular acceleration estimation algorithms with the most promising tuning parameters (see Appendix C) have been evaluated in a closed-loop simulation in absence of uncertainties, see Figure 6. That is, the estimated angular accelerations are used in an on-line fashion by the incremental controller. The numerical differentiator uses the two-point backward-difference formula. The bandwidth of the washout filter and the tuning parameter of the sliding mode differentiator have been respectively selected as 200 rad/s and $L = 5$. No loop synchronization has been introduced,[16,59] because the noise power is relatively low; therefore a high bandwidth of the washout filters can be used resulting in a very small effective time delay. From these simulation results can be concluded that all three approaches lead to almost identical closed-loop performance. For this reason, the most simplest approach, i.e. the two-point numerical differentiator, has been selected for all further simulations to provide the angular accelerations.

Table 7. Incremental Backstepping control gains

c_{11}	c_{12}	c_{13}	c_{21}	c_{22}	c_{23}
0.5	1.5	2	1.5	2	5

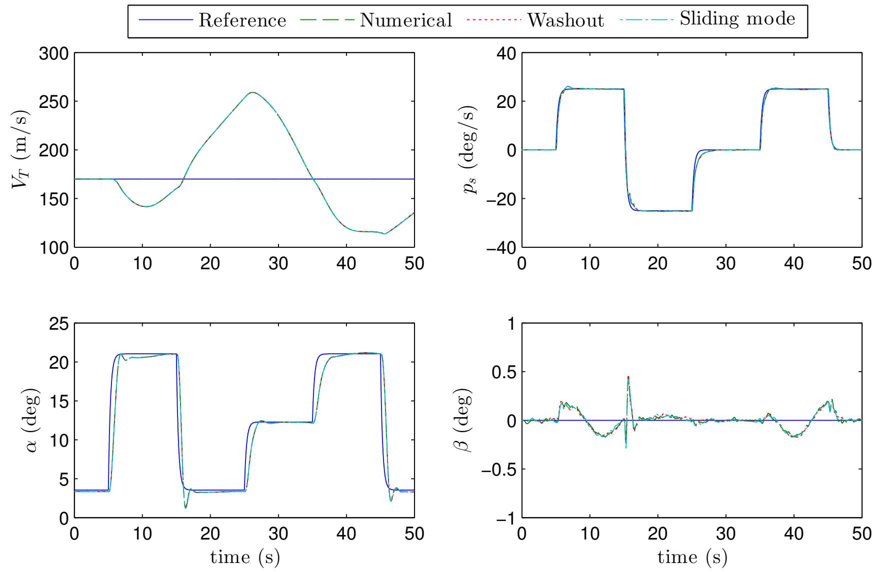

Figure 6. Tracking performance of the Incremental Backstepping controller in absence of uncertainties by using three different approaches to estimate the angular accelerations.

From the simulation of the IBS controller (see Figure 7) it can be concluded that, in contrary to the conventional BS controller, the incremental control law is robust to uncertainties in the aerodynamic damping coefficients. This is as expected because the incremental controller does not depend on the system dynamics $\boldsymbol{f}_2$.

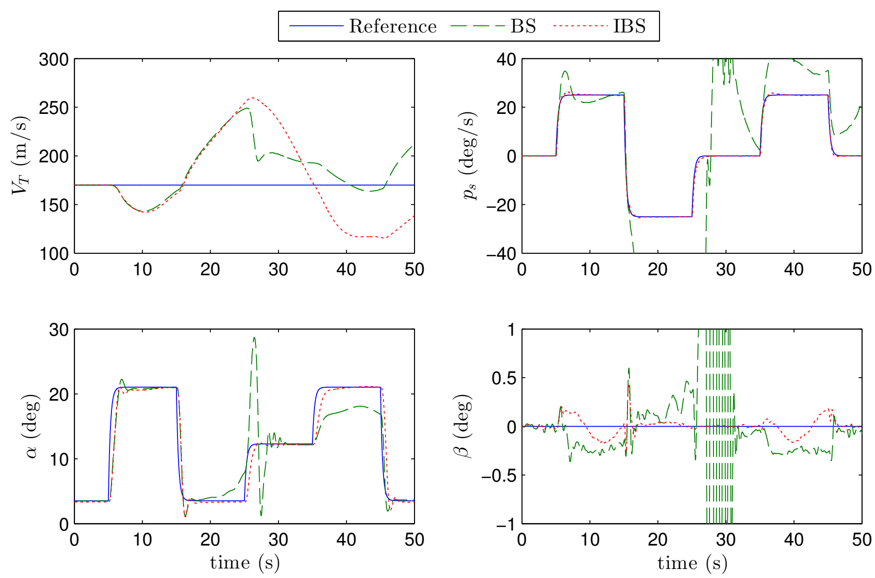

Figure 7. Tracking performance of the Backstepping (BS) and Incremental Backstepping (IBS) controller with uncertainties in the aerodynamic damping coefficients ($F_{var} = -F_{mag} = 0.4$).

Uncertainties in the control efficiency matrix $B_{2,0}$ are now introduced to further asses the robustness of the (Incremental) BS controller. This is achieved by magnitude scaling of the aerodynamic coefficient $C_M(\alpha, \delta_e)$. Note from Eqs. (22e) and (48) that an uncertainty in coefficient $C_M(\alpha, \delta_e)$ results in an uncertain C_{M_0} and $C_{M_{\delta_e}}$ coefficient, this results in respectively $\hat{\boldsymbol{f}}_2 \neq \boldsymbol{f}_2$ and $\hat{B}_{2,0} \neq B_{2,0}$. In reality such an uncertainty might be caused due to structural damage of the all-moving tail of the F-16. The simulation results of the (incremental) BS control laws with an uncertain pitching coefficient can be seen in Figure 8. The

Root-Mean-Square Deviation (RMSD) of the angle of attack has been defined as follows:

$$RMSD = \sqrt{\frac{1}{n}\sum_{i=1}^{n}\left(\alpha_{ref}[i] - \alpha[i]\right)^2}\,, \tag{92}$$

where n is the total number of samples. From Figure 8 can be seen that the incremental controller tracks the angle of attack reference signal more accurately compared to the conventional BS controller now coefficient $C_M(\alpha, \delta_e)$ is uncertain. However, when we keep increasing the uncertainty in the pitching moment coefficient, then also the incremental controller is no longer able to provide accurate tracking performance. This is as expected because the incremental controller still relies on accurate knowledge of matrix $B_{2,0}$.

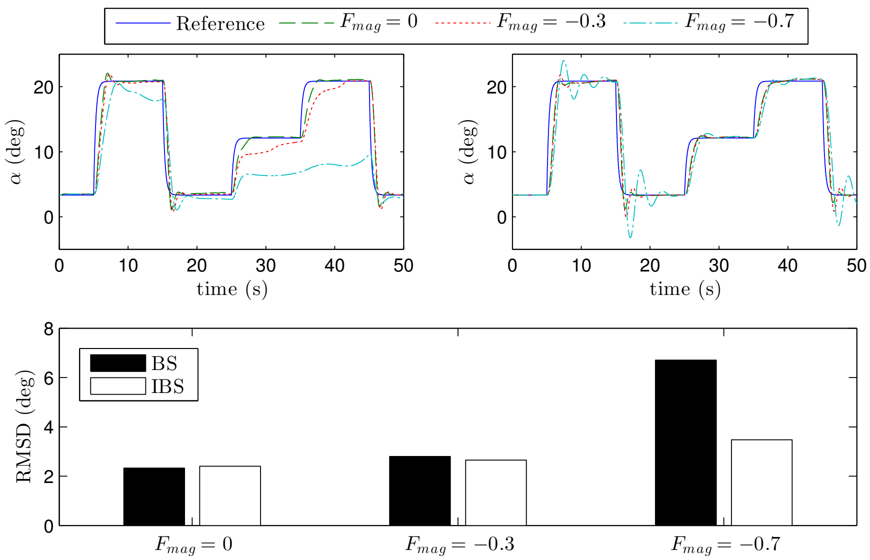

Figure 8. Tracking performance of Backstepping (upper left) and Incremental Backstepping (upper right) in case of uncertainties in the pitching moment coefficient $C_M(\alpha, \delta_e)$.

IV.C. Adaptive Incremental Backstepping

Now a time-varying magnitude uncertainty in the pitching moment coefficient $C_M(\alpha, \delta_e)$ is introduced in order to evaluate the (adaptive, incremental) BS control laws, see Figure 9. Note from Eqs. (22e) and (48) that an uncertainty in coefficient $C_M(\alpha, \delta_e)$ results in an uncertain C_{M_0} and $C_{M_{\delta_e}}$ coefficient. By using an incremental control law, the parameter estimator now only has to estimate the control derivative $C_{M_{\delta_e}}$, see also the discussion in Section III.B. The initial parameter estimates of function approximators Eq. (61) have been set as

$$a_0(0) = b_0(0) = c_0(0) = \hat{C}_{M_{\delta_e,nom}}(0) \tag{93a}$$

$$b_1(0) = b_2(0) = c_1(0) = c_2(0) = c_3(0) = c_4(0) = c_5(0) = 0\,, \tag{93b}$$

where $\hat{C}_{M_{\delta_e,nom}}(0)$ is given by the polynomial approximation of aerodynamic data table $C_M(\alpha, \delta_e)$, see also Section III.A.4. The gains of the incremental controller have been set similar as in Table 7. The adaptation gain matrices have been found through experimental tuning, see Table 8. The forgetting factor of the LS estimator has been set as $\lambda = 0.9999$.

The simulation results of the (adaptive, incremental) BS control laws with constant function approximator Eq. (61a) can be seen in Figure 10. Note that the reference value of $\hat{C}_{M_{\delta_e}}$ in Figure 10(c) is *not* the actual $C_{M_{\delta_e}}$, but follows from scaling the magnitude of the (accurate) polynomial approximation of aerodynamic

Table 8. **Adaptation gains. The coefficients in the top row correspond to function approximators Eq. (61).**

	a_0	b_0	b_1	b_2	c_0	c_1	c_2	c_3	c_4	c_5
Tuning Functions Γ	3	3	7	7	3	7	7	7	7	7
Least-Squares P_0	0.1	0.1	0.2	0.2	0.1	0.2	0.2	1	1	1
Immersion & Invariance Γ	1.8	1.8	5	5	1.8	5	5	5	5	5

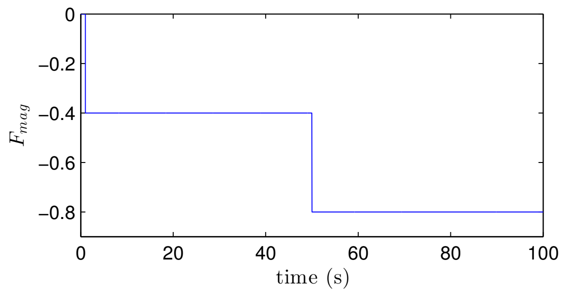

Figure 9. Magnitude scaling of the pitching moment coefficient $C_M(\alpha, \delta_e)$ to introduce a time-varying uncertainty.

data table $C_M(\alpha, \delta_e)$:

$$\hat{C}_{M_{\delta_e,ref}} = [1 + F_{mag}]\frac{\partial \hat{C}_M}{\partial \delta_e} = [1 + F_{mag}]\frac{\partial}{\partial \delta_e}\sum_{i=0}^{5}\sum_{j=0}^{3} p_{ij}\alpha^i\delta_e^j\,, \quad i + j \leq 5\,. \tag{94}$$

The RMSD of the angle of attack in Figure 10(d) has been calculated by using simulation data of the last 45 seconds, which is the region in which the introduced uncertainty is largest after the maneuver starts. The IBS controller reduces the RMSD with more than 50% compared to conventional BS. An additional reduce of the RMSD with about 20% is achieved by augmenting the incremental control law with parameter estimators based on TF, LS or I&I. Although these parameter estimators yield different estimates, the closed-loop performance of the adaptive IBS approaches is almost identical. This can be explained by the fact that the IBS controller is already robust to some degree to uncertainties in the control efficiency parameter as we have seen in Section IV.B; therefore it is not necessary to obtain very accurate estimates for satisfactory tracking performance. From Figure 10(c) can be seen that all parameter estimates converge to the (accurate) polynomial approximation $\hat{C}_{M_{\delta_e,ref}}$.

Because the LSAIBS simulation only runs for 100 seconds and there are no long periods in which the system is working in the steady state, there was no need to take measures to avoid estimator saturation or covariance windup, see also the discussion in Section III.D.

The time derivative $\Delta\dot{\delta}_e$ required for the I&I update laws (see Eqs. (85), (108) and (113)) has been obtained by using (delayed) outputs of the command filter, while the time derivatives $(\dot{\delta}_e, \dot{\alpha}, \dot{\bar{q}})$ are approximated by using two-point backward-difference schemes, see Eq. (101). These numerical derivatives result in more noise in the parameter estimate of the I&I controller compared to these of the TF and LS estimator. However, these high frequency oscillations do not appear in the input and output of the F-16 model because the noise is filtered by the low-pass command filters and actuator dynamics.

In Figure 11 the parameter estimate of the I&I estimator with constant function approximator Eq. (61a) is shown together with the *theoretical* estimate that follows from the estimator error dynamics Eq. (89). Naturally, the theoretical estimate does not exactly equal the parameter estimate that follows from the simulation. This is due to the fact that the estimator error dynamics Eq. (89) have been derived by neglecting sensor dynamics, actuator dynamics and the higher order terms in Eq. (46). Furthermore, these error dynamics were derived on the assumption that the unknown parameter $C_{M_{\delta_e}}$ is constant, which it is not. However, the derived estimator error dynamics render a good impression of the speed of converge of the I&I estimator as a function of the adaptation gain. Therefore, the estimator error dynamics Eq. (89) may be used for initial tuning of the I&I estimator; thereby simplifying the tuning process of the I&I estimator compared to that of the TF and LS estimators.

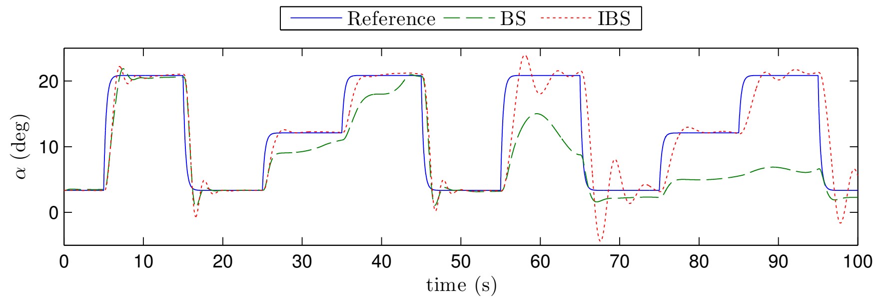

(a) (Incremental) Backstepping

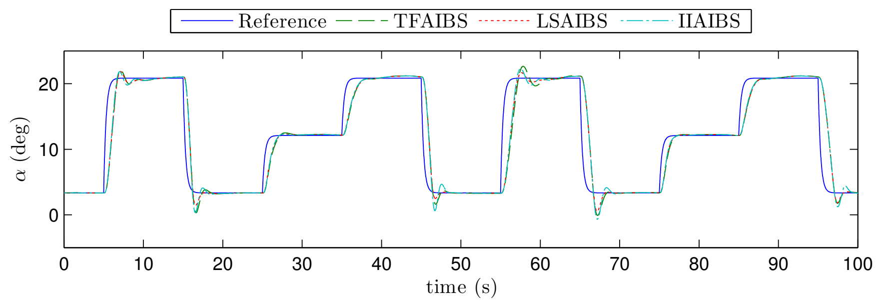

(b) Adaptive Incremental Backstepping

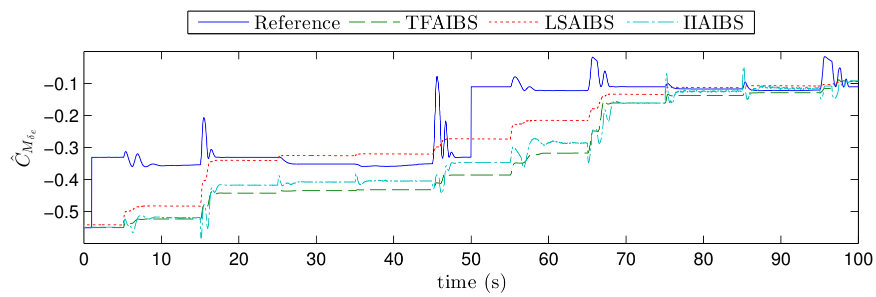

(c) Parameter estimates

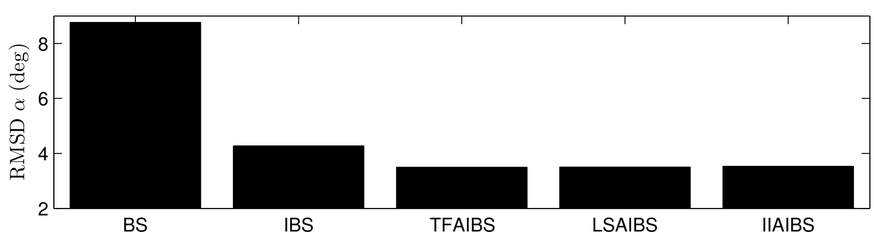

(d) RMSD values of the angle of attack

Figure 10. Tracking performance of the (Incremental) Backstepping controller and the Adaptive Incremental Backstepping controllers with a constant function approximator in case of uncertainties in the pitching moment $C_M(\alpha, \delta_e)$.

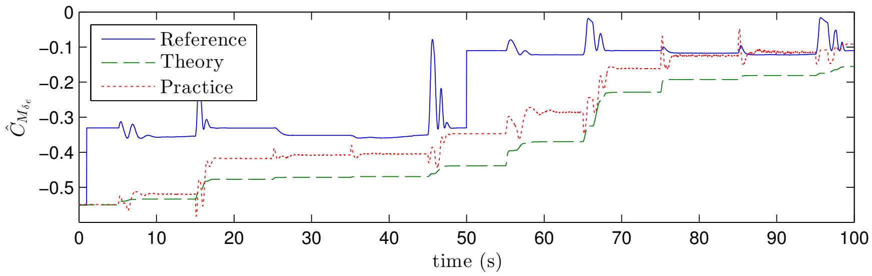

Figure 11. Parameter estimates of the Immersion & Invariance estimator. The *theoretical* estimate follows from estimator error dynamics Eq. (89) while the *practical* estimate follows from a simulation with function approximator Eq. (61a).

IV.C.1. Influence of the adaptation gain

The influence of the adaptation gain of the TF estimator on the closed-loop performance and the parameter estimation is shown in Figure 16 of Appendix E. Changing the adaptation gain of the TF estimator has a similar effect as changing the adaptation gain of the I&I estimator and the initial covariance matrix of the LS estimator, therefore the plots of the LSAIBS and Immersion and Invariance Adaptive Incremental Backstepping (IIAIBS) controllers are omitted. As expected, increasing the adaptation gain results in faster convergence of the parameter estimate. However, by increasing the adaptation gain, the sensitivity to noise and model error increases which may result in unstable closed-loop performance.

From Figure 16 we can see that the parameter estimates for the different gains seem to converge to constant values, but not necessarily converge to $\hat{C}_{M_{\delta_e,ref}}$. However, because the IBS controller is already robust to some degree to uncertainties in the control efficiency parameter, the tracking performance for the three different adaptation gains is nearly identical. The reason why the parameter estimates do not always converge to $\hat{C}_{M_{\delta_e,ref}}$ may be due to model mismatch which results from neglecting the sensor dynamics, actuator dynamics and the higher order terms in Eq. (46). Furthermore, by using the constant function approximator we have assumed that unknown parameter $C_{M_{\delta_e}}$ is constant, which it is not. Finally, $\hat{C}_{M_{\delta_e,ref}}$ is only an *approximation* of uncertain parameter $C_{M_{\delta_e}}$, and therefore additional errors are introduced.

IV.C.2. Influence of the forgetting factor

The forgetting factor of the LS estimator is set as $\lambda < 1$ to allow parameter estimation of time-varying coefficient $C_{M_{\delta_e}}$. In Figure 17 of Appendix E the effect of this forgetting factor can be seen on the closed-loop performance and the parameter estimates. As can be seen, a lower forgetting factor leads to a faster parameter estimation. However, by decreasing the forgetting factor the sensitivity to noise and model error increases which may result in unstable closed-loop performance. From Figure 17 we can see that not all parameter estimates converge to $\hat{C}_{M_{\delta_e,ref}}$. Note that the RLS estimator only results in *unbiased* estimates when we are dealing with zero mean white noise in the observation vector $\boldsymbol{y}$ and when the data matrix A is exactly known.[60] However, in this paper matrix A is not free or error because of sensor noise and neglecting the sensor dynamics, actuator dynamics and the higher order terms in Eq. (46). In order to keep the LS estimate unbiased and efficient in case of errors in both the data matrix A and the observation vector $\boldsymbol{y}$, the Total Least-Squares method may be considered.[61,62]

IV.C.3. Influence of the function approximator

In Figure 18 of Appendix E the three function approximators of Eq. (61) have been simulated for the IIAIBS control law. The results of the different function approximators for the TF and LS estimator are nearly identical, therefore the plots of the TFAIBS and LSAIBS controllers are omitted. Note that the tracking performance of the IIAIBS controller is not noticeably influenced by selecting a function approximator with a higher approximation power. This is caused by the fact that only coefficients (a_0, b_0, c_0) of the function approximators are estimated accurately, while the remaining coefficients appear to be unidentifiable. However, because the terms related to the angle of attack and elevator deflection are much smaller compared to these constant terms, the closed-loop performance is not influenced by these inaccurate estimates.

More accurate estimates of the α and δ_e dependent terms of the function approximators may be obtained by increasing the "richness" of the reference trajectory by, for example, superimposing a sinusoidal signal on the reference signal. The amplitude of this excitation signal may be modulated dependent upon the tracking error to guarantee parameter convergence.[63,64] Although this extra excitation might improve the parameter estimates, the closed-loop performance will hardly benefit from this because the IBS controller is already robust to a large degree to uncertainties in the control efficiency parameter as we have seen in Section IV.B.

V. Conclusions and Recommendations

V.A. Conclusions

In this paper nonlinear Backstepping (BS) control laws have been derived for a high-performance aircraft (F-16). Initial results have confirmed that the conventional BS control law does not provide accurate tracking performance when parametric uncertainties are introduced. By comparing the simulation results of the BS and the Incremental Backstepping (IBS) control law, we have seen that the IBS controller is more robust to uncertainties in the *system dynamics*. This finding is in line with the existing literature.[8,15,16] Furthermore, it has been shown that the IBS control law is more robust to uncertainties in the *control efficiency matrix*. To the best knowledge of the authors of this paper, this has not earlier been concluded in the literature on basis of simulation results. However, when we keep increasing the uncertainty of the control efficiency matrix, then also the incremental controller will no longer be able to provide accurate tracking performance.

The incremental control law derived in this paper requires the angular accelerations. Sensors to measure these accelerations exist, however, they are not common. Therefore, three algorithms with varying complexity have been evaluated to estimate the angular accelerations on basis of noisy angular rate measurements. From the simulation results can be concluded that all three approaches lead to almost identical closed-loop performance for the noise standard deviation and sampling frequency considered in this research.

The main contribution of this paper is the design of three *Adaptive* IBS control laws for the highly nonlinear F-16 model. By using an incremental control law, the estimator now only has to estimate the control efficiency matrix. This simplifies the controller design significantly compared to the Adaptive *non-Incremental* BS controllers of Sonneveldt.[7] The IBS controller is already robust to some degree to uncertainties in the control efficiency matrix; therefore the parameter estimations do not have to be very accurate in order to obtain satisfactory tracking performance. The closed-loop performance of the three designed Adaptive IBS approaches is almost identical; a reduce of the Root-Mean-Square Deviation (RMSD) with about 20% is achieved by augmenting the incremental control law with parameter estimators based on Tuning Function (TF), Least-Squares (LS) or Immersion and Invariance (I&I) in case of an uncertain pitching moment coefficient. This increase of performance is more significant compared to the findings of Ali *et al*.[26]

The advantage of the modular LS estimator is the very low design complexity. However, guaranteed closed-loop stability in case of uncertainties can not be proven. The design complexity of the I&I estimator is highest, however, the advantage is that an analytical expression of the estimator error can easily be derived. The dynamics of the estimator error may be used for initial tuning of the I&I estimator; thereby simplifying the tuning process of the I&I estimator compared to that of the TF and LS estimators.

Three function approximators with different complexity have been used for estimation of an uncertain control derivative. From the simulations can be concluded that the tracking performance of the Incremental Adaptive Backstepping (ABS) controllers is not noticeably influenced by selecting a function approximator with a higher approximation power. These simulation results are not in agreement with the hypothesis of Ali *et al*,[26] in which the authors suggest that better performance of the Immersion and Invariance Adaptive Incremental Backstepping (IIAIBS) controller may be obtained by using a more detailed regressor model in the identifier.

In conclusion, the results of this study show the great potential of Adaptive Incremental Backstepping in increasing the survivability of damaged aircraft.

V.B. Recommendations

This paper contains the development and evaluation of three Adaptive IBS control laws for a high-performance aircraft (F-16) with a large flight envelope. Because we have seen that these adaptive control laws have great potential, the research described in this paper can be extended into various directions. In the following, considerations are discussed that require further attention.

- Structural failure models are not available for the F-16 model that is used in this research. Therefore simulation scenarios of the F-16 model are limited to actuator hard-overs or lock-ups, center of gravity shift and uncertainties in the aerodynamic coefficients. However, it would be interesting to see how the developed Adaptive IBS control laws perform in more complex and asymmetric structural failure scenarios. Furthermore, the F-16 model may be extended with Failure Detection, Isolation and Estimation for health monitoring to simplify the task of on-line model identification.
- No formal proof for the Least-Squares Adaptive Incremental Backstepping (LSAIBS) controller is included in this paper that guarantees closed-loop stability in case of uncertainties, this is likely to impede certification of this control strategy. If the real-time identification routine is not able to provide accurate estimates of the control derivatives, then the possibility exists that this control approach leads to an unsatisfactory result. Therefore, robust BS could be considered for application in this context.[51–53] Another option is to include nonlinear damping terms in the control law to robustify the design against parameter estimation errors.[49]
- Because the goal of this paper was to evaluate three approaches to Adaptive IBS control, handling characteristics of the closed-loop system have not been considered. Nonetheless, it would be interesting to evaluate the designed Adaptive IBS control laws by performing pilot-in-the-loop simulations to assess the handling qualities of damaged aircraft.
- In the simulations in this paper the sign of the parameter estimate did not change, therefore there was no need to implement parameter projection operators to prevent singularities of the incremental control law in the domain of operation. Furthermore, because the simulation only ran for 100 seconds and there were no long periods in which the system was working in the steady state, there was no need to take measures to avoid estimator saturation or covariance windup of the LS estimator. It would be interesting to incorporate parameter project operators and time-varying forgetting factors to allow for an evaluation of the controllers in a larger domain of operation.
- The control objective of this paper was to make the airplane robustly seek references in roll rate and angle of attack at a constant airspeed while minimizing sideslip. Because the body orientation of the F-16 model is not controlled, the total velocity V_T does not accurately follow the reference value due to physical constraints. To keep the F-16 model within the speed range for which the aerodynamic data is valid, the freedom to select the α-reference signal was rather limited. More variety in the reference signals can be introduced for testing the parameter estimators when an outer loop is added to control the flight path angle of the F-16 model.
- As we have seen in the derivations in this paper, the incremental control law is robust to uncertainties in the *system dynamics* when the sampling rate is sufficiently high. Furthermore, the IBS control law appears to be robust to some degree to uncertainties in the control efficiency matrix. It would be interesting to see the influence of the sampling rate on the closed-loop performance and robustness properties of the incremental controller; preferably with a supporting theoretical analysis to obtain an expression between the sampling rate and the accompanying level of robustness.
- In this paper four control variables have been selected: the engine trust force, elevator, aileron and rudder. The number of control variables is equal to the amount of states appearing in the control objective. However, if we have complete failure of an actuator, then the BS and IBS control laws are no longer well-defined. In this case a control allocation module is required to distribute the required moments and forces over the available control effectors in some "optimal" way. Adaptive IBS augmented with control allocation algorithms to cope with complete actuator failures would make an interesting research topic.
- Very few actual flight tests have been performed with incremental control laws.[59, 65] The limited flight results with Unmanned Aerial Vehicles (UAVs) have shown that this incremental control approach is very sensitive to small time delays, which may lead to oscillations on the control surfaces. Therefore additional off-line research should be performed on phase differences between the measured and estimated signals before *adaptive* incremental control laws can be tested on actual flight tests. Next, incremental control laws rely on more measurements compared to conventional controllers, therefore additional research on sensor redundancy and failure detection methods now becomes even more important.

Appendices

Appendix A. Aerodynamic Coefficients F-16 Model

In this appendix the total coefficient equations are listed that are used to sum the various aerodynamic contributions to a given force or moment coefficient of the F-16 model.[30,31]

A.1 Force coefficients

X-axis force coefficient:

$$\begin{aligned} C_{X,T} &= f(\alpha, \delta_e) \\ &= C_X(\alpha, \delta_e) + \frac{q\bar{c}}{2V_T} C_{X_q}(\alpha) \end{aligned} \tag{95}$$

Y-axis force coefficient:

$$\begin{aligned} C_{Y,T} &= f(\alpha, \beta) + g\delta_a + h\delta_r \\ &= -0.02\beta + 0.021\delta_a + 0.086\delta_r + \frac{rb}{2V_T}\delta C_{Y_r}(\alpha) + \frac{pb}{2V_T} C_{Y_p}(\alpha) \end{aligned} \tag{96}$$

Z-axis force coefficient:

$$\begin{aligned} C_{Z,T} &= f(\alpha) + g(\alpha, \beta)\delta_e \\ &= \delta C_{Z_{\delta_e}}(\alpha, \beta)\left(\frac{\delta_e}{25}\right) + \frac{q\bar{c}}{2V_T} C_{Z_q}(\alpha) \end{aligned} \tag{97}$$

A.2 Moment coefficients

Rolling-moment coefficient:

$$\begin{aligned} C_{L,T} &= f(\alpha, \beta) + g(\alpha, \beta)\delta_a + h(\alpha, \beta)\delta_r \\ &= C_L(\alpha, \beta) + \delta C_{L_{\delta_a}}(\alpha, \beta)\left(\frac{\delta_a}{21.5}\right) + \delta C_{L_{\delta_r}}(\alpha, \beta)\left(\frac{\delta_r}{30}\right) + \frac{rb}{2V_T} C_{L_r}(\alpha) + \frac{pb}{2V_T} C_{L_p}(\alpha) \end{aligned} \tag{98}$$

Pitching-moment coefficient:

$$\begin{aligned} C_{M,T} &= f(\alpha, \beta, \delta_e) \\ &= C_M(\alpha, \delta_e) + C_{Z,T}[x_{cg_r} - x_{cg}] + \frac{q\bar{c}}{2V_T} C_{M_q}(\alpha) \end{aligned} \tag{99}$$

Yawing-moment coefficient:

$$\begin{aligned} C_{N,T} &= f(\alpha, \beta) + g(\alpha, \beta)\delta_a + h(\alpha, \beta)\delta_r \\ &= C_N(\alpha, \beta) - C_{Y_T}\left[x_{cg_r} - x_{cg}\right]\frac{\bar{c}}{b} + \delta C_{N_{\delta_a}}(\alpha, \beta)\left(\frac{\delta_a}{21.5}\right) + \delta C_{N_{\delta_r}}(\alpha, \beta)\left(\frac{\delta_r}{30}\right) \\ &+ \frac{rb}{2V_T} C_{N_r}(\alpha) + \frac{pb}{2V_T} C_{N_p}(\alpha) \end{aligned} \tag{100}$$

Appendix B. Approximation of Non-Affine Force and Moment Coefficient

In the figures below the non-affine force coefficient C_X and moment coefficient C_M, together with their polynomial approximation and model error, are displayed. These polynomial approximations are used to allow the Backstepping procedure to be applied to the F-16 model.

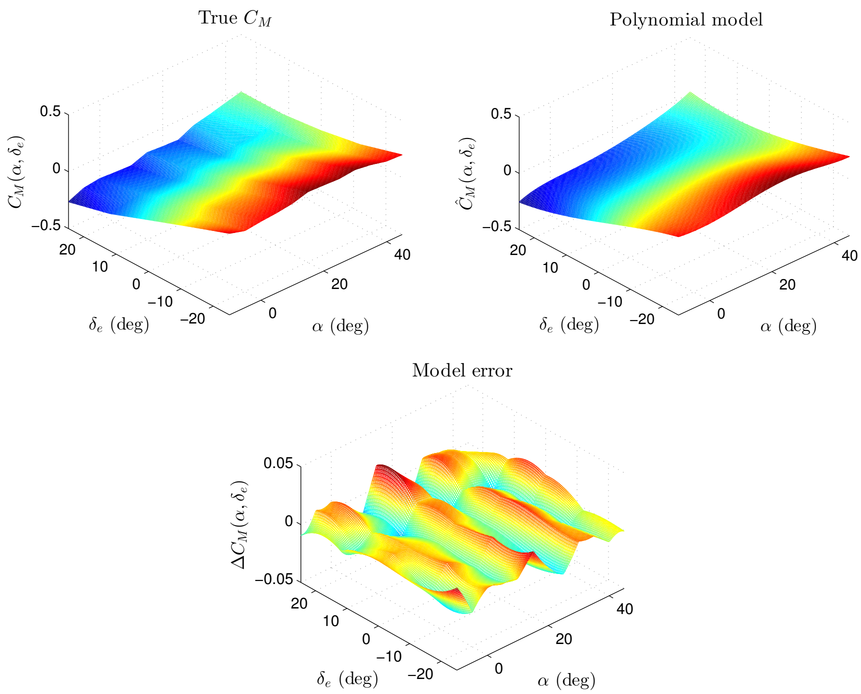

Figure 12. C_M **surface plots**

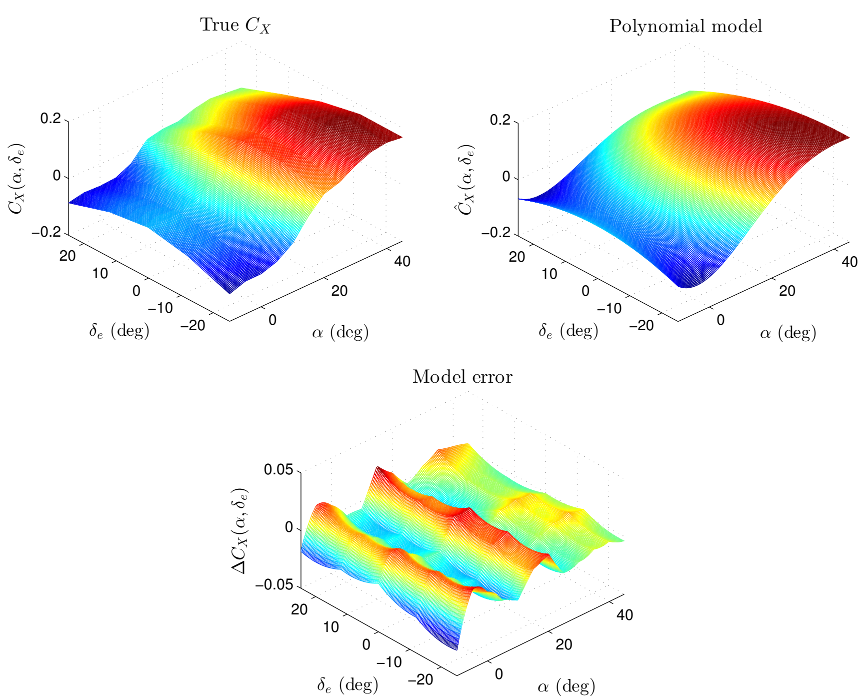

Figure 13. C_X **surface plots**

Appendix C. Estimation of Angular Accelerations

As can be seen from Eq. (51), the incremental control law requires the angular accelerations. Sensors to measure these accelerations exist, however, they are not common. Therefore noisy angular rate measurements are used to estimate the angular accelerations. The following three approaches have earlier been used to estimate the angular accelerations within the incremental control framework:[26,66,67]

- **Numerical differentiation**

  Two-point backward-difference:[68]

$$\dot{\boldsymbol{\omega}}_t = \frac{1}{dt}\left[\boldsymbol{\omega}_t - \boldsymbol{\omega}_{t-dt}\right] + \frac{dt}{2}\boldsymbol{\omega}_t^{(2)}(\xi)\,, \tag{101}$$

  for some ξ between t and $t-dt$, where dt is the sampling time, $\boldsymbol{\omega}$ is a vector containing the angular rate measurements $[p_m \;\; q_m \;\; r_m]^T$ and where $\boldsymbol{\omega}^{(2)}$ is the second time derivative of $\boldsymbol{\omega}$.

  Five-point backward-difference:[68]

$$\dot{\boldsymbol{\omega}}_t = -\frac{1}{12dt}\left[-25\boldsymbol{\omega}_t + 48\boldsymbol{\omega}_{t-dt} - 36\boldsymbol{\omega}_{t-2dt} + 16\boldsymbol{\omega}_{t-3dt} - 3\boldsymbol{\omega}_{t-4dt}\right] - \frac{dt^4}{5}\boldsymbol{\omega}_t^{(5)}(\xi)\,, \tag{102}$$

  for some ξ between t and $t-4dt$. Note that the last term of Eqs. (101) and (102) are the truncation errors. The disadvantage of numerically differentiating a noisy signal is that the noise is amplified. Moreover, when the sampling frequency is increased, the noise will be amplified even more. Nevertheless, this approach has been successfully taken in the literature to provide the angular accelerations for an incremental control law.[26]

- **Filtering**

  Second-order washout filter (Figure 14):[69]

$$H(s)_{washout} = \frac{s\Omega_{del}(s)}{\Omega(s)} = \frac{s\omega_n^2}{s^2 + 2\omega_n s + \omega_n^2}\,, \tag{103}$$

  where ω_n is the bandwidth of the filter and where $\Omega(s)$ and $\Omega_{del}(s)$ are respectively the Laplace transform of $\boldsymbol{\omega}$ and $\boldsymbol{\omega}_{del}$, where $\boldsymbol{\omega}_{del}$ is the delayed $\boldsymbol{\omega}$ signal. This washout filter eliminates the need for numerical differentiation. The second-order washout filter provides a filtered angular acceleration at the price of a time delay. The order of the washout filter can be increased to further suppress noise, however, this will increase the time delay between the output and input signal.

- **Sliding mode differentiator**

  5th-order sliding mode differentiator:[70]

$$\dot{z}_0 = v_0, \quad v_0 = -12L|z_0 - \omega(t)|^{5/6}\,\mathrm{sgn}(z_0 - \omega(t)) + z_1 \tag{104a}$$
$$\dot{z}_1 = v_1, \quad v_1 = -8L|z_1 - v_0|^{4/5}\,\mathrm{sgn}(z_1 - v_0) + z_2 \tag{104b}$$
$$\dot{z}_2 = v_2, \quad v_2 = -5L|z_2 - v_1|^{3/4}\,\mathrm{sgn}(z_2 - v_1) + z_3 \tag{104c}$$
$$\dot{z}_3 = v_3, \quad v_3 = -3L|z_3 - v_2|^{2/3}\,\mathrm{sgn}(z_3 - v_2) + z_4 \tag{104d}$$
$$\dot{z}_4 = v_4, \quad v_4 = -1.5L|z_4 - v_3|^{1/2}\,\mathrm{sgn}(z_4 - v_3) + z_5 \tag{104e}$$
$$\dot{z}_5 = -1.1L\,\mathrm{sgn}(z_5 - v_4)\,, \tag{104f}$$

  in which z_1 is the estimated derivative and L is a tuning parameter. Increasing the value of L results in faster convergence but higher sensitivity to input noise. This approach has been successfully taken in the literature to provide the angular accelerations for an incremental control law.[66,67]

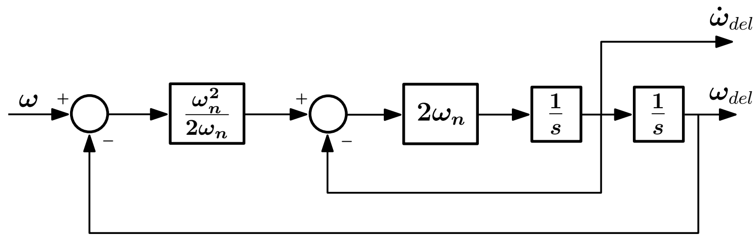

Figure 14. Second-order washout filter that generates a filtered angular acceleration at the price of a time delay.

In order to test these three approaches, a simulation has been run with conventional BS control law Eq. (32) in which the estimated and true angular accelerations are compared, see Figure 15. The RMSD of the angular acceleration estimation has been defined as follows:

$$RMSD = \sum_{j=1}^{3} \sqrt{\frac{1}{n} \sum_{i=1}^{n} \left(\dot{x}_{2,j}[i] - \dot{x}_{2,j_{est}}[i] \right)^2}, \tag{105}$$

where n is the number of samples and $\dot{\boldsymbol{x}}_{2_{est}}$ is the estimate of the true angular acceleration $\dot{\boldsymbol{x}}_2$. The RMSD values have been averaged over five simulation runs for each combination of estimation algorithm and tuning parameter. The results of the simulations for two sampling rates f_s and two different noise standard deviations σ can be found in Table 9.

From these results can be concluded that for three out of four combinations of f_s and σ the sliding mode differentiator with $L = 5$ gives the most accurate estimation of the angular acceleration in terms of the RMSD. Note that the 5-point numerical differentiation scheme performs worse compared to the 2-point numerical scheme. The reason for this is that the error term of the 5-point method contains the term $\omega^{(5)}$, which is much larger compared to $\omega^{(2)}$ of the 2-point scheme because taking derivatives enhances noise. Furthermore, note that the optimal bandwidth ω_n of the washout filter decreases when the noise standard deviation increases. This is explained as follows: when the noise power increases, the frequency reduces where the signal-to-noise ratio [dB] equals zero. Therefore, to effectively attenuate the noise for larger σ, the bandwidth ω_n of the washout filter should be reduced, which results in a larger effective time delay. Incremental control is known to be sensitive to these time delays,[8,39,71] and therefore compensation of this time delay (loop synchronization) might be required to achieve satisfactory closed-loop performance.[16,59] At last, note that all *estimated* angular accelerations lag behind the *real* angular accelerations, including the ones obtained by numerical differentiation. This is because the inertial sensor dynamics introduce a small effective time delay on the measured rates, see Eq. (8).

Because a small RMSD value for the angular acceleration estimator does not guarantee satisfactory tracking performance of the IBS controller; the algorithms of this section have been evaluated in closed-loop simulations in Section IV.B.

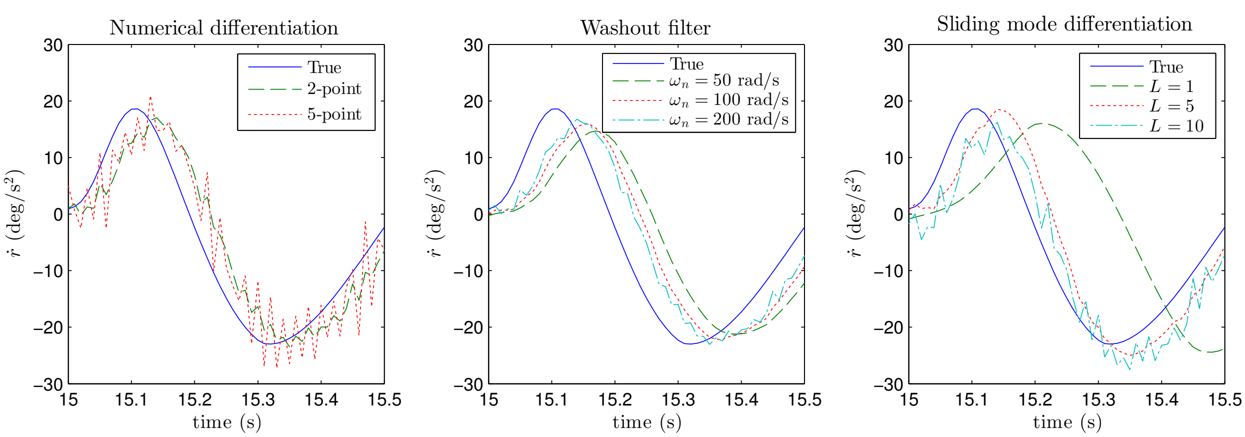

Figure 15. Estimation of the yaw acceleration by using a noisy rate measurement r_m for $f_s = 100\,\mathrm{Hz}$ and $\sigma_r = 0.01\,\mathrm{deg/s}$.

Table 9. Root-mean-square deviations of the estimated angular acceleration.

	Numerical		Washout filter			Sliding mode		
	2-point	5-point	$\omega_n = 50$	$\omega_n = 100$	$\omega_n = 200$	$L = 1$	$L = 5$	$L = 10$
$f_s = 100\,\text{Hz},\ \sigma_{p,q,r} = 0.01\,\text{deg/s}$	0.11	0.30	0.16	0.12	0.11	0.35	0.09	0.20
$f_s = 500\,\text{Hz},\ \sigma_{p,q,r} = 0.01\,\text{deg/s}$	0.38	1.46	0.16	0.11	0.10	0.34	0.08	0.08
$f_s = 100\,\text{Hz},\ \sigma_{p,q,r} = 0.1\,\text{deg/s}$	0.74	2.90	0.18	0.21	0.55	0.35	0.22	0.61
$f_s = 500\,\text{Hz},\ \sigma_{p,q,r} = 0.1\,\text{deg/s}$	3.70	14.58	0.16	0.16	0.29	0.35	0.15	0.26

Appendix D. Immersion & Invariance Update Laws

D.1 Function approximator (2)

The regressor $\boldsymbol{\varphi}_{2,2}$ and the $\boldsymbol{\beta}_{2,2}$-function are given by

$$\boldsymbol{\varphi}_{2,2}^T = c_7 \bar{q} S b \Delta\delta_e \begin{bmatrix} 1 & \alpha & \delta_e \end{bmatrix} \tag{106}$$

$$\boldsymbol{\beta}_{2,2} = \Gamma_{2,2} \boldsymbol{\varphi}_{2,2} x_{2,2}\,. \tag{107}$$

Following from Eq. (74), the update law becomes

$$\dot{\boldsymbol{\xi}}_{2,2} = -\Gamma_{2,2}\boldsymbol{\varphi}_{2,2}\left[f_2 + \boldsymbol{\varphi}_{2,2}^T(\boldsymbol{\xi}_{2,2} + \boldsymbol{\beta}_{2,2})\right] - \Gamma_{2,2} c_7 S b x_{2,2} \begin{bmatrix} \bar{q}\Delta\dot{\delta}_e + \dot{\bar{q}}\Delta\delta_e \\ \bar{q}\Delta\delta_e\dot{\alpha} + \bar{q}\Delta\dot{\delta}_e\alpha + \dot{\bar{q}}\Delta\delta_e\alpha \\ \bar{q}\Delta\delta_e\dot{\delta}_e + \bar{q}\Delta\dot{\delta}_e\delta_e + \dot{\bar{q}}\Delta\delta_e\delta_e \end{bmatrix}. \tag{108}$$

The estimate of the control efficiency $C_{M_{\delta_e}}$ is now given by

$$\hat{C}_{M_{\delta_e}} = \mathcal{P}\left\{\begin{bmatrix} 1 & \alpha & \delta_e \end{bmatrix}\left(\boldsymbol{\xi}_{2,2} + \Gamma_{2,2}\boldsymbol{\varphi}_{2,2} x_{2,2}\right)\right\}, \tag{109}$$

where $\mathcal{P}$ represents the parameter projection operator to prevent singularities of IBS control law Eq. (51). The dynamics of the estimation error $\boldsymbol{\sigma}_{2,2}$ now become

$$\dot{\boldsymbol{\sigma}}_{2,2} = -\Gamma_{2,2}\boldsymbol{\varphi}_{2,2}\boldsymbol{\varphi}_{2,2}^T\boldsymbol{\sigma}_{2,2}\,. \tag{110}$$

D.2 Function approximator (3)

The regressor $\boldsymbol{\varphi}_{2,3}$ and the $\boldsymbol{\beta}_{2,3}$-function are now given by

$$\boldsymbol{\varphi}_{2,3}^T = c_7 \bar{q} S b \Delta\delta_e \begin{bmatrix} 1 & \alpha & \delta_e & \alpha^2 & \alpha\delta_e & \delta_e^2 \end{bmatrix} \tag{111}$$

$$\boldsymbol{\beta}_{2,3} = \Gamma_{2,3}\boldsymbol{\varphi}_{2,3} x_{2,2}\,. \tag{112}$$

Following from Eq. (74), the update law becomes

$$\dot{\boldsymbol{\xi}}_{2,3} = -\Gamma_{2,3}\boldsymbol{\varphi}_{2,3}\left[f_2 + \boldsymbol{\varphi}_{2,3}^T(\boldsymbol{\xi}_{2,3} + \boldsymbol{\beta}_{2,3})\right] - \Gamma_{2,3} c_7 S b x_{2,2} \begin{bmatrix} \bar{q}\Delta\dot{\delta}_e + \dot{\bar{q}}\Delta\delta_e \\ \bar{q}\Delta\delta_e\dot{\alpha} + \bar{q}\Delta\dot{\delta}_e\alpha + \dot{\bar{q}}\Delta\delta_e\alpha \\ \bar{q}\Delta\delta_e\dot{\delta}_e + \bar{q}\Delta\dot{\delta}_e\delta_e + \dot{\bar{q}}\Delta\delta_e\delta_e \\ 2\bar{q}\Delta\delta_e\alpha\dot{\alpha} + \bar{q}\Delta\dot{\delta}_e\alpha^2 + \dot{\bar{q}}\Delta\delta_e\alpha^2 \\ \bar{q}\Delta\delta_e\alpha\dot{\delta}_e + \bar{q}\Delta\delta_e\dot{\alpha}\delta_e + \bar{q}\Delta\dot{\delta}_e\alpha\delta_e + \dot{\bar{q}}\Delta\delta_e\alpha\delta_e \\ 2\bar{q}\Delta\delta_e\delta_e\dot{\delta}_e + \bar{q}\Delta\dot{\delta}_e\delta_e^2 + \dot{\bar{q}}\Delta\delta_e\delta_e^2 \end{bmatrix}. \tag{113}$$

The estimate of the control efficiency $C_{M_{\delta_e}}$ is now given by

$$\hat{C}_{M_{\delta_e}} = \mathcal{P}\left\{\begin{bmatrix} 1 & \alpha & \delta_e & \alpha^2 & \alpha\delta_e & \delta_e^2 \end{bmatrix}\left(\boldsymbol{\xi}_{2,3} + \Gamma_{2,3}\boldsymbol{\varphi}_{2,3} x_{2,2}\right)\right\}, \tag{114}$$

where $\mathcal{P}$ represents the parameter projection operator to prevent singularities of IBS control law Eq. (51). The dynamics of the estimation error $\boldsymbol{\sigma}_{2,3}$ now become

$$\dot{\boldsymbol{\sigma}}_{2,3} = -\Gamma_{2,3}\boldsymbol{\varphi}_{2,3}\boldsymbol{\varphi}_{2,3}^T\boldsymbol{\sigma}_{2,3}\,. \tag{115}$$

Appendix E. Additional simulation results

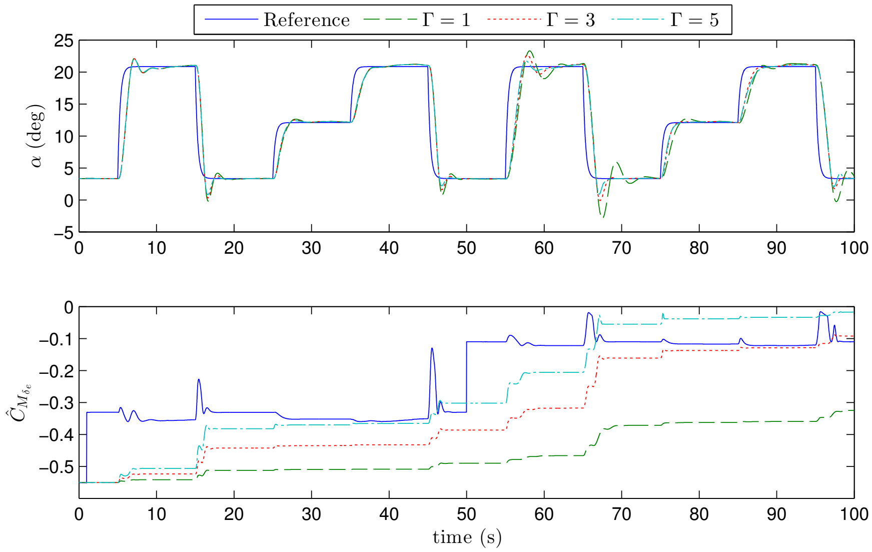

Figure 16. The performance of the Tuning Function estimator with constant function approximator (61a) for different values of the adaptation gain Γ in the presence of uncertainties in the pitching moment coefficient $C_{M_{\delta_e}}(\alpha, \delta_e)$.

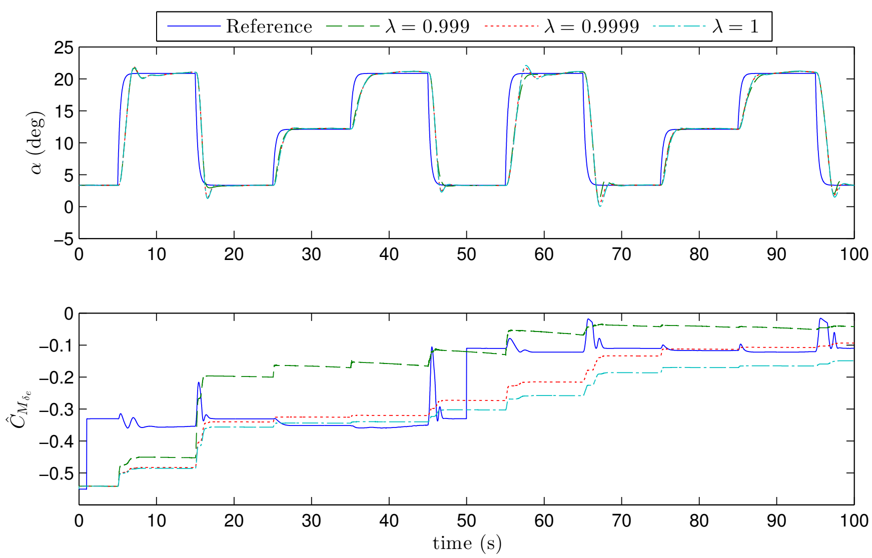

Figure 17. The performance of the Least-Squares Adaptive Incremental Backstepping controller with constant function approximator (61a) for $P_0 = 0.1$ and different values of the forgetting factor λ in the presence of uncertainties in the pitching moment coefficient $C_{M_{\delta_e}}(\alpha, \delta_e)$.

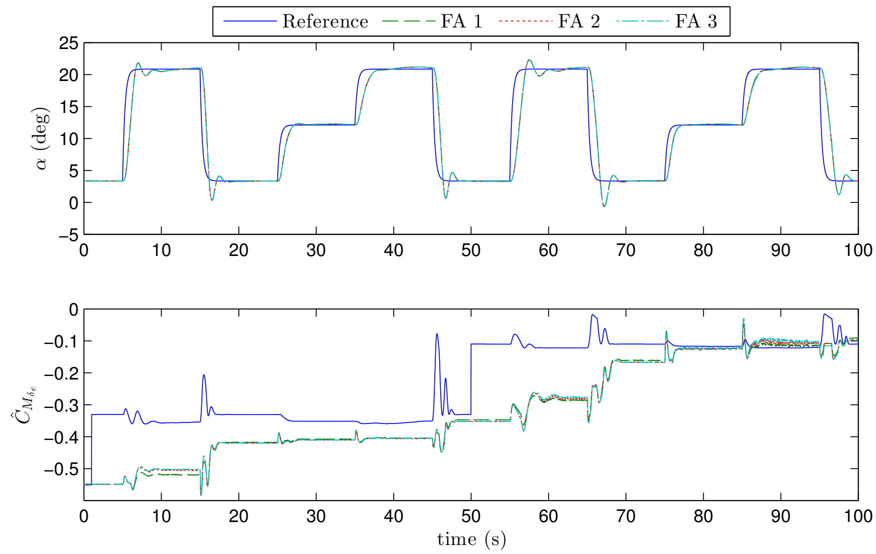

Figure 18. The performance of the Immersion & Invariance Adaptive Incremental Backstepping controller for three different Function Approximators (FAs) (see Eq. (61)) in the presence of uncertainties in the pitching moment $C_{M_{\delta_e}}(\alpha, \delta_e)$.

References

[1]European Aviation Safety Agency, "Annual Safety Review 2013," Tech. rep., 2013.

[2]Williams, K. W., "A Summary of Unmanned Aircraft Accident / Incident Data: Human Factors Implications," Tech. rep., Office of Aerospace Medicine, 2004.

[3]Schaefer, R., "Unmanned Aerial Vehicle Reliability Study," Tech. rep., Office of the Secretary of Defense, Washington DC, 2003.

[4]Smaili, M. H., Breeman, J., Lombaerts, T. J. J., and Joosten, D. A., "A Simulation Benchmark for Integrated Fault Tolerant Flight Control Evaluation," *AIAA Modeling and Simulation Technologies Conference and Exhibit*, American Institute of Aeronautics and Astronautics, Reston, Virigina, Aug. 2006, pp. 1–23.

[5]Lombaerts, T. J. J., Smaili, M. H., Stroosma, O., Chu, Q. P., Mulder, J. A., and Joosten, D. A., "Piloted Simulator Evaluation Results of New Fault-Tolerant Flight Control Algorithm," *Journal of Guidance, Control, and Dynamics*, Vol. 32, No. 6, Nov. 2009, pp. 1747–1765.

[6]Lombaerts, T. J. J., Huisman, H. O., Chu, Q. P., Mulder, J. A., and Joosten, D. A., "Nonlinear Reconfiguring Flight Control Based on Online Physical Model Identification," *Journal of Guidance, Control, and Dynamics*, Vol. 32, No. 3, May 2009, pp. 727–748.

[7]Sonneveldt, L., *Adaptive Backstepping Flight Control for Modern Fighter Aircraft*, Ph.D. thesis, Delft University of Technology, 2010.

[8]Falkena, W., *Investigation of Practical Flight Control Systems for Small Aircraft*, Ph.D. thesis, Delft University of Technology, 2012.

[9]Lombaerts, T. J. J., *Fault Tolerant Flight Control, A Physical Model Approach*, Ph.D. thesis, Delft University of Technology, 2010.

[10]van Oort, E. R., *Adaptive Backstepping Control and Safety Analysis for Modern Fighter Aircraft*, Ph.D. thesis, Delft University of Technology, 2011.

[11]Sonneveldt, L., Chu, Q. P., and Mulder, J. A., "Nonlinear Flight Control Design Using Constrained Adaptive Backstepping," *Journal of Guidance, Control, and Dynamics*, Vol. 30, No. 2, March 2007, pp. 322–336.

[12]Polycarpou, M., Farrell, J., and Sharma, M., "On-line Approximation Control of Uncertain Nonlinear Systems: Issues with Control Input Saturation," *Proceedings of the 2003 American Control Conference*, Vol. 1, IEEE, 2003, pp. 543–548.

[13]Sonneveldt, L., Chu, Q. P., and Mulder, J. A., "Constrained Adaptive Backstepping Flight Control: Application to a Nonlinear F-16/MATV Model," *AIAA Guidance, Navigation, and Control Conference and Exhibit*, American Institute of Aeronautics and Astronautics, Reston, Virigina, Aug. 2006.

[14]Farrell, J. A., Polycarpou, M. M., Sharma, M., and Dong, W., "Command Filtered Backstepping," *IEEE Transactions on Automatic Control*, Vol. 54, No. 6, 2009, pp. 1391–1395.

[15]Acquatella, P., *Robust Nonlinear Spacecraft Attitude Control: An Incremental Backstepping Approach*, Master's thesis, Delft University of Technology, 2011.

[16]Koschorke, J., *Advanced Flight Control Design and Evaluation*, Master's thesis, Delft University of Technology, 2012.

[17]Falkena, W., van Oort, E. R., and Chu, Q. P., "Towards Certifiable Advanced Flight Control Systems, A Sensor Based Backstepping Approach," *AIAA Guidance, Navigation, and Control Conference*, American Institute of Aeronautics and Astronautics, Aug. 2011.

[18]Falkena, W., Borst, C., van Oort, E. R., and Chu, Q. P., "Sensor-Based Backstepping," *Journal of Guidance, Control, and Dynamics*, Vol. 36, No. 2, March 2013, pp. 606–610.

[19]Sun, L. G., de Visser, C. C., Chu, Q. P., and Falkena, W., "Hybrid Sensor-Based Backstepping Control Approach with Its Application to Fault-Tolerant Flight Control," *Journal of Guidance, Control, and Dynamics*, Vol. 37, No. 1, Jan. 2014, pp. 59–71.

[20]van Oort, E. R., Sonneveldt, L., Chu, Q. P., and Mulder, J. A., "Modular Adaptive Input-to-State Stable Backstepping of a Nonlinear Missile Model," *Navigation and Control*, American Institute of Aeronautics and Astronautics, Reston, Virigina, Aug. 2007.

[21]Choi, I. and Bang, H., "Adaptive Command Filtered Backstepping Tracking Controller Design for Quadrotor Unmanned Aerial Vehicle," *Proceedings of the Institution of Mechanical Engineers, Part G: Journal of Aerospace Engineering*, Vol. 226, Oct. 2011, pp. 483–497.

[22]Farrell, J. A., Polycarpou, M. M., Djapic, V., and Sharma, M., "Command Filtered Adaptive Backstepping," *IEEE Transactions on Control Systems Technology*, Vol. 20, No. 3, May 2012, pp. 566–580.

[23]Sonneveldt, L., van Oort, E. R., Chu, Q. P., and Mulder, J. A., "Immersion and Invariance Based Nonlinear Adaptive Flight Control," *AIAA Guidance, Navigation, and Control Conference*, Aug. 2010.

[24]Karagiannis, D. and Astolfi, A., "Non-linear and Adaptive Flight Control of Autonomous Aircraft Using Invariant Manifolds," *Proceedings of the Institution of Mechanical Engineers, Part G: Journal of Aerospace Engineering*, Vol. 224, No. 4, 2010, pp. 403–415.

[25]Hu, J. and Zhang, H., "Immersion and Invariance Based Command-Filtered Adaptive Backstepping Control of VTOL Vehicles," *Automatica*, Vol. 49, No. 7, July 2013, pp. 2160–2167.

[26]Ali, A. A. H., Chu, Q. P., van Kampen, E., and de Visser, C. C., "Exploring Adaptive Incremental Backstepping using Immersion and Invariance for an F-16 Aircraft," *AIAA Guidance, Navigation, and Control Conference*, Jan. 2014.

[27]Krstić, M., Kanellakopoulos, I., and Kokotović, P., *Nonlinear and Adaptive Control Design*, Wiley, 1995.

[28]Russell, R. S., "Non-linear F-16 Simulation using Simulink and Matlab," Tech. rep., University of Minnesota, 2003.

[29]Sonneveldt, L., "Nonlinear F-16 Model Description," Tech. rep., Delft University of Technology, 2006.

[30]Nguyen, L. T., Ogburn, M. E., Gilbert, W. P., Kibler, K. S., Brown, P. W., and Deal, P. L., "Simulator Study of Stall/Post-Stall Characteristics of a Fighter Airplane with Relaxed Longitudinal Static Stability (F-16)," Tech. Rep. December, NASA Technical Paper 1538, 1979.

[31]Lewis, F. L. and Stevens, B. L., *Aircraft Control and Simulation*, John Wiley & Sons, 1992.

[32]Ruijgrok, G., *Elements of Aircraft Performance*, Delft University Press, 2004.

[33]Hagström, M., *Nonlinear Analysis and Synthesis Techniques for Aircraft Control*, Springer Berlin Heidelberg, 2007.

[34]Härkegård, O., *Backstepping and Control Allocation with Applications to Flight Control*, Ph.D. thesis, Linköping University, 2003.

[35]Farrell, J. A., Polycarpou, M. M., and Sharma, M., "On-line Approximation Based Control of Uncertain Nonlinear Systems with Magnitude, Rate and Bandwidth Constraints on the States and Actuators," *Proceeding of the 2004 American Control Conference*, Vol. 3, 2004, pp. 2557–2562.

[36]Etkin, B. and Reid, L. D., *Dynamics of Flight: Stability and Control*, Vol. 3, Wiley New York, 1996.

[37]Enns, D., "Control Allocation Approaches," *AIAA Guidance, Navigation, and Control Conference and Exhibit*, American Institute of Aeronautics and Astronautics, Reston, Virigina, Aug. 1998, pp. 98–108.

[38]Farrell, J. A., Sharma, M., and Polycarpou, M. M., "Backstepping-Based Flight Control with Adaptive Function Approximation," *Journal of Guidance, Control, and Dynamics*, Vol. 28, No. 6, 2005, pp. 1089–1102.

[39]Sieberling, S., Chu, Q. P., and Mulder, J. A., "Robust Flight Control Using Incremental Nonlinear Dynamic Inversion and Angular Acceleration Prediction," *Journal of Guidance, Control, and Dynamics*, Vol. 33, No. 6, Nov. 2010, pp. 1732–1742.

[40]Acquatella, P., Falkena, W., van Kampen, E., and Chu, Q. P., "Robust Nonlinear Spacecraft Attitude Control using Incremental Nonlinear Dynamic Inversion," *AIAA Guidance, Navigation, and Control Conference*, American Institute of Aeronautics and Astronautics, Aug. 2012.

[41]Simplício, P., Pavel, M. D., van Kampen, E., and Chu, Q. P., "An Acceleration Measurements-Based Approach for Helicopter Nonlinear Flight Control using Incremental Nonlinear Dynamic Inversion," *Control Engineering Practice*, Vol. 21, No. 8, Aug. 2013, pp. 1065–1077.

[42]Ali, A. A. H., *Adaptive Incremental Backstepping using Immersion and Invariance*, Master's thesis, Delft University of Technology, 2013.

[43]Krstić, M., "Invariant Manifolds and Asymptotic Properties of Adaptive Nonlinear Stabilizers," *IEEE Transactions on Automatic Control*, Vol. 41, No. 6, June 1996, pp. 817–829.

[44]Boyd, S. and Sastry, S. S., "Necessary and Sufficient Conditions for Parameter Convergence in Adaptive Control," *Automatica*, Vol. 22, No. 6, Nov. 1986, pp. 629–639.

[45]Dayal, B. S. and MacGregor, J. F., "Recursive Exponentially Weighted PLS and its Applications to Adaptive Control and Prediction," *Journal of Process Control*, Vol. 7, No. 3, Jan. 1997, pp. 169–179.

[46]Fortescue, T. R., Kershenbaum, L. S., and Ydstie, B. E., "Implementation of Self-Tuning Regulators with Variable Forgetting Factors," *Automatica*, Vol. 17, No. 6, 1981, pp. 831–835.

[47]Malik, O. P., Hope, G. S., and Cheng, S. J., "Some Issues on the Practical Use of Recursive Least Squares Identification in Self-Tuning Control," *International Journal of Control*, Vol. 53, No. 5, 1991, pp. 1021–1033.

[48]Stenlund, B. and Gustafsson, F., "Avoiding Windup in Recursive Parameter Estimation," *Preprints of Reglermöte 2002*, 2002, pp. 148–153.

[49]Van Oort, E. R., Sonneveldt, L., Chu, Q. P., and Mulder, J. A., "Full-Envelope Modular Adaptive Control of a Fighter Aircraft Using Orthogonal Least Squares," *Journal of Guidance, Control, and Dynamics*, Vol. 33, No. 5, Sept. 2010, pp. 1461–1472.

[50]Tol, H. J., de Visser, C. C., van Kampen, E., and Chu, Q. P., "Nonlinear and Fault-Tolerant Flight Control Using Multivariate Splines," *Proceedings of the 3rd CEAS EuroGNC, Specialist Conference on Guidance, Navigation & Control*, April 2015.

[51] Freeman, R. A. and Kokotović, P. V., *Robust Nonlinear Control Design: State-Space and Lyapunov Techniques*, Springer Science & Business Media, 2008.

[52] Kim, K. and Kim, Y., "Robust Backstepping Control for Slew Maneuver using Nonlinear Tracking Function," *IEEE Transactions on Control Systems Technology*, Vol. 11, No. 6, Nov. 2003, pp. 822–829.

[53] Lee, J., Yeon, J. S., Park, J. H., and Lee, S., "Robust Back-Stepping Control for Flexible-Joint Robot Manipulators," *2007 IEEE/RSJ International Conference on Intelligent Robots and Systems*, IEEE, Oct. 2007, pp. 183–188.

[54] Tol, H. J., de Visser, C. C., van Kampen, E., and Chu, Q. P., "Nonlinear Multivariate Spline-Based Control Allocation for High-Performance Aircraft," *Journal of Guidance, Control, and Dynamics*, Vol. 37, No. 6, Nov. 2014, pp. 1840–1862.

[55] Karagiannis, D. and Astolfi, A., "Nonlinear Adaptive Control of Systems in Feedback Form: An Alternative to Adaptive Backstepping," *Systems & Control Letters*, Vol. 57, No. 9, 2008, pp. 733–739.

[56] Karagiannis, D. and Astolfi, A., "Observer Design for a Class of Nonlinear Systems using Dynamic Scaling with Application to Adaptive Control," *CDC*, 2008, pp. 2314–2319.

[57] Sun, L. G., *Model and Sensor Based Nonlinear Adaptive Flight Control with Online System Identification*, Ph.D. thesis, Delft University of Technology, 2014.

[58] Choi, J. Y., Chwa, D., and Kim, M., "Adaptive Control for Feedback-Linearized Missiles with Uncertainties," *IEEE Transactions on Aerospace and Electronic Systems*, Vol. 36, No. 2, April 2000, pp. 467–481.

[59] Vlaar, C. M., *Incremental Nonlinear Dynamic Inversion Flight Control - Implementation and Flight Test on a Fixed Wing UAV*, Master's thesis, Delft University of Technology, 2014.

[60] van Huffel, S. and Vandewalle, J., *The Total Least Squares Problem*, Society for Industrial and Applied Mathematics, 1991.

[61] Markovsky, I. and Van Huffel, S., "Overview of Total Least-Squares Methods," *Signal Processing*, Vol. 87, No. 10, Oct. 2007, pp. 2283–2302.

[62] Edwards, C., Lombaerts, T. J. J., and Smaili, M. H., *Fault Tolerant Flight Control: A Benchmark Challenge*, Vol. 399 of *Lecture Notes in Control and Information Sciences*, Springer Berlin Heidelberg, Berlin, Heidelberg, 2010.

[63] Cao, C., Hovakimyan, N., and Wang, J., "Intelligent Excitation for Adaptive Control With Unknown Parameters in Reference Input," *IEEE Transactions on Automatic Control*, Vol. 52, No. 8, Aug. 2007, pp. 1525–1532.

[64] Stepanyan, V. and Hovakimyan, N., "Adaptive Disturbance Rejection Controller for Visual Tracking of a Maneuvering Target," *Journal of Guidance, Control, and Dynamics*, Vol. 30, No. 4, July 2007, pp. 1090–1106.

[65] Smith, P. and Berry, A., "Flight Test Experience of a Non-Linear Dynamic Inversion Control Law on the VAAC Harrier," *Atmospheric Flight Mechanics Conference*, 2000, pp. 132–142.

[66] Sun, L. G., de Visser, C. C., Chu, Q. P., and Falkena, W., "A Joint Sensor Based Backstepping Approach For Fault-Tolerant Flight Control of a Large Civil Aircraft," *AIAA Guidance, Navigation, and Control (GNC) Conference*, American Institute of Aeronautics and Astronautics, Reston, Virginia, Aug. 2013, pp. 1–22.

[67] Sun, L. G., de Visser, C. C., Chu, Q. P., and Mulder, J. A., "Joint Sensor Based Backstepping for Fault-Tolerant Flight Control," *Journal of Guidance, Control, and Dynamics*, Vol. 38, No. 1, Jan. 2015, pp. 62–75.

[68] Burden, R. L. and Faires, J. D., *Numerical Analysis*, Cengage Learning, 9th ed., 2010.

[69] Bacon, B. J., Ostroff, A. J., and Joshi, S. M., "Reconfigurable NDI Controller Using Inertial Sensor Failure Detection & Isolation," *IEEE Transactions on Aerospace and Electronic Systems*, Vol. 37, No. 4, 2001, pp. 1373–1383.

[70] Levant, A., "Higher-Order Sliding Modes, Differentiation and Output-Feedback Control," *International Journal of Control*, Vol. 76, No. 9-10, Jan. 2003, pp. 924–941.

[71] Koschorke, J., Falkena, W., Van Kampen, E., and Chu, Q. P., "Time Delayed Incremental Nonlinear Control," *AIAA Guidance, Navigation, and Control (GNC) Conference*, American Institute of Aeronautics and Astronautics, Reston, Virginia, Aug. 2013, pp. 1–18.

Appendix A

Research Context

This appendix contains a summary of the literature survey on Fault Tolerant Flight Control (FTFC). This fault tolerant approach to flight control is of paramount importance for safety-critical systems such as (unmanned) aircraft to enhance the survivability during an incident. First, the different classifications of FTFC and previous achievements are discussed in Appendix A-1. One of the subcategories of FTFC is Adaptive Control, which has the inherent ability to adapt to changes in the system parameters. This promising control strategy is discussed in more detail in Appendix A-2. These Adaptive Control schemes generally contain nonlinear flight control laws, that do not suffer from the drawbacks of gain-scheduled linear controllers, see Appendix A-3.

A-1 Fault Tolerant Flight Control

There are different approaches to FTFC, a simplified classification of these can be found in Figure A-1. A complete overview of FTFC including a detailed description of each method can be found in (Lombaerts, 2010). Generally speaking, FTFC systems can be classified into Passive Fault Tolerant Flight Control (PFTFC) and Active Fault Tolerant Flight Control (AFTFC). These two approaches are elaborated in respectively Appendices A-1-1 and A-1-2. Active Fault Tolerant Flight Control is a flexible control strategy with more potential compared to Passive Fault Tolerant Flight Control, and is further subdivided into on-line redesign and projection-based methods, see Appendix A-1-3.

A-1-1 Passive Fault Tolerant Flight Control

The controllers of PFTFC systems are fixed and are only robust inside a predefined uncertainty region around the nominal model. Passive Fault Tolerant Flight Control is therefore robust to presumed faults, but is generally not able to stabilize the aircraft during unanticipated failures. Another disadvantage of these schemes is that large stability radii lead to

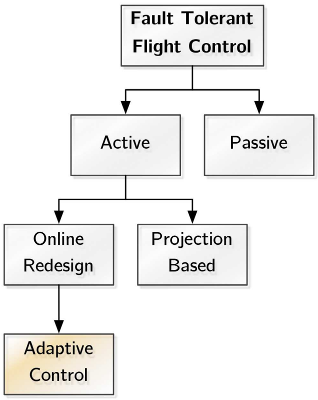

Figure A-1: The location of Adaptive Control within Fault Tolerant Flight Control. A complete classification of Fault Tolerant Flight Control can be found in (Lombaerts, 2010).

unnecessary conservativeness of the controller (Lombaerts, 2010; van Oort, 2011). However, PFTFC systems are generally less complex than AFTFC systems, because PFTFC does not require a reconfigurable controller and a Fault Detection and Isolation (FDI) module that provides on-line fault information.

In for example (Reiner, Balas, & Garrard, 1996), PFTFC has been applied by using a Nonlinear Dynamic Inversion (NDI)-based control law that has been augmented with a linear μ-controller. The resulting controller enhances the robustness to parameter variations and requires no gain scheduling with flight condition. This design technique appears to provide excellent performance, is robust to parametric uncertainties and results in a low-order linear controller. However, this design only guarantees stability of parametric uncertainties up to 20%. Therefore, it is not guaranteed that this design can anticipate for modeling errors or larger parametric uncertainties.

A-1-2 Active Fault Tolerant Flight Control

A flexible control strategy with more potential compared to PFTFC is AFTFC, which is also known as reconfigurable flight control. These active schemes are able to cope with unanticipated failures, without resulting in unnecessary conservativeness of the controller. This property is achieved by an FDI that provides on-line fault information to reconfigure the controller. Although this control strategy does not lead to unnecessary conservativeness, often degraded performance with respect to the nominal model has to be accepted during failures due to a downsized safe flight envelope (van Oort, 2011). As mentioned in (Jacklin, 2008), when AFTFC systems are able to make rapid and automatic adjustments to stabilize the aircraft during failures, they also have the ability to make a healthy aircraft unflyable in case of a malfunction of the flight control computer. Therefore, AFTFC needs to be proven to be highly safe and reliable before such systems can be possibly certified. Note that even AFTFC systems require some form of robustness, because generally the on-line estimated aircraft model is only an approximation of the real aircraft dynamics.

The components of an AFTFC system can be seen in Figure A-2. Flight Envelope Protection (FEP) is used to determine the safe flight envelope of the (damaged) aircraft in an on-line fashion. In (van Oort, 2011) the following definition for the safe flight envelope is given:

> ***Safe Flight Envelope:*** *the part of the state space for which safe operation of the aircraft and safety of its cargo can be guaranteed and externally posed constraints will not be violated.*

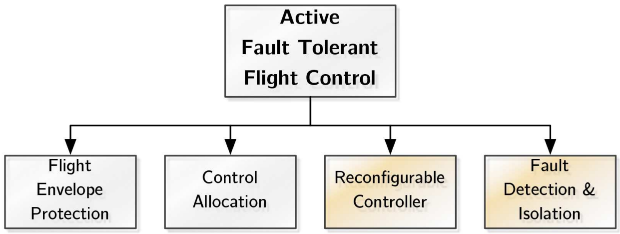

Figure A-2: The components of an Active Fault Tolerant Flight Control system.

Knowledge of the safe flight envelope during flight is essential in order to prevent Loss Of Control In-flight (LOC-I). The FEP modifies the reference signals provided by the (auto)pilot to make them consistent with the predicted safe flight envelope. More information on FEP can be found in (van Oort, 2011; Holzapfel & Theil, 2011; Lombaerts, Schuet, Wheeler, Acosta, & Kaneshige, 2013; Schuet, Lombaerts, Acosta, Wheeler, & Kaneshige, 2014).

The goal of Control Allocation (CA) is to determine the commanded actuator positions based on the output of the controller, i.e. the commanded forces and moments. Because generally the amount of actuators (flight control surfaces and engines) is larger than the six degrees of freedom of a rigid aircraft, a solution or approximation have to be found to an *underdetermined* system subject to constraints. These constraints arise from the actuator dynamics; which are subject to bandwidth, rate and magnitude limits. The CA module has to account for actuator failures in real-time based on on-line fault information provided by the FDI. The FDI provides estimates of the control efficiencies, which are used by the CA module to transform the commanded forces and moments into control deflections of the (remaining) actuators. Control Allocation can be implemented without actually modifying the controller itself, and is therefore a convenient method to implement in current systems. Control Allocation techniques are generally based on linear or quadratic programming, see (Enns, 1998; Lombaerts, 2010).

The remaining components of an AFTFC system are a reconfigurable controller and the FDI. A reconfigurable controller consists of a control law and parameters that can be updated. The well-known gain scheduling control technique uses look-up tables and interpolation functions to update the controller gains. When Adaptive Control is used, a compensation mechanism is used to provide gains that guarantee desired closed-loop properties. The FDI module is the heart of AFTFC systems, and provides on-line fault information to the FEP, CA and reconfigurable controller based on the input and output measurements of the controlled system. The interaction between the AFTFC components can be seen in Figure A-3. The focus of this thesis lies on the reconfigurable controller and the FDI.

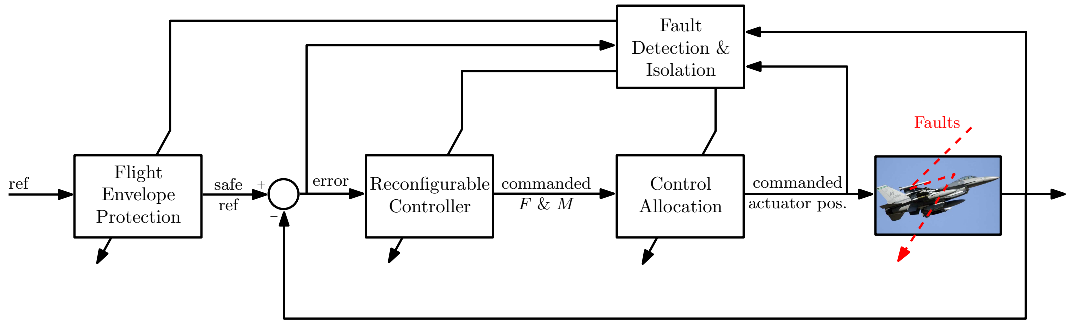

Figure A-3: A general structure of Active Fault Tolerant Flight Control.

A-1-3 On-line Redesign vs Projection-Based methods

Active Fault Tolerant Flight Control systems can be subdivided into on-line redesign and projection-based methods (Figure A-4). The difference between these methods is the way in which the post-fault controller is formed. For projection-based control a set of off-line controllers is designed (Figure A-4a). One of these controllers may be designed for a rudder runaway failure, while another controller can cope with an engine separation. The fault must be detected by an FDI to activate a reconfiguration mechanism that selects the controller which can stabilize the damaged aircraft. Note that similar to PFTFC systems, projection-based methods are generally not able to stabilize the aircraft during *unanticipated* failures.

A flexible control strategy with more potential compared to projection-based methods is on-line redesign (Figure A-4b). These active schemes are, as opposed to project-based methods, able to cope with unanticipated failures. This property is achieved by an FDI that provides on-line fault information to update the parameters of the controller. The disadvantage of such control schemes is that they are computationally expensive (Lombaerts, 2010).

In (Tang, 2014) a fault-tolerant Sensor-Based Backstepping (SBB) controller in combination with a projection-based method is applied to a Boeing 747-100/200 aircraft. In case of a rudder runaway failure, this projection method switches from a control law in which the rudder is used, to a control law in which differential thrust is applied to improve the lateral control. In this research the switch from one controller to another is performed manually, however, this could be automatized by implementation of an FDI.

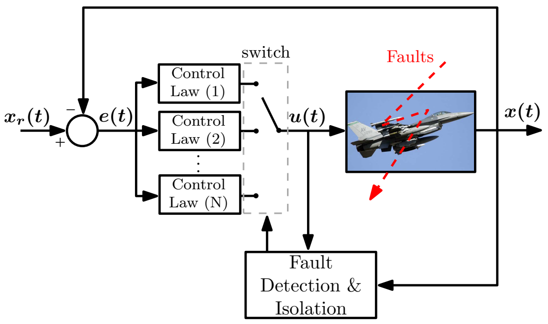

(a) Projection-Based Control

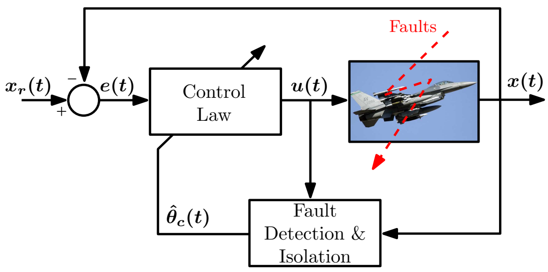

(b) On-line Redesign Control

Figure A-4: Two different implementations of Adaptive Control.

A-2 Adaptive Control

Adaptive Control is a method of on-line redesign AFTFC. This control approach has a high potential because it is able to compensate for inaccuracies in the nominal aircraft model. Moreover, sudden changes in the dynamic behavior of the aircraft can be identified and isolated to avoid LOC-I. A classification of Adaptive Control often found in literature is that of Direct and Indirect Adaptive Control; these two approaches are elaborated in respectively Appendices A-2-1 and A-2-2. Adaptive Control generally uses a *model-based* flight control law, because this is a more transparent approach compared to *model-free* control laws. This can be a major benefit for certification of these control laws. In order to apply model-based flight control, an accurate aerodynamic model is required during flight. System identification is the process of creating such a model based on the system's input-output behavior, see Appendix A-2-3.

A-2-1 Direct Adaptive Control

In Direct Adaptive Control (Figure A-5a), the control parameters $\boldsymbol{\theta}_c$ are obtained on-line without first identifying the model parameters $\boldsymbol{\theta}_m$ (Duarte & Narendra, 1989). This direct method is also known as Integrated or Implicit Adaptive Control (Lombaerts, 2010). The control parameters are updated by use of update laws that are selected in order to obtain favorable closed-loop properties. The proof of stability often depends on Lyapunov theory, therefore these schemes are sometimes referred to as Lyapunov-based Adaptive Control. In some applications the model parameters $\boldsymbol{\theta}_m$ are approximated based on the estimated control parameters $\hat{\boldsymbol{\theta}}_c$ (Duarte & Narendra, 1989). These model parameter estimations $\hat{\boldsymbol{\theta}}_m$ can then be used in health monitoring algorithms to detect failures such as structural damage or control surface runaway.

A well-known Integrated, Lyapunov-based Adaptive Control approach is Tuning Functions Adaptive Backstepping (Farrell, Polycarpou, & Sharma, 2004; Choi & Bang, 2011; Farrell et al., 2012). This technique has been widely applied to guarantee stability of nonlinear systems with parametric uncertainties. The parameter estimates converge to the real parameters when a "sufficiently rich" reference signal is injected.

A-2-2 Indirect Adaptive Control

In Indirect Adaptive Control (Figure A-5b), first the model parameters $\boldsymbol{\theta}_m$ are estimated on-line by using a separate module for model identification. In the next step, the control parameters $\boldsymbol{\theta}_c$ are estimated by using the provided model parameter estimates $\hat{\boldsymbol{\theta}}_m$. This indirect method is also known as modular, explicit or estimated-based Adaptive Control (Lombaerts, 2010). Indirect Adaptive Control schemes are based on the *certainty equivalence principle* (Krstić, Kanellakopoulos, & Kokotović, 1995; van Oort, 2011). This means that the controller is designed by assuming perfect knowledge of the model. Next, the model parameters are estimated by a separate module. The certainty equivalence controller is then simply obtained by replacing the model parameters $\boldsymbol{\theta}_m$ by their estimates $\hat{\boldsymbol{\theta}}_m$. The advantage of estimation-based designs is that they are more broadly applicable and allow a great choice

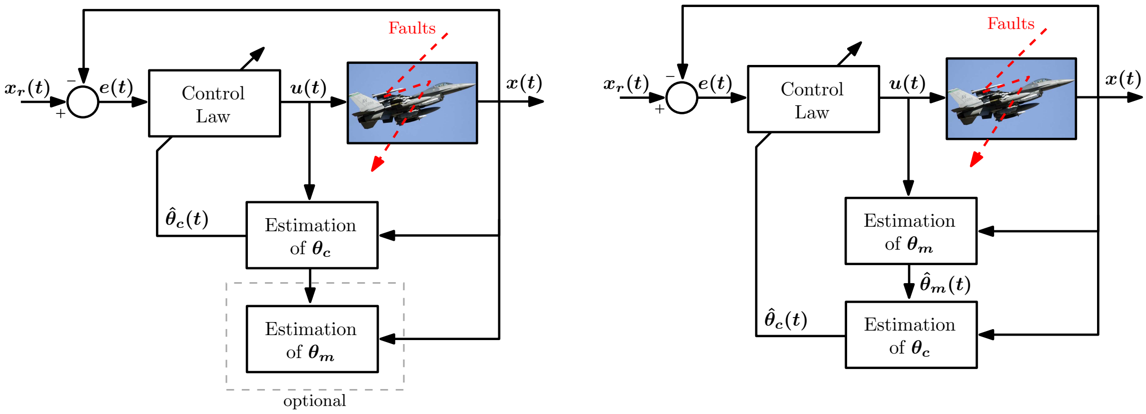

(a) Direct Adaptive Control **(b)** Indirect Adaptive Control

Figure A-5: Two different implementations of Adaptive Control.

of parameter update laws, such as gradient and least-squares algorithms. The disadvantage of these schemes is that stability of the closed-loop system is difficult to prove (Krstić et al., 1995).

In (Lombaerts, Smaili, et al., 2009; Lombaerts, Huisman, et al., 2009) an Indirect Adaptive Control approach has been adopted for a piloted simulator evaluation of a new FTFC algorithm. A nonlinear control law is developed that is a function of the model parameters $\boldsymbol{\theta}_m$. An identification module based on state and parameter estimation is used to provide estimates of these model parameters. It is assumed that the identifier is able to provide a sufficient accurate aircraft model, to avoid instability of the closed-loop system. The proposed Indirect Adaptive Control scheme has been shown to be successful in recovering damaged aircraft.

A-2-3 System Identification

Earlier in Appendix A-1 we subdivided FTFC systems into active and passive systems. Another classification often found in literature, independent of the active / passive categorization, is that of (1) model-based and (2) model-free schemes. Examples of model-based FTFC are Adaptive Backstepping (ABS) and Adaptive Nonlinear Dynamic Inversion (ANDI). A commonly used model-free flight control scheme is (robust) Proportional-Integral-Derivative (PID) control. Model-based schemes have advantages over model-free control with respect to reconfigurable flight control and from the aspect of on-line flight envelope protection (Sun, 2014). Model-based flight control is generally a more transparent approach which can be a major benefit for the certification of these advanced control laws.

In order to apply model-based flight control, an accurate aerodynamic model is required during flight. System identification is the process of creating such a model based on the system's input-output behavior (Figure A-6). For AFTFC this identification must be carried out in real-time in order to account for changes in the nominal aircraft model during flight (e.g. structural damage).

The most important steps of (on-line) aircraft system identification are:

- Model structure selection;
- State estimation;
- Parameter estimation.

These three phases are elaborated in the next sections.

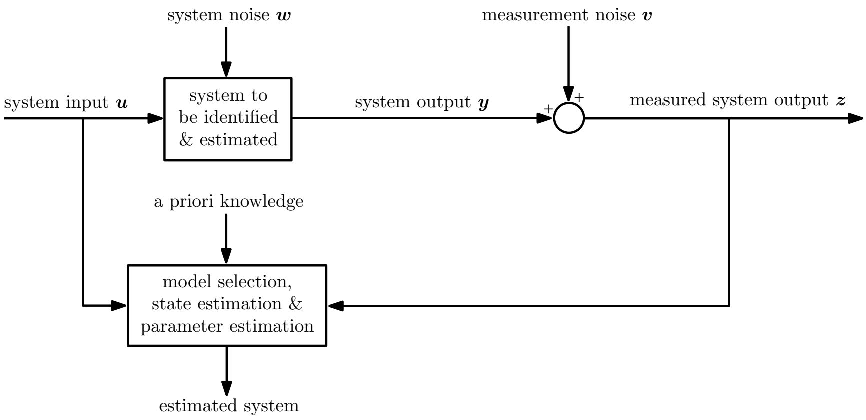

Figure A-6: General overview of the setup of system identification.

Model structure selection

The aircraft model describes the dynamic motion of the aircraft. Popular types of models are state space models, differential equations and transfer functions (Lombaerts, 2010). These models can be linear or nonlinear, time-invariant or time-varying, continuous or discrete and deterministic or stochastic. The choice of model depends on for example the equipment on board of the aircraft, the required accuracy and the choice whether or not to consider Gaussian processes. Independent of the type of model, three different modeling approaches can be distinguished (van Oort, 2011; de Visser, 2012):

White-box models are fully derived by first principles and assume underlying physics are completely understood. All equations and parameters of these models can be determined by theoretical modeling. An example of a white-box model are the rotational kinematic equations, which are essentially a transformation between two reference frames. The advantage of using white-box models is that they have a high prediction power and are valid for the complete operating domain of the system.

Black-box models are solely based on input-output measurements of the real system. The model structure as well as the parameters are determined from experimental modeling. The advantage of black-box models is that no knowledge of the physical workings of the system is required. However, the disadvantage of such models is that they are only valid inside the domain of the given input data, because the prediction power is generally difficult or impossible to verify. An example of black-box modeling are neural networks, see for instance (Kim & Calise, 1997).

Gray-box models combine the strengths of white and black-box models. These models are based on the integration of physical principles that are known together with input-output measurements. An example are the aerodynamic model equations, where we assume a structure of the forces and moments based on a priori knowledge, and subsequently determine the aerodynamic coefficients by using collected measurement data.

An important criterion in model structure selection is the principle of Parsimony (also known as Occam's razor), which seeks for a trade-off between good data fitting and prediction capabilities (Lombaerts, 2010).

> *Principle of parsimony: if there are two mathematical models to represent the same system with equal accuracy, then the model with the fewest parameters is preferable.*

By applying this principle we try to avoid *overfitting* of the measurement data, which could result in unnecessary complexity and poor prediction capabilities of the model.

One method for on-line aerodynamic model structure selection is called the Ordinary Polynomial Basis Based (OPBB) identification method (van Oort, 2011; Sun, 2014). In this technique a regressor is selected from a pre-determined regressor pool on basis of the output fitting error. In (van Oort, 2011) the whole flight envelope is split into partitions with locally valid models in order to reduce the computational load of the model structure selection. The model structure is recursively and locally updated during flight to obtain an accurate fit with the measurement data. Continuity in between the local models is achieved by using smooth interpolation functions. In (de Visser, 2011) multivariate simplex spline functions are used as model structure. These splines consist of a geometric component and a polynomial component. Current research at the Delft University of Technology (DUT) is aimed at optimizing the B-coefficients and vertex coordinates of these simplex splines.

State estimation

A realistic system, i.e. a system including system and sensor noise, can be represented by the following equations (de Visser, 2011, 2012):

$$\dot{\boldsymbol{x}}(t) = \boldsymbol{f}(\boldsymbol{\theta}(t), \boldsymbol{x}(t), \boldsymbol{u}(t), t) + G\boldsymbol{w}(t) \tag{A-1a}$$

$$\boldsymbol{z}(t) = \boldsymbol{h}(\boldsymbol{\theta}(t), \boldsymbol{x}(t), \boldsymbol{u}(t), t) + \boldsymbol{v}(t)\,, \tag{A-1b}$$

where $\boldsymbol{x}$ is the state vector, $\boldsymbol{f}$ is the system model, $\boldsymbol{\theta}$ is the parameter vector, $\boldsymbol{u}$ is the control input, G is the system noise input matrix, $\boldsymbol{w}$ is the system noise, $\boldsymbol{z}$ is the measured system output, $\boldsymbol{h}$ is the observation model and $\boldsymbol{v}$ is the measurement noise. State estimation is the technique in which we search for the best estimate of the states $\boldsymbol{x}$ while the parameters $\boldsymbol{\theta}$ are known. This is achieved by making use of the measured system inputs $\boldsymbol{u}$ and outputs $\boldsymbol{z}$ (see Figure A-6).

State estimation is necessary because the system's controller requires accurate knowledge of the states for adequate tracking performance and to restrain the aircraft to its safe operating envelope. Sensors alone are not sufficient for this purpose, because these measurements contain biases and noise. Moreover, important aircraft states like the true geometric angle of attack and angle of sideslip are not measurable directly (Mulder, Chu, Sridhar, Breeman, & Laban, 1999). At last, by combining different sensors such as Global Positioning System (GPS) and inertial sensors, more accurate estimates can be obtained.

If Eq. (A-1) is a linear system, a Kalman Filter (KF) can be used to estimate the states based on past and present measurements of input $\boldsymbol{u}(t)$ and output $\boldsymbol{z}(t)$. By applying a KF (see for instance (Kalman, 1960; de Visser, 2012)), a weighted least-squares estimate is obtained by minimizing a quadratic cost function that penalizes the state prediction error and the measurement prediction error. The selected weight depends on the uncertainty in the measurements. The KF obtains an optimal estimate of the states when (1) the model perfectly matches the system, (2) the noise is white and (3) the covariances are exactly known (Kalman, 1960).

The Extended Kalman Filter (EKF) has been developed because the KF only applies to linear systems, while most systems for aerospace applications turn out to be nonlinear. The EKF is a non-optimal extension of the KF to nonlinear systems of the form Eq. (A-1). This filter is a recursive estimator and linearizes the system at each time-step and subsequently applies the regular KF to obtain the state estimates. The main disadvantage of the EKF is that the linearization of the system at each time-step can introduce large errors, which generally leads to sub-optional performance and sometimes even divergence (Wan & Van Der Merwe, 2000).

The approximation issues of the EKF are addressed in the Iterated Extended Kalman Filter (IEKF) (see (Lombaerts, Huisman, et al., 2009; de Visser, 2011, 2012)) and the Unscented Kalman Filter (UKF) (see (Wan & Van Der Merwe, 2000; Zhan & Wan, 2007)). The IEKF uses iterations to compensate for the inaccuracies resulting from the linearization (de Visser, 2011). The UKF makes use of sample points (also known as sigma points) that are propagated through the non-linear system to achieve a better level of accuracy compared to the EKF at a comparable level of complexity (Wan & Van Der Merwe, 2000). Because the UKF avoids the cumbersome evaluation of Jacobian and Hessian matrices, the algorithm is generally easier to implement. Finally, in (Zhan & Wan, 2007) the Iterated Unscented Kalman Filter (IUKF) is developed, which is based on the IEKF and UKF. The IUKF further improves the tracking performance and robustness of the state estimator, while having a similar computational complexity as that of the UKF and IEKF.

Parameter estimation

Parameter estimation is the technique in which we search for the best estimate of the parameters $\boldsymbol{\theta}$ while the states $\boldsymbol{x}$ are known. This is achieved by making use of the measured system inputs $\boldsymbol{u}$ and outputs $\boldsymbol{z}$ (see Figure A-6). Note that parameter estimation is the inverse problem of state estimation. Estimation of parameters is necessary in order to derive accurate mathematical models of aircraft, which are required for simulators, model-based flight control systems and health monitoring algorithms. These parameter estimates are generally obtained by synthesis of Computational Fluid Dynamics (CFD), wind tunnel measurements and flight test data and result in a nominal aircraft model. For AFTFC systems fault-induced changes in parameters should be detected and estimated in real-time in order to enhance the survivability of damaged aircraft.

A simple form of parameter estimation can be seen in Figure A-7, in which the slope and the intercept of the straight line are the two parameters to be estimated based on measurements. A standard approach to obtain this approximation is Least-Squares (LS), in which the best fit is obtained by minimizing the sum of squared residuals, called the cost function. The LS method is credited to Carl Friedrich Gauss, who already applied this method early in the 19th century to calculate the orbits of celestial bodies (Eason, 1976).

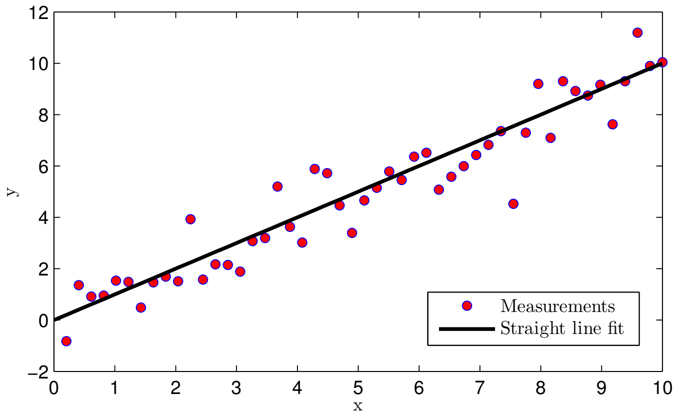

Figure A-7: Simulated measurement data. A typical problem would be to estimate the slope and the intercept of the straight line by minimizing some function of the error between model and measurement data.

Least-Squares can be applied in an on-line fashion by using the efficient Recursive Least-Squares (RLS) algorithm (see for instance (Li, 1999)). In (Lauzon & Bates, 1991; Lombaerts, Smaili, et al., 2009; Lombaerts, Huisman, et al., 2009) RLS has been applied to estimate time-varying parameters. In (Farrell et al., 2004; Choi & Bang, 2011; Farrell et al., 2012) Tuning Functions (TFs) in combination with a Backstepping (BS) control law are used to guarantee stability of a nonlinear system with parametric uncertainties. The parameter estimates converge to the real parameters when a "sufficiently rich" reference signal is injected. In (Astolfi & Ortega, 2003; Karagiannis & Astolfi, 2008b, 2008a, 2010; Sonneveldt, Oort, Chu, & Mulder, 2010; Hu & Zhang, 2013) a parameter estimator based on Immersion and Invariance (I&I) is used to guarantee global asymptotic stability of the closed-loop system and parameter convergence for uncertain nonlinear systems.

Note that in order to obtain satisfactory closed-loop performance, i.e. for example a zero steady-state error, it is not necessary that the parameters converge to their true values (Narendra, 1994). However, if we make use of a CA module (see Appendix A-1-2), accurate estimates of some of the parameters might be required.

Two important notions in parameter estimation are *identifiability* of the parameters and *richness* of the input. Model parameters are identifiable when they can be *uniquely* estimated from a set of observations (Pronzato & Pázman, 2013). In general it is very difficult to solve the problem of parameter identifiability of highly nonlinear systems (Serban & Freeman, 2001). One approach based on computing algorithms is presented in (Floret-Pontet & Lamnabhi-Lagarrigue, 2002). Identifiability of a parametric model not only depends on the model structure, but also on the input signal. Richness of the input, also known as the requirement of Persistent Excitation (PE), basically means that the input signal must "contain enough frequencies" for the parameter estimation error to converge to zero (Boyd & Sastry, 1986).

In (Chowdhary & Jategaonkar, 2010; Edwards, Lombaerts, & Smaili, 2010) a method is presented to simultaneously tackle the problem of state and parameter estimation by transforming the parameter estimation problem into a state estimation problem. This is accomplished by augmenting the state vector $\boldsymbol{x}$ with the unknown parameter vector $\boldsymbol{\theta}$. In (Chowdhary & Jategaonkar, 2010) the EKF and UKF have been used for recursive parameter estimation. It has been found that the UKF filter is the fastest in terms of convergence, but is also the costliest in terms of computational power.

An alternative to the joint-method for state and parameter estimation is presented in (Laban, 1994; Mulder et al., 1999; Lombaerts, Smaili, et al., 2009; Lombaerts, Huisman, et al., 2009; Sun, 2014). In these references the Two-Step Method (TSM), developed at the DUT, is applied that separates the steps of state and parameter estimation. First, an IEKF is used to estimate the states based upon redundant, contaminated information from all sensors. The system model that is used within the IEKF is the well-known nonlinear aircraft kinematics model. The output of the first step, the filtered and estimated aircraft states, provide the input to the next step. In this second step a RLS is used to estimate the aerodynamic model parameters. A trigger for re-identification is implemented that artificially increases the covariance matrix when the current model is not reliable anymore. By resetting this covariance matrix the parameter estimates are more influenced by new measurements, resulting in faster adaptation. In (Lombaerts, Smaili, et al., 2009; Lombaerts, Huisman, et al., 2009) it is shown that the TSM combined with a NDI controller is successful in recovering damaged aircraft. Moreover, the TSM has proven to be implementable in real-time by using standard desktop computers.

A-3 Nonlinear Flight Control

Traditionally, and even today, gain-scheduling of linear feedback controllers is applied to achieve stabilization and satisfactory tracking performance of aircraft over a wide range of flight conditions. Because the dynamic behavior of an aircraft changes throughout the flight envelope, many different linear flight control laws must be designed. In flight envelope regions with significant nonlinearities, or in case of failures (e.g. structural damage), gain-scheduling is not able to provide good performance because it is based on linearized and nominal aircraft models (Sonneveldt, 2010; Falkena, 2012). Next, it is difficult to guarantee satisfactory stability and tracking performance over the complete flight envelope (Sonneveldt, 2010). At last, gain-scheduling of linear controllers is an extensive task. The main reason why this control strategy is still applied nowadays is because it is based on well-developed classical linear control theory. Furthermore, certification authorities are used to dealing with them. In (Jacklin, 2008) this certification gap in adaptive flight control software is discussed. Furthermore, research efforts are considered that will likely be needed to make adaptive flight control become certifiable.

The nonlinear control methods that are discussed in this section do not suffer from the drawbacks of gain-scheduled linear controllers. The DUT has performed extensive research on these advanced control laws since the last decade. In this section the following two prominent nonlinear control methods are discussed:

1. Nonlinear Dynamic Inversion;
2. Backstepping.

A-3-1 Nonlinear Dynamic Inversion

The concept of NDI is to cancel the nonlinear aircraft dynamics, resulting in a system that behaves like a pure integrator that is easily controllable. One of the main advantages of NDI is the absence of any need for gain scheduling over the flight envelope (Lombaerts, Smaili, et al., 2009). Another advantage is a complete decoupling between the input-output relations. Nonlinear Dynamic Inversion is a special form of feedback linearization suited for flight control applications (Sonneveldt, 2010). This nonlinear control method has successfully been applied during actual flight tests already in the late seventies (Meyer, Su, & Hunt, 1984; Kim & Calise, 1997). Incorporation of pilot inputs into the design technique was accomplished in (Wehrend, 1979).

Nonlinear Dynamic Inversion has been applied in two different ways by the DUT:

1. Conventional Nonlinear Dynamic Inversion;
2. Incremental Nonlinear Dynamic Inversion.

These two nonlinear flight control methods are discussed in the next two sections.

Conventional nonlinear dynamic inversion

To illustrate the basic concept behind NDI we consider the following Multiple-Input and Multiple-Output (MIMO) system:

$$\dot{\boldsymbol{x}} = \boldsymbol{f}(\boldsymbol{x}) + G(\boldsymbol{x})\boldsymbol{u} \tag{A-2a}$$

$$\boldsymbol{y} = \boldsymbol{x}\,, \tag{A-2b}$$

where $\boldsymbol{x} \in \mathbb{R}^n$ is the state vector, $\boldsymbol{f}$ is a known vector field on $\mathbb{R}^n$, $G \in \mathbb{R}^{n\times m}$ is a known matrix whose columns are vector fields, $\boldsymbol{u} \in \mathbb{R}^m$ is the control input vector and $\boldsymbol{y} \in \mathbb{R}^n$ is the system output vector. The control task is to make sure that the output $\boldsymbol{y}$ follows a predefined reference output $\boldsymbol{y}_{ref}$, whose first derivative is assumed to be known and bounded.

If the matrix $G(\boldsymbol{x})$ is non-singular (i.e. invertible), all nonlinearities can be canceled by selecting the following NDI control input:

$$\boldsymbol{u} = G^{-1}(\boldsymbol{x})\left[\boldsymbol{v} - \boldsymbol{f}(\boldsymbol{x})\right]\,, \tag{A-3}$$

where $\boldsymbol{v}$ is the new input, also known as *virtual* control. Substituting control law (A-3) in Eq. (A-2) yields

$$\dot{\boldsymbol{x}} = \dot{\boldsymbol{y}} = \boldsymbol{v}\,. \tag{A-4}$$

As we can see, by canceling the nonlinear dynamics, the resulting system behaves like a pure integrator. Now the vector to be controlled $\boldsymbol{y}$ can easily be stabilized or tracked by using, for example, a proportional controller based on the tracking error $\boldsymbol{e} = \boldsymbol{y}_{ref} - \boldsymbol{y}$. Selecting the virtual control law as

$$\boldsymbol{v} = \dot{\boldsymbol{y}}_{ref} + K\boldsymbol{e}\,, \tag{A-5}$$

results in exponentially stable error dynamics

$$\dot{\boldsymbol{e}} = -K\boldsymbol{e}\,, \tag{A-6}$$

where K is a square matrix with positive diagonal entries. These control gains can be selected in a way to obtain favorable closed-loop performance based on well-known classical *linear* control theory.

From Figure A-8 can be seen that the entire control problem basically consists of two parts: the inner linearization loop based on Eq. (A-3) and an outer control loop based on Eq. (A-5) which is used to stabilize the pure integrator dynamics.

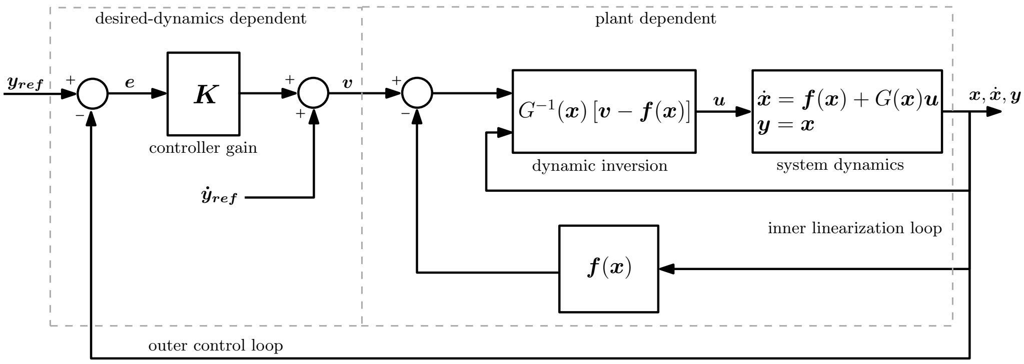

Figure A-8: Tracking of a Multiple-Input and Multiple-Output system with Nonlinear Dynamic Inversion, based on (Acquatella et al., 2012).

Note that system (A-2) is affine in the control vector $\boldsymbol{u}$, and therefore no nonlinear solvers are required to obtain control input (A-3). In (Hovakimyan, Lavretsky, & Sasane, 2007) a method is presented for dynamic inversion of *nonaffine*-in-control systems via Time-Scale Separation (TSS).

When the first-order time derivative of the control variable vector $\boldsymbol{y}$ does not contain the control input $\boldsymbol{u}$, subsequent time derivatives of the control variable vector should be derived until the control input appears. Then, similar to Eq. (A-3), we can cancel the nonlinearities and define the virtual input to stabilize the resulting linear system. Examples of this approach can be found in the literature (Looye, 2008; Sieberling, Chu, & Mulder, 2010).

In general, the number of physical control effectors on aircraft exceeds the number of variables to be controlled. In this case G^{-1} may be interpreted as a pseudoinverse of matrix G. In (Lombaerts, 2010) methods are described to handle the four cases that can be considered for calculation of this inverse. These four cases are the over-determined solution, the exactly determined solution, the under-determined solution and the singular matrix.

In the derivation of control law (A-3), we have implicitly made the following two assumptions (Acquatella et al., 2012):

1. The model of the system is accurately known;
2. There is complete and accurate knowledge of all system states.

If the first assumption is not satisfied, the (partially) unknown nonlinear dynamics cannot be completely canceled, and therefore system identification or robust control will have to be applied. If the sensors cannot provide accurate knowledge of all the states, nonlinear observers or estimators have to be implemented.

In (Reiner et al., 1996) NDI has been augmented with a linear μ-controller that enhances robustness to parameter variations and requires no gain scheduling with flight condition. This design technique appears to provide excellent performance, is robust to parametric uncertainties and results in a low-order linear controller. However, this design only guarantees stability of parametric uncertainties up to 20%. Therefore, it is not guaranteed that this design can anticipate for modeling errors or larger parametric uncertainties.

An adaptive tracking control architecture is discussed in (Kim & Calise, 1997) that combines NDI and Neural Networks (NNs). The NNs are used to represent the nonlinear inverse transformation. These NNs are able to learn on-line and therefore can be used to compensate for the nominal inversion error, which may arise from imperfect modeling or sudden changes in aircraft dynamics. On basis of simulations for an F-18 aircraft model, it is concluded that NDI augmented with on-line adaptive NNs shows outstanding potential for rapid and accurate adaptation in case of sudden changes in aircraft configuration.

In (Lombaerts, Smaili, et al., 2009; Lombaerts, Huisman, et al., 2009) NDI control has been augmented with an Aircraft State Estimator (ASE) and Aerodynamic Model Identification (AMI). The resulting control method is referred to as ANDI. A dual NDI loop has been implemented, consisting of an inner-loop body angular rate and an outer-loop sideslip angle control loop. In this research the ASE and AMI are performed in real-time in two separate steps. First, an IEKF is used that merges redundant and contaminated data resulting in accurate knowledge of the system states. Next, the a priori aerodynamic model is updated by means of an RLS operation that uses the accurate state information obtained from the first step. Physical experiments of this control strategy on the SIMONA research simulator of the DUT have shown that this approach greatly increases the ability to reconfigure aircraft in presence of component as well as structural failures.

Incremental nonlinear dynamic inversion

In (Sieberling et al., 2010; Acquatella et al., 2012; Vlaar, 2014) Incremental Nonlinear Dynamic Inversion (INDI) has been applied in order to improve the robustness of the closed-loop system with respect to conventional NDI-based control. This is achieved by reducing its dependency on the exact knowledge of the plant dynamics. To illustrate the basic concept behind INDI we again consider the following system:

$$\dot{\boldsymbol{x}} = \boldsymbol{f}(\boldsymbol{x}) + G(\boldsymbol{x})\boldsymbol{u} \tag{A-2a revisited}$$

$$\boldsymbol{y} = \boldsymbol{x}\,, \tag{A-2b revisited}$$

where $\boldsymbol{x} \in \mathbb{R}^n$ is the state vector, $\boldsymbol{f}$ is a smooth vector field on $\mathbb{R}^n$, $G \in \mathbb{R}^{n \times m}$ is a known matrix whose columns are smooth vector fields, $\boldsymbol{u} \in \mathbb{R}^m$ is the control input vector and $\boldsymbol{y} \in \mathbb{R}^n$ is the system output vector. It is assumed that the output $\boldsymbol{y}$ is the vector to be controlled.

Taking the first-order Taylor series expansion of Eq. (A-2a) around the current solution $[\boldsymbol{x}_0, \boldsymbol{u}_0]$ results in

$$\dot{\boldsymbol{x}} \cong \boldsymbol{f}(\boldsymbol{x}_0) + G(\boldsymbol{x_0})\boldsymbol{u}_0 + \frac{\partial}{\partial \boldsymbol{x}} \Big[\boldsymbol{f}(\boldsymbol{x}) + G(\boldsymbol{x})\boldsymbol{u}\Big]\Big|_{\substack{\boldsymbol{x}=\boldsymbol{x}_0 \\ \boldsymbol{u}=\boldsymbol{u}_0}} (\boldsymbol{x} - \boldsymbol{x}_0) + \frac{\partial}{\partial \boldsymbol{u}} \Big[G(\boldsymbol{x})\boldsymbol{u}\Big]\Big|_{\substack{\boldsymbol{x}=\boldsymbol{x}_0 \\ \boldsymbol{u}=\boldsymbol{u}_0}} (\boldsymbol{u} - \boldsymbol{u}_0)\,. \tag{A-8}$$

The linearization error is small when the sampling rate is sufficiently high. Eq. (A-8) can be written as

$$\dot{\boldsymbol{x}} \cong \dot{\boldsymbol{x}}_0 + A_0 \Delta \boldsymbol{x} + B_0 \Delta \boldsymbol{u}\,, \tag{A-9}$$

where

$$\Delta \boldsymbol{x} = \boldsymbol{x} - \boldsymbol{x}_0\,, \quad \Delta \boldsymbol{u} = \boldsymbol{u} - \boldsymbol{u}_0 \tag{A-10a}$$

$$A_0 = \frac{\partial}{\partial \boldsymbol{x}} \Big[\boldsymbol{f}(\boldsymbol{x}) + G(\boldsymbol{x})\boldsymbol{u}\Big]\Big|_{\substack{\boldsymbol{x}=\boldsymbol{x}_0 \\ \boldsymbol{u}=\boldsymbol{u}_0}} \tag{A-10b}$$

$$B_0 = \frac{\partial}{\partial \boldsymbol{u}} \Big[G(\boldsymbol{x})\boldsymbol{u}\Big]\Big|_{\substack{\boldsymbol{x}=\boldsymbol{x}_0 \\ \boldsymbol{u}=\boldsymbol{u}_0}} = G(\boldsymbol{x}_0)\,. \tag{A-10c}$$

The variables $\Delta \boldsymbol{x}$ and $\Delta \boldsymbol{u}$ are known as respectively the *incremental* state vector and the *incremental* control input. Similar as for conventional NDI-based control we can now invert the dynamics to obtain an expression for the incremental input:

$$\Delta \boldsymbol{u} = B_0^{-1} \Big[\boldsymbol{v} - \big(\dot{\boldsymbol{x}}_0 + A_0 \Delta \boldsymbol{x}\big)\Big] = G^{-1}(\boldsymbol{x}_0) \Big[\boldsymbol{v} - \big(\dot{\boldsymbol{x}}_0 + A_0 \Delta \boldsymbol{x}\big)\Big]\,, \tag{A-11}$$

where $\boldsymbol{v}$ is the new (virtual) input. Substituting the incremental control law (A-11) in Eq. (A-9) results in

$$\dot{\boldsymbol{x}} = \dot{\boldsymbol{y}} \cong \boldsymbol{v}\,. \tag{A-12}$$

As we can see, by canceling the dynamics, the resulting system behaves like a pure integrator when the sampling rate is sufficiently high. Similar as for conventional NDI, the vector to be controlled $\boldsymbol{y}$ can easily be stabilized or tracked by using, for example, a proportional controller based on the tracking error. Note that if B_0 is a non-square matrix or a square matrix without full rank, some form of control allocation would be required, see for instance (Enns, 1998; Lombaerts, 2010).

The control law (A-11) results in increments of control commands; these changes must be added to the current input to obtain the full input signal. If we assume a sufficiently time-scale separated system, that is the increment in state $\Delta \boldsymbol{x}$ is much smaller than the increment in both state derivative $\Delta \dot{\boldsymbol{x}}$ and input $\Delta \boldsymbol{u}$, we can neglect the former (Falkena, 2012; Sieberling et al., 2010; Acquatella et al., 2012; Simplício, Pavel, Kampen, & Chu, 2013). This is allowed for many aerospace applications because the deflections of the control surfaces directly effect the angular accelerations, while the angular rates only change by integrating these angular accelerations. Hence Eqs. (A-9) and (A-11) can be further simplified as respectively

$$\dot{\boldsymbol{x}} \cong \dot{\boldsymbol{x}}_0 + B_0 \Delta \boldsymbol{u} \tag{A-13}$$

$$\Delta \boldsymbol{u} = G^{-1}(\boldsymbol{x}_0) \left[\boldsymbol{v} - \dot{\boldsymbol{x}}_0 \right] . \tag{A-14}$$

By comparing respectively the conventional NDI-based and INDI control laws for a time-scale separated system of the form (A-2):

$$\boldsymbol{u} = G^{-1}(\boldsymbol{x}) \left[\boldsymbol{v} - \boldsymbol{f}(\boldsymbol{x}) \right] \tag{A-3 revisited}$$

$$\boldsymbol{u} = \boldsymbol{u}_0 + G^{-1}(\boldsymbol{x}_0) \left[\boldsymbol{v} - \dot{\boldsymbol{x}}_0 \right] , \tag{A-14 revisited}$$

we can see that the incremental controller does not rely on exact knowledge of the system dynamics $\boldsymbol{f}(\boldsymbol{x})$, but instead on the current control input $\boldsymbol{u}_0$ and state derivative $\dot{\boldsymbol{x}}_0$. Therefore, by implementing INDI instead of conventional-NDI, the system robustness against model mismatch and model uncertainties is largely increased. However, because INDI relies on more measurements (or estimates) compared to conventional-NDI, sensor redundancy and failure detection methods now become even more important.

In (Vlaar, 2014) an INDI rate controller has been implemented and tested during actual flights on an electrically powered fixed wing aircraft. In this research the angular accelerations and current actuator positions are both estimated, because the Unmanned Aerial Vehicle (UAV) was not equipped with sensors to measure these directly. The angular accelerations were obtained by a technique which differentiates the measured angular rates. The current actuator positions were estimated on basis of an actuator model. These flight tests have proven that INDI using estimated signals is feasible and leads to good tracking performance.

The disadvantage of NDI or INDI in combination with a separate identifier for system identification is that the certainty equivalence property does not hold for nonlinear systems (Krstić et al., 1995; Sonneveldt, 2010; van Oort et al., 2007). Therefore, the closed-loop system might become unstable when the parameter estimates do not exactly equal the real parameters. One way to achieve strong parametric robustness properties is to apply robust control, as has been done in for example (Reiner et al., 1996). However, robust control tends to yield rather conservative control laws, resulting in poor closed-loop performance (Sonneveldt, 2010; van Oort, Chu, & Mulder, 2006). Another disadvantage of NDI and INDI is the lack of any inherent stability characteristics in the controller's design procedure, which is likely to cause problems during the certification process of the controller (Ali, 2013). Therefore a better way to deal with large model uncertainties is to integrate the controller and identifier design, which is possible by using ABS (van Oort et al., 2007; Sonneveldt, 2010; Choi & Bang, 2011).

A-3-2 Backstepping

Backstepping is a recursive, Lyapunov-based, nonlinear design method. The concept of BS is to design a controller in a recursive way by considering some of the state variables as "virtual controls" and designing intermediate control laws for these, starting at the scalar equation which is separated by the largest number of integrations from the control input (Sonneveldt, 2010). Backstepping is a design method that is, in contrary to NDI, based on Lyapunov stability theory. This can be a major benefit for certification of BS control laws, because the goals of global asymptotic stabilization and tracking can be guaranteed. Another advantage of BS is that it is applicable to a broad class of systems. At last, BS is flexible in the choice of control law and can avoid wasteful cancellations as opposed to NDI (Sonneveldt, 2010).

Backstepping has been applied in the beginning of the 1990s as a recursive design for systems with nonlinearities not constrained by linear bounds. Not much later, adaptive and robust BS has been applied to achieve global stabilization in the presence of unknown parameters (Kokotović & Arcak, 2001). The BS design method is discussed in detail in the literature (Khalil & Grizzle, 2002; Sonneveldt, 2010; Ali, 2013). To illustrate the basic concept behind BS we consider the following pure feedback (lower triangular) system:

$$\dot{x}_1 = f_1(x_1) + g_1(x_1)x_2 \tag{A-15a}$$
$$\dot{x}_2 = f_2(x_1, x_2) + g_2(x_1, x_2)u \tag{A-15b}$$
$$y = x_1 \,, \tag{A-15c}$$

where $x_i \in \mathbb{R}$ for $i = 1, 2$ are the state variables, f_i and g_i for $i = 1, 2$ are known functions, $u \in \mathbb{R}$ is the physical control input and $g_i \neq 0$ for $i = 1, 2$. It is assumed that the first-order derivatives of f_1 and g_1 are continuous, that is f_1 and $g_1 \in C^1$. The control task is to make sure that the output y follows a predefined reference output y_r, whose first and second-order time derivative are assumed to be known and bounded.

We start the BS procedure by defining the tracking errors as

$$z_1 = x_1 - y_r \tag{A-16a}$$
$$z_2 = x_2 - \alpha_1 \,, \tag{A-16b}$$

where x_2 will be considered as virtual control and α_1 is the stabilizing control law yet to be defined. We start by considering the first subsystem (A-15a), which is the equation separated by the largest number of integrations from the control input u. This subsystem can now be rewritten in terms of the error states:

$$\dot{z}_1 = f_1 + g_1 \left(z_2 + \alpha_1\right) - \dot{y}_r \,. \tag{A-17}$$

To stabilize this nonlinear system, a Control Lyapunov Function (CLF) $\mathcal{V}$ is selected and the time derivative of this CLF will be rendered negative definite by proper selection of the stabilizing control law α_1 and real physical input u in a later stage. The first CLF is selected as

$$\mathcal{V}_1(z_1) = \frac{1}{2} z_1^2 \,. \tag{A-18}$$

Taking the time derivative of this CLF along the trajectories of Eq. (A-17) results in

$$\dot{\mathcal{V}}_1 = z_1 \left[f_1 + g_1 \left(z_2 + \alpha_1\right) - \dot{y}_r\right] \,. \tag{A-19}$$

An obvious choice for a stabilizing control law α_1 is

$$\alpha_1 = g_1^{-1} \left(-c_1 z_1 - f_1 + \dot{y}_r\right) \,, \tag{A-20}$$

which results in the following expression for $\dot{\mathcal{V}}_1$:

$$\dot{\mathcal{V}}_1 = -c_1 z_1^2 + g_1 z_1 z_2 \, . \tag{A-21}$$

Note that $\dot{\mathcal{V}}_1$ is currently not a negative definite function, due to presence of the cross term $g_1 z_1 z_2$. This term will be removed in the next design step.

Now we consider the dynamics of the second tracking error:

$$\dot{z}_2 = f_2 + g_2 u - \dot{\alpha}_1 \, . \tag{A-22}$$

Augmenting the earlier CLF to penalize the second error state as well results in

$$\mathcal{V}_2(z_1, z_2) = \frac{1}{2} z_1^2 + \frac{1}{2} z_2^2 \, . \tag{A-23}$$

Taking the time derivative along the solutions of Eqs. (A-17) and (A-22) yields

$$\dot{\mathcal{V}}_2 = -c_1 z_1^2 + g_1 z_1 z_2 + z_2 \left[f_2 + g_2 u - \dot{\alpha}_1 \right] \, . \tag{A-24}$$

By selecting the following physical control law:

$$u = g_2^{-1} \left[-c_2 z_2 - f_2 + \dot{\alpha}_1 - z_1 g_1 \right] \, , \tag{A-25}$$

we yield the CLF negative definite

$$\dot{\mathcal{V}}_2 = -c_1 z_1^2 - c_2 z_2^2 \, . \tag{A-26}$$

According to the theorem of *LaSalle-Yoshizawa* (see e.g. Theorem B.9 in (Sonneveldt, 2010)) the equilibrium $\boldsymbol{z} = \mathbf{0}$ is globally uniformly asymptotically stable when $c_1 > 0$ and $c_2 > 0$, implying that the reference output state y_r is successfully tracked by y, that is:

$$\lim_{t \to \infty} \left[y_r - y \right] = 0 \, . \tag{A-27}$$

Note that the time derivative of $\alpha_1(x_1, y_r, \dot{y}_r)$ which appears in the control law (A-25) can be computed analytically from Eq. (A-20):

$$\begin{aligned} \dot{\alpha}_1 &= \frac{\partial \alpha_1}{\partial x_1} \dot{x}_1 + \frac{\partial \alpha_1}{\partial y_r} \dot{y}_r + \frac{\partial \alpha_1}{\partial \dot{y}_r} \ddot{y}_r \\ &= \frac{\partial \alpha_1}{\partial x_1} \left[f_1(x_1) + g_1(x_1) x_2 \right] + \frac{\partial \alpha_1}{\partial y_r} \dot{y}_r + \frac{\partial \alpha_1}{\partial \dot{y}_r} \ddot{y}_r \, . \end{aligned} \tag{A-28}$$

Calculating the time derivatives of the stabilizing functions can be complicated and tedious in applications where the number of states is large. In (Farrell, Polycarpou, Sharma, & Dong, 2009) Command-Filtered BS is presented, which obviates the need for analytic computation of stabilizing function derivatives. Other advantages of this approach are the elimination of the Backstepping's restriction to nonlinear systems of a lower triangular form and to improve the performance of parameter update laws, by implementing constraints on the (virtual) controls (Farrell et al., 2009; Sonneveldt, 2010).

In (van Oort et al., 2007) the BS procedure has been augmented with an identification module based on RLS. The resulting control approach has been applied to control a nonlinear missile model. The combination of the BS controller and the identification module results in ABS that guarantees global boundedness of the tracking errors despite parametric uncertainties. The RLS implementation consists of a forgetting factor, thereby speeding up the identification process by exponential data weighing. A change detection algorithm is implemented to reset the covariance matrix in order to rapidly respond to sudden changes in the system's behavior. The resulting controller shows excellent tracking performance before and after a sudden failure in the system dynamics. Furthermore, the estimated parameters converge to their true values after a certain time of maneuvering.

Backstepping has been augmented with command filters and Lyapunov-based on-line parameter update laws in (Sonneveldt et al., 2007; Choi & Bang, 2011). The command filters are used for constraint handling and to obviate the need for analytic computation of the virtual control derivatives. In this first reference nonlinear Adaptive Control method has been applied to an F-16 aircraft model. Neural Networks are used inside the parameter update laws to approximate the uncertain aerodynamic forces and moments. Computer simulations have indicated that good tracking performance can be obtained even when large sudden actuator or symmetric structural failures occur. It was found that the main drawback of the implementation with Lyapunov-based on-line parameter update laws is that the experimental tuning of the update gains is a tedious task.

In (Choi & Bang, 2011) a similar control strategy without NNs has been implemented for a quadrotor UAV. In this reference the controller is tuned by subsequently tuning the control law gains, the command filter parameters and finally the update law gains. Computer simulations have shown that the estimated parameters converge to values close to the true parameters. However, the main purpose of the estimates is to enhance controller performance, and not necessarily good parameter estimates. Computer simulations demonstrate that this control approach results in good tracking performance even under physically constrained inputs and uncertainties.

In (Sonneveldt, 2010) an Inverse Optimal ABS control approach is developed. This control strategy is optimal with respect to some meaningful cost function in order to simplify the tuning of the ABS controller. The resulting controller possesses certain robustness properties, but the numerical sensitivity makes this approach less suitable than the other ABS controllers for complex flight control design problems (Sonneveldt, 2010). Moreover, the complexity of this approach does not simplify the tuning of the controller and update laws.

Backstepping has been augmented with a parameter estimator based on I&I in (Hu & Zhang, 2013; Ali et al., 2014). In both references use is made of a command filter for constraint handling and to obviate the need for analytic computation of the virtual control derivatives. In the first reference this nonlinear adaptive control method has been applied to a Vertical Take-Off and Landing (VTOL) vehicle. The designed I&I adaptive law guarantees that the mass' estimation error is a monotonically non-increasing function. Simulations have been run to illustrate the effectiveness of the BS controller with the I&I estimator.

In (Ali et al., 2014) the robustness properties of different BS flight controllers applied to an F-16 model are evaluated. An Incremental Backstepping (IBS) controller is derived that uses angular acceleration measurements and current actuator states to reduce the dependency on the on-board aircraft model. However, this controller still depends on a small portion of the aircraft model. An IBS augmented with an I&I estimator is shown to further improve the tracking performance in presence of parametric uncertainties related to the control effectiveness. However, the development of such an I&I identifier is rather complex. Moreover, the improvements in robustness appear to be marginal. According to (Ali, 2013; Ali et al., 2014) it is likely that better performance can be obtained when a more detailed regressor model is used as a function approximator for the I&I identifier.

In (Falkena et al., 2011, 2013; Galrinho et al., 2013; Galrinho, 2013; Tang, 2014) SBB has been applied, this BS based control strategy is based on the singular perturbation theory (see (Khalil & Grizzle, 2002)) and removes the dependency on the system dynamics by using measurements of the state derivatives. This is something we have earlier seen for IBS and INDI. However, the SBB controller uses even less model information compared to the incremental control laws. In (Falkena et al., 2011) an attitude rate controller is designed based on SBB. The only model-dependent part of the resulting control law is the *sign* of the control effectiveness matrix. Furthermore, the influence of sensor noise on the SBB controller has been addressed by computer simulations. It has been found that the influence of noise, including angular acceleration noise, on the system's response is small.

In (Falkena et al., 2013) an outer-loop based on BS is added to the SBB-based attitude rate loop to control the body orientation of a Piper Seneca II model. In both references the sign of the control effectiveness matrix is assumed to be known, however, a crude form of on-line aerodynamic model identification can be used to obtain this information in real-time (Lombaerts, Huisman, et al., 2009). In these references it is concluded that SBB provides good tracking performance with and without model uncertainties. Furthermore, because the SBB controller is Lyapunov-based, stability of the controlled system is guaranteed. The SBB approach makes use of a time-scale tuning parameter ϵ, which is in some articles considered to be a constant (Sun, 2014; Falkena et al., 2013), and in other publications a function of the Mach number (Galrinho, 2013; Galrinho et al., 2013).

Concluding, BS is a Lyapunov-based, nonlinear design method. Therefore the goals of global asymptotic stabilization and tracking can be guaranteed, which can be a major benefit for certification of these advanced control laws. Another advantage of BS-based control is that it is applicable to a broad class of systems. At last, BS is flexible in the choice of control law and can avoid wasteful cancellations as opposed to NDI (Sonneveldt, 2010). However, BS is sensitive to model uncertainties. As we have seen, this drawback can be mitigated by applying robust control or adaptive control that incorporates a parameter estimator, such as TF or I&I. A promising control strategy is SBB, because it almost completely removes the need for adaptation to uncertain parameters or unknown model structures. Because the flexible and Lyapunov-based BS control method offers many benefits compared to NDI and gain-scheduled linear control, the remainder of this thesis only focuses on reconfigurable *Backstepping* control laws.

Appendix B

Pendulum Model

The state space equations of a simple pendulum with a rigid, massless rod are given by (Khalil & Grizzle, 2002)

$$\dot{x}_1 = x_2 \tag{B-1a}$$

$$\dot{x}_2 = -\frac{g}{l}\sin(x_1) - \frac{k}{m}x_2 + \frac{1}{ml^2}u\,, \tag{B-1b}$$

where x_1 is the angle subtended by the rod and the vertical axis through the pivot point (Figure B-1). The length of the rod is denoted by l, m denotes the mass of the bob, g is the acceleration due to gravity, k is the coefficient of friction and u is the torque applied to the pendulum. The control task is to track the smooth reference state $x_{1,r}$ with the state x_1.

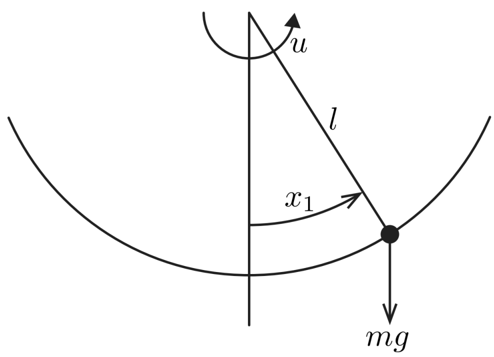

Figure B-1: Pendulum.

By introducing the following parameters for notational convenience:

$$\boldsymbol{\theta}_2 = \begin{bmatrix}\theta_{2,1} & \theta_{2,2} & \theta_{2,3}\end{bmatrix}^T = \begin{bmatrix}-\frac{g}{l} & -\frac{k}{m} & \frac{1}{ml^2}\end{bmatrix}^T\,, \tag{B-2}$$

we can write system (B-1) as

$$\dot{x}_1 = x_2 \tag{B-3a}$$

$$\dot{x}_2 = \theta_{2,1} \sin(x_1) + \theta_{2,2} x_2 + \theta_{2,3} u \,. \tag{B-3b}$$

In (Zinober & Owens, 2003) it is verified that system (B-3) is globally identifiable, indicating that the pendulum model is described by a unique parameter vector. This identifiability analysis is based on Lie derivatives (see (Floret-Pontet & Lamnabhi-Lagarrigue, 2002)).

In the next appendices controllers and parameter estimators will be designed for system (B-3) by neglecting the relationships of Eq. (B-2), i.e. uncertainties will be added to the elements of $\boldsymbol{\theta}_2$ independently of each other.

Appendix C

Backstepping Control

Backstepping (BS) is a recursive, Lyapunov-based, nonlinear design method. The main advantage of BS is that it is based on Lyapunov stability theory, and thereby guarantees the goals of global asymptotic stabilization and tracking (C-1). The concept of BS is to design a controller in a recursive way by considering some of the state variables as "virtual controls" and designing intermediate control laws for these, starting at the scalar equation which is separated by the largest number of integrations from the control input (C-2). In order to evaluate this nonlinear control approach, a BS control law is derived and simulated for the pendulum model (C-3).

C-1 Lyapunov Theory

In this section a brief overview of Lyapunov theory is given on which BS is based. A more extensive review of Lyapunov theory can be found in for example (Krstić et al., 1995; Khalil & Grizzle, 2002; Sonneveldt, 2010). First of all, the definitions of Lyapunov stability are introduced. Next, Lyapunov's direct method is discussed which can be applied to determine stability of nonlinear dynamical systems without explicitly solving the differential equations. At last, the Lyapunov theory is extended for control design in order to create a closed-loop system with desirable stability properties.

C-1-1 Lyapunov Stability

In this section we consider the nonlinear dynamical system

$$\dot{\boldsymbol{x}} = \boldsymbol{f}(\boldsymbol{x}), \quad \boldsymbol{x}(t_0) = \boldsymbol{x}_0\,, \tag{C-1}$$

where $\boldsymbol{x} \in \mathbb{R}^n$ is the state and $\boldsymbol{f}$ is locally Lipschitz in $\boldsymbol{x}$ (see definition 3.1 in (Sonneveldt, 2010)). We assume that system (C-1) has an equilibrium point $\boldsymbol{x}_e \in \mathbb{R}^n$ that by definition satisfies the relation $\boldsymbol{f}(\boldsymbol{x}_e) = \boldsymbol{0}$. Without loss of generality, we will assume that this equilibrium point is located at the origin, that is $\boldsymbol{x}_e = \mathbf{0}$. Note that any equilibrium of the system (C-1) can be shifted to the origin by a change of variables.

The equilibrium point $\boldsymbol{x}_e$ is *stable* when all solutions that start nearby $\boldsymbol{x}_e$ stay nearby this point, otherwise $\boldsymbol{x}_e$ is called *unstable*. The equilibrium point $\boldsymbol{x}_e$ is called *asymptotically stable* when the solutions that start nearby $\boldsymbol{x}_e$, converge to this equilibrium point as time approaches infinity. When this convergence takes place with an exponential rate, one speaks of *exponential stability*. In for example definition 3.2 of (Sonneveldt, 2010) and definition 4.1 of (Khalil & Grizzle, 2002) these notions are made more precise.

The *region of attaction* of an asymptotically stable equilibrium point is defined as the set of all initial conditions that converge to the given equilibrium point. When this domain of attraction is equal to $\mathbb{R}^n$, $\boldsymbol{x}_e$ is called *globally* asymptotically stable, otherwise $\boldsymbol{x}_e$ is called *locally* asymptotically stable. Note that if a system has more than one equilibrium point, none of the equilibrium points can be globally stable.

Another classification is that of *uniform* and *non-uniform* stable equilibrium points. An equilibrium point is uniformly (asymptotically) stable when $\boldsymbol{x}_e$ is (asymptotically) stable for all initial times t_0.

C-1-2 Lyapunov's Direct Method

The advantage of Lyapunov's direct method, also known as Lyapunov's second method, is that we can apply it to determine stability of system (C-1) without explicitly solving the differential equation. Lyapunov's direct method turns the question of determining stability into a search for a suitable Lyapunov function. The main difficulty of this method is to find such a Lyapunov function. Fortunately, approaches for searching Lyapunov functions exist and are discussed in for instance (Khalil & Grizzle, 2002).

We start by introducing the definitions for positive (semi-)definite and negative (semi-)definite functions (Sonneveldt, 2010):

Definition C.1
A continuously differentiable scalar function $\mathcal{V}(\boldsymbol{x})$ is:

- **positive definite** if $\mathcal{V}(\mathbf{0}) = 0$ and $\mathcal{V}(\boldsymbol{x}) > 0$ for $\boldsymbol{x} \neq \mathbf{0}$;
- **positive semi-definite** if $\mathcal{V}(\mathbf{0}) = 0$ and $\mathcal{V}(\boldsymbol{x}) \geq 0$ for $\boldsymbol{x} \neq \mathbf{0}$;
- **negative (semi-)definite** if $-\mathcal{V}(\boldsymbol{x})$ is positive (semi-)definite.

On basis of these definitions, the energy-like *Lyapunov function* can be defined as

---

Definition C.2 (Lyapunov function)
A continuously differentiable and positive definite scalar function $\mathcal{V}(\boldsymbol{x})$, where the domain is an open set containing the origin, is said to be a **Lyapunov function** for system (C-1) if its time derivative along the system's trajectories, that is:

$$\dot{\mathcal{V}} = \frac{\partial \mathcal{V}}{\partial \boldsymbol{x}} \dot{\boldsymbol{x}} = \frac{\partial \mathcal{V}}{\partial \boldsymbol{x}} \boldsymbol{f}(\boldsymbol{x}), \tag{C-2}$$

is negative semi-definite. Before these conditions are verified, the function $\mathcal{V}(\boldsymbol{x})$ is generally indicated as a Lyapunov Candidate Function (LCF).

Stability of system (C-1) can now be determined without explicitly solving the differential equation by using the following theorem (Khalil & Grizzle, 2002):

Theorem C.1 (Lyapunov's Direct Method)
Let $\mathcal{V}(\boldsymbol{x})$ be a continuous differentiable and positive definite function on $\mathbb{R}^n$ and let $\dot{\mathcal{V}}$ represent the time derivative of $\mathcal{V}$ along the trajectories of system (C-1). Furthermore, let $\mathcal{D}$ be an open region containing the equilibrium point $\boldsymbol{x}_e = \mathbf{0}$. The equilibrium state $\boldsymbol{x}_e$ of system (C-1) is:

- **stable**, if $\dot{\mathcal{V}}$ is negative semi-definite for $\boldsymbol{x} \in \mathcal{D}$;
- **asymptotically stable**, if $\dot{\mathcal{V}}$ is negative definite for $\boldsymbol{x} \in \mathcal{D}$;
- **exponentially stable**, if there exists three positive constant c_1, c_2 and c_3 such that $c_1|\boldsymbol{x}|^2 \leq \mathcal{V}(\boldsymbol{x}) \leq c_2|\boldsymbol{x}|^2$ and $\dot{\mathcal{V}} \leq -c_3|\boldsymbol{x}|^2$ for all $\boldsymbol{x} \in \mathcal{D}$.

The proof of this theorem can be found in chapter 4 of (Khalil & Grizzle, 2002). This theorem can be conveniently summarized as follows (Khalil & Grizzle, 2002):

> ***Lyapunov's Direct Method:*** *the origin of system (C-1) is stable if there is a continuously differentiable positive definite function $\mathcal{V}(\boldsymbol{x})$ so that $\dot{\mathcal{V}}(\boldsymbol{x})$ is negative semi-definite, and it is asymptotically stable if $\dot{\mathcal{V}}(\boldsymbol{x})$ is negative definite.*

According to Theorem C.1, when the time derivative of the Lyapunov function along the trajectories of system (C-1) is negative definite, the equilibrium $\boldsymbol{x}_e = 0$ is asymptotically stable. Finding such a Lyapunov function is generally very difficult. Fortunately, the powerful *LaSalle-Yoshizawa* theorem may be used to conclude asymptotic convergence even when $\dot{\mathcal{V}}$ is only negative semi-definite (Krstić et al., 1995).

Theorem C.2 (LaSalle-Yoshizawa)
Let $\boldsymbol{x}_e$ be an equilibrium point of

$$\dot{\boldsymbol{x}} = \boldsymbol{f}(\boldsymbol{x}, t)\,, \tag{C-3}$$

where $\boldsymbol{x} \in \mathbb{R}^n$, and $\boldsymbol{f} : \mathbb{R}^n \times \mathbb{R}^+ \to \mathbb{R}^n$ is locally Lipschitz in $\boldsymbol{x}$ uniformly in t. Let $\mathcal{V} : \mathbb{R}^n \to \mathbb{R}^+$ be a continuously differentiable function $\mathcal{V}(\boldsymbol{x})$ satisfying:

1. $\mathcal{V}(\boldsymbol{x}) > 0$ and $\mathcal{V}(\mathbf{0}) = 0$;
2. $\dot{\mathcal{V}} = \frac{\partial \mathcal{V}}{\partial \boldsymbol{x}} \boldsymbol{f}(\boldsymbol{x}, t) \leq -W(\boldsymbol{x}) \leq 0$;
3. $\mathcal{V}(\boldsymbol{x}) \to \infty$ as $|\boldsymbol{x}| \to \infty$.

$\forall \boldsymbol{x} \in \mathbb{R}^n$ and where $W(\boldsymbol{x})$ is a continuous function. Then all solutions $\boldsymbol{x}(t)$ of system (C-3) are uniformly globally bounded and

$$\lim_{t\to\infty} W(\boldsymbol{x}(t)) = 0\,. \tag{C-4}$$

In addition, if $W(\boldsymbol{x}) > 0$, then the equilibrium point $\boldsymbol{x}_e$ of system (C-3) is globally uniformly asymptotically stable.

Note that Theorem C.2 for checking stability is global in nature. If the LCF does satisfy this theorem in some open region $\mathcal{D} \in \mathbb{R}^n$ containing the equilibrium point $\boldsymbol{x}_e$ and $\mathcal{D} \neq \mathbb{R}^n$, then we can only guarantee that $\boldsymbol{x}_e$ is *locally* uniformly asymptotically stable.

Failure of a LCF to satisfy the conditions for stability does not mean that the equilibrium is not stable (Khalil & Grizzle, 2002). All we can conclude in this case is that the stability of the system cannot be determined by use of this LCF. However, it turns out that when an equilibrium point is stable, there exists a Lyapunov function $\mathcal{V}(\boldsymbol{x})$ for the corresponding system (Sonneveldt, 2010).

C-1-3 Lyapunov Control Design

In the previous section Lyapunov's direct method has been discussed which can be applied to analyze the stability properties of *autonomous* systems. In this section the Lyapunov theory is extended for control design to create a closed-loop system with desirable stability properties. We now consider the following nonlinear system that needs to be controlled:

$$\dot{\boldsymbol{x}} = \boldsymbol{f}(\boldsymbol{x}, u)\,, \tag{C-5}$$

where $\boldsymbol{x} \in \mathbb{R}^n$ is the state, $u \in \mathbb{R}$ is the control input and $\boldsymbol{f}(\boldsymbol{0}, 0) = \boldsymbol{0}$. The control objective is to find a feedback control law $\alpha(\boldsymbol{x})$ for the control input u, such that the equilibrium $\boldsymbol{x}_e = \boldsymbol{0}$ is globally asymptotically stable.

Theorem C.2 can be applied to system (C-5) resulting in the following relationship:

$$\dot{\mathcal{V}} = \frac{\partial \mathcal{V}}{\partial \boldsymbol{x}} \boldsymbol{f}(\boldsymbol{x}, \alpha(\boldsymbol{x})) \leq -W(\boldsymbol{x}) \leq 0\,, \quad \forall \boldsymbol{x} \in \mathbb{R}^n\,. \tag{C-6}$$

If we can find a Lyapunov function $\mathcal{V}(\boldsymbol{x})$ and a stabilizing control law $\alpha(\boldsymbol{x})$ such that this equation is satisfied, then the equilibrium $\boldsymbol{x}_e = \boldsymbol{0}$ of system (C-5) is rendered globally asymptotically stable. If such a choice for $\mathcal{V}(\boldsymbol{x})$ exists, then the corresponding system is said to possess a Control Lyapunov Function (CLF) (Sonneveldt, 2010; Koschorke, 2012).

Definition C.3 (Control Lyapunov Function)
A smooth positive definite and radially unbounded function $\mathcal{V}$, with $\mathcal{V}(\boldsymbol{0}) = 0$ and $\mathcal{V}(\boldsymbol{x}) > 0$ for $\boldsymbol{x} \neq \boldsymbol{0}$, is called a CLF for the system (C-5) if there exists a $u \in \mathbb{R}$ that satisfies

$$\left\{ \frac{\partial \mathcal{V}}{\partial \boldsymbol{x}} f(\boldsymbol{x}, u) \right\} \leq 0\,, \quad \forall \boldsymbol{x} \in \mathbb{R}^n\,. \tag{C-7}$$

In (Artstein, 1983) it is proven that the existence of a CLF for system (C-5) is equivalent to the existence of a global asymptotic stabilizing control law $\alpha(\boldsymbol{x})$ of that system. In other words, when there exists a control law $\alpha(\boldsymbol{x})$ that renders the equilibrium point $\boldsymbol{x}_e$ of system (C-5) globally asymptotically stable, it is guaranteed that a CLF exists. The difficulty now is to find such a CLF. Fortunately there is a group of functions meeting the requirements to become a CLF, of which a selection is listed in Table C-1 (Koschorke, 2012). The nonlinear control technique BS which is explained in the following sections makes use of CLF# 1. The advantage of this CLF is that sign definiteness can easily be checked.

Table C-1: Commonly used candidate Control Lyapunov Functions (Koschorke, 2012).

CLF#	$\mathcal{V}(x)$	$\dot{\mathcal{V}}(x)$
1	$\frac{1}{2}x^2$	$x\dot{x}$
2	$\lvert x\rvert$	$\text{sgn}(x)$
3	$\sqrt{\lvert x\rvert}$	$\text{sgn}(x)\frac{1}{2}\lvert x\rvert^{-\frac{1}{2}}\dot{x}$
4	$\ln(x^2+1)$	$2x\dot{x}\left(x^2+1\right)^{-1}$
5	$[\ln(x+1)]^2$	$x\dot{x}\cdot\log[x+1](x+1)^{-1}$

C-2 Recursive Backstepping

Backstepping is a recursive, Lyapunov-based, nonlinear design method. The main advantage of BS is that it is based on Lyapunov stability theory, and thereby guarantees the goals of global asymptotic stabilization and tracking. The concept of BS is to design a controller in a recursive way by considering some of the state variables as "virtual controls" and designing intermediate control laws for these, starting at the scalar equation which is separated by the largest number of integrations from the control input. The recursive BS control approach can be subdivided into three parts (Sonneveldt, 2010):

1. Define tracking errors $z_\star$ and rewrite the current state equation in terms of these errors;
2. Augment the CLF with a quadratic term that penalizes the new tracking error;
3. Select a stabilizing control law that renders the time derivative of the augmented CLF negative definite.

We consider the following lower triangular, strict-feedback system:

$$\dot{x}_i = f_i(\bar{\boldsymbol{x}}_i) + g_i(\bar{\boldsymbol{x}}_i)x_{i+1}\,, \quad i = 1,\ldots,n-1 \tag{C-8a}$$
$$\dot{x}_n = f_n(\boldsymbol{x}) + g_n(\boldsymbol{x})u\,, \tag{C-8b}$$

where $\bar{\boldsymbol{x}}_{\boldsymbol{i}} = [x_1,\cdots,x_i]^T$ and $\boldsymbol{x} = [x_1,\cdots,x_n]^T$ are the states, $x_i \in \mathbb{R}$, $u \in \mathbb{R}$ the control signal and $g_i \neq 0$ for $i = 1,\ldots,n$. The control objective is to track a smooth reference signal $x_{1,r}$, for which the n-order time derivatives are assumed to be known and bounded, with the state x_1. Furthermore, the signals x_i for $i = 2,\ldots,n$ must remain bounded. It is assumed that f_i and g_i are known and have $n-i$ continuous derivatives, that is f_i and $g_i \in C^{n-i}$ for $i = 1,\ldots,n$.

Subsystem 1

We start by considering the first subsystem, which is the subsystem "furthest" away from the actual control u:

$$\dot{x}_1 = f_1(x_1) + g_1(x_1)x_2\,. \tag{C-9}$$

Now we regard state x_2 as the control input for this subsystem. However, because x_2 is just a state variable and not the real control input u, we call x_2 the *virtual control.*

The tracking errors are defined as

$$z_1 = x_1 - x_{1,r} \tag{C-10a}$$
$$z_2 = x_2 - x_{2,r} \equiv x_2 - \alpha_1 \,, \tag{C-10b}$$

where $x_{2,r} \equiv \alpha_1$ is called the *stabilizing function*, which is the desired value of x_2. Rewriting the current subsystem in terms of the tracking error z_1 results in

$$\begin{aligned} \dot{z}_1 &= \dot{x}_1 - \dot{x}_{1,r} \\ &= f_1 + g_1 x_2 - \dot{x}_{1,r} \\ &= f_1 + g_1 \left(z_2 + \alpha_1\right) - \dot{x}_{1,r} \,. \end{aligned} \tag{C-11}$$

Now we formulate a quadratic scalar CLF for the first subsystem (C-9):

$$\mathcal{V}_1(z_1) = \frac{1}{2} z_1^2 \,. \tag{C-12}$$

The reason for choosing a quadratic scalar function is to allow for ease of checking sign definiteness. Taking the time derivative of the CLF along the trajectories of subsystem (C-11) results in

$$\dot{\mathcal{V}}_1 = z_1 \left[f_1 + g_1 \left(z_2 + \alpha_1\right) - \dot{x}_{1,r}\right] \,. \tag{C-13}$$

In order to yield the CLF negative definite, an obvious choice for stabilizing control law α_1 is

$$\alpha_1 = g_1^{-1} \left[-c_1 z_1 - f_1 + \dot{x}_{1,r}\right] \,, \tag{C-14}$$

which results in the following expression for $\dot{\mathcal{V}}_1$:

$$\dot{\mathcal{V}}_1 = -c_1 z_1^2 + z_1 g_1 z_2 \,. \tag{C-15}$$

Note that $\dot{\mathcal{V}}_1$ is not negative definite for all values of z_1 and z_2. The cross term $z_1 g_1 z_2$ will be removed in the next design step. By selecting the stabilizing function as Eq. (C-14) we have canceled the natural dynamics of the system. However, if certain nonlinearities are stabilizing, they need not to be canceled (Farrell et al., 2009).

Subsystem i, i = 2, ..., n - 1

Now we consider the i-th subsystem:

$$\dot{x}_i = f_i(\bar{\boldsymbol{x}}_i) + g_i(\bar{\boldsymbol{x}}_i) x_{i+1} \,, \quad i = 2, \ldots, n-1 \,. \tag{C-16}$$

We regard state x_{i+1} as the control input for the i-th subsystem. However, because x_{i+1} is just a state variable and not the real control input u, we call x_{i+1} the *virtual control.*

Now we introduce the tracking errors:

$$z_i = x_i - \alpha_{i-1}\,, \quad i = 3, \ldots, n\,, \tag{C-17}$$

and rewrite the i-th subsystem in terms of the tracking error:

$$\begin{aligned}\dot{z}_i &= \dot{x}_i - \dot{\alpha}_{i-1}\,, \quad i = 2, \ldots, n-1 \\ &= f_i + g_i x_{i+1} - \dot{\alpha}_{i-1} \\ &= f_i + g_i \left(z_{i+1} + \alpha_i\right) - \dot{\alpha}_{i-1}\,. \end{aligned} \tag{C-18}$$

Augmenting scalar CLF $\mathcal{V}_1$ yields:

$$\begin{aligned}\mathcal{V}_i(\bar{\boldsymbol{z}}_i) &= \frac{1}{2}\sum_{j=1}^{i} z_j^2\,, \quad i = 2, \ldots, n-1 \\ &= \mathcal{V}_1(z_1) + \frac{1}{2}\sum_{j=2}^{i} z_j^2\,, \end{aligned} \tag{C-19}$$

where $\bar{\boldsymbol{z}}_{\boldsymbol{i}} = [z_1, \cdots, z_i]^T$. Taking the time derivative of the CLF along the trajectories of Eqs. (C-11) and (C-18) results in

$$\begin{aligned}\dot{\mathcal{V}}_i &= \dot{\mathcal{V}}_1 + \sum_{j=2}^{i} z_j \dot{z}_j\,, \quad i = 2, \ldots, n-1 \\ &= -c_1 z_1^2 + z_1 g_1 z_2 + \sum_{r=2}^{i} z_j \left[f_j + g_j \left(z_{j+1} + \alpha_j\right) - \dot{\alpha}_{j-1}\right]\,. \end{aligned} \tag{C-20}$$

In order to yield the i-th CLF negative definite, an obvious choice for stabilizing control α_j is

$$\alpha_j = g_j^{-1}\left[-c_j z_j - f_j + \dot{\alpha}_{j-1} - z_{j-1} g_{j-1}\right]\,, \quad j = 2, \ldots, i\,, \tag{C-21}$$

which results in the following expression for $\dot{\mathcal{V}}_i$:

$$\dot{\mathcal{V}}_i = \sum_{j=1}^{i} -c_j z_j^2 + z_i g_i z_{i+1}\,, \quad i = 2, \ldots, n-1\,. \tag{C-22}$$

Note that $\dot{\mathcal{V}}_{n-1}$ is not negative definite for all values of z_{n-1} and z_n. The cross term $z_{n-1}g_{n-1}z_n$ will be removed in the final step.

Subsystem n

Now we consider the final subsystem:

$$\dot{x}_n = f_n(\boldsymbol{x}) + g_n(\boldsymbol{x})u\,, \tag{C-23}$$

and rewrite this subsystem in terms of the tracking error

$$\begin{aligned}\dot{z}_n &= \dot{x}_n - \dot{\alpha}_{n-1} \\ &= f_n + g_n u - \dot{\alpha}_{n-1} \,. \end{aligned} \tag{C-24}$$

The final Lyapunov function is now defined as

$$\begin{aligned}\mathcal{V}_n(\boldsymbol{z}) &= \frac{1}{2}\sum_{j=1}^{n} z_j^2 \\ &= \mathcal{V}_{n-1}(\bar{\boldsymbol{z}}_{n-1}) + \frac{1}{2}z_n^2 \,. \end{aligned} \tag{C-25}$$

Taking the time derivative of the CLF along the trajectories of Eqs. (C-11), (C-18) and (C-24) results in

$$\begin{aligned}\dot{\mathcal{V}}_n &= \dot{\mathcal{V}}_{n-1} + z_n \dot{z}_n \\ &= \sum_{j=1}^{n-1} -c_j z_j^2 + z_{n-1} g_{n-1} z_n + z_n \left[f_n + g_n u - \dot{\alpha}_{n-1}\right] \,. \end{aligned} \tag{C-26}$$

In order to yield $\dot{\mathcal{V}}_n$ negative definite, an obvious choice for the real control u is

$$u = g_n^{-1}\left[-c_n z_n - f_n + \dot{\alpha}_{n-1} - z_{n-1} g_{n-1}\right] \,, \tag{C-27}$$

which results in the following expression for $\dot{\mathcal{V}}_n$:

$$\dot{\mathcal{V}}_n = \sum_{j=1}^{n} -c_j z_j^2 \,. \tag{C-28}$$

According to the theorem of *LaSalle-Yoshizawa* (see Theorem C.2, page 71) the equilibrium $\boldsymbol{z} = \mathbf{0}$ is globally uniformly asymptotically stable when $c_1 > 0$ and $c_2 > 0$, implying that the reference output state $x_{1,r}$ is successfully tracked by x_1, that is:

$$\lim_{t\to\infty}\left[x_1 - x_{1,r}\right] = 0 \,. \tag{C-29}$$

Note that the BS control approach is restricted to lower triangular (strict-feedback) systems, because when we we apply the BS approach to non-triangular feedback passive systems, one or more (virtual) control laws become *differential* equations instead of *algebraic* equations.

C-3 Simulations

In this section a BS control law is derived for the pendulum model, which is for convenience repeated below:

$$\dot{x}_1 = x_2 \tag{B-3a revisited}$$

$$\dot{x}_2 = \theta_{2,1}\sin(x_1) + \theta_{2,2}x_2 + \theta_{2,3}u \,. \tag{B-3b revisited}$$

The control task is to track the smooth reference state $x_{1,r}$ with the state x_1. The BS procedure starts by defining the tracking errors as

$$z_1 = x_1 - x_{1,r} \tag{C-31a}$$
$$z_2 = x_2 - \alpha_1\,, \tag{C-31b}$$

where α_1 is a stabilizing control law which is later defined. Now system (B-3) can be rewritten in terms of the error states:

$$\dot{z}_1 = z_2 + \alpha_1 - \dot{x}_{1,r} \tag{C-32a}$$
$$\dot{z}_2 = \theta_{2,1}\sin(x_1) + \theta_{2,2}x_2 + \theta_{2,3}u - \dot{\alpha}_1\,. \tag{C-32b}$$

We start by formulating a quadratic scalar CLF for the first subsystem (C-32a):

$$\mathcal{V}_1(z_1) = \frac{1}{2}z_1^2\,. \tag{C-33}$$

The reason for choosing a quadratic scalar function is to allow for ease of checking sign definiteness. Taking the time derivative of the CLF along the trajectories of subsystem (C-32a) results in

$$\dot{\mathcal{V}}_1 = z_1\left[z_2 + \alpha_1 - \dot{x}_{1,r}\right]\,. \tag{C-34}$$

An obvious choice for a stabilizing control law α_1 is

$$\alpha_1 = -c_1 z_1 + \dot{x}_{1,r}\,, \tag{C-35}$$

which results in the following expression for $\dot{\mathcal{V}}_1$:

$$\dot{\mathcal{V}}_1 = -c_1 z_1^2 + z_1 z_2\,. \tag{C-36}$$

The cross term $z_1 z_2$ will be dealt with in the next design step. Now we move on to the second and last subsystem (C-32b). The earlier formulated quadratic CLF is augmented to penalize the second tracking error as well:

$$\mathcal{V}(\boldsymbol{z}) = \mathcal{V}_1 + \frac{1}{2}z_2^2\,. \tag{C-37}$$

Taking the time derivative of the CLF along the trajectories of system (C-32) yields

$$\begin{aligned}\dot{\mathcal{V}} &= \dot{\mathcal{V}}_1 + z_2\dot{z}_2 \\ &= -c_1 z_1^2 + z_1 z_2 + z_2\left[\theta_{2,1}\sin(x_1) + \theta_{2,2}x_2 + \theta_{2,3}u - \dot{\alpha}_1\right]\,. \end{aligned}\tag{C-38}$$

An obvious choice for the control torque u is:

$$u = \frac{1}{\theta_{2,3}}\left[-c_2 z_2 - z_1 - \theta_{2,1}\sin(x_1) - \theta_{2,2}x_2 + \dot{\alpha}_1\right]\,, \tag{C-39}$$

which results in the following expression for $\dot{\mathcal{V}}$:

$$\dot{\mathcal{V}} = -c_1 z_1^2 - c_2 z_2^2 \,. \tag{C-40}$$

According to the theorem of *LaSalle-Yoshizawa* (see Theorem C.2, page 71) the equilibrium $\boldsymbol{z} = \mathbf{0}$ is globally uniformly asymptotically stable when $c_1 > 0$ and $c_2 > 0$, implying that the reference output state $x_{1,r}$ is successfully tracked by x_1, that is:

$$\lim_{t \to \infty} \left[x_1 - x_{1,r} \right] = 0 \,. \tag{C-41}$$

Note that it is physically impossible for $\theta_{2,3} = \frac{1}{ml^2}$ to equal zero, therefore the control law (C-39) does not contain a singularity. The time derivative $\dot{\alpha}_1$ can be analytically obtained from Eq. (C-35):

$$\begin{aligned} \dot{\alpha}_1 &= -c_1 \dot{z}_1 + \ddot{x}_{1,r} \\ &= -c_1 \left(z_2 + \alpha_1 - \dot{x}_{1,r} \right) + \ddot{x}_{1,r} \,. \end{aligned} \tag{C-42}$$

Because we generally do not have exact information on the model parameters $\boldsymbol{\theta}_2$, the following controller might be applied in practice:

$$u = \frac{1}{\hat{\theta}_{2,3}} \left[-c_2 z_2 - z_1 - \hat{\theta}_{2,1} \sin(x_1) - \hat{\theta}_{2,2} x_2 + \dot{\alpha}_1 \right] \,, \tag{C-43}$$

where $\hat{\boldsymbol{\theta}}_2 = \begin{bmatrix} \hat{\theta}_{2,1} & \hat{\theta}_{2,2} & \hat{\theta}_{2,3} \end{bmatrix}^T$ is the estimate of $\boldsymbol{\theta}_2$. In order to obtain a singularity-free controller, a parameter projection method should be used to guarantee that $\hat{\theta}_{2,3} \neq 0$ (Krstić et al., 1995; Sonneveldt, 2010). Because in general $\hat{\boldsymbol{\theta}}_2 \neq \boldsymbol{\theta}_2$, nothing can be said about the stability of system (B-3) when we use control law (C-43).

Simulations of BS control law (C-43) have been performed in `Matlab` / `Simulink` with a sampling time of 0.01 s. The following initial conditions and parameters have been used for the *model*:

$$\begin{aligned} x_1(0) &= 1 \,, & x_2(0) &= -1 \,, \\ \theta_{2,1} &= -9.81 \,, & \theta_{2,2} &= -0.5 \,, \\ \theta_{2,3} &= 0.1 \,. \end{aligned} \tag{C-44}$$

The following *control* parameters have been selected:

$$\begin{aligned} c_1 &= 10 \,, & c_2 &= 10 \,, \\ \hat{\theta}_{2,1} &= \theta_{2,1} \,, & \hat{\theta}_{2,2} &= \theta_{2,2} \,, \\ \hat{\theta}_{2,3} &= \theta_{2,3} \,. \end{aligned} \tag{C-45}$$

The results of the simulation can be seen in Figure C-1. As expected, the full-information BS controller performs well in the absence of any parametric uncertainties.

To find out whether this BS controller can cope with parametric uncertainties, the parameter estimates now equal the real model parameters multiplied by an uncertainty factor. Simulations have been performed with an uncertainty factor of 5 and 10 and a sampling time of 0.01 s, the results can be seen in Figure C-2. Clearly, the BS controller is no longer able to accurately track the reference signal with the introduced uncertainties.

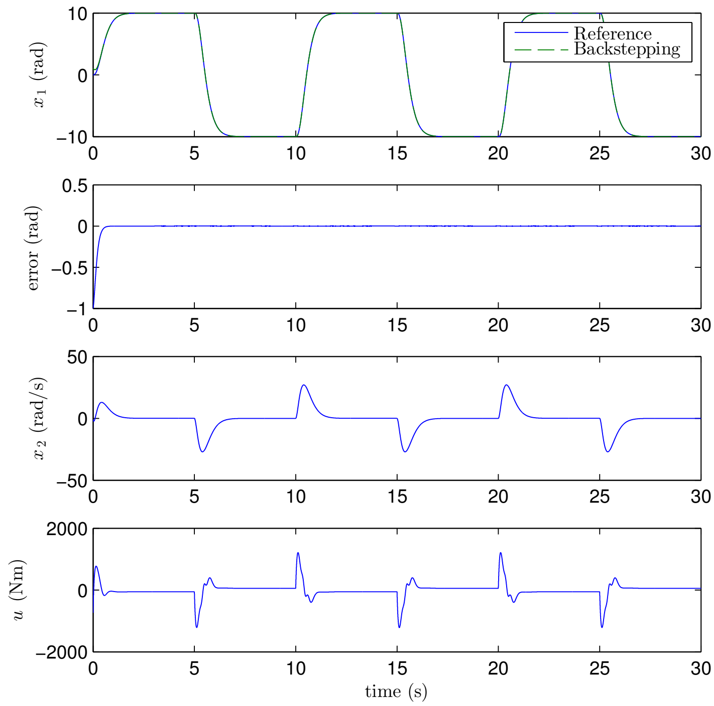

Figure C-1: The control performance of a Backstepping controller in the absence of any uncertainties.

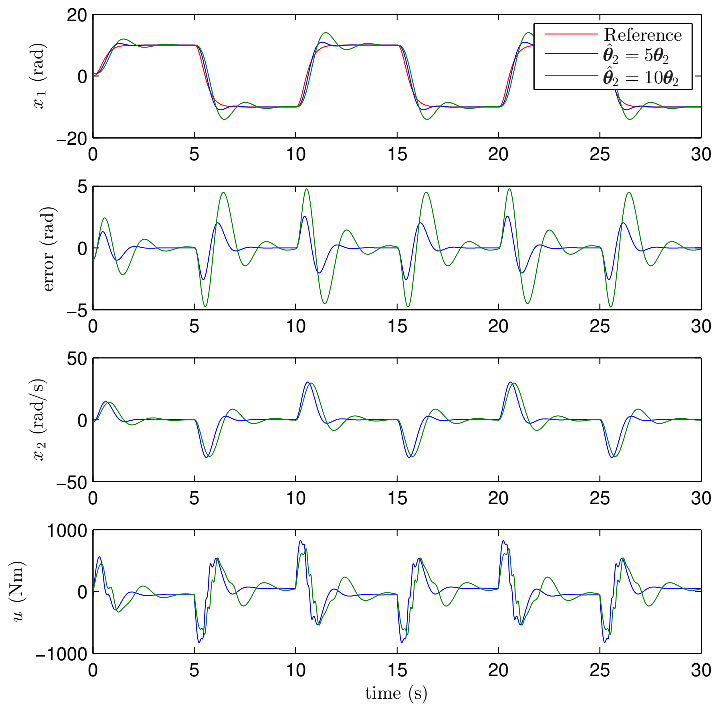

Figure C-2: The control performance of a Backstepping controller in the presence of parametric uncertainties.

Appendix D

Command-Filtered Backstepping

In this appendix the conventional Backstepping (BS) technique is augmented with command filters. Advantages of implementing command filters are (Sonneveldt, 2010):

- Obviating the need for analytic computation of virtual control derivatives, which becomes very tedious when working with high-order systems;
- Eliminating the Backstepping's restriction to nonlinear systems of a lower triangular form;
- Improving the performance of parameter update laws; by implementing magnitude, rate, and bandwidth constraints on the (virtual) controls.

The derivation of the Command-Filtered BS controller for non-triangular, feedback passive systems can be found in Appendix D-1. In this derivation command filters are used to produce magnitude, rate and bandwidth-limited signals and their time derivative. For this purpose generally first or second-order, low-pass filters with unity low-frequency (DC) gain are used (D-2). In order to evaluate this nonlinear control approach, a Command-Filtered BS control law is derived and simulated for the pendulum model (D-3).

D-1 Theory

We now consider the following non-triangular, feedback passive system:

$$\dot{x}_i = f_i(\boldsymbol{x}) + g_i(\boldsymbol{x})x_{i+1}\,, \quad i = 1, \ldots, n-1 \tag{D-1a}$$
$$\dot{x}_n = f_n(\boldsymbol{x}) + g_n(\boldsymbol{x})u\,, \tag{D-1b}$$

where $\boldsymbol{x} \in \mathbb{R}^n$ is the state vector, $x_i \in \mathbb{R}$, $u \in \mathbb{R}$ the control signal and $g_i \neq 0$ for $i = 1, \ldots, n$. The control objective is to track a smooth reference signal $x_{1,r}$, for which the time derivative is assumed to be known and bounded, with the state x_1. Furthermore, the signals x_i for

$i = 2, \ldots, n$ must remain bounded. It is assumed that the functions f_i and g_i are known and that their first-order derivatives are continuous, that is f_i and $g_i \in C^1$ for $i = 1, \ldots, n$. Note that the difference with system (C-8) is that functions f_i and g_i may now depend on all states $\boldsymbol{x}$.

Subsystem 1

We start by considering the first subsystem, which is the subsystem "furthest" away from the actual control u:

$$\dot{x}_1 = f_1(\boldsymbol{x}) + g_1(\boldsymbol{x})x_2 \,. \tag{D-2}$$

Now we regard state x_2 as the control input for this subsystem. However, because x_2 is just a state variable and not the real control input u, we call x_2 the *virtual control.*

Now we introduce the tracking errors:

$$z_1 = x_1 - x_{1,r} \tag{D-3a}$$
$$z_2 = x_2 - x_{2,r} \,, \tag{D-3b}$$

where $x_{2,r}$ is the new virtual control law to be designed. As with the standard BS procedure, the first stabilizing control law is defined as

$$\alpha_1 = g_1^{-1} \left[-c_1 z_1 - f_1 + \dot{x}_{1,r} \right] \,. \tag{C-14 revisited}$$

However, instead of directly applying this virtual control, a new signal $x_{2,r}^0$ is defined as

$$x_{2,r}^0 = \alpha_1 - \chi_2 \,, \tag{D-4}$$

where χ_2 will be defined later on. The raw signal $x_{2,r}^0$ is led through a command filter to obtain $x_{2,r}$ and its time derivative $\dot{x}_{2,r}$. The effect that the use of this command filter has on the tracking error z_1 is estimated by the stable linear filter:

$$\dot{\chi}_1 = -c_1 \chi_1 + g_1 \left(x_{2,r} - x_{2,r}^0 \right) \,, \tag{D-5}$$

with $\chi_1(0) = 0$. This auxiliary system compensates for the constraint effects due to magnitude, rate and bandwidth limitations of the command filter. Now we introduce the *compensated* tracking errors:

$$\bar{z}_1 = z_1 - \chi_1 \tag{D-6a}$$
$$\bar{z}_2 = z_2 - \chi_2 \,. \tag{D-6b}$$

The $\bar{z}_1$-dynamics are given by

$$\begin{aligned}
\dot{\bar{z}}_1 &= \dot{z}_1 - \dot{\chi}_1 \\
&= \dot{x}_1 - \dot{x}_{1,r} - \dot{\chi}_1 \\
&= f_1 + g_1 x_2 - \dot{x}_{1,r} + c_1 \chi_1 - g_1 \left(x_{2,r} - x_{2,r}^0 \right) \\
&= f_1 + g_1 \left(z_2 + x_{2,r} \right) - \dot{x}_{1,r} + c_1 \chi_1 - g_1 \left(x_{2,r} - x_{2,r}^0 \right) \,.
\end{aligned} \tag{D-7}$$

Now we formulate a quadratic scalar Control Lyapunov Function (CLF) for the first compensated tracking error:

$$\mathcal{V}_1(\bar{z}_1) = \frac{1}{2}\bar{z}_1^2 \,. \tag{D-8}$$

Taking the time derivative of the CLF along the trajectories of subsystem (D-7) yields

$$\begin{aligned}
\dot{\mathcal{V}}_1 &= \bar{z}_1 \left[f_1 + g_1 \left(z_2 + x_{2,r} \right) - \dot{x}_{1,r} + c_1\chi_1 - g_1 \left(x_{2,r} - x_{2,r}^0 \right) \right] \\
&= \bar{z}_1 \left[f_1 + g_1 \left(z_2 + x_{2,r} \right) - g_1 x_{2,r}^0 + g_1 x_{2,r}^0 - \dot{x}_{1,r} + c_1\chi_1 - g_1 \left(x_{2,r} - x_{2,r}^0 \right) \right] \\
&= \bar{z}_1 \left[f_1 + g_1 \left(z_2 + x_{2,r} \right) - g_1 x_{2,r}^0 + g_1 \left(\alpha_1 - \chi_2 \right) - \dot{x}_{1,r} + c_1\chi_1 - g_1 \left(x_{2,r} - x_{2,r}^0 \right) \right] \\
&= \bar{z}_1 \left[-c_1 z_1 + g_1 \left(z_2 + x_{2,r} \right) - g_1 x_{2,r}^0 - g_1\chi_2 + c_1\chi_1 - g_1 \left(x_{2,r} - x_{2,r}^0 \right) \right] \\
&= \bar{z}_1 \left[-c_1 z_1 + g_1 \bar{z}_2 + c_1\chi_1 \right] \\
&= \bar{z}_1 \left[-c_1 \left(z_1 - \chi_1 \right) + g_1 \bar{z}_2 \right] \\
&= -c_1 \bar{z}_1^2 + \bar{z}_1 g_1 \bar{z}_2 \,.
\end{aligned} \tag{D-9}$$

Note that $\dot{\mathcal{V}}_1$ is not negative definite for all values of $\bar{z}_1$ and $\bar{z}_2$. The cross term $\bar{z}_1 g_1 \bar{z}_2$ will be removed in the next design step.

Subsystem i, i = 2, ..., n - 1

Now we consider the i-th subsystem:

$$\dot{x}_i = f_i(\boldsymbol{x}) + g_i(\boldsymbol{x}) x_{i+1} \,, \quad i = 2, \ldots, n-1 \,. \tag{D-10}$$

We regard state x_{i+1} as the control input for the i-th subsystem. However, because x_{i+1} is just a state variable and not the real control input u, we call x_{i+1} the *virtual control.*

Now we introduce the tracking errors:

$$z_i = x_i - x_{i,r}, \quad i = 3, \ldots, n \,, \tag{D-11}$$

where $x_{i,r}$ are the new virtual control laws to be designed. As with the standard BS procedure, the stabilizing control laws are defined as

$$\alpha_i = g_i^{-1} \left[-c_i z_i - f_i + \dot{x}_{i,r} - \bar{z}_{i-1} g_{i-1} \right] , \quad i = 2, \ldots, n-1 \,. \tag{D-12}$$

Note that the variables $\dot{\alpha}_{i-1}$ and z_{i-1} in Eq. (C-21) have been replaced by respectively $\dot{x}_{i,r}$ and $\bar{z}_{i-1}$ because of the new definitions of the tracking error.

However, instead of directly applying this virtual control, new signals $x_{i,r}^0$ are defined by

$$x_{i,r}^0 = \alpha_{i-1} - \chi_i \,, \quad i = 3, \ldots, n \,, \tag{D-13}$$

where χ_i will be defined later on. The raw signals $x_{i,r}^0$ are led through command filters to obtain $x_{i,r}$ and their time derivatives $\dot{x}_{i,r}$. The effect that the use of these command filters have on the tracking error z_i is estimated by the stable linear filters:

$$\dot{\chi}_i = -c_i\chi_i + g_i \left(x_{i+1,r} - x_{i+1,r}^0 \right) \,, \quad i = 2, \ldots, n-1 \,, \tag{D-14}$$

with $\chi_i(0) = 0$. These auxiliary systems compensate for the constraint effects due to magnitude, rate and bandwidth limitations of the command filter. Now we introduce the *compensated* tracking errors:

$$\bar{z}_i = z_i - \chi_i\,, \quad i = 3, \ldots, n\,. \tag{D-15}$$

The $\bar{z}_i$-dynamics are given by

$$\begin{aligned}
\dot{\bar{z}}_i &= \dot{z}_i - \dot{\chi}_i, \quad i = 2, \ldots, n-1 \\
&= \dot{x}_i - \dot{x}_{i,r} - \dot{\chi}_i \\
&= f_i + g_i x_{i+1} - \dot{x}_{i,r} + c_i\chi_i - g_i\left(x_{i+1,r} - x^0_{i+1,r}\right) \\
&= f_i + g_i\left(z_{i+1} + x_{i+1,r}\right) - \dot{x}_{i,r} + c_i\chi_i - g_i\left(x_{i+1,r} - x^0_{i+1,r}\right)\,.
\end{aligned} \tag{D-16}$$

Augmenting the scalar CLF $\mathcal{V}_1$ yields

$$\begin{aligned}
\mathcal{V}_i(\bar{\boldsymbol{z}}_i) &= \frac{1}{2}\sum_{j=1}^{i}\bar{z}_j^2, \quad i = 2, \ldots, n-1 \\
&= \mathcal{V}_1(\bar{z}_1) + \frac{1}{2}\sum_{j=2}^{i}\bar{z}_j^2\,,
\end{aligned} \tag{D-17}$$

where $\bar{\boldsymbol{z}}_i = [\bar{z}_1, \cdots, \bar{z}_i]^T$. Taking the time derivative of the CLF along the trajectories of Eqs. (D-7) and (D-16) results in

$$\begin{aligned}
\dot{\mathcal{V}}_i &= \dot{\mathcal{V}}_1 + \sum_{j=2}^{i}\bar{z}_j\left[f_j + g_j\left(z_{j+1} + x_{j+1,r}\right) - \dot{x}_{j,r} + c_j\chi_j - g_j\left(x_{j+1,r} - x^0_{j+1,r}\right)\right], \quad i = 2, \ldots, n-1 \\
&= -c_1\bar{z}_1^2 + \bar{z}_1 g_1 \bar{z}_2 \\
&\quad + \sum_{j=2}^{i}\bar{z}_j\left[f_j + g_j\left(z_{j+1} + x_{j+1,r}\right) - g_j x^0_{j+1,r} + g_j x^0_{j+1,r} - \dot{x}_{j,r} + c_j\chi_j - g_j\left(x_{j+1,r} - x^0_{j+1,r}\right)\right] \\
&= -c_1\bar{z}_1^2 + \bar{z}_1 g_1 \bar{z}_2 \\
&\quad + \sum_{j=2}^{i}\bar{z}_j\left[f_j + g_j\left(z_{j+1} + x_{j+1,r}\right) + g_j\left(\alpha_j - \chi_{j+1}\right) - \dot{x}_{j,r} + c_j\chi_j - g_j x_{j+1,r} - x^0_{j+1,r}\right] \\
&= -c_1\bar{z}_1^2 + \bar{z}_1 g_1 \bar{z}_2 + \sum_{j=2}^{i}\bar{z}_j\left[-c_j z_j + g_j\bar{z}_{j+1} + c_j\chi_j - \bar{z}_{j-1}g_{j-1}\right] \\
&= -\sum_{j=1}^{i}c_j\bar{z}_j^2 + \bar{z}_i g_i \bar{z}_{i+1}\,.
\end{aligned} \tag{D-18}$$

Note that $\dot{\mathcal{V}}_{n-1}$ is not negative definite for all values of $\bar{z}_{n-1}$ and $\bar{z}_n$. The cross term $\bar{z}_{n-1}g_{n-1}\bar{z}_n$ will be removed in the final step.

Subsystem n

Now we consider the final subsystem:

$$\dot{x}_n = f_n(\boldsymbol{x}) + g_n(\boldsymbol{x})u\,. \tag{D-19}$$

The raw signal u^0 is led through a command filter to obtain u and its time derivative $\dot{u}$. The effect that the use of this command filter has on the tracking error z_n is estimated by the stable linear filter:

$$\dot{\chi}_n = -c_n\chi_n + g_n\left(u - u^0\right)\,, \tag{D-20}$$

with $\chi_n(0) = 0$. The $\bar{z}_n$-dynamics are given by

$$\begin{aligned}\dot{\bar{z}}_n &= \dot{z}_n - \dot{\chi}_n \\ &= \dot{x}_n - \dot{x}_{n,r} - \dot{\chi}_n \\ &= f_n + g_n u - \dot{x}_{n,r} + c_n\chi_n - g_n\left(u - u^0\right)\,.\end{aligned} \tag{D-21}$$

The final Lyapunov function is now defined as

$$\begin{aligned}\mathcal{V}_n(\boldsymbol{z}) &= \frac{1}{2}\sum_{j=1}^{n}\bar{z}_j^2 \\ &= \mathcal{V}_{n-1}(\bar{\boldsymbol{z}}_{n-1}) + \frac{1}{2}\bar{z}_n^2\,.\end{aligned} \tag{D-22}$$

Taking the time derivative of the CLF along the trajectories of Eqs. (D-7), (D-16) and (D-21) results in

$$\begin{aligned}\dot{\mathcal{V}}_n &= \dot{\mathcal{V}}_{n-1} + \bar{z}_n\dot{\bar{z}}_n \\ &= \sum_{j=1}^{n-1} -c_j\bar{z}_j^2 + \bar{z}_{n-1}g_{n-1}\bar{z}_n + \bar{z}_n\left[f_n + g_n u - \dot{x}_{n,r} + c_n\chi_n - g_n\left(u - u^0\right)\right] \\ &= \sum_{j=1}^{n-1} -c_j\bar{z}_j^2 + \bar{z}_{n-1}g_{n-1}\bar{z}_n + \bar{z}_n\left[f_n + g_n u^0 - \dot{x}_{n,r} + c_n\chi_n\right]\,.\end{aligned} \tag{D-23}$$

In order to yield $\dot{\mathcal{V}}_n$ negative definite, an obvious choice for the raw control law u^0 is

$$u^0 = \frac{1}{g_n}\left[-c_n z_n - f_n + \dot{x}_{n,r} - \bar{z}_{n-1}g_{n-1}\right]\,, \tag{D-24}$$

this yields

$$\begin{aligned}\dot{\mathcal{V}}_n &= \sum_{j=1}^{n-1} -c_j\bar{z}_j^2 + \bar{z}_{n-1}g_{n-1}\bar{z}_n + \bar{z}_n\left[-c_n z_n - \bar{z}_{n-1}g_{n-1} + c_n\chi_n\right] \\ &= \sum_{j=1}^{n-1} -c_j\bar{z}_j^2 + \bar{z}_n\left[-c_n\left(z_n - \chi_n\right)\right] \\ &= \sum_{j=1}^{n} -c_j\bar{z}_j^2\,.\end{aligned} \tag{D-25}$$

By the theorem of *LaSalle-Yoshizawa* (see Theorem C.2, page 71) it now follows that the equilibrium $\bar{\boldsymbol{z}} = \mathbf{0}$ is globally uniformly asymptotically stable. Note that this derivation only guarantees desirable properties for the *compensated* tracking error $\bar{\boldsymbol{z}}$ and not the *actual* tracking error $\boldsymbol{z}$. According to (Farrell, Sharma, & Polycarpou, 2005), in the absence of physical limitations (i.e. magnitude, rate, and bandwidth constraints on the commanded state $x_{2,r}$ and control u), convergence of the tracking error $\boldsymbol{z}$ is still guaranteed. When the inputs are too aggressive, the implemented limits can come into effect. During such a period $\boldsymbol{z}$ and $\boldsymbol{\chi}$ become nonzero because the desired control signals are not able to be implemented. However, the $\boldsymbol{\chi}$-signals and therefore also the tracking error $\boldsymbol{z}$ will remain bounded, because $\boldsymbol{\chi}$ is the output of a stable linear system with a bounded input. When the limits are no longer in effect, the tracking error $\boldsymbol{z}$ will converge to $\mathbf{0}$.

D-2 Command Filters

In the previous section command filters are mentioned that transform $x^0_{i,r}$ to produce magnitude, rate and bandwidth-limited signals $x_{i,r}$ and their time derivatives $\dot{x}_{i,r}$. For this purpose first-order, low-pass filters with unity low-frequency (DC) gain and bandwidth w_n can be used:

$$\dot{x}_{i,r} = S_R\left(\left\{S_M\left[x^0_{i,r}\right] - x_{i,r}\right\}\omega_n\right) \,, \tag{D-26}$$

with initial condition:

$$x_{i,r}(0) = \alpha_1\left(z_{i-1}(0), x_{i-1,r}(0)\right) \,. \tag{D-27}$$

The saturation functions S_M and S_R are defined similarly as

$$S_M(x) = \begin{cases} M & \text{if} \quad x \geq M \\ x & \text{if} \quad |x| < M \\ -M & \text{if} \quad x \leq M \,. \end{cases} \tag{D-28}$$

In the linear range of the functions S_M and S_R the transfer function of Eq. (D-26) is given by

$$\frac{X_{i,r}(s)}{X^0_{i,r}(s)} = \frac{\omega_n}{s + \omega_n} \,. \tag{D-29}$$

The corresponding block diagram of Eq. (D-29) can be seen in Figure D-1.

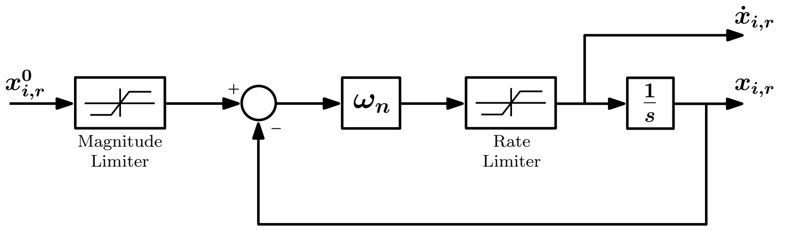

Figure D-1: First-order filter that generates the command and command derivative while enforcing magnitude, bandwidth and rate limit constraints.

Many other filters are possible as long as the order is at least one. In (Farrell et al., 2005) the following second-order command filter is used:

$$\begin{bmatrix}\dot{q}_1\\ \dot{q}_2\end{bmatrix} = \begin{bmatrix} q_2 \\ 2\zeta\omega_n\left(S_R\left\{\frac{\omega_n^2}{2\zeta\omega_n}\left[S_M\left(x_{i,r}^0\right)-q_1\right]\right\}-q_2\right)\end{bmatrix} \tag{D-30a}$$

$$\begin{bmatrix}x_{i,r}\\ \dot{x}_{i,r}\end{bmatrix} = \begin{bmatrix}q_1\\ q_2\end{bmatrix}, \tag{D-30b}$$

with initial conditions:

$$q_1(0) = \alpha_1\left(z_{i-1}(0), x_{i-1,r}(0)\right) \tag{D-31a}$$

$$q_2(0) = 0\,. \tag{D-31b}$$

In the linear range of the functions S_M and S_R the transfer function of Eq. (D-30) is given by

$$\frac{\begin{bmatrix}X_{i,r}(s)\\ sX_{i,r}(s)\end{bmatrix}}{X_{i,r}^0} = \frac{\begin{bmatrix}\omega_n^2\\ s\omega_n^2\end{bmatrix}}{s^2+2\zeta\omega_n s+\omega_n^2}\,. \tag{D-32}$$

The corresponding block diagram of Eq. (D-30) can be seen in Figure D-2.

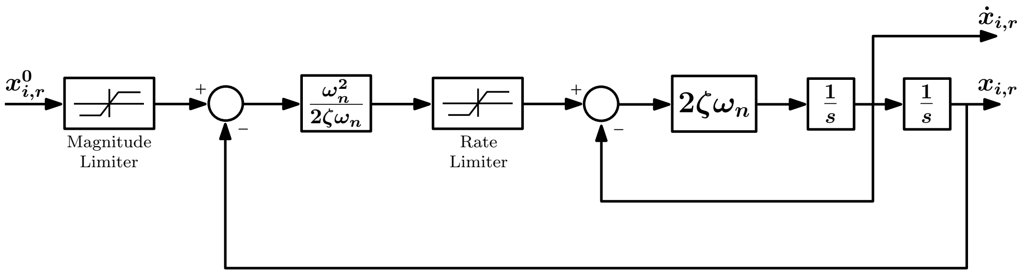

Figure D-2: Second-order filter that generates the command and command derivative while enforcing magnitude, bandwidth and rate limit constraints.

A second-order filter can be obtained by combining two first-order filters. The advantage of increasing the order of the filter is that noise is further suppressed, however, the time delay between the output and input signal will increase.

When the only purpose of the command filter is to compute a command and its derivative (i.e. there are no rate, magnitude, or bandwidth limitations), then we can simply select $S_R = 1$, $S_M = 1$. Note that if a magnitude limit is required, then we should set the damping ratio as $\zeta \geq 1$ in order to prevent x_r from overshooting the limit M. According to (Farrell et al., 2009), by increasing the command filter natural frequency ω_n, the solution to the Command-Filtered BS closed-loop system can be made arbitrarily close to the BS solution that relies on analytic derivatives. However, the sampling rate of the simulation should be consistent with ω_n, i.e. the sampling rate should be sufficiently large to capture the high frequent dynamics to avoid instability.

Note that even when we derive an exact analytical expression for the derivative of the stabilizing function α_1, it is still an approximation because the model is only an approximate representation of the plant. Therefore, the choice is not between a correct analytic expression or a filtered estimate of the command derivative, but between two *estimates* of the command derivative (Farrell et al., 2009).

Note from Figures D-1 and D-2 that we can only implement rate, magnitude and bandwidth limitations on the *commanded* states $\boldsymbol{x}_r$ and the *commanded* inputs $\boldsymbol{u}_r$, and not on the actual states $\boldsymbol{x}$ and the actual inputs $\boldsymbol{u}$. When the magnitude, rate and bandwidth limitations implemented on $\boldsymbol{u}_r$ are within the actuation system, then we have $\boldsymbol{u} = \boldsymbol{u}_r$. In that case, the limitations will not only apply to the commanded control $\boldsymbol{u}_r$, but also to the real control $\boldsymbol{u}$.

D-3 Simulations

In order to evaluate the Command-Filtered BS approach, two simulations are performed by using the pendulum model:

1. Command-Filtered Backstepping without constraints;
2. Command-Filtered Backstepping with constraints.

D-3-1 Command-Filtered Backstepping without constraints

In this section a Command-Filtered BS control law is derived for the pendulum model, which is for convenience repeated below:

$$\dot{x}_1 = x_2 \tag{B-3a revisited}$$

$$\dot{x}_2 = \theta_{2,1}\sin(x_1) + \theta_{2,2}x_2 + \theta_{2,3}u\,. \tag{B-3b revisited}$$

The control task is to track the smooth reference state $x_{1,r}$ with the state x_1. We start by defining the tracking errors as

$$z_1 = x_1 - x_{1,r} \tag{D-34a}$$

$$z_2 = x_2 - x_{2,r}\,, \tag{D-34b}$$

where $x_{2,r}$ is the new virtual control law to be designed. As with the standard BS procedure, the first virtual control is defined as

$$\alpha_1 = -c_1 z_1 + \dot{x}_{1,r}\,, \quad c_1 > 0\,. \tag{C-35 revisited}$$

However, instead of directly applying this virtual control, a new signal $x_{2,r}^0$ is defined as

$$x_{2,r}^0 = \alpha_1 - \chi_2\,, \tag{D-35}$$

where χ_2 will be defined later on. The raw signal $x_{2,r}^0$ is led through a command filter to obtain $x_{2,r}$ and its derivative $\dot{x}_{2,r}$. The effect that the use of this command filter has on the tracking error z_1 is estimated by the stable linear filter

$$\dot{\chi}_1 = -c_1\chi_1 + \left(x_{2,r} - x_{2,r}^0\right)\,, \tag{D-36}$$

with $\chi_1(0) = 0$. The auxiliary system (D-36) compensates for the constraint effects due to magnitude, rate and bandwidth limitations of the command filter. Now we introduce the *compensated* tracking errors:

$$\bar{z}_1 = z_1 - \chi_1 \tag{D-37a}$$
$$\bar{z}_2 = z_2 - \chi_2 \,. \tag{D-37b}$$

The $\bar{z}_1$-dynamics are given by

$$\dot{\bar{z}}_1 = z_2 + x_{2,r} - \dot{x}_{1,r} - \dot{\chi}_1 \,. \tag{D-38}$$

We start by formulating a quadratic scalar CLF for the first compensated tracking error:

$$\mathcal{V}_1(\bar{z}_1) = \frac{1}{2}\bar{z}_1^2 \,. \tag{D-39}$$

Taking the time derivative of $\mathcal{V}_1$ along the trajectories of Eq. (D-38) results in

$$\begin{aligned}
\dot{\mathcal{V}}_1 &= \bar{z}_1 \left(z_2 + x_{2,r} - \dot{x}_{1,r} - \dot{\chi}_1\right) \\
&= \bar{z}_1 \left(z_2 + x_{2,r} - x^0_{2,r} + x^0_{2,r} - \dot{x}_{1,r} - \dot{\chi}_1\right) \\
&= \bar{z}_1 \left(z_2 + x_{2,r} - x^0_{2,r} + \alpha_1 - \chi_2 - \dot{x}_{1,r} - \dot{\chi}_1\right) \\
&= \bar{z}_1 \left(-c_1 z_1 + \bar{z}_2 + x_{2,r} - x^0_{2,r} + c_1\chi_1 - x_{2,r} + x^0_{2,r}\right) \\
&= \bar{z}_1 \left(-c_1 \left(z_1 - \chi_1\right) + \bar{z}_2\right) \\
&= -c_1\bar{z}_1^2 + \bar{z}_1\bar{z}_2 \,.
\end{aligned} \tag{D-40}$$

The cross term $\bar{z}_1\bar{z}_2$ will be dealt with in the next design step. Now we move on to the second and final compensated subsystem. The $\bar{z}_2$-dynamics are given by

$$\dot{\bar{z}}_2 = \theta_{2,1}\sin(x_1) + \theta_{2,2}x_2 + \theta_{2,3}u - \dot{x}_{2,r} - \dot{\chi}_2 \,. \tag{D-41}$$

Now we augment the quadratic CLF function to penalize the second compensated tracking error as well:

$$\mathcal{V}(\bar{\boldsymbol{z}}) = \mathcal{V}_1 + \frac{1}{2}\bar{z}_2^2 \,. \tag{D-42}$$

Taking the time derivative of $\mathcal{V}$ along the solutions of Eqs. (D-38) and (D-41) results in

$$\dot{\mathcal{V}} = -c_1\bar{z}_1^2 + \bar{z}_1\bar{z}_2 + \bar{z}_2\left[\theta_{2,1}\sin(x_1) + \theta_{2,2}x_2 + \theta_{2,3}u - \dot{x}_{2,r} - \dot{\chi}_2\right] \,. \tag{D-43}$$

A raw control signal u^0 is led through a command filter to obtain u. The effect that the use of this command filter has on the tracking error z_2 is estimated by the stable linear filter

$$\dot{\chi}_2 = -c_2\chi_2 + \theta_{2,3}\left(u - u^0\right) \,, \tag{D-44}$$

with $\chi_2(0) = 0$. This yields

$$\dot{\mathcal{V}} = -c_1\bar{z}_1^2 + \bar{z}_1\bar{z}_2 + \bar{z}_2\left[\theta_{2,1}\sin(x_1) + \theta_{2,2}x_2 - \dot{x}_{2,r} + c_2\chi_2 + \theta_{2,3}u^0\right] \,. \tag{D-45}$$

Selecting the following raw control law:

$$u^0 = \frac{1}{\theta_{2,3}} \left[-c_2 z_2 - \bar{z}_1 - \theta_{2,1} \sin(x_1) - \theta_{2,2} x_2 + \dot{x}_{2,r} \right] , \quad c_2 > 0 , \tag{D-46}$$

renders the CLF negative definite

$$\begin{aligned} \dot{\mathcal{V}} &= -c_1 \bar{z}_1^2 + \bar{z}_1 \bar{z}_2 + \bar{z}_2 \left(c_2 \chi_2 - c_2 z_2 - \bar{z}_1 \right) \\ &= -c_1 \bar{z}_1^2 + \bar{z}_1 \bar{z}_2 + \bar{z}_2 \left(-c_2 \bar{z}_2 - \bar{z}_1 \right) \\ &= -c_1 \bar{z}_1^2 - c_2 \bar{z}_2^2 . \end{aligned} \tag{D-47}$$

By Theorem C.2 it now follows that the equilibrium $\bar{\boldsymbol{z}} = \mathbf{0}$ is globally uniformly asymptotically stable. Note that this derivation only guarantees desirable properties for the *compensated* tracking error $\bar{\boldsymbol{z}}$ and not the *actual* tracking error $\boldsymbol{z}$. According to (Farrell et al., 2005), in the absence of physical limitations (i.e. magnitude, rate, and bandwidth constraints on the commanded state $x_{2,r}$ and control u), convergence of the tracking error $\boldsymbol{z}$ is still guaranteed. When the inputs are too aggressive, the implemented limits can come into effect. During such a period $\boldsymbol{z}$ and $\boldsymbol{\chi}$ become nonzero because the desired control signals are not able to be implemented. However, the $\boldsymbol{\chi}$-signals and therefore also the tracking error $\boldsymbol{z}$ will remain bounded, because $\boldsymbol{\chi}$ is the output of a stable linear system with a bounded input. When the limits are no longer in effect, the tracking error $\boldsymbol{z}$ will converge to $\mathbf{0}$.

The controller structure developed in this section can be seen in Figure D-3. In this diagram CF represents the Command Filter (see Appendix D-2) and AF represents the Auxiliary Filter (see Eqs. (D-36) and (D-44)).

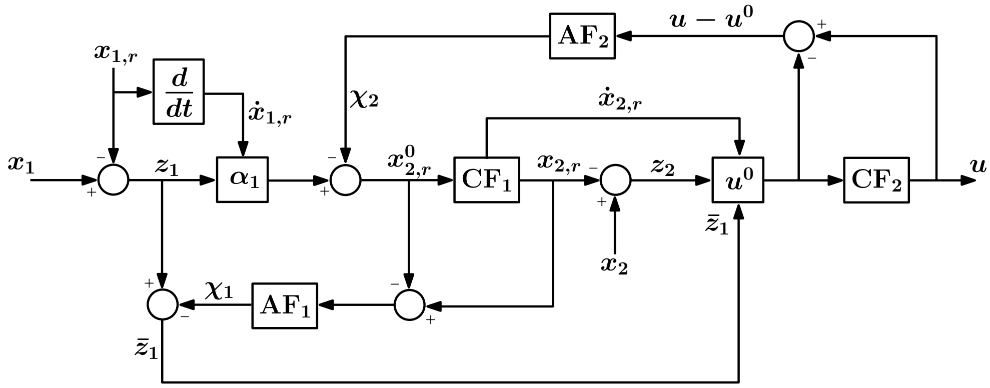

Figure D-3: Command-Filtered Backstepping controller structure.

Note that if magnitude, rate and bandwidth constraints on the control u are not necessary, then we can omit the second command filter and the second auxiliary filter (D-44).

If we compare the earlier designed conventional BS controller with the Command-Filtered BS control law:

$$u = \frac{1}{\theta_{2,3}} \left[-c_2 \left(x_2 - \alpha_1 \right) - z_1 - \theta_{2,1} \sin(x_1) - \theta_{2,2} x_2 + \dot{\alpha}_1 \right] \tag{C-39 revisited}$$

$$u^0 = \frac{1}{\theta_{2,3}} \left[-c_2 \left(x_2 - x_{2,r} \right) - \bar{z}_1 - \theta_{2,1} \sin(x_1) - \theta_{2,2} x_2 + \dot{x}_{2,r} \right] , \tag{D-46 revisited}$$

we can see that the Command-Filtered BS control law depends on $x_{2,r}$ and $\dot{x}_{2,r}$. These signals are the output of the command filter and therefore the analytical derivative $\dot{\alpha}_1$ is no longer required. In the absence of physical limitations (i.e. magnitude, rate and bandwidth constraints on the commanded state $x_{2,r}$ and control u), convergence of the tracking errors is still guaranteed.

Simulations of the full-information BS controller augmented with a first-order, low-pass command filter with unity DC gain and bandwidth ω_n have been run with a sampling time of 0.01 s. The command filter is used to obtain an estimate of the stabilizing function α_1 and its time derivative $\dot{\alpha}_1$. Note that we make use of a *first*-order filter because we are dealing with noise-free measurements. The initial conditions and parameters which have been used in this simulation for the model and controller can be found in respectively Eqs. (C-44) and (C-45). The results of the simulation can be seen in Figures D-4 and D-5. As expected, when ω_n increases, the solution of the Command-Filtered BS closed-loop system converges to the BS solution that relies on analytic derivatives. However, if we keep increasing the natural frequency of the command filter, then at around $\omega_n = 300\,\text{rad/s}$ the system becomes unstable because the high frequent dynamics cannot be captured with the relatively low sampling rate of 100 Hz. By increasing the sampling rate or by selecting a solver with a higher order of accuracy, the natural frequency of the command filter can be further increased.

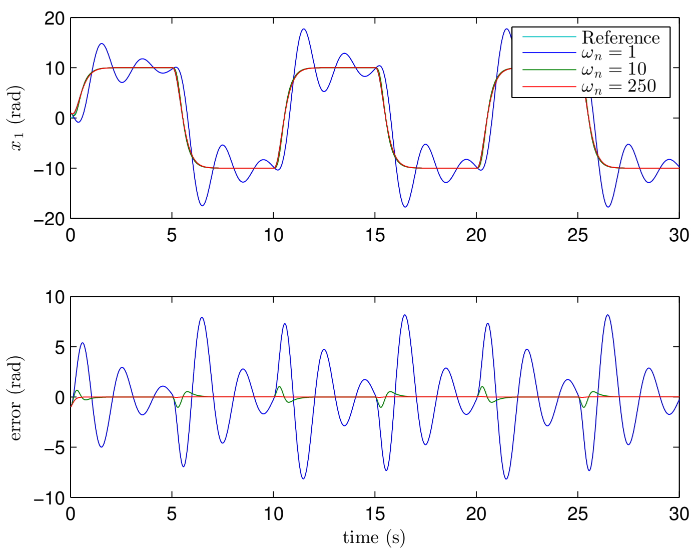

Figure D-4: The control performance of the Backstepping controller in the absence of any uncertainties. A first-order, low-pass filter with unity DC gain and bandwidth ω_n is used to obtain an estimate of the stabilizing function and its time derivative.

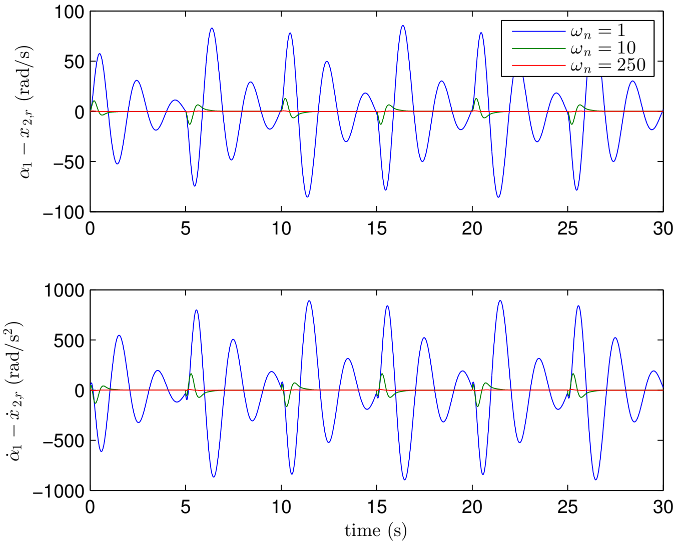

Figure D-5: Using a first-order, low-pass filter with unity DC gain and bandwidth ω_n to obtain an estimate of the stabilizing function and its time derivative.

D-3-2 Command-Filtered Backstepping with constraints

Now we introduce a magnitude limit for the control u of 1000 Nm. This control limit has been implemented in two different ways. In the first simulation, referred to as *BS + 1CF* in Figures D-6 and D-7, this control limit has been implemented as follows:

$$u = S_{1000} \left\{ \frac{1}{\theta_{2,3}} \left[-c_2 z_2 - \bar{z}_1 - \theta_{2,1} \sin(x_1) - \theta_{2,2} x_2 + \dot{x}_{2,r} \right] \right\} , \tag{D-48}$$

where S_M is defined in Eq. (D-28). In this simulation only one command filter is used to obviate the need for analytic computation of the virtual control derivative. That is, we only define a raw signal $x^0_{2,r}$ but not a raw control signal u^0. In the second simulation, referred to as *BS + 2CF* in Figures D-6 and D-7, this control limit has been introduced by implementation of a very simple second command filter:

$$\begin{aligned} u &= S_{1000} \left\{ u^0 \right\} \\ &= S_{1000} \left\{ \frac{1}{\theta_{2,3}} \left[-c_2 z_2 - \bar{z}_1 - \theta_{2,1} \sin(x_1) - \theta_{2,2} x_2 + \dot{x}_{2,r} \right] \right\} . \end{aligned} \tag{D-49}$$

A second stable linear filter Eq. (D-44) is used to estimate the effect that the use of this command filter has on the tracking error z_2. The initial conditions and parameters which have been used in this simulation for the model and controller can be found in respectively Eqs. (C-44) and (C-45). The results of the simulation with a sampling time of 0.01 s can be seen in Figures D-6 and D-7.

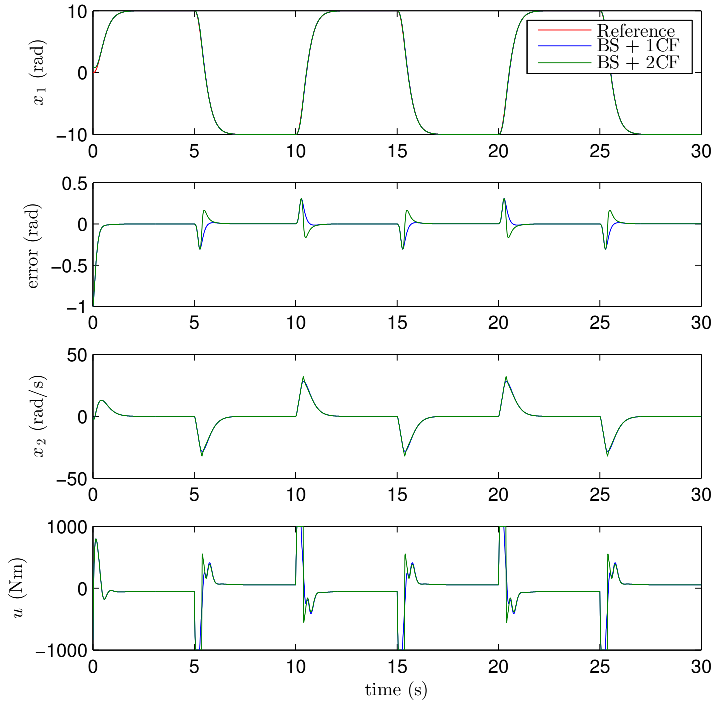

Figure D-6: Using two different ways of implementing the control magnitude limitation of $1000\,\mathrm{Nm}$. The bandwidths of the command filters are selected as $\omega_{n,1} = \omega_{n,2} = 200$ rad/s.

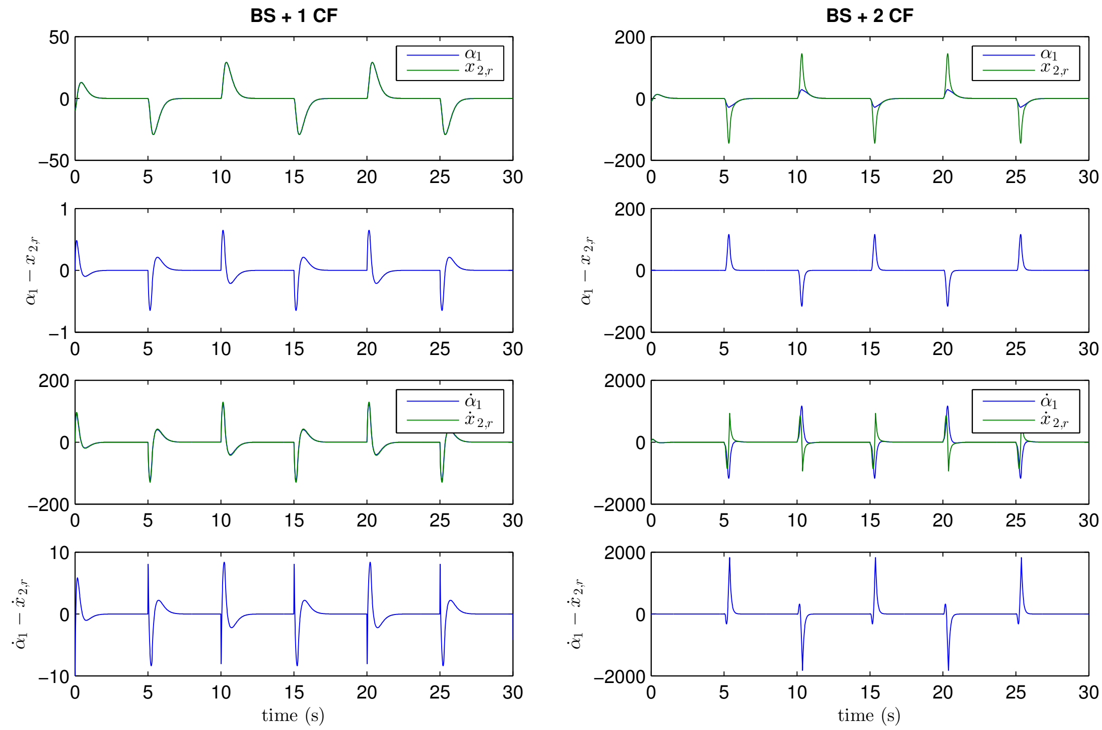

Figure D-7: Using two different ways of implementing the control magnitude limitation of $1000\,\mathrm{Nm}$. The bandwidths of the command filters are selected as $\omega_{n,1} = \omega_{n,2} = 200\,\mathrm{rad/s}$. The variables $x_{2,r}$ and $\dot{x}_{2,r}$ are approximations of the virtual control law α_1 and its derivative $\dot{\alpha}_1$.

From Figure D-6 we can conclude that both implementations of the control magnitude limit result in good tracking performance. The small tracking errors during the maneuver are due to the physical constraints. From Figure D-7 it can be seen that the variables $x_{2,r}$ and $\dot{x}_{2,r}$ for the *BS + 2CF* implementation are much larger compared to the more simpler implementation *BS + 1CF*. This can be explained as follows: when the control is saturated, the term $\left(u - u^0\right)$ in Eq. (D-44) will no longer equal 0, resulting in an increase of magnitude of signal χ_2. Following Eq. (D-35), the variable $x^0_{2,r}$ and thus the command-filtered signal $x_{2,r}$ will increase in magnitude. Now note that the raw control input u^0 is given by

$$u^0 = \frac{1}{\theta_{2,3}} \left[-c_2 \left(x_2 - x_{2,r}\right) - \bar{z}_1 - \theta_{2,1} \sin(x_1) - \theta_{2,2} x_2 + \dot{x}_{2,r} \right] . \qquad \text{(D-46 revisited)}$$

By analyzing this formula we expect to encounter saturation problems for the *BS + 2CF* implementation when the variables $x_{2,r}$ and $\dot{x}_{2,r}$ become very large. To verify this, we now make the control input u more restrictive by setting its magnitude limit to only 800 Nm with the same initial conditions and control parameters as before. The results of this simulation can be found in Figure D-8. Clearly, the *BS + 2CF* implementation results in unsatisfactory tracking performance. The reason is that the variables $x_{2,r}$ and $\dot{x}_{2,r}$ now become even larger compared to the previous simulation due to the lower magnitude limit of the control, resulting in a larger raw control signal u^0 according to Eq. (D-46). From Figure D-9 we can conclude that this results in almost continuous saturation of the control input, and therefore we can no longer guarantee desirable properties of the actual tracking error $\boldsymbol{z}$.

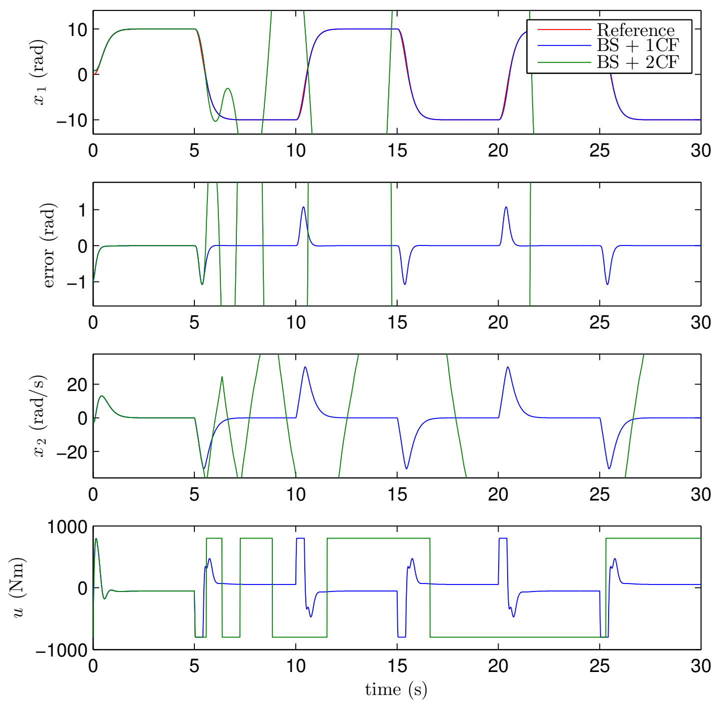

Figure D-8: Using two different ways of implementing the control magnitude limitation of 800 Nm. The bandwidths of the command filters are selected as $\omega_{n,1} = \omega_{n,2} = 200$ rad/s.

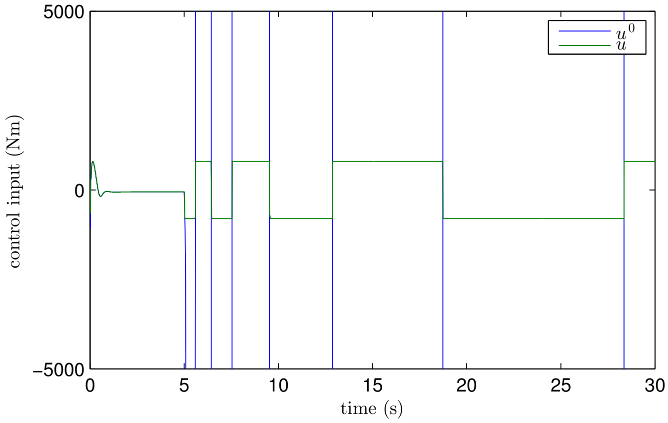

Figure D-9: The raw control input u^0 and the actual control input u with a magnitude limitation of $800\,\mathrm{Nm}$ for the BS + 2CF implementation.

Note that we can set a magnitude limit on $x_{2,r}$ using the command filter in order to prevent continuous saturation of the control (see Eq. (D-46)), and thereby improve the tracking performance of the *BS + 2CF* implementation. A new simulation has been run with the same initial conditions, control parameters and real control magnitude limit as before, but now also with a magnitude limit on the variable $x_{2,r}$. From Figure D-10 we can conclude that the performance of the two different implementations is now almost identical. From these simulation results it seems that when we only need to apply magnitude limits to the actual control, it is advantageous to use the *BS + 1CF* implementation because it is simpler and the performance is almost identical to that of the *BS + 2CF* implementation. However, in later sections it will become evident that the use of the second command filter significantly improves the parameter estimation of adaptive controllers when control limits come into effect.

Note that the command filters as in Figures D-1 and D-2 cannot be used to implement rate, magnitude or bandwidth constraints on the *actual* state x_2, but only on the *commanded* state $x_{2,r}$. Setting a limit on $x_{2,r}$ does not guarantee that x_2 will not exceed this limit, as can be seen from Figure D-11.

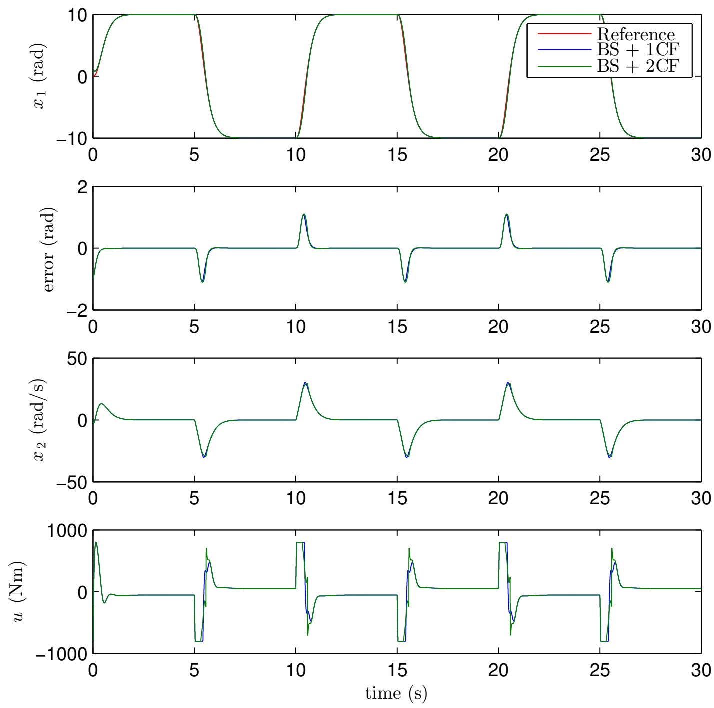

Figure D-10: Using two different ways of implementing the control magnitude limitation of $800\,\mathrm{Nm}$. The bandwidths of the command filters are selected as $\omega_{n,1} = \omega_{n,2} = 200\,\mathrm{rad/s}$. The variable $x_{2,r}$ is constrained to $\pm 40\,\mathrm{rad/s}$ for the BS + 2CF implementation to avoid continuous saturation of the input signal.

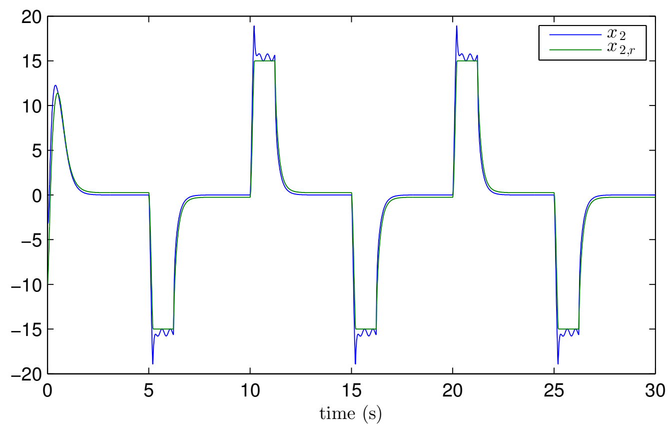

Figure D-11: The angular rate x_2 and the commanded angular rate $x_{2,r}$, the latter is magnitude limited to $\pm 15\,\mathrm{rad/s}$.

Appendix E

Incremental Backstepping

Incremental Backstepping (IBS) improves the robustness of the closed-loop system with respect to conventional Backstepping (BS). This is achieved by reducing the dependency on the exact knowledge of the plant dynamics (E-1). In order to evaluate this nonlinear control approach, (Command-Filtered) IBS control laws are derived and simulated for the pendulum model (E-2).

E-1 Theory

In order to apply IBS, a first-order Taylor series expansion of the nonlinear system needs to be derived. The *incremental* control law is then obtained on basis of the *linearized* system (E-1-1). Similar as for conventional BS, IBS can be extended with command filters to obviate the need for analytic computation of virtual control derivatives (E-1-2).

E-1-1 Incremental Backstepping

We consider the following cascaded nonlinear system:

$$\dot{\boldsymbol{x}}_1 = \boldsymbol{h}(\boldsymbol{x}_1) + K(\boldsymbol{x}_1)\boldsymbol{x}_2 \tag{E-1a}$$

$$\dot{\boldsymbol{x}}_2 = \boldsymbol{f}(\boldsymbol{x}_1, \boldsymbol{x}_2) + G(\boldsymbol{x}_1, \boldsymbol{x}_2)\boldsymbol{u}\,, \tag{E-1b}$$

where $\boldsymbol{x}_1 \in \mathbb{R}^{n_1}$ and $\boldsymbol{x}_2 \in \mathbb{R}^{n_2}$ are the state vectors, $\boldsymbol{u} \in \mathbb{R}^m$ is the input vector, $\boldsymbol{h}$ and $\boldsymbol{f}$ are smooth vector fields on respectively $\mathbb{R}^{n_1}$ and $\mathbb{R}^{n_2}$, and $K \in \mathbb{R}^{n_1 \times n_2}$ and $G \in \mathbb{R}^{n_2 \times m}$ are known matrices whose columns are smooth vector fields. The control task is to track a smooth reference signal $\boldsymbol{x}_{1,r}$, for which the first and second-order time derivative are assumed to be known and bounded. Furthermore, the signal $\boldsymbol{x}_2$ must remain bounded. It is assumed that the $\boldsymbol{x}_1$-subsystem is fully known while subsystem $\boldsymbol{x}_2$ contains uncertainties. This is a valid assumption in many aerospace control applications, because the $\boldsymbol{x}_1$-subsystem generally contains the *known* kinematic equations, while subsystem $\boldsymbol{x}_2$ contains the *uncertain* dynamic equations.

The design procedure for the IBS controller is as follows:

Subsystem $\boldsymbol{x}_1$

Similar as in the recursive BS approach, we start by considering the subsystem which is located "furthest" away from the control vector $\boldsymbol{u}$, that is:

$$\dot{\boldsymbol{x}}_1 = \boldsymbol{h}(\boldsymbol{x}_1) + K(\boldsymbol{x}_1)\boldsymbol{x}_2 \,. \tag{E-1a revisited}$$

Now we regard state vector $\boldsymbol{x}_2$ as the control input for this subsystem. However, because $\boldsymbol{x}_2$ is just a state vector and not the real control vector $\boldsymbol{u}$, we call $\boldsymbol{x}_2$ the *virtual control.*

The tracking errors are defined as

$$\boldsymbol{z}_1 = \boldsymbol{x}_1 - \boldsymbol{x}_{1,r} \tag{E-2a}$$

$$\boldsymbol{z}_2 = \boldsymbol{x}_2 - \boldsymbol{x}_{2,r} \equiv \boldsymbol{x}_2 - \boldsymbol{\alpha}_1 \,, \tag{E-2b}$$

where $\boldsymbol{x}_{2,r} \equiv \boldsymbol{\alpha}_1$ is called the *stabilizing vector field*, which is the desired value of $\boldsymbol{x}_2$. Rewriting the current subsystem in terms of the tracking error $\boldsymbol{z}_1$ results in

$$\begin{aligned}\dot{\boldsymbol{z}}_1 &= \dot{\boldsymbol{x}}_1 - \dot{\boldsymbol{x}}_{1,r}\\ &= \boldsymbol{h} + K\boldsymbol{x}_2 - \dot{\boldsymbol{x}}_{1,r}\\ &= \boldsymbol{h} + K\left(\boldsymbol{z}_2 + \boldsymbol{\alpha}_1\right) - \dot{\boldsymbol{x}}_{1,r} \,.\end{aligned} \tag{E-3}$$

Now we formulate a quadratic scalar Control Lyapunov Function (CLF) for the first subsystem:

$$\mathcal{V}_1(\boldsymbol{z}_1) = \frac{1}{2}\boldsymbol{z}_1^T\boldsymbol{z}_1 \,. \tag{E-4}$$

The reason for choosing a quadratic scalar function is to allow for ease of checking sign definiteness. Taking the time derivative of the CLF along the trajectories of subsystem (E-3) results in

$$\dot{\mathcal{V}}_1 = \boldsymbol{z}_1\big[\boldsymbol{h} + K\left(\boldsymbol{z}_2 + \boldsymbol{\alpha}_1\right) - \dot{\boldsymbol{x}}_{1,r}\big] \,. \tag{E-5}$$

In order to yield the CLF negative definite, an obvious choice for stabilizing control law $\boldsymbol{\alpha}_1$ is

$$\boldsymbol{\alpha}_1 = K^{-1}\left[-c_1\boldsymbol{z}_1 - \boldsymbol{h} + \dot{\boldsymbol{x}}_{1,r}\right] \,, \quad c_1 > 0 \,, \tag{E-6}$$

which results in the following expression for $\dot{\mathcal{V}}_1$:

$$\dot{\mathcal{V}}_1 = -\boldsymbol{z}_1^T c_1 \boldsymbol{z}_1 + \boldsymbol{z}_1^T K \boldsymbol{z}_2 \,. \tag{E-7}$$

The time derivative of the CLF $\dot{\mathcal{V}}_1$ is not negative definite for all values of $\boldsymbol{z}_1$ and $\boldsymbol{z}_2$. The cross term $\boldsymbol{z}_1^T K\boldsymbol{z}_2$ will be removed in the next design step. By selecting the stabilizing function as Eq. (E-6) we have canceled the natural dynamics of the system. However, if certain nonlinearities are stabilizing, they need not to be canceled (Farrell et al., 2009).

Note that if K is a non-square matrix or a square matrix without full rank, some form of virtual control allocation would be required, see for instance (Enns, 1998; Lombaerts, 2010). Also note that the approach taken so far is identical to that of recursive BS, see Appendix C-2. This is as expected because the first subsystem is assumed to be fully known.

Subsystem $\boldsymbol{x}_2$

Now we consider the final subsystem:

$$\dot{\boldsymbol{x}}_2 = \boldsymbol{f}(\boldsymbol{x}_1, \boldsymbol{x}_2) + G(\boldsymbol{x}_1, \boldsymbol{x}_2)\boldsymbol{u} \,. \tag{E-1b revisited}$$

Taking the first-order Taylor series expansion of Eq. (E-1b) around the current solution $[\boldsymbol{x}_0, \boldsymbol{u}_0]$ results in

$$\dot{\boldsymbol{x}}_2 \cong \boldsymbol{f}(\boldsymbol{x}_0) + G(\boldsymbol{x}_0)\boldsymbol{u}_0 + \frac{\partial}{\partial \boldsymbol{x}}\left[\boldsymbol{f}(\boldsymbol{x}) + G(\boldsymbol{x})\boldsymbol{u}\right]\Big|_{\substack{\boldsymbol{x}=\boldsymbol{x}_0\\ \boldsymbol{u}=\boldsymbol{u}_0}} (\boldsymbol{x}-\boldsymbol{x}_0) + \frac{\partial}{\partial \boldsymbol{u}}\left[G(\boldsymbol{x})\boldsymbol{u}\right]\Big|_{\substack{\boldsymbol{x}=\boldsymbol{x}_0\\ \boldsymbol{u}=\boldsymbol{u}_0}} (\boldsymbol{u}-\boldsymbol{u}_0) \,. \tag{E-8}$$

The linearization error is small when the sampling rate is sufficiently high. Eq. (E-8) can be written as

$$\dot{\boldsymbol{x}}_2 \cong \dot{\boldsymbol{x}}_{2,0} + A_0 \Delta \boldsymbol{x} + B_0 \Delta \boldsymbol{u} \,, \tag{E-9}$$

where

$$\Delta \boldsymbol{x} = \boldsymbol{x} - \boldsymbol{x}_0 \,, \quad \Delta \boldsymbol{u} = \boldsymbol{u} - \boldsymbol{u}_0 \tag{E-10a}$$

$$A_0 = \frac{\partial}{\partial \boldsymbol{x}}\left[\boldsymbol{f}(\boldsymbol{x}) + G(\boldsymbol{x})\boldsymbol{u}\right]\Big|_{\substack{\boldsymbol{x}=\boldsymbol{x}_0\\ \boldsymbol{u}=\boldsymbol{u}_0}} \tag{E-10b}$$

$$B_0 = \frac{\partial}{\partial \boldsymbol{u}}\left[G(\boldsymbol{x})\boldsymbol{u}\right]\Big|_{\substack{\boldsymbol{x}=\boldsymbol{x}_0\\ \boldsymbol{u}=\boldsymbol{u}_0}} = G(\boldsymbol{x}_0) \,, \tag{E-10c}$$

and where $\boldsymbol{x}_0$ and $\boldsymbol{u}_0$ are the current state and control commands. The variables $\Delta \boldsymbol{x}$ and $\Delta \boldsymbol{u}$ are known as respectively the *incremental* state vector and the *incremental* control input.

If we assume a sufficiently time-scale separated system, that is the increment in state $\Delta \boldsymbol{x}$ is much smaller than the increment in both state derivative $\Delta \dot{\boldsymbol{x}}_2$ and input $\Delta \boldsymbol{u}$, we can neglect the former (Falkena, 2012; Sieberling et al., 2010; Acquatella et al., 2012; Simplício et al., 2013). This is allowed for many aerospace applications because the deflections of the control surfaces directly effect the angular accelerations, while the angular rates only change by integrating these angular accelerations. Hence Eq. (E-9) can be further simplified as follows:

$$\dot{\boldsymbol{x}}_2 \cong \dot{\boldsymbol{x}}_{2,0} + B_0 \Delta \boldsymbol{u} \,. \tag{E-11}$$

Now the $\boldsymbol{x}_2$-subsystem is written in incremental form, the BS procedure can be continued. Rewriting Eq. (E-11) in terms of the tracking error yields

$$\begin{aligned} \dot{\boldsymbol{z}}_2 &= \dot{\boldsymbol{x}}_2 - \dot{\boldsymbol{\alpha}}_1 \\ &\cong \dot{\boldsymbol{x}}_{2,0} + B_0 \Delta \boldsymbol{u} - \dot{\boldsymbol{\alpha}}_1 \,. \end{aligned} \tag{E-12}$$

The final Lyapunov function is now defined as

$$\mathcal{V}_2(\boldsymbol{z}_1, \boldsymbol{z}_2) = \frac{1}{2}\boldsymbol{z}_1^T \boldsymbol{z}_1 + \frac{1}{2}\boldsymbol{z}_2^T \boldsymbol{z}_2 \,. \tag{E-13}$$

Taking the time derivative of the CLF along the solutions of the error dynamics results in

$$\begin{aligned}\dot{\mathcal{V}}_2 &= \dot{\mathcal{V}}_1 + \boldsymbol{z}_2^T \dot{\boldsymbol{z}}_2 \\ &\cong -\boldsymbol{z}_1^T c_1 \boldsymbol{z}_1 + \boldsymbol{z}_1^T K \boldsymbol{z}_2 + \boldsymbol{z}_2^T \left[\dot{\boldsymbol{x}}_{2,0} + B_0 \Delta \boldsymbol{u} - \dot{\boldsymbol{\alpha}}_1\right] \\ &= -\boldsymbol{z}_1^T c_1 \boldsymbol{z}_1 + \boldsymbol{z}_2^T \left[\dot{\boldsymbol{x}}_{2,0} + B_0 \Delta \boldsymbol{u} - \dot{\boldsymbol{\alpha}}_1 + K^T \boldsymbol{z}_1\right] .\end{aligned} \tag{E-14}$$

In order to yield $\dot{\mathcal{V}}_2$ negative definite, an obvious choice for the incremental control vector $\Delta \boldsymbol{u}$ is

$$\Delta \boldsymbol{u} = B_0^{-1} \big[-c_2 \boldsymbol{z}_2 - \dot{\boldsymbol{x}}_{2,0} + \dot{\boldsymbol{\alpha}}_1 - K^T \boldsymbol{z}_1 \big] , \quad c_2 > 0 , \tag{E-15}$$

which results in the following expression for $\dot{\mathcal{V}}_2$:

$$\dot{\mathcal{V}}_2 \cong -\boldsymbol{z}_1^T c_1 \boldsymbol{z}_1 - \boldsymbol{z}_2^T c_2 \boldsymbol{z}_2 . \tag{E-16}$$

If the sampling rate is sufficiently high, then according to the theorem of *LaSalle-Yoshizawa* (see Theorem C.2, page 71) the equilibrium $\boldsymbol{z} = \boldsymbol{0}$ is globally uniformly asymptotically stable when $c_1 > 0$ and $c_2 > 0$, implying that the reference output state $\boldsymbol{x}_{1,r}$ is successfully tracked by $\boldsymbol{x}_1$, that is:

$$\lim_{t \to \infty} \left[\boldsymbol{x}_1 - \boldsymbol{x}_{1,r}\right] = \boldsymbol{0} . \tag{E-17}$$

Note that if B_0 is a non-square matrix or a square matrix without full rank, some form of control allocation would be required, see for instance (Enns, 1998; Lombaerts, 2010).

In order to obtain the *total* control signal $\boldsymbol{u}$, the *current* control deflection $\boldsymbol{u}_0$ needs to be added to the *incremental* control signal $\Delta \boldsymbol{u}$:

$$\boldsymbol{u} = \boldsymbol{u}_0 + B_0^{-1} \big[-c_2 \boldsymbol{z}_2 - \dot{\boldsymbol{x}}_{2,0} + \dot{\boldsymbol{\alpha}}_1 - K^T \boldsymbol{z}_1 \big] . \tag{E-18}$$

If we compare this incremental control with that of the recursive BS approach:

$$u = g_n^{-1} \left[-c_n z_n - f_n + \dot{\alpha}_{n-1} - z_{n-1} g_{n-1}\right] , \tag{C-27 revisited}$$

we can see that the newly developed IBS controller does not rely on exact knowledge of the system dynamics $\boldsymbol{f}$. However, from Eq. (E-18) we can see that that the incremental controller still depends on the control efficiency matrix B_0.

In the derivation of incremental control law (E-18), we have implicitly made Assumption E.1 (Acquatella et al., 2012).

Assumption E.1 (Incremental Backstepping)

1. Complete and accurate knowledge of the states is available. Note that IBS control law (E-18) requires information of the angular acceleration $\dot{\boldsymbol{x}}_{2,0}$. Sensors to measure these accelerations exist, however, they are not common. Therefore the angular accelerations are generally estimated on basis of (noisy) angular rate data.
   Moreover, incremental control law (E-18) requires actuator output measurements. If these are not available, they need to be estimated on basis of a high-fidelity model of the actuator dynamics.
2. The sampling rate is sufficiently high and the control actions are instantaneous. This suggests that the term $A_0 \Delta \boldsymbol{x}$ can be left out of incremental equation (E-9). Only when this assumption is valid, the incremental control law is robust to uncertainties in the system dynamics $\boldsymbol{f}$.

E-1-2 Command-Filtered Incremental Backstepping

We consider the following cascaded nonlinear system:

$$\dot{\boldsymbol{x}}_1 = \boldsymbol{h}(\boldsymbol{x}_1, \boldsymbol{x}_2) + K(\boldsymbol{x}_1, \boldsymbol{x}_2)\boldsymbol{x}_2 \tag{E-19a}$$

$$\dot{\boldsymbol{x}}_2 = \boldsymbol{f}(\boldsymbol{x}_1, \boldsymbol{x}_2) + G(\boldsymbol{x}_1, \boldsymbol{x}_2)\boldsymbol{u}\,, \tag{E-19b}$$

where $\boldsymbol{x}_1 \in \mathbb{R}^{n_1}$ and $\boldsymbol{x}_2 \in \mathbb{R}^{n_2}$ are the state vectors, $\boldsymbol{u} \in \mathbb{R}^m$ is the input vector, $\boldsymbol{h}$ and $\boldsymbol{f}$ are smooth vector fields on respectively $\mathbb{R}^{n_1}$ and $\mathbb{R}^{n_2}$, and $K \in \mathbb{R}^{n_1 \times n_2}$ and $G \in \mathbb{R}^{n_2 \times m}$ are known matrices whose columns are smooth vector fields. The control task is to track a smooth reference signal $\boldsymbol{x}_{1,r}$, for which the time derivative is assumed to be known and bounded. Furthermore, the signal $\boldsymbol{x}_2$ must remain bounded. It is assumed that the $\boldsymbol{x}_1$-subsystem is fully known while subsystem $\boldsymbol{x}_2$ contains uncertainties. This is a valid assumption in many aerospace control applications, because the $\boldsymbol{x}_1$-subsystem generally contains the *known* kinematic equations, while subsystem $\boldsymbol{x}_2$ contains the *uncertain* dynamic equations. Note that the difference with system (E-1) is that vector function $\boldsymbol{h}$ and matrix K may now depend on all states $\boldsymbol{x}$.

The design procedure for the Command-Filtered IBS controller is as follows:

Subsystem $\boldsymbol{x}_1$

Similar as in the recursive BS approach, we start by considering the subsystem which is located "furthest" away from the control vector $\boldsymbol{u}$, that is:

$$\dot{\boldsymbol{x}}_1 = \boldsymbol{h}(\boldsymbol{x}_1, \boldsymbol{x}_2) + K(\boldsymbol{x}_1, \boldsymbol{x}_2)\boldsymbol{x}_2\,. \tag{E-19a revisited}$$

Now we regard state vector $\boldsymbol{x}_2$ as the control input for this subsystem. However, because $\boldsymbol{x}_2$ is just a state vector and not the real control vector $\boldsymbol{u}$, we call $\boldsymbol{x}_2$ the *stabilizing vector field.*

The tracking errors are defined as

$$\boldsymbol{z}_1 = \boldsymbol{x}_1 - \boldsymbol{x}_{1,r} \tag{E-20a}$$

$$\boldsymbol{z}_2 = \boldsymbol{x}_2 - \boldsymbol{x}_{2,r}\,, \tag{E-20b}$$

where $\boldsymbol{x}_{2,r}$ is the new virtual control law to be designed. As with the standard BS procedure, the first stabilizing control law is defined as

$$\boldsymbol{\alpha}_1 = K^{-1}\left[-c_1\boldsymbol{z}_1 - \boldsymbol{h} + \dot{\boldsymbol{x}}_{1,r}\right]\,, \quad c_1 > 0\,. \tag{E-6 revisited}$$

However, instead of directly applying this virtual control, a new signal $\boldsymbol{x}^0_{2,r}$ is defined as

$$\boldsymbol{x}^0_{2,r} = \boldsymbol{\alpha}_1 - \boldsymbol{\chi}_2\,, \tag{E-21}$$

where $\boldsymbol{\chi}_2$ will be defined later on. The raw signal $\boldsymbol{x}^0_{2,r}$ is led through a command filter to obtain $\boldsymbol{x}_{2,r}$ and its time derivative $\dot{\boldsymbol{x}}_{2,r}$. The effect that the use of this command filter has on the tracking error $\boldsymbol{z}_1$ is estimated by the stable linear filter

$$\dot{\boldsymbol{\chi}}_1 = -c_1\boldsymbol{\chi}_1 + K\left(\boldsymbol{x}_{2,r} - \boldsymbol{x}^0_{2,r}\right)\,, \tag{E-22}$$

with $\boldsymbol{\chi}_1(0) = \mathbf{0}$. This auxiliary system compensates for the constraint effects due to magnitude, rate and bandwidth limitations of the command filter. Now we introduce the *compensated* tracking errors

$$\bar{\boldsymbol{z}}_1 = \boldsymbol{z}_1 - \boldsymbol{\chi}_1 \tag{E-23a}$$
$$\bar{\boldsymbol{z}}_2 = \boldsymbol{z}_2 - \boldsymbol{\chi}_2 \,. \tag{E-23b}$$

The $\bar{\boldsymbol{z}}_1$-dynamics are given by

$$\begin{aligned}
\dot{\bar{\boldsymbol{z}}}_1 &= \dot{\boldsymbol{z}}_1 - \dot{\boldsymbol{\chi}}_1 \\
&= \boldsymbol{h} + K\boldsymbol{x}_2 - \dot{\boldsymbol{x}}_{1,r} + c_1\boldsymbol{\chi}_1 - K\left(\boldsymbol{x}_{2,r} - \boldsymbol{x}_{2,r}^0\right) \\
&= \boldsymbol{h} + K\left(\boldsymbol{z}_2 + \boldsymbol{x}_{2,r}\right) - \dot{\boldsymbol{x}}_{1,r} + c_1\boldsymbol{\chi}_1 - K\left(\boldsymbol{x}_{2,r} - \boldsymbol{x}_{2,r}^0\right) \,.
\end{aligned} \tag{E-24}$$

Now we formulate a quadratic scalar CLF for the first compensated tracking error

$$\mathcal{V}_1(\bar{\boldsymbol{z}}_1) = \frac{1}{2}\bar{\boldsymbol{z}}_1^T\bar{\boldsymbol{z}}_1 \,. \tag{E-25}$$

Taking the time derivative of the CLF along the trajectories of subsystem (E-24) results in

$$\begin{aligned}
\dot{\mathcal{V}}_1 &= \bar{\boldsymbol{z}}_1^T\left[\boldsymbol{h} + K\left(\boldsymbol{z}_2 + \boldsymbol{x}_{2,r}\right) - \dot{\boldsymbol{x}}_{1,r} + c_1\boldsymbol{\chi}_1 - K\left(\boldsymbol{x}_{2,r} - \boldsymbol{x}_{2,r}^0\right)\right] \\
&= \bar{\boldsymbol{z}}_1^T\left[\boldsymbol{h} + K\left(\boldsymbol{z}_2 + \boldsymbol{x}_{2,r}\right) - K\boldsymbol{x}_{2,r}^0 + K\boldsymbol{x}_{2,r}^0 - \dot{\boldsymbol{x}}_{1,r} + c_1\boldsymbol{\chi}_1 - K\left(\boldsymbol{x}_{2,r} - \boldsymbol{x}_{2,r}^0\right)\right] \\
&= \bar{\boldsymbol{z}}_1^T\left[\boldsymbol{h} + K\left(\boldsymbol{z}_2 + \boldsymbol{x}_{2,r}\right) - K\boldsymbol{x}_{2,r}^0 + K\left(\boldsymbol{\alpha}_1 - \boldsymbol{\chi}_2\right) - \dot{\boldsymbol{x}}_{1,r} + c_1\boldsymbol{\chi}_1 - K\left(\boldsymbol{x}_{2,r} - \boldsymbol{x}_{2,r}^0\right)\right] \\
&= \bar{\boldsymbol{z}}_1^T\left[-c_1\boldsymbol{z}_1 + K\left(\boldsymbol{z}_2 + \boldsymbol{x}_{2,r}\right) - K\boldsymbol{x}_{2,r}^0 - K\boldsymbol{\chi}_2 + c_1\boldsymbol{\chi}_1 - K\left(\boldsymbol{x}_{2,r} - \boldsymbol{x}_{2,r}^0\right)\right] \\
&= \bar{\boldsymbol{z}}_1^T\left[-c_1\boldsymbol{z}_1 + K\bar{\boldsymbol{z}}_2 + c_1\boldsymbol{\chi}_1\right] \\
&= \bar{\boldsymbol{z}}_1^T\left[-c_1\left(\boldsymbol{z}_1 - \boldsymbol{\chi}_1\right) + K\bar{\boldsymbol{z}}_2\right] \\
&= -\bar{\boldsymbol{z}}_1^T c_1\bar{\boldsymbol{z}}_1 + \bar{\boldsymbol{z}}_1^T K\bar{\boldsymbol{z}}_2 \,.
\end{aligned} \tag{E-26}$$

The time derivative $\dot{\mathcal{V}}_1$ is not negative define for all values of $\bar{\boldsymbol{z}}_1$ and $\bar{\boldsymbol{z}}_2$. The cross term $\bar{\boldsymbol{z}}_1^T K\bar{\boldsymbol{z}}_2$ will be removed in the next design step. Note that if K is a non-square matrix or a square matrix without full rank, some form of virtual control allocation would be required, see for instance (Enns, 1998; Lombaerts, 2010). Also note that the approach taken so far is identical to that of Command-Filtered BS, see Appendix D. This is as expected because the first subsystem is assumed to be fully known.

Subsystem $\boldsymbol{x}_2$

Now we consider the final subsystem:

$$\dot{\boldsymbol{x}}_2 = \boldsymbol{f}(\boldsymbol{x}_1, \boldsymbol{x}_2) + G(\boldsymbol{x}_1, \boldsymbol{x}_2)\boldsymbol{u} \,. \tag{E-19b revisited}$$

Taking the first-order Taylor series expansion of Eq. (E-19b) around the current solution $[\boldsymbol{x}_0, \boldsymbol{u}_0]$ results in

$$\dot{\boldsymbol{x}}_2 \cong \boldsymbol{f}(\boldsymbol{x}_0) + G(\boldsymbol{x}_0)\boldsymbol{u}_0 + \frac{\partial}{\partial \boldsymbol{x}}\left[\boldsymbol{f}(\boldsymbol{x}) + G(\boldsymbol{x})\boldsymbol{u}\right]\Big|_{\substack{\boldsymbol{x}=\boldsymbol{x}_0 \\ \boldsymbol{u}=\boldsymbol{u}_0}}\left(\boldsymbol{x} - \boldsymbol{x}_0\right) + \frac{\partial}{\partial \boldsymbol{u}}\left[G(\boldsymbol{x})\boldsymbol{u}\right]\Big|_{\substack{\boldsymbol{x}=\boldsymbol{x}_0 \\ \boldsymbol{u}=\boldsymbol{u}_0}}\left(\boldsymbol{u} - \boldsymbol{u}_0\right) . \tag{E-27}$$

The linearization error is small when the sampling rate is sufficiently high. Eq. (E-27) can be written as

$$\dot{\boldsymbol{x}}_2 \cong \dot{\boldsymbol{x}}_{2,0} + A_0 \Delta \boldsymbol{x} + B_0 \Delta \boldsymbol{u}\,, \tag{E-28}$$

where

$$\Delta \boldsymbol{x} = \boldsymbol{x} - \boldsymbol{x}_0\,, \quad \Delta \boldsymbol{u} = \boldsymbol{u} - \boldsymbol{u}_0 \tag{E-29a}$$

$$A_0 = \frac{\partial}{\partial \boldsymbol{x}} \left[\boldsymbol{f}(\boldsymbol{x}) + G(\boldsymbol{x})\boldsymbol{u} \right] \Big|_{\substack{\boldsymbol{x}=\boldsymbol{x}_0 \\ \boldsymbol{u}=\boldsymbol{u}_0}} \tag{E-29b}$$

$$B_0 = \frac{\partial}{\partial \boldsymbol{u}} \left[G(\boldsymbol{x})\boldsymbol{u} \right] \Big|_{\substack{\boldsymbol{x}=\boldsymbol{x}_0 \\ \boldsymbol{u}=\boldsymbol{u}_0}} = G(\boldsymbol{x}_0)\,, \tag{E-29c}$$

and where $\boldsymbol{x}_0$ and $\boldsymbol{u}_0$ are respectively the *current* state and the *current* control input. The variables $\Delta \boldsymbol{x}$ and $\Delta \boldsymbol{u}$ are known as respectively the *incremental* state vector and the *incremental* control input.

If we assume a sufficiently time-scale separated system, that is the increment in state $\Delta \boldsymbol{x}$ is much smaller than the increment in both state derivative $\Delta \dot{\boldsymbol{x}}_2$ and input $\Delta \boldsymbol{u}$, we can neglect the former (Falkena, 2012; Sieberling et al., 2010; Acquatella et al., 2012; Simplício et al., 2013). This is allowed for many aerospace applications because the deflections of the control surfaces directly effect the angular accelerations, while the angular rates only change by integrating these angular accelerations. Hence Eq. (E-28) can be further simplified as follows:

$$\dot{\boldsymbol{x}}_2 \cong \dot{\boldsymbol{x}}_{2,0} + B_0 \Delta \boldsymbol{u}\,. \tag{E-30}$$

Now the $\boldsymbol{x}_2$-subsystem is written in incremental form, the Command-Filtered IBS procedure can be continued. The raw signal $\boldsymbol{u}^0$ is led through a command filter to obtain $\boldsymbol{u}$. The effect that the use of this command filter has on the tracking error $\boldsymbol{z}_2$ is estimated by the stable linear filter:

$$\dot{\boldsymbol{\chi}}_2 = -c_2 \boldsymbol{\chi}_2 + B_0 \left(\boldsymbol{u} - \boldsymbol{u}^0 \right)\,, \tag{E-31}$$

with $\boldsymbol{\chi}_2(0) = \boldsymbol{0}$. The $\bar{\boldsymbol{z}}_2$-dynamics are given by

$$\begin{aligned} \dot{\bar{\boldsymbol{z}}}_2 &= \dot{\boldsymbol{z}}_2 - \dot{\boldsymbol{\chi}}_2 \\ &= \dot{\boldsymbol{x}}_2 - \dot{\boldsymbol{x}}_{2,r} - \dot{\boldsymbol{\chi}}_2 \\ &\cong \dot{\boldsymbol{x}}_{2,0} + B_0 \Delta \boldsymbol{u} - \dot{\boldsymbol{x}}_{2,r} + c_2 \boldsymbol{\chi}_2 - B_0 \left(\boldsymbol{u} - \boldsymbol{u}^0 \right)\,. \end{aligned} \tag{E-32}$$

The final Lyapunov function is now defined as

$$\mathcal{V}_2(\bar{\boldsymbol{z}}_1, \bar{\boldsymbol{z}}_2) = \frac{1}{2} \bar{\boldsymbol{z}}_1^T \bar{\boldsymbol{z}}_1 + \frac{1}{2} \bar{\boldsymbol{z}}_2^T \bar{\boldsymbol{z}}_2\,. \tag{E-33}$$

Taking the time derivative of the CLF along the solutions of the compensated error dynamics results in

$$\begin{aligned} \dot{\mathcal{V}}_2 &= \dot{\mathcal{V}}_1 + \bar{\boldsymbol{z}}_2^T \dot{\bar{\boldsymbol{z}}}_2 \\ &\cong -\bar{\boldsymbol{z}}_1^T c_1 \bar{\boldsymbol{z}}_1 + \bar{\boldsymbol{z}}_1^T K \bar{\boldsymbol{z}}_2 + \bar{\boldsymbol{z}}_2^T \left[\dot{\boldsymbol{x}}_{2,0} + B_0 \Delta \boldsymbol{u} - \dot{\boldsymbol{x}}_{2,r} + c_2 \boldsymbol{\chi}_2 - B_0 \left(\boldsymbol{u} - \boldsymbol{u}^0 \right) \right] \\ &= -\bar{\boldsymbol{z}}_1^T c_1 \bar{\boldsymbol{z}}_1 + \bar{\boldsymbol{z}}_1^T K \bar{\boldsymbol{z}}_2 + \bar{\boldsymbol{z}}_2^T \left[\dot{\boldsymbol{x}}_{2,0} + B_0 \left(\boldsymbol{u}^0 - \boldsymbol{u}_0 \right) - \dot{\boldsymbol{x}}_{2,r} + c_2 \boldsymbol{\chi}_2 \right]\,. \end{aligned} \tag{E-34}$$

Selecting the following raw control law:

$$\boldsymbol{u}^0 = \boldsymbol{u}_0 + B_0^{-1}\left[-c_2\boldsymbol{z}_2 - \dot{\boldsymbol{x}}_{2,0} + \dot{\boldsymbol{x}}_{2,r} - K^T\bar{\boldsymbol{z}}_1\right], \quad c_2 > 0\,, \tag{E-35}$$

yields the CLF negative definite

$$\begin{aligned}\dot{\mathcal{V}}_2 &\cong -\bar{\boldsymbol{z}}_1^T c_1\bar{\boldsymbol{z}}_1 + \bar{\boldsymbol{z}}_1^T K\bar{\boldsymbol{z}}_2 + \bar{\boldsymbol{z}}_2^T\left[-c_2\boldsymbol{z}_2 + c_2\boldsymbol{\chi}_2 - K^T\bar{\boldsymbol{z}}_1\right] \\ &= -\bar{\boldsymbol{z}}_1^T c_1\bar{\boldsymbol{z}}_1 + \bar{\boldsymbol{z}}_1^T K\bar{\boldsymbol{z}}_2 + \bar{\boldsymbol{z}}_2^T\left[-c_2\bar{\boldsymbol{z}}_2 - K^T\bar{\boldsymbol{z}}_1\right] \\ &= -\bar{\boldsymbol{z}}_1^T c_1\bar{\boldsymbol{z}}_1 + -\bar{\boldsymbol{z}}_2^T c_2\bar{\boldsymbol{z}}_2\,. \end{aligned}\tag{E-36}$$

By Theorem C.2 it now follows that:

$$\lim_{t\to\infty}\bar{\boldsymbol{z}} = \boldsymbol{0}\,, \tag{E-37}$$

when the sampling rate is sufficiently high. The new incremental control law (E-35) depends on $\boldsymbol{x}_{2,r}$ and $\dot{\boldsymbol{x}}_{2,r}$, which are the output of the command filter and therefore the analytical derivative $\dot{\boldsymbol{\alpha}}_1$ is no longer required. In the absence of physical limitations (i.e. magnitude, rate and bandwidth constraints on the intermediate state $\boldsymbol{x}_2$ and control $\boldsymbol{u}$) and for sufficiently high update rate, closed-loop stability is still guaranteed even when uncertainties are introduced in either the system dynamics or the control effectiveness matrix.

Note that if B_0 is a non-square matrix or a square matrix without full rank, some form of control allocation would be required, see for instance (Enns, 1998; Lombaerts, 2010).

E-2 Simulations

In order to evaluate the IBS approach, four simulations are performed by using the pendulum model:

1. Incremental Backstepping with Time-Scale Separation;
2. Command-Filtered Incremental Backstepping with Time-Scale Separation;
3. Incremental Backstepping without Time-Scale Separation;
4. Command-Filtered Incremental Backstepping without Time-Scale Separation.

E-2-1 Incremental Backstepping with Time-Scale Separation

In this section an IBS control law is derived for the pendulum model, which is for convenience repeated below:

$$\dot{x}_1 = x_2 \tag{B-3a revisited}$$

$$\dot{x}_2 = \theta_{2,1}\sin(x_1) + \theta_{2,2}x_2 + \theta_{2,3}u\,. \tag{B-3b revisited}$$

The control task is to track the smooth reference state $x_{1,r}$ with the state x_1. Similar as before, we start by introducing the following tracking errors:

$$z_1 = x_1 - x_{1,r} \tag{E-39a}$$

$$z_2 = x_2 - \alpha_1 \,. \tag{E-39b}$$

The derivations for subsystem x_1 remain exactly the same as in Appendix C-3 (see Eqs. (C-32) to (C-36)), because this subsystem is assumed to be fully known. Therefore we directly move on to the second and final subsystem. Taking the first-order Taylor series expansion of this system around the current solution $[\boldsymbol{x}_0, u_0]$ results in

$$\dot{x}_2 \cong \dot{x}_{2,0} + \theta_{2,1}\cos(x_{1,0})\Delta x_1 + \theta_{2,2}\Delta x_2 + \theta_{2,3}\Delta u \,, \tag{E-40}$$

where $\Delta x_i = x_i - x_{i,0}$ and $\Delta u = u - u_0$ are respectively the incremental state and incremental control. The linearization error is small when the sampling rate is sufficiently high. The terms appearing in Eq. (E-40) have been plotted for a simulation with conventional BS control law (C-43) and with model and control parameters as in Eqs. (C-44) and (C-45), see Figure E-1. From this simulation it is clear that:

$$\theta_{2,3}\Delta u \gg \theta_{2,1}\cos(x_{1,0})\Delta x_1 + \theta_{2,2}\Delta x_2 \,, \tag{E-41}$$

which allows us to simplify Eq. (E-40) even further:

$$\dot{x}_2 \cong \dot{x}_{2,0} + \theta_{2,3}\Delta u \,. \tag{E-42}$$

Note that this simplification only holds when Eq. (E-41) is satisfied, and thus may not be justified for a different selection of the model parameters $\boldsymbol{\theta}_2$.

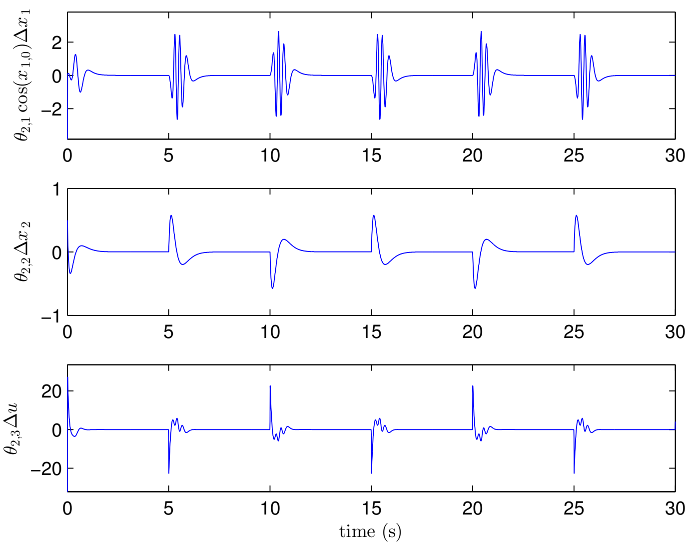

Figure E-1: The terms of incremental equation (E-46) for a sampling time of $0.01\,\text{s}$.

The dynamics of the second error state can now be written as

$$\begin{aligned} \dot{z}_2 &= \dot{x}_2 - \dot{\alpha}_1 \\ &\cong \dot{x}_{2,0} + \theta_{2,3}\Delta u - \dot{\alpha}_1 \,. \end{aligned} \tag{E-43}$$

Now the quadratic CLF is augmented to penalize the second tracking error as well:

$$\mathcal{V}(\boldsymbol{z}) = \mathcal{V}_1 + \frac{1}{2}z_2^2 \,. \tag{E-44}$$

Taking the time derivative of $\mathcal{V}$ along the trajectories of the error dynamics yields

$$\begin{aligned} \dot{\mathcal{V}} &= \dot{\mathcal{V}}_1 + z_2\dot{z}_2 \\ &\cong -c_1 z_1^2 + z_1 z_2 + z_2\left[\dot{x}_{2,0} + \theta_{2,3}\Delta u - \dot{\alpha}_1\right] \,. \end{aligned} \tag{E-45}$$

An obvious choice for the incremental control law Δu is

$$\Delta u = \frac{1}{\theta_{2,3}}\left[-\dot{x}_{2,0} + \dot{\alpha}_1 - z_1 - c_2 z_2\right] \,, \tag{E-46}$$

which results in the following expression for $\dot{\mathcal{V}}$:

$$\dot{\mathcal{V}} \cong -c_1 z_1^2 - c_2 z_2^2 \,. \tag{E-47}$$

When our assumptions on the sampling rate and Time-Scale Separation (TSS) are valid, this CLF is a negative definite function and therefore according to Theorem C.2:

$$\lim_{t\to\infty}\left[x_1 - x_{1,r}\right] = 0 \,. \tag{E-48}$$

To find the actual IBS control law, the incremental input needs to be added to the current input:

$$\begin{aligned} u &= u_0 + \Delta u \\ &= u_0 + \frac{1}{\theta_{2,3}}\left[-\dot{x}_{2,0} + \dot{\alpha}_1 - z_1 - c_2 z_2\right] \,. \end{aligned} \tag{E-49}$$

If we compare this control law with the earlier designed conventional BS controller:

$$u = \frac{1}{\theta_{2,3}}\left[-\theta_{2,1}\sin(x_1) - \theta_{2,2}x_2 + \dot{\alpha}_1 - z_1 - c_2 z_2\right] \,, \tag{C-39 revisited}$$

we can see that the newly developed IBS controller does not rely on exact knowledge of the system dynamics. From Eq. (E-49) we can see that the incremental controller still depends on the control effectiveness, i.e. parameter $\theta_{2,3}$. In (Chu, 2014) it is shown that for sufficiently high update rate, closed-loop stability is still guaranteed even when uncertainties are introduced in the control effectiveness matrix.

The IBS controller Eq. (E-49) relies on measurements of the angular acceleration $\dot{x}_{2,0}$ and the control input u_0, therefore sensor redundancy and failure detection methods now become mandatory.

Simulations of the newly designed IBS controller have been performed to compare its robustness properties with the full-information BS controller. The uncertainties that have been introduced in the parameters of the system dynamics are $\hat{\theta}_{2,1} = 30 \cdot \theta_{2,1}$ and $\hat{\theta}_{2,2} = 30 \cdot \theta_{2,2}$. The initial conditions and model parameters which have been used in this simulation can be found in Eq. (C-44). The sampling time has been selected as 0.01 s, the results can be seen in Figure E-2. As expected, the IBS controller is able to accurately track the reference signal even in case of uncertainties in the parameters of the system dynamics.

Another simulation has been run with an uncertainty in the control effectiveness, see Figure E-3. Because the incremental control law (E-49) still depends on $\theta_{2,3}$, the tracking performance degrades when this parameter becomes uncertain. However, we can see that by increasing the sampling rate f_s, the control law becomes less sensitive to this uncertainty.

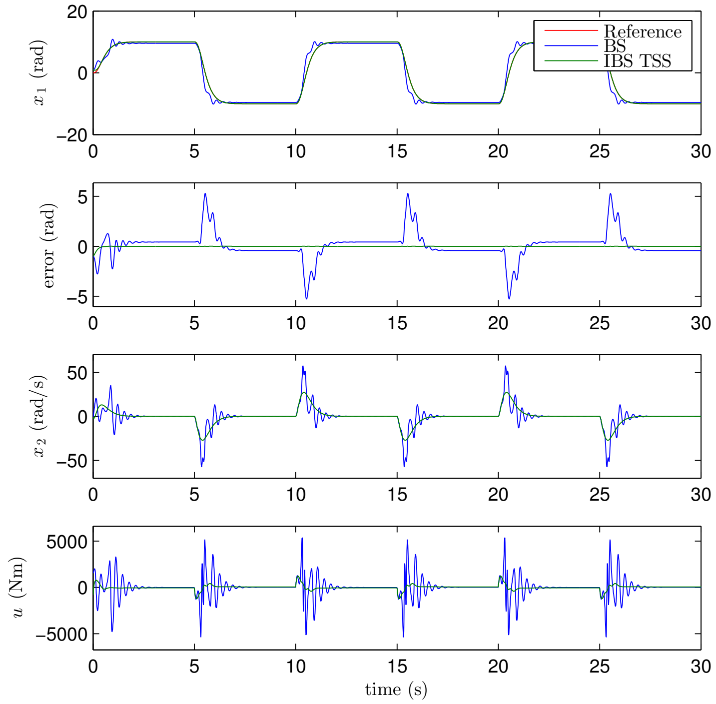

Figure E-2: The control performance of two control laws in the presence of parametric uncertainties in the system dynamics. The uncertainties that have been introduced are $\hat{\theta}_{2,1} = 30 \cdot \theta_{2,1}$ and $\hat{\theta}_{2,2} = 30 \cdot \theta_{2,2}$.

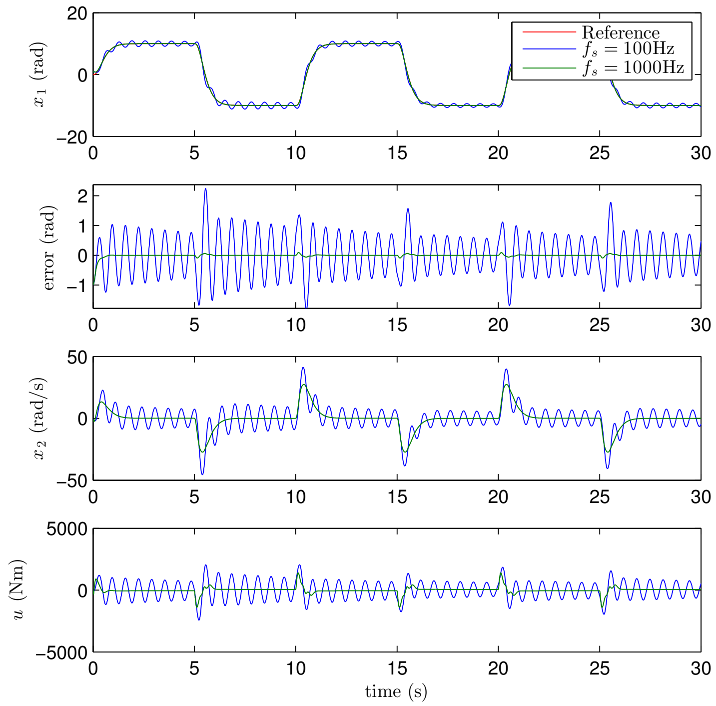

Figure E-3: The control performance of the Incremental Backstepping control law in the presence of an uncertain control effectiveness. The uncertainty that have been introduced is $\hat{\theta}_{2,3} = 20 \cdot \theta_{2,3}$.

E-2-2 Command-Filtered Incremental Backstepping with Time-Scale Separation

In this section the design procedure of a Command-Filtered IBS controller for the pendulum is discussed. We now consider the following time-scale separated incremental pendulum model (see Eqs. (E-41) and (E-42)):

$$\dot{x}_1 = x_2 \tag{E-50a}$$
$$\dot{x}_2 = \dot{x}_{2,0} + \theta_{2,3}\Delta u\,. \tag{E-50b}$$

The control task is to track the smooth reference state $x_{1,r}$ with the state x_1. Similar as before, we start by defining the tracking errors as

$$z_1 = x_1 - x_{1,r} \tag{E-51a}$$
$$z_2 = x_2 - x_{2,r}\,, \tag{E-51b}$$

and the *compensated* tracking errors as

$$\bar{z}_1 = z_1 - \chi_1 \tag{E-52a}$$
$$\bar{z}_2 = z_2 - \chi_2\,. \tag{E-52b}$$

The derivations for subsystem x_1 remain exactly the same as in Appendix D-3 (see Eqs. (D-35) to (D-40)), because this subsystem is assumed to be fully known. Therefore we directly move on to the second and final compensated subsystem. The $\bar{z}_2$-dynamics are given by

$$\dot{\bar{z}}_2 = \dot{x}_{2,0} + \theta_{2,3}\Delta u - \dot{x}_{2,r} - \dot{\chi}_2\,. \tag{E-53}$$

Augmenting the quadratic CLF function to penalize the second compensated tracking error yields

$$\mathcal{V}(\bar{\boldsymbol{z}}) = \mathcal{V}_1 + \frac{1}{2}\bar{z}_2^2 \,. \tag{E-54}$$

Taking the time derivative of $\mathcal{V}$ along the compensated error dynamics results in

$$\dot{\mathcal{V}} = -c_1\bar{z}_1^2 + \bar{z}_1\bar{z}_2 + \bar{z}_2\left[\dot{x}_{2,0} + \theta_{2,3}\Delta u - \dot{x}_{2,r} - \dot{\chi}_2\right] \,. \tag{E-55}$$

Now there are two options for implementation of the second command filter, see Figure E-4. We start with the derivations for command filter (1).

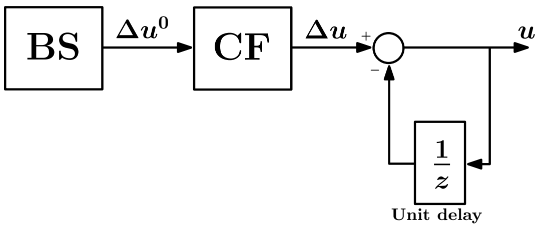

(a) Command filter (1)

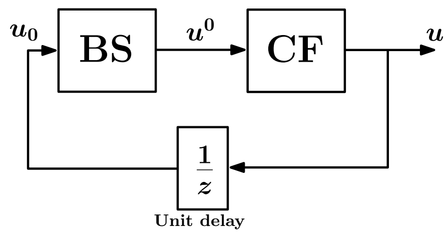

(b) Command filter (2)

Figure E-4: Two different implementations for the second command filter. The Backstepping (BS) control laws refer to Eqs. (E-58) and (E-63).

Command Filter (1)

The effect that the use of command filter (1) (see Figure E-4a) has on the tracking error z_2 is estimated by the stable linear filter:

$$\dot{\chi}_2 = -c_2\chi_2 + \theta_{2,3}\left(\Delta u - \Delta u^0\right) \,, \tag{E-56}$$

with $\chi_2(0) = 0$. Substituting this expression in Eq. (E-55) yields

$$\dot{\mathcal{V}} = -c_1\bar{z}_1^2 + \bar{z}_1\bar{z}_2 + \bar{z}_2\left[\dot{x}_{2,0} + \theta_{2,3}\Delta u^0 - \dot{x}_{2,r} + c_2\chi_2\right] \,. \tag{E-57}$$

Selecting the following raw incremental control law Δu^0:

$$\Delta u^0 = \frac{1}{\theta_{2,3}}\left[-c_2 z_2 - \bar{z}_1 - \dot{x}_{2,0} + \dot{x}_{2,r}\right] \,, \quad c_2 > 0 \,, \tag{E-58}$$

yields the CLF negative definite

$$\begin{aligned}\dot{\mathcal{V}} &= -c_1\bar{z}_1^2 + \bar{z}_1\bar{z}_2 + \bar{z}_2\left[c_2\chi_2 - c_2 z_2 - \bar{z}_1\right] \\ &= -c_1\bar{z}_1^2 + \bar{z}_1\bar{z}_2 + \bar{z}_2\left[-c_2\bar{z}_2 - \bar{z}_1\right] \\ &= -c_1\bar{z}_1^2 - c_2\bar{z}_2^2 \,.\end{aligned} \tag{E-59}$$

By Theorem C.2 it now follows that:

$$\lim_{t\to\infty} \bar{\boldsymbol{z}} = 0 \,. \tag{E-60}$$

The new incremental control law (E-58) depends on $x_{2,r}$ and $\dot{x}_{2,r}$, which are the output of the command filter and therefore the analytical derivative $\dot{\alpha}_1$ is no longer required. In the absence of physical limitations (i.e. magnitude, rate and bandwidth constraints on the intermediate state x_2 and control u) and for sufficiently high update rate, closed-loop stability is still guaranteed even when uncertainties are introduced in either the system dynamics or the control effectiveness matrix.

Command Filter (2)

The effect that the use of command filter (2) (see Figure E-4b) has on the tracking error z_2 is estimated by the stable linear filter:

$$\dot{\chi}_2 = -c_2\chi_2 + \theta_{2,3}\left(u - u^0\right) , \tag{E-61}$$

with $\chi_2(0) = 0$. Substituting this expression in Eq. (E-55) yields

$$\dot{\mathcal{V}} = -c_1\bar{z}_1^2 + \bar{z}_1\bar{z}_2 + \bar{z}_2\left[\dot{x}_{2,0} + \theta_{2,3}\left(u^0 - u_0\right) - \dot{x}_{2,r} + c_2\chi_2\right] . \tag{E-62}$$

Selecting the following raw control law:

$$u^0 = u_0 + \frac{1}{\theta_{2,3}}\left[-c_2 z_2 - \bar{z}_1 - \dot{x}_{2,0} + \dot{x}_{2,r}\right] , \quad c_2 > 0 , \tag{E-63}$$

yields the CLF negative definite

$$\begin{aligned}
\dot{\mathcal{V}} &= -c_1\bar{z}_1^2 + \bar{z}_1\bar{z}_2 + \bar{z}_2\left[c_2\chi_2 - c_2 z_2 - \bar{z}_1\right] \\
&= -c_1\bar{z}_1^2 + \bar{z}_1\bar{z}_2 + \bar{z}_2\left[-c_2\bar{z}_2 - \bar{z}_1\right] \\
&= -c_1\bar{z}_1^2 - c_2\bar{z}_2^2 .
\end{aligned} \tag{E-64}$$

By Theorem C.2 it now follows that:

$$\lim_{t\to\infty} \bar{\boldsymbol{z}} = 0 . \tag{E-65}$$

The new incremental control law (E-63) depends on $x_{2,r}$ and $\dot{x}_{2,r}$, which are the output of the command filter and therefore the analytical derivative $\dot{\alpha}_1$ is no longer required. In the absence of physical limitations (i.e. magnitude, rate, and bandwidth constraints on the intermediate state x_2 and control u) and for sufficiently high update rate, closed-loop stability is still guaranteed even when uncertainties are introduced in either the system dynamics or the control effectiveness matrix.

Simulations of the full-information Command-Filtered IBS controller with two different implementations of the command filter (see Figure E-4) have been run with a sampling time of 0.01 s. The parameters which have been used in this simulation for the model and controller can be found in respectively Eqs. (C-44) and (C-45). The results of the simulation can be seen in Figure E-5. Clearly, the implementation with the command filter (1) (see Figure E-4a) appears to be very sensitive to the delay that this filter introduces, resulting in an unstable closed-loop system. On the contrary, the second implementation of the command filter (see Figure E-4b) performs satisfactory. On basis of these results, the second option is used in all future simulations that involve the Command-Filtered IBS controller.

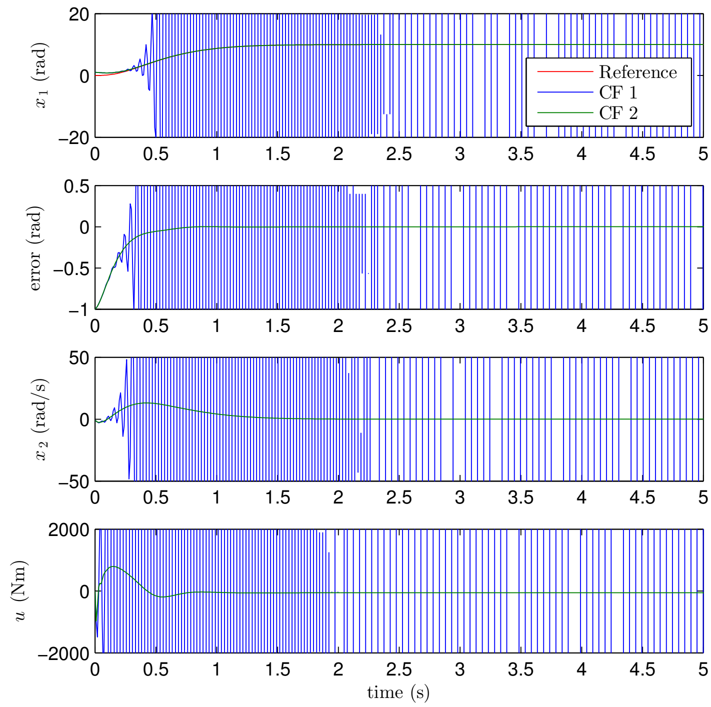

Figure E-5: The control performance of the Command-Filtered Incremental Backstepping controller with two different implementations of the command filter (see Figure E-4) in the absence of any uncertainties.

E-2-3 Incremental Backstepping without Time-Scale Separation

In this section the design procedure of an IBS controller for the pendulum is discussed. This time we do not make the assumption of TSS (see Eq. (E-41)), thus when the sampling rate is sufficiently high we can write the pendulum model as

$$\dot{x}_1 = x_2 \tag{E-66a}$$

$$\dot{x}_2 = \dot{x}_{2,0} + \theta_{2,1}\cos(x_{1,0})\Delta x_1 + \theta_{2,2}\Delta x_2 + \theta_{2,3}\Delta u\,. \tag{E-66b}$$

The control task is to track the smooth reference state $x_{1,r}$ with the state x_1. Similar as before, we start by introducing the following tracking errors:

$$z_1 = x_1 - x_{1,r} \tag{E-67a}$$
$$z_2 = x_2 - \alpha_1\,. \tag{E-67b}$$

The derivations for subsystem x_1 remain exactly the same as in Appendix C-3 (see Eqs. (C-32) to (C-36)), because this subsystem is assumed to be fully known. Therefore we directly move on to the second and final subsystem. Augmenting the quadratic CLF yields

$$\mathcal{V}(\boldsymbol{z}) = \mathcal{V}_1 + \frac{1}{2}z_2^2\,. \tag{E-68}$$

Taking the time derivative of $\mathcal{V}$ along the trajectories of the error dynamics results in

$$\begin{aligned}\dot{\mathcal{V}} &= \dot{\mathcal{V}}_1 + z_2\dot{z}_2 \\ &= -c_1z_1^2 + z_1z_2 + z_2\left[\dot{x}_{2,0} + \theta_{2,1}\cos(x_{1,0})\Delta x_1 + \theta_{2,2}\Delta x_2 + \theta_{2,3}\Delta u - \dot{\alpha}_1\right]\,.\end{aligned} \tag{E-69}$$

An obvious choice for the incremental control law Δu is

$$\Delta u = \frac{1}{\theta_{2,3}}\left[-\dot{x}_{2,0} + \dot{\alpha}_1 - \theta_{2,1}\cos(x_{1,0})\Delta x_1 - \theta_{2,2}\Delta x_2 - z_1 - c_2z_2\right]\,, \tag{E-70}$$

which results in the following expression for $\dot{\mathcal{V}}$:

$$\dot{\mathcal{V}} = -c_1z_1^2 - c_2z_2^2\,. \tag{E-71}$$

By Theorem C.2 it now follows that:

$$\lim_{t\to\infty} z_1 = 0 \to \lim_{t\to\infty}\left[x_1 - x_{1,r}\right] = 0 \tag{E-72a}$$
$$\lim_{t\to\infty} z_2 = 0\,. \tag{E-72b}$$

Now the performance of the conventional BS controller is compared to that of the incremental control laws with Time-Scale Separation (IBS TSS) and without Time-Scale Separation (IBS). The control laws are respectively:

$$u = \frac{1}{\theta_{2,3}}\left[-z_1 - c_2z_2 - \theta_{2,1}\sin(x_1) - \theta_{2,2}x_2 + \dot{\alpha}_1\right] \tag{C-39 revisited}$$
$$u = u_0 + \frac{1}{\theta_{2,3}}\left[-z_1 - c_2z_2 - \dot{x}_{2,0} + \dot{\alpha}_1\right] \tag{E-49 revisited}$$
$$u = u_0 + \frac{1}{\theta_{2,3}}\left[-z_1 - c_2z_2 - \theta_{2,1}\cos(x_{1,0})\Delta x_1 - \theta_{2,2}\Delta x_2 - \dot{x}_{2,0} + \dot{\alpha}_1\right]\,. \tag{E-70 revisited}$$

We see that both Eqs. (C-39) and (E-70) rely on exact knowledge of the plant dynamics and that both control laws depend on the control effectiveness parameter, i.e. $\theta_{2,3}$. A difference is that control law (E-70) also needs to measure/estimate $\dot{x}_{2,0}$ and u_0, making it more dependent on the corresponding sensors/estimators.

Simulations have been run with a sampling time of 0.01 s. The selected initial conditions and model parameters can be found in Eq. (C-44). The following control parameters have been used:

$$\begin{aligned} c_1 &= 10\,, & c_2 &= 10\,, \\ \hat{\theta}_{2,1} &= 25 \cdot \theta_{2,1}\,, & \hat{\theta}_{2,2} &= 25 \cdot \theta_{2,2}\,, \\ \hat{\theta}_{2,3} &= \theta_{2,3}\,. \end{aligned} \tag{E-73}$$

That is, uncertainties have been implemented in the system dynamics. The results of the simulation can be seen in Figure E-6. It is clear that the conventional BS controller (C-39) is not able to accurately track the reference signal now uncertainties have been introduced. The incremental controller (E-49) performs well because the following assumption holds (see Figure E-1):

$$\theta_{2,3}\Delta u \gg \theta_{2,1}\cos(x_{1,0})\Delta x_1 + \theta_{2,2}\Delta x_2\,, \tag{E-41 revisited}$$

which we used when deriving this control law, and therefore it is robust to uncertainties in parameters $\theta_{2,1}$ and $\theta_{2,2}$. The control law (E-70) performs slightly worse compared to the IBS controller with TSS because it depends on the uncertain parameters $\theta_{2,1}$ and $\theta_{2,2}$. However, this controller performs much better compared to the full-information BS controller because the uncertainties are now multiplied by the very small difference variables Δx_1 and Δx_2.

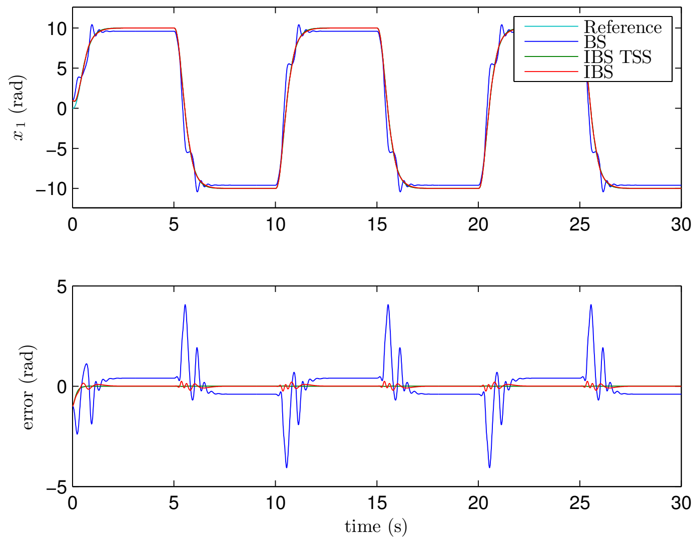

Figure E-6: The control performance of three control laws in the presence of parametric uncertainties in the system dynamics.

Now we change the model parameters to find out whether the IBS TSS controller will still perform satisfactory. The following initial conditions and parameters have been used for the model:

$$\begin{aligned} x_1(0) &= 1\,, & x_2(0) &= -1\,, \\ \theta_{2,1} &= -9.81\,, & \theta_{2,2} &= -200\,, \\ \theta_{2,3} &= 0.1\,. \end{aligned} \tag{E-74}$$

Simulations have been run with a sampling time of 0.01 s, no uncertainties have been introduced. The results of the simulation can be found in Figure E-7. From this figure it is clear that the IBS TSS controller is no longer able to accurately track the reference signal. This can be explained on basis of Figure E-8, where we can see that assumption (E-41) which we made during the derivation of this control law no longer holds.

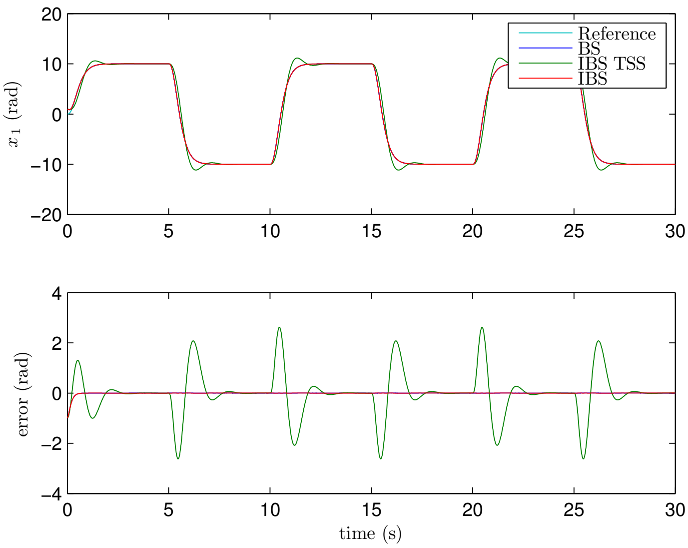

Figure E-7: The control performance of three control laws in the absence of any uncertainties.

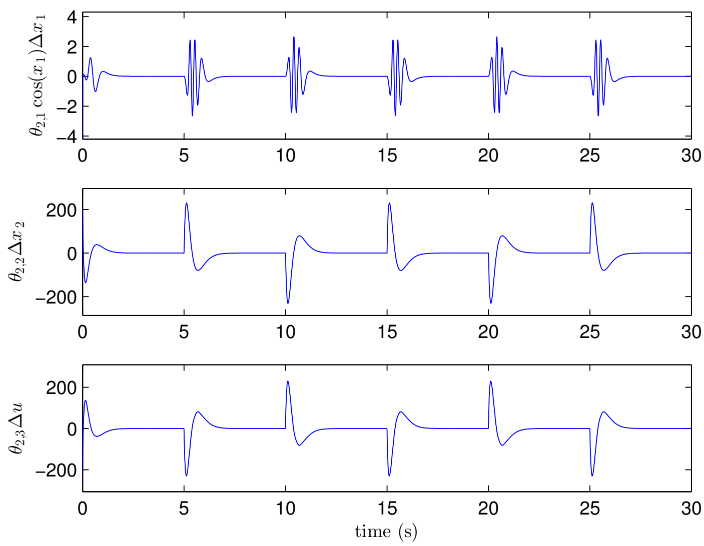

Figure E-8: The terms of incremental equation (E-46) for a sampling time of $0.01\,\mathrm{s}$.

Now we select the control parameters as follows:

$$\begin{aligned} c_1 &= 10\,, & c_2 &= 10\,, \\ \hat{\theta}_{2,1} &= \theta_{2,1}\,, & \hat{\theta}_{2,2} &= 1.1 \cdot \theta_{2,2}\,, \\ \hat{\theta}_{2,3} &= \theta_{2,3}\,. \end{aligned} \tag{E-75}$$

The results of the simulation with a sampling time of $0.01\,\mathrm{s}$ can be seen in Figure E-9. Clearly, only the IBS controller is now able to provide accurate tracking of the reference signal. However, we can see that even for this controller there is a small tracking error during the maneuvers. This small error is caused by the parametric uncertainty and can be reduced by increasing the sampling rate of the simulation, as can be seen in Figure E-10. Note that the tracking capability of the IBS TSS controller now also significantly improves, this is because the terms $\Delta \boldsymbol{x}$ and Δu in Eqs. (E-49) and (E-70) become even smaller for very high sampling rates. That is, both incremental controllers become model independent for sufficiently high sampling rates.

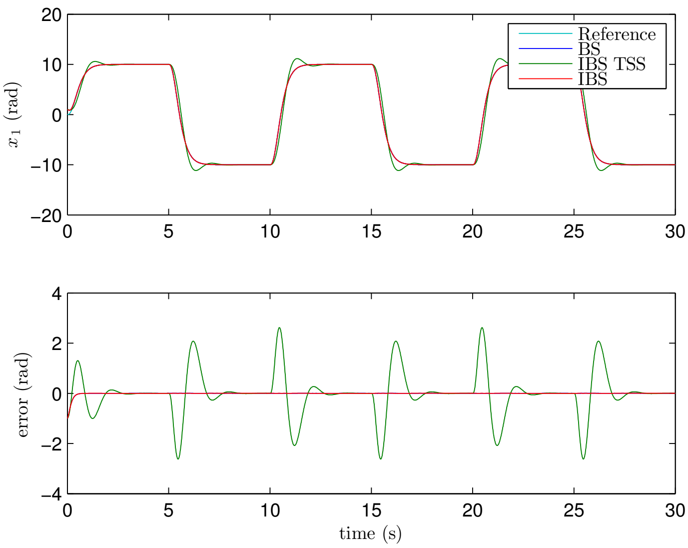

Figure E-9: The control performance of three control laws in the presence of parametric uncertainty $\hat{\theta}_{2,2} = 1.1 \cdot \theta_{2,2}$ with a sampling time of $0.01\,\mathrm{s}$.

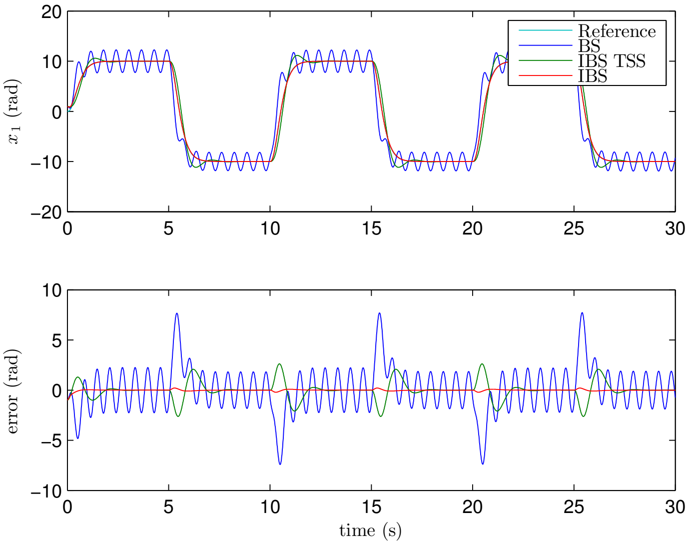

Figure E-10: The control performance of three control laws in the presence of parametric uncertainty $\hat{\theta}_{2,2} = 1.1 \cdot \theta_{2,2}$ with a sampling time of $0.001\,\mathrm{s}$.

E-2-4 Command-Filtered Incremental Backstepping without Time-Scale Separation

In this section the design procedure of a Command-Filtered IBS controller for the pendulum model is discussed. We do not make the assumption of TSS (see Eq. (E-41)), thus when the sampling rate is sufficiently high we can write the pendulum model as

$$\dot{x}_1 = x_2 \tag{E-66a revisited}$$
$$\dot{x}_2 = \dot{x}_{2,0} + \theta_{2,1}\cos(x_{1,0})\Delta x_1 + \theta_{2,2}\Delta x_2 + \theta_{2,3}\Delta u\,. \tag{E-66b revisited}$$

The control task is to track the smooth reference state $x_{1,r}$ with the state x_1. Earlier we obtained the following control laws for the complete nonlinear pendulum:

$$u = \frac{1}{\theta_{2,3}}\left[-c_2\left(x_2 - \alpha_1\right) - z_1 - \theta_{2,1}\sin(x_1) - \theta_{2,2}x_2 + \dot{\alpha}_1\right] \tag{C-39 revisited}$$
$$u^0 = \frac{1}{\theta_{2,3}}\left[-c_2\left(x_2 - x_{2,r}\right) - \bar{z}_1 - \theta_{2,1}\sin(x_1) - \theta_{2,2}x_2 + \dot{x}_{2,r}\right]\,, \tag{D-46 revisited}$$

which are respectively the conventional full-information BS controller and the Command-Filtered BS control law. In the last section we obtained the following IBS control law:

$$u = u_0 + \frac{1}{\theta_{2,3}}\left[-c_2\left(x_2 - \alpha_1\right) - z_1 - \dot{x}_{2,0} - \theta_{2,1}\cos(x_{1,0})\Delta x_1 - \theta_{2,2}\Delta x_2 + \dot{\alpha}_1\right]\,. \tag{E-70 revisited}$$

Now the following Command-Filtered IBS control seems viable:

$$u^0 = u_0 + \frac{1}{\theta_{2,3}}\left[-c_2\left(x_2 - x_{2,r}\right) - z_1 - \dot{x}_{2,0} - \theta_{2,1}\cos(x_{1,0})\Delta x_1 - \theta_{2,2}\Delta x_2 + \dot{x}_{2,r}\right]\,. \tag{E-77}$$

In order to proof stability of the closed-loop system, we consider the following quadratic Lyapunov function:

$$\mathcal{V}(\bar{\boldsymbol{z}}) = \frac{1}{2}\bar{z}_1^2 + \frac{1}{2}\bar{z}_2^2 \,, \tag{E-78}$$

where $\bar{\boldsymbol{z}}$ and the $\bar{z}_1$-dynamics are similar as in Eqs. (D-37) and (D-38). The $\bar{z}_2$-dynamics are now given by

$$\dot{\bar{z}}_2 = \dot{x}_{2,0} + \theta_{2,1}\cos(x_{1,0})\Delta x_1 + \theta_{2,2}\Delta x_2 + \theta_{2,3}\Delta u - \dot{x}_{2,r} - \dot{\chi}_2 \,. \tag{E-79}$$

Taking the time derivative of $\mathcal{V}$ along the trajectories of Eqs. (D-38) and (E-79) yields

$$\dot{\mathcal{V}} = -c_1\bar{z}_1^2 + \bar{z}_1\bar{z}_2 + \bar{z}_2\left[\dot{x}_{2,0} + \theta_{2,1}\cos(x_{1,0})\Delta x_1 + \theta_{2,2}\Delta x_2 + \theta_{2,3}\Delta u - \dot{x}_{2,r} - \dot{\chi}_2\right] \,. \tag{E-80}$$

Now χ_2 is the output of the following stable linear filter:

$$\dot{\chi}_2 = -c_2\chi_2 + \theta_{2,3}\left(u - u^0\right) \,, \tag{E-81}$$

with $\chi_2(0) = 0$. This yields:

$$\begin{aligned}
\dot{\mathcal{V}} &= -c_1\bar{z}_1^2 + \bar{z}_1\bar{z}_2 + \bar{z}_2\left[\dot{x}_{2,0} + \theta_{2,1}\Delta x_1 + \theta_{2,2}\Delta x_2 + \theta_{2,3}\left(u^0 - u_0\right) - \dot{x}_{2,r} + c_2\chi_2\right] \\
&= -c_1\bar{z}_1^2 + \bar{z}_1\bar{z}_2 + \bar{z}_2\left[-\bar{z}_1 - c_2 z_2 + c_2\chi_2\right] \\
&= -c_1\bar{z}_1^2 + \bar{z}_1\bar{z}_2 + \bar{z}_2\left[-\bar{z}_1 - c_2\bar{z}_2\right] \\
&= -c_1\bar{z}_1^2 - c_2\bar{z}_2^2 \,.
\end{aligned} \tag{E-82}$$

By Theorem C.2 it now follows that:

$$\lim_{t\to\infty} \bar{\boldsymbol{z}} = 0 \,. \tag{E-83}$$

The new incremental control law (E-77) depends on $x_{2,r}$ and $\dot{x}_{2,r}$, which are the output of the command filter and therefore the analytical derivative $\dot{\alpha}_1$ is no longer required. In the absence of physical limitations (i.e. magnitude, rate and bandwidth constraints on the intermediate state x_2 and control u) and for sufficiently high update rate, closed-loop stability is still guaranteed even when uncertainties are introduced in either the system dynamics or the control effectiveness matrix.

Appendix F

Tuning Functions Adaptive Backstepping

In this appendix the Tuning Functions Adaptive Backstepping (TFABS) control approach is derived and evaluated that makes use of Lyapunov-based on-line parameter update laws to increase the robustness against parametric uncertainties (F-1). In order to evaluate this nonlinear control approach, (Command-Filtered) TFABS control laws are derived and simulated for the pendulum model (F-2).

F-1 Theory

First the recursive Adaptive Backstepping (ABS) procedure is derived, in which the update laws are recursively build up in order to prevent overparameterization (F-1-1). Next, this approach is augmented with command filters to reduce the complexity (F-1-2).

F-1-1 Recursive Adaptive Backstepping

We consider the following strict-feedback system:

$$\dot{x}_i = f_i(\bar{\boldsymbol{x}}_i) + g_i(\bar{\boldsymbol{x}}_i)x_{i+1}\,, \quad i = 1, \ldots, n-1 \tag{F-1a}$$

$$\dot{x}_n = f_n(\boldsymbol{x}) + g_n(\boldsymbol{x})u\,, \tag{F-1b}$$

where $\boldsymbol{x} \in \mathbb{R}^n$ is the state, $\bar{\boldsymbol{x}}_i = [x_1, \cdots, x_i]^T$, $x_i \in \mathbb{R}$ and $u \in \mathbb{R}$ the control signal and $g_i \neq 0$ for $i = 1, \ldots, n$. The control objective is to track a smooth reference signal $x_{1,r}$, for which the n-order time derivatives are assumed to be known and bounded, with the state x_1. Furthermore, the signals x_i for $i = 2, \ldots, n$ must remain bounded. The smooth functions f_i and $g_i \in C^{n-i}$ for $i = 1, \ldots, n$ contain the unknown dynamics of the system and will have to be approximated. It is assumed there exist vectors $\boldsymbol{\theta}_{f_i}$ and $\boldsymbol{\theta}_{g_i}$ such that

$$f_i(\bar{\boldsymbol{x}}_i) = \boldsymbol{\varphi}_{f_i}(\bar{\boldsymbol{x}}_i)^T \boldsymbol{\theta}_{f_i}\,, \quad i = 1, \ldots, n \tag{F-2a}$$

$$g_i(\bar{\boldsymbol{x}}_i) = \boldsymbol{\varphi}_{g_i}(\bar{\boldsymbol{x}}_i)^T \boldsymbol{\theta}_{g_i}\,. \tag{F-2b}$$

Now we can write system (F-1) as

$$\dot{x}_i = \boldsymbol{\varphi}_{f_i}(\bar{\boldsymbol{x}}_i)^T \boldsymbol{\theta}_{f_i} + \boldsymbol{\varphi}_{g_i}(\bar{\boldsymbol{x}}_i)^T \boldsymbol{\theta}_{g_i} x_{i+1}\,, \quad i = 1, \ldots, n-1 \tag{F-3a}$$

$$\dot{x}_n = \boldsymbol{\varphi}_{f_n}(\boldsymbol{x})^T \boldsymbol{\theta}_{f_n} + \boldsymbol{\varphi}_{g_n}(\boldsymbol{x})^T \boldsymbol{\theta}_{g_n} u\,. \tag{F-3b}$$

The estimates of the nonlinear functions f_i and g_i are defined as

$$\hat{f}_i(\bar{\boldsymbol{x}}_i, \hat{\boldsymbol{\theta}}_{f_i}) = \boldsymbol{\varphi}_{f_i}(\bar{\boldsymbol{x}}_i)^T \hat{\boldsymbol{\theta}}_{f_i}\,, \quad i = 1, \ldots, n \tag{F-4a}$$

$$\hat{g}_i(\bar{\boldsymbol{x}}_i, \hat{\boldsymbol{\theta}}_{g_i}) = \boldsymbol{\varphi}_{g_i}(\bar{\boldsymbol{x}}_i)^T \hat{\boldsymbol{\theta}}_{g_i}\,, \tag{F-4b}$$

and the parameter errors as

$$\tilde{\boldsymbol{\theta}}_{f_i} = \boldsymbol{\theta}_{f_i} - \hat{\boldsymbol{\theta}}_{f_i} \quad \rightarrow \quad \dot{\tilde{\boldsymbol{\theta}}}_{f_i} = -\dot{\hat{\boldsymbol{\theta}}}_{f_i} \tag{F-5a}$$

$$\tilde{\boldsymbol{\theta}}_{g_i} = \boldsymbol{\theta}_{g_i} - \hat{\boldsymbol{\theta}}_{g_i} \quad \rightarrow \quad \dot{\tilde{\boldsymbol{\theta}}}_{g_i} = -\dot{\hat{\boldsymbol{\theta}}}_{g_i}\,. \tag{F-5b}$$

Subsystem 1

We start by considering the first subsystem, which is the subsystem "furthest" away from the actual control u:

$$\dot{x}_1 = \boldsymbol{\varphi}_{f_1}(x_1)^T \boldsymbol{\theta}_{f_1} + \boldsymbol{\varphi}_{g_1}(x_1)^T \boldsymbol{\theta}_{g_1} x_2\,. \tag{F-6}$$

Now we regard state x_2 as the control input for this subsystem. However, because x_2 is just a state variable and not the real control input u, we call x_2 the *virtual control.*

Now we introduce the tracking errors:

$$z_1 = x_1 - x_{1,r} \tag{F-7a}$$

$$z_2 = x_2 - x_{2,r} \equiv x_2 - \alpha_1\,, \tag{F-7b}$$

where $x_{2,r} \equiv \alpha_1$ is the desired value of x_2, called the *stabilizing function.* Rewriting the current subsystem in terms of the tracking error z_1 results in

$$\begin{aligned}\dot{z}_1 &= \dot{x}_1 - \dot{x}_{1,r} \\ &= \boldsymbol{\varphi}_{f_1}^T \boldsymbol{\theta}_{f_1} + \boldsymbol{\varphi}_{g_1}^T \boldsymbol{\theta}_{g_1} x_2 - \dot{x}_{1,r} \\ &= \boldsymbol{\varphi}_{f_1}^T \boldsymbol{\theta}_{f_1} + \boldsymbol{\varphi}_{g_1}^T \boldsymbol{\theta}_{g_1} \left[z_2 + \alpha_1\right] - \dot{x}_{1,r}\,.\end{aligned} \tag{F-8}$$

Now we formulate a quadratic scalar Control Lyapunov Function (CLF) for the first subsystem:

$$\mathcal{V}_1(z_1, \tilde{\boldsymbol{\theta}}_{\star_1}) = \frac{1}{2} z_1^2 + \frac{1}{2} \tilde{\boldsymbol{\theta}}_{f_1}^T \Gamma_{f_1}^{-1} \tilde{\boldsymbol{\theta}}_{f_1} + \frac{1}{2} \tilde{\boldsymbol{\theta}}_{g_1}^T \Gamma_{g_1}^{-1} \tilde{\boldsymbol{\theta}}_{g_1}\,. \tag{F-9}$$

Taking the time derivative along the trajectories of Eqs. (F-5) and (F-8) yields

$$\begin{aligned}
\dot{\mathcal{V}}_1 &= z_1\left[\boldsymbol{\varphi}_{f_1}^T\boldsymbol{\theta}_{f_1} + \boldsymbol{\varphi}_{g_1}^T\boldsymbol{\theta}_{g_1}(z_2+\alpha_1) - \dot{x}_{1,r}\right] - \tilde{\boldsymbol{\theta}}_{f_1}^T\Gamma_{f_1}^{-1}\dot{\hat{\boldsymbol{\theta}}}_{f_1} - \tilde{\boldsymbol{\theta}}_{g_1}^T\Gamma_{g_1}^{-1}\dot{\hat{\boldsymbol{\theta}}}_{g_1} \\
&= z_1\left[\boldsymbol{\varphi}_{f_1}^T\left(\tilde{\boldsymbol{\theta}}_{f_1}+\hat{\boldsymbol{\theta}}_{f_1}\right) + \boldsymbol{\varphi}_{g_1}^T\left(\tilde{\boldsymbol{\theta}}_{g_1}+\hat{\boldsymbol{\theta}}_{g_1}\right)(z_2+\alpha_1) - \dot{x}_{1,r}\right] - \tilde{\boldsymbol{\theta}}_{f_1}^T\Gamma_{f_1}^{-1}\dot{\hat{\boldsymbol{\theta}}}_{f_1} - \tilde{\boldsymbol{\theta}}_{g_1}^T\Gamma_{g_1}^{-1}\dot{\hat{\boldsymbol{\theta}}}_{g_1} \\
&= z_1\left[\boldsymbol{\varphi}_{f_1}^T\hat{\boldsymbol{\theta}}_{f_1} + \boldsymbol{\varphi}_{g_1}^T\hat{\boldsymbol{\theta}}_{g_1}(z_2+\alpha_1) - \dot{x}_{1,r}\right] - \tilde{\boldsymbol{\theta}}_{f_1}^T\Gamma_{f_1}^{-1}\left[\dot{\hat{\boldsymbol{\theta}}}_{f_1} - \Gamma_{f_1}\boldsymbol{\varphi}_{f_1}z_1\right] \\
&\quad -\tilde{\boldsymbol{\theta}}_{g_1}^T\Gamma_{g_1}^{-1}\left[\dot{\hat{\boldsymbol{\theta}}}_{g_1} - \Gamma_{g_1}\boldsymbol{\varphi}_{g_1}x_2z_1\right]\,.
\end{aligned} \tag{F-10}$$

The stabilizing control law α_1 and the *intermediate* update laws $\boldsymbol{\tau}_{f_{11}}$ and $\boldsymbol{\tau}_{g_{11}}$ are now selected as

$$\alpha_1 = \frac{1}{\boldsymbol{\varphi}_{g_1}^T\hat{\boldsymbol{\theta}}_{g_1}}\left[-c_1z_1 - \boldsymbol{\varphi}_{f_1}^T\hat{\boldsymbol{\theta}}_{f_1} + \dot{x}_{1,r}\right] \tag{F-11a}$$

$$\boldsymbol{\tau}_{f_{11}} = \Gamma_{f_1}\boldsymbol{\varphi}_{f_1}z_1 \tag{F-11b}$$

$$\boldsymbol{\tau}_{g_{11}} = \Gamma_{g_1}\boldsymbol{\varphi}_{g_1}x_2z_1\,, \tag{F-11c}$$

this yields

$$\dot{\mathcal{V}}_1 = -c_1z_1^2 + z_1\boldsymbol{\varphi}_{g_1}^T\hat{\boldsymbol{\theta}}_{g_1}z_2 - \tilde{\boldsymbol{\theta}}_{f_1}^T\Gamma_{f_1}^{-1}\left[\dot{\hat{\boldsymbol{\theta}}}_{f_1} - \boldsymbol{\tau}_{f_{11}}\right] - \tilde{\boldsymbol{\theta}}_{g_1}^T\Gamma_{g_1}^{-1}\left[\dot{\hat{\boldsymbol{\theta}}}_{g_1} - \boldsymbol{\tau}_{g_{11}}\right]\,. \tag{F-12}$$

Note that by selecting $\dot{\hat{\boldsymbol{\theta}}}_{f_1} = \boldsymbol{\tau}_{f_{11}}$ and $\dot{\hat{\boldsymbol{\theta}}}_{g_1} = \boldsymbol{\tau}_{g_{11}}$ we can cancel the last two indefinite terms. However, doing this at every design step will result in overparameterization of the estimator (Sonneveldt, 2010). In the TFABS approach, the Tuning Functions (TFs) $\boldsymbol{\tau}_\star$ are updated every step to prevent overparameterization.

Subsystem 2

Now we consider the second subsystem:

$$\dot{x}_2 = \boldsymbol{\varphi}_{f_2}(\bar{\boldsymbol{x}}_2)^T\boldsymbol{\theta}_{f_2} + \boldsymbol{\varphi}_{g_2}(\bar{\boldsymbol{x}}_2)^T\boldsymbol{\theta}_{g_2}x_3\,. \tag{F-13}$$

We regard state x_3 as the control input for the second subsystem. However, because x_3 is just a state variable and not the real control input u, we call x_3 the *virtual control*.

Now we introduce the tracking error:

$$z_3 = x_3 - \alpha_2\,, \tag{F-14}$$

and rewrite the second subsystem in terms of the tracking errors

$$\begin{aligned}
\dot{z}_2 &= \dot{x}_2 - \dot{\alpha}_1 \\
&= \boldsymbol{\varphi}_{f_2}^T\boldsymbol{\theta}_{f_2} + \boldsymbol{\varphi}_{g_2}^T\boldsymbol{\theta}_{g_2}x_3 - \dot{\alpha}_1 \\
&= \boldsymbol{\varphi}_{f_2}^T\boldsymbol{\theta}_{f_2} + \boldsymbol{\varphi}_{g_2}^T\boldsymbol{\theta}_{g_2}(z_3+\alpha_2) - \dot{\alpha}_1\,.
\end{aligned} \tag{F-15}$$

The time derivative of the first stabilizing function $\alpha_1 = f\big(x_1, x_{1,r}, \dot{x}_{1,r}, \dot{\theta}_{f_1}, \dot{\theta}_{g_1}\big)$ can be written as

$$\begin{aligned}
\dot{\alpha}_1 &= \frac{\partial \alpha_1}{\partial x_1}\left(\boldsymbol{\varphi}_{f_1}^T \boldsymbol{\theta}_{f_1} + \boldsymbol{\varphi}_{g_1}^T \boldsymbol{\theta}_{g_1} x_2\right) + \frac{\partial \alpha_1}{\partial x_{1,r}} \dot{x}_{1,r} + \frac{\partial \alpha_1}{\partial \dot{x}_{1,r}} \ddot{x}_{1,r} + \frac{\partial \alpha_1}{\partial \hat{\boldsymbol{\theta}}_{f_1}} \dot{\hat{\boldsymbol{\theta}}}_{f_1} + \frac{\partial \alpha_1}{\partial \hat{\boldsymbol{\theta}}_{g_1}} \dot{\hat{\boldsymbol{\theta}}}_{g_1} \\
&= \frac{\partial \alpha_1}{\partial x_1}\left(\boldsymbol{\varphi}_{f_1}^T \tilde{\boldsymbol{\theta}}_{f_1} + \boldsymbol{\varphi}_{g_1}^T \tilde{\boldsymbol{\theta}}_{g_1} x_2\right) + \lambda_1 \,,
\end{aligned} \tag{F-16}$$

where

$$\lambda_1 = \frac{\partial \alpha_1}{\partial x_1}\left(\boldsymbol{\varphi}_{f_1}^T \hat{\boldsymbol{\theta}}_{f_1} + \boldsymbol{\varphi}_{g_1}^T \hat{\boldsymbol{\theta}}_{g_1} x_2\right) + \frac{\partial \alpha_1}{\partial x_{1,r}} \dot{x}_{1,r} + \frac{\partial \alpha_1}{\partial \dot{x}_{1,r}} \ddot{x}_{1,r} + \frac{\partial \alpha_1}{\partial \hat{\boldsymbol{\theta}}_{f_1}} \dot{\hat{\boldsymbol{\theta}}}_{f_1} + \frac{\partial \alpha_1}{\partial \hat{\boldsymbol{\theta}}_{g_1}} \dot{\hat{\boldsymbol{\theta}}}_{g_1} \,. \tag{F-17}$$

Now we augment the scalar CLF $\mathcal{V}_1$:

$$\mathcal{V}_2(\bar{\boldsymbol{z}}_2, \tilde{\boldsymbol{\theta}}_{\star_2}) = \mathcal{V}_1 + \frac{1}{2} z_2^2 + \frac{1}{2} \tilde{\boldsymbol{\theta}}_{f_2}^T \Gamma_{f_2}^{-1} \tilde{\boldsymbol{\theta}}_{f_2} + \frac{1}{2} \tilde{\boldsymbol{\theta}}_{g_2}^T \Gamma_{g_2}^{-1} \tilde{\boldsymbol{\theta}}_{g_2} \,, \tag{F-18}$$

where $\bar{\boldsymbol{z}}_2 = [z_1, z_2]^T$ and $\tilde{\boldsymbol{\theta}}_{\star_2} = [\tilde{\boldsymbol{\theta}}_{f_1}, \tilde{\boldsymbol{\theta}}_{g_1}, \tilde{\boldsymbol{\theta}}_{f_2}, \tilde{\boldsymbol{\theta}}_{g_2}]^T$. Taking the time derivative of the CLF along the trajectories of Eqs. (F-5), (F-8) and (F-15) results in

$$\begin{aligned}
\dot{\mathcal{V}}_2 &= \dot{\mathcal{V}}_1 + z_2 \left[\boldsymbol{\varphi}_{f_2}^T \boldsymbol{\theta}_{f_2} + \boldsymbol{\varphi}_{g_2}^T \boldsymbol{\theta}_{g_2} (z_3 + \alpha_2) - \frac{\partial \alpha_1}{\partial x_1}\left(\boldsymbol{\varphi}_{f_1}^T \tilde{\boldsymbol{\theta}}_{f_1} + \boldsymbol{\varphi}_{g_1}^T \tilde{\boldsymbol{\theta}}_{g_1} x_2\right) - \lambda_1\right] \\
&\quad - \tilde{\boldsymbol{\theta}}_{f_2}^T \Gamma_{f_2}^{-1} \dot{\hat{\boldsymbol{\theta}}}_{f_2} - \tilde{\boldsymbol{\theta}}_{g_2}^T \Gamma_{g_2}^{-1} \dot{\hat{\boldsymbol{\theta}}}_{g_2} \\
&= -c_1 z_1^2 + z_1 \boldsymbol{\varphi}_{g_1}^T \hat{\boldsymbol{\theta}}_{g_1} z_2 + z_2 \left[\boldsymbol{\varphi}_{f_2}^T \hat{\boldsymbol{\theta}}_{f_2} + \boldsymbol{\varphi}_{g_2}^T \hat{\boldsymbol{\theta}}_{g_2} (z_3 + \alpha_2) - \lambda_1\right] \\
&\quad - \tilde{\boldsymbol{\theta}}_{f_1}^T \Gamma_{f_1}^{-1} \left[\dot{\hat{\boldsymbol{\theta}}}_{f_1} - \boldsymbol{\tau}_{f_{11}} + \Gamma_{f_1} \boldsymbol{\varphi}_{f_1} \frac{\partial \alpha_1}{\partial x_1} z_2\right] - \tilde{\boldsymbol{\theta}}_{g_1}^T \Gamma_{g_1}^{-1} \left[\dot{\hat{\boldsymbol{\theta}}}_{g_1} - \boldsymbol{\tau}_{g_{11}} + \Gamma_{g_1} \boldsymbol{\varphi}_{g_1} \frac{\partial \alpha_1}{\partial x_1} x_2 z_2\right] \\
&\quad - \tilde{\boldsymbol{\theta}}_{f_2}^T \Gamma_{f_2}^{-1} \left[\dot{\hat{\boldsymbol{\theta}}}_{f_2} - \Gamma_{f_2} \boldsymbol{\varphi}_{f_2} z_2\right] - \tilde{\boldsymbol{\theta}}_{g_2}^T \Gamma_{g_2}^{-1} \left[\dot{\hat{\boldsymbol{\theta}}}_{g_2} - \Gamma_{g_2} \boldsymbol{\varphi}_{g_2} x_3 z_2\right] \,.
\end{aligned} \tag{F-19}$$

The stabilizing control law α_2 and the *intermediate* update laws are now selected as

$$\alpha_2 = \frac{1}{\boldsymbol{\varphi}_{g_2}^T \hat{\boldsymbol{\theta}}_{g_2}} \left[-c_2 z_2 - \boldsymbol{\varphi}_{g_1}^T \hat{\boldsymbol{\theta}}_{g_1} z_1 - \boldsymbol{\varphi}_{f_2}^T \hat{\boldsymbol{\theta}}_{f_2} + \lambda_1\right] \tag{F-20a}$$

$$\boldsymbol{\tau}_{f_{12}} = \boldsymbol{\tau}_{f_{11}} - \Gamma_{f_1} \boldsymbol{\varphi}_{f_1} \frac{\partial \alpha_1}{\partial x_1} z_2 = \Gamma_{f_1} \boldsymbol{\varphi}_{f_1} \left[z_1 - \frac{\partial \alpha_1}{\partial x_1} z_2\right] \tag{F-20b}$$

$$\boldsymbol{\tau}_{g_{12}} = \boldsymbol{\tau}_{g_{11}} - \Gamma_{g_1} \boldsymbol{\varphi}_{g_1} \frac{\partial \alpha_1}{\partial x_1} x_2 z_2 = \Gamma_{g_1} \boldsymbol{\varphi}_{g_1} x_2 \left[z_1 - \frac{\partial \alpha_1}{\partial x_1} z_2\right] \tag{F-20c}$$

$$\boldsymbol{\tau}_{f_{22}} = \Gamma_{f_2} \boldsymbol{\varphi}_{f_2} z_2 \tag{F-20d}$$

$$\boldsymbol{\tau}_{g_{22}} = \Gamma_{g_2} \boldsymbol{\varphi}_{g_2} x_3 z_2 \,, \tag{F-20e}$$

this yields

$$\begin{aligned}
\dot{\mathcal{V}}_2 &= -c_1 z_1^2 - c_2 z_2^2 + z_2 \boldsymbol{\varphi}_{g_2}^T \hat{\boldsymbol{\theta}}_{g_2} z_3 - \tilde{\boldsymbol{\theta}}_{f_1}^T \Gamma_{f_1}^{-1} \left[\dot{\hat{\boldsymbol{\theta}}}_{f_1} - \boldsymbol{\tau}_{f_{12}}\right] - \tilde{\boldsymbol{\theta}}_{g_1}^T \Gamma_{g_1}^{-1} \left[\dot{\hat{\boldsymbol{\theta}}}_{g_1} - \boldsymbol{\tau}_{g_{12}}\right] \\
&\quad - \tilde{\boldsymbol{\theta}}_{f_2}^T \Gamma_{f_2}^{-1} \left[\dot{\hat{\boldsymbol{\theta}}}_{f_2} - \boldsymbol{\tau}_{f_{22}}\right] - \tilde{\boldsymbol{\theta}}_{g_2}^T \Gamma_{g_2}^{-1} \left[\dot{\hat{\boldsymbol{\theta}}}_{g_2} - \boldsymbol{\tau}_{g_{22}}\right] \,.
\end{aligned} \tag{F-21}$$

Subsystem i, i = 3, ..., n - 1

Now we consider the i-th subsystem:

$$\dot{x}_i = \boldsymbol{\varphi}_{f_i}(\bar{\boldsymbol{x}}_i)^T \boldsymbol{\theta}_{f_i} + \boldsymbol{\varphi}_{g_i}(\bar{\boldsymbol{x}}_i)^T \boldsymbol{\theta}_{g_i} x_{i+1}\,, \quad i = 3, \ldots, n-1\,. \tag{F-22}$$

We regard state x_{i+1} as the control input for the i-th subsystem. However, because x_{i+1} is just a state variable and not the real control input u, we call x_{i+1} the *virtual control.*

Now we introduce the tracking errors:

$$z_i = x_i - \alpha_{i-1}\,, \quad i = 4, \ldots, n\,, \tag{F-23}$$

and rewrite the i-th subsystem in terms of the tracking errors

$$\begin{aligned} \dot{z}_i &= \dot{x}_i - \dot{\alpha}_{i-1}\,, \quad i = 3, \ldots, n-1 \\ &= \boldsymbol{\varphi}_{f_i}^T \boldsymbol{\theta}_{f_i} + \boldsymbol{\varphi}_{g_i}^T \boldsymbol{\theta}_{g_i} x_{i+1} - \dot{\alpha}_{i-1} \\ &= \boldsymbol{\varphi}_{f_i}^T \boldsymbol{\theta}_{f_i} + \boldsymbol{\varphi}_{g_i}^T \boldsymbol{\theta}_{g_i} \left(z_{i+1} + \alpha_i\right) - \dot{\alpha}_{i-1}\,. \end{aligned} \tag{F-24}$$

The time derivative of the stabilizing function α_{i-1} can be written as

$$\begin{aligned} \dot{\alpha}_{i-1} &= \sum_{j=1}^{i-1} \frac{\partial \alpha_{i-1}}{\partial x_j} \left(\boldsymbol{\varphi}_{f_j}^T \boldsymbol{\theta}_{f_j} + \boldsymbol{\varphi}_{g_j}^T \boldsymbol{\theta}_{g_j} x_{j+1} \right) + \sum_{j=1}^{i-1} \left(\frac{\partial \alpha_{i-1}}{\partial \hat{\boldsymbol{\theta}}_{f_j}} \dot{\hat{\boldsymbol{\theta}}}_{f_j} + \frac{\partial \alpha_{i-1}}{\partial \hat{\boldsymbol{\theta}}_{g_j}} \dot{\hat{\boldsymbol{\theta}}}_{g_j} \right) + \sum_{j=1}^{i} \frac{\partial \alpha_{i-1}}{\partial x_{1,r}^{(j-1)}} x_{1,r}^{(j)} \\ &= \sum_{j=1}^{i-1} \frac{\partial \alpha_{i-1}}{\partial x_j} \left(\boldsymbol{\varphi}_{f_j}^T \tilde{\boldsymbol{\theta}}_{f_j} + \boldsymbol{\varphi}_{g_j}^T \tilde{\boldsymbol{\theta}}_{g_j} x_{j+1} \right) + \lambda_{i-1}\,, \end{aligned} \tag{F-25}$$

where

$$\lambda_{i-1} = \sum_{j=1}^{i-1} \frac{\partial \alpha_{i-1}}{\partial x_j} \left(\boldsymbol{\varphi}_{f_j}^T \hat{\boldsymbol{\theta}}_{f_j} + \boldsymbol{\varphi}_{g_j}^T \hat{\boldsymbol{\theta}}_{g_j} x_{j+1} \right) + \sum_{j=1}^{i-1} \left(\frac{\partial \alpha_{i-1}}{\partial \hat{\boldsymbol{\theta}}_{f_j}} \dot{\hat{\boldsymbol{\theta}}}_{f_j} + \frac{\partial \alpha_{i-1}}{\partial \hat{\boldsymbol{\theta}}_{g_j}} \dot{\hat{\boldsymbol{\theta}}}_{g_j} \right) + \sum_{j=1}^{i} \frac{\partial \alpha_{i-1}}{\partial x_{1,r}^{(j-1)}} x_{1,r}^{(j)}\,. \tag{F-26}$$

Now we augment the scalar CLF:

$$\mathcal{V}_i(\bar{\boldsymbol{z}}_i, \tilde{\boldsymbol{\theta}}_{\star_i}) = V_{i-1} + \frac{1}{2} z_i^2 + \frac{1}{2} \tilde{\boldsymbol{\theta}}_{f_i}^T \Gamma_{f_i}^{-1} \tilde{\boldsymbol{\theta}}_{f_i} + \frac{1}{2} \tilde{\boldsymbol{\theta}}_{g_i}^T \Gamma_{g_i}^{-1} \tilde{\boldsymbol{\theta}}_{g_i}\,, \quad i = 3, \ldots, n-1\,, \tag{F-27}$$

where $\bar{\boldsymbol{z}}_i = [z_1, \cdots, z_i]^T$ and $\tilde{\boldsymbol{\theta}}_{\star_i} = [\tilde{\boldsymbol{\theta}}_{f_1}, \cdots, \tilde{\boldsymbol{\theta}}_{f_i}, \tilde{\boldsymbol{\theta}}_{g_1}, \cdots, \tilde{\boldsymbol{\theta}}_{g_i}]^T$. Taking the time derivative of the CLF along the trajectories of Eqs. (F-5), (F-8), (F-15) and (F-24) results in

$$\begin{aligned}
\dot{\mathcal{V}}_i &= \dot{\mathcal{V}}_{i-1} + z_i \left[\boldsymbol{\varphi}_{f_i}^T \boldsymbol{\theta}_{f_i} + \boldsymbol{\varphi}_{g_i}^T \boldsymbol{\theta}_{g_i} \left(z_{i+1} + \alpha_i \right) - \frac{\partial \alpha_{i-1}}{\partial x_{i-1}} \left(\boldsymbol{\varphi}_{f_{i-1}}^T \tilde{\boldsymbol{\theta}}_{f_{i-1}} + \boldsymbol{\varphi}_{g_{i-1}}^T \tilde{\boldsymbol{\theta}}_{g_{i-1}} x_i \right) - \lambda_{i-1} \right] \\
&\quad - \tilde{\boldsymbol{\theta}}_{f_i}^T \Gamma_{f_i}^{-1} \dot{\hat{\boldsymbol{\theta}}}_{f_i} - \tilde{\boldsymbol{\theta}}_{g_i}^T \Gamma_{g_i}^{-1} \dot{\hat{\boldsymbol{\theta}}}_{g_i} \qquad \text{(F-28)} \\
&= - \sum_{j=1}^{i-1} c_j z_j^2 + z_{i-1} \boldsymbol{\varphi}_{g_{i-1}}^T \hat{\boldsymbol{\theta}}_{g_{i-1}} z_i + z_i \left[\boldsymbol{\varphi}_{f_i}^T \hat{\boldsymbol{\theta}}_{f_i} + \boldsymbol{\varphi}_{g_i}^T \hat{\boldsymbol{\theta}}_{g_i} \left(z_{i+1} + \alpha_i \right) - \lambda_{i-1} \right] \\
&\quad - \sum_{j=1}^{i-1} \tilde{\boldsymbol{\theta}}_{f_j}^T \Gamma_{f_j}^{-1} \left[\dot{\hat{\boldsymbol{\theta}}}_{f_j} - \boldsymbol{\tau}_{f_{j(i-1)}} + \Gamma_{f_j} \varphi_{f_j} \frac{\partial \alpha_{i-1}}{\partial x_j} z_i \right] - \tilde{\boldsymbol{\theta}}_{f_i}^T \Gamma_{f_i}^{-1} \left[\dot{\hat{\boldsymbol{\theta}}}_{f_i} - \Gamma_{f_i} \boldsymbol{\varphi}_{f_i} z_i \right] \\
&\quad - \sum_{j=1}^{i-1} \tilde{\boldsymbol{\theta}}_{g_j}^T \Gamma_{g_j}^{-1} \left[\dot{\hat{\boldsymbol{\theta}}}_{g_j} - \boldsymbol{\tau}_{g_{j(i-1)}} + \Gamma_{g_j} \varphi_{g_j} \frac{\partial \alpha_{i-1}}{\partial x_j} x_{j+1} z_i \right] - \tilde{\boldsymbol{\theta}}_{g_i}^T \Gamma_{g_i}^{-1} \left[\dot{\hat{\boldsymbol{\theta}}}_{g_i} - \Gamma_{g_i} \boldsymbol{\varphi}_{g_i} x_{i+1} z_i \right] .
\end{aligned}$$

The stabilizing control law α_i and the *intermediate* update laws are now selected as

$$\alpha_i = \frac{1}{\boldsymbol{\varphi}_{g_i}^T \hat{\boldsymbol{\theta}}_{g_i}} \left[-c_i z_i - \boldsymbol{\varphi}_{g_{i-1}}^T \hat{\boldsymbol{\theta}}_{g_{i-1}} z_{i-1} - \boldsymbol{\varphi}_{f_i}^T \hat{\boldsymbol{\theta}}_{f_i} + \lambda_{i-1} \right] \qquad \text{(F-29a)}$$

$$\boldsymbol{\tau}_{f_{ji}} = \boldsymbol{\tau}_{f_{j(i-1)}} - \Gamma_{f_j} \boldsymbol{\varphi}_{f_j} \frac{\partial \alpha_{i-1}}{\partial x_j} z_i = \Gamma_{f_j} \boldsymbol{\varphi}_{f_j} \left[z_j - \sum_{k=j}^{i-1} \frac{\partial \alpha_k}{\partial x_j} z_{k+1} \right] \qquad \text{(F-29b)}$$

$$\boldsymbol{\tau}_{g_{ji}} = \boldsymbol{\tau}_{g_{j(i-1)}} - \Gamma_{g_j} \boldsymbol{\varphi}_{g_j} \frac{\partial \alpha_{i-1}}{\partial x_j} x_{j+1} z_i = \Gamma_{g_j} \boldsymbol{\varphi}_{g_j} x_{j+1} \left[z_j - \sum_{k=j}^{i-1} \frac{\partial \alpha_k}{\partial x_j} z_{k+1} \right] \qquad \text{(F-29c)}$$

$$\boldsymbol{\tau}_{f_{ii}} = \Gamma_{f_i} \varphi_{f_i} z_i \qquad \text{(F-29d)}$$

$$\boldsymbol{\tau}_{g_{ii}} = \Gamma_{g_i} \varphi_{g_i} x_{i+1} z_i \, , \qquad \text{(F-29e)}$$

this yields

$$\dot{\mathcal{V}}_i = - \sum_{j=1}^{i} c_j z_j^2 + z_i \boldsymbol{\varphi}_{g_i}^T \hat{\boldsymbol{\theta}}_{g_i} z_{i+1} - \sum_{j=1}^{i} \tilde{\boldsymbol{\theta}}_{f_j}^T \Gamma_{f_j}^{-1} \left[\dot{\hat{\boldsymbol{\theta}}}_{f_j} - \boldsymbol{\tau}_{f_{ji}} \right] - \sum_{j=1}^{i} \tilde{\boldsymbol{\theta}}_{g_j}^T \Gamma_{g_j}^{-1} \left[\dot{\hat{\boldsymbol{\theta}}}_{g_j} - \boldsymbol{\tau}_{g_{ji}} \right] . \qquad \text{(F-30)}$$

Subsystem n

Now we consider the final subsystem:

$$\dot{x}_n = \boldsymbol{\varphi}_{f_n}(\boldsymbol{x})^T \boldsymbol{\theta}_{f_n} + \boldsymbol{\varphi}_{g_n}(\boldsymbol{x})^T \boldsymbol{\theta}_{g_n} u \, . \qquad \text{(F-31)}$$

The $\bar{z}_n$-dynamics are given by

$$\begin{aligned}
\dot{z}_n &= \dot{x}_n - \dot{\alpha}_{n-1} \\
&= \boldsymbol{\varphi}_{f_n}^T \boldsymbol{\theta}_{f_n} + \boldsymbol{\varphi}_{g_n}^T \boldsymbol{\theta}_{g_n} u - \dot{\alpha}_{n-1} \, . \qquad \text{(F-32)}
\end{aligned}$$

The final Lyapunov function is now defined as

$$\begin{aligned}\mathcal{V}_n(\bar{\boldsymbol{z}}_n, \tilde{\boldsymbol{\theta}}_{\star_n}) &= V_{n-1} + \frac{1}{2}z_n^2 + \frac{1}{2}\tilde{\boldsymbol{\theta}}_{f_n}^T \Gamma_{f_n}^{-1}\tilde{\boldsymbol{\theta}}_{f_n} + \frac{1}{2}\tilde{\boldsymbol{\theta}}_{g_n}^T \Gamma_{g_n}^{-1}\tilde{\boldsymbol{\theta}}_{g_n} \\ &= \frac{1}{2}\sum_{j=1}^{n}\left(z_j^2 + \tilde{\boldsymbol{\theta}}_{f_j}^T \Gamma_{f_j}^{-1}\tilde{\boldsymbol{\theta}}_{f_j} + \tilde{\boldsymbol{\theta}}_{g_j}^T \Gamma_{g_j}^{-1}\tilde{\boldsymbol{\theta}}_{g_j}\right) .\end{aligned} \tag{F-33}$$

Taking the time derivative of the CLF along the trajectories of Eqs. (F-5), (F-8), (F-15), (F-24) and (F-32) results in

$$\begin{aligned}\dot{\mathcal{V}}_n &= \dot{\mathcal{V}}_{n-1} + z_n\left[\boldsymbol{\varphi}_{f_n}^T\boldsymbol{\theta}_{f_n} + \boldsymbol{\varphi}_{g_n}^T\boldsymbol{\theta}_{g_n}u - \frac{\partial\alpha_{n-1}}{\partial x_{n-1}}\left(\boldsymbol{\varphi}_{f_{n-1}}^T\tilde{\boldsymbol{\theta}}_{f_{n-1}} + \boldsymbol{\varphi}_{g_{n-1}}^T\tilde{\boldsymbol{\theta}}_{g_{n-1}}x_n\right) - \lambda_{n-1}\right] \\ &\quad -\tilde{\boldsymbol{\theta}}_{f_n}^T\Gamma_{f_n}^{-1}\dot{\hat{\boldsymbol{\theta}}}_{f_n} - \tilde{\boldsymbol{\theta}}_{g_n}^T\Gamma_{g_n}^{-1}\dot{\hat{\boldsymbol{\theta}}}_{g_n} \qquad\qquad \text{(F-34)} \\ &= -\sum_{j=1}^{n-1}c_j z_j^2 + z_{n-1}\boldsymbol{\varphi}_{g_{n-1}}^T\hat{\boldsymbol{\theta}}_{g_{n-1}}z_n + z_n\left[\boldsymbol{\varphi}_{f_n}^T\hat{\boldsymbol{\theta}}_{f_n} + \boldsymbol{\varphi}_{g_n}^T\hat{\boldsymbol{\theta}}_{g_n}u - \lambda_{n-1}\right] \\ &\quad -\sum_{j=1}^{n-1}\tilde{\boldsymbol{\theta}}_{f_j}^T\Gamma_{f_j}^{-1}\left[\dot{\hat{\boldsymbol{\theta}}}_{f_j} - \boldsymbol{\tau}_{f_{j(n-1)}} + \Gamma_{f_j}\varphi_{f_j}\frac{\partial\alpha_{n-1}}{\partial x_j}z_n\right] - \tilde{\boldsymbol{\theta}}_{f_n}^T\Gamma_{f_n}^{-1}\left[\dot{\hat{\boldsymbol{\theta}}}_{f_n} - \Gamma_{f_n}\boldsymbol{\varphi}_{f_n}z_n\right] \\ &\quad -\sum_{j=1}^{n-1}\tilde{\boldsymbol{\theta}}_{g_j}^T\Gamma_{g_j}^{-1}\left[\dot{\hat{\boldsymbol{\theta}}}_{g_j} - \boldsymbol{\tau}_{g_{j(n-1)}} + \Gamma_{g_j}\varphi_{g_j}\frac{\partial\alpha_{n-1}}{\partial x_j}x_{j+1}z_n\right] - \tilde{\boldsymbol{\theta}}_{g_n}^T\Gamma_{g_n}^{-1}\left[\dot{\hat{\boldsymbol{\theta}}}_{g_n} - \Gamma_{g_n}\boldsymbol{\varphi}_{g_n}uz_n\right] .\end{aligned}$$

The control law u and the final update laws are now selected as

$$u = \frac{1}{\boldsymbol{\varphi}_{g_n}^T\hat{\boldsymbol{\theta}}_{g_n}}\left[-c_n z_n - \boldsymbol{\varphi}_{g_{n-1}}^T\hat{\boldsymbol{\theta}}_{g_{n-1}}z_{n-1} - \boldsymbol{\varphi}_{f_n}^T\hat{\boldsymbol{\theta}}_{f_n} + \lambda_{n-1}\right] \tag{F-35a}$$

$$\dot{\hat{\boldsymbol{\theta}}}_{f_j} = \boldsymbol{\tau}_{f_{j(n-1)}} - \Gamma_{f_j}\boldsymbol{\varphi}_{f_j}\frac{\partial\alpha_{n-1}}{\partial x_j}z_n = \Gamma_{f_j}\boldsymbol{\varphi}_{f_j}\left[z_j - \sum_{k=j}^{n-1}\frac{\partial\alpha_k}{\partial x_j}z_{k+1}\right] \tag{F-35b}$$

$$\dot{\hat{\boldsymbol{\theta}}}_{g_j} = \boldsymbol{\tau}_{g_{j(n-1)}} - \Gamma_{g_j}\boldsymbol{\varphi}_{g_j}\frac{\partial\alpha_{n-1}}{\partial x_j}x_{j+1}z_n = \Gamma_{g_j}\boldsymbol{\varphi}_{g_j}x_{j+1}\left[z_j - \sum_{k=j}^{n-1}\frac{\partial\alpha_k}{\partial x_j}z_{k+1}\right] \tag{F-35c}$$

$$\dot{\hat{\boldsymbol{\theta}}}_{f_n} = \Gamma_{f_n}\varphi_{f_n}z_n \tag{F-35d}$$

$$\dot{\hat{\boldsymbol{\theta}}}_{g_n} = \Gamma_{g_n}\varphi_{g_n}uz_n , \tag{F-35e}$$

this yields

$$\dot{\mathcal{V}}_n = -\sum_{j=1}^{n}c_j z_j^2 . \tag{F-36}$$

According to the theorem of *LaSalle-Yoshizawa* (see Theorem C.2, page 71) the equilibrium $\boldsymbol{z} = \boldsymbol{0}$ is globally uniformly asymptotically stable when $c_1 > 0$ and $c_2 > 0$, implying that the reference output state $x_{1,r}$ is successfully tracked by x_1, that is:

$$\lim_{t\to\infty}[x_1 - x_{1,r}] = 0 . \tag{F-37}$$

F-1-2 Command-Filtered Adaptive Backstepping

In this section the TFABS technique is augmented with command filters to obviate the need for analytic computation of the virtual control derivatives. Another advantage of using command filters is that systems no longer have to be in triangular form. Moreover, command filters allow the engineer to include magnitude, rate and bandwidth limits on the (virtual) controls.

We consider the following non-triangular, feedback passive system:

$$\dot{x}_i = f_i(\boldsymbol{x}) + g_i(\boldsymbol{x})x_{i+1}\,, \quad i = 1, \ldots, n-1 \tag{F-38a}$$

$$\dot{x}_n = f_n(\boldsymbol{x}) + g_n(\boldsymbol{x})u\,, \tag{F-38b}$$

where $\boldsymbol{x} \in \mathbb{R}^n$ is the state, $x_i \in \mathbb{R}$ and $u \in \mathbb{R}$ the control signal and $g_i \neq 0$ for $i = 1, \ldots, n$. The control objective is to track a smooth reference signal $x_{1,r}$, for which the first-order time derivative is assumed to be known and bounded, with the state x_1. Furthermore, the signals x_i for $i = 2, \ldots, n$ must remain bounded. The smooth functions f_i and g_i contain the unknown dynamics of the system and will have to be approximated. It is assumed there exist vectors $\boldsymbol{\theta}_{f_i}$ and $\boldsymbol{\theta}_{g_i}$ such that

$$f_i(\boldsymbol{x}) = \boldsymbol{\varphi}_{f_i}(\boldsymbol{x})^T\boldsymbol{\theta}_{f_i}\,, \quad i = 1, \ldots, n \tag{F-39a}$$

$$g_i(\boldsymbol{x}) = \boldsymbol{\varphi}_{g_i}(\boldsymbol{x})^T\boldsymbol{\theta}_{g_i}\,. \tag{F-39b}$$

Now we can write Eq. (F-38) as

$$\dot{x}_i = \boldsymbol{\varphi}_{f_i}(\boldsymbol{x})^T\boldsymbol{\theta}_{f_i} + \boldsymbol{\varphi}_{g_i}(\boldsymbol{x})^T\boldsymbol{\theta}_{g_i}x_{i+1}\,, \quad i = 1, \ldots, n-1 \tag{F-40a}$$

$$\dot{x}_n = \boldsymbol{\varphi}_{f_n}(\boldsymbol{x})^T\boldsymbol{\theta}_{f_n} + \boldsymbol{\varphi}_{g_n}(\boldsymbol{x})^T\boldsymbol{\theta}_{g_n}u\,. \tag{F-40b}$$

The estimates of the nonlinear functions f_i and g_i are defined as

$$\hat{f}_i(\boldsymbol{x}, \hat{\boldsymbol{\theta}}_{f_i}) = \boldsymbol{\varphi}_{f_i}(\boldsymbol{x})^T\hat{\boldsymbol{\theta}}_{f_i}\,, \quad i = 1, \ldots, n \tag{F-41a}$$

$$\hat{g}_i(\boldsymbol{x}, \hat{\boldsymbol{\theta}}_{g_i}) = \boldsymbol{\varphi}_{g_i}(\boldsymbol{x})^T\hat{\boldsymbol{\theta}}_{g_i}\,, \tag{F-41b}$$

and the parameter errors as

$$\tilde{\boldsymbol{\theta}}_{f_i} = \boldsymbol{\theta}_{f_i} - \hat{\boldsymbol{\theta}}_{f_i} \quad \rightarrow \quad \dot{\tilde{\boldsymbol{\theta}}}_{f_i} = -\dot{\hat{\boldsymbol{\theta}}}_{f_i} \tag{F-42a}$$

$$\tilde{\boldsymbol{\theta}}_{g_i} = \boldsymbol{\theta}_{g_i} - \hat{\boldsymbol{\theta}}_{g_i} \quad \rightarrow \quad \dot{\tilde{\boldsymbol{\theta}}}_{g_i} = -\dot{\hat{\boldsymbol{\theta}}}_{g_i}\,. \tag{F-42b}$$

Subsystem 1

We start by considering the first subsystem, which is the subsystem "furthest" away from the actual control u:

$$\dot{x}_1 = \boldsymbol{\varphi}_{f_1}(\boldsymbol{x})^T\boldsymbol{\theta}_{f_1} + \boldsymbol{\varphi}_{g_1}(\boldsymbol{x})^T\boldsymbol{\theta}_{g_1}x_2\,. \tag{F-43}$$

Now we regard state x_2 as the control input for this subsystem. However, because x_2 is just a state variable and not the real control input u, we call x_2 the *virtual control*.

The tracking errors are defined as

$$z_1 = x_1 - x_{1,r} \tag{F-44a}$$
$$z_2 = x_2 - x_{2,r}\,, \tag{F-44b}$$

where $x_{2,r}$ is the new virtual control law to be designed. As with TFABS, the first stabilizing control law is defined as

$$\alpha_1 = \frac{1}{\boldsymbol{\varphi}_{g_1}^T \hat{\boldsymbol{\theta}}_{g_1}} \left[-c_1 z_1 - \boldsymbol{\varphi}_{f_1}^T \hat{\boldsymbol{\theta}}_{f_1} + \dot{x}_{1,r} \right]\,. \tag{F-11a revisited}$$

However, instead of directly applying this virtual control, a new signal $x_{2,r}^0$ is defined as

$$x_{2,r}^0 = \alpha_1 - \chi_2\,, \tag{F-45}$$

where χ_2 will be defined later on. The raw signal $x_{2,r}^0$ is led through a command filter to obtain $x_{2,r}$ and its time derivative $\dot{x}_{2,r}$. The effect that the use of this command filter has on the tracking error z_1 is estimated by the stable linear filter:

$$\dot{\chi}_1 = -c_1 \chi_1 + \boldsymbol{\varphi}_{g_1}^T \hat{\boldsymbol{\theta}}_{g_1} \left(x_{2,r} - x_{2,r}^0 \right)\,, \tag{F-46}$$

with $\chi_1(0) = 0$. This auxiliary system compensates for the constraint effects due to magnitude, rate and bandwidth limitations of the command filter. Now we introduce the *compensated* tracking errors:

$$\bar{z}_1 = z_1 - \chi_1 \tag{F-47a}$$
$$\bar{z}_2 = z_2 - \chi_2\,. \tag{F-47b}$$

The $\bar{z}_1$-dynamics are given by

$$\begin{aligned}
\dot{\bar{z}}_1 &= \dot{z}_1 - \dot{\chi}_1 \\
&= \dot{x}_1 - \dot{x}_{1,r} - \dot{\chi}_1 \\
&= \boldsymbol{\varphi}_{f_1}^T \boldsymbol{\theta}_{f_1} + \boldsymbol{\varphi}_{g_1}^T \boldsymbol{\theta}_{g_1} x_2 - \dot{x}_{1,r} + c_1 \chi_1 - \boldsymbol{\varphi}_{g_1}^T \hat{\boldsymbol{\theta}}_{g_1} \left(x_{2,r} - x_{2,r}^0 \right) \\
&= \boldsymbol{\varphi}_{f_1}^T \boldsymbol{\theta}_{f_1} + \boldsymbol{\varphi}_{g_1}^T \boldsymbol{\theta}_{g_1} \left(z_2 + x_{2,r} \right) - \dot{x}_{1,r} + c_1 \chi_1 - \boldsymbol{\varphi}_{g_1}^T \hat{\boldsymbol{\theta}}_{g_1} \left(x_{2,r} - x_{2,r}^0 \right)\,.
\end{aligned} \tag{F-48}$$

Now we formulate a quadratic scalar CLF for the first subsystem:

$$\mathcal{V}_1(\bar{z}_1, \tilde{\boldsymbol{\theta}}_{\star_1}) = \frac{1}{2}\bar{z}_1^2 + \frac{1}{2}\tilde{\boldsymbol{\theta}}_{f_1}^T \Gamma_{f_1}^{-1} \tilde{\boldsymbol{\theta}}_{f_1} + \frac{1}{2}\tilde{\boldsymbol{\theta}}_{g_1}^T \Gamma_{g_1}^{-1} \tilde{\boldsymbol{\theta}}_{g_1}\,. \tag{F-49}$$

Taking the time derivative of $\mathcal{V}_1$ along the trajectories of Eqs. (F-42) and (F-48) results in

$$\begin{aligned}
\dot{\mathcal{V}}_1 &= \bar{z}_1 \left[\boldsymbol{\varphi}_{f_1}^T \boldsymbol{\theta}_{f_1} + \boldsymbol{\varphi}_{g_1}^T \boldsymbol{\theta}_{g_1}\left(z_2 + x_{2,r}\right) - \dot{x}_{1,r} + c_1\chi_1 - \boldsymbol{\varphi}_{g_1}^T \hat{\boldsymbol{\theta}}_{g_1}\left(x_{2,r} - x_{2,r}^0\right)\right] \\
&\quad - \tilde{\boldsymbol{\theta}}_{f_1}^T \Gamma_{f_1}^{-1} \dot{\hat{\boldsymbol{\theta}}}_{f_1} - \tilde{\boldsymbol{\theta}}_{g_1}^T \Gamma_{g_1}^{-1} \dot{\hat{\boldsymbol{\theta}}}_{g_1} \\
&= \bar{z}_1 \left[\boldsymbol{\varphi}_{f_1}^T \boldsymbol{\theta}_{f_1} + \boldsymbol{\varphi}_{g_1}^T \boldsymbol{\theta}_{g_1}\left(z_2 + x_{2,r}\right) - \boldsymbol{\varphi}_{g_1}^T \hat{\boldsymbol{\theta}}_{g_1} x_{2,r}^0 + \boldsymbol{\varphi}_{g_1}^T \hat{\boldsymbol{\theta}}_{g_1} x_{2,r}^0 - \dot{x}_{1,r} + c_1\chi_1 \right. \\
&\qquad \left. - \boldsymbol{\varphi}_{g_1}^T \hat{\boldsymbol{\theta}}_{g_1}\left(x_{2,r} - x_{2,r}^0\right)\right] - \tilde{\boldsymbol{\theta}}_{f_1}^T \Gamma_{f_1}^{-1} \dot{\hat{\boldsymbol{\theta}}}_{f_1} - \tilde{\boldsymbol{\theta}}_{g_1}^T \Gamma_{g_1}^{-1} \dot{\hat{\boldsymbol{\theta}}}_{g_1} \\
&= \bar{z}_1 \left[\boldsymbol{\varphi}_{f_1}^T \boldsymbol{\theta}_{f_1} + \boldsymbol{\varphi}_{g_1}^T \boldsymbol{\theta}_{g_1}\left(z_2 + x_{2,r}\right) - \boldsymbol{\varphi}_{g_1}^T \hat{\boldsymbol{\theta}}_{g_1} x_{2,r}^0 + \boldsymbol{\varphi}_{g_1}^T \hat{\boldsymbol{\theta}}_{g_1}\left(\alpha_1 - \chi_2\right) - \dot{x}_{1,r} + c_1\chi_1 \right. \\
&\qquad \left. - \boldsymbol{\varphi}_{g_1}^T \hat{\boldsymbol{\theta}}_{g_1}\left(x_{2,r} - x_{2,r}^0\right)\right] - \tilde{\boldsymbol{\theta}}_{f_1}^T \Gamma_{f_1}^{-1} \dot{\hat{\boldsymbol{\theta}}}_{f_1} - \tilde{\boldsymbol{\theta}}_{g_1}^T \Gamma_{g_1}^{-1} \dot{\hat{\boldsymbol{\theta}}}_{g_1} \\
&= \bar{z}_1 \left[-c_1 z_1 + \boldsymbol{\varphi}_{f_1}^T \tilde{\boldsymbol{\theta}}_{f_1} + \boldsymbol{\varphi}_{g_1}^T \boldsymbol{\theta}_{g_1}\left(z_2 + x_{2,r}\right) - \boldsymbol{\varphi}_{g_1}^T \hat{\boldsymbol{\theta}}_{g_1} x_{2,r}^0 - \boldsymbol{\varphi}_{g_1}^T \hat{\boldsymbol{\theta}}_{g_1}\chi_2 + c_1\chi_1 \right. \\
&\qquad \left. - \boldsymbol{\varphi}_{g_1}^T \hat{\boldsymbol{\theta}}_{g_1}\left(x_{2,r} - x_{2,r}^0\right)\right] - \tilde{\boldsymbol{\theta}}_{f_1}^T \Gamma_{f_1}^{-1} \dot{\hat{\boldsymbol{\theta}}}_{f_1} - \tilde{\boldsymbol{\theta}}_{g_1}^T \Gamma_{g_1}^{-1} \dot{\hat{\boldsymbol{\theta}}}_{g_1} \\
&= \bar{z}_1 \left[-c_1\left(z_1 - \chi_1\right) + \boldsymbol{\varphi}_{f_1}^T \tilde{\boldsymbol{\theta}}_{f_1} + \boldsymbol{\varphi}_{g_1}^T \tilde{\boldsymbol{\theta}}_{g_1} x_2 + \boldsymbol{\varphi}_{g_1}^T \hat{\boldsymbol{\theta}}_{g_1} \bar{z}_2\right] - \tilde{\boldsymbol{\theta}}_{f_1}^T \Gamma_{f_1}^{-1} \dot{\hat{\boldsymbol{\theta}}}_{f_1} - \tilde{\boldsymbol{\theta}}_{g_1}^T \Gamma_{g_1}^{-1} \dot{\hat{\boldsymbol{\theta}}}_{g_1} \\
&= -c_1 \bar{z}_1^2 + \bar{z}_1 \boldsymbol{\varphi}_{g_1}^T \hat{\boldsymbol{\theta}}_{g_1} \bar{z}_2 - \tilde{\boldsymbol{\theta}}_{f_1}^T \Gamma_{f_1}^{-1}\left[\dot{\hat{\boldsymbol{\theta}}}_{f_1} - \Gamma_{f_1} \boldsymbol{\varphi}_{f_1} \bar{z}_1\right] - \tilde{\boldsymbol{\theta}}_{g_1}^T \Gamma_{g_1}^{-1}\left[\dot{\hat{\boldsymbol{\theta}}}_{g_1} - \Gamma_{g_1} \boldsymbol{\varphi}_{g_1} x_2 \bar{z}_1\right] . \qquad \text{(F-50)}
\end{aligned}$$

The parameter update laws are now selected as

$$\dot{\hat{\boldsymbol{\theta}}}_{f_1} = \Gamma_{f_1} \boldsymbol{\varphi}_{f_1} \bar{z}_1 \qquad \text{(F-51a)}$$

$$\dot{\hat{\boldsymbol{\theta}}}_{g_1} = \Gamma_{g_1} \boldsymbol{\varphi}_{g_1} x_2 \bar{z}_1 , \qquad \text{(F-51b)}$$

this yields

$$\dot{\mathcal{V}}_1 = -c_1 \bar{z}_1^2 + \bar{z}_1 \boldsymbol{\varphi}_{g_1}^T \hat{\boldsymbol{\theta}}_{g_1} \bar{z}_2 . \qquad \text{(F-52)}$$

Subsystem i, i = 2, ..., n - 1

Now we consider the i-th subsystem:

$$\dot{x}_i = \boldsymbol{\varphi}_{f_i}(\boldsymbol{x})^T \boldsymbol{\theta}_{f_i} + \boldsymbol{\varphi}_{g_i}(\boldsymbol{x})^T \boldsymbol{\theta}_{g_i} x_{i+1} , \quad i = 2, \ldots, n-1 . \qquad \text{(F-53)}$$

We regard state x_{i+1} as the control input for the i-th subsystem. However, because x_{i+1} is just a state variable and not the real control input u, we call x_{i+1} the *virtual control.*

Now we introduce the tracking errors:

$$z_i = x_i - x_{i,r} , \quad i = 3, \ldots, n , \qquad \text{(F-54)}$$

where $x_{i,r}$ are the new virtual control laws to be designed. As with TFABS, the stabilizing control laws are defined as

$$\alpha_i = \frac{1}{\boldsymbol{\varphi}_{g_i}^T \hat{\boldsymbol{\theta}}_{g_i}}\left[-c_i z_i - \boldsymbol{\varphi}_{g_{i-1}}^T \hat{\boldsymbol{\theta}}_{g_{i-1}} \bar{z}_{i-1} - \boldsymbol{\varphi}_{f_i}^T \hat{\boldsymbol{\theta}}_{f_i} + \dot{x}_{i,r}\right] , \quad i = 2, \ldots, n-1 . \qquad \text{(F-55)}$$

Note that the variables λ_{i-1} and z_{i-1} in Eq. (C-21) have been replaced by respectively $\dot{x}_{i,r}$ and $\bar{z}_{i-1}$ because of the new definitions of the tracking error.

However, instead of directly applying this virtual control, new signals $x_{i,r}^0$ are defined by

$$x_{i,r}^0 = \alpha_{i-1} - \chi_i \,, \quad i = 3, \dots, n \,, \tag{F-56}$$

where χ_i will be defined later on. The raw signals $x_{i,r}^0$ are led through command filters to obtain $x_{i,r}$ and their time derivative $\dot{x}_{i,r}$. The effect that the use of these command filters have on the tracking error z_i is estimated by the stable linear filters:

$$\dot{\chi}_i = -c_i \chi_i + \boldsymbol{\varphi}_{g_i}^T \hat{\boldsymbol{\theta}}_{g_i} \left(x_{i+1,r} - x_{i+1,r}^0 \right) \,, \quad i = 2, \dots, n-1 \,, \tag{F-57}$$

with $\chi_i(0) = 0$. These auxiliary systems compensate for the constraint effects due to magnitude, rate and bandwidth limitations of the command filter. Now we introduce the *compensated* tracking errors:

$$\bar{z}_i = z_i - \chi_i, \quad i = 3, \dots, n \,. \tag{F-58}$$

The $\bar{z}_i$-dynamics are given by

$$\begin{aligned}
\dot{\bar{z}}_i &= \dot{z}_i - \dot{\chi}_i, \quad i = 2, \dots, n-1 \\
&= \dot{x}_i - \dot{x}_{i,r} - \dot{\chi}_i \\
&= \boldsymbol{\varphi}_{f_i}^T \boldsymbol{\theta}_{f_i} + \boldsymbol{\varphi}_{g_i}^T \boldsymbol{\theta}_{g_i} x_{i+1} - \dot{x}_{i,r} + c_i \chi_i - \boldsymbol{\varphi}_{g_i}^T \hat{\boldsymbol{\theta}}_{g_i} \left(x_{i+1,r} - x_{i+1,r}^0 \right) \\
&= \boldsymbol{\varphi}_{f_i}^T \boldsymbol{\theta}_{f_i} + \boldsymbol{\varphi}_{g_i}^T \boldsymbol{\theta}_{g_i} \left(z_{i+1} + x_{i+1,r} \right) - \dot{x}_{i,r} + c_i \chi_i - \boldsymbol{\varphi}_{g_i}^T \hat{\boldsymbol{\theta}}_{g_i} \left(x_{i+1,r} - x_{i+1,r}^0 \right) \,.
\end{aligned} \tag{F-59}$$

Augmenting the scalar CLF $\mathcal{V}_1$:

$$\begin{aligned}
\mathcal{V}_i(\bar{\boldsymbol{z}}_i, \tilde{\boldsymbol{\theta}}_{\star_i}) &= \frac{1}{2} \sum_{j=1}^{i} \left[\bar{z}_j^2 + \frac{1}{2} \tilde{\boldsymbol{\theta}}_{f_j}^T \Gamma_{f_j}^{-1} \tilde{\boldsymbol{\theta}}_{f_j} + \frac{1}{2} \tilde{\boldsymbol{\theta}}_{g_j}^T \Gamma_{g_j}^{-1} \tilde{\boldsymbol{\theta}}_{g_j} \right], \quad i = 2, \dots, n-1 \\
&= \frac{1}{2} \bar{z}_1^2 + \frac{1}{2} \tilde{\boldsymbol{\theta}}_{f_1}^T \Gamma_{f_1}^{-1} \tilde{\boldsymbol{\theta}}_{f_1} + \frac{1}{2} \tilde{\boldsymbol{\theta}}_{g_1}^T \Gamma_{g_1}^{-1} \tilde{\boldsymbol{\theta}}_{g_1} + \frac{1}{2} \sum_{j=2}^{i} \left[\bar{z}_j^2 + \frac{1}{2} \tilde{\boldsymbol{\theta}}_{f_j}^T \Gamma_{f_j}^{-1} \tilde{\boldsymbol{\theta}}_{f_j} + \frac{1}{2} \tilde{\boldsymbol{\theta}}_{g_j}^T \Gamma_{g_j}^{-1} \tilde{\boldsymbol{\theta}}_{g_j} \right] \\
&= \mathcal{V}_1(\bar{z}_1) + \frac{1}{2} \sum_{j=2}^{i} \left[\bar{z}_j^2 + \frac{1}{2} \tilde{\boldsymbol{\theta}}_{f_j}^T \Gamma_{f_j}^{-1} \tilde{\boldsymbol{\theta}}_{f_j} + \frac{1}{2} \tilde{\boldsymbol{\theta}}_{g_j}^T \Gamma_{g_j}^{-1} \tilde{\boldsymbol{\theta}}_{g_j} \right] \,.
\end{aligned} \tag{F-60}$$

where $\bar{\boldsymbol{z}}_i = [\bar{z}_1, \cdots, \bar{z}_i]^T$ and $\tilde{\boldsymbol{\theta}}_{\star_i} = [\tilde{\boldsymbol{\theta}}_{f_1}, \cdots, \tilde{\boldsymbol{\theta}}_{f_i}, \tilde{\boldsymbol{\theta}}_{g_1}, \cdots, \tilde{\boldsymbol{\theta}}_{g_i}]^T$. Taking the time derivative of the CLF along the trajectories of Eqs. (F-42), (F-48) and (F-59) results in

$$
\begin{aligned}
\dot{\mathcal{V}}_i &= \dot{\mathcal{V}}_1 + \sum_{j=2}^{i} \bar{z}_j \left[\boldsymbol{\varphi}_{f_j}^T \boldsymbol{\theta}_{f_j} + \boldsymbol{\varphi}_{g_j}^T \boldsymbol{\theta}_{g_j} \left(z_{j+1} + x_{j+1,r}\right) - \dot{x}_{j,r} + c_j \chi_j - \varphi_{g_j}^T \hat{\boldsymbol{\theta}}_{g_j} \left(x_{j+1,r} - x_{j+1,r}^0\right) \right] \\
&\quad - \sum_{j=2}^{i} \left[\tilde{\boldsymbol{\theta}}_{f_j}^T \Gamma_{f_j}^{-1} \dot{\hat{\boldsymbol{\theta}}}_{f_j} + \tilde{\boldsymbol{\theta}}_{g_j}^T \Gamma_{g_j}^{-1} \dot{\hat{\boldsymbol{\theta}}}_{g_j} \right] \\
&= -c_1 \bar{z}_1^2 + \bar{z}_1 \varphi_{g_1}^T \hat{\boldsymbol{\theta}}_{g_1} \bar{z}_2 - \sum_{j=2}^{i} \left[\tilde{\boldsymbol{\theta}}_{f_j}^T \Gamma_{f_j}^{-1} \dot{\hat{\boldsymbol{\theta}}}_{f_j} + \tilde{\boldsymbol{\theta}}_{g_j}^T \Gamma_{g_j}^{-1} \dot{\hat{\boldsymbol{\theta}}}_{g_j} \right] \\
&\quad + \sum_{j=2}^{i} \bar{z}_j \left[\boldsymbol{\varphi}_{f_j}^T \boldsymbol{\theta}_{f_j} + \boldsymbol{\varphi}_{g_j}^T \boldsymbol{\theta}_{g_j} \left(z_{j+1} + x_{j+1,r}\right) - \dot{x}_{j,r} + c_j \chi_j - \varphi_{g_j}^T \hat{\boldsymbol{\theta}}_{g_j} \left(x_{j+1,r} - x_{j+1,r}^0\right) \right] \\
&= -c_1 \bar{z}_1^2 + \bar{z}_1 \varphi_{g_1}^T \hat{\boldsymbol{\theta}}_{g_1} \bar{z}_2 - \sum_{j=2}^{i} \left[\tilde{\boldsymbol{\theta}}_{f_j}^T \Gamma_{f_j}^{-1} \dot{\hat{\boldsymbol{\theta}}}_{f_j} + \tilde{\boldsymbol{\theta}}_{g_j}^T \Gamma_{g_j}^{-1} \dot{\hat{\boldsymbol{\theta}}}_{g_j} \right] \\
&\quad + \sum_{j=2}^{i} \bar{z}_j \left[\boldsymbol{\varphi}_{f_j}^T \boldsymbol{\theta}_{f_j} + \boldsymbol{\varphi}_{g_j}^T \boldsymbol{\theta}_{g_j} \left(z_{j+1} + x_{j+1,r}\right) - \varphi_{g_j}^T \hat{\boldsymbol{\theta}}_{g_j} x_{j+1,r}^0 + \varphi_{g_j}^T \hat{\boldsymbol{\theta}}_{g_j} \left(\alpha_j - \chi_{j+1}\right) \right. \\
&\qquad\qquad \left. - \dot{x}_{j,r} + c_1 \chi_1 - \varphi_{g_j}^T \hat{\boldsymbol{\theta}}_{g_j} \left(x_{j+1,r} - x_{j+1,r}^0\right) \right] \\
&= -c_1 \bar{z}_1^2 + \bar{z}_1 \varphi_{g_1}^T \hat{\boldsymbol{\theta}}_{g_1} \bar{z}_2 - \sum_{j=2}^{i} \left[\tilde{\boldsymbol{\theta}}_{f_j}^T \Gamma_{f_j}^{-1} \dot{\hat{\boldsymbol{\theta}}}_{f_j} + \tilde{\boldsymbol{\theta}}_{g_j}^T \Gamma_{g_j}^{-1} \dot{\hat{\boldsymbol{\theta}}}_{g_j} \right] \\
&\quad + \sum_{j=2}^{i} \bar{z}_j \left[-c_j z_j - \boldsymbol{\varphi}_{g_{j-1}}^T \hat{\boldsymbol{\theta}}_{g_{j-1}} \bar{z}_{j-1} + \boldsymbol{\varphi}_{f_j}^T \tilde{\boldsymbol{\theta}}_{f_j} + \boldsymbol{\varphi}_{g_j}^T \boldsymbol{\theta}_{g_j} \left(z_{j+1} + x_{j+1,r}\right) - \varphi_{g_j}^T \hat{\boldsymbol{\theta}}_{g_j} x_{j+1,r}^0 \right. \\
&\qquad\qquad \left. - \varphi_{g_j}^T \hat{\boldsymbol{\theta}}_{g_j} \chi_{j+1} + c_j \chi_j - \varphi_{g_j}^T \hat{\boldsymbol{\theta}}_{g_j} \left(x_{j+1,r} - x_{j+1,r}^0\right) \right] \\
&= -c_1 \bar{z}_1^2 + \bar{z}_1 \varphi_{g_1}^T \hat{\boldsymbol{\theta}}_{g_1} \bar{z}_2 - \sum_{j=2}^{i} \left[\tilde{\boldsymbol{\theta}}_{f_j}^T \Gamma_{f_j}^{-1} \dot{\hat{\boldsymbol{\theta}}}_{f_j} + \tilde{\boldsymbol{\theta}}_{g_j}^T \Gamma_{g_j}^{-1} \dot{\hat{\boldsymbol{\theta}}}_{g_j} \right] \\
&\quad + \sum_{j=2}^{i} \bar{z}_j \left[-c_j \left(z_j - \chi_j\right) - \boldsymbol{\varphi}_{g_{j-1}}^T \hat{\boldsymbol{\theta}}_{g_{j-1}} \bar{z}_{j-1} + \boldsymbol{\varphi}_{f_j}^T \tilde{\boldsymbol{\theta}}_{f_j} + \boldsymbol{\varphi}_{g_j}^T \tilde{\boldsymbol{\theta}}_{g_j} x_{j+1} + \varphi_{g_j}^T \hat{\boldsymbol{\theta}}_{g_j} \bar{z}_{j+1} \right] \\
&= -\sum_{j=1}^{i} c_j \bar{z}_j^2 + \bar{z}_i \varphi_{g_i}^T \hat{\boldsymbol{\theta}}_{g_i} \bar{z}_{i+1} - \sum_{j=2}^{i} \tilde{\boldsymbol{\theta}}_{f_j}^T \Gamma_{f_j}^{-1} \left[\dot{\hat{\boldsymbol{\theta}}}_{f_j} - \Gamma_{f_j} \boldsymbol{\varphi}_{f_j} \bar{z}_j \right] \\
&\quad - \sum_{j=2}^{i} \tilde{\boldsymbol{\theta}}_{g_j}^T \Gamma_{g_j}^{-1} \left[\dot{\hat{\boldsymbol{\theta}}}_{g_j} - \Gamma_{g_j} \boldsymbol{\varphi}_{g_j} x_{j+1} \bar{z}_j \right] .
\end{aligned}
\tag{F-61}
$$

The parameter update laws are now selected as

$$
\dot{\hat{\boldsymbol{\theta}}}_{f_j} = \Gamma_{f_j} \boldsymbol{\varphi}_{f_j} \bar{z}_j \tag{F-62a}
$$

$$
\dot{\hat{\boldsymbol{\theta}}}_{g_j} = \Gamma_{g_j} \boldsymbol{\varphi}_{g_j} x_{j+1} \bar{z}_j , \tag{F-62b}
$$

this yields

$$\dot{\mathcal{V}}_i = -\sum_{j=1}^{i} c_j \bar{z}_j^2 + \bar{z}_i \varphi_{g_i}^T \hat{\boldsymbol{\theta}}_{g_i} \bar{z}_{i+1} \,. \tag{F-63}$$

Subsystem n

Now we consider the final subsystem:

$$\dot{x}_n = \boldsymbol{\varphi}_{f_n}(\boldsymbol{x})^T \boldsymbol{\theta}_{f_n} + \boldsymbol{\varphi}_{g_n}(\boldsymbol{x})^T \boldsymbol{\theta}_{g_n} u \,. \tag{F-64}$$

The raw signal u^0 is led through a command filter to obtain u. The effect that the use of this command filter has on the tracking error z_n is estimated by the stable linear filter:

$$\dot{\chi}_n = -c_n \chi_n + \boldsymbol{\varphi}_{g_n}^T \hat{\boldsymbol{\theta}}_{g_n} \left(u - u^0\right) \,, \tag{F-65}$$

with $\chi_n(0) = 0$. The $\bar{z}_n$-dynamics are given by

$$\begin{aligned} \dot{\bar{z}}_n &= \dot{z}_n - \dot{\chi}_n \\ &= \dot{x}_n - \dot{x}_{n,r} - \dot{\chi}_n \\ &= \boldsymbol{\varphi}_{f_n}^T \boldsymbol{\theta}_{f_n} + \boldsymbol{\varphi}_{g_n}^T \boldsymbol{\theta}_{g_n} u - \dot{x}_{n,r} + c_n \chi_n - \boldsymbol{\varphi}_{g_n}^T \hat{\boldsymbol{\theta}}_{g_n} \left(u - u^0\right) \,. \end{aligned} \tag{F-66}$$

The final Lyapunov function is now defined as

$$\begin{aligned} \mathcal{V}_n(\bar{\boldsymbol{z}}_n, \tilde{\boldsymbol{\theta}}_{\star_n}) &= \frac{1}{2} \sum_{j=1}^{n} \left[\bar{z}_j^2 + \frac{1}{2} \tilde{\boldsymbol{\theta}}_{f_j}^T \Gamma_{f_j}^{-1} \tilde{\boldsymbol{\theta}}_{f_j} + \frac{1}{2} \tilde{\boldsymbol{\theta}}_{g_j}^T \Gamma_{g_j}^{-1} \tilde{\boldsymbol{\theta}}_{g_j} \right] \\ &= \mathcal{V}_{n-1}(\bar{\boldsymbol{z}}_{n-1}) + \frac{1}{2} \bar{z}_n^2 + \frac{1}{2} \tilde{\boldsymbol{\theta}}_{f_n}^T \Gamma_{f_n}^{-1} \tilde{\boldsymbol{\theta}}_{f_n} + \frac{1}{2} \tilde{\boldsymbol{\theta}}_{g_n}^T \Gamma_{g_n}^{-1} \tilde{\boldsymbol{\theta}}_{g_n} \,. \end{aligned} \tag{F-67}$$

Taking the time derivative of the CLF along the trajectories of Eqs. (F-42), (F-48), (F-59) and (F-66) results in

$$\begin{aligned} \dot{\mathcal{V}}_n &= \dot{\mathcal{V}}_{n-1} + \bar{z}_n \left[\boldsymbol{\varphi}_{f_n}^T \boldsymbol{\theta}_{f_n} + \boldsymbol{\varphi}_{g_n}^T \boldsymbol{\theta}_{g_n} u - \dot{x}_{n,r} + c_n \chi_n - \boldsymbol{\varphi}_{g_n}^T \hat{\boldsymbol{\theta}}_{g_n} \left(u - u^0\right) \right] \\ &\quad - \tilde{\boldsymbol{\theta}}_{f_n}^T \Gamma_{f_n}^{-1} \dot{\hat{\boldsymbol{\theta}}}_{f_n} - \tilde{\boldsymbol{\theta}}_{g_n}^T \Gamma_{g_n}^{-1} \dot{\hat{\boldsymbol{\theta}}}_{g_n} \\ &= -\sum_{j=1}^{n-1} c_j \bar{z}_j^2 + \bar{z}_{n-1} \varphi_{g_{n-1}}^T \hat{\boldsymbol{\theta}}_{g_{n-1}} \bar{z}_n - \tilde{\boldsymbol{\theta}}_{f_n}^T \Gamma_{f_n}^{-1} \dot{\hat{\boldsymbol{\theta}}}_{f_n} - \tilde{\boldsymbol{\theta}}_{g_n}^T \Gamma_{g_n}^{-1} \dot{\hat{\boldsymbol{\theta}}}_{g_n} \\ &\quad + \bar{z}_n \left[\boldsymbol{\varphi}_{f_n}^T \boldsymbol{\theta}_{f_n} + \boldsymbol{\varphi}_{g_n}^T \hat{\boldsymbol{\theta}}_{g_n} u^0 - \dot{x}_{n,r} + c_n \chi_n + \boldsymbol{\varphi}_{g_n}^T \tilde{\boldsymbol{\theta}}_{g_n} u \right] \,. \end{aligned} \tag{F-68}$$

Now we select the following control law

$$u^0 = \frac{1}{\boldsymbol{\varphi}_{g_n}^T \hat{\boldsymbol{\theta}}_{g_n}} \left[-c_n z_n - \boldsymbol{\varphi}_{g_{n-1}}^T \hat{\boldsymbol{\theta}}_{g_{n-1}} \bar{z}_{n-1} - \boldsymbol{\varphi}_{f_n}^T \hat{\boldsymbol{\theta}}_{f_n} + \dot{x}_{n,r} \right] \,, \tag{F-69}$$

this yields

$$\begin{aligned}
\dot{\mathcal{V}}_n = & -\sum_{j=1}^{n-1} c_j \bar{z}_j^2 + \bar{z}_{n-1}\varphi_{g_{n-1}}^T \hat{\boldsymbol{\theta}}_{g_{n-1}} \bar{z}_n - \tilde{\boldsymbol{\theta}}_{f_n}^T \Gamma_{f_n}^{-1} \dot{\hat{\boldsymbol{\theta}}}_{f_n} - \tilde{\boldsymbol{\theta}}_{g_n}^T \Gamma_{g_n}^{-1} \dot{\hat{\boldsymbol{\theta}}}_{g_n} \\
& + \bar{z}_n \left[-c_n z_n - \boldsymbol{\varphi}_{g_{n-1}}^T \hat{\boldsymbol{\theta}}_{g_{n-1}} \bar{z}_{n-1} + \boldsymbol{\varphi}_{f_n}^T \tilde{\boldsymbol{\theta}}_{f_n} + \boldsymbol{\varphi}_{g_n}^T \tilde{\boldsymbol{\theta}}_{g_n} u + c_n \chi_n \right] \\
= & -\sum_{j=1}^{n-1} c_j \bar{z}_j^2 - \tilde{\boldsymbol{\theta}}_{f_n}^T \Gamma_{f_n}^{-1} \dot{\hat{\boldsymbol{\theta}}}_{f_n} - \tilde{\boldsymbol{\theta}}_{g_n}^T \Gamma_{g_n}^{-1} \dot{\hat{\boldsymbol{\theta}}}_{g_n} + \bar{z}_n \left[-c_n (z_n - \chi_n) + \boldsymbol{\varphi}_{f_n}^T \tilde{\boldsymbol{\theta}}_{f_n} + \boldsymbol{\varphi}_{g_n}^T \tilde{\boldsymbol{\theta}}_{g_n} u \right] \\
= & -\sum_{j=1}^{n} c_j \bar{z}_j^2 - \tilde{\boldsymbol{\theta}}_{f_n}^T \Gamma_{f_n}^{-1} \left[\dot{\hat{\boldsymbol{\theta}}}_{f_n} - \Gamma_{f_n} \boldsymbol{\varphi}_{f_n} \bar{z}_n \right] - \tilde{\boldsymbol{\theta}}_{g_n}^T \Gamma_{g_n}^{-1} \left[\dot{\hat{\boldsymbol{\theta}}}_{g_n} - \Gamma_{g_n} \boldsymbol{\varphi}_{g_n} u \bar{z}_n \right] . \qquad \text{(F-70)}
\end{aligned}$$

The parameter update laws are now selected as

$$\dot{\hat{\boldsymbol{\theta}}}_{f_n} = \Gamma_{f_n} \boldsymbol{\varphi}_{f_n} \bar{z}_n \qquad \text{(F-71a)}$$

$$\dot{\hat{\boldsymbol{\theta}}}_{g_n} = \Gamma_{g_n} \boldsymbol{\varphi}_{g_n} u \bar{z}_n \,, \qquad \text{(F-71b)}$$

this yields

$$\dot{\mathcal{V}}_n = -\sum_{j=1}^{n} c_j \bar{z}_j^2 \,. \qquad \text{(F-72)}$$

By the theorem of *LaSalle-Yoshizawa* (see Theorem C.2, page 71) it now follows that the equilibrium $\bar{\boldsymbol{z}} = \mathbf{0}$ is globally uniformly asymptotically stable. Note that this derivation only guarantees desirable properties for the *compensated* tracking error $\bar{\boldsymbol{z}}$ and not the *actual* tracking error $\boldsymbol{z}$. According to (Farrell et al., 2005), in the absence of physical limitations (i.e. magnitude, rate and bandwidth constraints on the commanded state $x_{2,r}$ and control u), convergence of the tracking error $\boldsymbol{z}$ is still guaranteed. When the inputs are too aggressive, the implemented limits can come into effect. During such a period $\boldsymbol{z}$ and $\boldsymbol{\chi}$ become nonzero because the desired control signals are not able to be implemented. However, the $\boldsymbol{\chi}$-signals and therefore also the tracking error $\boldsymbol{z}$ will remain bounded, because $\boldsymbol{\chi}$ is the output of a stable linear system with a bounded input. When the limits are no longer in effect, the tracking error $\boldsymbol{z}$ will converge to $\mathbf{0}$.

F-2 Simulations

In order to evaluate the TFABS approach, six simulations are performed by using the pendulum model:

1. Adaptive Backstepping with one unknown parameter;
2. Command-Filtered Adaptive Backstepping with one unknown parameter;
3. Adaptive Backstepping with one unknown time-varying parameter;
4. Adaptive Backstepping with three unknown parameters;
5. Adaptive Incremental Backstepping with Time-Scale Separation;
6. Adaptive Incremental Backstepping without Time-Scale Separation.

F-2-1 Adaptive Backstepping with one unknown parameter

In this section a Backstepping (BS) controller is augmented with a TF in order to cope with a parametric uncertainty of the pendulum model, which is for convenience repeated below:

$$\dot{x}_1 = x_2 \tag{B-3a revisited}$$
$$\dot{x}_2 = \theta_{2,1}\sin(x_1) + \theta_{2,2}x_2 + \theta_{2,3}u\,, \tag{B-3b revisited}$$

where we now assume $\theta_{2,2}$ is an unknown *constant* parameter. The control task is to track the smooth reference state $x_{1,r}$ with the state x_1. Similar as before, we start by defining the tracking errors as

$$z_1 = x_1 - x_{1,r} \tag{F-74a}$$
$$z_2 = x_2 - \alpha_1\,. \tag{F-74b}$$

The derivations for subsystem x_1 remain exactly the same as in Appendix C-3 (see Eqs. (C-32) to (C-36)), because this subsystem is assumed to be fully known. Therefore we directly move on to the second and final subsystem. Now we introduce the parameter estimation error $\tilde{\theta}_{2,2}$:

$$\tilde{\theta}_{2,2} = \theta_{2,2} - \hat{\theta}_{2,2} \quad \rightarrow \quad \dot{\tilde{\theta}}_{2,2} = -\dot{\hat{\theta}}_{2,2}\,, \tag{F-75}$$

where $\hat{\theta}_{2,2}$ is the estimate of $\theta_{2,2}$. Now we can rewrite the dynamics of the second error state as follows:

$$\dot{z}_2 = \theta_{2,1}\sin(x_1) + \left(\tilde{\theta}_{2,2} + \hat{\theta}_{2,2}\right)x_2 + \theta_{2,3}u - \dot{\alpha}_1\,. \tag{F-76}$$

The earlier formulated Lyapunov function $\mathcal{V}_1$ is now augmented to penalize the second tracking error and the parameter estimation error as well:

$$\mathcal{V}(\boldsymbol{z}, \tilde{\theta}_{2,2}) = \frac{1}{2}z_1^2 + \frac{1}{2}z_2^2 + \frac{1}{2\gamma_2}\tilde{\theta}_{2,2}^2\,, \tag{F-77}$$

where $\gamma_2 > 0$ is the adaptation gain. Taking the time derivative of $\mathcal{V}$ along the trajectories of the error dynamics and Eq. (F-75) results in

$$\begin{aligned}\dot{\mathcal{V}} &= -c_1z_1^2 + z_1z_2 + z_2\left[\theta_{2,1}\sin(x_1) + \left(\tilde{\theta}_{2,2} + \hat{\theta}_{2,2}\right)x_2 + \theta_{2,3}u - \dot{\alpha}_1\right] - \frac{1}{\gamma_2}\tilde{\theta}_{2,2}\dot{\hat{\theta}}_{2,2}\\ &= -c_1z_1^2 + z_1z_2 + z_2\left[\theta_{2,1}\sin(x_1) + \hat{\theta}_{2,2}x_2 + \theta_{2,3}u - \dot{\alpha}_1\right] - \frac{1}{\gamma_2}\tilde{\theta}_{2,2}\left(\dot{\hat{\theta}}_{2,2} - \gamma_2z_2x_2\right)\,.\end{aligned} \tag{F-78}$$

Now we introduce the following real control u:

$$u = \frac{1}{\theta_{2,3}}\left[-c_2z_2 - z_1 - \theta_{2,1}\sin(x_1) - \hat{\theta}_{2,2}x_2 + \dot{\alpha}_1\right]\,, \tag{F-79}$$

which reduces $\dot{\mathcal{V}}$ to

$$\dot{\mathcal{V}} = -c_1z_1^2 - c_2z_2^2 - \frac{1}{\gamma_{2,2}}\tilde{\theta}_{2,2}\left(\dot{\hat{\theta}}_{2,2} - \gamma_2z_2x_2\right)\,. \tag{F-80}$$

By selecting the following update law:

$$\dot{\hat{\theta}}_{2,2} = \gamma_2 z_2 x_2 \,, \tag{F-81}$$

we render $\dot{\mathcal{V}}$ negative definite:

$$\dot{\mathcal{V}} = -c_1 z_1^2 - c_2 z_2^2 \,. \tag{F-82}$$

By Theorem C.2 it now follows that

$$\lim_{t\to\infty} z_1 = 0 \to \lim_{t\to\infty} [x_1 - x_{1,r}] = 0 \tag{F-83a}$$

$$\lim_{t\to\infty} z_2 = 0 \,. \tag{F-83b}$$

Note that the parameter estimation error is completely canceled in Eq. (F-80) by selecting the parameter update law as (F-81), therefore we cannot guarantee that the parameter estimate $\hat{\theta}_{2,2}$ actually converges to the real parameter $\theta_{2,2}$. All we can conclude from Eqs. (F-77) and (F-82) with respect to the parameter estimation error $\tilde{\theta}_{2,2}$ is that it is bounded. In (Krstić, 1996) it is proven that convergence of the parameter estimate to a constant value is always achieved. In case of Persistent Excitation (PE), the parameter estimate converges to the actual parameter value. The requirement of PE basically means that the reference signal must be "rich enough", i.e. "contain enough frequencies" for the parameter estimation error to converge to zero (Boyd & Sastry, 1986).

Simulations of the TFABS controller have been run for the system (B-3) with one unknown parameter and a sampling time of 0.01 s. The initial conditions and parameters which have been used in this simulation for the model can be found in Eq. (C-44). The following control and estimator parameters have been selected:

$$\begin{aligned} c_1 &= 10\,, & c_2 &= 10\,, \\ \hat{\theta}_{2,1} &= \theta_{2,1}\,, & \hat{\theta}_{2,2}(0) &= -50 \cdot \theta_{2,2}\,, \\ \hat{\theta}_{2,3} &= \theta_{2,3}\,. \end{aligned} \tag{F-84}$$

Different values of the adaptation gain γ_2 have been selected. From Figure F-1 we can clearly see that the TFABS controller performs much better compared to the conventional BS controller (C-39) in presence of the introduced parametric uncertainty. From Figure F-2 we can see that the parameter estimates for the different values of γ_2 seem to converge to the real parameter. Increasing the adaptation gain γ_2 results in faster convergence of the parameter estimate. However, if we keep increasing γ_2, the overshoot of the parameter estimate becomes significant which might results in an undesired transient response of the closed-loop system.

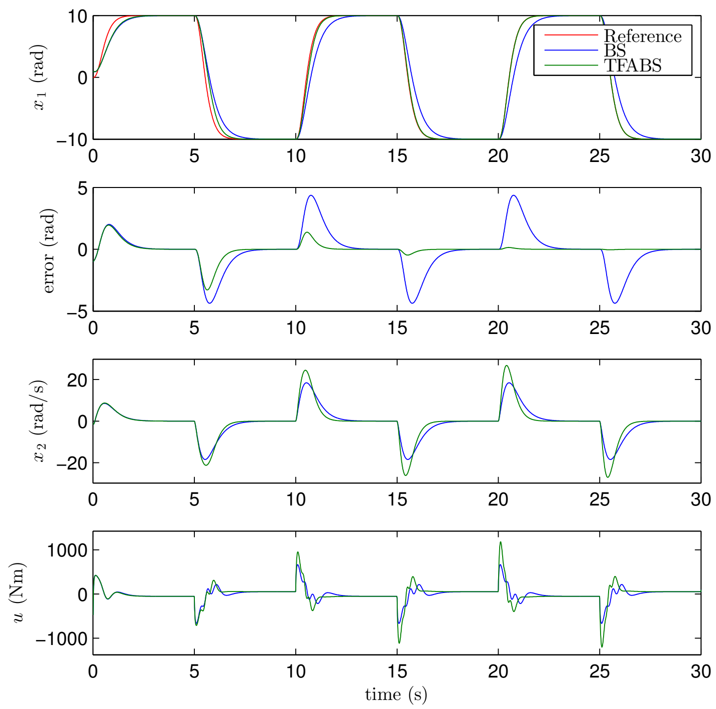

Figure F-1: The control performance of the Tuning Functions Adaptive Backstepping controller with $\gamma_2 = 0.03$ in the presence of a parametric uncertainty.

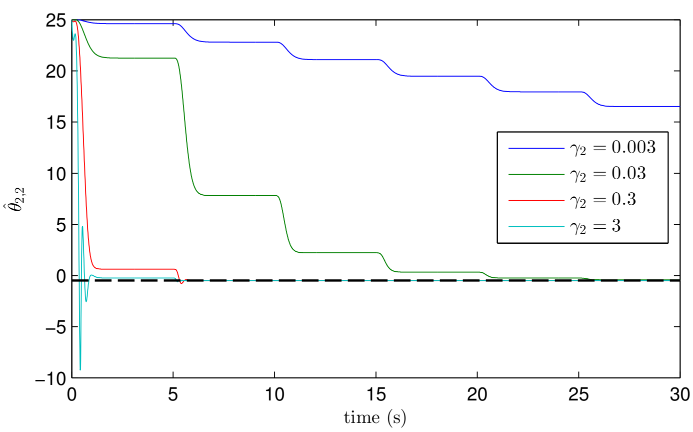

Figure F-2: The performance of the Tuning Function estimator for different values of γ_2. The dashed black line represents the value of the real parameter $\theta_{2,2}$.

Now we introduce a magnitude limit for the control u of $\pm 850\,\mathrm{Nm}$ to find out how the TFABS controller performs in case of such a constraint. The results can be found in Figures F-3 and F-4. As can be seen, the TFABS control law still performs better compared to the conventional BS controller in case of the introduced parametric uncertainty and the magnitude limit for the control. However, the introduction of the magnitude limit considerably decreases the performance of the TF estimator. The reason for this is that the adaptation is driven by the tracking error z_2 (see Eq. (F-81)), which is now no longer due to the parameter estimation error exclusively. Therefore, as soon as the input is saturated the estimator starts to “unlearn”, resulting in less accurate tracking of the reference signal.

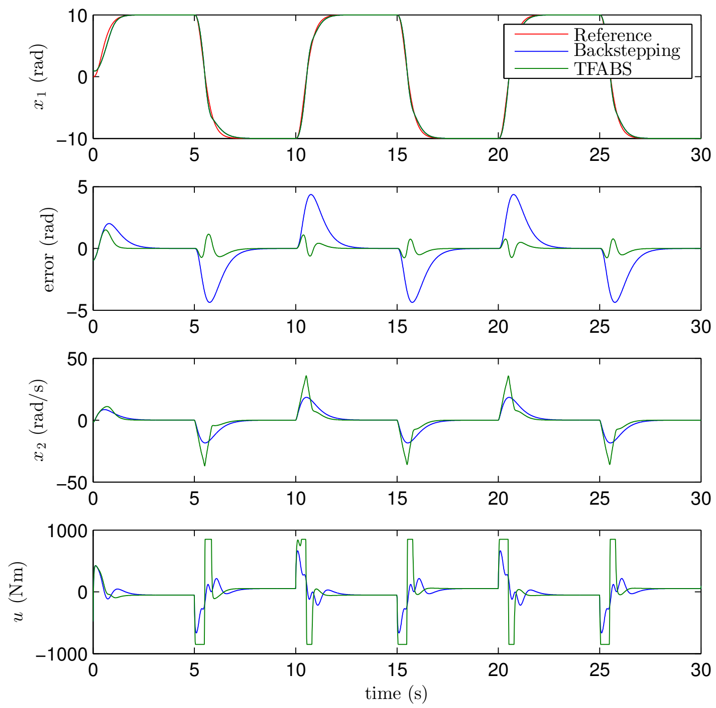

Figure F-3: The control performance of the Tuning Functions Adaptive Backstepping controller with $\gamma_2 = 0.3$ in the presence of a parametric uncertainty. The control u has been magnitude limited to $\pm 850\,\mathrm{Nm}$.

Note that if a priori knowledge is available in terms of a lower and/or upper bound on the value of the unknown parameter, a projection method may be adopted to possibly improve the robustness and closed-loop transient response (Akella & Subbarao, 2005). In this example, a projection method could have forced the parameter estimate of $\theta_{2,2} = -k/m$ to be negative at all time instances. This technique is not further discussed in this report, but more information can be found in the literature (Krstić et al., 1995; Timmons, Chizeck, Casas, Chankong, & Katona, 1997; Akella & Subbarao, 2005).

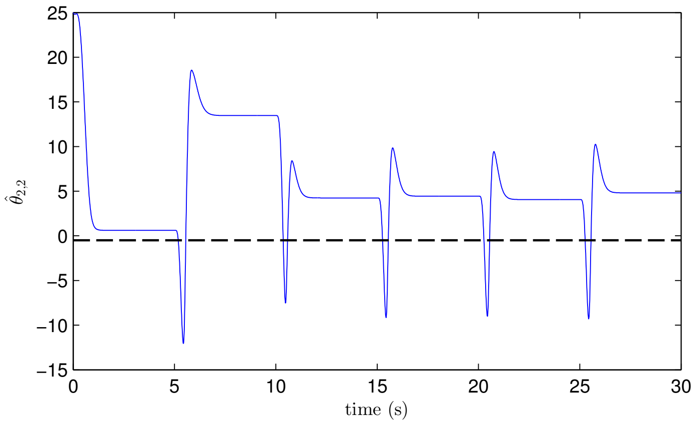

Figure F-4: The performance of the Tuning Function estimator with $\gamma_2 = 0.3$. The control u has been magnitude limited to $\pm 850\,\mathrm{Nm}$. The dashed black line represents the value of the real parameter $\theta_{2,2}$.

F-2-2 Command-Filtered Adaptive Backstepping with one unknown parameter

In the last section we saw that the TF estimator does not work satisfactory when the control input is saturated. Therefore we now augment the TFABS controller with command filters in order to simultaneously cope with parametric uncertainties and control limitations. The pendulum model is for convenience repeated below:

$$\dot{x}_1 = x_2 \tag{B-3a revisited}$$
$$\dot{x}_2 = \theta_{2,1}\sin(x_1) + \theta_{2,2}x_2 + \theta_{2,3}u\,, \tag{B-3b revisited}$$

where we assume $\theta_{2,2}$ is an unknown *constant* parameter. The control task is to track the smooth reference state $x_{1,r}$ with the state x_1. Similar as before, we start by defining the tracking errors as

$$z_1 = x_1 - x_{1,r} \tag{F-86a}$$
$$z_2 = x_2 - x_{2,r}\,, \tag{F-86b}$$

and the *compensated* tracking errors as

$$\bar{z}_1 = z_1 - \chi_1 \tag{F-87a}$$
$$\bar{z}_2 = z_2 - \chi_2\,. \tag{F-87b}$$

The derivations for subsystem x_1 remain exactly the same as in Appendix D-3 (see Eqs. (D-35) to (D-40)), because this subsystem is assumed to be fully known. Therefore we directly move on to the second and final compensated subsystem. The $\bar{z}_2$-dynamics are given by:

$$\dot{\bar{z}}_2 = \theta_{2,1}\sin(x_1) + \theta_{2,2}x_2 + \theta_{2,3}u - \dot{x}_{2,r} - \dot{\chi}_2\,. \tag{F-88}$$

Similar as in the last section we now introduce the parameter estimation error $\tilde{\theta}_{2,2}$:

$$\tilde{\theta}_{2,2} = \theta_{2,2} - \hat{\theta}_{2,2} \rightarrow \dot{\tilde{\theta}}_{2,2} = -\dot{\hat{\theta}}_{2,2}\,, \tag{F-89}$$

where $\hat{\theta}_{2,2}$ is the parameter estimate of $\theta_{2,2}$. Now we can rewrite the $\bar{z}_2$-dynamics as

$$\dot{\bar{z}}_2 = \theta_{2,1}\sin(x_1) + \left(\tilde{\theta}_{2,2} + \hat{\theta}_{2,2}\right) x_2 + \theta_{2,3}u - \dot{x}_{2,r} - \dot{\chi}_2 \,. \tag{F-90}$$

Now we augment the quadratic CLF function to penalize the second tracking compensated error and the parameter estimation error as well:

$$\mathcal{V}\left(\bar{\boldsymbol{z}}\right) = \mathcal{V}_1 + \frac{1}{2}\bar{z}_2^2 + \frac{1}{2\gamma_2}\tilde{\theta}_{2,2}^2 \,, \tag{F-91}$$

where $\gamma_2 > 0$ is the adaptation gain. Taking the time derivative of $\mathcal{V}$ along the trajectories of the compensated error dynamics and Eq. (F-89) results in

$$\begin{aligned}\dot{\mathcal{V}} &= -c_1\bar{z}_1^2 + \bar{z}_1\bar{z}_2 + \bar{z}_2\left[\theta_{2,1}\sin(x_1) + \left(\tilde{\theta}_{2,2} + \hat{\theta}_{2,2}\right) x_2 + \theta_{2,3}u - \dot{x}_{2,r} - \dot{\chi}_2\right] - \frac{1}{\gamma_2}\tilde{\theta}_{2,2}\dot{\hat{\theta}}_{2,2} \\ &= -c_1\bar{z}_1^2 + \bar{z}_1\bar{z}_2 + \bar{z}_2\left[\theta_{2,1}\sin(x_1) + \hat{\theta}_{2,2}x_2 + \theta_{2,3}u - \dot{x}_{2,r} - \dot{\chi}_2\right] - \frac{1}{\gamma_2}\tilde{\theta}_{2,2}\left(\dot{\hat{\theta}}_{2,2} - \gamma_2\bar{z}_2x_2\right) .\end{aligned} \tag{F-92}$$

A raw control signal u^0 is led through a command filter to obtain u. The effect that the use of this command filter has on the tracking error z_2 is estimated by the stable linear filter:

$$\dot{\chi}_2 = -c_2\chi_2 + \theta_{2,3}\left(u - u^0\right) \,, \tag{F-93}$$

with $\chi_2(0) = 0$. This yields

$$\dot{\mathcal{V}} = -c_1\bar{z}_1^2 + \bar{z}_1\bar{z}_2 + \bar{z}_2\left[\theta_{2,1}\sin(x_1) + \hat{\theta}_{2,2}x_2 + \theta_{2,3}u^0 - \dot{x}_{2,r} + c_2\chi_2\right] - \frac{1}{\gamma_2}\tilde{\theta}_{2,2}\left(\dot{\hat{\theta}}_{2,2} - \gamma_2\bar{z}_2x_2\right) . \tag{F-94}$$

Selecting the raw control law and update law as

$$u^0 = \frac{1}{\theta_{2,3}}\left[-c_2z_2 - \bar{z}_1 - \theta_{2,1}\sin(x_1) - \hat{\theta}_{2,2}x_2 + \dot{x}_{2,r}\right], \quad c_2 > 0 \tag{F-95a}$$

$$\dot{\hat{\theta}}_{2,2} = \gamma_2\bar{z}_2x_2 \,, \tag{F-95b}$$

yields the CLF negative definite:

$$\begin{aligned}\dot{\mathcal{V}} &= -c_1\bar{z}_1^2 + \bar{z}_1\bar{z}_2 + \bar{z}_2\left[c_2\chi_2 - c_2z_2 - \bar{z}_1\right] \\ &= -c_1\bar{z}_1^2 + \bar{z}_1\bar{z}_2 + \bar{z}_2\left[-c_2\bar{z}_2 - \bar{z}_1\right] \\ &= -c_1\bar{z}_1^2 - c_2\bar{z}_2^2 \,.\end{aligned} \tag{F-96}$$

By Theorem C.2 it now follows that the equilibrium $\bar{\boldsymbol{z}} = \boldsymbol{0}$ is globally uniformly asymptotically stable. Note that this derivation only guarantees desirable properties for the compensated tracking error $\bar{\boldsymbol{z}}$ and not the actual tracking error $\boldsymbol{z}$. When the inputs are too aggressive, the implemented limits can come into effect. During such a period $\boldsymbol{z}$ and $\boldsymbol{\chi}$ become nonzero because the desired control signals are not able to be implemented. However, the $\boldsymbol{\chi}$-signals

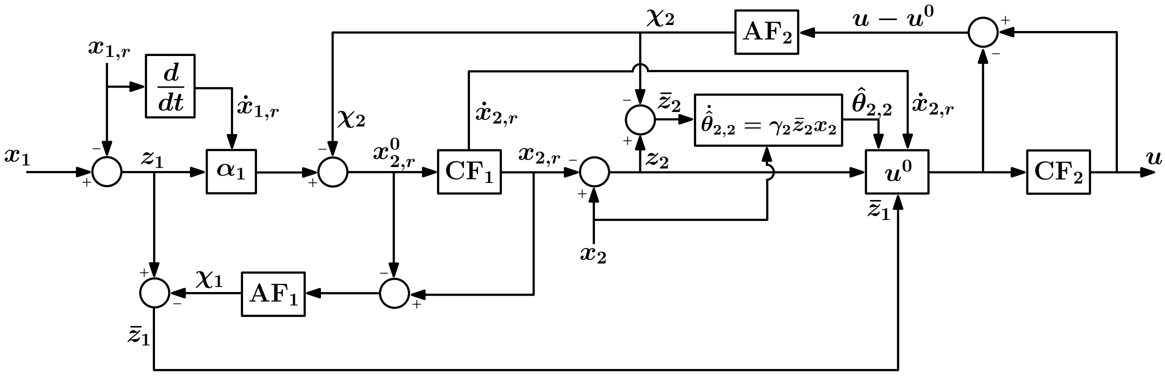

Figure F-5: Command-Filtered Tuning Functions Adaptive Backstepping controller structure.

and therefore also the tracking error $\boldsymbol{z}$ will remain bounded, because $\boldsymbol{\chi}$ is the output of a stable linear system with a bounded input. When the limits are no longer in effect, the tracking error $\boldsymbol{z}$ will converge to $\mathbf{0}$.

The controller structure developed in this section can be seen in Figure F-5. In this diagram CF represents the Command Filter (see Appendix D-2) and AF represents the Auxiliary Filter (see Eqs. (D-5) and (F-93)).

Similar as in the last section, a magnitude limit for the control input u has been introduced. The results of the simulation can be found in Figures F-6 and F-7. The variable $x_{2,r}$ is constrained to ± 40 rad/s for the TFABS (Command Filter (CF)) implementation to avoid continuous saturation of the input signal, see also the discussion in Appendix D-3-2. As can be seen, the command filters significantly increase the performance of the TFABS controller when control limitations are introduced. The reason for this is that when limits on the command filter are in effect, the real tracking errors z_i may increase, but the compensated tracking errors $\bar{z}_i$ that drive the estimation process are still unaffected (Sonneveldt, 2010). Another advantage of the TFABS (CF) implementation is that we now no longer need to analytically derive the time derivative of the stabilizing control law α_1.

F-2-3 Adaptive Backstepping with one unknown time-varying parameter

In the two previous sections we assumed that $\theta_{2,2}$ is an unknown *constant* parameter. Now a simulation has been performed in which this parameter changes halfway the simulation, in order to find out how the TF estimator performs in case of an abrupt parameter change. Simulations of the TFABS controller have been run for the system (B-3) with one unknown parameter and a sampling time of 0.01 s. The initial conditions and parameters which have been used in this simulation for the model can be found in Eq. (C-44), the control and estimator parameters are similar as in Eq. (F-84). The estimation results can be seen in Figure F-8. Clearly, the TF estimator is able to cope with the sudden parameter change.

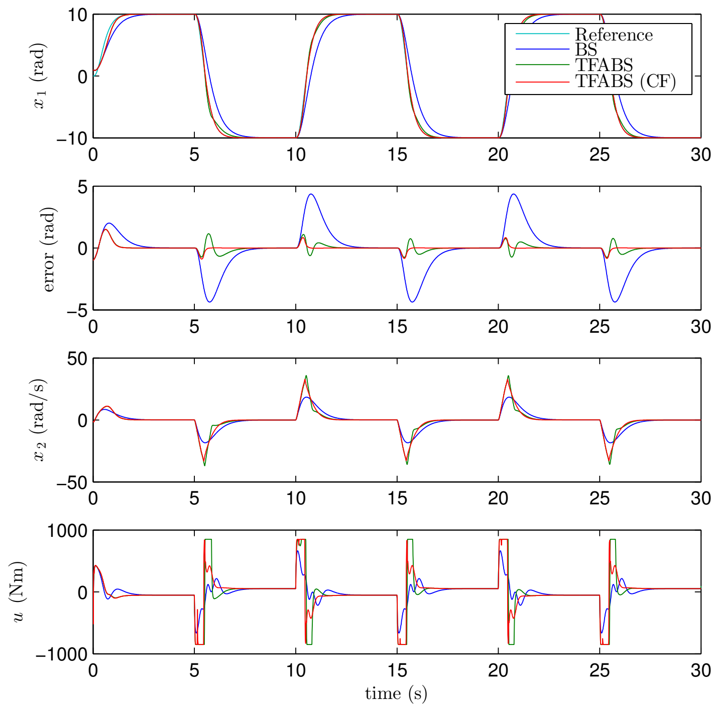

Figure F-6: The control performance of the Tuning Functions Adaptive Backstepping controller with $\gamma_2 = 0.3$ in the presence of a parametric uncertainty. The control u has been magnitude limited to $\pm 850\,\mathrm{Nm}$.

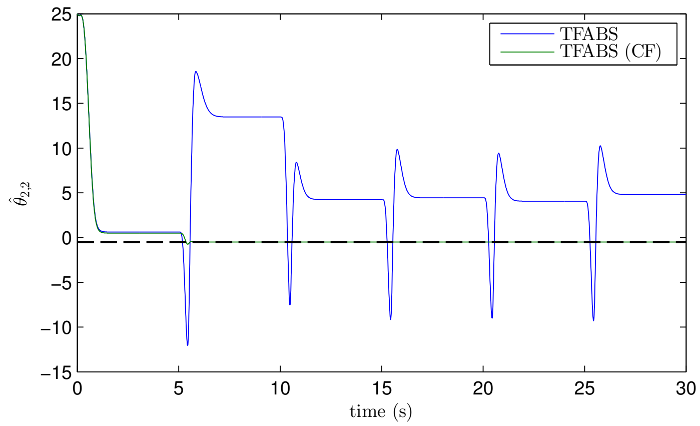

Figure F-7: The performance of the Tuning Function estimator with $\gamma_2 = 0.3$. The control u has been magnitude limited to $\pm 850\,\mathrm{Nm}$. The dashed black line represents the value of the real parameter $\theta_{2,2}$.

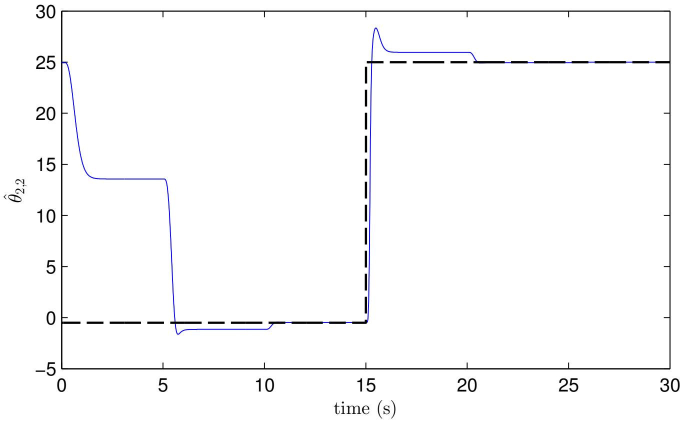

Figure F-8: The performance of the Tuning Function estimator with $\gamma_2 = 0.1$ in case of an abrupt parameter change. The dashed black line represents the value of the real parameter $\theta_{2,2}$.

Now a simulation is performed in which the uncertain parameter $\theta_{2,2}$ is a linear function of state $x_1(t)$. The simulation has been run for different values of the adaptation gain γ_2 and with $\hat{\theta}_{2,2}(0) = -1$. The initial conditions and parameters which have been used in this simulation for the model can be found in Eq. (C-44). From Figure F-9 we can see that the parameter estimator, which has been derived by assuming a *constant* unknown parameter $\theta_{2,2}$, is not able to accurately track the time-varying parameter $\theta_{2,2}(t)$. By increasing the adaptation gain, the estimator tracks the changes of parameter $\theta_{2,2}$ more accurately, however, this also leads to an undesired transient behavior. Moreover, by increasing the adaptation gain, the sensitivity to noise and actuator dynamics increases (Karagiannis & Astolfi, 2010).

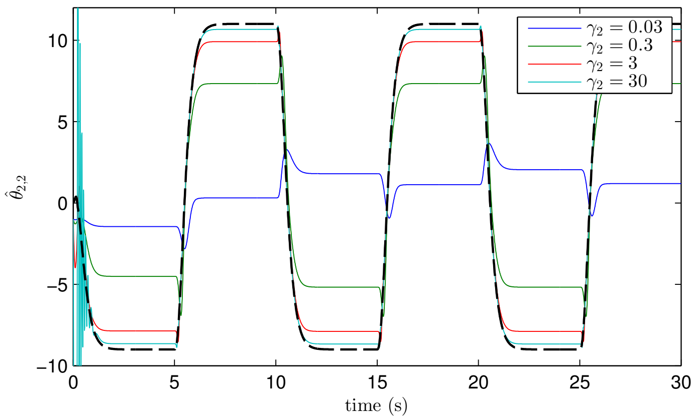

Figure F-9: The performance of the Tuning Function estimator for different values of γ_2 in case of a time-varying parameter. The dashed black line represents the real parameter $\theta_{2,2}(t)$.

A better way to estimate time-varying parameters with TF estimators is to use function approximators that are capable of approximating the (unknown) functions. If we know that $\theta_{2,2}(t)$ is a linear function of state $x_1(t)$, we may use the following function approximator:

$$\hat{\theta}_{2,2}(t) = \hat{a}x_1(t) + \hat{b}\,, \tag{F-97}$$

where $\hat{a}$ and $\hat{b}$ are now the parameter estimates. Now we introduce the parameter estimation errors:

$$\tilde{a} = a - \hat{a} \quad \rightarrow \quad \dot{\tilde{a}} = -\dot{\hat{a}} \tag{F-98a}$$

$$\tilde{b} = b - \hat{b} \quad \rightarrow \quad \dot{\tilde{b}} = -\dot{\hat{b}} \,. \tag{F-98b}$$

The z_2-dynamics are now given by

$$\dot{z}_2 = \theta_{2,1}\sin(x_1) + \underbrace{(ax_1 + b)}_{\theta_{2,2}(t)} x_2 + \theta_{2,3}u - \dot{\alpha}_1 \,. \tag{F-99}$$

The earlier formulated Lyapunov function $\mathcal{V}_1$ is now augmented to penalize the second tracking error and both parameter estimation errors as well:

$$\mathcal{V}(\boldsymbol{z}, \tilde{\theta}_{2,2}) = \frac{1}{2}z_1^2 + \frac{1}{2}z_2^2 + \frac{1}{2\gamma_{2,1}}\tilde{a}^2 + \frac{1}{2\gamma_{2,2}}\tilde{b}^2 \,, \tag{F-100}$$

where $\gamma_{2,1} > 0$ and $\gamma_{2,2} > 0$ are the adaptation gains. Taking the time derivative of $\mathcal{V}$ along the trajectories of the error dynamics and Eq. (F-98) results in

$$\begin{aligned}
\dot{\mathcal{V}} &= -c_1 z_1^2 + z_1 z_2 + z_2 \left[\theta_{2,1}\sin(x_1) + \left(\left[\tilde{a} + \hat{a}\right] x_1 + \tilde{b} + \hat{b}\right) x_2 + \theta_{2,3}u - \dot{\alpha}_1\right] \\
&\quad - \frac{1}{\gamma_{2,1}}\tilde{a}\dot{\hat{a}} - \frac{1}{\gamma_{2,2}}\tilde{b}\dot{\hat{b}} \\
&= -c_1 z_1^2 + z_1 z_2 + z_2 \left[\theta_{2,1}\sin(x_1) + \left(\hat{a}x_1 + \hat{b}\right) x_2 + \theta_{2,3}u - \dot{\alpha}_1\right] \\
&\quad - \frac{1}{\gamma_{2,1}}\tilde{a}\left(\dot{\hat{a}} - \gamma_{2,1}x_1 x_2 z_2\right) - \frac{1}{\gamma_{2,2}}\tilde{b}\left(\dot{\hat{b}} - \gamma_{2,2}x_2 z_2\right) \,.
\end{aligned} \tag{F-101}$$

By selecting real control u as (F-79) and the following update laws:

$$\dot{\hat{a}} = \gamma_{2,1}x_1 x_2 z_2 \tag{F-102a}$$

$$\dot{\hat{b}} = \gamma_{2,2}x_2 z_2 \,, \tag{F-102b}$$

we render $\dot{\mathcal{V}}$ negative definite

$$\dot{\mathcal{V}} = -c_1 z_1^2 - c_2 z_2^2 \,. \tag{F-103}$$

By Theorem C.2 it now follows that

$$\lim_{t\to\infty} z_1 = 0 \rightarrow \lim_{t\to\infty}\left[x_1 - x_{1,r}\right] = 0 \tag{F-104a}$$

$$\lim_{t\to\infty} z_2 = 0 \,. \tag{F-104b}$$

Note that the parameter estimation errors are completely canceled in Eq. (F-101) by selecting the parameter update laws as (F-102), therefore we cannot guarantee that the parameter estimates $\hat{a}$ and $\hat{b}$ actually converge to the real parameters a and b. All we can conclude from Eqs. (F-100) and (F-103) with respect to the parameter estimation errors $\tilde{a}$ and $\tilde{b}$ is that they are bounded. In (Krstić, 1996) it is proven that convergence of the parameter estimates to constant values is always achieved. In case of PE, the parameter estimates converge to the actual parameter values. The requirement of PE basically means that the reference signal must be "rich enough", i.e. "contain enough frequencies" for the parameter estimation errors to converge to zero (Boyd & Sastry, 1986).

A simulation has been run to estimate unknown time-varying parameter $\theta_{2,2}(t)$ by using function approximator (F-97) and a sampling time of 0.01 s. The initial conditions and parameters which have been used in this simulation for the model can be found in Eq. (C-44). The following control and estimator parameters have been selected:

$$\begin{aligned} c_1 &= 10\,, & c_2 &= 10\,, \\ \hat{\theta}_{2,1} &= \theta_{2,1}\,, & \hat{\theta}_{2,3} &= \theta_{2,3}\,, \\ a &= 1\,, & \hat{a}(0) &= -1\,, \\ b &= 1\,, & \hat{b}(0) &= 0\,, \\ \gamma_{2,1} &= 0.1\,, & \gamma_{2,2} &= 0.3\,. \end{aligned} \tag{F-105}$$

By comparing Figure F-10 with Figure F-9, we can clearly see that the performance of the parameter estimator significantly improves when using a function approximator that is capable of approximating the (unknown) function.

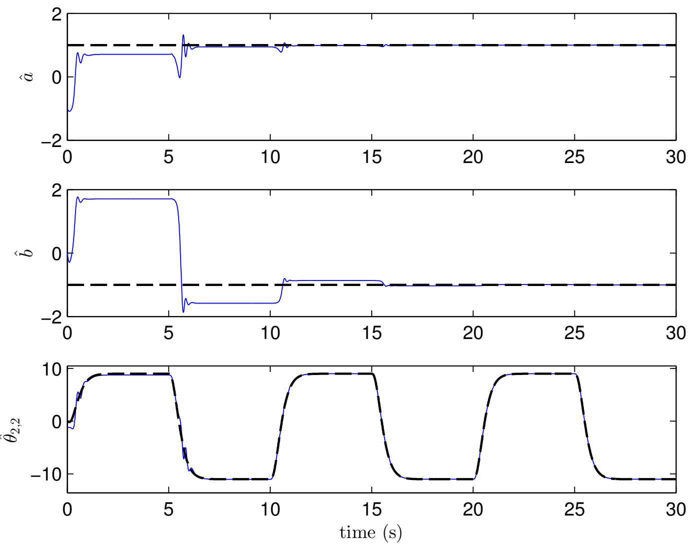

Figure F-10: The performance of the Tuning Function estimator with $\gamma_{2,1} = 0.1$ and $\gamma_{2,2} = 0.3$ in case of a time-varying parameter. The dashed black lines represent the real parameters.

F-2-4 Adaptive Backstepping with three unknown parameters

In this section a BS controller is augmented with TFs in order to cope with parametric uncertainties. The pendulum model is for convenience repeated below:

$$\dot{x}_1 = x_2 \tag{B-3a revisited}$$
$$\dot{x}_2 = \theta_{2,1}\sin(x_1) + \theta_{2,2}x_2 + \theta_{2,3}u\,, \tag{B-3b revisited}$$

where $\theta_{2,1}$, $\theta_{2,2}$ and $\theta_{2,3}$ are assumed to be unknown *constant* parameters. The control task is to track the smooth reference state $x_{1,r}$ with the state x_1. Similar as before, we start by defining the tracking errors as

$$z_1 = x_1 - x_{1,r} \tag{F-107a}$$
$$z_2 = x_2 - \alpha_1\,. \tag{F-107b}$$

The derivations for subsystem x_1 remain exactly the same as in Appendix C-3 (see Eqs. (C-32) to (C-36)), because this subsystem is assumed to be fully known. Therefore we directly move on to the second and final subsystem. Now we introduce the parameter estimation error $\tilde{\boldsymbol{\theta}}_2$:

$$\tilde{\boldsymbol{\theta}}_2 = \begin{bmatrix}\tilde{\theta}_{2,1} & \tilde{\theta}_{2,2} & \tilde{\theta}_{2,3}\end{bmatrix}^T = \boldsymbol{\theta}_2 - \hat{\boldsymbol{\theta}}_2 \rightarrow \dot{\tilde{\boldsymbol{\theta}}}_2 = -\dot{\hat{\boldsymbol{\theta}}}_2\,, \tag{F-108}$$

where $\hat{\boldsymbol{\theta}}_2$ is estimate of $\boldsymbol{\theta}_2$. Now we can rewrite the dynamics of the second error state as follows:

$$\dot{z}_2 = \left(\tilde{\theta}_{2,1} + \hat{\theta}_{2,1}\right)\sin(x_1) + \left(\tilde{\theta}_{2,2} + \hat{\theta}_{2,2}\right)x_2 + \left(\tilde{\theta}_{2,3} + \hat{\theta}_{2,3}\right)u - \dot{\alpha}_1\,. \tag{F-109}$$

The earlier formulated Lyapunov function $\mathcal{V}_1$ is now augmented to penalize the second tracking error and the parameter estimation errors as well:

$$\mathcal{V}(\boldsymbol{z}, \tilde{\boldsymbol{\theta}}_2) = \frac{1}{2}z_1^2 + \frac{1}{2}z_2^2 + \frac{1}{2\gamma_{2,1}}\tilde{\theta}_{2,1}^2 + \frac{1}{2\gamma_{2,2}}\tilde{\theta}_{2,2}^2 + \frac{1}{2\gamma_{2,3}}\tilde{\theta}_{2,3}^2\,, \tag{F-110}$$

where $\gamma_{2,i} > 0$ for $i = 1, 2, 3$ are the adaptation gains. Taking the time derivative of $\mathcal{V}$ along the trajectories of the error dynamics and Eq. (F-108) results in

$$\begin{aligned}\dot{\mathcal{V}} &= -c_1z_1^2 + z_1z_2 + z_2\left[\left(\tilde{\theta}_{2,1} + \hat{\theta}_{2,1}\right)\sin(x_1) + \left(\tilde{\theta}_{2,2} + \hat{\theta}_{2,2}\right)x_2 + \left(\tilde{\theta}_{2,3} + \hat{\theta}_{2,3}\right)u - \dot{\alpha}_1\right] \\ &\quad - \frac{1}{\gamma_{2,1}}\tilde{\theta}_{2,1}\dot{\hat{\theta}}_{2,1} - \frac{1}{\gamma_{2,2}}\tilde{\theta}_{2,2}\dot{\hat{\theta}}_{2,2} - \frac{1}{\gamma_{2,3}}\tilde{\theta}_{2,3}\dot{\hat{\theta}}_{2,3} \\ &= -c_1z_1^2 + z_1z_2 + z_2\left[\hat{\theta}_{2,1}\sin(x_1) + \hat{\theta}_{2,2}x_2 + \hat{\theta}_{2,3}u - \dot{\alpha}_1\right] \\ &\quad - \frac{1}{\gamma_{2,1}}\tilde{\theta}_{2,1}\left[\dot{\hat{\theta}}_{2,1} - \gamma_{2,1}z_2\sin(x_1)\right] - \frac{1}{\gamma_{2,2}}\tilde{\theta}_{2,2}\left[\dot{\hat{\theta}}_{2,2} - \gamma_{2,2}z_2x_2\right] - \frac{1}{\gamma_{2,3}}\tilde{\theta}_{2,3}\left[\dot{\hat{\theta}}_{2,3} - \gamma_{2,3}z_2u\right]\,.\end{aligned} \tag{F-111}$$

We introduce the following real control u:

$$u = \frac{1}{\hat{\theta}_{2,3}}\left[-c_2z_2 - z_1 - \hat{\theta}_{2,1}\sin(x_1) - \hat{\theta}_{2,2}x_2 + \dot{\alpha}_1\right]\,, \tag{F-112}$$

which reduces $\dot{\mathcal{V}}$ to:

$$\dot{\mathcal{V}} = -c_1 z_1^2 - c_2 z_2^2 - \frac{1}{\gamma_{2,1}}\tilde{\theta}_{2,1}\left[\dot{\hat{\theta}}_{2,1} - \gamma_{2,1} z_2 \sin(x_1)\right] - \frac{1}{\gamma_{2,2}}\tilde{\theta}_{2,2}\left[\dot{\hat{\theta}}_{2,2} - \gamma_{2,2} z_2 x_2\right]$$
$$-\frac{1}{\gamma_{2,3}}\tilde{\theta}_{2,3}\left[\dot{\hat{\theta}}_{2,3} - \gamma_{2,3} z_2 u\right]\,. \tag{F-113}$$

By selecting the following parameter update laws:

$$\dot{\hat{\theta}}_{2,1} = \gamma_{2,1} z_2 \sin(x_1) \tag{F-114a}$$
$$\dot{\hat{\theta}}_{2,2} = \gamma_{2,2} z_2 x_2 \tag{F-114b}$$
$$\dot{\hat{\theta}}_{2,3} = \gamma_{2,3} z_2 u\,, \tag{F-114c}$$

we render $\dot{\mathcal{V}}$ negative definite:

$$\dot{\mathcal{V}} = -c_1 z_1^2 - c_2 z_2^2\,. \tag{F-115}$$

By Theorem C.2 it now follows that:

$$\lim_{t\to\infty} z_1 = 0 \to \lim_{t\to\infty}\left[x_1 - x_{1,r}\right] = 0 \tag{F-116a}$$
$$\lim_{t\to\infty} z_2 = 0\,. \tag{F-116b}$$

Note that the parameter estimation error is completely canceled in Eq. (F-113) by selecting the parameter update laws as (F-114), therefore we cannot guarantee that the parameter estimate $\hat{\boldsymbol{\theta}}_2$ actually converges to the real parameter $\boldsymbol{\theta}_2$. All we can conclude from Eqs. (F-77) and (F-82) with respect to the parameter estimation error $\tilde{\boldsymbol{\theta}}_2$ is that it is bounded. In (Krstić, 1996) it is proven that convergence of the parameter estimate to a constant value is always achieved. In case of PE, the parameter estimate converges to the actual parameter value. The requirement of PE basically means that the reference signal must be "rich enough", i.e. "contain enough frequencies" for the parameter estimation error to converge to zero (Boyd & Sastry, 1986).

Simulations of the TFABS controller have been run for the system (B-3) with three unknown parameters and a sampling time of 0.01 s. The initial conditions and parameters which have been used in this simulation for the model can be found in Eq. (C-44). The following control and estimator parameters have been selected:

$$\begin{aligned} c_1 &= 10\,, & c_2 &= 10\,, \\ \gamma_{2,1} &= 10\,, & \hat{\theta}_{2,1} &= 20\cdot\theta_{2,1}\,, \\ \gamma_{2,2} &= 10^{-2}\,, & \hat{\theta}_{2,2} &= -20\cdot\theta_{2,2}\,, \\ \gamma_{2,3} &= 5^{-5}\,, & \hat{\theta}_{2,3} &= 5\cdot\theta_{2,3}\,. \end{aligned} \tag{F-117}$$

From Figure F-11 we can clearly see that the TFABS controller performs much better compared to the conventional BS controller (C-39) in presence of the introduced parametric uncertainties. From Figure F-12 we can see that the parameter estimation errors slowly converge to values around 0.

Similar as in the last section, we can implement command filters to cope with control limitations and to obviate the need for analytic computation of the virtual control derivative.

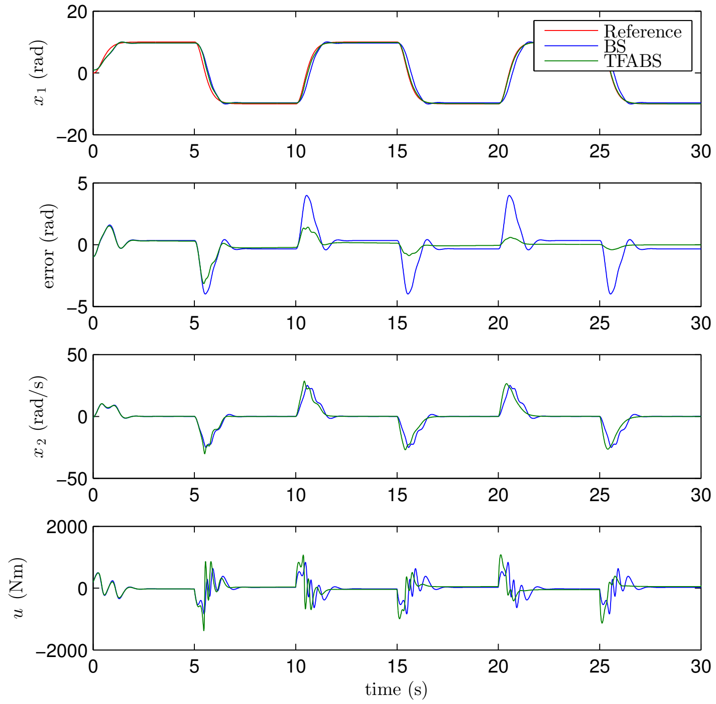

Figure F-11: The control performance of the Tuning Functions Adaptive Backstepping controller in the presence of parametric uncertainties.

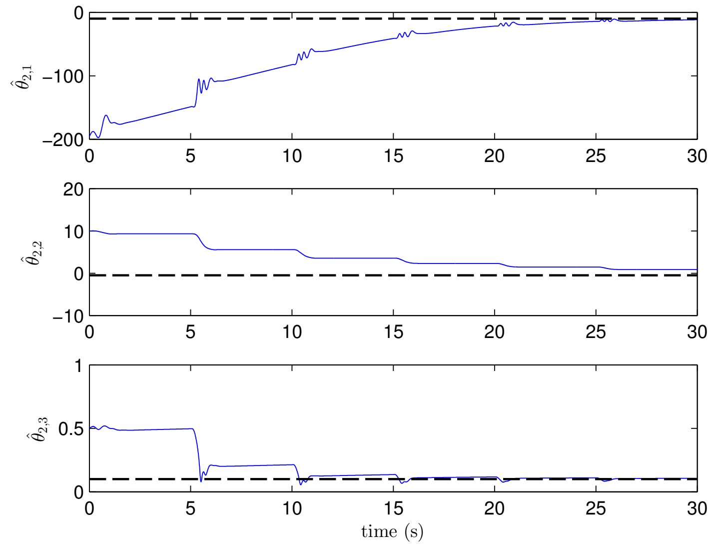

Figure F-12: The performance of the Tuning Function estimators. The dashed black lines represent the values of the real parameters.

F-2-5 Adaptive Incremental Backstepping with Time-Scale Separation

In this section a TFABS controller is designed to guarantee global asymptotic stability of the closed-loop system and parameter convergence for an uncertain nonlinear system. We now consider the following time-scale separated incremental pendulum model (see Eqs. (E-41) and (E-42)):

$$\dot{x}_1 = x_2 \tag{E-50a revisited}$$
$$\dot{x}_2 = \dot{x}_{2,0} + \theta_{2,3}\Delta u\,, \tag{E-50b revisited}$$

where we assume that $\theta_{2,3}$ is an unknown *constant* parameter. Note that Eq. (E-50b) is the incremental form of the full equation of the pendulum, see Eq. (B-3b). The control task is to track the smooth reference state $x_{1,r}$ with the state x_1. Similar as before, we start by defining the tracking errors as

$$z_1 = x_1 - x_{1,r} \tag{F-119a}$$
$$z_2 = x_2 - \alpha_1\,. \tag{F-119b}$$

The derivations for subsystem x_1 remain exactly the same as in Appendix C-3 (see Eqs. (C-32) to (C-36)), because this subsystem is assumed to be fully known. Therefore we directly move on to the second and final subsystem. Now we introduce the parameter estimation error $\tilde{\theta}_{2,3}$:

$$\tilde{\theta}_{2,3} = \theta_{2,3} - \hat{\theta}_{2,3} \rightarrow \dot{\tilde{\theta}}_{2,3} = -\dot{\hat{\theta}}_{2,3}\,, \tag{F-120}$$

where $\hat{\theta}_{2,3}$ is the estimate of $\theta_{2,3}$. Now we can rewrite the dynamics of the second error state as follows:

$$\dot{z}_2 = \dot{x}_{2,0} + \left(\tilde{\theta}_{2,3} + \hat{\theta}_{2,3}\right)\Delta u - \dot{\alpha}_1\,. \tag{F-121}$$

The earlier formulated Lyapunov function $\mathcal{V}_1$ is now augmented to penalize the second tracking error and the parameter estimation error as well:

$$\mathcal{V}(\boldsymbol{z}, \tilde{\theta}_{2,3}) = \frac{1}{2}z_1^2 + \frac{1}{2}z_2^2 + \frac{1}{2\gamma_2}\tilde{\theta}_{2,3}^2\,, \tag{F-122}$$

where $\gamma_2 > 0$ is the adaptation gain. Taking the time derivative of $\mathcal{V}$ along the trajectories of the error dynamics and Eq. (F-120) results in

$$\begin{aligned}\dot{\mathcal{V}} &= -c_1 z_1^2 + z_1 z_2 + z_2\left[\dot{x}_{2,0} + \left(\tilde{\theta}_{2,3} + \hat{\theta}_{2,3}\right)\Delta u - \dot{\alpha}_1\right] - \frac{1}{\gamma_2}\tilde{\theta}_{2,3}\dot{\hat{\theta}}_{2,3} \\ &= -c_1 z_1^2 + z_1 z_2 + z_2\left[\dot{x}_{2,0} + \hat{\theta}_{2,3}\Delta u - \dot{\alpha}_1\right] - \frac{1}{\gamma_2}\tilde{\theta}_{2,3}\left(\dot{\hat{\theta}}_{2,3} - \gamma_2 z_2 \Delta u\right)\,.\end{aligned} \tag{F-123}$$

Now we introduce the following real incremental control Δu:

$$\Delta u = \frac{1}{\hat{\theta}_{2,3}}\left[-c_2 z_2 - z_1 - \dot{x}_{2,0} + \dot{\alpha}_1\right]\,, \tag{F-124}$$

which reduces $\dot{\mathcal{V}}$ to:

$$\dot{\mathcal{V}} = -c_1 z_1^2 - c_2 z_2^2 - \frac{1}{\gamma_2}\tilde{\theta}_{2,3}\left(\dot{\hat{\theta}}_{2,3} - \gamma_2 z_2 \Delta u\right). \tag{F-125}$$

By selecting the following update law:

$$\dot{\hat{\theta}}_{2,3} = \gamma_2 z_2 \Delta u\,, \tag{F-126}$$

we render $\dot{\mathcal{V}}$ negative definite:

$$\dot{\mathcal{V}} = -c_1 z_1^2 - c_2 z_2^2\,. \tag{F-127}$$

By Theorem C.2 it now follows that:

$$\lim_{t\to\infty} z_1 = 0 \to \lim_{t\to\infty}\left[x_1 - x_{1,r}\right] = 0 \tag{F-128a}$$

$$\lim_{t\to\infty} z_2 = 0\,. \tag{F-128b}$$

Note that the parameter estimation error is completely canceled in Eq. (F-125) by selecting the parameter update law as (F-126), therefore we cannot guarantee that the parameter estimate $\hat{\theta}_{2,3}$ actually converges to the real parameter $\theta_{2,3}$. All we can conclude from Eqs. (F-122) and (F-127) with respect to the parameter estimation error $\tilde{\theta}_{2,3}$ is that it is bounded. In (Krstić, 1996) it is proven that convergence of the parameter estimate to a constant value is always achieved. In case of PE, the parameter estimate converges to the actual parameter value. The requirement of PE basically means that the reference signal must be "rich enough", i.e. "contain enough frequencies" for the parameter estimation error to converge to zero (Boyd & Sastry, 1986).

Simulations of the newly designed incremental TFABS controller have been run for system (B-3) with an uncertain control efficiency and a sampling time of 0.01 s. The initial conditions and parameters which have been used in this simulation for the model can be found in Eq. (C-44). The following control and estimator parameters have been selected:

$$\begin{aligned} c_1 &= 10\,, & c_2 &= 10\,, \\ \hat{\theta}_{2,3}(0) &= 20\cdot\theta_{2,3}\,. \end{aligned} \tag{F-129}$$

Different values of the adaptation gain γ_2 have been selected. From Figure F-13 we can clearly see that the TFABS controller performs much better compared to the conventional BS controller (C-39) in presence of the introduced parametric uncertainty. From Figure F-14 we can see that the parameter estimates for the different values of γ_2 seem to converge to the real parameter. Increasing the adaptation gain γ_2 results in faster convergence of the parameter estimate. However, if we keep increasing γ_2, the overshoot of the parameter estimate becomes significant which might results in an undesired transient response of the closed-loop system.

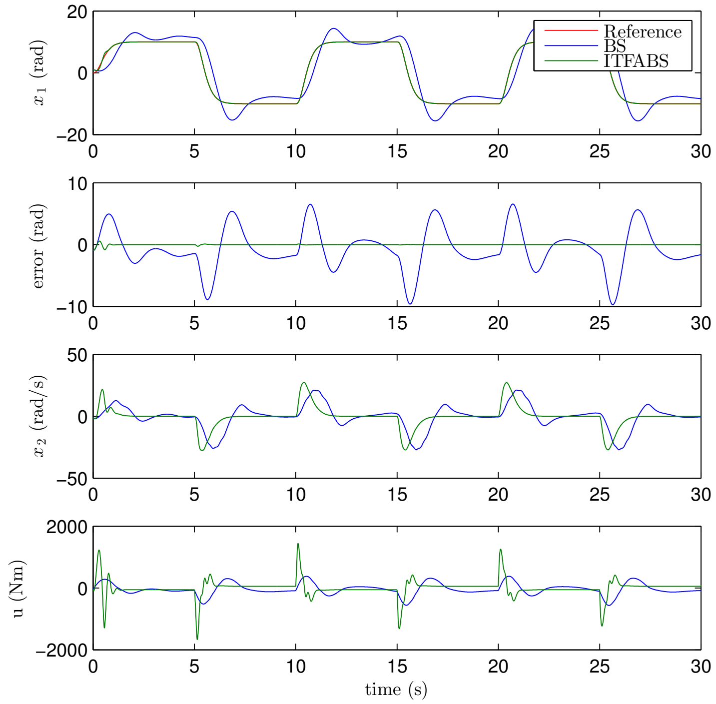

Figure F-13: The control performance of the Tuning Functions Adaptive Incremental Backstepping controller with $\gamma_2 = 5 \cdot 10^{-3}$ in the presence of a parametric uncertainty.

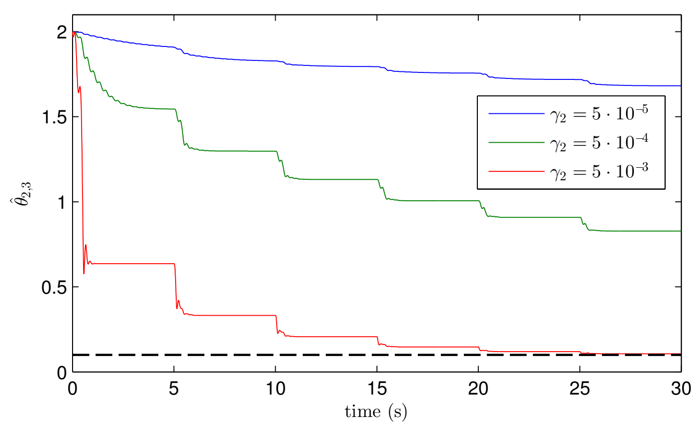

Figure F-14: The performance of the Tuning Function estimator for different values of γ_2. The dashed black line represents the value of the real parameter $\theta_{2,3}$.

F-2-6 Adaptive Incremental Backstepping without Time-Scale Separation

In this section a TFABS controller is designed to guarantee global asymptotic stability of the closed-loop system and parameter convergence for an uncertain nonlinear system. We do not make the assumption of Time-Scale Separation (TSS) (see Eq. (E-41)), thus when the sampling rate is sufficiently high we can write the pendulum model as

$$\dot{x}_1 = x_2 \tag{E-66a revisited}$$

$$\dot{x}_2 = \dot{x}_{2,0} + \theta_{2,1}\cos(x_{1,0})\Delta x_1 + \theta_{2,2}\Delta x_2 + \theta_{2,3}\Delta u\,, \tag{E-66b revisited}$$

where we assume $\theta_{2,1}$, $\theta_{2,2}$ and $\theta_{2,3}$ are unknown *constant* parameters. Note that Eq. (E-66b) is the incremental form of the full equation of the pendulum, see Eq. (B-3b).

Similar as before, we start by defining the tracking errors as

$$z_1 = x_1 - x_{1,r} \tag{F-131a}$$

$$z_2 = x_2 - \alpha_1\,. \tag{F-131b}$$

The derivations for subsystem x_1 remain exactly the same as in Appendix C-3 (see Eqs. (C-32) to (C-36)), because this subsystem is assumed to be fully known. Therefore we directly move on to the second and final subsystem. Now we introduce the parameter estimation error $\tilde{\boldsymbol{\theta}}_2$:

$$\tilde{\boldsymbol{\theta}}_2 = \begin{bmatrix}\tilde{\theta}_{2,1} & \tilde{\theta}_{2,2} & \tilde{\theta}_{2,3}\end{bmatrix}^T = \boldsymbol{\theta}_2 - \hat{\boldsymbol{\theta}}_2 \rightarrow \dot{\tilde{\boldsymbol{\theta}}}_2 = -\dot{\hat{\boldsymbol{\theta}}}_2\,, \tag{F-132}$$

where $\hat{\boldsymbol{\theta}}_2$ is the estimate of $\boldsymbol{\theta}_2$. Now we can rewrite the dynamics of the second error state as follows:

$$\dot{z}_2 = \dot{x}_{2,0} + \left(\tilde{\theta}_{2,1} + \hat{\theta}_{2,1}\right)\cos(x_{1,0})\Delta x_1 + \left(\tilde{\theta}_{2,2} + \hat{\theta}_{2,2}\right)\Delta x_2 + \left(\tilde{\theta}_{2,3} + \hat{\theta}_{2,3}\right)\Delta u - \dot{\alpha}_1\,. \tag{F-133}$$

The earlier formulated Lyapunov function $\mathcal{V}_1$ is now augmented to penalize the second tracking error and the parameter estimation errors as well:

$$\mathcal{V}(\boldsymbol{z}, \tilde{\boldsymbol{\theta}}_2) = \mathcal{V}_1 + \frac{1}{2}z_2^2 + \frac{1}{2\gamma_{2,1}}\tilde{\theta}_{2,1}^2 + \frac{1}{2\gamma_{2,2}}\tilde{\theta}_{2,2}^2 + \frac{1}{2\gamma_{2,3}}\tilde{\theta}_{2,3}^2\,, \tag{F-134}$$

where $\gamma_{2,i} > 0$ for $i = 1, 2, 3$ are the adaptation gains. Taking the time derivative of $\mathcal{V}$ along the trajectories of the error dynamics and Eq. (F-132) results in

$$\begin{aligned}
\dot{\mathcal{V}} &= -c_1 z_1^2 + z_1 z_2 - \frac{1}{\gamma_{2,1}}\tilde{\theta}_{2,1}\dot{\hat{\theta}}_{2,1} - \frac{1}{\gamma_{2,2}}\tilde{\theta}_{2,2}\dot{\hat{\theta}}_{2,2} - \frac{1}{\gamma_{2,3}}\tilde{\theta}_{2,3}\dot{\hat{\theta}}_{2,3} \\
&\quad + z_2\left[\dot{x}_{2,0} + \left(\tilde{\theta}_{2,1} + \hat{\theta}_{2,1}\right)\cos(x_{1,0})\Delta x_1 + \left(\tilde{\theta}_{2,2} + \hat{\theta}_{2,2}\right)\Delta x_2 + \left(\tilde{\theta}_{2,3} + \hat{\theta}_{2,3}\right)\Delta u - \dot{\alpha}_1\right] \\
&= -c_1 z_1^2 + z_1 z_2 - \frac{1}{\gamma_{2,1}}\tilde{\theta}_{2,1}\left(\dot{\hat{\theta}}_{2,1} - \gamma_{2,1}z_2\cos(x_{1,0})\Delta x_1\right) - \frac{1}{\gamma_{2,2}}\tilde{\theta}_{2,2}\left(\dot{\hat{\theta}}_{2,2} - \gamma_{2,2}z_2\Delta x_2\right) \\
&\quad - \frac{1}{\gamma_{2,3}}\tilde{\theta}_{2,3}\left(\dot{\hat{\theta}}_{2,3} - \gamma_{2,3}z_2\Delta u\right) + z_2\left[\dot{x}_{2,0} + \hat{\theta}_{2,1}\cos(x_{1,0})\Delta x_1 + \hat{\theta}_{2,2}\Delta x_2 + \hat{\theta}_{2,3}\Delta u - \dot{\alpha}_1\right]\,.
\end{aligned} \tag{F-135}$$

By selecting the following real incremental control:

$$\Delta u = \frac{1}{\hat{\theta}_{2,3}} \left[-c_2 z_2 - z_1 - \dot{x}_{2,0} - \hat{\theta}_{2,1} \cos(x_{1,0}) \Delta x_1 - \hat{\theta}_{2,2} \Delta x_2 + \dot{\alpha}_1 \right] , \tag{F-136}$$

and update laws:

$$\dot{\hat{\theta}}_{2,1} = \gamma_{2,1} z_2 \cos(x_{1,0}) \Delta x_1 \tag{F-137a}$$

$$\dot{\hat{\theta}}_{2,2} = \gamma_{2,2} z_2 \Delta x_2 \tag{F-137b}$$

$$\dot{\hat{\theta}}_{2,3} = \gamma_{2,3} z_2 \Delta u \, , \tag{F-137c}$$

we render $\dot{\mathcal{V}}$ negative definite:

$$\dot{\mathcal{V}} = -c_1 z_1^2 - c_2 z_2^2 \, . \tag{F-138}$$

By Theorem C.2 it now follows that:

$$\lim_{t \to \infty} z_1 = 0 \to \lim_{t \to \infty} [x_1 - x_{1,r}] = 0 \tag{F-139a}$$

$$\lim_{t \to \infty} z_2 = 0 \, . \tag{F-139b}$$

Note that the parameter estimation errors are completely canceled in Eq. (F-135) by selecting the parameter update laws as (F-137), therefore we cannot guarantee that the parameter estimate $\hat{\boldsymbol{\theta}}_2$ actually converges to the real parameter $\boldsymbol{\theta}_2$. All we can conclude from Eqs. (F-134) and (F-138) with respect to the parameter estimation error $\tilde{\boldsymbol{\theta}}_2$ is that it is bounded. In (Krstić, 1996) it is proven that convergence of the parameter estimate to a constant value is always achieved. In case of PE, the parameter estimates converge to the actual parameters. The requirement of PE basically means that the reference signal must be “rich enough”, i.e. “contain enough frequencies” for the parameter estimation error to converge to zero (Boyd & Sastry, 1986).

Appendix G

Least-Squares Adaptive Backstepping

In this appendix the Backstepping (BS) control approach is augmented with Least-Squares (LS) parameter estimators. This is a form of Indirect Adaptive Control that is based on the *certainty equivalence principle* (Krstić et al., 1995; van Oort, 2011). This means that the controller is designed by assuming perfect knowledge of the model. Next, the model parameters are estimated by a separate module (G-1). The certainty equivalence controller is then simply obtained by replacing the model parameters $\boldsymbol{\theta}_m$ by their estimates $\hat{\boldsymbol{\theta}}_m$. In order to evaluate this nonlinear control approach, Least-Squares Adaptive Backstepping (LSABS) control laws are derived and simulated for the pendulum model (G-2).

G-1 Theory

In order to apply LSABS, the non-triangular, feedback passive system is rewritten to obtain an overdetermined system (G-1-1). Subsequently, LS fitting is applied to obtain an estimate of the model parameters (G-1-2).

G-1-1 Obtaining an Overdetermined System

The overdetermined system that we need to obtain before we can apply the technique of LS fitting can be derived in two ways:

- Conventional method;
- Incremental method.

These two approaches are discussed in the next sections.

Conventional method

We consider the following non-triangular, feedback passive system:

$$\dot{x}_i = f_i(\boldsymbol{x}) + g_i(\boldsymbol{x})x_{i+1}\,, \quad i = 1, \ldots, n-1 \tag{G-1a}$$
$$\dot{x}_n = f_n(\boldsymbol{x}) + g_n(\boldsymbol{x})u\,, \tag{G-1b}$$

which can be written as

$$\dot{x}_i = f_i(\boldsymbol{x}) + g_i(\boldsymbol{x})x_{i+1}\,, \quad i = 1, \ldots, n\,, \tag{G-2}$$

where $\boldsymbol{x} = [x_1, \cdots, x_n]^T$ is the state vector, $x_i \in \mathbb{R}$ and $x_{n+1} \equiv u \in \mathbb{R}$ the control signal. The smooth functions f_i and g_i contain the unknown dynamics of the system and will have to be approximated. It is assumed there exist vectors $\boldsymbol{\theta}_{f_i}$ and $\boldsymbol{\theta}_{g_i}$ such that

$$f_i(\boldsymbol{x}) = \boldsymbol{\varphi}_{f_i}(\boldsymbol{x})^T\boldsymbol{\theta}_{f_i} \tag{G-3a}$$
$$g_i(\boldsymbol{x}) = \boldsymbol{\varphi}_{g_i}(\boldsymbol{x})^T\boldsymbol{\theta}_{g_i}\,, \tag{G-3b}$$

where $\boldsymbol{\varphi}_\star$ are the regressors and $\boldsymbol{\theta}_\star$ are vectors of unknown *constant* parameters. Now Eq. (G-2) can be written as

$$\dot{x}_i = \boldsymbol{\varphi}_{f_i}(\boldsymbol{x}_i)^T\boldsymbol{\theta}_{f_i} + \boldsymbol{\varphi}_{g_i}(\boldsymbol{x}_i)^T\boldsymbol{\theta}_{g_i}x_{i+1}\,. \tag{G-4}$$

At time k the following vector equations can be constructed by using the past N measurements:

$$\boldsymbol{y}_i \cong A_i\boldsymbol{\theta}_i\,, \quad i = 1, \ldots, n\,, \tag{G-5}$$

where

$$\boldsymbol{y}_i = \begin{bmatrix}\dot{x}_{i,k-N} & \cdots & \dot{x}_{i,k-1} & \dot{x}_{i,k}\end{bmatrix}^T\,, \qquad \boldsymbol{\theta}_i = \begin{bmatrix}\boldsymbol{\theta}_{f_i}^T & \boldsymbol{\theta}_{g_i}^T\end{bmatrix}^T\,, \tag{G-6}$$

$$A_i = \begin{bmatrix}\boldsymbol{\varphi}_{f_i}(\boldsymbol{x}_{i,k-N})^T & \boldsymbol{\varphi}_{g_i}(\boldsymbol{x}_{i,k-N})^T x_{i+1,k-N} \\ \vdots & \vdots \\ \boldsymbol{\varphi}_{f_i}(\boldsymbol{x}_{i,k-1})^T & \boldsymbol{\varphi}_{g_i}(\boldsymbol{x}_{i,k-1})^T x_{i+1,k-1} \\ \boldsymbol{\varphi}_{f_i}(\boldsymbol{x}_{i,k})^T & \boldsymbol{\varphi}_{g_i}(\boldsymbol{x}_{i,k})^T x_{i+1,k}\end{bmatrix}.$$

The method of Least-Squares can be applied to estimate the unknown constant parameters when we assume that $\dot{x}_i$ and x_i for $i = 1, \ldots, n$ and $x_{n+1} \equiv u$ are measurable or can be accurately estimated. The certainty equivalence controller is then simply obtained by replacing the model parameters $\boldsymbol{\theta}_m$ of the (incremental) BS control law by their estimates $\hat{\boldsymbol{\theta}}_m$.

Incremental method

Again, we consider the following non-triangular, feedback passive system:

$$\dot{x}_i = f_i(\boldsymbol{x}) + g_i(\boldsymbol{x})x_{i+1}\,, \quad i = 1, \ldots, n-1 \tag{G-7a}$$
$$\dot{x}_n = f_n(\boldsymbol{x}) + g_n(\boldsymbol{x})u\,, \tag{G-7b}$$

Taking the first-order Taylor series expansion around the current solution $[\boldsymbol{x_0}, u_0]$ of Eq. (G-7) results in

$$\dot{x}_i \cong f_i(\boldsymbol{x}_0) + g_i(\boldsymbol{x}_0)x_{i+1,0} + \frac{\partial}{\partial \boldsymbol{x}} \left[f_i(\boldsymbol{x}) + g_i(\boldsymbol{x})x_{i+1}\right]\Big|_{\boldsymbol{x}=\boldsymbol{x}_0} (\boldsymbol{x} - \boldsymbol{x}_0) \ , \quad i = 1, \ldots, n-1 \tag{G-8a}$$

$$\dot{x}_n \cong f_n(\boldsymbol{x}_0) + g_n(\boldsymbol{x}_0)u_0 + \frac{\partial}{\partial \boldsymbol{x}} \left[f_n(\boldsymbol{x}) + g_n(\boldsymbol{x})u\right]\Big|_{\substack{\boldsymbol{x}=\boldsymbol{x}_0 \\ u=u_0}} (\boldsymbol{x} - \boldsymbol{x}_0) + \frac{\partial}{\partial u} \left[g_n(\boldsymbol{x})u\right]\Big|_{\substack{\boldsymbol{x}=\boldsymbol{x}_0 \\ u=u_0}} (u - u_0) \ . \tag{G-8b}$$

By definition, the current state rates satisfy

$$\dot{x}_{i,0} = f_i(\boldsymbol{x}_0) + g_i(\boldsymbol{x}_0)x_{i+1,0} \, , \quad i = 1, \ldots, n-1 \tag{G-9a}$$

$$\dot{x}_{n,0} = f_n(\boldsymbol{x}_0) + g_n(\boldsymbol{x}_0)u_0 \, , \tag{G-9b}$$

resulting in

$$\dot{x}_i \cong \dot{x}_{i,0} + \frac{\partial}{\partial \boldsymbol{x}} \left[f_i(\boldsymbol{x}) + g_i(\boldsymbol{x})x_{i+1}\right]\Big|_{\boldsymbol{x}=\boldsymbol{x}_0} (\boldsymbol{x} - \boldsymbol{x}_0) \ , \quad i = 1, \ldots, n-1 \tag{G-10a}$$

$$\dot{x}_n \cong \dot{x}_{n,0} + \frac{\partial}{\partial \boldsymbol{x}} \left[f_n(\boldsymbol{x}) + g_n(\boldsymbol{x})u\right]\Big|_{\substack{\boldsymbol{x}=\boldsymbol{x}_0 \\ u=u_0}} (\boldsymbol{x} - \boldsymbol{x}_0) + g_n(\boldsymbol{x}_0) (u - u_0) \ . \tag{G-10b}$$

By using Eq. (G-3) and the following notation

$$\Delta\dot{x}_i = \dot{x}_i - \dot{x}_{i,0} \, , \quad i = 1, \ldots, n \tag{G-11a}$$

$$\Delta\boldsymbol{x} = \boldsymbol{x} - \boldsymbol{x}_0 \, , \quad \Delta u = u - u_0 \, , \tag{G-11b}$$

we can write Eq. (G-10) as

$$\Delta\dot{x}_i \cong \frac{\partial}{\partial \boldsymbol{x}} \left[\boldsymbol{\varphi}_{f_i}(\boldsymbol{x})^T\boldsymbol{\theta}_{f_i} + \boldsymbol{\varphi}_{g_i}(\boldsymbol{x})^T\boldsymbol{\theta}_{g_i}x_{i+1}\right]\Big|_{\boldsymbol{x}=\boldsymbol{x}_0} \Delta\boldsymbol{x} \, , \quad i = 1, \ldots, n-1 \tag{G-12a}$$

$$\Delta\dot{x}_n \cong \frac{\partial}{\partial \boldsymbol{x}} \left[\boldsymbol{\varphi}_{f_n}(\boldsymbol{x})^T\boldsymbol{\theta}_{f_n} + \boldsymbol{\varphi}_{g_n}(\boldsymbol{x})^T\boldsymbol{\theta}_{g_n}u\right]\Big|_{\substack{\boldsymbol{x}=\boldsymbol{x}_0 \\ u=u_0}} \Delta\boldsymbol{x} + \boldsymbol{\varphi}_{g_n}(\boldsymbol{x}_0)^T\boldsymbol{\theta}_{g_n}\Delta u \, , \tag{G-12b}$$

rewriting yields

$$\Delta\dot{x}_i \cong \Delta\boldsymbol{x}^T \frac{\partial}{\partial \boldsymbol{x}} \left[\boldsymbol{\varphi}_{f_i}(\boldsymbol{x})^T\boldsymbol{\theta}_{f_i} + \boldsymbol{\varphi}_{g_i}(\boldsymbol{x})^T\boldsymbol{\theta}_{g_i}x_{i+1}\right]\Big|^T_{\boldsymbol{x}=\boldsymbol{x}_0} \, , \quad i = 1, \ldots, n-1 \tag{G-13a}$$

$$\Delta\dot{x}_n \cong \Delta\boldsymbol{x}^T \frac{\partial}{\partial \boldsymbol{x}} \left[\boldsymbol{\varphi}_{f_n}(\boldsymbol{x})^T\boldsymbol{\theta}_{f_n} + \boldsymbol{\varphi}_{g_n}(\boldsymbol{x})^T\boldsymbol{\theta}_{g_n}u\right]\Big|^T_{\substack{\boldsymbol{x}=\boldsymbol{x}_0 \\ u=u_0}} + \boldsymbol{\varphi}_{g_n}(\boldsymbol{x}_0)^T\Delta u\boldsymbol{\theta}_{g_n} \, , \tag{G-13b}$$

and further rewriting yields

$$\Delta\dot{x}_i \cong \Delta\boldsymbol{x}^T \frac{\partial}{\partial \boldsymbol{x}} \left[\boldsymbol{\varphi}_{f_i}(\boldsymbol{x})\right]\Big|^T_{\boldsymbol{x}=\boldsymbol{x}_0} \boldsymbol{\theta}_{f_i} + \Delta\boldsymbol{x}^T \frac{\partial}{\partial \boldsymbol{x}} \left[\boldsymbol{\varphi}_{g_i}(\boldsymbol{x})x_{i+1}\right]\Big|^T_{\boldsymbol{x}=\boldsymbol{x}_0} \boldsymbol{\theta}_{g_i} \, , \quad i = 1, \ldots, n-1 \tag{G-14a}$$

$$\Delta\dot{x}_n \cong \Delta\boldsymbol{x}^T \frac{\partial}{\partial \boldsymbol{x}} \left[\boldsymbol{\varphi}_{f_n}(\boldsymbol{x})\right]\Big|^T_{\boldsymbol{x}=\boldsymbol{x}_0} \boldsymbol{\theta}_{f_n} + \Delta\boldsymbol{x}^T \frac{\partial}{\partial \boldsymbol{x}} \left[\boldsymbol{\varphi}_{g_n}(\boldsymbol{x})\right]\Big|^T_{\boldsymbol{x}=\boldsymbol{x}_0} u_0\boldsymbol{\theta}_{g_n} + \boldsymbol{\varphi}_{g_n}(\boldsymbol{x}_0)^T\Delta u\boldsymbol{\theta}_{g_n} \, . \tag{G-14b}$$

At time k the following vector equations can be constructed by using the past N measurements:

$$\boldsymbol{y}_i \cong A_i \boldsymbol{\theta}_i\,, \quad i = 1, \ldots, n-1 \tag{G-15a}$$
$$\boldsymbol{y}_n \cong A_n \boldsymbol{\theta}_n\,, \tag{G-15b}$$

where

$$\boldsymbol{y}_i = \begin{bmatrix}\Delta \dot{x}_{i,k-N} & \cdots & \Delta \dot{x}_{i,k-1} & \Delta \dot{x}_{i,k}\end{bmatrix}^T, \qquad \boldsymbol{\theta}_i = \begin{bmatrix}\boldsymbol{\theta}_{f_i}^T & \boldsymbol{\theta}_{g_i}^T\end{bmatrix}^T, \tag{G-16}$$

$$A_i = \begin{bmatrix} \Delta \boldsymbol{x}_{k-N}^T \frac{\partial}{\partial \boldsymbol{x}} \boldsymbol{\varphi}_{f_i}\Big|_{\boldsymbol{x}=\boldsymbol{x}_{k-N-1}}^T & \Delta \boldsymbol{x}_{k-N}^T \frac{\partial}{\partial \boldsymbol{x}} \left[\boldsymbol{\varphi}_{g_i} x_{i+1}\right]^T\Big|_{\boldsymbol{x}=\boldsymbol{x}_{k-N-1}} \\ \vdots & \vdots \\ \Delta \boldsymbol{x}_{k-1}^T \frac{\partial}{\partial \boldsymbol{x}} \boldsymbol{\varphi}_{f_i}\Big|_{\boldsymbol{x}=\boldsymbol{x}_{k-2}}^T & \Delta \boldsymbol{x}_{k-1}^T \frac{\partial}{\partial \boldsymbol{x}} \left[\boldsymbol{\varphi}_{g_i} x_{i+1}\right]^T\Big|_{\boldsymbol{x}=\boldsymbol{x}_{k-2}} \\ \Delta \boldsymbol{x}_{k}^T \frac{\partial}{\partial \boldsymbol{x}} \boldsymbol{\varphi}_{f_i}\Big|_{\boldsymbol{x}=\boldsymbol{x}_{k-1}}^T & \Delta \boldsymbol{x}_{k}^T \frac{\partial}{\partial \boldsymbol{x}} \left[\boldsymbol{\varphi}_{g_i} x_{i+1}\right]^T\Big|_{\boldsymbol{x}=\boldsymbol{x}_{k-1}} \end{bmatrix},$$

and

$$\boldsymbol{y}_n = \begin{bmatrix}\Delta \dot{x}_{n,k-N} & \cdots & \Delta \dot{x}_{n,k-1} & \Delta \dot{x}_{n,k}\end{bmatrix}^T, \qquad \boldsymbol{\theta}_n = \begin{bmatrix}\boldsymbol{\theta}_{f_n}^T & \boldsymbol{\theta}_{g_n}^T\end{bmatrix}^T, \tag{G-17}$$

$$A_n = \begin{bmatrix} \Delta \boldsymbol{x}_{k-N}^T \frac{\partial}{\partial \boldsymbol{x}} \boldsymbol{\varphi}_{f_n}\Big|_{\boldsymbol{x}=\boldsymbol{x}_{k-N-1}}^T & \Delta \boldsymbol{x}_{k-N}^T \frac{\partial}{\partial \boldsymbol{x}} \boldsymbol{\varphi}_{g_n}\Big|_{\boldsymbol{x}=\boldsymbol{x}_{k-N-1}}^T u_{k-N-1} + \boldsymbol{\varphi}_{g_n}(\boldsymbol{x}_{k-N-1})^T \Delta u_{k-N} \\ \vdots & \vdots \\ \Delta \boldsymbol{x}_{k-1}^T \frac{\partial}{\partial \boldsymbol{x}} \boldsymbol{\varphi}_{f_n}\Big|_{\boldsymbol{x}=\boldsymbol{x}_{k-2}}^T & \Delta \boldsymbol{x}_{k-1}^T \frac{\partial}{\partial \boldsymbol{x}} \boldsymbol{\varphi}_{g_n}\Big|_{\boldsymbol{x}=\boldsymbol{x}_{k-2}}^T u_{k-2} + \boldsymbol{\varphi}_{g_n}(\boldsymbol{x}_{k-2})^T \Delta u_{k-1} \\ \Delta \boldsymbol{x}_{k}^T \frac{\partial}{\partial \boldsymbol{x}} \boldsymbol{\varphi}_{f_n}\Big|_{\boldsymbol{x}=\boldsymbol{x}_{k-1}}^T & \Delta \boldsymbol{x}_{k}^T \frac{\partial}{\partial \boldsymbol{x}} \boldsymbol{\varphi}_{g_n}\Big|_{\boldsymbol{x}=\boldsymbol{x}_{k-1}}^T u_{k-1} + \boldsymbol{\varphi}_{g_n}(\boldsymbol{x}_{k-1})^T \Delta u_{k} \end{bmatrix}.$$

The method of Least-Squares can be applied to estimate the unknown constant parameters when we assume that $\dot{x}_i$ and x_i for $i = 1, \ldots, n$ and $x_{n+1} \equiv u$ are measurable or can be accurately estimated. The certainty equivalence controller is then simply obtained by replacing the model parameters $\boldsymbol{\theta}_m$ of the (incremental) BS control law by their estimates $\hat{\boldsymbol{\theta}}_m$.

Note that if we assume a sufficiently time-scale separated system, that is the increment in state $\Delta \boldsymbol{x}$ is much smaller than the increment in both state derivative $\Delta \dot{\boldsymbol{x}}_2$ and input $\Delta \boldsymbol{u}$, we can neglect the former. In that case Eq. (G-15b) simplifies to:

$$\begin{bmatrix}\Delta \dot{x}_{n,k-N} \\ \vdots \\ \Delta \dot{x}_{n,k-1} \\ \Delta \dot{x}_{n,k}\end{bmatrix} \cong \begin{bmatrix}\boldsymbol{\varphi}_{g_n}(\boldsymbol{x}_{k-N-1})^T \Delta u_{k-N} \\ \vdots \\ \boldsymbol{\varphi}_{g_n}(\boldsymbol{x}_{k-2})^T \Delta u_{k-1} \\ \boldsymbol{\varphi}_{g_n}(\boldsymbol{x}_{k-1})^T \Delta u_{k}\end{bmatrix} \boldsymbol{\theta}_{g_n}\,. \tag{G-18}$$

G-1-2 Least-Squares Fitting

In the previous section we have obtained systems of linear equations in the form

$$\boldsymbol{y} = A\boldsymbol{\theta}\,, \tag{G-19}$$

where $\boldsymbol{\theta}$ are the parameters to be estimated. In the next sections the following linear Least-Squares approaches will be discussed to approximate the unknown parameter vector $\boldsymbol{\theta}$:

- Ordinary least-squares
- Weighted least-squares
- Recursive least-squares
- Recursive least-squares with forgetting
- Total least-squares

Ordinary least-squares

The Ordinary Least-Squares (OLS) algorithm is obtained by minimizing the following cost function:

$$J(\boldsymbol{\theta}) = (\boldsymbol{y} - A\boldsymbol{\theta})^T(\boldsymbol{y} - A\boldsymbol{\theta})\,. \tag{G-20}$$

This results in the well-known OLS solution:

$$\hat{\boldsymbol{\theta}}_{OLS} = \left(A^T A\right)^{-1} A^T \boldsymbol{y}\,. \tag{G-21}$$

The OLS-estimator results in unbiased parameter estimates when we are dealing with zero mean white noise in the observation vector $\boldsymbol{y}$ and when the data matrix A is exactly known (van Huffel & Vandewalle, 1991). However, the assumption that measurements in matrix A are free of error is frequently unrealistic resulting in biased parameter estimates.

Weighted least-squares

The Weighted Least-Squares (WLS) algorithm is obtained by minimizing the following cost function:

$$J(\boldsymbol{\theta}) = (\boldsymbol{y} - A\boldsymbol{\theta})^T W(\boldsymbol{y} - A\boldsymbol{\theta})\,, \tag{G-22}$$

where W is a diagonal weighting matrix. This results in the well-known WLS solution:

$$\hat{\boldsymbol{\theta}}_{WLS} = \left(A^T W A\right)^{-1} A^T W \boldsymbol{y}\,. \tag{G-23}$$

With WLS we are able to give the data points the proper amount of influence over the parameter estimate. This is different from OLS in which all data is treated equally.

Recursive least-squares

The cost function as used for deriving the OLS solution (see Eq. (G-20)) is now split into a new and an old part as follows:

$$\begin{aligned} J(\boldsymbol{\theta}_{k+1}) &= (\boldsymbol{y}_{k+1} - A_{k+1}\boldsymbol{\theta}_{k+1})^T(\boldsymbol{y}_{k+1} - A_{k+1}\boldsymbol{\theta}_{k+1}) \\ &= \underbrace{(\boldsymbol{y}_k - A_k\boldsymbol{\theta}_{k+1})^T(\boldsymbol{y}_k - A_k\boldsymbol{\theta}_{k+1})}_{\text{old data}} + \underbrace{(y_{k+1} - \boldsymbol{a}_{k+1}\boldsymbol{\theta}_{k+1})^T(y_{k+1} - \boldsymbol{a}_{k+1}\boldsymbol{\theta}_{k+1})}_{\text{new data}}\,, \end{aligned} \tag{G-24}$$

where

$$A_{k+1} = \begin{bmatrix} A_k & \boldsymbol{a}_{k+1} \end{bmatrix}^T \tag{G-25a}$$
$$\boldsymbol{y}_k = \begin{bmatrix} y_1 & y_2 & \dots & y_k \end{bmatrix}^T \tag{G-25b}$$
$$\boldsymbol{y}_{k+1} = \begin{bmatrix} \boldsymbol{y}_k^T & y_{k+1} \end{bmatrix}^T . \tag{G-25c}$$

Minimizing cost function (G-24) results in the Recursive Least-Squares (RLS) algorithm (Zhu & Li, 1999):

$$\hat{\boldsymbol{\theta}}_{k+1} = \hat{\boldsymbol{\theta}}_k + K_{k+1} \underbrace{\left(y_{k+1} - \boldsymbol{a}_{k+1}\hat{\boldsymbol{\theta}}_k \right)}_{\Delta_k} , \tag{G-26}$$

where Δ is the innovation, $\boldsymbol{a}$ the regression vector and K the Kalman gain given by

$$K_{k+1} = P_k \boldsymbol{a}_{k+1}^T \left(\boldsymbol{a}_{k+1} P_k \boldsymbol{a}_{k+1}^T + 1 \right)^{-1} \tag{G-27a}$$
$$P_{k+1} = \left(I_N - K_{k+1}\boldsymbol{a}_{k+1} \right) P_k , \tag{G-27b}$$

and where P is the covariance matrix. For this algorithm we need an initial estimate of the unknown parameter and the covariance matrix. The advantage of the RLS algorithm is that it can be executed very efficiently in on-line applications.

Recursive least-squares with forgetting

The cost function as used for deriving the WLS solution (see Eq. (G-22)) is now split into a new and an old part as follows:

$$\begin{aligned} J(\boldsymbol{\theta}_{k+1}) &= (\boldsymbol{y}_{k+1} - A_{k+1}\boldsymbol{\theta}_{k+1})^T W_{k+1} (\boldsymbol{y}_{k+1} - A_{k+1}\boldsymbol{\theta}_{k+1}) \\ &= \underbrace{(\boldsymbol{y}_k - A_k\boldsymbol{\theta}_{k+1})^T W_k (\boldsymbol{y}_k - A_k\boldsymbol{\theta}_{k+1})}_{\text{old data}} + \underbrace{(y_{k+1} - \boldsymbol{a}_{k+1}\boldsymbol{\theta}_{k+1})^T w_{k+1} (y_{k+1} - \boldsymbol{a}_{k+1}\boldsymbol{\theta}_{k+1})}_{\text{new data}} , \end{aligned} \tag{G-28}$$

where

$$A_{k+1} = \begin{bmatrix} A_k & \boldsymbol{a}_{k+1} \end{bmatrix}^T \tag{G-29a}$$
$$\boldsymbol{y}_k = \begin{bmatrix} y_1 & y_2 & \dots & y_k \end{bmatrix}^T \tag{G-29b}$$
$$\boldsymbol{y}_{k+1} = \begin{bmatrix} \boldsymbol{y}_k^T & y_{k+1} \end{bmatrix}^T \tag{G-29c}$$
$$W_{k+1} = \begin{bmatrix} W_k & 0 \\ 0 & w_{k+1} \end{bmatrix}^T , \tag{G-29d}$$

where k is the current instant and N is the amount of past measurements used to obtain the WLS solution. By applying *exponential* forgetting, the weighting matrix is as follows:

$$W_{k+1} = \begin{bmatrix} \lambda^{N-1} & 0 & 0 & 0 \\ 0 & \ddots & 0 & 0 \\ 0 & 0 & \lambda^1 & 0 \\ 0 & 0 & 0 & \lambda^0 \end{bmatrix} . \tag{G-30}$$

For the forgetting factor we have $0 < \lambda \leq 1$. Setting $\lambda = 1$ corresponds to "no forgetting" and estimating constant coefficients. Setting $\lambda < 1$ implies that past measurements are less significant for parameter estimation and can be "forgotten". $\lambda < 1$ should be set to estimate time-varying coefficients.

Minimizing cost function (G-28) results in the RLS algorithm with exponential forgetting (Dayal & MacGregor, 1997):

$$\hat{\boldsymbol{\theta}}_{k+1} = \hat{\boldsymbol{\theta}}_k + K_{k+1}\left(y_{k+1} - \boldsymbol{a}_{k+1}\hat{\boldsymbol{\theta}}_k\right) \tag{G-31a}$$

$$K_{k+1} = P_k \boldsymbol{a}_{k+1}^T \left(\boldsymbol{a}_{k+1} P_k \boldsymbol{a}_{k+1}^T + \lambda\right)^{-1} \tag{G-31b}$$

$$P_{k+1} = \frac{1}{\lambda}\left(I_N - K_{k+1}\boldsymbol{a}_{k+1}\right) P_k \, . \tag{G-31c}$$

Total least-squares

The OLS-estimator results in unbiased parameter estimates only when we are dealing with zero mean white noise in the observation vector $\boldsymbol{y}$ and when the data matrix A is exactly known (van Huffel & Vandewalle, 1991). However, the assumption that measurements in matrix A are free of error is frequently unrealistic. In for example (Laban, 1994; Mulder et al., 1999; Lombaerts, Smaili, et al., 2009; Lombaerts, Huisman, et al., 2009; Sun, 2014) the Two-Step Method (TSM) is applied for state and parameter estimation. The parameter estimation in this approach uses direct measurements and estimated states which are the output of the first step (flight path reconstruction). The OLS provides an unbiased estimate of the aerodynamic parameters only in case of *perfect* flight path reconstruction. Once the output of the first step contains errors, the OLS estimator becomes biased (Edwards et al., 2010).

In order to keep the Least-Squares estimate unbiased and efficient in case of errors in both the data matrix A and the observation vector $\boldsymbol{y}$, the Total Least-Squares (TLS) method may be applied, which is also known as errors-in-variables or orthogonal regression. The TLS gives the "best" estimate (in a statistical sense) of the parameter vector when all variables are subject to zero mean white noise and common covariance matrix equal to the identity matrix up to a scaling factor (van Huffel & Vandewalle, 1991). In the TLS approach, the sum of squares of residuals on *all* the variables in Eq. (G-19) is minimized.

The TLS solution of the overdetermined system of linear equations $\boldsymbol{y} = A\boldsymbol{\theta}$ is given by (van Huffel & Vandewalle, 1991; Markovsky & Van Huffel, 2007)

$$\hat{\boldsymbol{\theta}}_{TLS} = -1/(v_{n+1,n+1})[v_{1,n+1}, \cdots, v_{n,n+1}]^T \, , \tag{G-32}$$

where v_{ij} refers to the (i,j)-th entry of V which is given by the Singular Value Decomposition (SVD) of $A \in \mathbb{R}^{m\times n}$ and $\boldsymbol{y} \in \mathbb{R}^m$, where $m > n$:

$$\begin{bmatrix} A & \boldsymbol{y} \end{bmatrix} = U\Sigma V^\dagger \, , \tag{G-33}$$

and where U is a $m \times m$ unitary matrix, Σ is a $m \times n$ diagonal matrix with non-negative real numbers on the diagonal and $V^\dagger$ denotes the *conjugate* transpose of the $n \times n$ unitary matrix V. In (van Huffel & Vandewalle, 1991) this basic TLS solution has been extended to avoid the singularity at $v_{n+1,n+1} = 0$. In order to reduce the computational load of the TLS algorithm in on-line applications, the TLS can be calculated in a sequential manner (Soijer, 2004; Edwards et al., 2010).

In Figure G-1 the difference between the OLS and TLS is visualized for $\theta \in \mathbb{R}$. In the OLS cost function the sum of the squared blue line segments is penalized, while in the TLS cost function the sum of the squared red line segments is penalized.

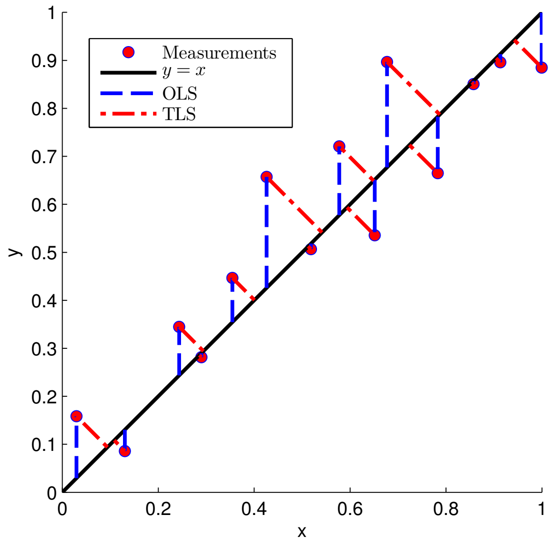

Figure G-1: Simulated measurement data of a system with equation $y = x$. In the OLS cost function the sum of the squared blue line segments is penalized, while in the TLS cost function the sum of the squared red line segments is penalized.

G-2 Simulations

In order to evaluate the LSABS approach, seven simulations are performed by using the pendulum model:

1. Adaptive Backstepping with one unknown parameter;
2. Adaptive Backstepping with one unknown time-varying parameter;
3. Adaptive Backstepping with three unknown parameters;
4. Adaptive Incremental Backstepping with one unknown parameter;
5. Adaptive Incremental Backstepping with one unknown time-varying parameter;
6. Adaptive Incremental Backstepping with three unknown parameters;
7. Adaptive Incremental Backstepping with Time-Scale Separation.

G-2-1 Adaptive Backstepping with one unknown parameter

In this section a Least-Squares estimator is combined with a BS controller by using the certainty equivalence principle. The pendulum model is for convenience repeated below:

$$\dot{x}_1 = x_2 \tag{B-3a revisited}$$

$$\dot{x}_2 = \theta_{2,1}\sin(x_1) + \theta_{2,2}x_2 + \theta_{2,3}u\,, \tag{B-3b revisited}$$

where we assume $\theta_{2,2}$ is an unknown *constant* parameter. The control task is to track the smooth reference state $x_{1,r}$ with the state x_1. At time k the following vector equation can be constructed from Eq. (B-3b) by using the past N measurements:

$$\begin{bmatrix} \dot{x}_{2,k-N} \\ \vdots \\ \dot{x}_{2,k-1} \\ \dot{x}_{2,k} \end{bmatrix} = \begin{bmatrix} \sin(x_{1,k-N}) & x_{2,k-N} & u_{k-N} \\ \vdots & \vdots & \vdots \\ \sin(x_{1,k-1}) & x_{2,k-1} & u_{k-1} \\ \sin(x_{1,k}) & x_{2,k} & u_k \end{bmatrix} \begin{bmatrix} \theta_{2,1} \\ \theta_{2,2} \\ \theta_{2,3} \end{bmatrix}, \tag{G-35}$$

which can be rewritten as

$$\underbrace{\begin{bmatrix} \dot{x}_{2,k-N} - \sin(x_{1,k-N})\theta_{2,1} - u_{k-N}\theta_{2,3} \\ \vdots \\ \dot{x}_{2,k-1} - \sin(x_{1,k-1})\theta_{2,1} - u_{k-1}\theta_{2,3} \\ \dot{x}_{2,k} - \sin(x_{1,k})\theta_{2,1} - u_k\theta_{2,3} \end{bmatrix}}_{\boldsymbol{y}} = \underbrace{\begin{bmatrix} x_{2,k-N} \\ \vdots \\ x_{2,k-1} \\ x_{2,k} \end{bmatrix}}_{A} \theta_{2,2}\,. \tag{G-36}$$

If we assume measurements or accurate estimates of $\dot{x}_2$, x_1, x_2 and u are available, then parameter $\theta_{2,2}$ can simply be estimated by applying the OLS solution:

$$\hat{\theta}_{2,2} = \left(A^T A\right)^{-1} A^T \boldsymbol{y}\,, \tag{G-21 revisited}$$

where $\hat{\theta}_{2,2}$ is the Least-Squares estimate for $\theta_{2,2}$. Earlier we derived the following control laws for the non-time scale separated system Eq. (B-3):

$$u = \frac{1}{\theta_{2,3}}\left[-c_2 z_2 - z_1 - \theta_{2,1}\sin(x_1) - \theta_{2,2}x_2 + \dot{\alpha}_1\right] \tag{C-39 revisited}$$

$$\Delta u = \frac{1}{\theta_{2,3}}\left[-c_2 z_2 - z_1 - \theta_{2,1}\cos(x_{1,0})\Delta x_1 - \theta_{2,2}\Delta x_2 + \dot{\alpha}_1 - \dot{x}_{2,0}\right]. \tag{E-70 revisited}$$

The corresponding certainty equivalence adaptive controllers when $\theta_{2,2}$ is unknown are simply obtained by replacing the parameter $\theta_{2,2}$ with its estimate $\hat{\theta}_{2,2}$:

$$u = \frac{1}{\theta_{2,3}}\left[-c_2 z_2 - z_1 - \theta_{2,1}\sin(x_1) - \hat{\theta}_{2,2}x_2 + \dot{\alpha}_1\right] \tag{G-37}$$

$$\Delta u = \frac{1}{\theta_{2,3}}\left[-c_2 z_2 - z_1 - \theta_{2,1}\cos(x_{1,0})\Delta x_1 - \hat{\theta}_{2,2}\Delta x_2 + \dot{\alpha}_1 - \dot{x}_{2,0}\right]. \tag{G-38}$$

The adaptive implementation consisting of the LS estimator and control law (G-37) is from now on referred to as LSABS, while the implementation with the LS estimator and control law (G-38) is referred to as Least-Squares Adaptive Incremental Backstepping (LSAIBS).

Because the OLS solution should be calculated on-line, i.e. while the simulation is running, the efficient RLS algorithm has been implemented in `Matlab/Simulink` to obtain the LS solution, see Eq. (G-27).

Simulations of the LSABS and LSAIBS controllers have been run for system (B-3) with one unknown parameter and a sampling time of 0.01 s. The initial conditions and parameters which have been used in this simulation for the model can be found in Eq. (C-44). The following control and estimator parameters have been selected:

$$\begin{aligned} c_1 &= 10\,, & c_2 &= 10\,, \\ \hat{\theta}_{2,1} &= \theta_{2,1}\,, & \hat{\theta}_{2,2}(0) &= -50 \cdot \theta_{2,2}\,, \\ \hat{\theta}_{2,3} &= \theta_{2,3}\,. \end{aligned} \tag{G-39}$$

Different values of the initial parameter variance P_0 have been selected. From Figure G-2 we can clearly see that the LSABS and LSAIBS controllers perform much better compared to the conventional BS controller (C-39) in presence of the introduced parametric uncertainty. The control performance of the LSABS and LSAIBS controllers are nearly identical, this is as expected because the linearization error is small due to the high sampling rate. However, initially the LSAIBS controller performs slightly better because in Eq. (G-38) the uncertainty $\theta_{2,2}$ is multiplied by the small difference variable Δx_2, making this control law more robust to uncertainties. From Figure G-3 we can see that the parameter estimates for the different values of P_0 seem to converge to the real parameter. Increasing the initial parameter variance P_0 results in faster convergence of the parameter estimate, and therefore we can consider this parameter as an adaptation gain similar to what we have seen for the Tuning Function (TF) and Immersion and Invariance (I&I) estimators.

G-2-2 Adaptive Backstepping with one unknown time-varying parameter

In the previous section we assumed that $\theta_{2,2}$ is an unknown *constant* parameter. Now a simulation has been performed in which this parameter changes halfway the simulation, in order to find out how the LS estimator performs in case of an abrupt parameter change. Simulations of the LSABS controller have been run for system (B-3) with one unknown parameter and a sampling time of 0.01 s. The initial conditions and parameters which have been used in this simulation for the model can be found in Eq. (C-44), the control and estimator parameters are similar as in Eq. (F-84). The parameter estimation results can be seen in Figure G-4. Clearly, the LS estimator is not able to cope with the sudden parameter change. This can be explained on basis of the fact that the RLS-based estimate after $t = 15$ s is contaminated by the old data. One way to counteract this problem is to apply RLS with exponential forgetting. From Figure G-4 we can see that by applying RLS with a forgetting factor $\lambda < 1$, the LS estimator is able to cope with the sudden parameter change. However, by decreasing the forgetting factor, the estimator will become more sensitive to noise.

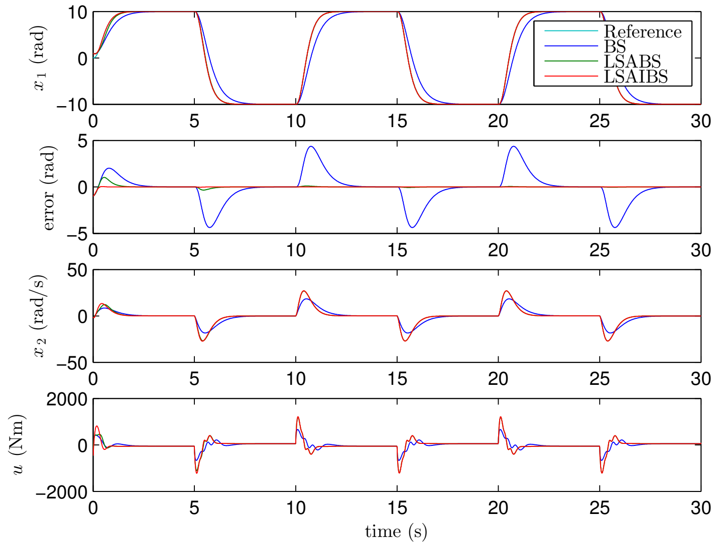

Figure G-2: The control performance of the Least-Squares Adaptive Backstepping controllers with $P_0 = 10^{-3}$ in the presence of a parametric uncertainty.

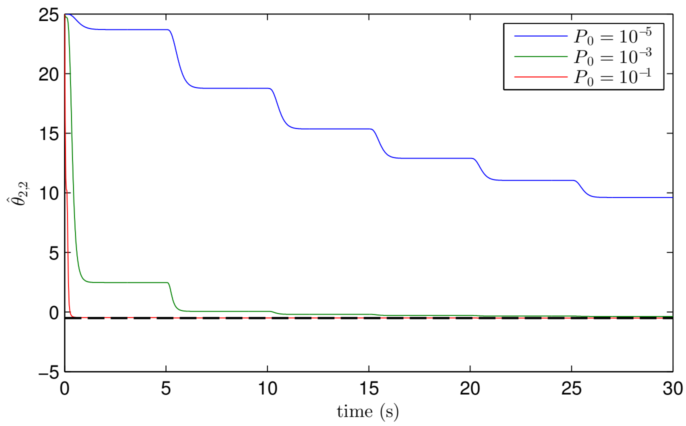

Figure G-3: The performance of the Least-Squares parameter estimator for different values of P_0. The dashed black line represents the value of the real parameter $\theta_{2,2}$.

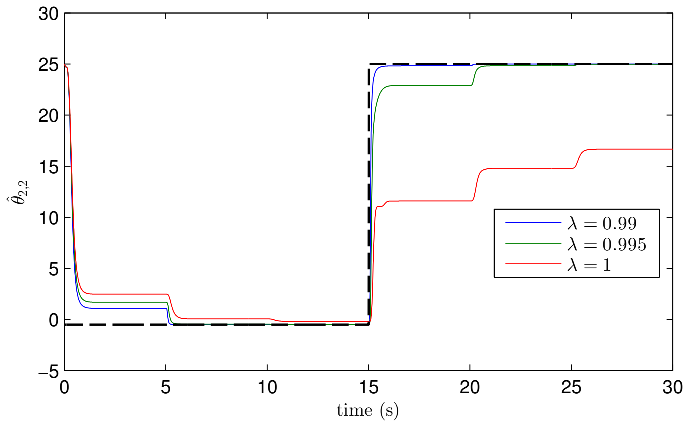

Figure G-4: The performance of the Least-Squares estimator with $P_0 = 10^{-3}$ and different values of the forgetting factor λ in case of an abrupt parameter change. The dashed black line represents the value of the real parameter $\theta_{2,2}$.

Now a simulation is performed in which the uncertain parameter $\theta_{2,2}$ is a linear function of state $x_1(t)$. The simulation has been run for different values of the forgetting factor λ and with $\hat{\theta}_{2,2}(0) = -1$. The initial conditions and parameters which have been used in this simulation for the model can be found in Eq. (C-44). From Figure H-8 we can see that the parameter estimator, which has been derived by assuming a *constant* unknown parameter $\theta_{2,2}$, is able to accurately track the time-varying parameter $\theta_{2,2}(t)$ with a forgetting factor $\lambda < 1$. However, by decreasing the forgetting factor, the estimator will become more sensitive to noise. Therefore it is more judicious to use a function approximator that is capable of approximating the time-varying parameter, in a way similar as explained in Appendix F-2-3.

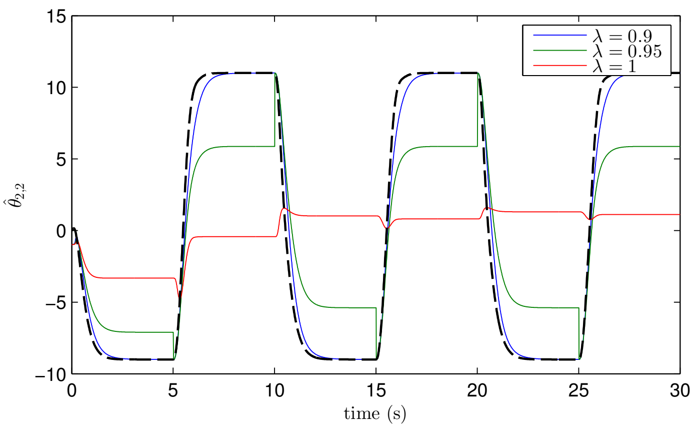

Figure G-5: The performance of the Least-Squares estimator for different values of the forgetting factor λ in case of a time-varying parameter. The dashed black line represents the real parameter $\theta_{2,2}(t)$.

G-2-3 Adaptive Backstepping with three unknown parameters

In this section a LS estimator is combined with a BS controller based on the certainty equivalence principle. The pendulum model is for convenience repeated below:

$$\dot{x}_1 = x_2 \tag{B-3a revisited}$$
$$\dot{x}_2 = \theta_{2,1}\sin(x_1) + \theta_{2,2}x_2 + \theta_{2,3}u\,, \tag{B-3b revisited}$$

where $\theta_{2,1}$, $\theta_{2,2}$ and $\theta_{2,3}$ are assumed to be unknown *constant* parameters. The control task is to track the smooth reference state $x_{1,r}$ with the state x_1. At time k the following vector equation can be constructed from Eq. (B-3b) by using the past N measurements:

$$\underbrace{\begin{bmatrix} \dot{x}_{2,k-N} \\ \vdots \\ \dot{x}_{2,k-1} \\ \dot{x}_{2,k} \end{bmatrix}}_{\boldsymbol{y}} = \underbrace{\begin{bmatrix} \sin(x_{1,k-N}) & x_{2,k-N} & u_{k-N} \\ \vdots & \vdots & \vdots \\ \sin(x_{1,k-1}) & x_{2,k-1} & u_{k-1} \\ \sin(x_{1,k}) & x_{2,k} & u_k \end{bmatrix}}_{A} \underbrace{\begin{bmatrix} \theta_{2,1} \\ \theta_{2,2} \\ \theta_{2,3} \end{bmatrix}}_{\boldsymbol{\theta}_2}\,. \tag{G-41}$$

If we assume measurements or accurate estimates of $\dot{x}_2$, x_1, x_2 and u are available, then parameters $\boldsymbol{\theta}_2$ can simply be estimated by applying the OLS solution:

$$\hat{\boldsymbol{\theta}}_2 = \left(A^T A\right)^{-1} A^T \boldsymbol{y}\,, \tag{G-21 revisited}$$

where $\hat{\boldsymbol{\theta}}_2$ is the Least-Squares estimate for $\boldsymbol{\theta}_2$. Earlier we derived the following (incremental) BS control laws for system (B-3):

$$u = \frac{1}{\theta_{2,3}}\left[-c_2z_2 - z_1 - \theta_{2,1}\sin(x_1) - \theta_{2,2}x_2 + \dot{\alpha}_1\right] \tag{C-39 revisited}$$
$$\Delta u = \frac{1}{\theta_{2,3}}\left[-c_2z_2 - z_1 - \theta_{2,1}\cos(x_{1,0})\Delta x_1 - \theta_{2,2}\Delta x_2 + \dot{\alpha}_1 - \dot{x}_{2,0}\right]. \tag{E-70 revisited}$$

The corresponding certainty equivalence adaptive controllers when the parameters $\boldsymbol{\theta}_2$ are unknown are simply obtained by replacing these parameters by their estimate:

$$u = \frac{1}{\hat{\theta}_{2,3}}\left[-c_2z_2 - z_1 - \hat{\theta}_{2,1}\sin(x_1) - \hat{\theta}_{2,2}x_2 + \dot{\alpha}_1\right] \tag{G-42}$$
$$\Delta u = \frac{1}{\hat{\theta}_{2,3}}\left[-c_2z_2 - z_1 - \hat{\theta}_{2,1}\cos(x_{1,0})\Delta x_1 - \hat{\theta}_{2,2}\Delta x_2 + \dot{\alpha}_1 - \dot{x}_{2,0}\right]. \tag{G-43}$$

The adaptive implementation consisting of the LS estimator and control law (G-42) is referred to as LSABS, while the implementation with the LS estimator and control law (G-43) is referred to as LSAIBS.

Because the OLS solution should be calculated on-line, i.e. while the simulation is running, the efficient RLS algorithm has been implemented in `Matlab/Simulink` to obtain the LS solution, see Eq. (G-27).

Simulations of the BS and Incremental Backstepping (IBS) control laws with and without LS estimator have been run for system (B-3) with three unknown parameters and a sampling time of 0.01 s. The initial conditions and parameters which have been used in this simulation for the model can be found in Eq. (C-44). The following control and estimator parameters have been selected:

$$\begin{aligned} c_1 &= 10\,, & c_2 &= 10\,, \\ P_{0,1} &= 10\,, & \hat{\theta}_{2,1} &= 20 \cdot \theta_{2,1}\,, \\ P_{0,2} &= 0.1\,, & \hat{\theta}_{2,2} &= -20 \cdot \theta_{2,2}\,, \\ P_{0,3} &= 1\,, & \hat{\theta}_{2,3} &= 5 \cdot \theta_{2,3}\,. \end{aligned} \tag{G-44}$$

From Figure G-6 we can clearly see that the IBS, LSABS and LSAIBS controllers perform much better compared to the conventional BS controller (C-39) in presence of the introduced parametric uncertainties. The IBS control law performs better compared to the full-information BS controller because the uncertainties are now multiplied by the very small difference variables Δx_1 and Δx_2. The control performances of the LSABS and LSAIBS controllers are nearly identical after the parameters have converged, this is as expected because the linearization error is small due to the high sampling rate. However, initially the LSAIBS controller performs better compared to the LSABS controller because in Eq. (G-43) the uncertainties are multiplied by small difference variables. From Figure G-7 we can see that the parameter estimates for both the LSABS and LSAIBS controller quickly converge to the real parameters.

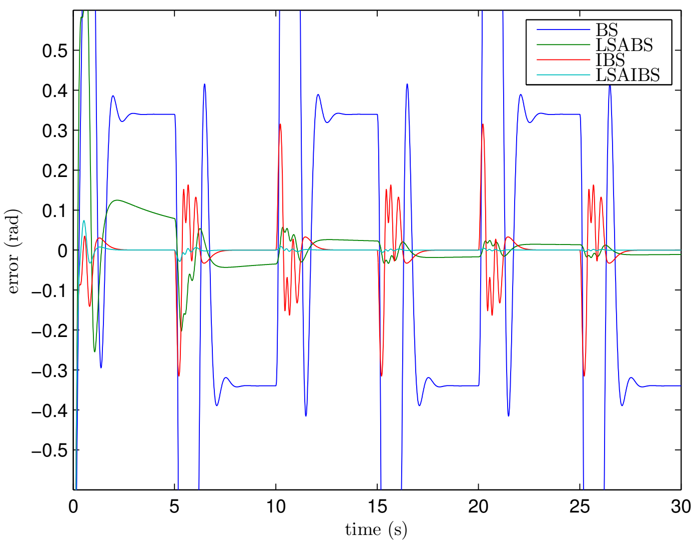

Figure G-6: The tracking errors of two different control laws with and without adaptation in the presence of parametric uncertainties.

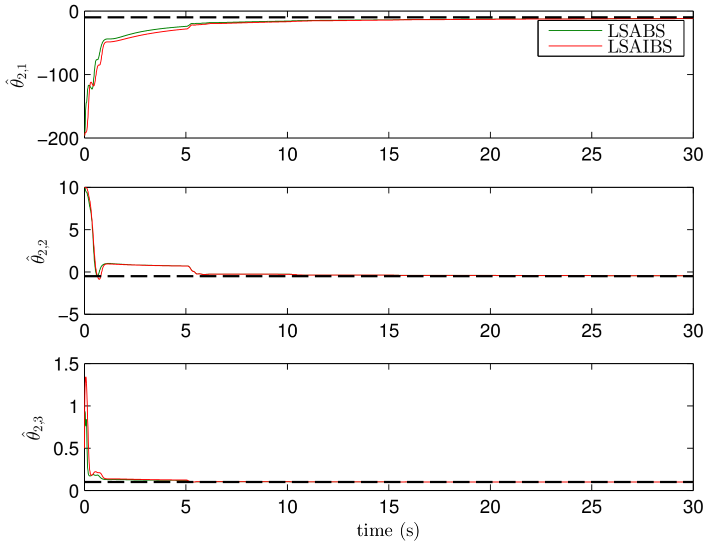

Figure G-7: The performance of the Least-Squares parameter estimators. The dashed black lines represent the value of the real parameter.

G-2-4 Adaptive Incremental Backstepping with one unknown parameter

In this section an incremental LS estimator is combined with a BS controller based on the certainty equivalence principle. Now we consider the following incremental system:

$$\dot{x}_1 = x_2 \qquad \text{(E-66a revisited)}$$
$$\dot{x}_2 = \dot{x}_{2,0} + \theta_{2,1}\cos(x_{1,0})\Delta x_1 + \theta_{2,2}\Delta x_2 + \theta_{2,3}\Delta u\,, \qquad \text{(E-66b revisited)}$$

where we assume $\theta_{2,2}$ is an unknown *constant* parameter. The control task is to track the smooth reference state $x_{1,r}$ with the state x_1. At time k the following vector equation can be constructed from Eq. (E-66b) by using the past N measurements:

$$\begin{bmatrix} \Delta\dot{x}_{2,k-N} \\ \vdots \\ \Delta\dot{x}_{2,k-1} \\ \Delta\dot{x}_{2,k} \end{bmatrix} = \begin{bmatrix} \cos(x_{1,k-N-1})\Delta x_{1,k-N} & \Delta x_{2,k-N} & \Delta u_{k-N} \\ \vdots & \vdots & \vdots \\ \cos(x_{1,k-2})\Delta x_{1,k-1} & \Delta x_{2,k-1} & \Delta u_{k-1} \\ \cos(x_{1,k-1})\Delta x_{1,k} & \Delta x_{2,k} & \Delta u_k \end{bmatrix} \begin{bmatrix} \theta_{2,1} \\ \theta_{2,2} \\ \theta_{2,3} \end{bmatrix}, \qquad \text{(G-46)}$$

which can be rewritten as

$$\underbrace{\begin{bmatrix} \Delta\dot{x}_{2,k-N} - \cos(x_{1,k-N-1})\Delta x_{1,k-N}\theta_{2,1} - \Delta u_{k-N}\theta_{2,3} \\ \vdots \\ \Delta\dot{x}_{2,k-1} - \cos(x_{1,k-2})\Delta x_{1,k-1}\theta_{2,1} - \Delta u_{k-1}\theta_{2,3} \\ \Delta\dot{x}_{2,k} - \cos(x_{1,k-1})\Delta x_{1,k}\theta_{2,1} - \Delta u_k\theta_{2,3} \end{bmatrix}}_{\boldsymbol{y}} = \underbrace{\begin{bmatrix} \Delta x_{2,k-N} \\ \vdots \\ \Delta x_{2,k-1} \\ \Delta x_{2,k} \end{bmatrix}}_{A} \theta_{2,2}\,. \qquad \text{(G-47)}$$

If we assume measurements or accurate estimates of $\dot{x}_2$, x_1, x_2 and u are available, then parameter $\theta_{2,2}$ can simply be estimated by applying the OLS solution:

$$\hat{\theta}_{2,2} = \left(A^T A\right)^{-1} A^T \boldsymbol{y}\,, \qquad \text{(G-21 revisited)}$$

where $\hat{\theta}_{2,2}$ is the Least-Squares estimate for $\theta_{2,2}$. Earlier we derived the following control laws for the non-time scale separated system Eq. (B-3):

$$u = \frac{1}{\theta_{2,3}}\left[-c_2z_2 - z_1 - \theta_{2,1}\sin(x_1) - \theta_{2,2}x_2 + \dot{\alpha}_1\right] \tag{C-39 revisited}$$

$$\Delta u = \frac{1}{\theta_{2,3}}\left[-c_2z_2 - z_1 - \theta_{2,1}\cos(x_{1,0})\Delta x_1 - \theta_{2,2}\Delta x_2 + \dot{\alpha}_1 - \dot{x}_{2,0}\right]. \tag{E-70 revisited}$$

The corresponding certainty equivalence adaptive controllers when $\theta_{2,2}$ is unknown are simply obtained by replacing the parameter $\theta_{2,2}$ with its estimate $\hat{\theta}_{2,2}$:

$$u = \frac{1}{\theta_{2,3}}\left[-c_2z_2 - z_1 - \theta_{2,1}\sin(x_1) - \hat{\theta}_{2,2}x_2 + \dot{\alpha}_1\right] \tag{G-48}$$

$$\Delta u = \frac{1}{\theta_{2,3}}\left[-c_2z_2 - z_1 - \theta_{2,1}\cos(x_{1,0})\Delta x_1 - \hat{\theta}_{2,2}\Delta x_2 + \dot{\alpha}_1 - \dot{x}_{2,0}\right]. \tag{G-49}$$

The adaptive implementation consisting of the incremental estimator and control law (G-48) is from now on referred to as Incremental Parameter Estimation Backstepping (IPEBS), while the implementation with the estimator and control law (G-49) is referred to as Incremental Parameter Estimation Incremental Backstepping (IPEIBS).

Because the OLS solution should be calculated on-line, i.e. while the simulation is running, the efficient RLS algorithm has been implemented in `Matlab/Simulink` to obtain the Least-Squares solution, see Eq. (G-27).

Simulations of the IPEBS and IPEIBS controllers have been run for system (B-3) with one unknown parameter and a sampling time of 0.01 s. The initial conditions and parameters which have been used in this simulation for the model can be found in Eq. (C-44). The following control and estimator parameters have been selected:

$$\begin{aligned} c_1 &= 10\,, & c_2 &= 10\,, \\ \hat{\theta}_{2,1} &= \theta_{2,1}\,, & \hat{\theta}_{2,2}(0) &= -50\cdot\theta_{2,2}\,, \\ \hat{\theta}_{2,3} &= \theta_{2,3}\,. \end{aligned} \tag{G-50}$$

Different values of the initial parameter variance P_0 have been selected. From Figure G-8 we can clearly see that the IPEBS and IPEIBS controllers perform much better compared to the conventional BS controller (C-39) in presence of the introduced parametric uncertainty. The control performance of the IPEBS and IPEIBS controllers are nearly identical, this is as expected because the linearization error is small due to the high sampling rate. From Figure G-9 we can see that the parameter estimates for the different values of P_0 seem to converge to values close to the real parameter. Increasing the initial parameter variance P_0 results in faster convergence of the parameter estimate, and therefore we can consider this parameter as an adaptation gain similar to what we have seen for the TF and I&I estimators.

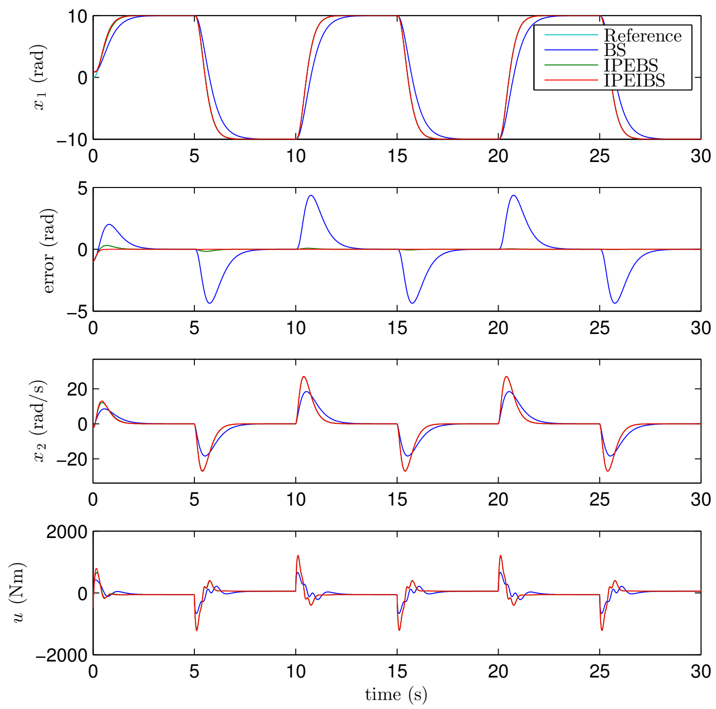

Figure G-8: The control performance of the Incremental Parameter Estimation Backstepping controller with $P_0 = 1$ in the presence of a parametric uncertainty.

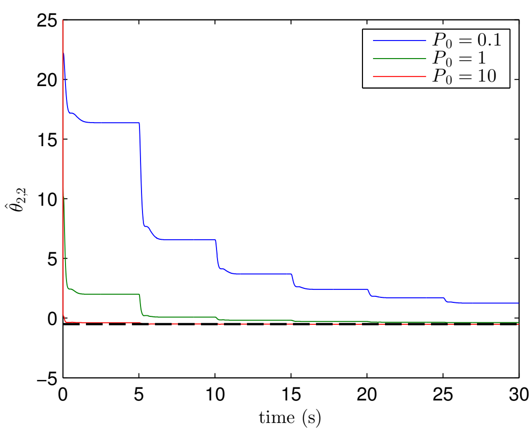

Figure G-9: The performance of the Incremental Parameter Estimator for different values of P_0. The dashed black line represents the value of the real parameter $\theta_{2,2}$.

G-2-5 Adaptive Incremental Backstepping with one unknown time-varying parameter

In the previous section we assumed that $\theta_{2,2}$ is an unknown *constant* parameter. Now a simulation has been performed in which this parameter changes halfway the simulation, in order to find out how the Incremental Parameter Estimator (IPE) performs in case of an abrupt parameter change. Simulations of the IPEBS controller have been run for the system (B-3) with one unknown parameter and a sampling time of 0.01 s. The initial conditions and parameters which have been used in this simulation for the model can be found in Eq. (C-44), the control and estimator parameters are similar as in Eq. (F-84). The estimation results can be seen in Figure G-10. Clearly, the IPE is not able to cope with the sudden parameter change. This can be explained on basis of the fact that the RLS-based estimate after $t = 15$ s is contaminated by the old data.

One way to counteract this problem is to apply RLS with exponential forgetting. From Figure G-10 we can see that by applying RLS with a forgetting factor $\lambda < 1$, the IPE is able to cope with the sudden parameter change. However, by decreasing the forgetting factor, the estimator will become more sensitive to the linearization error and to noise.

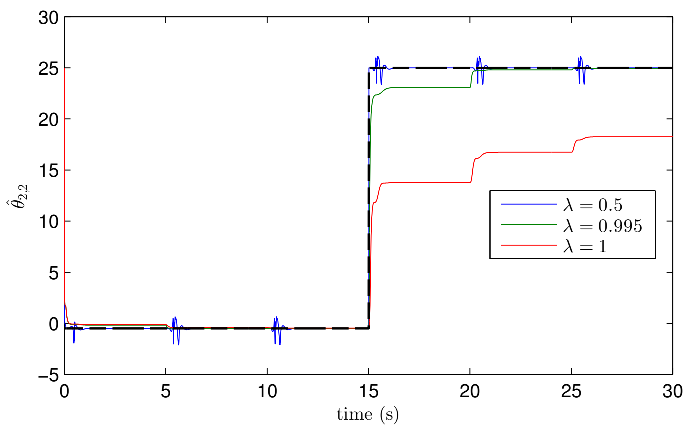

Figure G-10: The performance of the Incremental Parameter Estimator with $P_0 = 5$ and different values of the forgetting factor λ in case of an abrupt parameter change. The dashed black line represents the value of the real parameter $\theta_{2,2}$.

Now a simulation is performed in which the uncertain parameter $\theta_{2,2}$ is a linear function of state $x_1(t)$. The simulation has been run for different values of the forgetting factor λ and with $\hat{\theta}_{2,2}(0) = -1$. The initial conditions and parameters which have been used in this simulation for the model can be found in Eq. (C-44). From Figure H-8 we can see that the parameter estimator, which has been derived by assuming a *constant* unknown parameter $\theta_{2,2}$, is not able to accurately track the time-varying parameter $\theta_{2,2}(t)$. Therefore a function approximator should be used that is capable of approximating the time-varying parameter, in a way similar as explained in Appendix F-2-3.

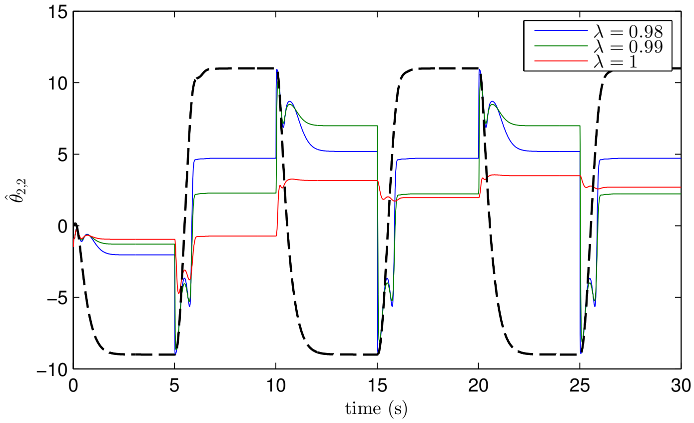

Figure G-11: The performance of the Incremental Parameter Estimator for different values of the forgetting factor λ in case of a time-varying parameter. The dashed black line represents the real parameter $\theta_{2,2}(t)$.

G-2-6 Adaptive Incremental Backstepping with three unknown parameters

In this section an IPE is combined with a BS controller based on the certainty equivalence principle. Again we consider the following incremental system:

$$\dot{x}_1 = x_2 \qquad \text{(E-66a revisited)}$$

$$\dot{x}_2 = \dot{x}_{2,0} + \theta_{2,1}\cos(x_{1,0})\Delta x_1 + \theta_{2,2}\Delta x_2 + \theta_{2,3}\Delta u\,, \qquad \text{(E-66b revisited)}$$

where we assume $\theta_{2,1}$, $\theta_{2,2}$ and $\theta_{2,3}$ are unknown *constant* parameters. The control task is to track the smooth reference state $x_{1,r}$ with the state x_1. At time k the following vector equation can be constructed from Eq. (E-66b) by using the past N measurements:

$$\underbrace{\begin{bmatrix} \Delta\dot{x}_{2,k-N} \\ \vdots \\ \Delta\dot{x}_{2,k-1} \\ \Delta\dot{x}_{2,k} \end{bmatrix}}_{\boldsymbol{y}} = \underbrace{\begin{bmatrix} \cos(x_{1,k-N-1})\Delta x_{1,k-N} & \Delta x_{2,k-N} & \Delta u_{k-N} \\ \vdots & \vdots & \\ \cos(x_{1,k-2})\Delta x_{1,k-1} & \Delta x_{2,k-1} & \Delta u_{k-1} \\ \cos(x_{1,k-1})\Delta x_{1,k} & \Delta x_{2,k} & \Delta u_k \end{bmatrix}}_{A} \underbrace{\begin{bmatrix} \theta_{2,1} \\ \theta_{2,2} \\ \theta_{2,3} \end{bmatrix}}_{\boldsymbol{\theta}_2}. \qquad \text{(G-52)}$$

If we assume measurements or accurate estimates of $\dot{x}_2$, x_1, x_2 and u are available, then parameters $\boldsymbol{\theta}_2$ can simply be estimated by applying the OLS solution:

$$\hat{\boldsymbol{\theta}}_2 = \left(A^T A\right)^{-1} A^T \boldsymbol{y}\,, \qquad \text{(G-21 revisited)}$$

where $\hat{\boldsymbol{\theta}}_2$ is the Least-Squares estimate for $\boldsymbol{\theta}_2$. Earlier we derived the following control laws for the non-time scale separated system Eq. (B-3):

$$u = \frac{1}{\theta_{2,3}}\left[-c_2 z_2 - z_1 - \theta_{2,1}\sin(x_1) - \theta_{2,2}x_2 + \dot{\alpha}_1\right] \qquad \text{(C-39 revisited)}$$

$$\Delta u = \frac{1}{\theta_{2,3}}\left[-c_2 z_2 - z_1 - \theta_{2,1}\cos(x_{1,0})\Delta x_1 - \theta_{2,2}\Delta x_2 + \dot{\alpha}_1 - \dot{x}_{2,0}\right]. \qquad \text{(E-70 revisited)}$$

The corresponding certainty equivalence adaptive controllers when the parameters $\boldsymbol{\theta}_2$ are unknown are simply obtained by replacing these parameters by their estimate:

$$u = \frac{1}{\hat{\theta}_{2,3}} \left[-c_2 z_2 - z_1 - \hat{\theta}_{2,1} \sin(x_1) - \hat{\theta}_{2,2} x_2 + \dot{\alpha}_1 \right] \tag{G-53}$$

$$\Delta u = \frac{1}{\hat{\theta}_{2,3}} \left[-c_2 z_2 - z_1 - \hat{\theta}_{2,1} \cos(x_{1,0}) \Delta x_1 - \hat{\theta}_{2,2} \Delta x_2 + \dot{\alpha}_1 - \dot{x}_{2,0} \right] . \tag{G-54}$$

Because the OLS solution should be calculated on-line, i.e. while the simulation is running, the efficient RLS algorithm has been implemented in `Matlab/Simulink` to obtain the Least-Squares solution, see Eq. (G-27).

Simulations of the BS and IBS control laws with and without IPE have been run for the system (B-3) with three unknown parameters and a sampling time of 0.01 s. The initial conditions and parameters which have been used in this simulation for the model can be found in Eq. (C-44). The following control and estimator parameters have been selected:

$$\begin{aligned} c_1 &= 10\,, & c_2 &= 10\,, \\ P_{0,1} &= 10\,, & \hat{\theta}_{2,1} &= 20 \cdot \theta_{2,1}\,, \\ P_{0,2} &= 0.1\,, & \hat{\theta}_{2,2} &= -20 \cdot \theta_{2,2}\,, \\ P_{0,3} &= 1\,, & \hat{\theta}_{2,3} &= 5 \cdot \theta_{2,3}\,. \end{aligned} \tag{G-55}$$

From Figure G-12 we can clearly see that the IBS, IPEBS and IPEIBS controllers perform much better compared to the conventional BS controller (C-39) in presence of the introduced parametric uncertainties. The IBS control law performs better compared to the full-information BS controller because the uncertainties are now multiplied by the very small difference variables Δx_1 and Δx_2. The IPEIBS controller performs better compared to the IPEBS controller because in Eq. (G-54) the uncertainties are multiplied by small difference variables. From Figure G-13 we can see that the parameter estimates for both the IPEBS and IPEIBS controller quickly converge to the real parameters.

G-2-7 Adaptive Incremental Backstepping with Time-Scale Separation

In this section an IPE is designed and combined with a BS controller based on the certainty equivalence principle for the pendulum system. We now consider the following time-scale separated incremental pendulum model (see Eqs. (E-41) and (E-42)):

$$\dot{x}_1 = x_2 \tag{G-56a}$$

$$\dot{x}_2 = \dot{x}_{2,0} + \theta_{2,3} \Delta u\,, \tag{G-56b}$$

where we assume that $\theta_{2,3}$ is an unknown *constant* parameter.

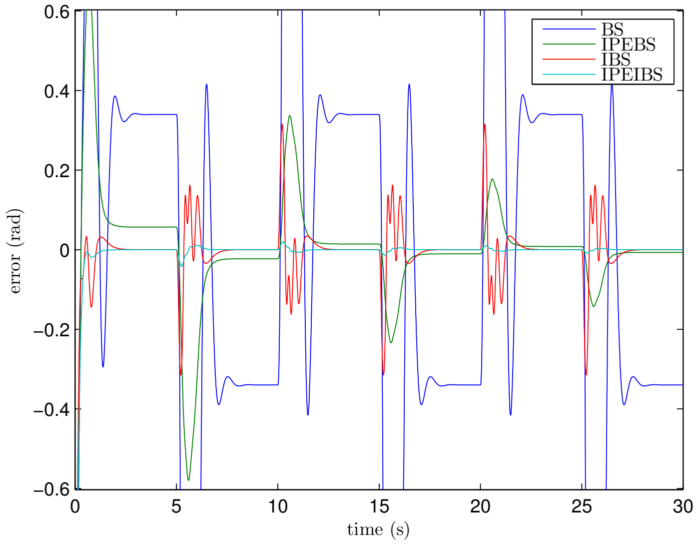

Figure G-12: The tracking errors of two different control laws with and without adaptation in the presence of parametric uncertainties.

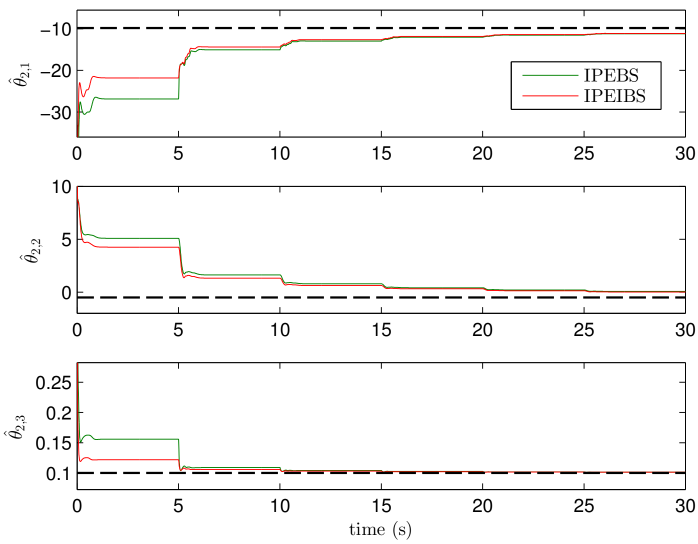

Figure G-13: The performance of the incremental parameter estimators. The dashed black lines represent the value of the real parameter.

Note that Eq. (G-56b) is the incremental form of the full equation of the pendulum, see Eq. (B-3b). At time k the following vector equation can be constructed from Eq. (G-56b) by using the past N measurements:

$$\underbrace{\begin{bmatrix} \Delta\dot{x}_{2,k-N} \\ \vdots \\ \Delta\dot{x}_{2,k-1} \\ \Delta\dot{x}_{2,k} \end{bmatrix}}_{\boldsymbol{y}} \cong \underbrace{\begin{bmatrix} \Delta u_{k-N} \\ \vdots \\ \Delta u_{k-1} \\ \Delta u_{k} \end{bmatrix}}_{A} \theta_{2,3}\,. \tag{G-57}$$

If we assume measurements or accurate estimates of $\dot{x}_2$ and u are available, then parameter $\theta_{2,3}$ can simply be estimated by applying the OLS solution:

$$\hat{\theta}_{2,3} = \left(A^T A\right)^{-1} A^T \boldsymbol{y}\,, \tag{G-21 revisited}$$

where $\hat{\theta}_{2,3}$ is the Least-Squares estimate for $\theta_{2,3}$. Earlier we derived the following control law for the time-scale separated system Eq. (G-56):

$$\Delta u = \frac{1}{\theta_{2,3}} \left[-c_2 z_2 - z_1 + \dot{\alpha}_1 - \dot{x}_{2,0}\right]\,. \tag{E-46 revisited}$$

The corresponding certainty equivalence adaptive controller when the parameter $\theta_{2,3}$ is unknown is simply obtained by replacing this parameter by its estimate:

$$\Delta u = \frac{1}{\hat{\theta}_{2,3}} \left[-c_2 z_2 - z_1 + \dot{\alpha}_1 - \dot{x}_{2,0}\right]\,. \tag{G-58}$$

Note that we can rewrite Eq. (G-57) as follows:

$$\underbrace{\begin{bmatrix} \Delta u_{k-N} \\ \vdots \\ \Delta u_{k-1} \\ \Delta u_{k} \end{bmatrix}}_{\boldsymbol{y}} \cong \underbrace{\begin{bmatrix} \Delta\dot{x}_{2,k-N} \\ \vdots \\ \Delta\dot{x}_{2,k-1} \\ \Delta\dot{x}_{2,k} \end{bmatrix}}_{A} \theta_{2,3}^{-1}\,. \tag{G-59}$$

Now we can determine the *inverse* of the control efficiency parameter directly by applying the OLS solution:

$$\hat{\theta}_{2,3}^{-1} = \left(A^T A\right)^{-1} A^T \boldsymbol{y}\,. \tag{G-60}$$

This approach is computationally more efficient because IBS control law (G-58) depends on the *inverse* of the control efficiency $\theta_{2,3}$. Because the OLS solution should be calculated online, i.e. while the simulation is running, the efficient RLS algorithm has been implemented in `Matlab/Simulink` to obtain the Least-Squares solution, see Eq. (G-27).

Simulations of the IBS control law with and without IPE have been run for the system (B-3) with an unknown control efficiency $\theta_{2,3}$ and a sampling time of 0.01 s. The initial conditions and parameters which have been used in this simulation for the model can be found in Eq. (C-44). The following control and estimator parameters have been selected:

$$
\begin{aligned}
c_1 &= 10\,, & c_2 &= 10\,,\\
P_0 &= 1\cdot 10^{-4}\,, & \hat{\theta}_{2,1} &= \theta_{2,1}\,,\\
\hat{\theta}_{2,2} &= \theta_{2,2}\,, & \hat{\theta}_{2,3} &= 20\cdot\theta_{2,3}\,.
\end{aligned}
\tag{G-61}
$$

From Figure G-14 we can clearly see that the IBS and IPEIBS controllers perform much better compared to the conventional BS controller (C-39) in presence of the introduced parametric uncertainty. The IBS control law performs better compared to the full-information BS controller because the uncertainties are now multiplied by the very small difference variables Δx_1 and Δx_2. From Figure G-15 we can see that the parameter estimate for the IPEIBS controller quickly converges to the real parameter.

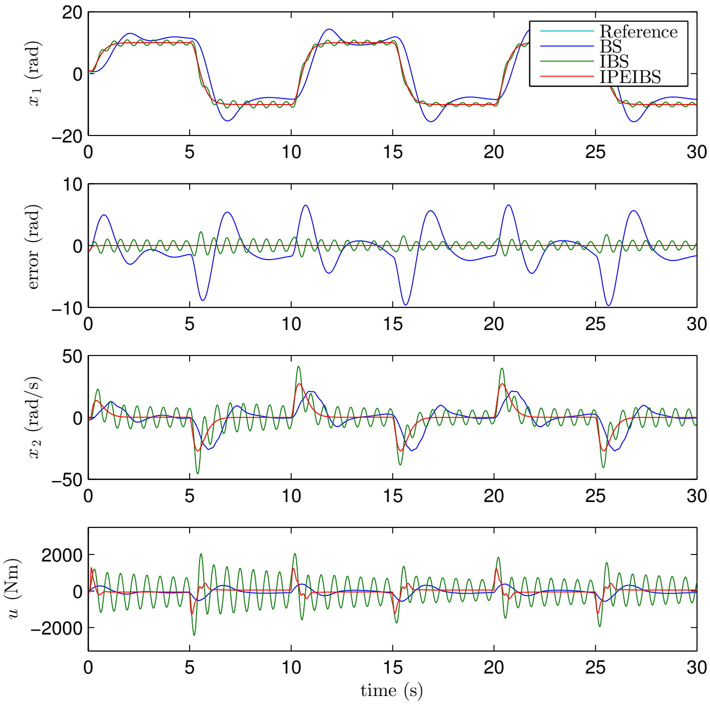

Figure G-14: The control performance of the Incremental Parameter Estimation Backstepping controller with Time-Scale Separation and $P_0 = 1\cdot 10^{-4}$.

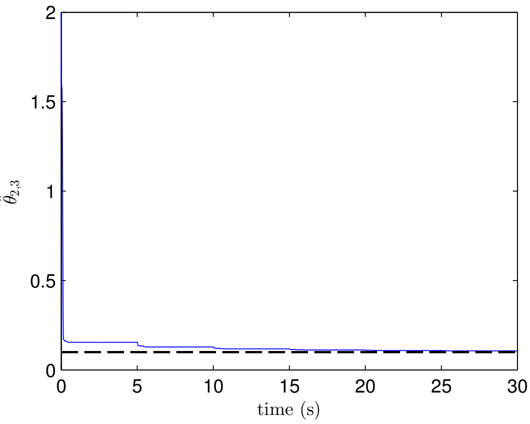

Figure G-15: The performance of the Incremental Parameter Estimator with Time-Scale Separation. The dashed black line represents the value of the real parameter $\theta_{2,3}$.

Appendix H

Immersion and Invariance Adaptive Backstepping

In this appendix the Immersion and Invariance Adaptive Backstepping (IIABS) control approach is derived and evaluated that makes use of update laws that are based on Immersion and Invariance (I&I). This control technique guarantees asymptotic stability of the closed-loop system and parameter convergence for uncertain nonlinear systems (H-1). In order to evaluate this nonlinear control approach, IIABS control laws are derived and simulated for the pendulum model (H-2).

H-1 Theory

We consider the following cascaded nonlinear system:

$$\dot{\boldsymbol{x}}_1 = \boldsymbol{h}(\boldsymbol{x}_1, \boldsymbol{x}_2) + K(\boldsymbol{x}_1, \boldsymbol{x}_2)\boldsymbol{x}_2 \tag{H-1a}$$

$$\dot{\boldsymbol{x}}_2 = \boldsymbol{f}(\boldsymbol{x}_1, \boldsymbol{x}_2) + G(\boldsymbol{x}_1, \boldsymbol{x}_2)\boldsymbol{u}\,, \tag{H-1b}$$

where $\boldsymbol{x}_1 \in \mathbb{R}^{n_1}$ and $\boldsymbol{x}_2 \in \mathbb{R}^{n_2}$ are the state vectors, $\boldsymbol{u} \in \mathbb{R}^m$ is the input vector, $\boldsymbol{h}$ is a known and $\boldsymbol{f}$ an unknown smooth vector field on respectively $\mathbb{R}^{n_1}$ and $\mathbb{R}^{n_2}$, and $K \in \mathbb{R}^{n_1 \times n_2}$ is a known and $G \in \mathbb{R}^{n_2 \times m}$ an unknown matrix whose columns are smooth vector fields. The control task is to track a smooth reference signal $\boldsymbol{x}_{1,r}$, for which the time derivative is assumed to be known and bounded. Furthermore, the signal $\boldsymbol{x}_2$ must remain bounded. It is assumed that the $\boldsymbol{x}_1$-subsystem is fully known while subsystem $\boldsymbol{x}_2$ contains uncertainties. This is a valid assumption in many aerospace control applications, because the $\boldsymbol{x}_1$-subsystem generally contains the *known* kinematic equations, while subsystem $\boldsymbol{x}_2$ contains the *uncertain* dynamic equations.

It is assumed that Eq. (H-1b) can be written as follows to facilitate the design procedure of the I&I estimator:

$$\dot{x}_{2,i} = f_i(\boldsymbol{x}_1, \boldsymbol{x}_2, \boldsymbol{u}) + \boldsymbol{\varphi}_i(\boldsymbol{x}_1, x_{2,1}, \ldots, x_{2,i}, \boldsymbol{u})^T \boldsymbol{\theta}\,, \qquad \text{for } i = 1, \ldots, n_2 \tag{H-2a}$$

$$\dot{\boldsymbol{\xi}}_i = \boldsymbol{w}_i\,, \tag{H-2b}$$

where f_i represents the certain part of system (H-1b), $\boldsymbol{\varphi}_i \in \mathbb{R}^r$ are the smooth and known regressor functions, $\boldsymbol{\theta} \in \mathbb{R}^r$ is a vector with unknown *constant* parameters, $\boldsymbol{\xi}_i \in \mathbb{R}^r$ is the estimator state and $\boldsymbol{w}_i \in \mathbb{R}^r$ is the update law to be determined. The design of the *overparameterized* I&I estimator of order $n_2 \times r$ starts by defining the estimation errors as

$$\boldsymbol{\sigma}_i = \boldsymbol{\xi}_i + \boldsymbol{\beta}_i\left(\boldsymbol{x}_1, x_{2,1}, \ldots, x_{2,i}, \boldsymbol{u}\right) - \boldsymbol{\theta}\,, \qquad \text{for } i = 1, \ldots, n_2\,, \tag{H-3}$$

where $\boldsymbol{\beta}_i(\cdot)$ are continuous functions yet to be specified. The dynamics of the estimation error are given by

$$\begin{aligned}
\dot{\boldsymbol{\sigma}}_i &= \dot{\boldsymbol{\xi}}_i + \dot{\boldsymbol{\beta}}_i\left(\boldsymbol{x}_1, x_{2,1}, \ldots, x_{2,i}, \boldsymbol{u}\right) \\
&= \dot{\boldsymbol{\xi}}_i + \frac{\partial \boldsymbol{\beta}_i}{\partial \boldsymbol{x}_1}\dot{\boldsymbol{x}}_1 + \sum_{j=1}^{i} \frac{\partial \boldsymbol{\beta}_i}{\partial x_{2,j}}\dot{x}_{2,j} + \sum_{k=1}^{m} \frac{\partial \boldsymbol{\beta}_i}{\partial u_k}\dot{u}_k \\
&= \dot{\boldsymbol{\xi}}_i + \frac{\partial \boldsymbol{\beta}_i}{\partial \boldsymbol{x}_1}\dot{\boldsymbol{x}}_1 + \sum_{j=1}^{i} \frac{\partial \boldsymbol{\beta}_i}{\partial x_{2,j}}\left[f_j + \boldsymbol{\varphi}_j^T\left(\boldsymbol{\xi}_i + \boldsymbol{\beta}_i - \boldsymbol{\sigma}_i\right)\right] + \sum_{k=1}^{m} \frac{\partial \boldsymbol{\beta}_i}{\partial u_k}\dot{u}_k\,.
\end{aligned} \tag{H-4}$$

The update laws $\boldsymbol{w}_i$ are selected as

$$\boldsymbol{w}_i \equiv \dot{\boldsymbol{\xi}}_i = -\frac{\partial \boldsymbol{\beta}_i}{\partial \boldsymbol{x}_1}\dot{\boldsymbol{x}}_1 - \sum_{j=1}^{i} \frac{\partial \boldsymbol{\beta}_i}{\partial x_{2,j}}\left[f_j + \boldsymbol{\varphi}_j^T\left(\boldsymbol{\xi}_i + \boldsymbol{\beta}_i\right)\right] - \sum_{k=1}^{m} \frac{\partial \boldsymbol{\beta}_i}{\partial u_k}\dot{u}_k\,, \tag{H-5}$$

which yields the following estimator error dynamics:

$$\dot{\boldsymbol{\sigma}}_i = -\sum_{j=1}^{i} \frac{\partial \boldsymbol{\beta}_i}{\partial x_{2,j}}\boldsymbol{\varphi}_j^T \boldsymbol{\sigma}_i\,. \tag{H-6}$$

Note that the update laws $\boldsymbol{w}_i$ are selected such that the estimation error dynamics (H-6) have an equilibrium at zero. In order to obtain an asymptotically converging estimate of each unknown term $\boldsymbol{\varphi}_i^T\boldsymbol{\theta}$, we can select the $\boldsymbol{\beta}_i$-functions as (Karagiannis & Astolfi, 2008a; Sonneveldt, 2010):

$$\boldsymbol{\beta}_i(\boldsymbol{x}_1, x_{2,1}, \ldots, x_{2,i}, \boldsymbol{u}) = \Gamma_i \int_0^{x_{2,i}} \boldsymbol{\varphi}_i(\boldsymbol{x}_1, x_{2,1}, \ldots, x_{2,i-1}, \chi, \boldsymbol{u})\, d\chi + \boldsymbol{\epsilon}_i(x_{2,i})\,, \tag{H-7}$$

where Γ_i is a *positive* diagonal matrix containing the update gain parameters:

$$\Gamma_i = \begin{bmatrix} \gamma_{i,1} & 0 & 0 \\ 0 & \ddots & 0 \\ 0 & 0 & \gamma_{i,r} \end{bmatrix}, \tag{H-8}$$

and where $\boldsymbol{\epsilon}_i$ are continuously differentiable functions that satisfy the partial differential matrix inequality:

$$F_i(\boldsymbol{x}_1, x_{2,1}, \ldots, x_{2,i}, \boldsymbol{u})^T + F_i(\boldsymbol{x}_1, x_{2,1}, \ldots, x_{2,i}, \boldsymbol{u}) \geq 0\,, \tag{H-9}$$

where

$$\begin{aligned} F_i(\boldsymbol{x}_1, x_{2,1}, \ldots, x_{2,i}, \boldsymbol{u}) = \Gamma_i \sum_{j=1}^{i-1} \frac{\partial}{\partial x_{2,j}} \left[\int_0^{x_{2,i}} \boldsymbol{\varphi}_i(\boldsymbol{x}_1, x_{2,1}, \ldots, x_{2,i-1}, \chi, \boldsymbol{u})\, d\chi \right] \\ \cdot\, \boldsymbol{\varphi}_j(\boldsymbol{x}_1, x_{2,1}, \ldots, x_{2,j}, \boldsymbol{u})^T + \frac{\partial \boldsymbol{\epsilon}_i}{\partial x_{2,i}} \boldsymbol{\varphi}_i(\boldsymbol{x}_1, x_{2,1}, \ldots, x_{2,i}, \boldsymbol{u})^T\,. \end{aligned} \tag{H-10}$$

In the special case in which $\boldsymbol{\varphi}_i(\cdot)$ is *not* a function of $x_{2,l}$ for $i \neq l$ and $l = 1, 2, 3$, the trivial solution $\boldsymbol{\epsilon}_i(x_{2,i}) = \mathbf{0}$ satisfies inequality (H-10). The same simplification occurs when only one of the functions $\boldsymbol{\varphi}_i(\cdot)$ is non-zero. In general, it is not easy to find functions $\boldsymbol{\epsilon}_i$ that satisfy Eq. (H-10). The problem of finding the $\boldsymbol{\epsilon}_i$-functions can be prevented by using dynamic scaling and output filters, which is demonstrated in (Karagiannis & Astolfi, 2008b; Sonneveldt, 2010).

In order to proof that the I&I estimator (H-5) and (H-7) yields an asymptotically converging estimate of each unknown term $\boldsymbol{\varphi}_i^T \boldsymbol{\theta}$, we consider the following Lyapunov function:

$$\mathcal{V}(\boldsymbol{\sigma}) = \sum_{i=1}^{n_2} \boldsymbol{\sigma}_i^T \boldsymbol{\sigma}_i\,. \tag{H-11}$$

Taking the time derivative of $\mathcal{V}$ along the trajectories of Eq. (H-6) yields

$$\dot{\mathcal{V}} = -2 \sum_{i=1}^{n_2} \boldsymbol{\sigma}_i^T \left[\sum_{j=1}^{i} \frac{\partial \boldsymbol{\beta}_i}{\partial x_{2,j}} \boldsymbol{\varphi}_j^T \right] \boldsymbol{\sigma}_i\,. \tag{H-12}$$

Note that the term between the square brackets can be written as

$$\begin{aligned} \sum_{j=1}^{i} \frac{\partial \boldsymbol{\beta}_i}{\partial x_{2,j}} \boldsymbol{\varphi}_j^T &= \sum_{j=1}^{i-1} \frac{\partial}{\partial x_{2,j}} \left[\Gamma_i \int_0^{x_{2,i}} \boldsymbol{\varphi}_i(\boldsymbol{x}_1, x_{2,1}, \ldots, x_{2,i-1}, \chi, \boldsymbol{u}) d\chi \right] \boldsymbol{\varphi}_j(\boldsymbol{x}_1, x_{2,1}, \ldots, x_{2,j}, \boldsymbol{u})^T \\ &\quad + \frac{\partial}{\partial x_{2,i}} \left[\Gamma_i \int_0^{x_{2,i}} \boldsymbol{\varphi}_i(\boldsymbol{x}_1, x_{2,1}, \ldots, x_{2,i-1}, \chi, \boldsymbol{u}) d\chi + \boldsymbol{\epsilon}_i(x_{2,i}) \right] \\ &\qquad \cdot\, \boldsymbol{\varphi}_i(\boldsymbol{x}_1, x_{2,1}, \ldots, x_{2,i}, \boldsymbol{u})^T \\ &= \sum_{j=1}^{i-1} \frac{\partial}{\partial x_{2,j}} \left[\Gamma_i \int_0^{x_{2,i}} \boldsymbol{\varphi}_i(\boldsymbol{x}_1, x_{2,1}, \ldots, x_{2,i-1}, \chi, \boldsymbol{u}) d\chi \right] \cdot \boldsymbol{\varphi}_j(\boldsymbol{x}_1, x_{2,1}, \ldots, x_{2,j}, \boldsymbol{u})^T \\ &\quad + \Gamma_i \boldsymbol{\varphi}_i(\boldsymbol{x}_1, x_{2,1}, \ldots, x_{2,i}, \boldsymbol{u}) \boldsymbol{\varphi}_i(\boldsymbol{x}_1, x_{2,1}, \ldots, x_{2,i}, \boldsymbol{u})^T \\ &\quad + \frac{\partial \boldsymbol{\epsilon}_i(x_{2,i})}{\partial x_{2,i}} \boldsymbol{\varphi}_i(\boldsymbol{x}_1, x_{2,1}, \ldots, x_{2,i}, \boldsymbol{u})^T \\ &= \Gamma_i \boldsymbol{\varphi}_i(\boldsymbol{x}_1, x_{2,1}, \ldots, x_{2,i}, \boldsymbol{u}) \boldsymbol{\varphi}_i(\boldsymbol{x}_1, x_{2,1}, \ldots, x_{2,i}, \boldsymbol{u})^T + F_i\,. \end{aligned} \tag{H-13}$$

Therefore the time derivative of $\mathcal{V}$ along the trajectories of Eq. (H-6) becomes

$$\begin{aligned}\dot{\mathcal{V}} &= -2\sum_{i=1}^{n_2}\boldsymbol{\sigma}_i^T\Big[\Gamma_i\boldsymbol{\varphi}_i(\boldsymbol{x}_1,x_{2,1},\ldots,x_{2,i},\boldsymbol{u})\boldsymbol{\varphi}_i(\boldsymbol{x}_1,x_{2,1},\ldots,x_{2,i},\boldsymbol{u})^T+F_i\Big]\boldsymbol{\sigma}_i\\ &= -\sum_{i=1}^{n_2}\boldsymbol{\sigma}_i^T\Big[2\Gamma_i\boldsymbol{\varphi}_i(\boldsymbol{x}_1,x_{2,1},\ldots,x_{2,i},\boldsymbol{u})\boldsymbol{\varphi}_i(\boldsymbol{x}_1,x_{2,1},\ldots,x_{2,i},\boldsymbol{u})^T+F_i^T+F_i\Big]\boldsymbol{\sigma}_i\\ &\le -2\sum_{i=1}^{n_2}\boldsymbol{\sigma}_i^T\Big[\Gamma_i\boldsymbol{\varphi}_i(\boldsymbol{x}_1,x_{2,1},\ldots,x_{2,i},\boldsymbol{u})\boldsymbol{\varphi}_i(\boldsymbol{x}_1,x_{2,1},\ldots,x_{2,i},\boldsymbol{u})^T\Big]\boldsymbol{\sigma}_i\\ &\le -2\sum_{i=1}^{n_2}\boldsymbol{\varphi}_i(\boldsymbol{x}_1,x_{2,1},\ldots,x_{2,i},\boldsymbol{u})^T\Gamma_i\boldsymbol{\sigma}_i\boldsymbol{\varphi}_i(\boldsymbol{x}_1,x_{2,1},\ldots,x_{2,i},\boldsymbol{u})^T\boldsymbol{\sigma}_i\,,\end{aligned}\tag{H-14}$$

where $\boldsymbol{\sigma}_i^T F_i\boldsymbol{\sigma}_i = \boldsymbol{\sigma}_i^T\left[0.5F_i^T+0.5F_i\right]\boldsymbol{\sigma}_i$ and Eq. (H-9) were used. By the theorem of *LaSalle-Yoshizawa* (see e.g. Theorem B.9 in (Sonneveldt, 2010)) it now follows that the equilibrium $\boldsymbol{\varphi}_i^T\boldsymbol{\sigma}_i$ is globally uniformly asymptotically stable.

The (Command-Filtered, Incremental) Backstepping (BS) control law for system (H-1) is derived as explained in Appendices C to E. The *adaptive* control law based on the I&I estimator is then obtained by replacing the unknown terms $\boldsymbol{\varphi}_i^T\boldsymbol{\theta}$ by their estimates $\boldsymbol{\varphi}_i^T(\boldsymbol{\xi}_i+\boldsymbol{\beta}_i)$. Stability of the closed-loop system can then be proved by using the following Lyapunov function $\mathcal{V}(\bar{\boldsymbol{z}},\boldsymbol{\sigma})=\sum_{i=1}^{n_2}\boldsymbol{\sigma}_i^T\boldsymbol{\sigma}_i+\sum_{j=1}^{2}\bar{\boldsymbol{z}}_j^T\bar{\boldsymbol{z}}_j$, see e.g. (Sonneveldt, 2010). This approach is also illustrated in the next section.

H-2 Simulations

In order to evaluate the IIABS approach, seven simulations are performed by using the pendulum model:

1. Adaptive Backstepping for one unknown parameter;
2. Command-Filtered Adaptive Backstepping with one unknown parameter;
3. Adaptive Backstepping with one unknown time-varying parameter;
4. Adaptive Backstepping with two unknown parameters;
5. Command-Filtered Adaptive Backstepping with three unknown parameters;
6. Command-Filtered Adaptive Incremental Backstepping with Time-Scale Separation;
7. Command-Filtered Adaptive Incremental Backstepping without Time-Scale Separation.

H-2-1 Adaptive Backstepping with one unknown parameter

In this section an I&I estimator is combined with a BS controller to guarantee global asymptotic stability of the closed-loop system and parameter convergence for an uncertain nonlinear system. Now we assume $\theta_{2,2}$ is an unknown *constant* parameter, and consider the following augmented pendulum model:

$$\dot{x}_1 = x_2 \tag{H-15a}$$
$$\dot{x}_2 = \theta_{2,1}\sin(x_1) + \theta_{2,2}x_2 + \theta_{2,3}u \tag{H-15b}$$
$$\dot{\xi}_{2,2} = w\,, \tag{H-15c}$$

in which $\xi_{2,2} \in \mathbb{R}$ is the estimator state and w is the update law to be determined. The control task is to track the smooth reference state $x_{1,r}$ with the state x_1. Now we introduce the following one-dimensional manifold:

$$\mathcal{M} = \left\{(\boldsymbol{x}, \xi_{2,2}) \in \mathbb{R}^3 | \xi_{2,2} + \beta_2(\boldsymbol{x}) - \theta_{2,2} = 0\right\}\,, \tag{H-16}$$

where $\beta_2(\boldsymbol{x})$ is a continuous function yet to be specified. The estimate of the unknown constant $\theta_{2,2}$ is given by

$$\hat{\theta}_{2,2} = \xi_{2,2} + \beta_2\,. \tag{H-17}$$

If the manifold $\mathcal{M}$ is *invariant* (see Definition H.1), the dynamics of the $\boldsymbol{x}$-subsystem of (H-15) restricted to this manifold can be written as

$$\dot{x}_1 = x_2 \tag{H-18a}$$
$$\dot{x}_2 = \theta_{2,1}\sin(x_1) + \left(\xi_{2,2} + \beta_2(\boldsymbol{x})\right)x_2 + \theta_{2,3}u\,. \tag{H-18b}$$

Definition H.1 (Invariant Manifold)
The manifold $\mathcal{M} = \{\boldsymbol{x} \in \mathbb{R}^n | \boldsymbol{s}(\boldsymbol{x}) = \boldsymbol{0}\}$, with $\boldsymbol{s}(\boldsymbol{x})$ smooth, is said to be (positively) invariant for $\dot{\boldsymbol{x}} = \boldsymbol{f}(\boldsymbol{x})$ if $\boldsymbol{s}(\boldsymbol{x}(0)) = \boldsymbol{0}$, which implies $\boldsymbol{s}(\boldsymbol{x}(t)) = \boldsymbol{0}$, for all $t \geq 0$.

The dynamics of this system are completely known, i.e. the dynamics are independent of the unknown parameter $\theta_{2,2}$. Now we define the off-the-manifold coordinate:

$$\sigma_2 = \hat{\theta}_{2,2} - \theta_{2,2} = \xi_{2,2} + \beta_2 - \theta_{2,2}\,, \tag{H-19}$$

which plays the role of estimation error. The off-the-manifold dynamics are given by

$$\dot{\sigma}_2 = w + \frac{\partial \beta_2}{\partial x_1}\dot{x}_1 + \frac{\partial \beta_2}{\partial x_2}\dot{x}_2\,. \tag{H-20}$$

Substituting Eqs. (H-15a), (H-15b) and (H-19) into Eq. (H-20) results in

$$\dot{\sigma}_2 = w + \frac{\partial \beta_2}{\partial x_1}x_2 + \frac{\partial \beta_2}{\partial x_2}\left[\theta_{2,1}\sin(x_1) + \left(\xi_{2,2} + \beta_2(\boldsymbol{x}) - \sigma_2\right)x_2 + \theta_{2,3}u\right]\,. \tag{H-21}$$

To render the manifold $\mathcal{M}$ invariant, the following update law is selected:

$$w = \dot{\xi}_{2,2} = -\frac{\partial \beta_2}{\partial x_1} x_2 - \frac{\partial \beta_2}{\partial x_2} \left[\theta_{2,1} \sin(x_1) + (\xi_{2,2} + \beta_2(\boldsymbol{x}))\, x_2 + \theta_{2,3} u\right] , \tag{H-22}$$

which results in the following off-the-manifold dynamics:

$$\dot{\sigma}_2 = -\frac{\partial \beta_2}{\partial x_2} \sigma_2 x_2 \,. \tag{H-23}$$

The Lyapunov function is now constructed as

$$\mathcal{V}(\sigma_2) = \frac{1}{2\gamma_2} \sigma_2^2 , \quad \gamma_2 > 0 , \tag{H-24}$$

where γ_2 is the adaptation gain. Taking the time derivative of this function along the trajectories of Eq. (H-23) results in

$$\dot{\mathcal{V}} = -\frac{1}{\gamma_2} \frac{\partial \beta_2}{\partial x_2} \sigma_2^2 x_2 \,. \tag{H-25}$$

To render $\dot{\mathcal{V}}$ negative definite, the following nonlinear function is selected:

$$\beta_2 = \frac{\gamma_2}{2} x_2^2 \to \frac{\partial \beta_2}{\partial x_2} = \gamma_2 x_2 , \tag{H-26}$$

which results in

$$\dot{\mathcal{V}} = -\left(x_2 \sigma_2\right)^2 , \tag{H-27}$$

and

$$\dot{\sigma}_2 = -\gamma_2 x_2^2 \sigma_2 \,. \tag{H-28}$$

Note that the dynamics of the parameter estimation error σ_2 are described by a first-order linear ordinary, homogeneous differential equation with a time-varying coefficient. The well-known solution to this differential equation is

$$\sigma_2(t) = \sigma_2(0) e^{-\gamma_2 \int_0^t x_2(\xi)^2 \, d\xi} , \tag{H-29}$$

which indicates that the parameter estimation error is a monotonically non-increasing function. Note that overparameterization of the derived I&I estimator is eliminated since we are dealing with only one uncertain equation.

Now we have succeeded in making the manifold $\mathcal{M}$ attractive and invariant. The next task is to find a BS control law such that the closed-loop system globally asymptotically tracks the reference signal $x_{1,r}$, whose derivatives are known and bounded.

We start by introducing the following tracking errors:

$$z_1 = x_1 - x_{1,r} \tag{H-30a}$$

$$z_2 = x_2 - \alpha_1 \,. \tag{H-30b}$$

The derivations for subsystem x_1 remain exactly the same as in Appendix C-3 (see Eqs. (C-32) to (C-36)), because this subsystem is assumed to be fully known. Therefore we directly move on to the second and final subsystem. We can rewrite this system by using the definition of the off-the-manifold coordinate, resulting in:

$$\dot{z}_2 = \theta_{2,1} \sin(x_1) + (\xi_{2,2} + \beta_2 - \sigma_2)\, x_2 + \theta_{2,3} u - \dot{\alpha}_1 \,. \tag{H-31}$$

Now the following real control u is introduced:

$$\begin{aligned} u &= \frac{1}{\theta_{2,3}} \left[-\rho - \theta_{2,1} \sin(x_1) - \hat{\theta}_{2,2} x_2 + \dot{\alpha}_1 \right] \\ &= \frac{1}{\theta_{2,3}} \left[-\rho - \theta_{2,1} \sin(x_1) - (\xi_{2,2} + \beta_2)\, x_2 + \dot{\alpha}_1 \right] , \end{aligned} \tag{H-32}$$

where ρ is a stabilizing function to be defined. This reduces the z_2-dynamics to

$$\dot{z}_2 = -\rho - \sigma_2 x_2 \,. \tag{H-33}$$

Augmenting the quadratic Control Lyapunov Function (CLF) to penalize the second tracking error and the off-the-manifold coordinate yields

$$\mathcal{V}(\boldsymbol{z}, \sigma_2) = \mathcal{V}_1 + z_2^2 + \frac{L}{2\gamma_2} \sigma_2^2 \,, \tag{H-34}$$

where L is a positive constant. Taking the time derivative of $\mathcal{V}$ along the trajectories of the error dynamics and Eq. (H-28) results in

$$\begin{aligned} \dot{\mathcal{V}} &= -2c_1 z_1^2 + 2z_1 z_2 + 2z_2(-\rho - \sigma_2 x_2) + L\sigma_2 \left(-x_2^2 \sigma_2 \right) \\ &= -2c_1 z_1^2 + 2z_1 z_2 - 2z_2 \rho - 2\sigma_2 x_2 z_2 - L\sigma_2^2 x_2^2 \\ &= -2c_1 z_1^2 + 2z_1 z_2 - 2z_2 \rho + \epsilon z_2^2 - \left(\frac{1}{\sqrt{\epsilon}} \sigma_2 x_2 + \sqrt{\epsilon} z_2 \right)^2 - \left(L - \frac{1}{\epsilon} \right) (\sigma_2 x_2)^2 \\ &\leq -2c_1 z_1^2 + 2z_1 z_2 - 2z_2 \rho + \epsilon z_2^2 - \left(L - \frac{1}{\epsilon} \right) (\sigma_2 x_2)^2 \,, \end{aligned} \tag{H-35}$$

where ϵ is a positive constant. The derivative $\dot{\mathcal{V}}$ is made negative definite by using the following expression for the stabilizing function ρ:

$$\rho = z_1 + c_2 z_2, \quad c_2 > 0 \,. \tag{H-36}$$

This renders $\dot{\mathcal{V}}$ into

$$\dot{\mathcal{V}} \leq -2c_1 z_1^2 - (2c_2 - \epsilon)\, z_2^2 - \left(L - \frac{1}{\epsilon} \right) (\sigma_2 x_2)^2 \,. \tag{H-37}$$

By Theorem C.2 it now follows that if $c_2 > \frac{\epsilon}{2}$ and $L > \frac{1}{\epsilon}$, then:

$$\lim_{t\to\infty} z_1 = 0 \to \lim_{t\to\infty} [x_1 - x_{1,r}] = 0 \tag{H-38a}$$

$$\lim_{t\to\infty} z_2 = 0 \tag{H-38b}$$

$$\lim_{t\to\infty} \sigma_2 x_2 = \left(\hat{\theta}_{2,2} - \theta_{2,2} \right) x_2 = 0 \,. \tag{H-38c}$$

Because ϵ and L are arbitrary positive constants, stability is guaranteed when $c_2 > 0$. Note that Eq. (H-38c) does not imply that the estimate $\hat{\theta}_{2,2}$ converges to the real parameter $\theta_{2,2}$. According to (Karagiannis & Astolfi, 2010) this requires a Persistent Excitation (PE) condition, and can be achieved only by injecting "sufficiently rich" reference signals. From Eqs. (H-29) and (H-38c) can be seen that this requires a reference signal that results in $x_2 \neq 0$.

If we substitute Eq. (H-26) into update law (H-22) we obtain:

$$\dot{\xi}_{2,2} = -\gamma_2 x_2 \left[\theta_{2,1}\sin(x_1) + \left(\xi_{2,2} + \frac{\gamma_2}{2}x_2^2\right)x_2 + \theta_{2,3}u\right] . \tag{H-39}$$

By substituting Eq. (H-36) into Eq. (H-32) we find the following control law:

$$u = \frac{1}{\theta_{2,3}}\left[-z_1 - c_2 z_2 - \theta_{2,1}\sin(x_1) - \hat{\theta}_{2,2}x_2 + \dot{\alpha}_1\right] . \tag{H-40}$$

By comparing the new control law with the earlier designed conventional BS controller:

$$u = \frac{1}{\theta_{2,3}}\left[-z_1 - c_2 z_2 - \theta_{2,1}\sin(x_1) - \theta_{2,2}x_2 + \dot{\alpha}_1\right] , \tag{C-39 revisited}$$

we can see that the new control law based on the I&I estimator can simply be obtained from the full-information BS controller by replacing the parameter $\theta_{2,2}$ by its estimate $\hat{\theta}_{2,2}$.

The controller structure developed in this section can be seen in Figure H-1. Note that the I&I-dynamics can be found in Eq. (H-39).

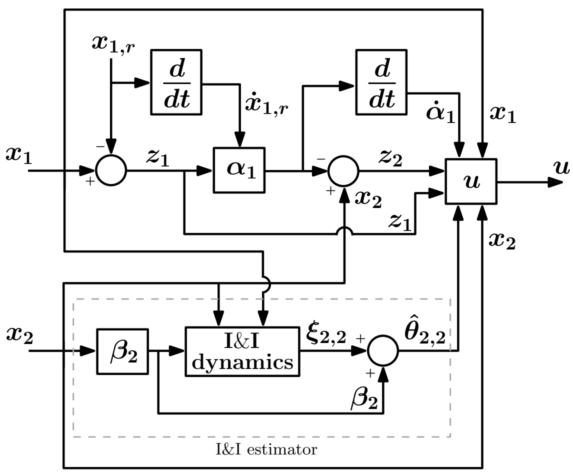

Figure H-1: Immersion & Invariance Adaptive Backstepping controller structure.

Note that the positive constant ϵ, which was introduced in Eq. (H-35), is only used to rewrite $\dot{\mathcal{V}}$ to prove stability of the closed-loop system. The constant ϵ does not turn up in the physical control law (H-40). This is an improvement compared to (Sonneveldt, 2010; Ali, 2013), in which the parameter ϵ is finally transformed into another tuning parameter. In these references the adaptation gain γ_2 also becomes a function of the parameter ϵ, which is not the case for the current derivation. Therefore, the way in which stability has been proved in this section significantly improves the ease of tuning compared to (Sonneveldt, 2010; Ali, 2013).

Simulations of the BS controller augmented with an I&I estimator have been run for system (H-15) with one unknown parameter and a sampling time of 0.01 s. The initial conditions and parameters which have been used in this simulation for the model can be found in Eq. (C-44). The following control and estimator parameters have been selected:

$$
\begin{aligned}
c_1 &= 10\,, & c_2 &= 10\,, \\
\hat{\theta}_{2,1} &= \theta_{2,1}\,, & \xi_{2,2}(0) &= -50 \cdot \theta_{2,2}\,, \\
\hat{\theta}_{2,3} &= \theta_{2,3}\,.
\end{aligned}
\tag{H-41}
$$

Different values of the parameter γ_2 have been selected. Increasing the gain γ_2 results in a better tracking performance as can be seen in Figure H-2. After the parameter estimate has converged, all three controllers are able to accurately follow the reference signal. As expected from Eq. (H-28), increasing the gain γ_2 results in faster convergence of the parameter estimate (see Figure H-3). The trade-off is that sensitivity to noise and actuator dynamics increases (Karagiannis & Astolfi, 2010). Also, if we keep increasing γ_2 without lowering the sample time, the closed-loop system might become unstable due to an unbounded $\dot{\xi}_{2,2}$, see Eq. (H-39). Note from Figure H-3 that the parameter estimation error is monotonically non-increasing, which is as expected from Eq. (H-28). In Figure H-4 we can see that the variables z_1, z_2 and $\sigma_2 x_2$ all converge to 0, which is in accordance with Eq. (H-38).

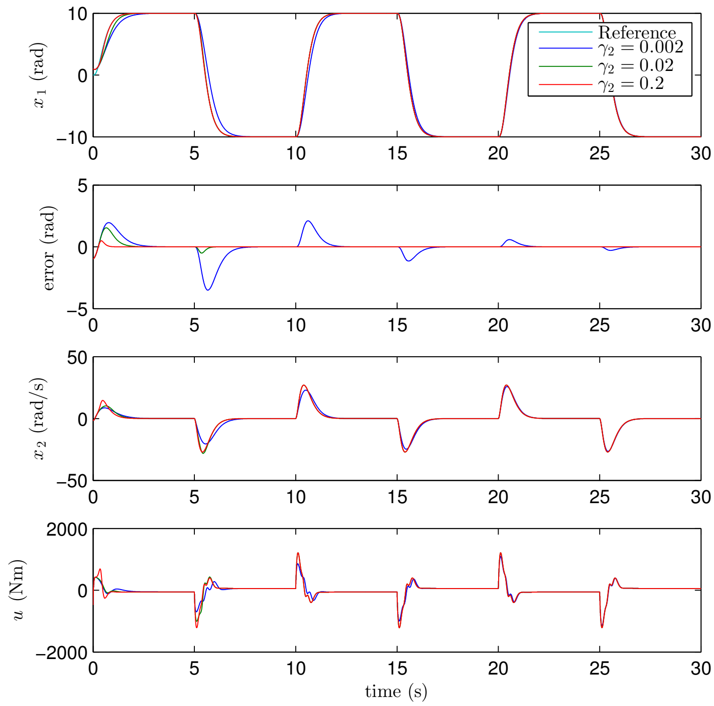

Figure H-2: The control performance of the Backstepping controller augmented with an Immersion & Invariance estimator for different values of γ_2 in the presence of a parametric uncertainty.

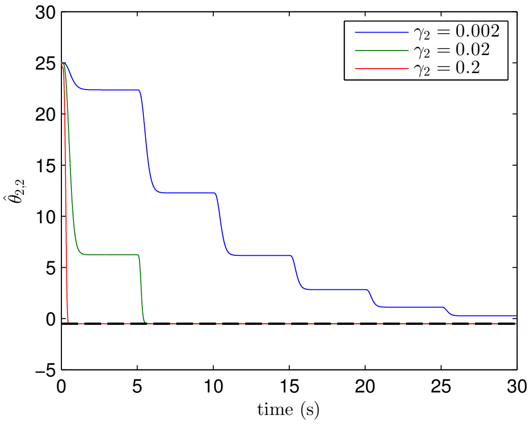

Figure H-3: The performance of the Immersion and Invariance estimator for different values of γ_2. The dashed black line represents the value of the real parameter $\theta_{2,2}$.

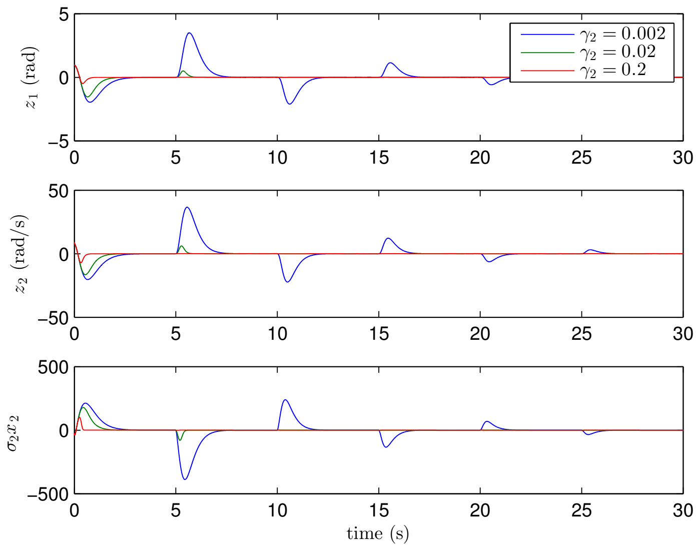

Figure H-4: The control performance of the Backstepping controller augmented with an Immersion & Invariance estimator for different values of γ_2.

Similar as in section (F-2-2), we now introduce a magnitude limit for the control u of $\pm 850\,\mathrm{Nm}$ to find out how this new controller and I&I estimator perform in case of such a limit. The results can be found in Figures H-5 and H-6. The small tracking errors during the maneuver are due to the physical constraints. Clearly, the I&I estimator is *not* influenced by the magnitude limit for the control, as opposed to the Tuning Function (TF) estimator (see Figure F-4). The reason for this is that the I&I update law (H-39) is *not* driven by the tracking error z_2, in contrary to the TF estimator (F-81).

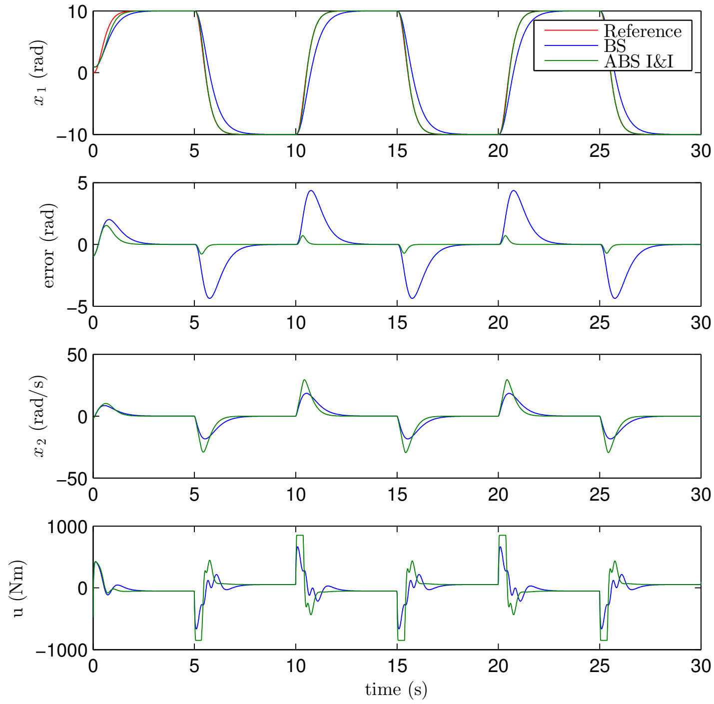

Figure H-5: The control performance of the Backstepping controller with and without an Immersion & Invariance estimator with $\gamma_2 = 0.02$ in the presence of a parametric uncertainty. The control u has been magnitude limited to $\pm 850\,\mathrm{Nm}$.

H-2-2 Command-Filtered Adaptive Backstepping with one unknown parameter

In this section the BS controller will be augmented with command filters to compute the commanded signals and their time derivatives, so that we no longer have to derive the analytical expression of the virtual control derivative. The design of the I&I estimator can be found in the previous section, and is independent of the command filter design. The pendulum model is for convenience repeated below:

$$\dot{x}_1 = x_2 \qquad \text{(B-3a revisited)}$$

$$\dot{x}_2 = \theta_{2,1}\sin(x_1) + \theta_{2,2}x_2 + \theta_{2,3}u\,. \qquad \text{(B-3b revisited)}$$

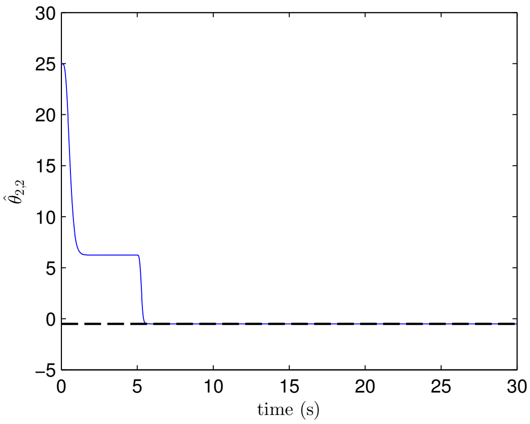

Figure H-6: The performance of the Immersion & Invariance estimator with $\gamma_2 = 0.02$. The control u has been magnitude limited to $\pm 850\,\mathrm{Nm}$. The dashed black line represents the value of the real parameter $\theta_{2,2}$.

The control task is to track the smooth reference state $x_{1,r}$ with the state x_1. Similar as before, we define the following tracking errors:

$$z_1 = x_1 - x_{1,r} \tag{H-43a}$$
$$z_2 = x_2 - x_{2,r}\,, \tag{H-43b}$$

and the *compensated* tracking errors as

$$\bar{z}_1 = z_1 - \chi_1 \tag{H-44a}$$
$$\bar{z}_2 = z_2 - \chi_2\,. \tag{H-44b}$$

The derivations for subsystem x_1 remain exactly the same as in Appendix D-3 (see Eqs. (D-35) to (D-40)), because this subsystem is assumed to be fully known. Therefore we directly move on to the second and final compensated subsystem. The $\bar{z}_2$-dynamics are given by

$$\begin{aligned}\dot{\bar{z}}_2 &= \theta_{2,1}\sin(x_1) + \theta_{2,2}x_2 + \theta_{2,3}u - \dot{x}_{2,r} - \dot{\chi}_2 \\ &= \theta_{2,1}\sin(x_1) + (\xi_{2,2} + \beta_2 - \sigma_2)\,x_2 + \theta_{2,3}u - \dot{x}_{2,r} - \dot{\chi}_2\,.\end{aligned} \tag{H-45}$$

Now we augment the quadratic CLF function to penalize the second compensated error and the off-the-manifold coordinate as well:

$$\mathcal{V}\left(\bar{\boldsymbol{z}}, \sigma_2\right) = \mathcal{V}_1 + \bar{z}_2^2 + \frac{L}{2\gamma_2}\sigma_2^2\,, \tag{H-46}$$

where L is a positive constant. Taking the time derivative of $\mathcal{V}$ along the trajectories of the compensated error dynamics and Eq. (H-28) results in

$$\begin{aligned}\dot{\mathcal{V}} = &-2c_1\bar{z}_1^2 + 2\bar{z}_1\bar{z}_2 + 2\bar{z}_2\left[\theta_{2,1}\sin(x_1) + (\xi_{2,2} + \beta_2 - \sigma_2)\,x_2 + \theta_{2,3}u - \dot{x}_{2,r} - \dot{\chi}_2\right] \\ &-L\sigma_2^2 x_2^2\,.\end{aligned} \tag{H-47}$$

The raw control signal u^0 is led through a command filter to obtain u. The effect that the use of the command filter has on the tracking error z_2 is estimated by the stable linear filter:

$$\dot{\chi}_2 = -c_2\chi_2 + \theta_{2,3}\left(u - u^0\right)\,, \tag{H-48}$$

with $\chi_2(0) = 0$. This yields

$$\begin{aligned}\dot{\mathcal{V}} = &-2c_1\bar{z}_1^2 + 2\bar{z}_1\bar{z}_2 + 2\bar{z}_2\left[\theta_{2,1}\sin(x_1) + (\xi_{2,2} + \beta_2 - \sigma_2)\,x_2 - \dot{x}_{2,r} + c_2\chi_2 + \theta_{2,3}u^0\right] \\ &-L\sigma_2^2 x_2^2\,.\end{aligned} \tag{H-49}$$

Now we select the following raw control law u^0:

$$\begin{aligned}u^0 &= \frac{1}{\theta_{2,3}}\left[-\rho - \theta_{2,1}\sin(x_1) - \hat{\theta}_{2,2}x_2 + \dot{x}_{2,r}\right] \\ &= \frac{1}{\theta_{2,3}}\left[-\rho - \theta_{2,1}\sin(x_1) - (\xi_{2,2} + \beta_2)\,x_2 + \dot{x}_{2,r}\right]\,,\end{aligned} \tag{H-50}$$

where ρ is a stabilizing function to be defined. This yields

$$\begin{aligned}\dot{\mathcal{V}} &= -2c_1\bar{z}_1^2 + 2\bar{z}_1\bar{z}_2 + 2\bar{z}_2\left(-\rho - \sigma_2x_2 + c_2\chi_2\right) - L\sigma_2^2x_2^2 \\ &= -2c_1\bar{z}_1^2 - 2c_2\bar{z}_2^2 + 2\bar{z}_1\bar{z}_2 + 2\bar{z}_2\left(-\rho - \sigma_2x_2 + c_2z_2\right) - L\sigma_2^2x_2^2 \\ &= -2c_1\bar{z}_1^2 - 2c_2\bar{z}_2^2 + 2\bar{z}_1\bar{z}_2 - 2\bar{z}_2\rho + 2c_2z_2\bar{z}_2 - 2\sigma_2x_2\bar{z}_2 - L\sigma_2^2x_2^2 \\ &= -2c_1\bar{z}_1^2 - 2c_2\bar{z}_2^2 + 2\bar{z}_1\bar{z}_2 - 2\bar{z}_2\rho + 2c_2z_2\bar{z}_2 + \epsilon\bar{z}_2^2 - \left(\frac{1}{\sqrt{\epsilon}}\sigma_2x_2 + \sqrt{\epsilon}\bar{z}_2^2\right)^2 \\ &\quad - \left(L - \frac{1}{\epsilon}\right)(\sigma_2x_2)^2 \\ &\leq -2c_1\bar{z}_1^2 - \left(2c_2 - \epsilon\right)\bar{z}_2^2 + 2\bar{z}_1\bar{z}_2 - 2\bar{z}_2\rho + 2c_2z_2\bar{z}_2 - \left(L - \frac{1}{\epsilon}\right)(\sigma_2x_2)^2\,.\end{aligned} \tag{H-51}$$

The derivative $\dot{\mathcal{V}}$ is now made negative definite by using the following expression for the stabilizing function ρ:

$$\rho = \bar{z}_1 + c_2z_2, \quad c_2 > 0\,, \tag{H-52}$$

which yields

$$\dot{\mathcal{V}} \leq -2c_1\bar{z}_1^2 - \left(2c_2 - \epsilon\right)\bar{z}_2^2 - \left(2\gamma - \frac{1}{\epsilon}\right)(\sigma_2x_2)^2\,. \tag{H-53}$$

By Theorem C.2 it now follows that if $c_2 > \frac{\epsilon}{2}$ and $L > \frac{1}{\epsilon}$, then:

$$\lim_{t\to\infty} \bar{\boldsymbol{z}} = \boldsymbol{0} \tag{H-54a}$$

$$\lim_{t\to\infty} \sigma_2x_2 = \left(\hat{\theta}_{2,2} - \theta_{2,2}\right)x_2 = 0\,. \tag{H-54b}$$

Because ϵ and L are arbitrary positive constants, stability of the equilibrium $\bar{\boldsymbol{z}} = \boldsymbol{0}$ is guaranteed when $c_2 > 0$. Note that Eq. (H-54b) does not imply that the estimate $\hat{\theta}_2$ converges to the real parameter θ_2. According to (Karagiannis & Astolfi, 2010) this requires a PE condition, and can be achieved only by injecting "sufficiently rich" reference signals. From Eqs. (H-29) and (H-54b) can be seen that this requires a reference signal that results in $x_2 \neq 0$.

If we compare the new raw control law with the earlier designed conventional BS controller and the BS controller based on the I&I estimator:

$$u^0 = \frac{1}{\theta_{2,3}}\left[-\bar{z}_1 - c_2\left(x_2 - x_{2,r}\right) - \theta_{2,1}\sin(x_1) - \hat{\theta}_{2,2}x_2 + \dot{x}_{2,r}\right] \tag{H-55}$$

$$u = \frac{1}{\theta_{2,3}}\left[-z_1 - c_2\left(x_2 - \alpha_1\right) - \theta_{2,1}\sin(x_1) - \theta_{2,2}x_2 + \dot{\alpha}_1\right] \tag{C-39 revisited}$$

$$u = \frac{1}{\theta_{2,3}}\left[-z_1 - c_2\left(x_2 - \alpha_1\right) - \theta_{2,1}\sin(x_1) - \hat{\theta}_{2,2}x_2 + \dot{\alpha}_1\right], \tag{H-40 revisited}$$

we can see that the new raw Command-Filtered BS control law based on the I&I estimator depends on $x_{2,r}$ and $\dot{x}_{2,r}$, which are the output of the command filter and therefore the analytical derivative $\dot{\alpha}_1$ is no longer required. In the absence of physical limitations (i.e. magnitude, rate and bandwidth constraints on the intermediate state x_2 and control u), convergence of the tracking errors is still guaranteed even when the parameter $\theta_{2,2}$ is an unknown constant.

H-2-3 Adaptive Backstepping with one unknown time-varying parameter

In the two previous sections we assumed that $\theta_{2,2}$ is an unknown *constant* parameter. Now a simulation has been performed in which this parameter changes halfway the simulation, in order to find out how the I&I estimator performs in case of an abrupt parameter change. Simulations of the I&I BS controller have been run for system (B-3) with one unknown parameter and a sampling time of 0.01 s. The initial conditions and parameters which have been used in this simulation for the model can be found in Eq. (C-44), the control and estimator parameters are similar as in Eq. (F-84). The estimation results can be seen in Figure H-7. Clearly, the I&I estimator is able to cope with the sudden parameter change. If we compare the performance of the I&I estimator with that of the TF estimator (see Figure F-8), we can see that the I&I estimator performs better because it does not exhibit any overshoot.

Now a simulation is performed in which the uncertain parameter $\theta_{2,2}$ is a linear function of state $x_1(t)$. The simulation has been run for different values of the adaptation gain γ_2 and with $\hat{\theta}_{2,2}(0) = -1$. The initial conditions and parameters which have been used in this simulation for the model can be found in Eq. (C-44). From Figure H-8 we can see that the parameter estimator, which has been derived by assuming a *constant* unknown parameter $\theta_{2,2}$, is not able to accurately track the time-varying parameter $\theta_{2,2}(t)$. By increasing the adaptation gain, the estimator tracks the changes of parameter $\theta_{2,2}$ more accurately. However, if we keep increasing the adaptation gain the estimator will become unstable, see also the discussion in Appendix H-2-1. Moreover, by increasing the adaptation gain, the sensitivity to noise and actuator dynamics increases (Karagiannis & Astolfi, 2010). A better way to estimate time-varying parameters with I&I estimators is to use function approximators that are capable of approximating the desired function, in a way similar as explained in Appendix F-2-3.

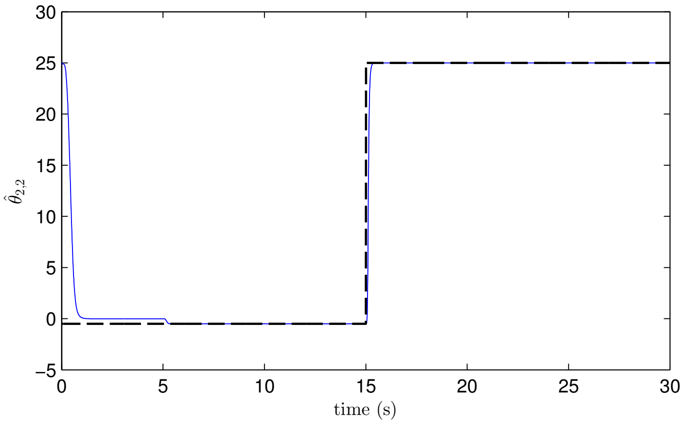

Figure H-7: The performance of the Immersion & Invariance estimator with $\gamma_2 = 0.05$ in case of an abrupt parameter change. The dashed black line represents the value of the real parameter $\theta_{2,2}$.

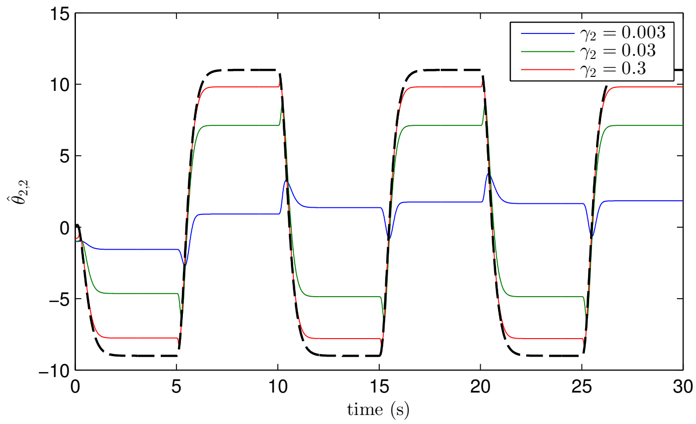

Figure H-8: The performance of the Immersion & Invariance estimator for different values of γ_2 in case of a time-varying parameter. The dashed black line represents the real parameter $\theta_{2,2}(t)$.

H-2-4 Adaptive Backstepping with two unknown parameters

In this section an I&I estimator is combined with a BS controller to guarantee global asymptotic stability of the closed-loop system and parameter convergence for an uncertain nonlinear system. Now we assume $\theta_{2,1}$ and $\theta_{2,2}$ are unknown *constant* parameters, and consider the following augmented pendulum model:

$$\dot{x}_1 = x_2 \tag{H-56a}$$
$$\dot{x}_2 = \theta_{2,1}\sin(x_1) + \theta_{2,2}x_2 + \theta_{2,3}u \tag{H-56b}$$
$$\dot{\boldsymbol{\xi}}_2 = \boldsymbol{w}\,, \tag{H-56c}$$

in which $\boldsymbol{\xi}_2 \in \mathbb{R}^2$ is the estimator state and $\boldsymbol{w}$ is the update law to be determined. The control task is to track the smooth reference state $x_{1,r}$ with the state x_1. The $\boldsymbol{x}$-subsystem can be written as

$$\dot{x}_1 = x_2 + \boldsymbol{\varphi}_1(x_1)^T\boldsymbol{\theta}_2 \tag{H-57a}$$
$$\dot{x}_2 = \theta_{2,3}u + \boldsymbol{\varphi}_2(\boldsymbol{x})^T\boldsymbol{\theta}_2\,, \tag{H-57b}$$

where

$$\boldsymbol{\varphi}_1(x_1) = \begin{bmatrix}0\\0\end{bmatrix}, \quad \boldsymbol{\varphi}_2(\boldsymbol{x}) = \begin{bmatrix}\sin(x_1)\\x_2\end{bmatrix}, \quad \boldsymbol{\theta}_2 = \begin{bmatrix}\theta_{2,1}\\\theta_{2,2}\end{bmatrix}. \tag{H-58}$$

Now we introduce the following two-dimensional manifold:

$$\mathcal{M} = \left\{(\boldsymbol{x},\boldsymbol{\xi}_2) \in \mathbb{R}^4 | \boldsymbol{\xi}_2 + \boldsymbol{\beta}_2(\boldsymbol{x}) - \boldsymbol{\theta}_2 = \boldsymbol{0}\right\}\,, \tag{H-59}$$

where $\boldsymbol{\beta}_2(\boldsymbol{x})$ is a continuous function yet to be specified. The estimate of the unknown constant $\boldsymbol{\theta}_2$ is given by

$$\hat{\boldsymbol{\theta}}_2 = \boldsymbol{\xi}_2 + \boldsymbol{\beta}_2\,. \tag{H-60}$$

If the manifold $\mathcal{M}$ is *invariant* (see Definition H.1 on page 181), the dynamics of the $\boldsymbol{x}$-subsystem of (H-56) restricted to this manifold can be written as

$$\dot{x}_1 = x_2 + \boldsymbol{\varphi}_1(x_1)^T\left(\boldsymbol{\xi}_2 + \boldsymbol{\beta}_2(\boldsymbol{x})\right) \tag{H-61a}$$
$$\dot{x}_2 = \theta_{2,3}u + \boldsymbol{\varphi}_2(\boldsymbol{x})^T\left(\boldsymbol{\xi}_2 + \boldsymbol{\beta}_2(\boldsymbol{x})\right)\,. \tag{H-61b}$$

The dynamics of this system are completely known, i.e. the dynamics are independent of the unknown parameters $\theta_{2,1}$ and $\theta_{2,2}$. Now we define the off-the-manifold coordinate:

$$\boldsymbol{\sigma}_2 = \hat{\boldsymbol{\theta}}_2 - \boldsymbol{\theta}_2 = \boldsymbol{\xi}_2 + \boldsymbol{\beta}_2 - \boldsymbol{\theta}_2\,, \tag{H-62}$$

which plays the role of estimation error. The off-the-manifold dynamics are given by

$$\dot{\boldsymbol{\sigma}}_2 = \boldsymbol{w} + \frac{\partial\boldsymbol{\beta}_2}{\partial x_1}\dot{x}_1 + \frac{\partial\boldsymbol{\beta}_2}{\partial x_2}\dot{x}_2\,. \tag{H-63}$$

Substituting Eqs. (H-56a), (H-56b) and (H-62) into Eq. (H-63) results in

$$\dot{\boldsymbol{\sigma}}_2 = \boldsymbol{w} + \frac{\partial \boldsymbol{\beta}_2}{\partial x_1}\left[x_2 + \boldsymbol{\varphi}_1(x_1)^T\left(\boldsymbol{\xi}_2 + \boldsymbol{\beta}_2(\boldsymbol{x}) - \boldsymbol{\sigma}_2\right)\right] + \frac{\partial \boldsymbol{\beta}_2}{\partial x_2}\left[\theta_{2,3}u + \boldsymbol{\varphi}_2(\boldsymbol{x})^T\left(\boldsymbol{\xi}_2 + \boldsymbol{\beta}_2(\boldsymbol{x}) - \boldsymbol{\sigma}_2\right)\right]. \tag{H-64}$$

To render the manifold $\mathcal{M}$ invariant, the following update law is selected:

$$\boldsymbol{w} = \dot{\boldsymbol{\xi}}_2 = -\frac{\partial \boldsymbol{\beta}_2}{\partial x_1}\left[x_2 + \boldsymbol{\varphi}_1(x_1)^T\left(\boldsymbol{\xi}_2 + \boldsymbol{\beta}_2(\boldsymbol{x})\right)\right] - \frac{\partial \boldsymbol{\beta}_2}{\partial x_2}\left[\theta_{2,3}u + \boldsymbol{\varphi}_2(\boldsymbol{x})^T\left(\boldsymbol{\xi}_2 + \boldsymbol{\beta}_2(\boldsymbol{x})\right)\right], \tag{H-65}$$

which results in the following off-the-manifold dynamics:

$$\dot{\boldsymbol{\sigma}}_2 = -\frac{\partial \boldsymbol{\beta}_2}{\partial x_1}\boldsymbol{\varphi}_1(x_1)^T\boldsymbol{\sigma}_2 - \frac{\partial \boldsymbol{\beta}_2}{\partial x_2}\boldsymbol{\varphi}_2(\boldsymbol{x})^T\boldsymbol{\sigma}_2\,. \tag{H-66}$$

In order to render the manifold $\mathcal{M}$ attractive, we can select the $\boldsymbol{\beta}_2$-function as (Karagiannis & Astolfi, 2008a):

$$\boldsymbol{\beta}_2(\boldsymbol{x}) = \gamma_2 \int_0^{x_2} \boldsymbol{\varphi}_2(x_1, \chi)\, d\chi\,, \tag{H-67}$$

which gives

$$\boldsymbol{\beta}_2(\boldsymbol{x}) = \gamma_2 \begin{bmatrix} x_2\sin(x_1) \\ \frac{1}{2}x_2^2 \end{bmatrix}. \tag{H-68}$$

The partial derivatives are given by

$$\frac{\partial \beta_{2,1}}{\partial x_1} = \gamma_2 x_2 \cos(x_1)\,, \quad \frac{\partial \beta_{2,1}}{\partial x_2} = \gamma_2 \sin(x_1)\,, \tag{H-69a}$$

$$\frac{\partial \beta_{2,2}}{\partial x_1} = 0\,, \quad \frac{\partial \beta_{2,2}}{\partial x_2} = \gamma_2 x_2\,. \tag{H-69b}$$

The off-the-manifold dynamics are now given by

$$\dot{\sigma}_{2,1} = -\gamma_2[\sigma_{2,1}\sin^2(x_1) + \sigma_{2,2}\sin(x_1)x_2] \tag{H-70a}$$

$$\dot{\sigma}_{2,2} = -\gamma_2[\sigma_{2,1}\sin(x_1)x_2 + \sigma_{2,2}x_2^2]\,. \tag{H-70b}$$

In order to proof that the manifold $\mathcal{M}$ is indeed attractive, we now select the following Lyapunov function:

$$\mathcal{V}(\boldsymbol{\sigma}_2) = \frac{1}{2\gamma_2}\sigma_{2,1}^2 + \frac{1}{2\gamma_2}\sigma_{2,2}^2\,, \quad \gamma_2 > 0\,. \tag{H-71}$$

Taking the time derivative of this function along the trajectories of Eq. (H-66) results in

$$\begin{aligned}
\dot{\mathcal{V}} &= \frac{1}{\gamma_2}\sigma_{2,1}\dot{\sigma}_{2,1} + \frac{1}{\gamma_2}\sigma_{2,2}\dot{\sigma}_{2,2} \\
&= -\frac{1}{\gamma_2}\sigma_{2,1}\frac{\partial \beta_{2,1}}{\partial x_2}\left[\sigma_{2,1}\sin(x_1) + \sigma_{2,2}x_2\right] - \frac{1}{\gamma_2}\sigma_{2,2}\frac{\partial \beta_{2,2}}{\partial x_2}\left[\sigma_{2,1}\sin(x_1) + \sigma_{2,2}x_2\right] \\
&= -\sigma_{2,1}\sin(x_1)\left[\sigma_{2,1}\sin(x_1) + \sigma_{2,2}x_2\right] - \sigma_{2,2}x_2\left[\sigma_{2,1}\sin(x_1) + \sigma_{2,2}x_2\right] \\
&= -\left[\sigma_{2,1}^2\sin^2(x_1) + 2\sigma_{2,1}\sigma_{2,2}\sin(x_1)x_2 + \sigma_{2,2}^2x_2^2\right] \\
&= -\left[\sigma_{2,1}\sin(x_1) + \sigma_{2,2}x_2\right]^2.
\end{aligned} \tag{H-72}$$

Now we have succeeded in making the manifold $\mathcal{M}$ attractive and invariant. The next task is to find a BS control law such that the closed-loop system globally asymptotically tracks the reference signal $x_{1,r}$, whose time derivatives are known and bounded.

Similar as before, we start by introducing the following tracking errors:

$$z_1 = x_1 - x_{1,r} \tag{H-73a}$$

$$z_2 = x_2 - \alpha_1 \,. \tag{H-73b}$$

The derivations for subsystem x_1 remain exactly the same as in Appendix C-3 (see Eqs. (C-32) to (C-36)), because this subsystem is assumed to be fully known. Therefore we directly move on to the second and final subsystem. We can rewrite this system by using the definition of the off-the-manifold coordinate, resulting in

$$\dot{z}_2 = (\xi_{2,1} + \beta_{2,1} - \sigma_{2,1}) \sin(x_1) + (\xi_{2,2} + \beta_{2,2} - \sigma_{2,2})\, x_2 + \theta_{2,3} u - \dot{\alpha}_1 \,. \tag{H-74}$$

We introduce the following real control u:

$$\begin{aligned} u &= \frac{1}{\theta_{2,3}} \left[-\rho - \hat{\theta}_{2,1} \sin(x_1) - \hat{\theta}_{2,2} x_2 + \dot{\alpha}_1 \right] \\ &= \frac{1}{\theta_{2,3}} \left[-\rho - (\xi_{2,1} + \beta_{2,1}) \sin(x_1) - (\xi_{2,2} + \beta_{2,2})\, x_2 + \dot{\alpha}_1 \right] , \end{aligned} \tag{H-75}$$

where ρ is a stabilizing function to be defined. This reduces the z_2-dynamics to

$$\dot{z}_2 = -\rho - \sigma_{2,1} \sin(x_1) - \sigma_{2,2} x_2 \,. \tag{H-76}$$

The quadratic CLF is augmented to penalize the second tracking error and the off-the-manifold coordinates as well:

$$\mathcal{V}(\boldsymbol{z}, \boldsymbol{\sigma}_2) = \mathcal{V}_1 + z_2^2 + \frac{L}{2\gamma_2} \sigma_{2,1}^2 + \frac{L}{2\gamma_2} \sigma_{2,2}^2 \,, \tag{H-77}$$

where L is a positive constant. Taking the time derivative of $\mathcal{V}$ along the trajectories of the error dynamics and Eq. (H-70) results in

$$\begin{aligned} \dot{\mathcal{V}} &= -2c_1 z_1^2 + 2z_1 z_2 + 2z_2 \left(-\rho - \sigma_{2,1} \sin(x_1) - \sigma_{2,2} x_2 \right) \\ &\quad -L\sigma_{2,1} \left[\sigma_{2,1} \sin^2(x_1) + \sigma_{2,2} \sin(x_1) x_2 \right] - L\sigma_{2,2} \left[\sigma_{2,1} \sin(x_1) x_2 + \sigma_{2,2} x_2^2 \right] \\ &= -2c_1 z_1^2 + 2z_1 z_2 - 2z_2 \rho - 2z_2 \left[\sigma_{2,1} \sin(x_1) + \sigma_{2,2} x_2 \right] \\ &\quad -L\sigma_{2,1}^2 \sin^2(x_1) - 2L\sigma_{2,1}\sigma_{2,2} \sin(x_1) x_2 - L\sigma_{2,2}^2 x_2^2 \\ &= -2c_1 z_1^2 + 2z_1 z_2 - 2z_2 \rho - 2z_2 \left[\sigma_{2,1} \sin(x_1) + \sigma_{2,2} x_2 \right] - L \left[\sigma_{2,1} \sin(x_1) + \sigma_{2,2} x_2 \right]^2 \\ &= -2c_1 z_1^2 + 2z_1 z_2 - 2z_2 \rho + \epsilon z_2^2 \\ &\quad - \left(\frac{1}{\sqrt{\epsilon}} \left[\sigma_{2,1} \sin(x_1) + \sigma_{2,2} x_2 \right] + \sqrt{\epsilon} z_2 \right)^2 - \left(L - \frac{1}{\epsilon} \right) \left[\sigma_{2,1} \sin(x_1) + \sigma_{2,2} x_2 \right]^2 \\ &\leq -2c_1 z_1^2 + 2z_1 z_2 - 2z_2 \rho + \epsilon z_2^2 - \left(L - \frac{1}{\epsilon} \right) \left[\sigma_{2,1} \sin(x_1) + \sigma_{2,2} x_2 \right]^2 , \end{aligned} \tag{H-78}$$

where ϵ is a positive constant. The derivative $\dot{\mathcal{V}}$ is made negative definite by using the following expression for the stabilizing function ρ:

$$\rho = z_1 + c_2 z_2\,, \quad c_2 > 0\,, \tag{H-79}$$

which yields

$$\dot{\mathcal{V}} \leq -2c_1 z_1^2 - (2c_2 - \epsilon)\, z_2^2 - \left(L - \frac{1}{\epsilon}\right) [\sigma_{2,1}\sin(x_1) + \sigma_{2,2}x_2]^2\,. \tag{H-80}$$

By Theorem C.2 it now follows that if $c_2 > \frac{\epsilon}{2}$ and $L > \frac{1}{\epsilon}$ then:

$$\lim_{t\to\infty} z_1 = 0 \rightarrow \lim_{t\to\infty} [x_1 - x_{1,r}] = 0 \tag{H-81a}$$

$$\lim_{t\to\infty} z_2 = 0 \tag{H-81b}$$

$$\lim_{t\to\infty} [\sigma_{2,1}\sin(x_1) + \sigma_{2,2}x_2] = \lim_{t\to\infty} \left[\boldsymbol{\varphi}_2^T \left(\hat{\boldsymbol{\theta}}_2 - \boldsymbol{\theta}_2\right)\right] = 0\,. \tag{H-81c}$$

Because ϵ and L are arbitrary positive constants, stability is guaranteed when $c_2 > 0$. Note that Eq. (H-81c) does not imply that the estimate $\hat{\boldsymbol{\theta}}_2$ converges to the real parameter $\boldsymbol{\theta}_2$. According to (Karagiannis & Astolfi, 2010) this requires a PE condition, and can be achieved only by injecting "sufficiently rich" reference signals. From Eqs. (H-70) and (H-81c) can be seen that this requires a reference signal that results in $x_1 \neq k\pi$ and $x_2 \neq 0$ with k an integer.

If we substitute Eqs. (H-68) and (H-69) into Eq. (H-65) we obtain:

$$w_1 = \dot{\xi}_{2,1} = -\gamma_2 \left[h(\boldsymbol{x}, u)\sin(x_1) + x_2^2\cos(x_{1,0})\right] \tag{H-82a}$$

$$w_2 = \dot{\xi}_{2,2} = -\gamma_2 \left[h(\boldsymbol{x}, u)x_2\right]\,, \tag{H-82b}$$

where

$$h(\boldsymbol{x}, u) = \theta_{2,3}u + \sin(x_1)\left(\xi_{2,1} + \beta_{2,1}\right) + x_2\left(\xi_{2,2} + \beta_{2,2}\right)\,. \tag{H-83}$$

If we substitute Eq. (H-79) into Eq. (H-75) we find the following control law:

$$u = \frac{1}{\theta_{2,3}} \left[-z_1 - c_2 z_2 - \hat{\theta}_{2,1}\sin(x_1) - \hat{\theta}_{2,2}x_2 + \dot{\alpha}_1\right]\,. \tag{H-84}$$

If we compare the new control law with the earlier designed conventional BS controller:

$$u = \frac{1}{\theta_{2,3}} [-z_1 - c_2 z_2 - \theta_{2,1}\sin(x_1) - \theta_{2,2}x_2 + \dot{\alpha}_1]\,, \tag{C-39 revisited}$$

we can see that the new control law based on the I&I estimator can simply be obtained from the full-information BS controller by replacing the parameters $\theta_{2,1}$ and $\theta_{2,2}$ by their estimates $\hat{\theta}_{2,1}$ and $\hat{\theta}_{2,2}$.

Simulations of the BS controller augmented with an I&I estimator have been run for system (H-56) with two unknown parameters and a sampling time of 0.01 s. The initial conditions and parameters which have been used in this simulation for the model can be found in Eq. (C-44). The following control and estimator parameters have been selected:

$$\begin{aligned} c_1 &= 10\,, & c_2 &= 10\,, \\ \xi_{2,1}(0) &= -50 \cdot \theta_{2,1}\,, & \xi_{2,2}(0) &= -50 \cdot \theta_{2,2}\,, \\ \hat{\theta}_{2,3} &= \theta_{2,3}\,. \end{aligned} \tag{H-85}$$

Different values for the adaptation gain γ_2 have been selected, the results of the simulations can be seen in Figures H-9 and H-10. From Figure H-9 it is clear that the tracking performance is best for the I&I estimator with the highest adaptation gain. However, from Figure H-10 we can conclude that the highest adaptation gain results in very large fluctuations for the estimate $\hat{\theta}_{2,2}$. These results, together with the fact that the parameter update laws (H-82) are significantly different from each other, makes it judicious to use distinct adaption gains for the parameter update laws. Using distinct adaption gains for the different update laws is an approach we earlier saw for the TF estimator, see for example Eq. (F-114).

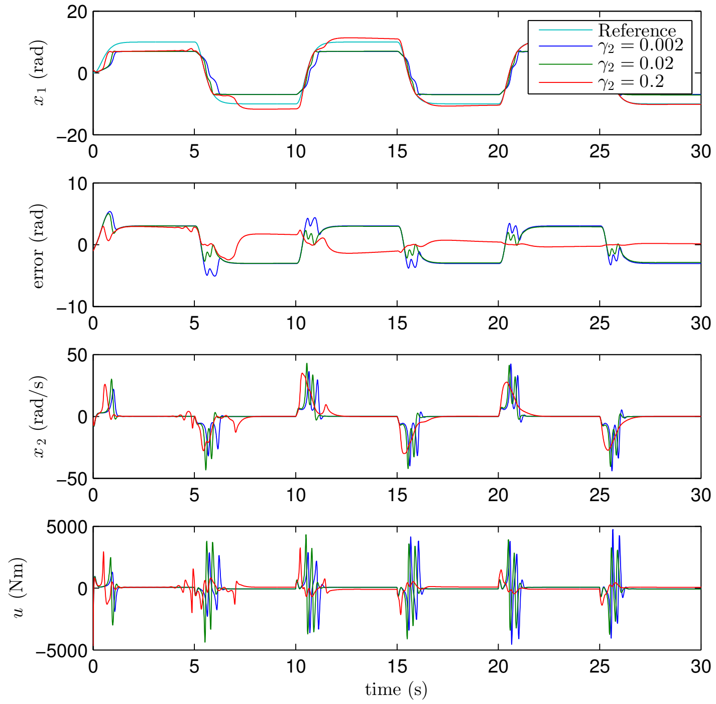

Figure H-9: The control performance of the Backstepping controller augmented with an Immersion & Invariance estimator for different values of γ_2 in the presence of parametric uncertainties.

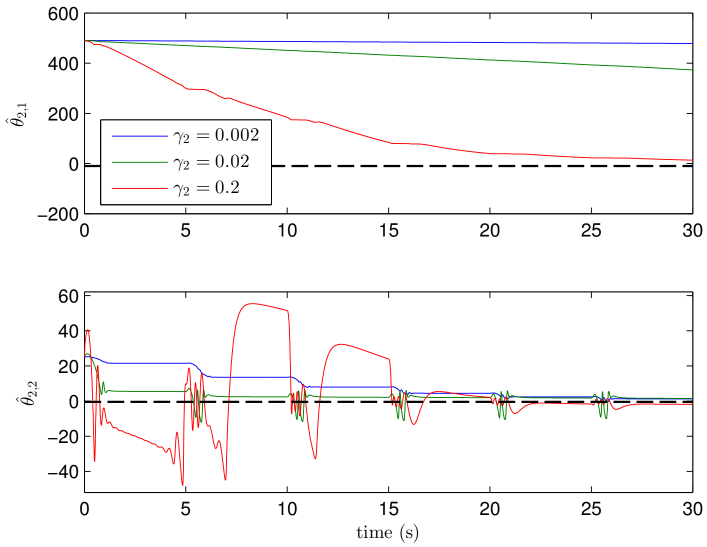

Figure H-10: The performance of the Immersion & Invariance estimators for different values of γ_2. The dashed black lines represent the values of the real parameters.

The $\boldsymbol{\beta}_2$-function, earlier defined in Eq. (H-68), is therefore now selected as

$$\boldsymbol{\beta}_2(\boldsymbol{x}) = \begin{bmatrix} \gamma_{2,1} x_2 \sin(x_1) \\ \frac{1}{2}\gamma_{2,2} x_2^2 \end{bmatrix}, \tag{H-86}$$

where $\gamma_{2,1}$ and $\gamma_{2,2}$ are the adaptation gains. The off-the-manifold dynamics are now given by

$$\dot{\sigma}_{2,1} = -\gamma_{2,1}[\sigma_{2,1}\sin^2(x_1) + \sigma_{2,2}\sin(x_1)x_2] \tag{H-87a}$$
$$\dot{\sigma}_{2,2} = -\gamma_{2,2}[\sigma_{2,1}\sin(x_1)x_2 + \sigma_{2,2}x_2^2]\,. \tag{H-87b}$$

Similar to Eqs. (H-71) and (H-72), the following Lyapunov function can now be used to demonstrate that the manifold $\mathcal{M}$ (see Eq. (H-59)) is attractive:

$$\mathcal{V}(\boldsymbol{\sigma}_2) = \frac{1}{2\gamma_{2,1}}\sigma_{2,1}^2 + \frac{1}{2\gamma_{2,2}}\sigma_{2,2}^2\,, \qquad \gamma_{2,1}\,, \gamma_{2,2} > 0\,. \tag{H-88}$$

Analogous to Eqs. (H-77) to (H-80), we can guarantee closed-loop stability by evaluating the following quadratic CLF:

$$\mathcal{V}(\boldsymbol{z}, \boldsymbol{\sigma}_2) = z_1^2 + z_2^2 + \frac{L}{2\gamma_{2,1}}\sigma_{2,1}^2 + \frac{L}{2\gamma_{2,2}}\sigma_{2,2}^2\,, \tag{H-89}$$

where L is a positive constant.

Simulations of the BS controller augmented with an I&I estimator have been run for the system (H-56) with two unknown parameters and a sampling time of 0.01 s. The initial conditions and parameters which have been used in this simulation for the model can be found in Eq. (C-44). The following control and estimator parameters have been selected:

$$\begin{aligned} c_1 &= 10\,, & c_2 &= 10, \\ \gamma_{2,1} &= 2\,, & \xi_{2,1}(0) &= -50 \cdot \theta_{2,1}\,, \\ \gamma_{2,2} &= 0.01\,, & \xi_{2,2}(0) &= -50 \cdot \theta_{2,2}\,, \\ \hat{\theta}_{2,3} &= \theta_{2,3}\,. \end{aligned} \tag{H-90}$$

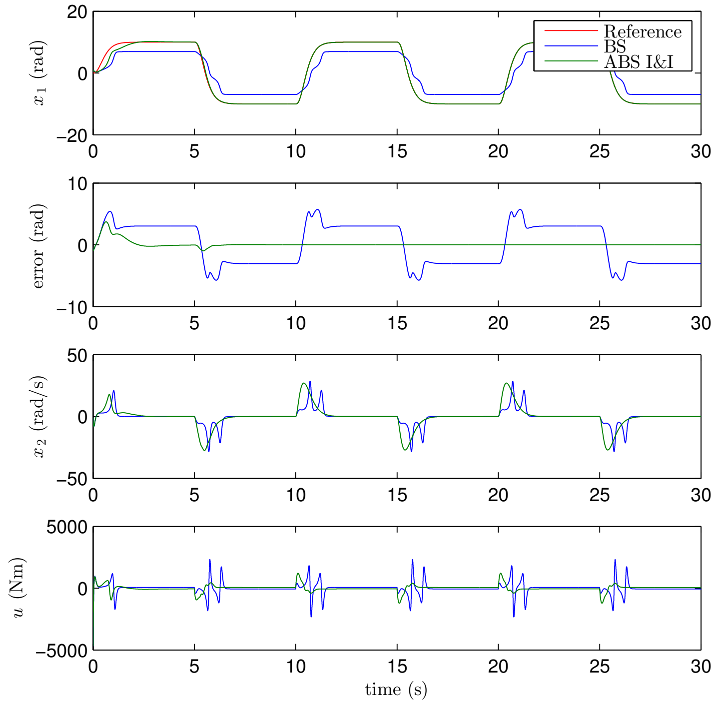

Figure H-11: The control performance of the Backstepping controller with and without Immersion & Invariance estimator in the presence of parametric uncertainties.

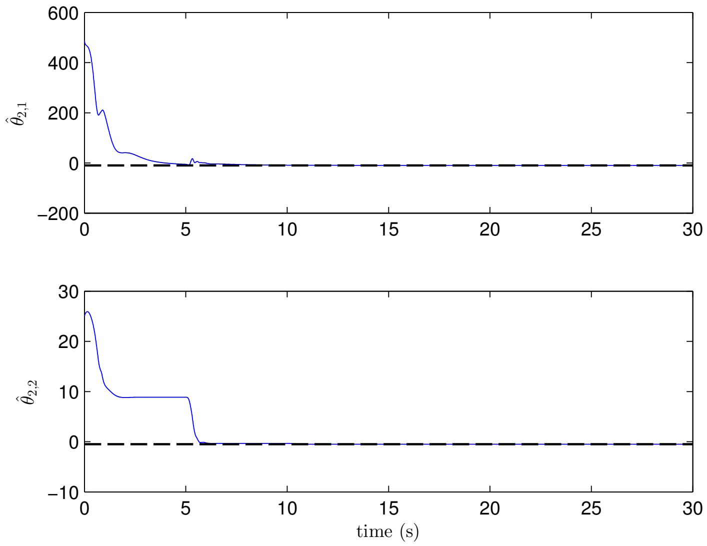

Figure H-12: The performance of the Immersion & Invariance estimators. The dashed black lines represent the values of the real parameters.

H-2-5 Command-Filtered Adaptive Backstepping with three unknown parameters

In this section an I&I estimator is combined with a BS controller to guarantee global asymptotic stability of the closed-loop system and parameter convergence for an uncertain nonlinear system. A command filter is designed to obtain the time derivative of the control input u, which is required in the estimator design.

We consider the following augmented pendulum model:

$$\dot{x}_1 = x_2 \tag{H-91a}$$
$$\dot{x}_2 = \theta_{2,1}\sin(x_1) + \theta_{2,2}x_2 + \theta_{2,3}u \tag{H-91b}$$
$$\dot{\boldsymbol{\xi}}_2 = \boldsymbol{w}\,, \tag{H-91c}$$

in which $\boldsymbol{\xi}_2 \in \mathbb{R}^3$ is the estimator state and $\boldsymbol{w}$ is the update law to be determined. Now we assume parameters $\theta_{2,1}$, $\theta_{2,2}$ and $\theta_{2,3}$ are unknown *constants*. The control task is to track the smooth reference state $x_{1,r}$ with the state x_1. The $\boldsymbol{x}$-subsystem can be written as

$$\dot{x}_1 = x_2 + \boldsymbol{\varphi}_1(x_1)^T\boldsymbol{\theta}_2 \tag{H-92a}$$
$$\dot{x}_2 = \boldsymbol{\varphi}_2(\boldsymbol{x}, u)^T\boldsymbol{\theta}_2\,, \tag{H-92b}$$

where

$$\boldsymbol{\varphi}_1(x_1) = \begin{bmatrix} 0 \\ 0 \\ 0 \end{bmatrix}, \quad \boldsymbol{\varphi}_2(\boldsymbol{x}, u) = \begin{bmatrix} \sin(x_1) \\ x_2 \\ u \end{bmatrix}, \quad \boldsymbol{\theta}_2 = \begin{bmatrix} \theta_{2,1} \\ \theta_{2,2} \\ \theta_{2,3} \end{bmatrix}. \tag{H-93}$$

Now we introduce the following three-dimensional manifold:

$$\mathcal{M} = \left\{(\boldsymbol{x}, u, \boldsymbol{\xi}_2) \in \mathbb{R}^6 | \boldsymbol{\xi}_2 + \boldsymbol{\beta}_2(\boldsymbol{x}, u) - \boldsymbol{\theta}_2 = \mathbf{0}\right\}\,, \tag{H-94}$$

where $\boldsymbol{\beta}_2(\boldsymbol{x}, u)$ is a continuous function yet to be specified. The estimate of the unknown constants $\boldsymbol{\theta}_2$ is given by

$$\hat{\boldsymbol{\theta}}_2 = \boldsymbol{\xi}_2 + \boldsymbol{\beta}_2 \,. \tag{H-95}$$

If the manifold $\mathcal{M}$ is *invariant* (see Definition H.1 on page 181), the dynamics of the $\boldsymbol{x}$-subsystem of (H-91) restricted to this manifold can be written as

$$\dot{x}_1 = x_2 + \boldsymbol{\varphi}_1^T \left(\boldsymbol{\xi}_2 + \boldsymbol{\beta}_2(\boldsymbol{x}, u)\right) \tag{H-96a}$$

$$\dot{x}_2 = \boldsymbol{\varphi}_2(\boldsymbol{x}, u)^T \left(\boldsymbol{\xi}_2 + \boldsymbol{\beta}_2(\boldsymbol{x}, u)\right) \,. \tag{H-96b}$$

The dynamics of this system are completely known, i.e. the dynamics are independent of the unknown parameters $\theta_{2,1}$, $\theta_{2,2}$ and $\theta_{2,3}$. Now we define the off-the-manifold coordinate:

$$\boldsymbol{\sigma}_2 = \hat{\boldsymbol{\theta}}_2 - \boldsymbol{\theta}_2 = \boldsymbol{\xi}_2 + \boldsymbol{\beta}_2 - \boldsymbol{\theta}_2 \,, \tag{H-97}$$

which plays the role of estimation error. The off-the-manifold dynamics are given by

$$\dot{\boldsymbol{\sigma}}_2 = \boldsymbol{w} + \frac{\partial \boldsymbol{\beta}_2}{\partial x_1}\dot{x}_1 + \frac{\partial \boldsymbol{\beta}_2}{\partial x_2}\dot{x}_2 + \frac{\partial \boldsymbol{\beta}_2}{\partial u}\dot{u} \,. \tag{H-98}$$

Substituting Eqs. (H-91a), (H-91b) and (H-97) into Eq. (H-98) results in

$$\begin{aligned} \dot{\boldsymbol{\sigma}}_2 = \boldsymbol{w} &+ \frac{\partial \boldsymbol{\beta}_2}{\partial x_1}\left[x_2 + \boldsymbol{\varphi}_1^T \left(\boldsymbol{\xi}_2 + \boldsymbol{\beta}_2(\boldsymbol{x}, u) - \boldsymbol{\sigma}_2\right)\right] \\ &+ \frac{\partial \boldsymbol{\beta}_2}{\partial x_2}\left[\boldsymbol{\varphi}_2(\boldsymbol{x}, u)^T \left(\boldsymbol{\xi}_2 + \boldsymbol{\beta}_2(\boldsymbol{x}, u) - \boldsymbol{\sigma}_2\right)\right] + \frac{\partial \boldsymbol{\beta}_2}{\partial u}\dot{u} \,. \end{aligned} \tag{H-99}$$

To render the manifold $\mathcal{M}$ invariant, the following update law is selected:

$$\begin{aligned} \boldsymbol{w} = \dot{\boldsymbol{\xi}}_2 = &- \frac{\partial \boldsymbol{\beta}_2}{\partial x_1}\left[x_2 + \boldsymbol{\varphi}_1^T \left(\boldsymbol{\xi}_2 + \boldsymbol{\beta}_2(\boldsymbol{x}, u)\right)\right] \\ &- \frac{\partial \boldsymbol{\beta}_2}{\partial x_2}\left[\boldsymbol{\varphi}_2(\boldsymbol{x}, u)^T \left(\boldsymbol{\xi}_2 + \boldsymbol{\beta}_2(\boldsymbol{x}, u)\right)\right] - \frac{\partial \boldsymbol{\beta}_2}{\partial u}\dot{u} \,, \end{aligned} \tag{H-100}$$

which results in the following off-the-manifold dynamics:

$$\dot{\boldsymbol{\sigma}}_2 = -\frac{\partial \boldsymbol{\beta}_2}{\partial x_1}\boldsymbol{\varphi}_1^T \boldsymbol{\sigma}_2 - \frac{\partial \boldsymbol{\beta}_2}{\partial x_2}\boldsymbol{\varphi}_2(\boldsymbol{x}, u)^T \boldsymbol{\sigma}_2 \,. \tag{H-101}$$

Note that the derivative of the control input is required in the estimator design. This derivative will be obtained from a command filter. In order to render the manifold $\mathcal{M}$ attractive, we can select the $\boldsymbol{\beta}_2$-function as

$$\boldsymbol{\beta}_2(\boldsymbol{x}, u) = \Gamma_2 \int_0^{x_2} \boldsymbol{\varphi}_2(x_1, \chi, u)\, d\chi \,, \tag{H-102}$$

which results in

$$\boldsymbol{\beta}_2(\boldsymbol{x}, u) = \Gamma_2 \begin{bmatrix} x_2 \sin(x_1) \\ \frac{1}{2}x_2^2 \\ x_2 u \end{bmatrix} \,, \tag{H-103}$$

where Γ_2 is a positive diagonal matrix:

$$\Gamma_2 = \begin{bmatrix} \gamma_{2,1} & 0 & 0 \\ 0 & \gamma_{2,2} & 0 \\ 0 & 0 & \gamma_{2,3} \end{bmatrix} . \tag{H-104}$$

The partial derivatives of $\boldsymbol{\beta}_2(\boldsymbol{x}, u)$ are given by

$$\frac{\partial \beta_{2,1}}{\partial x_1} = \gamma_{2,1} x_2 \cos(x_1) \,, \quad \frac{\partial \beta_{2,1}}{\partial x_2} = \gamma_{2,1} \sin(x_1) \,, \quad \frac{\partial \beta_{2,1}}{\partial u} = 0 \,, \tag{H-105a}$$
$$\frac{\partial \beta_{2,2}}{\partial x_1} = 0 \,, \quad \frac{\partial \beta_{2,2}}{\partial x_2} = \gamma_{2,2} x_2 \,, \quad \frac{\partial \beta_{2,2}}{\partial u} = 0 \,, \tag{H-105b}$$
$$\frac{\partial \beta_{2,3}}{\partial x_1} = 0 \,, \quad \frac{\partial \beta_{2,3}}{\partial x_2} = \gamma_{2,3} u \,, \quad \frac{\partial \beta_{2,3}}{\partial u} = \gamma_{2,3} x_2 \,. \tag{H-105c}$$

The off-the-manifold dynamics are now given by

$$\dot{\sigma}_{2,1} = -\gamma_{2,1} \left[\sigma_{2,1} \sin^2(x_1) + \sigma_{2,2} \sin(x_1) x_2 + \sigma_{2,3} \sin(x_1) u\right] \tag{H-106a}$$
$$\dot{\sigma}_{2,2} = -\gamma_{2,2} \left[\sigma_{2,1} \sin(x_1) x_2 + \sigma_{2,2} x_2^2 + \sigma_{2,3} x_2 u\right] \tag{H-106b}$$
$$\dot{\sigma}_{2,3} = -\gamma_{2,3} \left[\sigma_{2,1} \sin(x_1) u + \sigma_{2,2} x_2 u + \sigma_{2,3} u^2\right] \,. \tag{H-106c}$$

Note that we selected distinct adaptation gains for the different parameter update laws, the reason for doing so has earlier been explained in Appendix H-2-4. In order to proof that the manifold $\mathcal{M}$ is indeed attractive by selecting the $\boldsymbol{\beta}_2$ function as Eq. (H-103), we now select the following Lyapunov function:

$$\mathcal{V}(\boldsymbol{\sigma}_2) = \frac{1}{2\gamma_{2,1}} \sigma_{2,1}^2 + \frac{1}{2\gamma_{2,2}} \sigma_{2,2}^2 + \frac{1}{2\gamma_{2,3}} \sigma_{2,3}^2 \,. \tag{H-107}$$

Taking the time derivative of this function along the trajectories of Eq. (H-106) results in

$$\begin{aligned} \dot{\mathcal{V}} &= \frac{1}{\gamma_{2,1}} \sigma_{2,1} \dot{\sigma}_{2,1} + \frac{1}{\gamma_{2,2}} \sigma_{2,2} \dot{\sigma}_{2,2} + \frac{1}{\gamma_{2,3}} \sigma_{2,3} \dot{\sigma}_{2,3} \\ &= -\sigma_{2,1} \left[\sigma_{2,1} \sin^2(x_1) + \sigma_{2,2} \sin(x_1) x_2 + \sigma_{2,3} \sin(x_1) u\right] \\ &\quad -\sigma_{2,2} \left[\sigma_{2,1} \sin(x_1) x_2 + \sigma_{2,2} x_2^2 + \sigma_{2,3} x_2 u\right] - \sigma_{2,3} \left[\sigma_{2,1} \sin(x_1) u + \sigma_{2,2} x_2 u + \sigma_{2,3} u^2\right] \\ &= -\big[\sigma_{2,1}^2 \sin^2(x_1) + \sigma_{2,2}^2 x_2^2 + \sigma_{2,3}^2 u^2 + 2\sigma_{2,1}\sigma_{2,2} \sin(x_1) x_2 + 2\sigma_{2,1}\sigma_{2,3} \sin(x_1) u \\ &\qquad + 2\sigma_{2,2}\sigma_{2,3} x_2 u\big] \\ &= -\left[\sigma_{2,1} \sin(x_1) + \sigma_{2,2} x_2 + \sigma_{2,3} u\right]^2 \,. \end{aligned} \tag{H-108}$$

Now we have succeeded in making the manifold $\mathcal{M}$ attractive and invariant. The next task is to find a BS control law such that the closed-loop system globally asymptotically tracks the reference signal $x_{1,r}$, whose time derivative is known and bounded. Command filters will be used to obviate the need for analytic computation of the virtual control derivative and to obtain the time derivative of the real control u which is required for the I&I estimator, see Eq. (H-100).

Earlier we obtained the following control laws for the nonlinear pendulum:

$$u^0 = \frac{1}{\theta_{2,3}}\left[-\bar{z}_1 - c_2\left(x_2 - x_{2,r}\right) - \theta_{2,1}\sin(x_1) - \hat{\theta}_{2,2}x_2 + \dot{x}_{2,r}\right] \tag{H-55 revisited}$$

$$u = \frac{1}{\theta_{2,3}}\left[-z_1 - c_2\left(x_2 - \alpha_1\right) - \hat{\theta}_{2,1}\sin(x_1) - \hat{\theta}_{2,2}x_2 + \dot{\alpha}_1\right], \tag{H-109}$$

which are respectively the Command-Filtered BS controller with an I&I estimator for one unknown parameter, and the BS controller with an I&I estimator for two unknown parameters. Now the following Command-Filtered BS controller based on an I&I estimator for three unknowns seems viable:

$$\begin{aligned} u^0 &= \frac{1}{\hat{\theta}_{2,3}}\left[-\bar{z}_1 - c_2\left(x_2 - x_{2,r}\right) - \hat{\theta}_{2,1}\sin(x_1) - \hat{\theta}_{2,2}x_2 + \dot{x}_{2,r}\right] \\ &= \frac{1}{\xi_{2,3}+\beta_{2,3}}\left[-\bar{z}_1 - c_2\left(x_2 - x_{2,r}\right) - \left(\xi_{2,1}+\beta_{2,1}\right)\sin(x_1) - \left(\xi_{2,2}+\beta_{2,2}\right)x_2 + \dot{x}_{2,r}\right]. \end{aligned} \tag{H-110}$$

In order to proof stability of the closed-loop system, we consider the following quadratic Lyapunov function:

$$\mathcal{V}(\bar{\boldsymbol{z}}, \boldsymbol{\sigma}_2) = \bar{z}_1^2 + \bar{z}_2^2 + \frac{L}{2\gamma_{2,1}}\sigma_{2,1}^2 + \frac{L}{2\gamma_{2,2}}\sigma_{2,2}^2 + \frac{L}{2\gamma_{2,3}}\sigma_{2,3}^2, \tag{H-111}$$

where $\bar{\boldsymbol{z}}$ and the $\bar{z}_1$-dynamics are similar as in Eqs. (D-37) and (D-38) and L is a positive constant. The $\bar{z}_2$-dynamics are now given by

$$\dot{\bar{z}}_2 = \left(\xi_{2,1}+\beta_{2,1}-\sigma_{2,1}\right)\sin(x_1) + \left(\xi_{2,2}+\beta_{2,2}-\sigma_{2,2}\right)x_2 + \left(\xi_{2,3}+\beta_{2,3}-\sigma_{2,3}\right)u - \dot{x}_{2,r} - \dot{\chi}_2. \tag{H-112}$$

Taking the time derivative of $\mathcal{V}$ along the trajectories of Eqs. (D-38), (H-106) and (H-112) results in

$$\begin{aligned} \dot{\mathcal{V}} = & -2c_1\bar{z}_1^2 + 2\bar{z}_1\bar{z}_2 \\ & +2\bar{z}_2\left[\left(\xi_{2,1}+\beta_{2,1}-\sigma_{2,1}\right)\sin(x_1) + \left(\xi_{2,2}+\beta_{2,2}-\sigma_{2,2}\right)x_2 + \left(\xi_{2,3}+\beta_{2,3}-\sigma_{2,3}\right)u\right. \\ & \left.-\dot{x}_{2,r} - \dot{\chi}_2\right] - L\sigma_{2,1}\left[\sigma_{2,1}\sin^2(x_1) + \sigma_{2,2}\sin(x_1)x_2 + \sigma_{2,3}\sin(x_1)u\right] \\ & -L\sigma_{2,2}\left[\sigma_{2,1}\sin(x_1)x_2 + \sigma_{2,2}x_2^2 + \sigma_{2,3}x_2u\right] \\ & -L\sigma_{2,3}\left[\sigma_{2,1}\sin(x_1)u + \sigma_{2,2}x_2u + \sigma_{2,3}u^2\right]. \end{aligned} \tag{H-113}$$

Now χ_2 is the output of the following stable linear filter:

$$\dot{\chi}_2 = -c_2\chi_2 + \left(\xi_{2,3}+\beta_{2,3}\right)\left(u - u^0\right), \tag{H-114}$$

with $\chi_2(0) = 0$. This yields

$$\begin{aligned}
\dot{\mathcal{V}} &= -2c_1\bar{z}_1^2 + 2\bar{z}_1\bar{z}_2 \\
&\quad +2\bar{z}_2\big[(\xi_{2,1} + \beta_{2,1} - \sigma_{2,1})\sin(x_1) + (\xi_{2,2} + \beta_{2,2} - \sigma_{2,2})\,x_2 \\
&\quad + (\xi_{2,3} + \beta_{2,3})\,u^0 - \sigma_{2,3}u - \dot{x}_{2,r} + c_2\chi_2\big] \\
&\quad -L\sigma_{2,1}\left[\sigma_{2,1}\sin^2(x_1) + \sigma_{2,2}\sin(x_1)x_2 + \sigma_{2,3}\sin(x_1)u\right] \\
&\quad -L\sigma_{2,2}\left[\sigma_{2,1}\sin(x_1)x_2 + \sigma_{2,2}x_2^2 + \sigma_{2,3}x_2u\right] \\
&\quad -L\sigma_{2,3}\left[\sigma_{2,1}\sin(x_1)u + \sigma_{2,2}x_2u + \sigma_{2,3}u^2\right] \\
&= -2c_1\bar{z}_1^2 + 2\bar{z}_1\bar{z}_2 \\
&\quad +2\bar{z}_2\left[-\bar{z}_1 - c_2z_2 - \sigma_{2,1}\sin(x_1) - \sigma_{2,2}x_2 - \sigma_{2,3}u + c_2\chi_2\right] \\
&\quad -L\sigma_{2,1}\left[\sigma_{2,1}\sin^2(x_1) + \sigma_{2,2}\sin(x_1)x_2 + \sigma_{2,3}\sin(x_1)u\right] \\
&\quad -L\sigma_{2,2}\left[\sigma_{2,1}\sin(x_1)x_2 + \sigma_{2,2}x_2^2 + \sigma_{2,3}x_2u\right] \\
&\quad -L\sigma_{2,3}\left[\sigma_{2,1}\sin(x_1)u + \sigma_{2,2}x_2u + \sigma_{2,3}u^2\right] \\
&= -2c_1\bar{z}_1^2 - 2c_2\bar{z}_2^2 - 2\bar{z}_2\left[\sigma_{2,1}\sin(x_1) + \sigma_{2,2}x_2 + 2\sigma_{2,3}u\right] \\
&\quad -L\big[\sigma_{2,1}^2\sin^2(x_1) + \sigma_{2,2}^2x_2^2 + \sigma_{2,3}^2u^2 + 2\sigma_{2,1}\sigma_{2,2}\sin(x_1)x_2 + 2\sigma_{2,1}\sigma_{2,3}\sin(x_1)u \\
&\qquad +2\sigma_{2,2}\sigma_{2,3}x_2u\big] \\
&= -2c_1\bar{z}_1^2 - 2c_2\bar{z}_2^2 + \epsilon\bar{z}_2^2 - \left(\frac{1}{\sqrt{\epsilon}}\left[\sigma_{2,1}\sin(x_1) + \sigma_{2,2}x_2 + \sigma_{2,3}u\right] + \sqrt{\epsilon}\bar{z}_2\right)^2 \\
&\quad -\left(L - \frac{1}{\epsilon}\right)\left[\sigma_{2,1}\sin(x_1) + \sigma_{2,2}x_2 + \sigma_{2,3}u\right]^2 \\
&\leq -2c_1\bar{z}_1^2 - (2c_2 - \epsilon)\,\bar{z}_2^2 - \left(L - \frac{1}{\epsilon}\right)\left[\sigma_{2,1}\sin(x_1) + \sigma_{2,2}x_2 + \sigma_{2,3}u\right]^2 ,
\end{aligned} \tag{H-115}$$

where ϵ is a positive constant. If $c_2 > \frac{\epsilon}{2}$ and $L > \frac{1}{\epsilon}$, it follows according to Theorem C.2 that:

$$\lim_{t\to\infty} \bar{\boldsymbol{z}} = \mathbf{0} \tag{H-116a}$$

$$\lim_{t\to\infty} \left[\sigma_{2,1}\sin(x_1) + \sigma_{2,2}x_2 + \theta_{2,3}u\right] = \lim_{t\to\infty} \left[\boldsymbol{\varphi}_2^T\left(\hat{\boldsymbol{\theta}}_2 - \boldsymbol{\theta}_2\right)\right] = 0\,. \tag{H-116b}$$

Because ϵ and L are arbitrary positive constants, stability is guaranteed when $c_2 > 0$. Note that Eq. (H-116b) does not imply that the estimate $\hat{\boldsymbol{\theta}}_2$ converges to the real parameter $\boldsymbol{\theta}_2$. According to (Karagiannis & Astolfi, 2010) this requires a PE condition, and can be achieved only by injecting "sufficiently rich" reference signals. From Eqs. (H-106) and (H-116b) can be seen that this requires a reference signal $u \neq 0$ that results in $x_1 \neq k\pi$ and $x_2 \neq 0$ with k an integer.

The new control law (H-110) based on the I&I estimator depends on $x_{2,r}$ and $\dot{x}_{2,r}$, which are the output of the command filter and therefore the analytical derivative $\dot{\alpha}_1$ is no longer required. In the absence of physical limitations (i.e. magnitude, rate and bandwidth constraints on the intermediate state x_2 and control u), closed-loop stability is still guaranteed even when uncertainties are introduced in either the system dynamics or the control effectiveness matrix.

Simulations of the Command-Filtered BS controller augmented with an I&I estimator have been run for the system (H-56) with three unknown parameters and a sampling time of 0.01 s. The initial conditions and parameters which have been used in this simulation for the model can be found in Eq. (C-44). The following control, command filter and estimator parameters have been selected:

$$\begin{aligned} c_1 &= 10\,, & c_2 &= 10, \\ \omega_1 &= 200\,, & \omega_2 &= 200\,, \\ \gamma_{2,1} &= 2, & \xi_{2,1}(0) &= 20 \cdot \theta_{2,1}\,, \\ \gamma_{2,2} &= 5 \cdot 10^{-3}\,, & \xi_{2,2}(0) &= -20 \cdot \theta_{2,2}\,, \\ \gamma_{2,3} &= 5 \cdot 10^{-6}\,, & \xi_{2,3}(0) &= 5 \cdot \theta_{2,3}\,. \end{aligned} \tag{H-117}$$

From Figure H-13 we can clearly see that the Adaptive Backstepping (ABS) I&I controller performs much better compared to the conventional BS controller in presence of the introduced parametric uncertainties. From Figure H-14 we can see that the parameter estimates quickly converge to the real parameters.

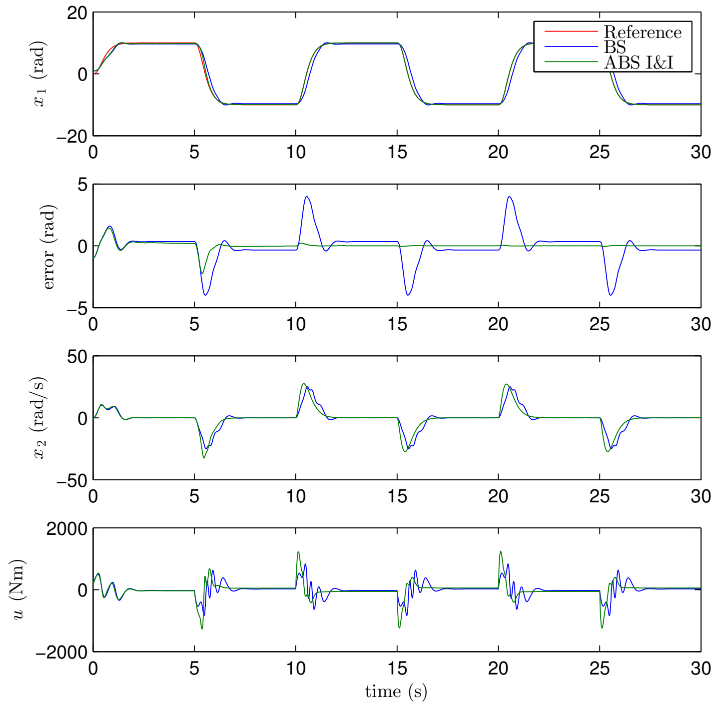

Figure H-13: The control performance of the Backstepping controller with and without an Immersion & Invariance estimator in the presence of parametric uncertainties.

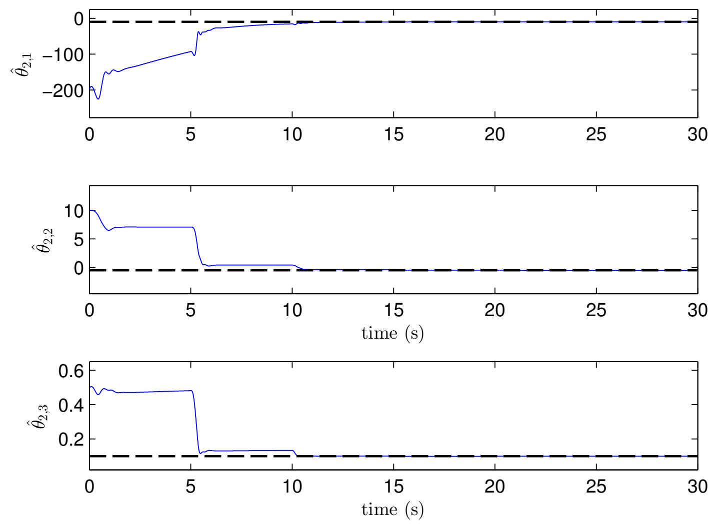

Figure H-14: The performance of the Immersion & Invariance estimators. The dashed black lines represent the values of the real parameters.

H-2-6 Command-Filtered Adaptive Incremental Backstepping with Time-Scale Separation

In this section an I&I estimator is combined with a BS controller to guarantee global asymptotic stability of the closed-loop system and parameter convergence for an uncertain nonlinear system.

We consider the following augmented incremental pendulum model:

$$\dot{x}_1 = x_2 \tag{H-118a}$$
$$\dot{x}_2 = \dot{x}_{2,0} + \theta_{2,3}\Delta u \tag{H-118b}$$
$$\dot{\xi}_{2,3} = w\,, \tag{H-118c}$$

where $\xi_{2,3}$ is the estimator state and w the update law to be determined. The control task is to track the smooth reference state $x_{1,r}$ with the state x_1. Note that Eq. (H-118b) is the incremental form of the full equation of the pendulum, see Eq. (B-3b). We now assume $\theta_{2,3}$ is an unknown *constant* parameter and define the following one-dimensional manifold:

$$\mathcal{M} = \left\{(x_2, \xi_{2,3}, \Delta u) \in \mathbb{R}^3 | \xi_{2,3} + \beta_2(x_2, \Delta u) - \theta_{2,3} = 0\right\}\,, \tag{H-119}$$

where $\beta_2(x_2, \Delta u)$ is a continuous function yet to be specified. The estimate of the unknown *constant* $\theta_{2,3}$ is given by

$$\hat{\theta}_{2,3} = \xi_{2,3} + \beta_2\,. \tag{H-120}$$

Provided that this manifold is *invariant* (see Definition H.1 on page 181), the dynamics of subsystem (H-118b) on the manifold $\mathcal{M}$ are given by

$$\dot{x}_2 = \dot{x}_{2,0} + (\xi_{2,3} + \beta_2)\,\Delta u\,, \tag{H-121}$$

which is completely known. Now we define the off-the-manifold coordinate σ_2:

$$\sigma_2 = \hat{\theta}_{2,3} - \theta_{2,3} = \xi_{2,3} + \beta_2 - \theta_{2,3}\,, \tag{H-122}$$

which plays the role of estimation error. The off-the-manifold dynamics are given by

$$\begin{aligned}\dot{\sigma}_2 &= w + \frac{\partial \beta_2}{\partial x_2}\left(\dot{x}_{2,0} + \theta_{2,3}\Delta u\right) + \frac{\partial \beta_2}{\partial \Delta u}\Delta \dot{u} \\ &= w + \frac{\partial \beta_2}{\partial x_2}\left(\dot{x}_{2,0} + \left(\xi_{2,3} + \beta_2 - \sigma_2\right)\Delta u\right) + \frac{\partial \beta_2}{\partial \Delta u}\Delta \dot{u}\,. \end{aligned}\tag{H-123}$$

To render the manifold $\mathcal{M}$ invariant, the following update law is selected:

$$w = \dot{\xi}_{2,3} = -\frac{\partial \beta_2}{\partial x_2}\left(\dot{x}_{2,0} + \left(\xi_{2,3} + \beta_2\right)\Delta u\right) - \frac{\partial \beta_2}{\partial \Delta u}\Delta \dot{u}\,, \tag{H-124}$$

which transforms the off-the-manifold dynamics into:

$$\dot{\sigma}_2 = -\frac{\partial \beta_2}{\partial x_2}\sigma_2 \Delta u\,. \tag{H-125}$$

Note that the time derivative of the incremental control input Δu is required in the estimator design. This derivative will be obtained by using (delayed) outputs of the command filter, see Figure H-15.

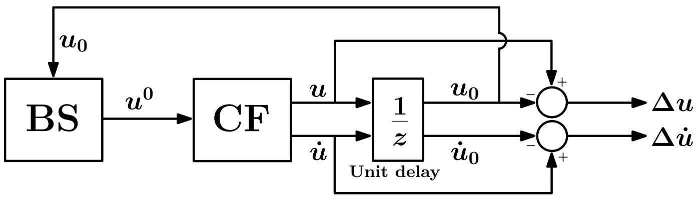

Figure H-15: Obtaining signal Δu and $\Delta \dot{u}$ by using (delayed) outputs of the command filter.

Now the next step is to find an expression for the function β_2 such that this system is globally asymptotically stable thereby making the manifold $\mathcal{M}$ attractive. We choose the following quadratic Lyapunov function:

$$\mathcal{V}(\sigma_2) = \frac{1}{2\gamma_2}\sigma_2^2\,, \quad \gamma_2 > 0\,. \tag{H-126}$$

Taking the time derivative of this function along the trajectories of Eq. (H-125) results in

$$\begin{aligned}\dot{\mathcal{V}} &= \frac{1}{\gamma_2}\sigma_2\dot{\sigma}_2 \\ &= -\frac{1}{\gamma_2}\frac{\partial \beta_2}{\partial x_2}\sigma_2^2 \Delta u\,. \end{aligned}\tag{H-127}$$

To render $\dot{\mathcal{V}}$ negative definite, β_2 can be chosen as

$$\beta_2 = \gamma_2 x_2 \Delta u \quad \rightarrow \quad \frac{\partial \beta_2}{\partial x_2} = \gamma_2 \Delta u\,, \quad \frac{\partial \beta_2}{\partial \Delta u} = \gamma_2 x_2\,, \tag{H-128}$$

resulting in

$$\dot{\mathcal{V}} = -(\sigma_2 \Delta u)^2 , \tag{H-129}$$

and

$$\dot{\sigma}_2 = -\gamma_2 \sigma_2 \Delta u^2 . \tag{H-130}$$

Note that the dynamics of the parameter estimation error σ_2 are described by a first-order linear ordinary, homogeneous differential equation with a time-varying coefficient. The well-known solution to this differential equation is

$$\sigma_2(t) = \sigma_2(0) e^{-\gamma_2 \int_0^t [\Delta u(\xi)]^2 \, d\xi} , \tag{H-131}$$

which indicates that the parameter estimation error is a monotonically non-increasing function. If we substitute Eq. (H-128) into update law (H-124) we obtain:

$$\dot{\xi}_{2,3} = -\gamma_2 \left[\dot{x}_{2,0} \Delta u + \left(\xi_{2,3} + \gamma_2 x_2 \Delta u \right) \Delta u^2 + x_2 \Delta \dot{u} \right] . \tag{H-132}$$

This concludes the estimator design of the controller. Now we have succeeded in making the manifold $\mathcal{M}$ invariant and attractive, it is time to find a BS control law such that the system (H-118) globally asymptotically tracks the reference signal $x_{1,r}$. Command filters will be used to obviate the need for analytic computation of the virtual control derivative and to obtain the time derivative of the incremental control input Δu which is required for the I&I estimator, see Eq. (H-124).

Earlier we obtained the following Command-Filtered Incremental Backstepping (IBS) control law for the incremental system with Time-Scale Separation (TSS):

$$u^0 = u_0 + \frac{1}{\theta_{2,3}} \left[-\bar{z}_1 - c_2 \left(x_2 - x_{2,r} \right) - \dot{x}_{2,0} + \dot{x}_{2,r} \right] . \tag{E-63 revisited}$$

For the incremental system with TSS we earlier obtained the following Tuning Functions Adaptive Backstepping (TFABS) control law:

$$u = u_0 + \frac{1}{\hat{\theta}_{2,3}} \left[-z_1 - c_2 \left(x_2 - \alpha_1 \right) - \dot{x}_{2,0} + \dot{\alpha}_1 \right] . \tag{F-124 revisited}$$

Now the following Command-Filtered IBS control law based on an I&I estimator seems viable for system (H-118):

$$\begin{aligned} u^0 &= u_0 + \frac{1}{\hat{\theta}_{2,3}} \left[-\bar{z}_1 - c_2 \left(x_2 - x_{2,r} \right) - \dot{x}_{2,0} + \dot{x}_{2,r} \right] \\ &= u_0 + \frac{1}{\xi_{2,3} + \beta_2} \left[-\bar{z}_1 - c_2 \left(x_2 - x_{2,r} \right) - \dot{x}_{2,0} + \dot{x}_{2,r} \right] . \end{aligned} \tag{H-133}$$

In order to proof stability of the closed-loop system, we consider the following quadratic Lyapunov function:

$$\mathcal{V}(\bar{\boldsymbol{z}}, \sigma_2) = \bar{z}_1^2 + \bar{z}_2^2 + \frac{L}{2\gamma_2} \sigma_2^2 , \tag{H-134}$$

where $\bar{\boldsymbol{z}}$ and the $\bar{z}_1$-dynamics are similar as in Eqs. (D-37) and (D-38). The $\bar{z}_2$-dynamics are now given by

$$\begin{aligned}\dot{\bar{z}}_2 &= \dot{x}_{2,0} + \theta_{2,3}\Delta u - \dot{x}_{2,r} - \dot{\chi}_2 \\ &= \dot{x}_{2,0} + (\xi_{2,3} + \beta_2)\,\Delta u - \sigma_2 \Delta u - \dot{x}_{2,r} - \dot{\chi}_2\,. \end{aligned} \tag{H-135}$$

Taking the time derivative of $\mathcal{V}$ along the trajectories of the compensated error dynamics and Eq. (H-130) results in

$$\dot{\mathcal{V}} = -2c_1\bar{z}_1^2 + 2\bar{z}_1\bar{z}_2 + 2\bar{z}_2\left[\dot{x}_{2,0} + (\xi_{2,3}+\beta_2)\,\Delta u - \sigma_2\Delta u - \dot{x}_{2,r} - \dot{\chi}_2\right] - L\sigma_2^2\Delta u^2\,. \tag{H-136}$$

Now χ_2 is the output of the following stable linear filter:

$$\dot{\chi}_2 = -c_2\chi_2 + (\xi_{2,3}+\beta_2)\left(u - u^0\right)\,, \tag{H-137}$$

with $\chi_2(0) = 0$. This yields

$$\begin{aligned}\dot{\mathcal{V}} &= -2c_1\bar{z}_1^2 + 2\bar{z}_1\bar{z}_2 + 2\bar{z}_2\left[\dot{x}_{2,0} + (\xi_{2,3}+\beta_2)\left(u^0 - u_0\right) - \sigma_2\Delta u - \dot{x}_{2,r} + c_2\chi_2\right] - L\sigma_2^2\Delta u^2 \\ &= -2c_1\bar{z}_1^2 + 2\bar{z}_1\bar{z}_2 + 2\bar{z}_2\left[-\bar{z}_1 - c_2 z_2 - \sigma_2\Delta u + c_2\chi_2\right] - L\sigma_2^2\Delta u^2 \\ &= -2c_1\bar{z}_1^2 + 2\bar{z}_2\left[-c_2 z_2 - \sigma_2\Delta u + c_2\chi_2\right] - L\sigma_2^2\Delta u^2 \\ &= -2c_1\bar{z}_1^2 - 2c_2\bar{z}_2^2 - 2\sigma_2\Delta u\bar{z}_2 - L\sigma_2^2\Delta u^2 \\ &= -2c_1\bar{z}_1^2 - 2c_2\bar{z}_2^2 + \epsilon\bar{z}_2^2 - \left(\frac{1}{\sqrt{\epsilon}}\sigma_2\Delta u + \sqrt{\epsilon}\bar{z}_2\right)^2 - \left(L - \frac{1}{\epsilon}\right)(\sigma_2\Delta u)^2 \\ &\leq -2c_1\bar{z}_1^2 - (2c_2 - \epsilon)\,\bar{z}_2^2 - \left(L - \frac{1}{\epsilon}\right)(\sigma_2\Delta u)^2\,, \end{aligned} \tag{H-138}$$

where ϵ is a positive constant. If $c_2 > \frac{\epsilon}{2}$ and $L > \frac{1}{\epsilon}$, it follows according to Theorem C.2 that:

$$\lim_{t\to\infty} \bar{\boldsymbol{z}} = \mathbf{0} \tag{H-139a}$$

$$\lim_{t\to\infty} \sigma_2\Delta u = \left(\hat{\theta}_{2,3} - \theta_{2,3}\right)\Delta u = 0\,. \tag{H-139b}$$

Because ϵ and L are arbitrary positive constants, stability is guaranteed when $c_2 > 0$. Note that Eq. (H-139b) does not imply that the estimate $\hat{\theta}_{2,3}$ converges to the real parameter $\theta_{2,3}$. According to (Karagiannis & Astolfi, 2010) this requires a PE condition, and can be achieved only by injecting "sufficiently rich" reference signals. From Eq. (H-139b) can be seen that this requires a reference signal $\Delta u \neq 0$.

The new incremental control law (H-133) depends on $x_{2,r}$ and $\dot{x}_{2,r}$, which are the output of the command filter and therefore the analytical derivative $\dot{\alpha}_1$ is no longer required. In the absence of physical limitations (i.e. magnitude, rate and bandwidth constraints on the intermediate state x_2 and control u) and for sufficiently high update rate, closed-loop stability is still guaranteed even when uncertainties are introduced in either the system dynamics or the control effectiveness matrix.

H-2-7 Command-Filtered Adaptive Incremental Backstepping without Time-Scale Separation

In this section a Command-Filtered BS controller with I&I estimator is designed to guarantee global asymptotic stability of the closed-loop system and parameter convergence for an uncertain nonlinear system. We do not make the assumption of TSS (see Eq. (E-41)), thus when the sampling rate is sufficiently high we can write the pendulum model as

$$\dot{x}_1 = x_2 \tag{H-140a}$$
$$\dot{x}_2 = \dot{x}_{2,0} + \theta_{2,1}\cos(x_1)\Delta x_1 + \theta_{2,2}\Delta x_2 + \theta_{2,3}\Delta u \tag{H-140b}$$
$$\dot{\boldsymbol{\xi}}_2 = \boldsymbol{w}\,, \tag{H-140c}$$

in which $\boldsymbol{\xi}_2 \in \mathbb{R}^3$ is the estimator state and $\boldsymbol{w}$ is the update law to be determined. The parameters $\theta_{2,1}$, $\theta_{2,2}$ and $\theta_{2,3}$ are assumed to be unknown *constant* parameters. Note that Eq. (E-66b) is the incremental form of the full equation of the pendulum, see Eq. (B-3b).

The $\boldsymbol{x}$-subsystem can be written as

$$\Delta\dot{x}_1 = \Delta x_2 + \boldsymbol{\varphi}_1^T\boldsymbol{\theta}_2 \tag{H-141a}$$
$$\Delta\dot{x}_2 = \boldsymbol{\varphi}_2(x_1, \Delta\boldsymbol{x}, \Delta u)^T\boldsymbol{\theta}_2\,, \tag{H-141b}$$

where

$$\boldsymbol{\varphi}_1 = \begin{bmatrix} 0 \\ 0 \\ 0 \end{bmatrix}, \quad \boldsymbol{\varphi}_2(x_1, \Delta\boldsymbol{x}, \Delta u) = \begin{bmatrix} \cos(x_1)\Delta x_1 \\ \Delta x_2 \\ \Delta u \end{bmatrix}, \quad \boldsymbol{\theta}_2 = \begin{bmatrix} \theta_{2,1} \\ \theta_{2,2} \\ \theta_{2,3} \end{bmatrix}. \tag{H-142}$$

Now we introduce the following three-dimensional manifold:

$$\mathcal{M} = \left\{(\Delta\boldsymbol{x}, \boldsymbol{\xi}_2, \Delta u) \in \mathbb{R}^6 | \boldsymbol{\xi}_2 + \boldsymbol{\beta}_2(x_1, \Delta\boldsymbol{x}, \Delta u) - \boldsymbol{\theta}_2 = \boldsymbol{0}\right\}, \tag{H-143}$$

where $\boldsymbol{\beta}_2(x_1, \Delta\boldsymbol{x}, \Delta u)$ is a continuous function yet to be specified. The estimate of the unknown constants $\boldsymbol{\theta}_2$ is given by

$$\hat{\boldsymbol{\theta}}_2 = \boldsymbol{\xi}_2 + \boldsymbol{\beta}_2\,. \tag{H-144}$$

If the manifold $\mathcal{M}$ is *invariant* (see Definition H.1 on page 181), the dynamics of system (H-141) restricted to this manifold can be written as

$$\Delta\dot{x}_1 = \Delta x_2 \tag{H-145a}$$
$$\Delta\dot{x}_2 = \boldsymbol{\varphi}_2(x_1, \Delta\boldsymbol{x}, \Delta u)^T\left(\boldsymbol{\xi}_2 + \boldsymbol{\beta}_2(x_1, \Delta\boldsymbol{x}, \Delta u)\right). \tag{H-145b}$$

The dynamics of this system are completely known, i.e. the dynamics are independent of the unknown parameters $\theta_{2,1}$, $\theta_{2,2}$ and $\theta_{2,3}$. Now we define the off-the-manifold coordinate:

$$\boldsymbol{\sigma}_2 = \hat{\boldsymbol{\theta}}_2 - \boldsymbol{\theta}_2 = \boldsymbol{\xi}_2 + \boldsymbol{\beta}_2(x_1, \Delta\boldsymbol{x}, \Delta u) - \boldsymbol{\theta}_2\,, \tag{H-146}$$

which plays the role of estimation error. Now the task is to guarantee that the off-the-manifold coordinate $\boldsymbol{\sigma}_2$ globally asymptotically converges to its zero equilibrium. The off-the-manifold dynamics are given by

$$\begin{aligned}
\dot{\boldsymbol{\sigma}}_2 &= \boldsymbol{w} + \frac{\partial \boldsymbol{\beta}_2}{\partial x_1}\dot{x}_1 + \frac{\partial \boldsymbol{\beta}_2}{\partial \Delta x_1}\Delta \dot{x}_1 + \frac{\partial \boldsymbol{\beta}_2}{\partial \Delta x_2}\Delta \dot{x}_2 + \frac{\partial \boldsymbol{\beta}_2}{\partial \Delta u}\Delta \dot{u} \\
&= \boldsymbol{w} + \frac{\partial \boldsymbol{\beta}_2}{\partial x_1}x_2 + \frac{\partial \boldsymbol{\beta}_2}{\partial \Delta x_1}\Delta x_2 + \frac{\partial \boldsymbol{\beta}_2}{\partial \Delta x_2}\left[\boldsymbol{\varphi}_2(x_1, \Delta \boldsymbol{x}, \Delta u)^T \boldsymbol{\theta}_2\right] + \frac{\partial \boldsymbol{\beta}_2}{\partial \Delta u}\Delta \dot{u} \\
&= \boldsymbol{w} + \frac{\partial \boldsymbol{\beta}_2}{\partial x_1}x_2 + \frac{\partial \boldsymbol{\beta}_2}{\partial \Delta x_1}\Delta x_2 + \frac{\partial \boldsymbol{\beta}_2}{\partial \Delta x_2}\left[\boldsymbol{\varphi}_2(x_1, \Delta \boldsymbol{x}, \Delta u)^T \left(\boldsymbol{\xi}_2 + \boldsymbol{\beta}_2 - \boldsymbol{\sigma}_2\right)\right] + \frac{\partial \boldsymbol{\beta}_2}{\partial \Delta u}\Delta \dot{u} \,.
\end{aligned} \tag{H-147}$$

We select the update law in order to render the manifold $\mathcal{M}$ invariant as

$$\boldsymbol{w} = \dot{\boldsymbol{\xi}}_2 = -\frac{\partial \boldsymbol{\beta}_2}{\partial x_1}x_2 - \frac{\partial \boldsymbol{\beta}_2}{\partial \Delta x_1}\Delta x_2 - \frac{\partial \boldsymbol{\beta}_2}{\partial \Delta x_2}\left[\boldsymbol{\varphi}_2(x_1, \Delta \boldsymbol{x}, \Delta u)^T \left(\boldsymbol{\xi}_2 + \boldsymbol{\beta}_2\right)\right] - \frac{\partial \boldsymbol{\beta}_2}{\partial \Delta u}\Delta \dot{u} \,, \tag{H-148}$$

which results in the following off-the-manifold dynamics:

$$\dot{\boldsymbol{\sigma}}_2 = -\frac{\partial \boldsymbol{\beta}_2}{\partial \Delta x_2}\boldsymbol{\varphi}_2^T \boldsymbol{\sigma}_2 \,. \tag{H-149}$$

Note that the time derivative of the incremental control input Δu is required in the estimator design. This derivative will be obtained by using (delayed) outputs of the command filter, see Figure H-15. In order to render the manifold $\mathcal{M}$ attractive, we can select the $\boldsymbol{\beta}_2$-function as

$$\boldsymbol{\beta}_2(x_1, \Delta \boldsymbol{x}, \Delta u) = \Gamma_2 \int_0^{\Delta x_2} \boldsymbol{\varphi}_2(x_1, \Delta x_1, \chi, \Delta u)\, d\chi \,, \tag{H-150}$$

which results into

$$\boldsymbol{\beta}_2(x_1, \Delta \boldsymbol{x}, \Delta u) = \Gamma_2 \begin{bmatrix} \Delta x_2 \cos(x_1)\Delta x_1 \\ \frac{1}{2}\Delta x_2^2 \\ \Delta x_2 \Delta u \end{bmatrix} , \tag{H-151}$$

where Γ_2 is a positive diagonal matrix:

$$\Gamma_2 = \begin{bmatrix} \gamma_{2,1} & 0 & 0 \\ 0 & \gamma_{2,2} & 0 \\ 0 & 0 & \gamma_{2,3} \end{bmatrix} . \tag{H-152}$$

The *nonzero* partial derivatives of function $\boldsymbol{\beta}_2$ are given by

$$\begin{aligned}
&\frac{\partial \beta_{2,1}}{\partial x_1} = -\gamma_{2,1}\Delta x_2 \sin(x_1)\Delta x_1 \,, &&\frac{\partial \beta_{2,1}}{\partial \Delta x_1} = \gamma_{2,1}\Delta x_2 \cos(x_1) \,, &&\frac{\partial \beta_{2,1}}{\partial \Delta x_2} = \gamma_{2,1} \cos(x_1)\Delta x_1 \,, \\
&\frac{\partial \beta_{2,2}}{\partial \Delta x_2} = \gamma_{2,2}\Delta x_2 \,, &&\frac{\partial \beta_{2,3}}{\partial \Delta x_2} = \gamma_{2,3}\Delta u \,, &&\frac{\partial \beta_{2,3}}{\partial \Delta u} = \gamma_{2,3}\Delta x_2 \,.
\end{aligned} \tag{H-153}$$

The off-the-manifold dynamics are now given by

$$\dot{\sigma}_{2,1} = -\gamma_{2,1}\left[\sigma_{2,1}\cos^2(x_1)\Delta x_1^2 + \sigma_{2,2}\cos(x_1)\Delta x_1 \Delta x_2 + \sigma_{2,3}\cos(x_1)\Delta x_1 \Delta u\right] \tag{H-154a}$$

$$\dot{\sigma}_{2,2} = -\gamma_{2,2}\left[\sigma_{2,1}\cos(x_1)\Delta x_1 \Delta x_2 + \sigma_{2,2}\Delta x_2^2 + \sigma_{2,3}\Delta x_2 \Delta u\right] \tag{H-154b}$$

$$\dot{\sigma}_{2,3} = -\gamma_{2,3}\left[\sigma_{2,1}\cos(x_1)\Delta x_1 \Delta u + \sigma_{2,2}\Delta x_2 \Delta u + \sigma_{2,3}\Delta u^2\right] \,. \tag{H-154c}$$

In order to proof that the manifold $\mathcal{M}$ is indeed attractive, we now select the following Lyapunov function:

$$\mathcal{V}(\boldsymbol{\sigma}_2) = \frac{1}{2\gamma_{2,1}}\sigma_{2,1}^2 + \frac{1}{2\gamma_{2,2}}\sigma_{2,2}^2 + \frac{1}{2\gamma_{2,3}}\sigma_{2,3}^2 \, . \tag{H-155}$$

Taking the time derivative of this function along the trajectories of Eq. (H-154) results in

$$\begin{aligned}
\dot{\mathcal{V}} &= \frac{1}{\gamma_{2,1}}\sigma_{2,1}\dot{\sigma}_{2,1} + \frac{1}{\gamma_{2,2}}\sigma_{2,2}\dot{\sigma}_{2,2} + \frac{1}{\gamma_{2,3}}\sigma_{2,3}\dot{\sigma}_{2,3} \\
&= -\sigma_{2,1}\left[\sigma_{2,1}\cos^2(x_1)\Delta x_1^2 + \sigma_{2,2}\cos(x_1)\Delta x_1 \Delta x_2 + \sigma_{2,3}\cos(x_1)\Delta x_1 \Delta u\right] \\
&\quad -\sigma_{2,2}\left[\sigma_{2,1}\cos(x_1)\Delta x_1\Delta x_2 + \sigma_{2,2}\Delta x_2^2 + \sigma_{2,3}\Delta x_2 \Delta u\right] \\
&\quad -\sigma_{2,3}\left[\sigma_{2,1}\cos(x_1)\Delta x_1 \Delta u + \sigma_{2,2}\Delta x_2 \Delta u + \sigma_{2,3}\Delta u^2\right] \\
&= -\left[\sigma_{2,1}^2\cos^2(x_1)\Delta x_1^2 + \sigma_{2,2}^2\Delta x_2^2 + \sigma_{2,3}^2\Delta u^2\right] \\
&\quad -\left[2\sigma_{2,1}\sigma_{2,2}\cos(x_1)\Delta x_1\Delta x_2 + 2\sigma_{2,1}\sigma_{2,3}\cos(x_1)\Delta x_1 \Delta u + 2\sigma_{2,2}\sigma_{2,3}\Delta x_2\Delta u\right] \\
&= -\left[\sigma_{2,1}\cos(x_1)\Delta x_1 + \sigma_{2,2}\Delta x_2 + \sigma_{2,3}\Delta u\right]^2 \, .
\end{aligned} \tag{H-156}$$

Now we have succeeded in making the manifold $\mathcal{M}$ attractive and invariant. The next task is to find a BS control law such that the closed-loop system globally asymptotically tracks the reference signal $x_{1,r}$, whose derivatives are known and bounded. Command filters will be used to obviate the need for analytic computation of the virtual control derivative and to obtain the time derivative of the real incremental control Δu which is required for the I&I estimator, see Eq. (H-148). Earlier we obtained the following control laws for the complete nonlinear pendulum:

$$u = \frac{1}{\theta_{2,3}}\left[-z_1 - c_2\left(x_2 - \alpha_1\right) - \theta_{2,1}\sin(x_1) - \theta_{2,2}x_2 + \dot{\alpha}_1\right] \tag{C-39 revisited}$$

$$u^0 = \frac{1}{\hat{\theta}_{2,3}}\left[-\bar{z}_1 - c_2\left(x_2 - x_{2,r}\right) - \hat{\theta}_{2,1}\sin(x_1) - \hat{\theta}_{2,2}x_2 + \dot{x}_{2,r}\right] \, , \tag{H-110 revisited}$$

which are respectively the full-information BS controller and the Command-Filtered BS controller based on an I&I estimator. Earlier we obtained the following Command-Filtered BS control law for the incremental system without TSS:

$$u^0 = u_0 + \frac{1}{\theta_{2,3}}\left[-z_1 - c_2\left(x_2 - x_{2,r}\right) - \dot{x}_{2,0} - \theta_{2,1}\cos(x_1)\Delta x_1 - \theta_{2,2}\Delta x_2 + \dot{x}_{2,r}\right] \, . \tag{E-77 revisited}$$

Now the following Command-Filtered IBS control law based on an I&I estimator seems viable:

$$\begin{aligned}
u^0 &= u_0 + \frac{1}{\hat{\theta}_{2,3}}\left[-\bar{z}_1 - c_2\left(x_2 - x_{2,r}\right) - \dot{x}_{2,0} - \hat{\theta}_{2,1}\cos(x_1)\Delta x_1 - \hat{\theta}_{2,2}\Delta x_2 + \dot{x}_{2,r}\right] \\
&= u_0 + \frac{1}{\xi_{2,3} + \beta_{2,3}}\Big[-\bar{z}_1 - c_2\left(x_2 - x_{2,r}\right) - \dot{x}_{2,0} - \left(\xi_{2,1} + \beta_{2,1}\right)\cos(x_1)\Delta x_1 \\
&\quad - \left(\xi_{2,2} + \beta_{2,2}\right)\Delta x_2 + \dot{x}_{2,r}\Big] \, .
\end{aligned} \tag{H-157}$$

In order to proof stability, we consider the following quadratic Lyapunov function:

$$\mathcal{V}(\bar{\boldsymbol{z}}, \boldsymbol{\sigma}_2) = \bar{z}_1^2 + \bar{z}_2^2 + \frac{L}{2\gamma_{2,1}}\sigma_{2,1}^2 + \frac{L}{2\gamma_{2,2}}\sigma_{2,2}^2 + \frac{L}{2\gamma_{2,3}}\sigma_{2,3}^2 \, , \tag{H-158}$$

where $\bar{\boldsymbol{z}}$ and the $\bar{z}_1$-dynamics are similar as in Eqs. (D-37) and (D-38) and L is a positive constant. The $\bar{z}_2$-dynamics are now given by

$$\begin{aligned}\dot{\bar{z}}_2 &= \dot{x}_{2,0} + \theta_{2,1}\cos(x_1)\Delta x_1 + \theta_{2,2}\Delta x_2 + \theta_{2,3}\Delta u - \dot{x}_{2,r} - \dot{\chi}_2 \\ &= \dot{x}_{2,0} + (\xi_{2,1} + \beta_{2,1} - \sigma_{2,1})\cos(x_1)\Delta x_1 + (\xi_{2,2} + \beta_{2,2} - \sigma_{2,2})\,\Delta x_2 \\ &\quad + (\xi_{2,3} + \beta_{2,3})\,\Delta u - \sigma_{2,3}\Delta u - \dot{x}_{2,r} - \dot{\chi}_2 \,. \end{aligned} \tag{H-159}$$

Taking the time derivative of $\mathcal{V}$ along the trajectories of the compensated error dynamics and Eq. (H-154) results in

$$\begin{aligned}\dot{\mathcal{V}} = &-2c_1\bar{z}_1^2 + 2\bar{z}_1\bar{z}_2 + 2\bar{z}_2\big[\dot{x}_{2,0} + (\xi_{2,1} + \beta_{2,1} - \sigma_{2,1})\cos(x_1)\Delta x_1 \\ &+ (\xi_{2,2} + \beta_{2,2} - \sigma_{2,2})\,\Delta x_2 + (\xi_{2,3} + \beta_{2,3})\,\Delta u - \sigma_{2,3}\Delta u - \dot{x}_{2,r} - \dot{\chi}_2\big] \\ &-L\sigma_{2,1}\left[\sigma_{2,1}\cos^2(x_1)\Delta x_1^2 + \sigma_{2,2}\cos(x_1)\Delta x_1\Delta x_2 + \sigma_{2,3}\cos(x_1)\Delta x_1\Delta u\right] \\ &-L\sigma_{2,2}\left[\sigma_{2,1}\cos(x_1)\Delta x_1\Delta x_2 + \sigma_{2,2}\Delta x_2^2 + \sigma_{2,3}\Delta x_2\Delta u\right] \\ &-L\sigma_{2,3}\left[\sigma_{2,1}\cos(x_1)\Delta x_1\Delta u + \sigma_{2,2}\Delta x_2\Delta u + \sigma_{2,3}\Delta u^2\right] \,. \end{aligned} \tag{H-160}$$

Signal χ_2 is the output of the following stable linear filter:

$$\dot{\chi}_2 = -c_2\chi_2 + (\xi_{2,3} + \beta_{2,3})\left(u - u^0\right) \,, \tag{H-161}$$

with $\chi_2(0) = 0$. This yields

$$\begin{aligned}\dot{\mathcal{V}} &= -2c_1\bar{z}_1^2 + 2\bar{z}_1\bar{z}_2 \\ &\quad +2\bar{z}_2\big[\dot{x}_{2,0} + (\xi_{2,1} + \beta_{2,1} - \sigma_{2,1})\cos(x_1)\Delta x_1 + (\xi_{2,2} + \beta_{2,2} - \sigma_{2,2})\,\Delta x_2 \\ &\quad + (\xi_{2,3} + \beta_{2,3})\left(u^0 - u_0\right) - \sigma_{2,3}u - \dot{x}_{2,r} + c_2\chi_2\big] \\ &\quad -L\sigma_{2,1}\left[\sigma_{2,1}\cos^2(x_1)\Delta x_1^2 + \sigma_{2,2}\cos(x_1)\Delta x_1\Delta x_2 + \sigma_{2,3}\cos(x_1)\Delta x_1\Delta u\right] \\ &\quad -L\sigma_{2,2}\left[\sigma_{2,1}\cos(x_1)\Delta x_1\Delta x_2 + \sigma_{2,2}\Delta x_2^2 + \sigma_{2,3}\Delta x_2\Delta u\right]) \\ &\quad -L\sigma_{2,3}\left[\sigma_{2,1}\cos(x_1)\Delta x_1\Delta u + \sigma_{2,2}\Delta x_2\Delta u + \sigma_{2,3}\Delta u^2\right] \\ &= -2c_1\bar{z}_1^2 + 2\bar{z}_1\bar{z}_2 \\ &\quad +2\bar{z}_2\left[-\bar{z}_1 - c_2z_2 - \sigma_{2,1}\cos(x_1)\Delta x_1 - \sigma_{2,2}\Delta x_2 - \sigma_{2,3}\Delta u + c_2\chi_2\right] \\ &\quad -L\sigma_{2,1}\left[\sigma_{2,1}\cos^2(x_1)\Delta x_1^2 + \sigma_{2,2}\cos(x_1)\Delta x_1\Delta x_2 + \sigma_{2,3}\cos(x_1)\Delta x_1\Delta u\right] \\ &\quad -L\sigma_{2,2}\left[\sigma_{2,1}\cos(x_1)\Delta x_1\Delta x_2 + \sigma_{2,2}\Delta x_2^2 + \sigma_{2,3}\Delta x_2\Delta u\right] \\ &\quad -L\sigma_{2,3}\left[\sigma_{2,1}\cos(x_1)\Delta x_1\Delta u + \sigma_{2,2}\Delta x_2\Delta u + \sigma_{2,3}\Delta u^2\right] \\ &= -2c_1\bar{z}_1^2 - 2c_2\bar{z}_2^2 - 2\bar{z}_2\left[\sigma_{2,1}\cos(x_1)\Delta x_1 + \sigma_{2,2}\Delta x_2 + 2\sigma_{2,3}\Delta u\right] \\ &\quad -L\big[\sigma_{2,1}^2\cos^2(x_1)\Delta x_1^2 + \sigma_{2,2}^2\Delta x_2^2 + \sigma_{2,3}^2\Delta u^2 + 2\sigma_{2,1}\sigma_{2,2}\cos(x_1)\Delta x_1\Delta x_2 \\ &\quad +2\sigma_{2,1}\sigma_{2,3}\cos(x_1)\Delta x_1\Delta u + 2\sigma_{2,2}\sigma_{2,3}\Delta x_2\Delta u\big] \\ &= -2c_1\bar{z}_1^2 - 2c_2\bar{z}_2^2 + \epsilon\bar{z}_2^2 - \left(\frac{1}{\sqrt{\epsilon}}\left[\sigma_{2,1}\cos(x_1)\Delta x_1 + \sigma_{2,2}\Delta x_2 + \sigma_{2,3}\Delta u\right] + \sqrt{\epsilon}\bar{z}_2\right)^2 \\ &\quad -\left(L - \frac{1}{\epsilon}\right)\left[\sigma_{2,1}\cos(x_1)\Delta x_1 + \sigma_{2,2}\Delta x_2 + \sigma_{2,3}\Delta u\right]^2 \\ &\leq -2c_1\bar{z}_1^2 - (2c_2 - \epsilon)\,\bar{z}_2^2 - \left(L - \frac{1}{\epsilon}\right)\left[\sigma_{2,1}\cos(x_1)\Delta x_1 + \sigma_{2,2}\Delta x_2 + \sigma_{2,3}\Delta u\right]^2 \,, \end{aligned} \tag{H-162}$$

where ϵ is a positive constant. If $c_2 > \frac{\epsilon}{2}$ and $L > \frac{1}{\epsilon}$, it follows according to Theorem C.2 that:

$$\lim_{t\to\infty} \bar{\boldsymbol{z}} = \mathbf{0} \tag{H-163a}$$

$$\lim_{t\to\infty} \left[\sigma_{2,1}\cos(x_1)\Delta x_1 + \sigma_{2,2}\Delta x_2 + \sigma_{2,3}\Delta u\right] = \lim_{t\to\infty}\left[\boldsymbol{\varphi}_2^T\left(\hat{\boldsymbol{\theta}}_2 - \boldsymbol{\theta}_2\right)\right] = 0\,. \tag{H-163b}$$

Because ϵ and L are arbitrary positive constants, stability is guaranteed when $c_2 > 0$. Note that Eq. (H-163b) does not imply that the estimate $\hat{\boldsymbol{\theta}}_2$ converges to the real parameter $\boldsymbol{\theta}_2$. According to (Karagiannis & Astolfi, 2010) this requires a PE condition, and can be achieved only by injecting "sufficiently rich" reference signals. From Eqs. (H-154) and (H-163b) can be seen that this requires a reference signal $\Delta u \neq 0$ that results in $x_1 \neq k\pi$ and $\Delta x_2 \neq 0$ with k an integer.

The new control law (H-157) based on an I&I estimator depends on $x_{2,r}$ and $\dot{x}_{2,r}$, which are the output of the command filter and therefore the analytical derivative $\dot{\alpha}_1$ is no longer required. In the absence of physical limitations (i.e. magnitude, rate and bandwidth constraints on the intermediate state x_2 and control u), closed-loop stability is still guaranteed even when uncertainties are introduced in either the system dynamics or the control effectiveness matrix.

Appendix I

Sensor-Based Backstepping

In this appendix the Sensor-Based Backstepping (SBB) control approach is derived and evaluated that is based on the singular perturbation theory (see (Khalil & Grizzle, 2002)) and removes the dependency on the system dynamics by using measurements of the state derivatives (I-1). The SBB controller uses even less model information compared to the incremental control laws (see Appendix E). In order to evaluate this nonlinear control approach, a SBB control law is derived and simulated for the pendulum model (I-2).

I-1 Theory

We consider the following scalar nonlinear system:

$$\dot{x} = f(t, x, u)\,, \tag{I-1}$$

where $x \in \mathbb{R}$ is the state of the system and $u \in \mathbb{R}$ is the control input and $(\partial f / \partial u) \neq 0$. In (Hovakimyan et al., 2007) the following controller is proposed for a time-scale separated system

$$\epsilon \dot{u} = -\operatorname{sgn}\left(\frac{\partial f}{\partial u}\right) f(t, z, u)\,, \quad \epsilon \ll 1\,, \tag{I-2}$$

with the tracking error $z = x - x_r$. This control law asymptotically stabilizes the error dynamics when the assumptions in Theorem 2 of (Hovakimyan et al., 2007) are met. These assumptions are also referred to as the Approximate Dynamic Inversion (ADI) assumptions. One of the advantages of the SBB controller is that it can be applied to nonaffine systems without the need for a nonlinear solver.

In (Falkena, 2012) the mapping $f(t, z, u)$ is selected as

$$f(t, z, u) = \dot{x} - \dot{x}_r + c\frac{\partial \mathcal{V}(z)}{\partial z}\,, \quad c > 0\,, \tag{I-3}$$

where $\dot{x}$ is a measurement or estimated value of the state derivative and $\dot{x}_r$ is the desired state derivative. A Backstepping (BS) controller can be designed for the latter using the positive definite, radially unbounded Control Lyapunov Function (CLF) $\mathcal{V}(z)$, of which the time derivative should be negative definite for asymptotic stability in the sense of Lyapunov. Substituting Eq. (I-3) in Eq. (I-2) yields

$$\epsilon \dot{u} = -\operatorname{sgn}\left(\frac{\partial f}{\partial u}\right)\left[\dot{x} - \dot{x}_r + c\frac{\partial \mathcal{V}(z)}{\partial z}\right] . \tag{I-4}$$

This controller will guarantee asymptotic stability of the error dynamics when the ADI assumptions are met. Note that the SBB control law (I-4) uses even less model information than the time-scaled separated Incremental Backstepping (IBS) control method of Appendix E.

I-2 Simulations

In this section an SBB controller is designed for the pendulum model, which is for convenience repeated below:

$$\dot{x}_1 = x_2 \tag{B-3a revisited}$$
$$\dot{x}_2 = \theta_{2,1}\sin(x_1) + \theta_{2,2}x_2 + \theta_{2,3}u \, . \tag{B-3b revisited}$$

The tracking errors are defined as

$$z_1 = x_1 - x_{1,r} \tag{I-6a}$$
$$z_2 = x_2 - \alpha_1 \, . \tag{I-6b}$$

The derivations for subsystem x_1 remain exactly the same as in Appendix C-3 (see Eqs. (C-32) to (C-36)), because this subsystem is assumed to be fully known. Now the following quadratic Lyapunov function is introduced:

$$\mathcal{V}(z_2) = \frac{1}{2}z_2^2 \rightarrow \frac{\partial \mathcal{V}}{\partial z_2} = z_2 \, . \tag{I-7}$$

From Eqs. (I-2), (I-6b) and (I-7) we now obtain the SBB control law:

$$\epsilon \dot{u} = -\operatorname{sgn}(\theta_{2,3})\left[\dot{x}_2 - \dot{\alpha}_1 + c_2 z_2\right] . \tag{I-8}$$

If the angular acceleration $\dot{x}_2$ cannot be measured, it can be estimated by using (noisy) angular rate data x_2. This will generally amplify the noise level and/or introduce time delays. Estimation of the angular acceleration can be avoided by integrating both sides of Eq. (I-8):

$$u = u(t_0) - \frac{\operatorname{sgn}(\theta_{2,3})}{\epsilon}\left[x_2 - x_2(t_0) - \alpha_1 + \alpha_1(t_0) + c_2\int_{t_0}^{t} z_2 \, dt\right] , \tag{I-9}$$

from which we can conclude that the input u can be calculated without knowledge of the angular acceleration $\dot{x}_2$ and the virtual control derivative $\dot{\alpha}_1$. Although Eqs. (I-8) and (I-9) are mathematically similar, control law (I-9) will result in better tracking performance when the system is not equipped with an angular acceleration sensor with a similar or higher precision compared to that of an angular rate sensor.

If we compare the earlier designed time-scaled separated IBS controller with the SBB controller:

$$u = u_0 + \frac{1}{\theta_{2,3}} \left[-\dot{x}_{2,0} + \dot{\alpha}_1 - z_1 - c_2 z_2 \right] \tag{E-49 revisited}$$

$$u = u(t_0) - \frac{\operatorname{sgn}(\theta_{2,3})}{\epsilon} \left[x_2 - x_2(t_0) - \alpha_1 + \alpha_1(t_0) + c_2 \int_{t_0}^{t} z_2 \, dt \right] , \tag{I-9 revisited}$$

we can see that the SBB controller uses even less model information than the IBS controller. The only information which the SBB controller requires from the model is the sign of the control effectiveness parameter $\theta_{2,3}$, which may be obtained by a crude form of online aerodynamic model identification.

Simulations of the SBB controller (I-9) have been run for the system (B-3) with a sampling time of 0.01 s. The initial conditions and parameters which have been used in this simulation for the model can be found in Eq. (C-44). The following control parameters have been selected:

$$c_1 = 10 , \qquad c_2 = 10 , \qquad \operatorname{sgn}\left(\hat{\theta}_{2,3}\right) = \operatorname{sgn}\left(\theta_{2,3}\right) . \tag{I-10}$$

The results of the simulation can be seen in Figure I-1. Clearly, the model-free SBB controller performs slightly worse than the conventional BS controller in absence of uncertainties. The tracking performance of the controller can be improved by decreasing the value of ϵ. However, the sampling rate of the simulation should be consistent with ϵ, i.e. the sampling rate should be high enough to capture the high frequent dynamics to avoid instability. The advantage of the SBB controller compared to the BS controller is that it is a model-free approach, and therefore it is not sensitive to model uncertainties. However, tuning of the parameter ϵ might be required in order to obtain satisfactory closed-loop performance over the complete state space (Galrinho, 2013; Galrinho et al., 2013).

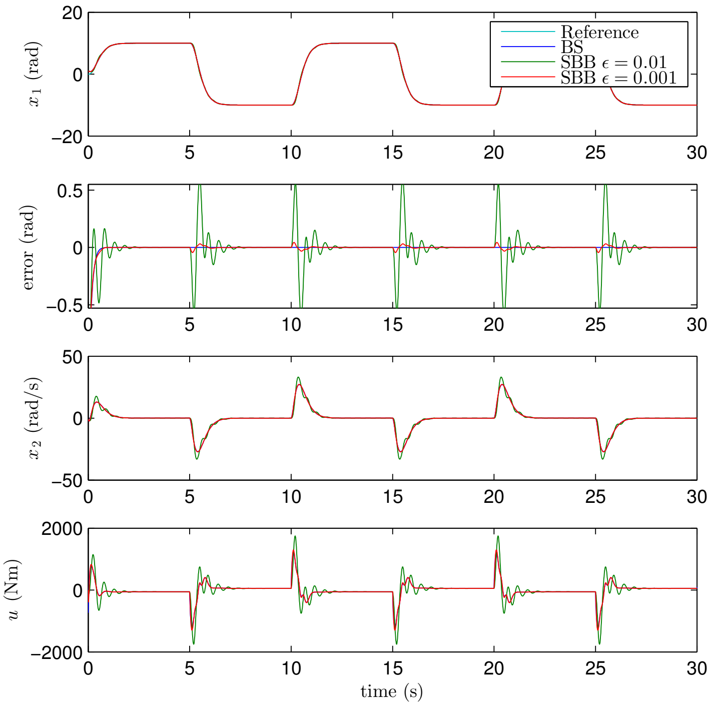

Figure I-1: The control performance of a Backstepping controller and a Sensor-Based Backstepping controller for different values of ϵ in absence of any uncertainties.

Appendix J

Overview of Backstepping Control Laws

In this appendix an overview is given of all the Backstepping control laws that have been derived for the pendulum model in the foregoing appendices.

Backstepping

$$u = \frac{1}{\theta_{2,3}} \left[-z_1 - c_2(x_2 - \alpha_1) - \theta_{2,1} \sin(x_1) - \theta_{2,2} x_2 + \dot{\alpha}_1 \right] \tag{C-43 revisited}$$

Command-Filtered Backstepping

$$u^0 = \frac{1}{\theta_{2,3}} \left[-\bar{z}_1 - c_2 \left(x_2 - x_{2,r} \right) - \theta_{2,1} \sin(x_1) - \theta_{2,2} x_2 + \dot{x}_{2,r} \right] \tag{D-46 revisited}$$

Incremental Backstepping with Time-Scale Separation

$$u = u_0 + \frac{1}{\theta_{2,3}} \left[-z_1 - c_2 \left(x_2 - \alpha_1 \right) - \dot{x}_{2,0} + \dot{\alpha}_1 \right] \tag{E-46 revisited}$$

Command-Filtered Incremental Backstepping with Time-Scale Separation

For command filter (1) (see Figure E-4a):

$$\Delta u^0 = \frac{1}{\theta_{2,3}} \left[-\bar{z}_1 - c_2 \left(x_2 - x_{2,r} \right) - \dot{x}_{2,0} + \dot{x}_{2,r} \right] \tag{E-58 revisited}$$

For command filter (2) (see Figure E-4b):

$$u^0 = u_0 + \frac{1}{\theta_{2,3}} \left[-\bar{z}_1 - c_2 \left(x_2 - x_{2,r} \right) - \dot{x}_{2,0} + \dot{x}_{2,r} \right] \tag{E-63 revisited}$$

Incremental Backstepping without Time-Scale Separation

$$u = u_0 + \frac{1}{\theta_{2,3}} \left[-z_1 - c_2 \left(x_2 - \alpha_1 \right) - \dot{x}_{2,0} - \theta_{2,1} \cos(x_{1,0}) \Delta x_1 - \theta_{2,2} \Delta x_2 + \dot{\alpha}_1 \right] \tag{E-70 revisited}$$

Command-Filtered Incremental Backstepping without Time-Scale Separation

$$u^0 = u_0 + \frac{1}{\theta_{2,3}} \left[-z_1 - c_2 \left(x_2 - x_{2,r} \right) - \dot{x}_{2,0} - \theta_{2,1} \cos(x_{1,0}) \Delta x_1 - \theta_{2,2} \Delta x_2 + \dot{x}_{2,r} \right] \tag{E-77 revisited}$$

Tuning Functions Adaptive Backstepping with one unknown parameter

$$u = \frac{1}{\theta_{2,3}} \left[-z_1 - c_2 (x_2 - \alpha_1) - \theta_{2,1} \sin(x_1) - \hat{\theta}_{2,2} x_2 + \dot{\alpha}_1 \right] \tag{F-79 revisited}$$

$$\dot{\hat{\theta}}_{2,2} = \gamma_2 z_2 x_2 \tag{F-81 revisited}$$

Command-Filtered Tuning Functions Adaptive Backstepping with one unknown parameter

$$u^0 = \frac{1}{\theta_{2,3}} \left[-\bar{z}_1 - c_2 \left(x_2 - x_{2,r} \right) - \theta_{2,1} \sin(x_1) - \hat{\theta}_{2,2} x_2 + \dot{x}_{2,r} \right] \tag{F-95a revisited}$$

$$\dot{\hat{\theta}}_{2,2} = \gamma_2 \bar{z}_2 x_2 \tag{F-95b revisited}$$

Tuning Functions Adaptive Backstepping with three unknown parameters

$$u = \frac{1}{\hat{\theta}_{2,3}} \left[-z_1 - c_2 \left(x_2 - \alpha_1 \right) - \hat{\theta}_{2,1} \sin(x_1) - \hat{\theta}_{2,2} x_2 + \dot{\alpha}_1 \right] \tag{F-112 revisited}$$

$$\dot{\hat{\theta}}_{2,1} = \gamma_{2,1} z_2 \sin(x_1) \tag{F-114a revisited}$$

$$\dot{\hat{\theta}}_{2,2} = \gamma_{2,2} z_2 x_2 \tag{F-114b revisited}$$

$$\dot{\hat{\theta}}_{2,3} = \gamma_{2,3} z_2 u \tag{F-114c revisited}$$

Tuning Functions Adaptive Incremental Backstepping with Time-Scale Separation

$$u = u_0 + \frac{1}{\hat{\theta}_{2,3}} \left[-z_1 - c_2 \left(x_2 - \alpha_1\right) - \dot{x}_{2,0} + \dot{\alpha}_1\right] \tag{F-124 revisited}$$

$$\dot{\hat{\theta}}_{2,3} = \gamma_2 z_2 \Delta u \tag{F-126 revisited}$$

Tuning Functions Adaptive Incremental Backstepping without Time-Scale Separation

$$\Delta u = \frac{1}{\hat{\theta}_{2,3}} \left[-z_1 - c_2 \left(x_2 - \alpha_1\right) - \dot{x}_{2,0} - \hat{\theta}_{2,1} \cos(x_{1,0}) \Delta x_1 - \hat{\theta}_{2,2} \Delta x_2 + \dot{\alpha}_1\right] \tag{F-136 revisited}$$

$$\dot{\hat{\theta}}_{2,1} = \gamma_{2,1} z_2 \cos(x_{1,0}) \Delta x_1 \tag{F-137a revisited}$$

$$\dot{\hat{\theta}}_{2,2} = \gamma_{2,2} z_2 \Delta x_2 \tag{F-137b revisited}$$

$$\dot{\hat{\theta}}_{2,3} = \gamma_{2,3} z_2 \Delta u \tag{F-137c revisited}$$

Least-Squares Adaptive Backstepping with one unknown parameter

$$u = \frac{1}{\theta_{2,3}} \left[-c_2 z_2 - z_1 - \theta_{2,1} \sin(x_1) - \hat{\theta}_{2,2} x_2 + \dot{\alpha}_1\right] \tag{G-37 revisited}$$

$$\Delta u = \frac{1}{\theta_{2,3}} \left[-c_2 z_2 - z_1 - \theta_{2,1} \cos(x_{1,0}) \Delta x_1 - \hat{\theta}_{2,2} \Delta x_2 + \dot{\alpha}_1 - \dot{x}_{2,0}\right] \tag{G-38 revisited}$$

$$\underbrace{\begin{bmatrix} \dot{x}_{2,k-N} - \sin(x_{1,k-N}) x_{1,k-N} \theta_{2,1} - u_{k-N} \theta_{2,3} \\ \vdots \\ \dot{x}_{2,k-1} - \sin(x_{1,k-1}) x_{1,k-1} \theta_{2,1} - u_{k-1} \theta_{2,3} \\ \dot{x}_{2,k} - \sin(x_{1,k}) x_{1,k} \theta_{2,1} - u_k \theta_{2,3} \end{bmatrix}}_{\boldsymbol{y}} \cong \underbrace{\begin{bmatrix} x_{2,k-N} \\ \vdots \\ x_{2,k-1} \\ x_{2,k} \end{bmatrix}}_{A} \theta_{2,2} \tag{G-36 revisited}$$

$$\hat{\theta}_{2,2} = \left(A^T A\right)^{-1} A^T \boldsymbol{y} \tag{G-21 revisited}$$

Least-Squares Adaptive Backstepping with three unknown parameter

$$u = \frac{1}{\hat{\theta}_{2,3}} \left[-c_2 z_2 - z_1 - \hat{\theta}_{2,1} \sin(x_1) - \hat{\theta}_{2,2} x_2 + \dot{\alpha}_1 \right] \tag{G-42 revisited}$$

$$\Delta u = \frac{1}{\hat{\theta}_{2,3}} \left[-c_2 z_2 - z_1 - \hat{\theta}_{2,1} \cos(x_{1,0}) \Delta x_1 - \hat{\theta}_{2,2} \Delta x_2 + \dot{\alpha}_1 - \dot{x}_{2,0} \right] \tag{G-43 revisited}$$

$$\underbrace{\begin{bmatrix} \dot{x}_{2,k-N} \\ \vdots \\ \dot{x}_{2,k-1} \\ \dot{x}_{2,k} \end{bmatrix}}_{\boldsymbol{y}} = \underbrace{\begin{bmatrix} \sin(x_{1,k-N}) x_{1,k-N} & x_{2,k-N} & u_{k-N} \\ \vdots & \vdots & \vdots \\ \sin(x_{1,k-1}) x_{1,k-1} & x_{2,k-1} & u_{k-1} \\ \sin(x_{1,k}) x_{1,k} & x_{2,k} & u_k \end{bmatrix}}_{A} \underbrace{\begin{bmatrix} \theta_{2,1} \\ \theta_{2,2} \\ \theta_{2,3} \end{bmatrix}}_{\boldsymbol{\theta}_2} \tag{G-41 revisited}$$

$$\hat{\boldsymbol{\theta}}_2 = \left(A^T A \right)^{-1} A^T \boldsymbol{y} \tag{G-21 revisited}$$

Least-Squares Adaptive Incremental Backstepping with one unknown parameter

$$u = \frac{1}{\theta_{2,3}} \left[-c_2 z_2 - z_1 - \theta_{2,1} \sin(x_1) - \hat{\theta}_{2,2} x_2 + \dot{\alpha}_1 \right] \tag{G-48 revisited}$$

$$\Delta u = \frac{1}{\theta_{2,3}} \left[-c_2 z_2 - z_1 - \theta_{2,1} \cos(x_{1,0}) \Delta x_1 - \hat{\theta}_{2,2} \Delta x_2 + \dot{\alpha}_1 - \dot{x}_{2,0} \right] \tag{G-49 revisited}$$

$$\underbrace{\begin{bmatrix} \Delta \dot{x}_{2,k-N} - \cos(x_{1,k-N-1}) \Delta x_{1,k-N} \theta_{2,1} - \Delta u_{k-N} \theta_{2,3} \\ \vdots \\ \Delta \dot{x}_{2,k-1} - \cos(x_{1,k-2}) \Delta x_{1,k-1} \theta_{2,1} - \Delta u_{k-1} \theta_{2,3} \\ \Delta \dot{x}_{2,k} - \cos(x_{1,k-1}) \Delta x_{1,k} \theta_{2,1} - \Delta u_k \theta_{2,3} \end{bmatrix}}_{\boldsymbol{y}} \cong \underbrace{\begin{bmatrix} \Delta x_{2,k-N} \\ \vdots \\ \Delta x_{2,k-1} \\ \Delta x_{2,k} \end{bmatrix}}_{A} \theta_{2,2} \tag{G-47 revisited}$$

$$\hat{\theta}_{2,2} = \left(A^T A \right)^{-1} A^T \boldsymbol{y} \tag{G-21 revisited}$$

Least-Squares Adaptive Incremental Backstepping with three unknown parameters

$$u = \frac{1}{\hat{\theta}_{2,3}} \left[-c_2 z_2 - z_1 - \hat{\theta}_{2,1} \sin(x_1) - \hat{\theta}_{2,2} x_2 + \dot{\alpha}_1 \right] \tag{G-53 revisited}$$

$$\Delta u = \frac{1}{\hat{\theta}_{2,3}} \left[-c_2 z_2 - z_1 - \hat{\theta}_{2,1} \cos(x_{1,0}) \Delta x_1 - \hat{\theta}_{2,2} \Delta x_2 + \dot{\alpha}_1 - \dot{x}_{2,0} \right] \tag{G-54 revisited}$$

$$\underbrace{\begin{bmatrix} \Delta \dot{x}_{2,k-N} \\ \vdots \\ \Delta \dot{x}_{2,k-1} \\ \Delta \dot{x}_{2,k} \end{bmatrix}}_{\boldsymbol{y}} \cong \underbrace{\begin{bmatrix} \cos(x_{1,k-N-1}) \Delta x_{1,k-N} & \Delta x_{2,k-N} & \Delta u_{k-N} \\ \vdots & \vdots & \\ \cos(x_{1,k-2}) \Delta x_{1,k-1} & \Delta x_{2,k-1} & \Delta u_{k-1} \\ \cos(x_{1,k-1}) \Delta x_{1,k} & \Delta x_{2,k} & \Delta u_k \end{bmatrix}}_{A} \underbrace{\begin{bmatrix} \theta_{2,1} \\ \theta_{2,2} \\ \theta_{2,3} \end{bmatrix}}_{\boldsymbol{\theta}_2} \tag{G-52 revisited}$$

$$\hat{\boldsymbol{\theta}}_2 = \left(A^T A \right)^{-1} A^T \boldsymbol{y} \tag{G-21 revisited}$$

Least-Squares Adaptive Incremental Backstepping with Time-Scale Separation

$$\Delta u = \frac{1}{\hat{\theta}_{2,3}} \left[-c_2 z_2 - z_1 + \dot{\alpha}_1 - \dot{x}_{2,0} \right] \tag{G-58 revisited}$$

$$\underbrace{\begin{bmatrix} \Delta \dot{x}_{2,k-N} \\ \vdots \\ \Delta \dot{x}_{2,k-1} \\ \Delta \dot{x}_{2,k} \end{bmatrix}}_{\boldsymbol{y}} \cong \underbrace{\begin{bmatrix} \Delta u_{k-N} \\ \vdots \\ \Delta u_{k-1} \\ \Delta u_k \end{bmatrix}}_{A} \theta_{2,3} \tag{G-57 revisited}$$

$$\hat{\theta}_{2,3} = \left(A^T A \right)^{-1} A^T \boldsymbol{y} \tag{G-21 revisited}$$

Immersion & Invariance Adaptive Backstepping with one unknown parameter

$$u = \frac{1}{\theta_{2,3}} \left[-z_1 - c_2 \left(x_2 - \alpha_1 \right) - \theta_{2,1} \sin(x_1) - \hat{\theta}_{2,2} x_2 + \dot{\alpha}_1 \right] \tag{H-40 revisited}$$

$$\hat{\theta}_{2,2} = \xi_{2,2} + \beta_2 \tag{H-17 revisited}$$

$$\dot{\xi}_{2,2} = -\frac{\partial \beta_2}{\partial x_2} \left[\theta_{2,1} \sin(x_1) + \left(\xi_{2,2} + \beta_2 \right) x_2 + \theta_{2,3} u \right] \tag{H-22 revisited}$$

$$\beta_2 = \frac{\gamma}{2} x_2^2 \tag{H-26 revisited}$$

Command-Filtered Immersion & Invariance Adaptive Backstepping with one unknown parameter

$$u^0 = \frac{1}{\theta_{2,3}} \left[-\bar{z}_1 - c_2 \left(x_2 - x_{2,r} \right) - \theta_{2,1} \sin(x_1) - \hat{\theta}_{2,2} x_2 + \dot{x}_{2,r} \right] \tag{H-55 revisited}$$

$$\hat{\theta}_{2,2} = \xi_{2,2} + \beta_2 \tag{H-17 revisited}$$

$$\dot{\xi}_{2,2} = -\frac{\partial \beta_2}{\partial x_2} \left[\theta_{2,1} \sin(x_1) + \hat{\theta}_{2,2} x_2 + \theta_{2,3} u \right] \tag{H-22 revisited}$$

$$\beta_2 = \frac{\gamma_2}{2} x_2^2 \tag{H-26 revisited}$$

Immersion & Invariance Adaptive Backstepping with two unknown parameters

$$u = \frac{1}{\theta_{2,3}}\left[-z_1 - c_2\left(x_2 - \alpha_1\right) - \hat{\theta}_{2,1}\sin(x_1) - \hat{\theta}_{2,2}x_2 + \dot{\alpha}_1\right] \qquad \text{(H-75 revisited)}$$

$$\hat{\boldsymbol{\theta}}_2 = \boldsymbol{\xi}_2 + \boldsymbol{\beta}_2 \qquad \text{(H-60 revisited)}$$

$$\dot{\boldsymbol{\xi}}_2 = -\frac{\partial \boldsymbol{\beta}_2}{\partial x_1}x_2 - \frac{\partial \boldsymbol{\beta}_2}{\partial x_2}\left[\hat{\theta}_{2,1}\sin(x_1) + \hat{\theta}_{2,2}x_2 + \theta_{2,3}u\right] \qquad \text{(H-65 revisited)}$$

$$\boldsymbol{\beta}_2 = \Gamma_2\left[x_2\sin(x_1) \quad \tfrac{1}{2}x_2^2\right]^T \qquad \text{(H-86 revisited)}$$

Command-Filtered Immersion & Invariance Backstepping with three unknown parameters

$$u^0 = \frac{1}{\hat{\theta}_{2,3}}\left[-\bar{z}_1 - c_2\left(x_2 - x_{2,r}\right) - \hat{\theta}_{2,1}\sin(x_1) - \hat{\theta}_{2,2}x_2 + \dot{x}_{2,r}\right] \qquad \text{(H-110 revisited)}$$

$$\hat{\boldsymbol{\theta}}_2 = \boldsymbol{\xi}_2 + \boldsymbol{\beta}_2 \qquad \text{(H-95 revisited)}$$

$$\dot{\boldsymbol{\xi}}_2 = -\frac{\partial \boldsymbol{\beta}_2}{\partial x_1}x_2 - \frac{\partial \boldsymbol{\beta}_2}{\partial x_2}\left[\hat{\theta}_{2,1}\sin(x_1) + \hat{\theta}_{2,2}x_2 + \hat{\theta}_{2,3}u\right] - \frac{\partial \boldsymbol{\beta}_2}{\partial u}\dot{u} \qquad \text{(H-100 revisited)}$$

$$\boldsymbol{\beta}_2 = \Gamma_2\left[x_2\sin(x_1) \quad \tfrac{1}{2}x_2^2 \quad x_2u\right]^T \qquad \text{(H-103 revisited)}$$

Command-Filtered Immersion & Invariance Incremental Backstepping with Time-Scale Separation

$$u^0 = u_0 + \frac{1}{\hat{\theta}_{2,3}}\left[-\bar{z}_1 - c_2\left(x_2 - x_{2,r}\right) - \dot{x}_{2,0} + \dot{x}_{2,r}\right] \qquad \text{(H-133 revisited)}$$

$$\hat{\theta}_{2,3} = \xi_{2,3} + \beta_2 \qquad \text{(H-120 revisited)}$$

$$\dot{\xi}_{2,3} = -\frac{\partial \beta_2}{\partial x_2}\left(\dot{x}_{2,0} + \left(\xi_{2,3} + \beta_2\right)\Delta u\right) - \frac{\partial \beta_2}{\partial \Delta u}\Delta\dot{u} \qquad \text{(H-124 revisited)}$$

$$\beta_2 = \gamma_2 x_2 \Delta u \qquad \text{(H-128 revisited)}$$

Command-Filtered Immersion & Invariance Incremental Backstepping without Time-Scale Separation

$$u^0 = u_0 + \frac{1}{\hat{\theta}_{2,3}} \left[-\bar{z}_1 - c_2 \left(x_2 - x_{2,r} \right) - \dot{x}_{2,0} - \hat{\theta}_{2,1} \cos(x_{1,0}) \Delta x_1 - \hat{\theta}_{2,2} \Delta x_2 + \dot{x}_{2,r} \right] \tag{H-157 revisited}$$

$$\hat{\boldsymbol{\theta}}_2 = \boldsymbol{\xi}_2 + \boldsymbol{\beta}_2 \tag{H-144 revisited}$$

$$\dot{\boldsymbol{\xi}}_2 = -\frac{\partial \boldsymbol{\beta}_2}{\partial x_1} x_2 - \frac{\partial \boldsymbol{\beta}_2}{\partial \Delta x_1} \Delta x_2 - \frac{\partial \boldsymbol{\beta}_2}{\partial \Delta x_2} \left[\hat{\theta}_{2,1} \cos(x_{1,0}) \Delta x_1 + \hat{\theta}_{2,2} \Delta x_2 + \hat{\theta}_{2,3} \Delta u \right] - \frac{\partial \boldsymbol{\beta}_2}{\partial \Delta u} \Delta \dot{u} \tag{H-148 revisited}$$

$$\boldsymbol{\beta}_2 = \Gamma_2 \begin{bmatrix} \Delta x_2 \cos(x_{1,0}) \Delta x_1 & \frac{1}{2} \Delta x_2^2 & \Delta x_2 \Delta u \end{bmatrix}^T \tag{H-151 revisited}$$

Sensor-Based Backstepping

$$\epsilon \dot{u} = -\operatorname{sgn}\left(\theta_{2,3}\right) \left[\dot{x}_2 - \dot{\alpha}_1 + c_2 z_2 \right] \tag{I-8 revisited}$$

$$u = u(t_0) - \frac{\operatorname{sgn}\left(\theta_{2,3}\right)}{\epsilon} \left[x_2 - x_2(t_0) - \alpha_1 + \alpha_1(t_0) + c_2 \int_{t_0}^{t} \left(x_2 - \alpha_1 \right) \, dt \right] \tag{I-9 revisited}$$

Appendix K

Conclusions Preliminary Analysis

In the literature survey we have seen that there are some blind spots in the Adaptive Backstepping (ABS) theory. First of all, a comprehensive comparison study of the closed-loop performance and sensitivity to parametric uncertainties of these ABS controllers does currently not exist. Next, most literature does not address the sensitivity of the developed controllers to sensor dynamics and noise. Because the ultimate goal is to use Fault Tolerant Flight Control (FTFC) systems to increase the aviation safety, it is of paramount importance to evaluate the performance of these Adaptive Control laws in a practical context. At last, in some of the literature only the closed-loop performance of the adaptive controller is addressed, and not the performance of the parameter estimator itself. Although it is not necessary that the parameters converge to their true values for satisfactory closed-loop performance, Control Allocation (CA) modules require accurate estimates of the control effectiveness parameters.

As a result of these findings, a simple nonlinear pendulum model was used for initial evaluation of five approaches to fault tolerant Backstepping (BS). Sensor noise was *not* yet considered in this preliminary analysis. Based on the derivations and simulations in the `Matlab/Simulink` environment, we can draw the following preliminary conclusions:

- The performance of the conventional BS controller is significantly degraded when uncertainties are introduced.
- Command filters obviate the need for analytic computation of virtual control derivatives. Furthermore, they improve the performance of Lyapunov-based parameter update laws by implementing magnitude, rate and bandwidth constraints on the (virtual) controls.
- Incremental Backstepping (IBS) reduces the sensitivity to parametric uncertainties and possibly model mismatch by using measurements or estimates of the state derivatives and current control deflections. This control approach still relies on a portion of the model. However, by increasing the sampling rate, we can further robustify the controller. Even when the IBS with Time-Scale Separation (TSS) controller is applied to a *non* time-scale separated system, accurate tracking performance is obtained when the sampling rate is sufficiently high.

- With the Tuning Functions Adaptive Backstepping (TFABS) approach we can guarantee closed-loop stability of uncertain systems. A larger adaptation gain of the Tuning Function (TF) estimator generally provides better tracking accuracy.
- By augmenting the BS control law with Immersion and Invariance (I&I) estimators, we can guarantee closed-loop stability of uncertain systems. Note that the way in which stability has been proved for the Immersion and Invariance Adaptive Backstepping (IIABS) controller in this preliminary thesis significantly improves the ease of tuning compared to (Sonneveldt, 2010; Ali, 2013). A larger adaptation gain of the I&I estimator generally provides better tracking accuracy. In contrast to the TFABS approach, the dynamics of the parameter estimation error are known and are monotonically non-increasing when we are dealing with *one* parametric uncertainty. Furthermore, as opposed to TFABS, the I&I estimator does *not* require command filters when we are dealing with magnitude, rate and bandwidth constraints on the (virtual) controls.
- With the Least-Squares Adaptive Backstepping (LSABS) approach, closed-loop stability cannot be (easily) guaranteed in case of uncertainties. However, the Least-Squares (LS) estimator is significantly less complex compared to the TF and I&I estimators. A larger initial covariance matrix P_0 generally provides better tracking accuracy.
- The TF, I&I and LS estimators can be used in combination with an *incremental* control law; in that case the estimator only has to estimate the control efficiency parameter.
- In order to accurately track time-varying parameters with the ABS approaches, function approximators must be used that are capable of approximating the unknown function.
- Sensor-Based Backstepping (SBB) removes the dependency on the system dynamics by using measurements or estimates of the state derivatives and current control deflections. This control strategy uses even less model information compared to the incremental control laws. The SBB controller performs slightly worse compared to the conventional BS controller in absence of uncertainties. The advantage of the SBB controller compared to the BS controller is that it is a model-free approach, and therefore it is not sensitive to model uncertainties. However, tuning might be required to obtain satisfactory closed-loop performance over the complete state space.

From the simulation results can be concluded that all fault tolerant BS control approaches that have been applied to control the uncertain pendulum model are promising. Based on these preliminary conclusions, the paper of this thesis will address the *practicability* of these control approaches. Furthermore, larger system nonlinearities are considered. To achieve this, an accurate high-fidelity aerodynamic Lockheed Martin F-16 `Matlab/Simulink` software package is used. According to (Sonneveldt, 2010), this highly nonlinear model is currently the most accurate aircraft model available. To limit the scope of the thesis, and because the *incremental* control laws significantly improve the robustness compared to the conventional BS controller, only *Adaptive Incremental* BS control laws are considered. The F-16 model will be augmented with sensor dynamics and noise to make the simulations more realistic. The angular accelerations that are necessary for the incremental control laws are estimated on basis of noisy angular rate measurements, because angular accelerometers are not widely available yet. Finally, the control laws as well as the tracking performance, parameter estimation errors and stability properties are compared and conclusions are drawn.

Bibliography

Acquatella, P. (2011). *Robust Nonlinear Spacecraft Attitude Control: An Incremental Backstepping Approach.* Unpublished master's thesis, Delft University of Technology.

Acquatella, P., Falkena, W., van Kampen, E., & Chu, Q. P. (2012, August). Robust Nonlinear Spacecraft Attitude Control using Incremental Nonlinear Dynamic Inversion. In *AIAA Guidance, Navigation, and Control Conference.* American Institute of Aeronautics and Astronautics.

Akella, M. R., & Subbarao, K. (2005). A Novel Parameter Projection Mechanism for Smooth and Stable Adaptive Control. *Systems & Control letters*, *54*(1), 43–51.

Ali, A. A. H. (2013). *Adaptive Incremental Backstepping using Immersion and Invariance.* Unpublished master's thesis, Delft University of Technology.

Ali, A. A. H., Chu, Q. P., van Kampen, E., & de Visser, C. C. (2014, January). Exploring Adaptive Incremental Backstepping using Immersion and Invariance for an F-16 Aircraft. In *AIAA Guidance, Navigation, and Control Conference.*

Artstein, Z. (1983, January). Stabilization with Relaxed Controls. *Nonlinear Analysis: Theory, Methods & Applications*, *7*(11), 1163–1173.

Astolfi, A., & Ortega, R. (2003). Immersion and Invariance: A New Tool for Stabilization and Adaptive Control of Nonlinear Systems. *IEEE Transactions on Automatic Control*, *48*(4), 590–606.

Boyd, S., & Sastry, S. S. (1986, November). Necessary and Sufficient Conditions for Parameter Convergence in Adaptive Control. *Automatica*, *22*(6), 629–639.

Choi, I., & Bang, H. (2011, October). Adaptive Command Filtered Backstepping Tracking Controller Design for Quadrotor Unmanned Aerial Vehicle. In *Proceedings of the Institution of Mechanical Engineers, Part G: Journal of Aerospace Engineering* (Vol. 226, pp. 483–497).

Chowdhary, G., & Jategaonkar, R. (2010, March). Aerodynamic Parameter Estimation from Flight Data Applying Extended and Unscented Kalman Filter. *Aerospace Science and Technology*, *14*(2), 106–117.

Chu, Q. P. (2014). *AE4311 - Advanced Flight Control.* Lecture Slides, Delft University of Technology.

Dayal, B. S., & MacGregor, J. F. (1997, January). Recursive Exponentially Weighted PLS and its Applications to Adaptive Control and Prediction. *Journal of Process Control*, *7*(3), 169–179.

Duarte, M. A., & Narendra, K. S. (1989). Combined Direct and Indirect Approach to Adaptive Control. *IEEE Transactions on Automatic Control*, *34*(10), 1071–1075.

Eason, E. D. (1976). A Review of Least-Squares Methods for Solving Partial Differential Equations. *International Journal for Numerical Methods in Engineering*, *10*(5), 1021–1046.

Edwards, C., Lombaerts, T. J. J., & Smaili, M. H. (2010). *Fault Tolerant Flight Control: A Benchmark Challenge* (Vol. 399; M. Thoma, F. Allgöwer, & M. Morari, Eds.). Springer Berlin Heidelberg.

Enns, D. (1998, August). Control Allocation Approaches. In *AIAA Guidance, Navigation, and Control Conference and Exhibit* (pp. 98–108). Reston, Virigina: American Institute of Aeronautics and Astronautics.

European Aviation Safety Agency. (2013). *Annual Safety Review 2013* (Tech. Rep.).

Falkena, W. (2012). Investigation of Practical Flight Control Systems for Small Aircraft (Doctoral dissertation, Delft University of Technology). *ISBN 978-94-6203-258-3*.

Falkena, W., Borst, C., van Oort, E. R., & Chu, Q. P. (2013, March). Sensor-Based Backstepping. *Journal of Guidance, Control, and Dynamics*, *36*(2), 606–610.

Falkena, W., van Oort, E. R., & Chu, Q. P. (2011, August). Towards Certifiable Advanced Flight Control Systems, A Sensor Based Backstepping Approach. In *AIAA Guidance, Navigation, and Control Conference.* American Institute of Aeronautics and Astronautics.

Farrell, J. A., Polycarpou, M. M., Djapic, V., & Sharma, M. (2012, May). Command Filtered Adaptive Backstepping. *IEEE Transactions on Control Systems Technology*, *20*(3), 566–580.

Farrell, J. A., Polycarpou, M. M., & Sharma, M. (2004). On-line Approximation Based Control of Uncertain Nonlinear Systems with Magnitude, Rate and Bandwidth Constraints on the States and Actuators. *Proceeding of the 2004 American Control Conference*, *3*, 2557–2562.

Farrell, J. A., Polycarpou, M. M., Sharma, M., & Dong, W. (2009). Command Filtered Backstepping. *IEEE Transactions on Automatic Control*, *54*(6), 1391–1395.

Farrell, J. A., Sharma, M., & Polycarpou, M. M. (2005). Backstepping-Based Flight Control with Adaptive Function Approximation. *Journal of Guidance, Control, and Dynamics*, *28*(6), 1089–1102.

Floret-Pontet, F., & Lamnabhi-Lagarrigue, F. (2002). Parameter Identification and State Estimation for Continuous-Time Nonlinear Systems. In *American Control Conference* (Vol. 1, pp. 394–399). American Automatic Control Council.

Galrinho, M. (2013). *A Full Flight Envelope Flight Control System for the Hypersonic UAV Hypresearch.* Unpublished master's thesis, Delft University of Technology.

Galrinho, M., de Visser, C. C., Chu, Q. P., van Kampen, E., & Walpot, L. (2013). *Designing the Flight Control System for a Hypersonic UAV - A Sensor Based Backstepping Approach.*

Holzapfel, F., & Theil, S. (Eds.). (2011). *Advances in Aerospace Guidance, Navigation and Control.* Springer Berlin Heidelberg.

Hovakimyan, N., Lavretsky, E., & Sasane, A. (2007). Dynamic Inversion for Nonaffine-in-Control Systems via Time-Scale Separation. Part I. *Journal of Dynamical and Control Systems*, *13*(4), 451–465.

Hu, J., & Zhang, H. (2013, July). Immersion and Invariance Based Command-Filtered Adaptive Backstepping Control of VTOL Vehicles. *Automatica*, *49*(7), 2160–2167.

van Huffel, S., & Vandewalle, J. (1991). *The Total Least Squares Problem.* Society for Industrial and Applied Mathematics.

Jacklin, S. A. (2008, August). Closing the Certification Gaps in Adaptive Flight Control Software. In *AIAA Guidance, Navigation and Control Conference and Exhibit* (pp. 1–14).

Kalman, R. E. (1960). A New Approach to Linear Filtering and Prediction Problems. *Journal of Basic Engineering*, *82*(1), 35.

Karagiannis, D., & Astolfi, A. (2008a). Nonlinear Adaptive Control of Systems in Feedback Form: An Alternative to Adaptive Backstepping. *Systems & Control Letters*, *57*(9), 733–739.

Karagiannis, D., & Astolfi, A. (2008b). Observer Design for a Class of Nonlinear Systems using Dynamic Scaling with Application to Adaptive Control. In *CDC* (pp. 2314–2319).

Karagiannis, D., & Astolfi, A. (2010). Non-linear and Adaptive Flight Control of Autonomous Aircraft Using Invariant Manifolds. *Proceedings of the Institution of Mechanical Engineers, Part G: Journal of Aerospace Engineering*, *224*(4), 403–415.

Khalil, H. K., & Grizzle, J. W. (2002). *Nonlinear Systems* (Vol. 3). Prentice hall Upper Saddle River.

Kim, B. S., & Calise, A. J. (1997, January). Nonlinear Flight Control Using Neural Networks. *Journal of Guidance, Control, and Dynamics*, *20*(1), 26–33.

Kokotović, P., & Arcak, M. (2001, May). Constructive Nonlinear Control: A Historical Perspective. *Automatica*, *37*(5), 637–662.

Koschorke, J. (2012). *Advanced Flight Control Design and Evaluation.* Unpublished master's thesis, Delft University of Technology.

Krstić, M. (1996, June). Invariant Manifolds and Asymptotic Properties of Adaptive Nonlinear Stabilizers. *IEEE Transactions on Automatic Control*, *41*(6), 817–829.

Krstić, M., Kanellakopoulos, I., & Kokotović, P. (1995). *Nonlinear and Adaptive Control Design.* Wiley.

Laban, M. (1994). On-line Aircraft Aerodynamic Model Identification (Doctoral dissertation, Delft University of Technology). *ISBN 90-6275-987-4*.

Lauzon, A. M., & Bates, J. H. T. (1991, September). Estimation of Time-Varying Respiratory Mechanical Parameters by Recursive Least Squares. *Journal of Applied Physiology*, *71*(3), 1159–65.

Li, X. R. (1999, dec). Recursive Least Squares with Linear Constraints. In *Proceedings of the 38th IEEE Conference on Decision and Control* (Vol. 3, pp. 2414–2419). IEEE.

Lombaerts, T. J. J. (2010). Fault Tolerant Flight Control, A Physical Model Approach (Doctoral dissertation, Delft University of Technology). *ISBN 978-90-815443-1-3*.

Lombaerts, T. J. J., Huisman, H. O., Chu, Q. P., Mulder, J. A., & Joosten, D. A. (2009, May). Nonlinear Reconfiguring Flight Control Based on Online Physical Model Identification. *Journal of Guidance, Control, and Dynamics*, *32*(3), 727–748.

Lombaerts, T. J. J., Schuet, S. R., Wheeler, K. R., Acosta, D. M., & Kaneshige, J. T. (2013, August). Safe Maneuvering Envelope Estimation based on a Physical Approach. *AIAA Guidance, Navigation, and Control Conference*, 1–20.

Lombaerts, T. J. J., Smaili, M. H., Stroosma, O., Chu, Q. P., Mulder, J. A., & Joosten, D. A. (2009, November). Piloted Simulator Evaluation Results of New Fault-Tolerant Flight Control Algorithm. *Journal of Guidance, Control, and Dynamics*, *32*(6), 1747–1765.

Looye, G. H. N. (2008). An Integrated Approach to Aircraft Modelling and Flight Control Law Design (Doctoral dissertation, Delft University of Technology). *ISBN 978-90-5335-148-2*.

Markovsky, I., & Van Huffel, S. (2007, October). Overview of Total Least-Squares Methods. *Signal Processing*, *87*(10), 2283–2302.

Meyer, G., Su, R., & Hunt, L. R. (1984). Application of Nonlinear Transformations to Automatic Flight Control. *Automatica*, *20*(1), 103–107.

Mulder, J. A., Chu, Q. P., Sridhar, J. K., Breeman, J. H., & Laban, M. (1999, October). Non-linear Aircraft Flight Path Reconstruction Review and New Advances. *Progress in Aerospace Sciences*, *35*(7), 673–726.

Narendra, K. S. (1994, December). Parameter Adaptive Control - The End... or The Beginning? In *Conference on Decision and Control* (Vol. 3, pp. 2117–2125). IEEE.

van Oort, E. R. (2011). Adaptive Backstepping Control and Safety Analysis for Modern Fighter Aircraft (Doctoral dissertation, Delft University of Technology). *ISBN 978-90-8570-735-6*.

van Oort, E. R., Chu, Q. P., & Mulder, J. A. (2006, August). Robust Model Predictive Control of a Feedback Linearized F-16/MATV Aircraft Model. In *AIAA Guidance, Navigation, and Control Conference and Exhibit.* Reston, Virigina: American Institute of Aeronautics and Astronautics.

van Oort, E. R., Sonneveldt, L., Chu, Q. P., & Mulder, J. A. (2007, August). Modular Adaptive Input-to-State Stable Backstepping of a Nonlinear Missile Model. In *Navigation and Control.* Reston, Virigina: American Institute of Aeronautics and Astronautics.

Pronzato, L., & Pázman, A. (2013). *Design of Experiments in Nonlinear Models* (Vol. 212). New York: Springer.

Reiner, J., Balas, G. J., & Garrard, W. L. (1996, November). Flight Control Design Using Robust Dynamic Inversion and Time-Scale Separation. *Automatica*, *32*(11), 1493–1504.

Schaefer, R. (2003). *Unmanned Aerial Vehicle Reliability Study* (Tech. Rep.). Washington DC: Office of the Secretary of Defense.

Schuet, S. R., Lombaerts, T. J. J., Acosta, D. M., Wheeler, K. R., & Kaneshige, J. T. (2014, January). An Adaptive Nonlinear Aircraft Maneuvering Envelope Estimation Approach for Online Applications. In *AIAA Guidance, Navigation, and Control Conference* (pp. 1–22). Reston, Virginia: American Institute of Aeronautics and Astronautics.

Serban, R., & Freeman, J. S. (2001, October). Identification and Identifiability of Unknown Parameters in Multibody Dynamic Systems. *Multibody System Dynamics*, *5*(4), 335–350.

Sieberling, S., Chu, Q. P., & Mulder, J. A. (2010, November). Robust Flight Control Using Incremental Nonlinear Dynamic Inversion and Angular Acceleration Prediction. *Journal of Guidance, Control, and Dynamics*, *33*(6), 1732–1742.

Simplício, P., Pavel, M. D., Kampen, E. van, & Chu, Q. P. (2013, August). An Acceleration Measurements-Based Approach for Helicopter Nonlinear Flight Control using Incremental Nonlinear Dynamic Inversion. *Control Engineering Practice*, *21*(8), 1065–1077.

Smaili, M. H., Breeman, J., Lombaerts, T. J. J., & Joosten, D. A. (2006, August). A Simulation Benchmark for Integrated Fault Tolerant Flight Control Evaluation. In *AIAA Modeling and Simulation Technologies Conference and Exhibit* (pp. 1–23). Reston, Virigina: American Institute of Aeronautics and Astronautics.

Soijer, M. W. (2004, May). Sequential Computation of Total Least-Squares Parameter Estimates. *Journal of Guidance, Control, and Dynamics*, *27*(3), 501–503.

Sonneveldt, L. (2010). Adaptive Backstepping Flight Control for Modern Fighter Aircraft (Doctoral dissertation, Delft University of Technology). *ISBN 978-90-8570-573-4*.

Sonneveldt, L., Chu, Q. P., & Mulder, J. A. (2007, March). Nonlinear Flight Control Design Using Constrained Adaptive Backstepping. *Journal of Guidance, Control, and Dynamics*, *30*(2), 322–336.

Sonneveldt, L., Oort, E. R. van, Chu, Q. P., & Mulder, J. A. (2010, August). Immersion and Invariance Based Nonlinear Adaptive Flight Control. In *AIAA Guidance, Navigation, and Control Conference.*

Sun, L. G. (2014). Model and Sensor Based Nonlinear Adaptive Flight Control with Online System Identification (Doctoral dissertation, Delft University of Technology). *ISBN 978-94-6186-350-8*.

Tang, S. H. (2014). *Piloted Simulator Evaluation of a Model-Independent Fault-Tolerant Flight Controller*. Unpublished master's thesis, Delft University of Technology.

Timmons, W. D., Chizeck, H. J., Casas, F., Chankong, V., & Katona, P. G. (1997). Parameter-Constrained Adaptive Control. *Industrial & Engineering Chemistry Research*, *36*(11), 4894–4905.

de Visser, C. C. (2011). Model Identification (Doctoral dissertation, Delft University of Technology). *ISBN 978-90-8570-770-7*.

de Visser, C. C. (2012). *AE4312 - Modern System Identification of Aerospace Vehicles.* Lecture Slides, Delft University of Technology.

Vlaar, C. M. (2014). *Incremental Nonlinear Dynamic Inversion Flight Control - Implementation and Flight Test on a Fixed Wing UAV*. Unpublished master's thesis, Delft University of Technology.

Wan, E. A., & Van Der Merwe, R. (2000). The Unscented Kalman Filter for Nonlinear Estimation. In *Proceedings of the IEEE 2000 Adaptive Systems for Signal Processing, Communications, and Control Symposium* (pp. 153–158).

Wehrend, W. R. J. (1979). *Pilot Control Through the TAFCOS Automatic Flight Control System* (Tech. Rep. No. NASA TM-81152).

Williams, K. W. (2004). *A Summary of Unmanned Aircraft Accident / Incident Data: Human Factors Implications* (Tech. Rep.). Office of Aerospace Medicine.

Zhan, R., & Wan, J. (2007, July). Iterated Unscented Kalman Filter for Passive Target Tracking. *IEEE Transactions on Aerospace and Electronic Systems*, *43*(3), 1155–1163.

Zhu, Y., & Li, X. R. (1999). Recursive Least Squares With Linear Constraints. In *Proceedings of the 38th IEEE Conference on Decision and Control* (Vol. 3, pp. 2414–2419).

Zinober, A., & Owens, D. (2003). *Nonlinear and Adaptive Control.* Springer.